frontiers | Research Topics

Genetics and genomics of plant reproduction for crop breeding, volume II

Edited by
Gianni Barcaccia, Fulvio Pupilli, Sara Zenoni, Emidio Albertini, Andrea Mazzucato, Silvia Vieira Coimbra, Luciana Baldoni and Soraya Mousavi

Published in
Frontiers in Plant Science

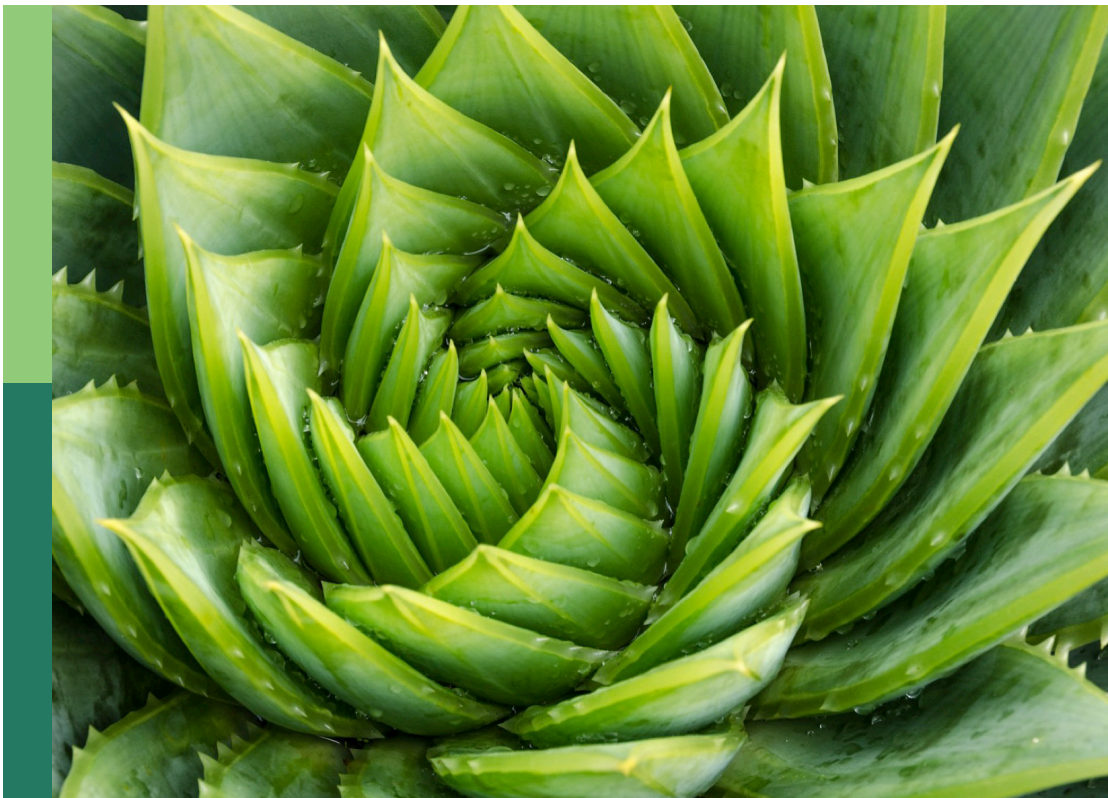

ISSN 1664-8714
ISBN 978-2-83251-788-8
DOI 10.3389/978-2-83251-788-8

About Frontiers

Frontiers is more than just an open access publisher of scholarly articles: it is a pioneering approach to the world of academia, radically improving the way scholarly research is managed. The grand vision of Frontiers is a world where all people have an equal opportunity to seek, share and generate knowledge. Frontiers provides immediate and permanent online open access to all its publications, but this alone is not enough to realize our grand goals.

Frontiers journal series

The Frontiers journal series is a multi-tier and interdisciplinary set of open-access, online journals, promising a paradigm shift from the current review, selection and dissemination processes in academic publishing. All Frontiers journals are driven by researchers for researchers; therefore, they constitute a service to the scholarly community. At the same time, the *Frontiers journal series* operates on a revolutionary invention, the tiered publishing system, initially addressing specific communities of scholars, and gradually climbing up to broader public understanding, thus serving the interests of the lay society, too.

Dedication to quality

Each Frontiers article is a landmark of the highest quality, thanks to genuinely collaborative interactions between authors and review editors, who include some of the world's best academicians. Research must be certified by peers before entering a stream of knowledge that may eventually reach the public - and shape society; therefore, Frontiers only applies the most rigorous and unbiased reviews. Frontiers revolutionizes research publishing by freely delivering the most outstanding research, evaluated with no bias from both the academic and social point of view. By applying the most advanced information technologies, Frontiers is catapulting scholarly publishing into a new generation.

What are Frontiers Research Topics?

Frontiers Research Topics are very popular trademarks of the *Frontiers journals series*: they are collections of at least ten articles, all centered on a particular subject. With their unique mix of varied contributions from Original Research to Review Articles, Frontiers Research Topics unify the most influential researchers, the latest key findings and historical advances in a hot research area.

Find out more on how to host your own Frontiers Research Topic or contribute to one as an author by contacting the Frontiers editorial office: frontiersin.org/about/contact

Genetics and genomics of plant reproduction for crop breeding, volume II

Topic editors

Gianni Barcaccia — University of Padua, Italy
Fulvio Pupilli — National Research Council (CNR), Italy
Sara Zenoni — University of Verona, Italy
Emidio Albertini — University of Perugia, Italy
Andrea Mazzucato — University of Tuscia, Italy
Silvia Vieira Coimbra — University of Porto, Portugal
Luciana Baldoni — Institute of Bioscience and Bioresources, National Research Council (CNR), Italy
Soraya Mousavi — National Research Council (CNR), Italy

Citation

Barcaccia, G., Pupilli, F., Zenoni, S., Albertini, E., Mazzucato, A., Coimbra, S. V., Baldoni, L., Mousavi, S., eds. (2023). *Genetics and genomics of plant reproduction for crop breeding, volume II*. Lausanne: Frontiers Media SA. doi: 10.3389/978-2-83251-788-8

Table of contents

frontiers | Frontiers in Plant Science

TYPE Editorial
PUBLISHED 14 February 2023
DOI 10.3389/fpls.2023.1145208

OPEN ACCESS

EDITED AND REVIEWED BY
Francisco Barro,
Institute for Sustainable Agriculture (CSIC), Spain

*CORRESPONDENCE
Gianni Barcaccia
gianni.barcaccia@unipd.it

SPECIALTY SECTION
This article was submitted to Plant Breeding, a section of the journal Frontiers in Plant Science

RECEIVED 15 January 2023
ACCEPTED 31 January 2023
PUBLISHED 14 February 2023

CITATION
Barcaccia G, Mazzucato A, Albertini E, Zenoni S, Baldoni L, Mousavi S, Mendes MA, Coimbra S, Granell A and Pupilli F (2023) Editorial: Genetics and genomics of plant reproduction for crop breeding, volume II.
Front. Plant Sci. 14:1145208.
doi: 10.3389/fpls.2023.1145208

Editorial: Genetics and genomics of plant reproduction for crop breeding, volume II

Gianni Barcaccia[1]*, Andrea Mazzucato[2], Emidio Albertini[3], Sara Zenoni[4], Luciana Baldoni[5], Soraya Mousavi[5], Marta Adelina Mendes[6], Silvia Coimbra[7], Antonio Granell[8] and Fulvio Pupilli[5]

[1]Department of Agronomy Food Natural resources Animals and Environment (DAFNAE), University of Padova, Padova, Italy, [2]Department of Agriculture and Forest Sciences (DAFNE), University of Tuscia, Viterbo, Italy, [3]Department of Agricultural, Food and Environmental Sciences (DSA3), University of Perugia, Perugia, Italy, [4]Department of Biotechnologies, University of Verona, Verona, Italy, [5]Institute of Biosciences and Bioresources, Research Division of Perugia, National Research Council (CNR), Perugia, Italy, [6]Department of Biosciences, University of Milan, Milan, Italy, [7]Department of Biology, Faculty of Sciences, University of Porto, Porto, Portugal, [8]Institute of Molecular and Cellular Biology of Plants, Spanish National Research Council (CSIC), Polytechnic University of Valencia, Valencia, Spain

KEYWORDS

apomixis, apomeiosis, parthenogenesis, male-sterility, self-incompatibility, parthenocarpy, polyploidy, plant breeding

Editorial on the Research Topic
Genetics and genomics of plant reproduction for crop breeding, volume II

The main challenges of modern agriculture deal with sustainably producing food and raw materials while contributing to environment preservation and mitigation of climate change risks worldwide. The actual unprecedented global economic and social crisis due to the Coronavirus pandemic, along with the current geo-politics instability due to Russia's war in Ukraine and the modified climate conditions, will likely mean a turning point to deal with the overall resilience of agriculture systems and sustainability of food supplies (Barcaccia et al., 2020).

In a not too far coming future, increasing the production per hectare of cultivated plants will be necessary to cope with the increasing human population and the gradual deterioration of environmental conditions, especially in developing countries. Suppose it is true that next-generation genotyping and phenotyping platforms enable to predict and select resistance to plant pathogens and tolerance to environmental stresses. In that case, it is also true that new breeding techniques allow the developing of improved varieties based on superior genotypes enriched or edited for single genes/traits so to ensure greater unit yields ("more with less" principle) and better quality for economically important plant species ("do no significant harm" principle). In this context, studying and understanding the mechanisms that regulate reproductive systems is crucial as, in many cases, the stability and yield of crop plants depend on genetic factors and networks controlling fundamental aspects of seed and fruit development.

Reproduction in angiosperms has a well-defined evolutionary meaning. If, on the one hand, it markedly determines the preservation of genetic diversity between species, limiting or avoiding an exchange of genes between different genomes, on the other hand, it equally

affects the genetic structure of populations, significantly contributing to the composition of genotypes within species and the organization of their genomes (Figure 1). Consequently, the opportunities and modalities for the genetic improvement of crop populations and the development of new varieties depend on plant reproductive systems and barriers, including male-sterility, self-incompatibility, parthenocarpy, and apomeiosis/parthenogenesis or apomixis. In a general view, comprehending the molecular basis of the reproductive systems of crop plants will help overcome the reproductive barriers that limit crop yield and quality, and serve to understand the evolution and structure of plant populations.

Our Research Topic, Genetics and Genomics of Plant Reproduction for Crop Breeding, includes a total of 25 articles in its first volume (Research Topic, vol. 1) and additional 12 articles in its second volume (Research Topic, vol. 2). It represents a valuable collection of both Original Research and Review Articles focused on the recent advances of our knowledge on the genetics of crop plant reproductive systems owing to the application and exploitation of novel biotechnological tools supported by information deriving from modern genomics. Several articles provided insights on identifying the genetic mechanisms and factors that control the expression of sexual barriers and molecular markers for their prediction in important horticultural crops and fruit trees. The latter include male-sterility in leaf chicory, tomato, and foxtail millet (Palumbo et al.; Takei et al.; Gao et al.), self-incompatibility in cabbage, pear, and olive (Alagna et al.; Claessen et al.; Mariotti et al.; Xiao et al.) and parthenocarpy in tomato and, more in general, in higher plants (Picarella and Mazzucato; Takei et al.). Other articles reported consistent findings from the identification and/or functional analysis of candidate genes for apomixis and its components (apomeiosis, i.e., aposporY or diplospory, parthenogenesis, and autonomous endosperm development) in apomictic model species (Mancini et al.; Galla et al.; Kaushal et al.; Vijverberg et al.; Zappacosta et al.; Cielo Pasten et al.; Singh Sidhu et al.; Xia et al.). Worth of mentioning several very interesting review articles on the topics of apomixis as a whole (i.e., The rise of apomixis in natural plant populations by Hojsgaard and Hörandl; Partitioning apomixis components to understand and utilize gametophytic apomixis by Kaushal et al.; Does Polyploidy inhibit sex chromosome evolution in Angiosperms? By He and Hörandl; Trends in apomixis research: the ten most cited research articles published in the pregenomic and genomic eras by Palumbo et al.), parthenogenesis (i.e., Identifying and engineering genes for parthenogenesis in plants by Vijverberg, Ozias-Akins, and Schranz), self-incompatibility (i.e., Finding a compatible partner: molecular control, genetic determination, and impact on fertilization and fruit set of self-incompatibility in European pear by Claessen et al.; The paradox of self-fertile varieties in the context of self-incompatible genotypes in olive by Alagna et al.) and parthenocarpy (i.e., The occurrence of seedlessness in higher plants, with insights on roles and mechanisms of parthenocarpy by Picarella and Mazzucato, 2019).

The potential use of new biotechnological approaches for either loss-of-function and gain-of-function applications, such as cisgenesis (for conspecific gene transfer or introgression) and genome editing (for endogenous gene knockout or silencing and gene editing or replacement), will assume strong relevance in the future of agriculture, as these methods would allow direct intervention at the genomic level in any variety without changing its genetic background (Pirrello et al., 2022). All these genome-wide biotechnological strategies contribute to the achievement of new rapidly increasing precision breeding methods that are potentially useful for developing cultivars genetically improved for single traits while preserving the rest of the genome. In addition, these methods reduce the time needed to fix a superior genotype in an elite cultivar, avoiding any genetic recombination or transfer of unwanted genetic material. Furthermore, in the coming years, it seems possible that biotechnological approaches could allow not only cisgenesis transfer or the editing of genes of interest but also the control of whole biosynthetic pathways and regulatory networks, making the improvement of crop plant cultivars for complex agronomic traits achievable by intervening in the development or composition of specific tissues and organs.

It is well known that the possibility to control fertilization to achieve full hybridization between genetically divergent parental lines is highly desirable for breeding F1 hybrid seeds and heterotic varieties, as farmers demand. Natural parthenocarpy is also desirable as a strategy for producing seedless fruits, increasingly

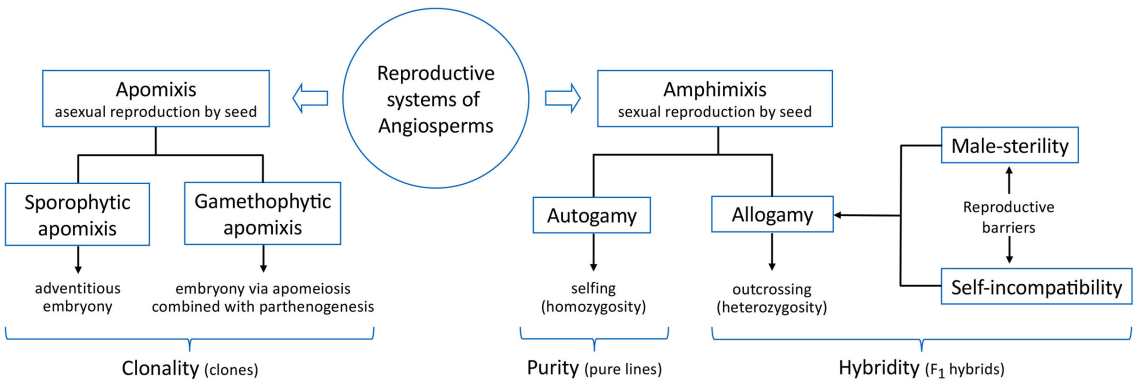

FIGURE 1
Main reproductive systems and barriers in crop plants: apomixis determines clonal populations by means of either sporophytic embryony or gamethophytic embryony, whereas amphimixis through selfing and outcrossing is exploited for breeding pure lines and F1 hybrids, respectively.

appreciated by consumers. With the strengthening of genomics, mapping and cloning the genes that control meiosis, gametogenesis, pollen-pistil interaction, and fertilization-independent hybrid seed and seedless fruit production is at our fingertips. For the most important crop plants, traditional breeding approaches have been used extensively to develop new cultivars with desirable characteristics, including resistance/tolerance to biotic and abiotic stresses, high yield, and a high content of compounds beneficial to human health. The technological progress of the last few decades has revolutionized our ability to study and manipulate genetic variation in crop plants. The development of high-throughput sequencing platforms and accompanying analytical methods have led to the sequencing and assembling of a large number of plant genomes, the construction of dense and ultra-dense molecular linkage maps, the identification of structural variants, and the application of molecular markers in breeding programs (Reviewed by Simko et al., 2021).

We are confident that the control of plant reproduction systems and barriers can potentially change the distribution and scale of investments for breeding new varieties, disrupt existing commercial supply chains and lead to greater uptake and use of agronomic sources and nutritional traits, contributing so to environmental quality traits and mitigation of climate change risks. We expect that genomics and biotechnologies can play a central role in modern plant breeding, as their main applicative tools and platforms are capable of making a pivotal contribution to renewing the varietal landscape for the main crops and restarting the whole primary sector and agri-food industry, also addressing social and environmental issues, and so accelerating the transition to sustainability (Barcaccia et al., 2020).

As technologies to overcome sexual barriers, as others related to genetic improvement of crops are mainly focused on guaranteeing sufficient, safe, and nutrient food worldwide, efforts in research and investments should be maintained under governmental control.

Author contributions

GB: conceptualization. GB: writing—original draft preparation. All authors listed have made a substantial, direct, and intellectual contribution to review and edit this version of the work and approved it for publication.

Acknowledgments

We wish to thank the authors of the articles published in this Research Topic for their valuable scientific contributions and the reviewers for their rigorous revisions. We also wish to thank the Editorial board for their qualified and continuous support.

Conflict of interest

The authors declare that the research was conducted in the absence of any commercial or financial relationships that could be construed as a potential conflict of interest.

The handling editor FB declared a shared parent affiliation with the author AG at the time of review.

Publisher's note

References

Barcaccia, G., D'Agostino, V., Zotti, A., and Cozzi, B. (2020). Impact of the SARS-CoV-2 on the Italian agri-food sector: an analysis of the quarter of pandemic lockdown and clues for a socio-economic and territorial restart. *Sustainability* 12 (14), 5651. doi: 10.3390/su12145651

Pirrello, C., Magon, G., Palumbo, F., Farinati, S., Lucchin, M., Barcaccia, G., et al. (2022). Past, present and future of genetic strategies to control tolerance to the main fungal and oomycete pathogens in grapevine. *J. Exp. Bot.* erac487. doi: 10.1093/jxb/erac487

Simko, I., Jia, M., Venkatesh, J., Kang, B.-C., Weng, Y., Barcaccia, G., et al. (2021). Genomics and marker-assisted improvement of vegetable crops. *Crit. Rev. Plant Sci.* 40 (4), 303–365. doi: 10.1080/07352689.2021.1941605

frontiers in Plant Science

ORIGINAL RESEARCH
published: 24 January 2022
doi: 10.3389/fpls.2021.817922

The Ethylene Biosynthesis Gene *CpACO1A*: A New Player in the Regulation of Sex Determination and Female Flower Development in *Cucurbita pepo*

Gustavo Cebrián[1†], Jessica Iglesias-Moya[1†], Jonathan Romero[1†], Cecilia Martínez[1†], Dolores Garrido[2†] and Manuel Jamilena[1*†]

[1] Department of Biology and Geology, Agrifood Campus of International Excellence and Research Centre CIAMBITAL, University of Almería, Almería, Spain, [2] Department of Plant Physiology, University of Granada, Granada, Spain

A methanesulfonate-generated mutant has been identified in *Cucurbita pepo* that alters sex determination. The mutation converts female into hermaphrodite flowers and disrupts the growth rate and maturation of petals and carpels, delaying female flower opening, and promoting the growth rate of ovaries and the parthenocarpic development of the fruit. Whole-genome resequencing allowed identification of the causal mutation of the phenotypes as a missense mutation in the coding region of *CpACO1A*, which encodes for a type I ACO enzyme that shares a high identity with *Cucumis sativus* CsACO3 and *Cucumis melo* CmACO1. The so-called *aco1a* reduced ACO1 activity and ethylene production in the different organs where the gene is expressed, and reduced ethylene sensitivity in flowers. Other sex-determining genes, such as *CpACO2B*, *CpACS11A,* and *CpACS27A*, were differentially expressed in the mutant, indicating that ethylene provided by CpACO1A but also the transcriptional regulation of *CpACO1A*, *CpACO2B*, *CpACS11A*, and *CpACS27A* are responsible for determining the fate of the floral meristem toward a female flower, promoting the development of carpels and arresting the development of stamens. The positive regulation of ethylene on petal maturation and flower opening can be mediated by inducing the biosynthesis of JA, while its negative control on ovary growth and fruit set could be mediated by its repressive effect on IAA biosynthesis.

Keywords: *ACO* gene regulation, andromonoecy, monoecy, ethylene, flower maturation, parthenocarpy

HIGHLIGHTS

- CpACO1A is a type I ACO enzyme involved in ethylene production in different *Cucurbita pepo* organs.
- A mutation in *CpACO1A* disrupts ethylene production and converts female into hermaphrodite flowers.
- Transcription of the ethylene biosynthesis genes is feedback-regulated in the female flower.
- The mutation *aco1a* alters the homeostasis of IAA, ABA, JA, and SA in the female flower.

OPEN ACCESS

Edited by:
Silvia Vieira Coimbra, University of Porto, Portugal

Reviewed by:
Ana Maria Rocha De Almeida, California State University, East Bay, United States
Tangren Cheng, Beijing Forestry University, China
Haifeng Li, Northwest A&F University, China
Simona Masiero, University of Milan, Italy

***Correspondence:**
Manuel Jamilena
mjamille@ual.es

†ORCID:
Gustavo Cebrián
orcid.org/0000-0001-8969-1976
Jessica Iglesias-Moya
orcid.org/0000-0002-4632-8162
Jonathan Romero
orcid.org/0000-0003-0812-0309
Cecilia Martínez
orcid.org/0000-0003-0464-1828
Dolores Garrido
orcid.org/0000-0002-0426-7146
Manuel Jamilena
orcid.org/0000-0001-7072-0458

Specialty section:
This article was submitted to Plant Breeding, a section of the journal Frontiers in Plant Science

Received: *18 November 2021*
Accepted: *27 December 2021*
Published: *24 January 2022*

Citation:
Cebrián G, Iglesias-Moya J, Romero J, Martínez C, Garrido D and Jamilena M (2022) The Ethylene Biosynthesis Gene CpACO1A: A New Player in the Regulation of Sex Determination and Female Flower Development in Cucurbita pepo. Front. Plant Sci. 12:817922. doi: 10.3389/fpls.2021.817922

INTRODUCTION

The cultivated species of the Cucurbitaceae family are a group of monoecious plants that have been utilized as a model for the study of the genetic control of sex determination in plants (Martínez and Jamilena, 2021). Many varieties in cultivated species are monoecious, developing male and female flower in the same plant, but some of the varieties are andromonoecious (male and hermaphroditic flowers), trimonoecious (male, female, and hermaphroditic flowers), gynoecious (only female flowers), and androecious (only male flowers). This natural variability makes this an ideal family to investigate the genetics of sex determination. The first sex-determining genes were discovered in *Cucumis sativus* (cucumber) and *Cucumis melo* (melon) (Boualem et al., 2008, 2009, 2015; Martin et al., 2009; Chen et al., 2016), but recent years have witnessed important discoveries in *Cucurbita pepo* (pumpkin and squash) (Martínez et al., 2014; García et al., 2020a,b) and *Citrullus lanatus* (watermelon) (Boualem et al., 2016; Ji et al., 2016; Manzano et al., 2016; Aguado et al., 2020; Zhang et al., 2020). Although many of the findings are similar in all species, the genetic control of sexual determination in some species differs slightly from the rest of the species (Aguado et al., 2020).

Ethylene is the key regulator of sex determination in cucurbits. External treatments with ethylene-releasing or -inhibiting agents have been used to determine the role of this hormone in the control of sex expression, i.e., female flowering transition and the number of female and male flowers per plant, as well as sex determination, which are the mechanisms that lead to a female or a male flower from a potentially hermaphrodite floral bud (Manzano et al., 2013, 2014). The latter was achieved by arresting the growth of the stamens or carpels, respectively (Bai et al., 2004). Ethylene increases the ratio of female to male flowers in *Cucumis* and *Cucurbita* (Rudich et al., 1969; Byers et al., 1972; Manzano et al., 2011, 2013), but reduces this ratio in *Citrullus* plants. Inhibition of ethylene biosynthesis or perception, on the other hand, reduces the number of female flowers per plant in *Cucumis* and *Cucurbita*, and transforms the female flowers into bisexual or hermaphrodite ones. In *Citrullus*, this last treatment increases the number of female flowers per plant, but also transforms female flowers into hermaphroditic flowers, indicating that ethylene is required to arrest the development of stamens in female flowers of all cucurbits (Manzano et al., 2014). Although gibberellins, auxins, and brassinosteroids have also been associated with sex control in cucurbits, some of their functions seem to be mediated by ethylene (Papadopoulou et al., 2005; Manzano et al., 2011; Zhang et al., 2014, 2017).

So far, all of the discovered sex-determining genes are either in the ethylene biosynthesis and signaling pathway, or are transcriptional factors that regulate the former. The gene that regulates abortion of stamens during the formation of a female flower in all studied cucurbits encodes for an ethylene biosynthesis enzyme: cucumber *ACS2* and its orthologs (Boualem et al., 2008, 2009, 2016; Martínez et al., 2014; Ji et al., 2016; Manzano et al., 2016). This female-forming gene is negatively regulated by the transcription factor *WIP1*, which is responsible for the arrest of carpels in the formation of male flowers (Martin et al., 2009; Hu et al., 2017; Zhang et al., 2020). The male-forming *WIP1* gene is negatively regulated by *ACS11* and *ACO2/ACO3* in cucumber and melon, which are expressed very early in the floral meristem and determine the formation of a female flower. The disruption of either of these genes promotes the conversion of monoecy into androecy (Boualem et al., 2015; Chen et al., 2016). EMS mutation in ethylene receptor genes of *C. pepo* has demonstrated that ethylene perception at early and late stages of flower development is crucial for female flower determination. The *etr1a*, *etr1a-1*, *etr1b*, and *etr2b* gain of function mutations, in fact, lead to andromonoecy and androecy concomitantly with a reduced ethylene sensitivity (García et al., 2018, 2020a,b).

The role of other ethylene biosynthesis genes in sex determination is unknown. In this paper, we demonstrate that the ethylene biosynthesis gene *CpACO1A* is involved in sex determination and flower development in *C. pepo*. Although the gene is not flower-specific, its role in ethylene biosynthesis is required for arresting stamen development, and the proper maturation and development of corolla and ovary of the female flower. *CpACO1A* and other sex-determining *ACO* and *ACS* ethylene biosynthesis genes were regulated by *CpACO1A*-producing ethylene in the female flower. The ethylene provided by CpACO1A also regulates hormonal balance in the female flowers. The increased indole-3-acetic acid (IAA) and the reduced abscisic acid (ABA) and jasmonic acid (JA) contents in the *aco1a* mutant may be responsible for the parthenocarpic fruit development and the delayed flower opening of the mutant female flower.

MATERIALS AND METHODS

Plant Material and Isolation of Mutants

The *aco1a* mutant analyzed in this study was isolated from a high-throughput screening of *C. pepo* EMS collection (García et al., 2018). M2 plants from 600 lines were grown to maturity under standard greenhouse conditions, and alterations in reproductive developmental traits were evaluated. A mutant family was detected that produced hermaphrodite flowers, instead of female flowers. This mutant was selected for further characterization, and named *aco1a*. The monitoring of the development of the growth of the female floral organs, corolla, and ovary, as well as the degree of their stamen development detected in the flowers, showed similarity with the phenotype found for other families of mutants previously described and characterized by García et al. (2020a,b) in *C. pepo*, which led us to deduce the possible relationship of ethylene with this new mutation. Prior to phenotyping, *aco1a* mutant plants were crossed twice with the background genotype MUC16, and the resulting BC_2 generation was selfed to obtain the BC_2S_1 generation.

Phenotyping for Monoecy Stability, Sex Expression, and Floral Traits

The total of 300 BC_2S_1 plants from wt/wt, wt/*aco1a*, and *aco1a*/*aco1a* were transplanted to a greenhouse and grown to

maturity under local greenhouse conditions without climate control, and under standard crop management of the region, in Almería, Spain. The sex phenotype of each plant was determined according to the sex of the flowers in the first 40 nodes of each plant. A minimum of 30 wt/wt, 30 wt/*aco1a*, and 30 *aco1a*/*aco1a* plants were phenotyped. Phenotypic evaluations were performed in the spring-summer seasons 2019 and 2020.

The sex expression of each genotype was assessed by determining the node at which plants transitioned to pistillate flowering, and the number of male or pistillate/hermaphrodite flower nodes. The sex phenotype of each individual pistillate/hermaphrodite flower was assessed by the so-called andromonoecy index (AI) (Martínez et al., 2014; Manzano et al., 2016). Pistillate flowers were separated into three phenotypic classes that were given a score from 0 to 3 according to the degree of their stamen development: female (AI = 0), showing no stamen development; bisexual or pistillate (AI = 1; AI = 2), showing partial development of stamens and no pollen; and hermaphrodite (AI = 3), showing complete development of stamens and pollen. The average AI of each plant and each genotype was then assessed from the resulting AI score of at least 10 individual female flowers from each plant, using a minimum of 30 plants for each genotype. To assess floral organ development, the growth rates of ovaries and petals in both female and male flowers of WT and *aco1a* mutant plants were determined by measuring the length and diameter of these floral organs every 2 day for 28 day in 20 flowers of each genotype, starting with flower buds ∼2 mm in length. The anthesis time was estimated as the number of days taken for a 2 mm pistillate or male floral bud to reach anthesis.

Identification of *aco1a* Mutation by Whole-Genome Sequencing Analysis

To identify the causal mutations of the *aco1a* phenotype, WT, and mutant plants derived from BC_1S_1-segregating populations were subjected to whole-genome sequencing (WGS). In total, 120 BC_1S_1 seedlings were transplanted to a greenhouse and grown to maturity. The phenotype of those seedlings was verified in the adult plants, as wt/wt and wt/*aco1a* plants were monoecious while *aco1a*/*aco1a* plants were andromonoecious or partially andromonoecious.

The genomic DNA from 30 WT and 30 *aco1a* plants was isolated by using the Gene JET Genomic DNA Purification Kit (Thermo Fisher Scientific®), and pooled into two different bulks: WT bulk and *aco1a* mutant bulk. DNA from each bulk was randomly sheared into short fragments of approximately 350 bp for library construction using the NEBNext® DNA Library Prep Kit[1], and fragments were briefly PCR enriched with indexed oligos. Pair-end sequencing was performed using the Illumina® sequencing platform, with a read length of PE150 bp at each end. The effective sequencing data were aligned with the reference *C. pepo* genome v.4.1 through BWA software (Li and Durbin, 2009). Single nucleotide polymorphisms (SNPs) were detected using the GATK HAPLOTYPECALLER (Depristo et al., 2011). ANNOVAR was used to annotate the detected SNPs (Wang et al., 2010). Common variants between these mutant families (and other sequenced mutant families in the laboratory) were discarded, as they are likely common genomic differences with the reference genome. The genotype of the WT bulk (wt/wt and wt/*aco1a* plants) was expected to be 0/1 with an alternative allelic frequency (AF) of 0.3, while the genotype of the mutant bulk (*aco1a*/*aco1a* plants) was expected to be 1/1 with an AF = 1. Therefore, the sequencing data were filtered according to the following parameters: genotype quality $\geq$ 90, read depth $\geq$ 10, AF = 1 in the mutant bulks, and AF $\leq$ 0.3 in the WT bulks. Once we had a set of positions that were differentially enriched in each bulk, we filtered out SNPs that were not canonical EMS changes (G > A or C > T transitions) (Till et al., 2004). All filters were performed with RStudio® software. The impact of this final set EMS SNPs on gene function was finally determined by using Integrative Genomics Viewer (IGV) software and the Cucurbit Genomics Database (CuGenDB)[2].

Validation of the Identified Mutations by High-Throughput Genotyping of Individual Segregating Plants

Segregation analysis was performed to confirm that the identified mutations were causal mutations of the *aco1a* phenotype. Approximately 300 BC_2S_1 plants segregating for the mutation were genotyped using Kompetitive allele-specific PCR (KASP) technology. Primers were synthesized by LGC Genomics®[3], and the KASP assay was performed in the FX96 Touch Real−Time PCR Detection System (Bio-Rad®) using the LGC protocol[4]. The multiplex PCRs were run with 10 μL final reaction volume containing 5 μL KASP V4.0 2× Master mix standard ROX (LCG Genomics®), 0.14 μL KASP-by-Design primer mix (LCG Genomics®), 2 μL of 10–20 ng/μL genomic DNA, and 2.86 μL of water. The PCR thermocycling conditions were 15 min at 94°C (hot-start activation) followed by 10 cycles of 94°C for 20 s and 61°C for 1 min (dropping −0.6°C per cycle to achieve a 55°C annealing temperature) followed by 26 cycles of 94°C for 20 s and 55°C for 1 min. Data were then analyzed using CFX Maestro™ Software (Bio-Rad®) to identify SNP genotypes.

1-Aminocyclopropane-1-Carboxylic Acid Oxidase Enzyme Activity

1-Aminocyclopropane-1-carboxylic acid oxidase (ACO) activity was assessed following the protocol described in Bulens et al. (2011). The enzyme activity was quantified in leaves, stems, roots, cotyledon, and flowers in triplicate. About 0.5 g of each material was pulverized in liquid nitrogen, and 1 mL of extraction buffer MOPS (pH 7.2) and 50 mg of polyvinylpolypyrrolidone (PVPP) were added to each sample. The samples were subsequently incubated for 10 min at 4°C and finally centrifuged for 30 min at 22,000 × *g* at 4°C. About 400 μL of the resulting supernatant

[1]https://international.neb.com

[2]http://cucurbitgenomics.org

[3]http://www.lgcgroup.com

[4]https://afly.co/xyn2

was mixed with 3.6 mL of MOPS reaction buffer (pH 7.2) in a 20 mL glass vial. After homogenizing the mixture for 5 s, samples were incubated in a water bath for 1 h at 30°C while gently shaking. The amount of ethylene formed was determined by analyzing 1 mL of gas from the headspace of the reaction tube on a Varian® 3900 gas chromatograph (GC) fitted with a flame ionisation detector (FID). A blank sample (3.6 mL reaction buffer + 400 μL DW) was used as a control for the whole process. Enzyme reactions and ethylene readings were done in triplicate. The activity of ACO was expressed as nmol $\times$ gFW^{-1} $\times$ h^{-1}.

Ethylene Production Measurements

The production of ethylene in WT and *aco1a* flowers was assessed throughout the different stages of development. Female and male floral buds of 8–55 mm in length (FFB/MFB) and the apical shoots of plants growing under climatic controlled conditions were collected and incubated at room temperature for 6 h in hermetic glass containers of 50–450 mL. Ethylene production was determined by analyzing 1 mL of gas from the headspace in a Varian® 3900 gas chromatograph (GC) fitted with a FID. The instrument was calibrated with standard ethylene gas. Four biological replicates were made for each one of the flower developmental stages analyzed and three measurements per sample. Ethylene production was expressed as nL $\times$ gFW^{-1} $\times$ $6\,h^{-1}$.

Assessing Ethylene Sensitivity

To evaluate the level of sensitivity to ethylene, flower abscission was assessed for male flowers in response to an external treatment with ethylene. Male flowers from WT and *aco1a* plants were collected at two stages of development: A (anthesis) and A-2 (2 day before anthesis). For each stage, 30 WT and *aco1a* flowers were placed in glass vases with water, and incubated in two culture chambers with equal humidity and temperature, 50% RH and 20°C. One of the chambers was used as a control (Ct), and the other was filled with 50 ppm of ethylene (ET). The tests were performed in triplicate. Both chambers remained closed for 72 h, and the percentage of abscission produced was evaluated after 24, 36, 48, and 72 h for each stage of development.

Hormone Concentration Measurements

Female flower buds of 5–8 mm from WT and *aco1a* plants were collected for hormone concentration measurements. Representative samples consisted of three bulks of approximately 30 female flowers each. To preserve the samples, WT and *aco1a* bulks were quickly stored on dry ice. Then, the samples were placed in a freeze dryer CRYODOS V3.1-50 (Telstar®), where they were lyophilized for 1 week and subsequently pulverized in a mixer mill MM200 (Retsch™). The concentration of salicylic acid (SA), indol-3-butyric acid (IBA), IAA, gibberellic acid (GA3), 6-benzyladenine (BA), ABA, and JA were determined in each triplicated sample through ultra-performance liquid chromatography coupled with a hybrid quadrupole orthogonal time-of-flight mass spectrometer (UPLC-Q-TOF/MS/MS) according to the hormone determination method of Müller and Munné-Bosch (2011).

Bioinformatics and Phylogenetic Analysis

Alignments and protein sequences analysis were performed using the BLAST alignment tools at NCBI[5]. Protein structure information and homology-modeling were analyzed using the Protein Data Bank RCSB PDB[6] and SWISS-MODEL[7]. The phylogenetic relationships between *C. pepo*, *Arabidopsis thaliana*, *Solanum lycopersicum*, *Oryza sativa*, *C. sativus*, and *C. melo* of *ACO* genes were studied using MEGA X software (Kumar et al., 2018), which allowed the alignment of proteins and the construction of phylogenetic trees using MUSCLE (Edgar, 2004) and the maximum likelihood method based on the Poisson correction model (Zuckerkandl and Pauling, 1965), with 2,000 bootstrap replicates. The protein sequences (**Supplementary Table 1**) were obtained using the Arabidopsis Information Resource[8], the Cucurbit Genomics Database (CuGenDB)[9], the Rice Database Oryzabase-SHIGEN[10], and the Sol Genomics Network[11]. Cucurbits *ACO* genes structure visualization, such as the composition and position of exons and introns, were performed with the Gene Structure Display Server (GSDS)[12]. Finally, Delta Delta G ($\Delta\Delta G$), a metric for predicting how a single point mutation will affect protein stability, was assessed with the tools SNAP2[13] and I-Mutant3.0.[14] MUpro[15] and CUPSAT[16] tools were also used to predict the stability of the CpACO1A protein.

Assessment of Relative Gene Expression by Quantitative RT-PCR

Gene expression analysis was carried out in samples of WT and *aco1a* plants growing in a greenhouse during the spring-summer season. The expression level was studied in male and female flowers' organs (corolla and ovaries) at different flower developmental stages, as well as in plant apical shoots, leaves, shoots, cotyledons, and roots. The analysis was performed in three biological replicates for each genotype, each of which was derived from a pool of four plants. Total RNA was isolated according to the protocol of the GeneJET Plant RNA Purification Kit (Thermo Fisher Scientific®). RNA was converted into cDNA with the ADNc RevertAid™ kit (Thermo Fisher Scientific®). The qRT-PCR was performed in 10 μL total volume with 1× Top Green qPCR Super Mix (Bio-Rad®) in the CFX96 Touch Real-Time PCR Detection System thermocycler (Bio-Rad®). The gene expression values were calculated using the $2^{-\Delta\Delta CT}$ method (Livak and Schmittgen, 2001). The constitutive *EF1α* gene was

[5]https://blast.ncbi.nlm.nih.gov/Blast.cgi
[6]https://www.rcsb.org
[7]https://swissmodel.expasy.org
[8]https://www.arabidopsis.org
[9]http://cucurbitgenomics.org
[10]https://shigen.nig.ac.jp/rice/oryzabase
[11]https://solgenomics.net
[12]http://gsds.gao-lab.org/Gsds_about.php
[13]https://rostlab.org/services/snap2web
[14]https://folding.biofold.org/i-mutant/i-mutant2.0.html
[15]http://mupro.proteomics.ics.uci.edu
[16]http://cupsat.tu-bs.de

used as the internal reference. **Supplementary Table 2** shows the primers used for each qRT-PCR reaction.

Statistical Analyses

Data were analyzed for multiple comparisons by analysis of variance (ANOVA) using the statistical software Statgraphic Centurion XVIII. Differences between genotypes and treatments were separated by least significant difference (LSD) at a significance level of $p \leq 0.05$.

RESULTS

aco1a Impairs Sex Determination and Petals and Ovary Development

The mutant *aco1a* was found in a high-throughput screening of a *C. pepo* mutant collection for alterations in flower and fruit development. To ensure accurate phenotyping, mutant plants were backcrossed with the background genotype MUC16 for two generations, and then selfed. The resulting BC_2S_1 generations segregated 3:1 for WT and *aco1a* phenotypes, indicating that the mutation is recessive (**Supplementary Table 3**).

The sex phenotype of *aco1a* was assessed in BC_2S_1 plants growing under spring-summer conditions (**Figure 1**). Male flowers were not affected, but most female flowers were converted into bisexual flowers with partially or totally developed stamens (**Figure 1A**). This partial conversion of monoecy into andromonoecy, also termed unstable monoecy, partial andromonoecy, or trimonoecy, indicates that *aco1a* impairs the sex determination mechanism which is responsible for arresting stamen development in the female flower. Pistillate flowers in the first 40 nodes were classified according to the andromonoecious index (AI) in either homozygous WT (wt/wt), heterozygous (wt/*aco1a*), or homozygous mutant (*aco1a*/*aco1a*) plants (**Figure 1B**). The wt/wt and wt/*aco1a* plants produced only female flowers (AI = 0), indicating a complete arrest of stamen development in the pistillate flowers of these plants (**Figure 1C**). The *aco1a*/*aco1a* pistillate flowers, however, exhibited different degrees of stamen development (AI ranging from 0 to 3), and plants had an average AI of 2.1 (**Figures 1B,C**).

Figure 2 shows the effects of the *aco1a* mutation on petal and ovary/fruit development. In the bisexual and hermaphrodite flowers of *aco1a* (AI = 2–3), the petal growth rate was reduced and resembled petal development in male flowers. Petal maturity and subsequent anthesis of the flower were delayed in the mutant with respect to WT (**Figures 2A,B**). Anthesis time, the period of time taken for a 2 mm floral bud to reach anthesis and to open, was longer in male WT flowers (average 21 days) than in female WT flowers (average 12 days) (**Figure 2B**). Bisexual and hermaphrodite *aco1a* flowers also took an average of 21 days to reach anthesis (range 20–25 days). No alterations in petal development or anthesis time were observed in WT and *aco1a* male flowers (**Figure 2B**).

Pollination was attempted in *aco1a* hermaphrodite flowers (AI = 2–3), but none of the fruits were able to set seeds. Since the pollen is fertile in other plants, this female sterility could be associated with the over-maturation of stigma and style because

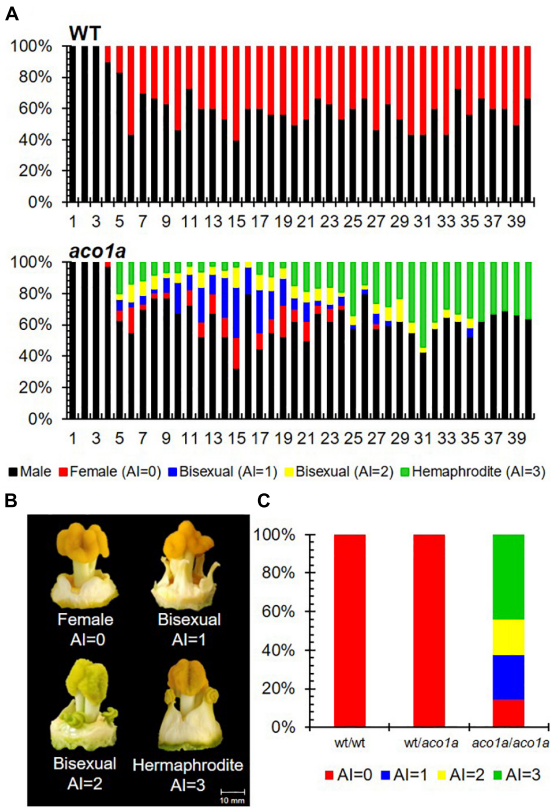

FIGURE 1 | Sex phenotype of WT and *aco1a* plants. **(A)** Distribution of male and pistillate flowers in the first 40 nodes of the main shoot. In each node, color bars indicate the percentages of male (black), female (red), and bisexual and hermaphrodite flowers (blue, yellow, and green) in the total number of plants analyzed ($n = 30$ for each genotype). **(B)** Phenotype of pistillate flowers with different stamen development and AI index. Female flowers (AI = 0) develop no stamen, bisexual flowers (AI = 1–2) develop intermediate stamens, and hermaphrodite flowers (AI = 3) develop entire stamens with pollen. **(C)** Percentage of each pistillate flower in each genotype.

of the delayed corolla aperture. However, we were able to self *aco1a*/*aco1a* plants by using the few female flowers with no stamen (AI = 0). Significant differences were detected in ovary size between WT and *aco1a* pistillate flowers (**Figures 2A,C**). At anthesis, the WT ovary reached approximately 12 cm in length and then aborted. The *aco1a* ovary, in contrast, continued to grow until it reached 18–30 cm at anthesis (**Figures 2A,C**). The growth rate of WT and *aco1a* ovary/fruit was similar during the first 16 days. After that time, WT ovaries aborted, and those of *aco1a* maintained growth up to anthesis (**Figure 2C**). The *aco1a* fruits can be considered parthenocarpic since they grew in the absence of pollination, as the corolla was closed.

aco1a Is a Missense Mutation Causing P5L Substitution in the Ethylene Biosynthesis Enzyme CpACO1A

To elucidate the causal mutation of *aco1a* phenotype, we performed WGS of two bulked DNA samples from a BC_2S_1 segregating population: the WT bulk, having DNA from 30 WT

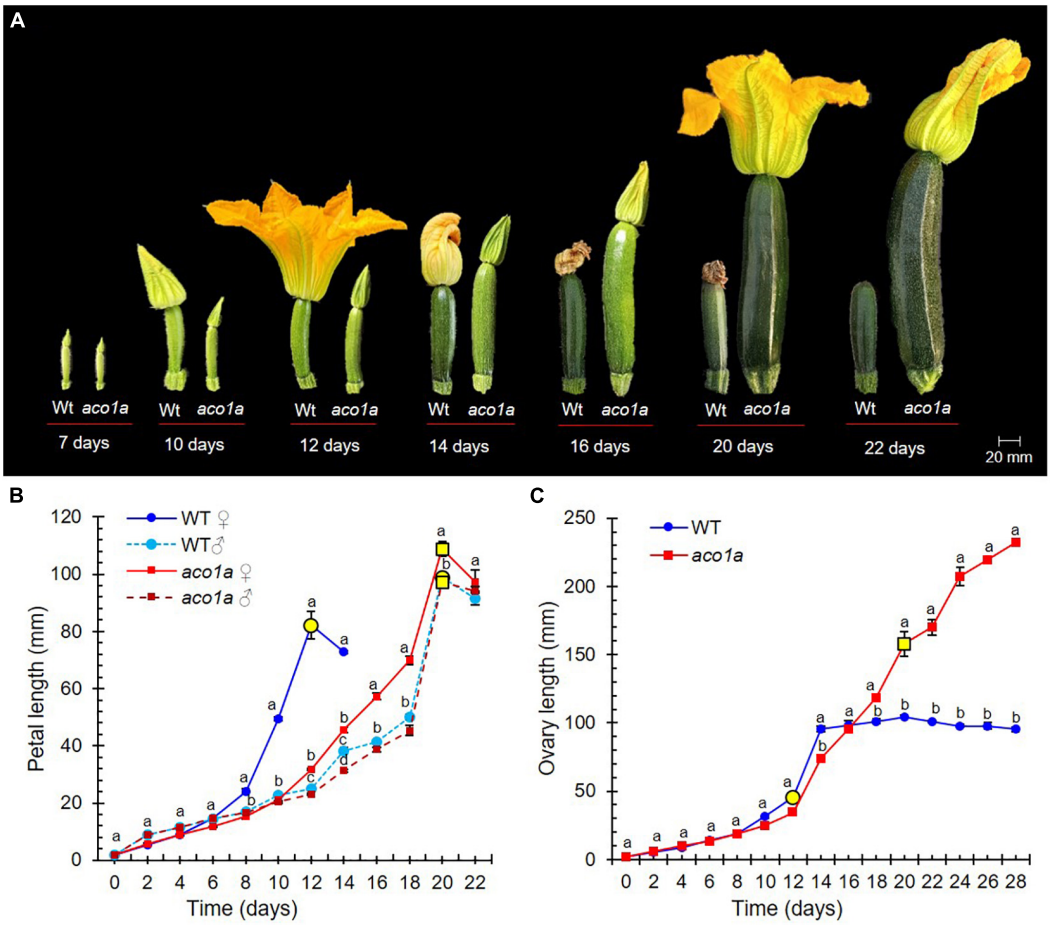

FIGURE 2 | Comparison of WT and *aco1a* flower development. **(A)** Effect of *aco1a* mutation on the development of ovary and corolla of the pistillate flower. Note that the mutant pistillate flower reaches anthesis later than the WT, and that the ovary continues its growth until producing a parthenocarpic fruit. **(B)** Comparison of the growth rate of WT and mutant corolla. Flowers were labeled when their ovaries were 2 mm long, and then measured every 2 days for 22 days. Yellow circles indicate the time at which more than 80% of the flowers reached anthesis. **(C)** Comparison of the growth rate of WT and mutant ovaries/fruits over a period of 22 days. Error bars represent SE. Different letters indicate significant differences in flowers of the different genotypes at each developmental time ($p \leq 0.05$).

plants (monoecious); and the *aco1a* bulk, having DNA from 30 mutant plants (partially andromonoecious). In the mutant bulk, only the plants that showed the most extreme andromonoecious phenotype were selected.

More than 98% of the sequencing reads (more than 80 million in each bulk) were mapped against the *C. pepo* reference genome version 4.1, which represented an average depth of 47.41 (**Table 1**). The identified SNPs (more than 370,000 in each of the bulks) were filtered for their mutant allele frequency (AF) in the WT and the mutant DNA bulks. For the causal mutation of the phenotype, it is expected that the genotype was 0/1 for WT bulk (alternative allele frequency AF = 0.25) and 1/1 for the mutant bulk (AF = 1). For the non-causal SNPs, however, we expected an AF of 0.5 in both bulks. A putative causal region in chromosome 4 was found that has the expected AF in WT and mutant bulk (**Figure 3A**). In fact, after filtering for AF = 1 in the mutant bulk and AF < 0.3 in the WT bulk, 412 SNPs were selected (**Table 1**). Among them, 145 corresponded to canonical EMS mutations (C > T and G > A), and only one on chromosome 4 was positioned on the exome and had a high impact on the protein (**Table 1** and **Figure 3**).

The sequence surrounding the candidate *aco1a* mutation (±500 bp) was then used in BLAST searches against the DNA and protein databases at NCBI. It was found that the C > T transition was a missense mutation changing proline by leucine at residue 5 (P5L) of the ethylene biosynthesis enzyme 1-aminocyclopropane-1-1carboxylate oxidase 1A (CpACO1A) (**Figure 3A**). To prove that the selected EMS mutation was the one responsible for *aco1a* phenotype, we genotyped the SNP alleles in 300 plants from a BC_2S_1 population. The results demonstrated a 100% co-segregation between the *aco1a* phenotype and the C > T mutation in *CpACO1A* (**Supplementary Table 4**). Other three EMS-induced mutations in chromosome 4 were also tested (**Supplementary Table 5**), but none of them co-segregated with the mutant phenotype in the 300 BC_2S_1 plants analyzed.

The identified mutation has a deleterious effect on CpACO1A enzyme (**Figure 3B**). Bioinformatics analysis with the SNAP[2] tool predicted a negative effect of P5L substitution on protein function

TABLE 1 | Summary sequencing data for WT and *aco1a*.

Sequencing				WT	*aco1a*
No. reads				106,448,438	84,600,742
Mapped reads (%)				98.10	98.06
Average depth				47.41	40.41
Coverage at least 4× (%)				95.81	95.41
SNPs filtering					
Total No. SNPs				381,666	374,917
AF (WT) < 0.3; AF (*aco1a*) = 1				412	412
EMS SNPs G > A or C > T				145	145
EMS SNPs (GQ > 90; DP > 10)				4	4
High impact SNPs				0	1
Candidate SNP					
Chr	**Position**	**Ref**	**Alt**	**Gene ID**	**Effect**	**Functional annotation**
4	7,715,975	C	T	Cp4.1LG04g02610	P5L	1-Aminocyclopropane-1-carboxylate oxidase 1

AF, allelic frequency; GQ, genotype quality; DP, read depth.

(**Figure 3B**). Other bioinformatics tools, such as PredictSNP, MAPP and iStable, among others, showed the same evidence (**Figure 3B**). Moreover, predicted Gibbs free energy changes ($\Delta\Delta G$), a metric for predicting how a single point mutation could affect protein stability, was assessed for P5L mutation by using I-mutant3.0 predictor, CUPSAT, and MUpro. The comparison of *aco1a* and WT CpACO1A resulted in negative $\Delta\Delta G$ values, which indicated a decreased stability of the mutated protein (**Figure 3B**).

Gene Structure and Phylogenetic Relationships of *CpACO1A*

Given that the genomes of *C. pepo* are duplicated (Sun et al., 2017; Montero-Pau et al., 2018), the gene *CpACO1A* on chromosome 4 (Cp4.1LG04g02610) has a paralog (*CpACO1B*) with more than 80% of homology on an syntenic block of chromosome 5 (Cp4.1LG05g15190). The duplicates did not maintain the same molecular structure: four exons for *CpACO1A* and three exons for *CpACO1B* (**Figure 4A**). *ACO1*, like genes in other plants, including those of *Cucurbita maxima*, *Cucurbita moschata*, *C. melo*, *C. lanatus,* and *C. sativus*, conserve the four exonic structure of *CpACO1A* (**Figure 4A**). All ACO proteins in the NCBI database were found to conserve the proline residue on position five, indicating that this is an essential residue for ACO activity (**Figure 4B**).

Based on residues conserved at specific positions toward the carboxylic end of the proteins, three types of ACO enzymes have been established in plants (**Figure 4B**), which also defines its specific functionality and biological activity. A phylogenetic tree was inferred by using ACO protein sequences from different cucurbit species, including different *Cucurbita* sp., *C. melo* and *C. sativus*, together with those of the most studied model species, *A. thaliana*, *S. lycopersicum*, and *O. sativa* (**Figures 4B,C**). The *C. pepo* CpACO1A is a type I ACO that clustered together with melon CmACO1 and cucumber CsACO3 (also called CsACO1-like). Furthermore, the genes coding for the type I ACO1 enzymes of these three cucurbits were found to be positioned in a syntenic block of *C. pepo*, *C. melo*, and *C. sativus* genomes. The paralogous CpACO1B is also a type I ACO, but clustered separately from CpACO1A, CsACO3, and CmACO1 (**Figure 4C**).

The *aco1a* Mutation Impairs *CpACO1A* Expression, ACO Activity, and Ethylene Production and Sensitivity

The expression of *CpACO1A* and *CpACO1B* in different WT and *aco1a* tissues is shown in **Figure 5A**. *CpACO1B* was not expressed in any of the analyzed tissues, indicating that this is a non-functional paralogous gene. *CpACO1A* was found to be expressed in all tissues, except in cotyledons. Its transcript was, however, much more accumulated in roots and flowers (**Figure 5A**). *CpACO1A* was similarly expressed in the different WT and mutant tissues, except in the female flower buds, where the gene showed a higher expression in the mutant. To understand the function of *CpACO1A* in flower development, its expression was compared in WT and *aco1a* apical shoots and female and male flowers buds (FFB/MFB) at different stages of development (**Figure 5B**). In the apical shoot, *CpACO1A* expression was similar in WT and *aco1a* plants. In the mutant female and male flowers, *CpACO1A* transcripts are similarly more highly accumulated in the mutants, suggesting that the andromonoecious *aco1a* phenotype is not caused by a reduction of gene expression.

Although there are other ACO isoenzymes in the *C. pepo* genome, we have assessed the total ACO activity and ethylene production in different WT and *aco1*a plant tissues (**Figure 5C**). The *aco1a* mutation was found to cause a reduction of ACO activity in all studied tissues, except in cotyledons, where the gene was not found to be expressed (**Figure 5C**). These data suggest that the mutation *aco1a* likely impairs CpACO1A activity.

The *aco1a* mutation significantly reduced the production of ethylene in the apical shoots of the plants, where a number of small floral buds are developing, and in pistillate flowers (**Figure 5D**). As previously reported, ethylene increased throughout the development of male, female (WT) and bisexual/hermaphrodite (*aco1a*) flowers, and pistillate flowers produced significantly more ethylene than male flowers at the same developmental stage (**Figure 5D**). The bisexual flowers of *aco1a* showed a significant reduction of ethylene production during their development, especially those flowers with more than 35 mm in length (**Figure 5D**). A slight reduction in ethylene production was also found in *aco1a* male flowers of 50–55 mm in length (**Figure 5D**).

Ethylene sensitivity in WT and *aco1a* plants was also assessed by measuring the abscission time of male flowers in response to external treatments with ethylene (**Figure 6**). The male floral buds were collected at two developmental stages: anthesis (A) and 2 day before anthesis (A-2). The flowers were put in a container with water and treated in an atmosphere with air (control) or ethylene (ET) up to 72 h, and floral abscission was evaluated

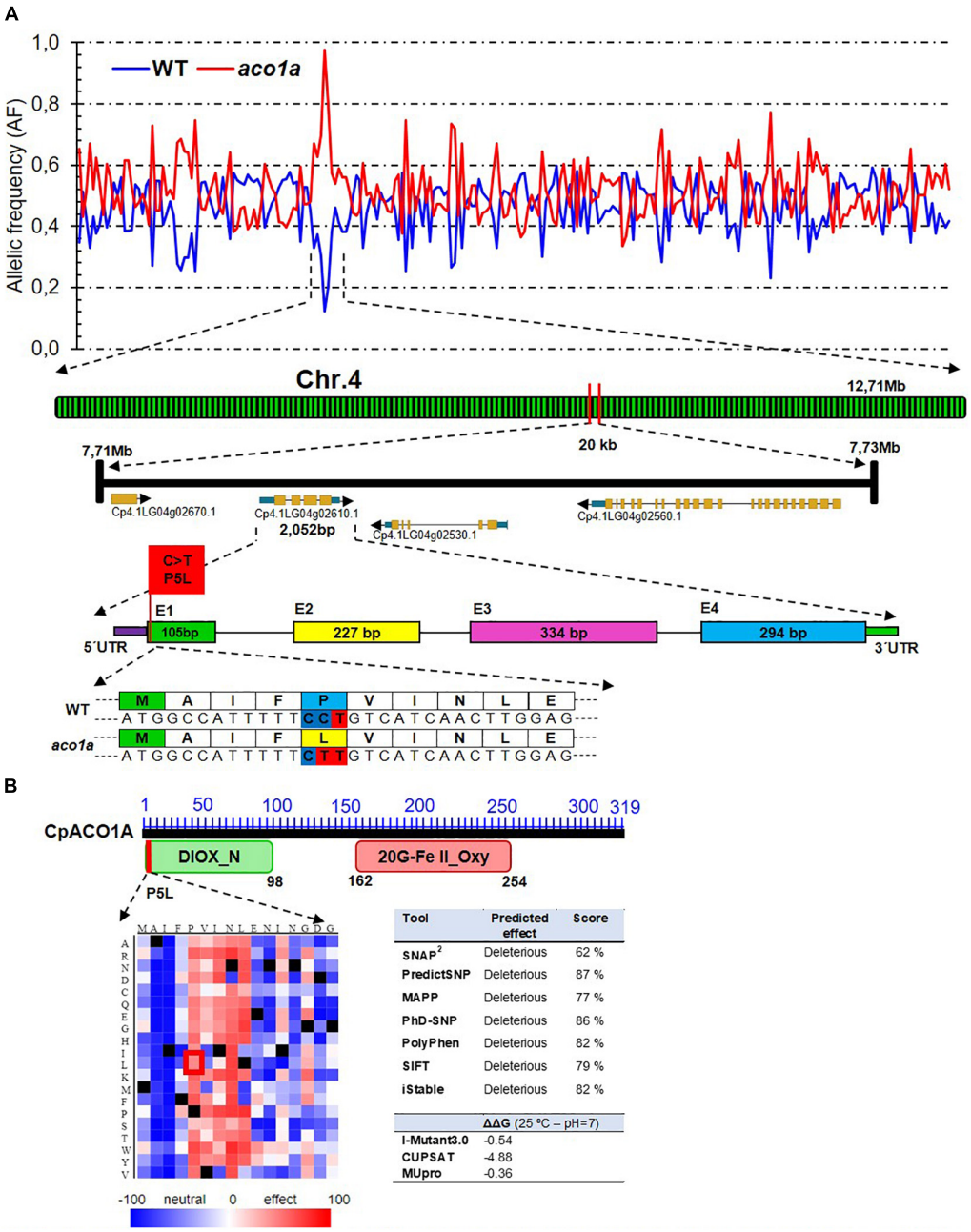

FIGURE 3 | Identification of *aco1a* causal mutation by BSA-sequencing. **(A)** Frequency of the alternate allele in the WT and *aco1a* bulks along the physical map of squash genome. The analysis indicates that a region of chromosome 4 is responsible for the mutant phenotype. A missense mutation on the gene *Cp4.1LG04g02610.1* (*CpACO1A*) produces a change of proline by leucine at residue 5 (P5L) of the ethylene biosynthesis enzyme CpACO1A. **(B)** Impact of P5L mutation in the N-terminal conservative non-heme dioxygenase DIOX_N region of ACO enzymes. The SNAP^2-generated heatmap of CpACO1A N-domain indicates that changes in residue 5–9 have a high impact on protein function. The red box indicates the impact of the *aco1a* mutation. The table on the right shows the predicted effect of the mutation on protein function and stability by using different bioinformatics tools.

every 12 h (**Figure 6A**). Both WT and *aco1a* flowers responded to ethylene by accelerating their senescence and abscission (**Figure 6B**). However, the increase in the percentage of flower abscission in response to ethylene was lower in *aco1a* than in WT flowers (**Figure 6B**), indicating a partially ethylene-insensitive phenotype of the mutant *aco1a* male flowers.

Expression of Different Sex-Determining Genes in WT and *aco1a* Flowers

The possible regulation of *CpACO1A* over other sex-determining genes was investigated by assessing the expression of those genes in WT and *aco1a* pistillate and male flowers (**Figure 7**). The ethylene biosynthesis genes *CpACO2B*, *CpACS11A*, and

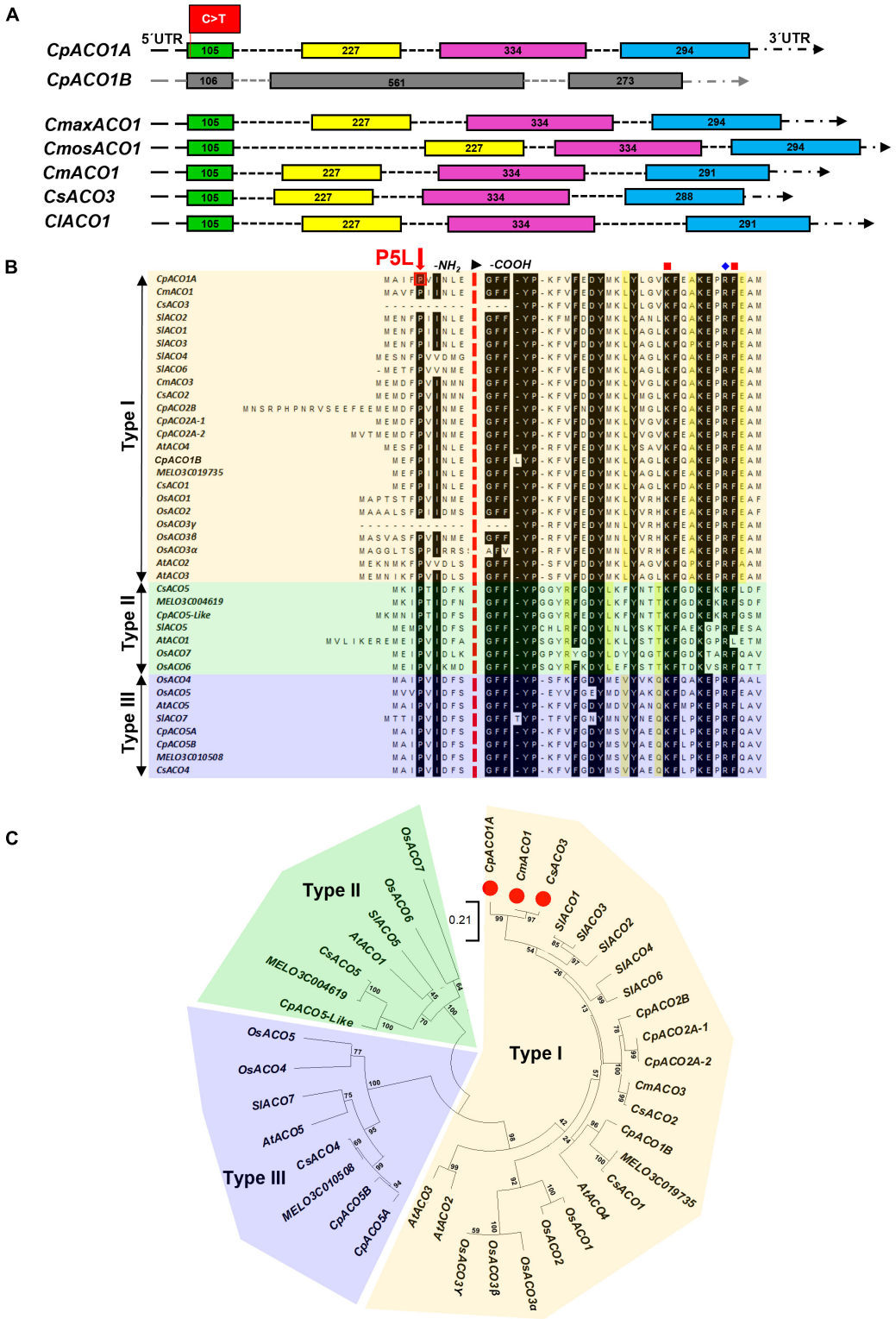

FIGURE 4 | Genetic relationships among ACO enzymes in different plant species. **(A)** Comparison of the gene structure of *CpACO1A* and *CpACO1B* of *C. pepo* with other homologs in cucurbit species: *Cucurbita maxima* (*CmaxACO1*), *Cucurbita moschata* (*CmosACO1*), *Cucumis melo* (*CmACO1*), *Cucumis sativus* (*CsACO3*), and *Citrullus lanatus* (*ClACO1*). **(B)** Consensus proline residue in position 5 and ACO classification according to conserved residues in a specific position toward the -COOH end of the proteins. **(C)** Phylogenetic ACO tree from different cucurbit species: *C. melo*, *C. sativus*, and *C. pepo* together with those of the most studied model species, *Arabidopsis thaliana*, *Solanum lycopersicum*, and *Oryza sativa*. Bootstrap values for the main branches are depicted on the tree.

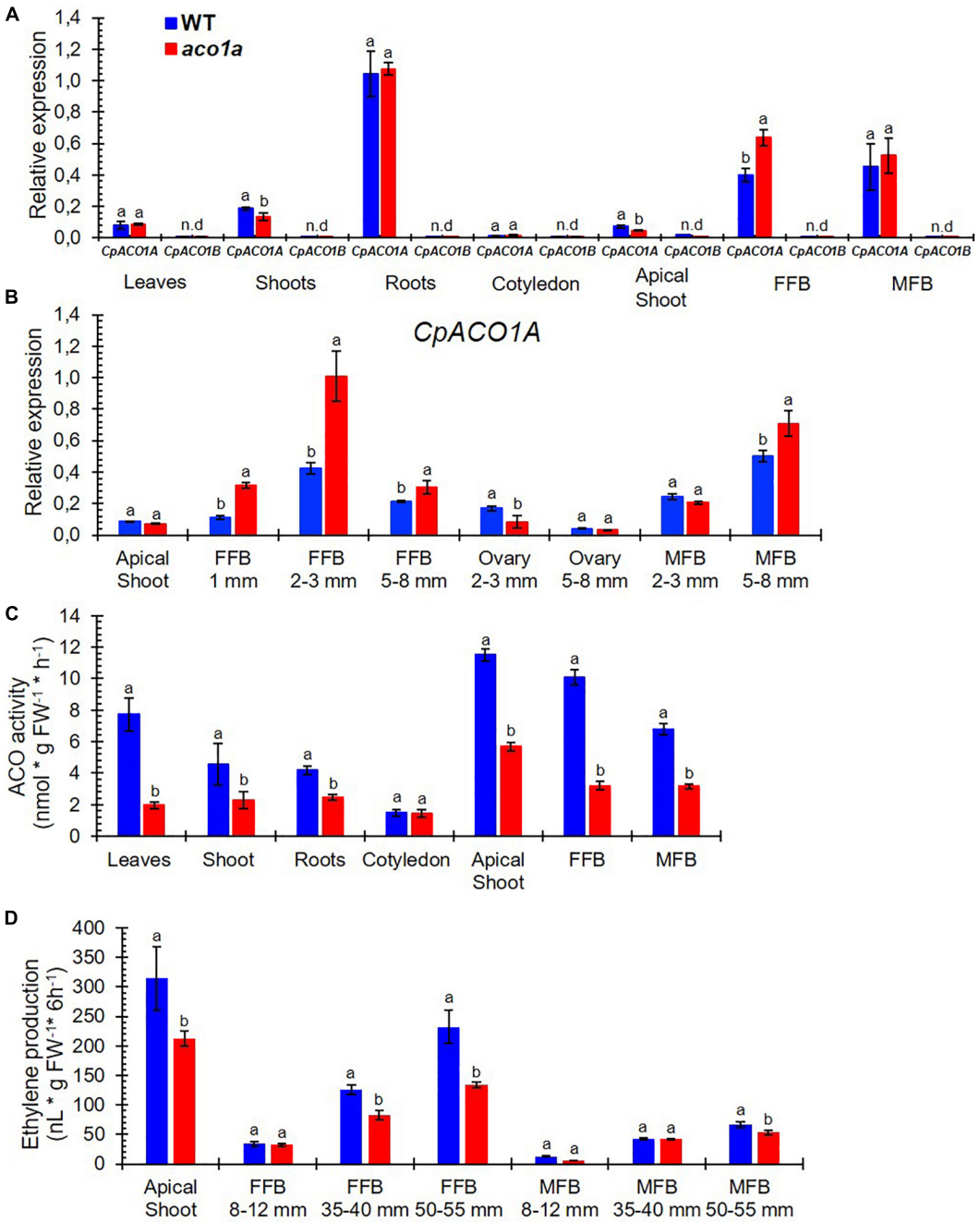

FIGURE 5 | Comparison of *CpACO1A* gene expression, ACO activity, and ethylene production in WT and *aco1a* plants. **(A)** Relative gene expression of *CpACO1A* and *CpACO1B* in different WT and *aco1a* plant organs. **(B)** Relative expression of *CpACO1A* in the apical shoots and in female and male floral buds at different stages of development. **(C)** ACO1 activity in different WT and *aco1a plant* organs. **(D)** Ethylene production in the apical shoot and in female and male floral buds of WT and *aco1a* plants. FFB, female floral bud excluding the ovary; MFB, male floral bud. The assessments were performed in three independent replicates for each tissue. Error bars represent SE. Different letters indicate significant differences between WT and mutant organs at the same stage of development ($p \leq 0.05$).

CpACS27A, which are expressed at early stages of female flower development and make the floral meristem to be determined as a female flower (Martínez and Jamilena, 2021), were differentially expressed in WT and *aco1a* pistillate flowers, but not in the apical shoots or in male flowers (**Figure 7**). In very small floral buds (1 mm), the *aco1a* mutation repressed the expression of the three genes. In 2–3 mm floral buds, the expression of the *CpACS11A* and *CpACS27A* was repressed in the ovary, and the expression of *CpACO2B* and *CpACS11A* was induced in the rest of the floral organs (petals, style, and stigma). In 5–8 mm female floral buds,

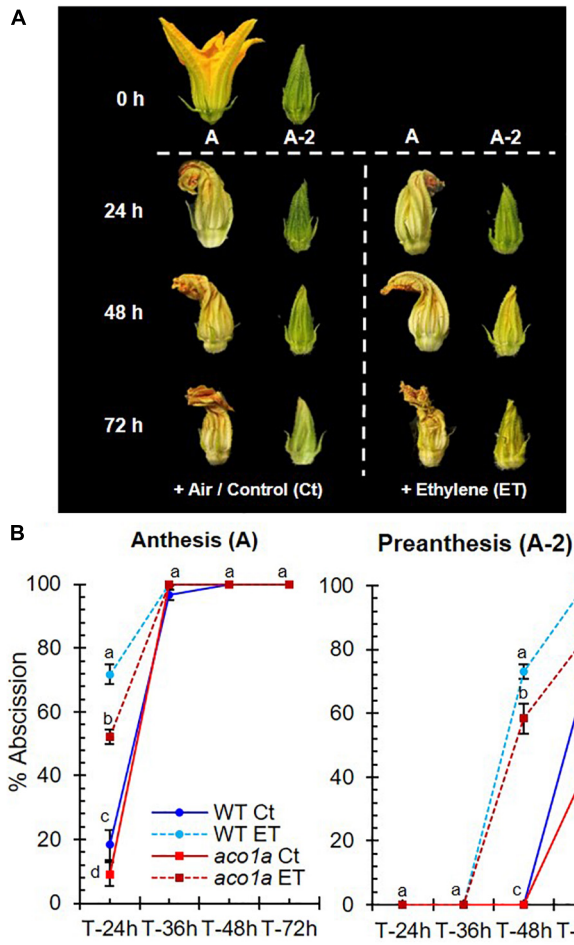

FIGURE 6 | Ethylene sensitivity of WT and *aco1a* plants. The sensitivity to ethylene was determined by assessing the percentage of flower abscission in response to ethylene in male flowers at two stages of development. **(A)** Phenotype of male flowers at two stages of development: anthesis **(A)** and 2 days before anthesis (A-2). Photographs were taken at harvest (0 h of treatment) and 24, 48, and 72 h after the treatment with air or ethylene (ET). **(B)** Percentage of abscission in male flowers harvested at anthesis **(A)** or 2 days before anthesis (A-2). Error bars represent SE. Different letters indicate significant differences between flower abscission of each treatment and genotype at the same time after the treatment ($p \leq 0.05$).

the expressions of these three ethylene biosynthesis genes were not altered by *aco1a* (**Figure 7**).

The mutation *aco1a* also diminished the expression of the ethylene receptor *CpETR1A* and the ethylene signaling gene *CpEIN3A* (**Figure 7**) at early stages of female flower development (female floral buds of 1 mm and 2–3 mm in length) and in ovaries of flowers 2–3 mm in length. In the rest of the analyzed tissues, including the apical shoot, female flowers at later stages of development and male flowers, no difference was found in the expression of these two ethylene signaling genes between WT and *aco1a* tissues (**Figure 7**). The expression *CpWIP1B*, a homolog of melon *WIP1* involved in the arrest of stamen during the development of male flowers, was unaltered by the mutation in most of the studied tissues, but in the apical shoot and in male floral buds of 5–8 mm in length, the gene was induced in the mutant.

Hormone Imbalance in Early Female Development of *aco1a* Flowers

To examine whether the mutation *aco1a* can change the hormonal balance of pistillate flower, we proceeded to compare phytohormone contents of WT female flower and *aco1a* hermaphrodite flowers. **Table 2** shows phytohormone concentrations of pistillate flower buds of 5–8 mm from WT and *aco1a* plants. No difference was detected for IBA, GA3, and BA contents. However, the *aco1a* flowers showed a considerable reduction in the content of ABA and JA, as well as SA (**Table 2**). In contrast, the auxin (IAA) content in the *aco1a* hermaphrodite flowers was much higher than that in female WT flowers (**Table 2**).

DISCUSSION

It has been assumed that not ACO, but ACS, is the rate-limiting enzyme in ethylene biosynthesis. However, there is an increasing amount of evidence demonstrating the importance of ACO in controlling ethylene production in plants (Houben and Van de Poel, 2019). In cucurbits, mutations in *CmACO1* are known to inhibit fruit ripening and extend fruit shelf life (Dahmani-Mardas et al., 2010). An essential role of *CsACO2* and *CmACO3* orthologs in carpel development has been recently reported in cucumber and melon (Chen et al., 2016). In this paper, we establish that *CpACO1A* is a key regulator in sex determination and female flower development of *C. pepo*.

aco1a Disrupts Ethylene Biosynthesis and Hormonal Balance During Female Flower Development

The ACO protein family can be divided in three phylogenetic groups based on amino-acid sequence similarity (Houben and Van de Poel, 2019). At a functional level, the ACO protein has two highly conserved and well-distinguished domains, one N-terminal, highly conservative non-heme dioxygenase DIOX_N region and a C-terminally located 2OG-FeII_Oxy region, both of which are critical for ACO activity (Ruduś et al., 2013). The sequence alignment and the phylogenetic tree constructed by using ACO proteins from diverse plant species have proven that CpACO1A is a type I ACO enzyme, and that the *aco1a* P5L mutation affects the first amino acid of the CpACO1A DIOX_N domain, which is a conserved proline residue in all analyzed plant ACOs. The reduced ACO activity and ethylene production in *aco1a* plant organs confirmed the disfunction of P5L isoform of CpACO1A and the importance of 5P residue for its activity.

CpACO1A transcript differentially accumulated in different tissues and stages of development. Comparison of ethylene production and gene expression in WT and *aco1a* organs indicated that *CpACO1A* may be regulated by ethylene in a tissue- and temporal-specific manner. This feedback regulation

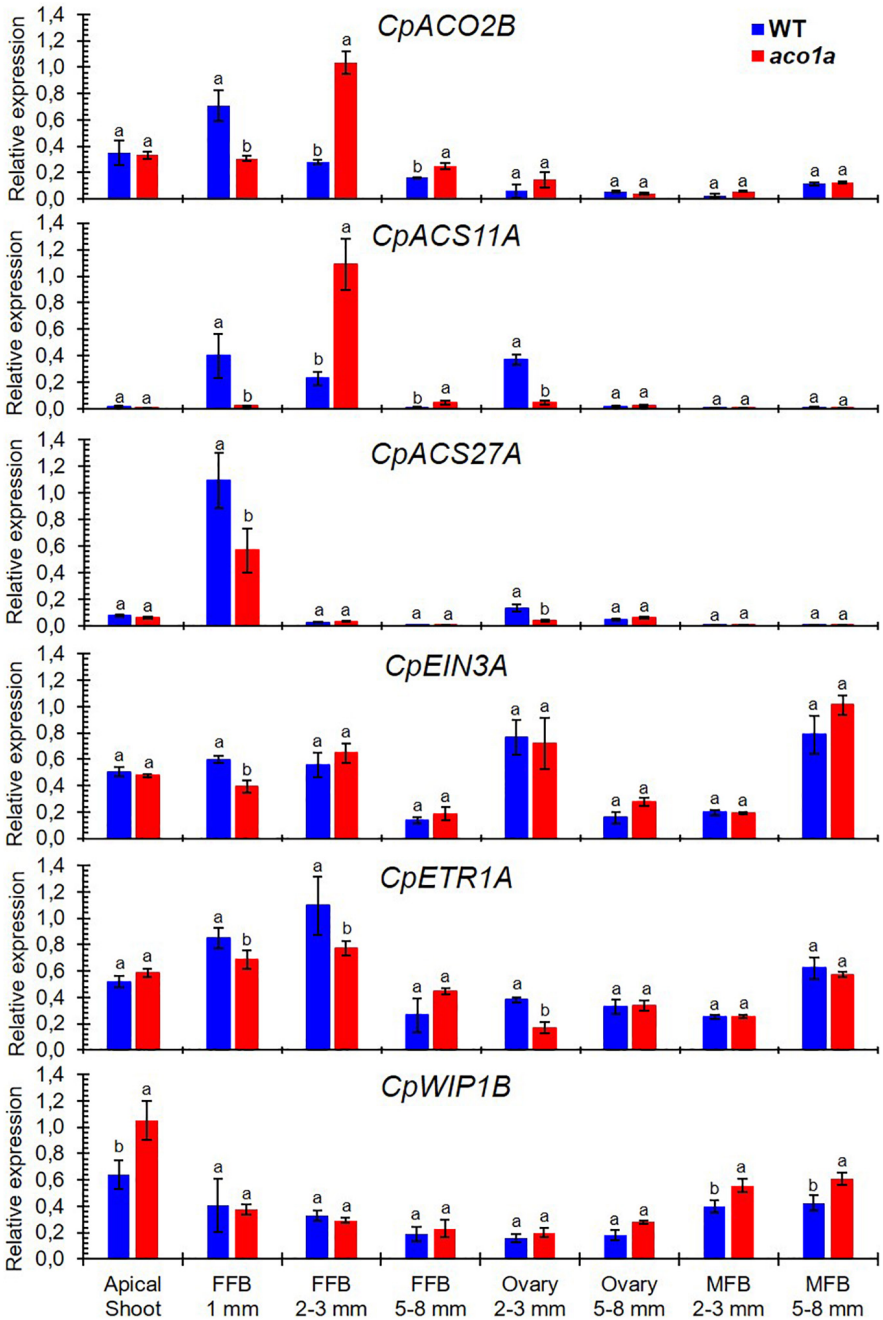

FIGURE 7 | Relative expression of different sex-determining genes in the apical shoots and flowers of WT and *aco1a* plants. The expression was assessed for genes involved in ethylene biosynthesis (*CpACO2B*, *CpACS11A*, and *CpACS27A*), ethylene perception and signaling (*CpETR1A* and *CpEIN3A*), and coding for the transcription factors (*CpWIP1B*) that are known to be involved in sex determination in cucurbit species. The relative level of each transcript was quantified by quantitative PCR in three independent replicates of each tissue. FFB, female floral bud excluding the ovary; MFB, male floral bud. Error bars represent SE. Different letters indicate significant differences between WT and mutant apical shoots and flowers at the same stage of development ($p \leq 0.05$).

could also affect other ethylene biosynthesis genes involved in flower development and sex determination, including *CpACO2B*, *CpACS11A*, and *CpACS27A*. Both positive and negative feedback ethylene-mediated regulation of *ACS* and *ACO* transcription have been reported in other systems in a tissue- and temporal-specific manner during flower and fruit development (Barry et al., 1996; Nakatsuka et al., 1998; Inaba et al., 2007; Trivellini et al., 2011; Houben and Van de Poel, 2019; Pattyn et al., 2020). However, we do not exclude the possibility that the regulation of *ACS* and *ACO* genes in the female flower is mediated by other hormones, such as IAA, which was found to be highly accumulated in the ethylene-deficient *aco1a* pistillate flowers.

TABLE 2 | Hormone concentrations ng/mL (ppb).

Hormones	WT	*aco1a*
Salicylic acid (SA)	4661.94 ± 41.00 **a**	3196.83 ± 46.34 **b**
Indole-3-butyric acid (IBA)	n.d	n.d
Indole-3-acetic acid (IAA)	<LOQ **b**	23.25 ± 2.47 **a**
Gibberellic acid (GA3)	n.d	n.d
6-Benzyladenine (BA)	n.d	n.d
Abscisic acid (ABA)	124.81 ± 4.06 **a**	36.02 ± 2.35 **b**
Jasmonic acid (JA)	656.65 ± 19.11 **a**	248.56 ± 5.41 **b**

Different letters within the same row indicate significant differences between WT and aco1a hormone content ($p < 0.05$); n = 3. LOQ, results below the limit of quantification (5 ppb). n.d, not detected.

The hormonal imbalance detected in *aco1a* female flowers reveals the existence of crosstalk between ethylene and other hormones, such as IAA, SA, ABA, and JA, during female flower development. The coaction of ethylene and auxin has been reported in various growth and developmental processes, including root elongation, lateral root formation, hypocotyl growth, and fruit development and ripening, where both hormones may act synergistically or antagonistically (Stepanova et al., 2007; Muday et al., 2012; Li et al., 2016; Yue et al., 2020). The reciprocal positive regulation between auxin and ethylene is well established; elevated levels of auxin trigger transcriptional activation of subsets of *ACS* and *ACO* genes, leading to increased ethylene production; and ethylene positively controls IAA biosynthesis by the up-regulation of *Weak ET Insensitive 2* (*WEI2*) and *WEI7* (Růžička et al., 2007; Stepanova et al., 2007; Swarup et al., 2007; Zemlyanskaya et al., 2018). However, ethylene has also been reported to negatively regulate auxin biosynthesis (Harkey et al., 2018; Li et al., 2018). We found that ethylene and auxin are mutually repressed, likely having an antagonistic action in squash female flower development. Auxin down-regulates the expression of ethylene biosynthesis and signaling genes in the female flower upon fruit set (Martínez et al., 2013), and here we demonstrated that ethylene has a negative regulation on auxin in female flowers, accumulating much higher content of IAA in ethylene-deficient *aco1a* than in WT. On the other hand, the reduced levels of ABA, JA, and SA in the ethylene-deficient mutant *aco1a* indicates that ethylene positively regulates the homeostasis of these three phytohormones in the female flower. As discussed below, all of these hormones have key functions in flower development (Chandler, 2011), and can cooperate with ethylene in the regulation of squash female flower development.

CpACO1A Prevents Stamen Development in Squash Female Flowers

Different sex-determining mechanisms prevent the development of either the stamens or the carpel in a primarily hermaphrodite floral meristem (Martínez and Jamilena, 2021). In Cucurbitaceae, ethylene arrests the development of stamens and promotes the development of carpels during the determination of female flowers. Early ethylene biosynthesis genes, such as *ACS11* and *ACO2*, in cucumber and melon are able to promote carpel development and determine the fate of floral meristem toward a female flower. The LOF mutation in these two ethylene biosynthesis genes leads to androecy in both cucumber and melon (Boualem et al., 2015; Chen et al., 2016), as occurs with mutation in some ethylene receptor genes (García et al., 2020a,b). Our results demonstrate that *aco1a* mutation led to a reduction in ACO activity and ethylene production, but induced the expression of *CpACO1A*. This upregulation also occurs for *CpACO2B* and *CpACS11A* in *aco1a*, but the induction of these two genes occurs in flowers where sex determination has already taken place (flowers above 2–3 mm in length). At earlier stages of female flower development (female floral buds less than 1 mm), the genes *CpACO2B* and *CpACS11A* were down-regulated in the mutant, and could not compensate for the reduced ethylene caused by *CpACO1A* disfunction.

The later-acting ethylene biosynthesis gene *ACS2* is specifically expressed in female flowers at early stages of development to control the arrest of stamen development. LOF mutations for *ACS2* orthologs (*CsACS2* in cucumber, *CmACS7* in melon, *CpACS27A* in *C. pepo*, and *CitACS4* in watermelon) promote the conversion of female into hermaphrodite flowers and monoecy into andromonoecy (Boualem et al., 2008, 2009, 2016; Martínez et al., 2014; Ji et al., 2016; Manzano et al., 2016). The phenotype of *aco1a* mutant described in this paper resembles those of *acs2-like* mutants, indicating that *CpACO1A* is, together with *CpACS27A*, the key enzymes that produce the requisite ethylene to prevent the development of stamens in squash female flowers. The reduced expression of *CpACS27A* in *aco1a* pistillate flowers at early stages of development suggests that the regulation of

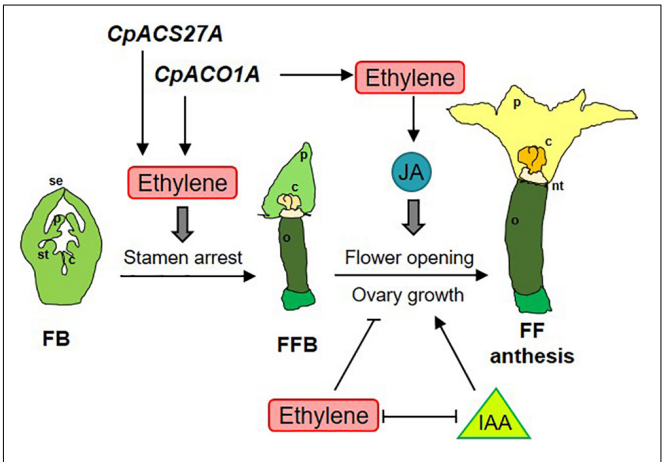

FIGURE 8 | Model integrating ethylene, jasmonate (JA) and auxin (IAA) in the regulation of sex determination (stamen arrest), female flower opening and ovary growth and fruit set and development in *Cucurbita pepo*. The genes *CpACO1A* and *CpACS27A* participate in the biosynthesis of the ethylene required for carpel promotion and stamen arrest at earlier stages of female floral bud (FFB) development. *CpACO1A* also participates in the ethylene produced at later stages of FFB for controlling flower opening and ovary growth and fruit set. Petal maturation and female flower opening is mediated by jasmonic acid (JA), while ovary growth and fruit set is coordinated by the antagonist action of ethylene and IAA, which are mutually repressed during the development of the female flower. se, sepal; p, petal; st, stamen; c, carpel; o, ovary; nt, nectary; FB, floral bud, FFB, female floral bud, FF, female flower.

these two key enzymes is coordinated, producing the required ethylene for the proper development of the female flower. This coordinated regulation may be mediated by ethylene, as occurs in other systems (Barry et al., 2000; Inaba et al., 2007).

CpACO1A Controls Flower Opening and Ovary Development in the Absence of Pollination

The phenotype of *aco1a* flowers also indicates that ethylene regulates the growth and development of other floral organs in the pistillate flowers of squash, including the corolla and the ovary/fruit. The delayed anthesis time of the *aco1a* pistillate flower demonstrates that ethylene is a positive regulator of petal growth and maturation in squash. This was also found in squash ethylene-insensitive mutants (García et al., 2020a,b), and seems to be associated with pistillate flower masculinization. Ethylene, which is the hormone that activates the developmental program of a female flower, is also used to promote the growing rate and maturation of female corolla. In the male flower, where ethylene production is very low, petals develop slower and anthesis is markedly more delayed. Given that male flowers are produced in the first nodes of the plant, this ethylene-mediated mechanism ensures that male and female flowers reach anthesis at the same time to achieve successful pollination. JA is known to be involved in anther and pollen maturation (Stintzi and Browse, 2000; Wang et al., 2005; Browse and Wallis, 2019), but also participates in petal maturation and flower opening (Reeves et al., 2012; Oh et al., 2013; Niwa et al., 2018; Schubert et al., 2019). The delayed flower opening and reduced JA in the ethylene-deficient hermaphrodite flowers of *aco1a* indicate that ethylene can regulate the maturation and opening of the female flower by inducing the biosynthesis of JA (**Figure 8**).

We have previously reported that external treatments with ethylene inhibitors were able induce fruit set and early fruit development in the absence of pollination (parthenocarpic fruit), and that fruit set is concomitant with a reduction in ethylene production, ethylene biosynthesis, and signaling gene expression in the days immediately after anthesis (Martínez et al., 2013). Mutations in ethylene receptor genes of squash confer partial ethylene insensitivity, and also result in parthenocarpic fruits (García et al., 2020a,b). The negative role of ethylene in fruit set has been also found in tomato, where ethylene and signaling genes are down-regulated in early-developing fruit (Vriezen et al., 2008; Wang et al., 2009), and the blocking of ethylene perception, using the ethylene-insensitive mutation *Sletr1-1* or treatments with 1MCP, leads to parthenocarpic fruits through the induction of auxin and gibberellin (Wang et al., 2009; Shinozaki et al., 2015, 2018; An et al., 2020). The up-regulation of IAA in *aco1a* may be responsible for the continued growth of *aco1a* ovaries in the absence of pollination. Auxins are the key hormones regulating fruit set in the Cucurbitaceae family (Trebitsh et al., 1987; Kim et al., 1992; Martínez et al., 2013), and were found to be highly induced in the *aco1a* flowers. This means that auxins not only repress the production, perception and signaling of ethylene in the squash developing fruit, as reported by Martínez et al. (2013), but can be negatively regulated by ethylene in the developing ovary (**Figure 8**). It is feasible that the two hormones are specifically accumulated in different floral organs, i.e., ethylene in the upper flower organs for promoting the development of carpels and petals and arresting the development of stamens, and auxin in the inferior ovary for inducing fruit set and development (**Figure 8**).

DATA AVAILABILITY STATEMENT

The datasets presented in this study can be found in online repositories. The names of the repository/repositories and accession number(s) can be found in the article/**Supplementary Material**.

AUTHOR CONTRIBUTIONS

MJ designed and coordinated the research. GC conducted most of the experiments and data analysis. JI-M and JR collaborated in phenotyping. CM and DG collaborated in data analysis. MJ and GC wrote the first version of the manuscript, and the other authors contributed later to improve it and approved the final version for submission. All authors contributed to the article and approved the submitted version.

FUNDING

This work was supported by grants AGL2017-82885-C2-1-R and PID2020-118080RB-C21, funded by the Spanish Ministry of Science and Innovation, and grant P12-AGR-1423, funded by Junta de Andalucía, Spain.

ACKNOWLEDGMENTS

GC and JI-M gratefully acknowledge the FPU and FPI scholarship program from MEC.

SUPPLEMENTARY MATERIAL

The Supplementary Material for this article can be found online at: https://www.frontiersin.org/articles/10.3389/fpls.2021.817922/full#supplementary-material

REFERENCES

Aguado, E., García, A., Iglesias-Moya, J., Romero, J., Wehner, T. C., Gómez-Guillamón, M. L., et al. (2020). Mapping a partial andromonoecy locus in *Citrullus lanatus* using BSA-Seq and GWAS approaches. *Front. Plant Sci.* 11:1243. doi: 10.3389/fpls.2020.01243

An, J., Althiab Almasaud, R., Bouzayen, M., Zouine, M., and Chervin, C. (2020). Auxin and ethylene regulation of fruit set. *Plant Sci.* 292:110381. doi: 10.1016/j.plantsci.2019.110381

Bai, S. L., Peng, Y.-B., Cui, J. X., Gu, H. T., Xu, L. Y., Li, Y. Q., et al. (2004). Developmental analyses reveal early arrests of the spore-bearing parts of reproductive organs in unisexual flowers of cucumber (*Cucumis sativus* L.). *Planta* 220, 230–240. doi: 10.1007/s00425-004-1342-2

Barry, C. S., Blume, B., Bouzayen, M., Cooper, W., Hamilton, A. J., and Grierson, D. (1996). Differential expression of the 1-aminocyclopropane-1-carboxylate oxidase gene family of tomato. *Plant J.* 9, 525–535. doi: 10.1046/j.1365-313X.1996.09040525.x

Barry, C. S., Llop-Tous, M. I., and Grierson, D. (2000). The regulation of 1-aminocyclopropane-1-carboxylic acid synthase gene expression during the transition from system-1 to system-2 ethylene synthesis in tomato. *Plant Physiol.* 123, 979–986. doi: 10.1104/pp.123.3.979

Boualem, A., Fergany, M., Fernandez, R., Troadec, C., Martin, A., Morin, H., et al. (2008). A conserved mutation in an ethylene biosynthesis enzyme leads to andromonoecy in melons. *Science* 321, 836–838. doi: 10.1126/science.1159023

Boualem, A., Lemhemdi, A., Sari, M. A., Pignoly, S., Troadec, C., Choucha, F. A., et al. (2016). The andromonoecious sex determination gene predates the separation of *Cucumis* and *Citrullus genera*. *PLoS One* 11:e0155444. doi: 10.1371/journal.pone.0155444

Boualem, A., Troadec, C., Camps, C., Lemhemdi, A., Morin, H., Sari, M.-A., et al. (2015). A cucurbit androecy gene reveals how unisexual flowers develop and dioecy emerges. *Science* 350, 688–691. doi: 10.1126/SCIENCE.AAC8370

Boualem, A., Troadec, C., Kovalski, I., Sari, M. A., Perl-Treves, R., and Bendahmane, A. (2009). A conserved ethylene biosynthesis enzyme leads to andromonoecy in two *Cucumis* species. *PLoS One* 4:e6144. doi: 10.1371/journal.pone.0006144

Browse, J., and Wallis, J. G. (2019). *Arabidopsis* flowers unlocked the mechanism of jasmonate signaling. *Plants* 8:285. doi: 10.3390/plants8080285

Bulens, I., Van de Poel, B., Hertog, M. L., De Proft, M. P., Geeraerd, A. H., and Nicolaï, B. M. (2011). Protocol: an updated integrated methodology for analysis of metabolites and enzyme activities of ethylene biosynthesis. *Plant Methods* 7:17. doi: 10.1186/1746-4811-7-17

Byers, R. E., Baker, L. R., Sell, H. M., Herner, R. C., and Dilley, D. R. (1972). Ethylene: a natural regulator of sex expression of *Cucumis melo* L. *Proc. Natl. Acad. Sci. U.S.A.* 69, 717–720. doi: 10.1073/pnas.69.3.717

Chandler, J. W. (2011). The hormonal regulation of flower development. *J. Plant Growth Regul.* 30, 242–254. doi: 10.1007/s00344-010-9180-x

Chen, H., Sun, J., Li, S., Cui, Q., Zhang, H., Xin, F., et al. (2016). An ACC oxidase gene essential for cucumber carpel development. *Mol. Plant* 9, 1315–1327. doi: 10.1016/J.MOLP.2016.06.018

Dahmani-Mardas, F., Troadec, C., Boualem, A., Lévêque, S., Alsadon, A. A., Aldoss, A. A., et al. (2010). Engineering melon plants with improved fruit shelf life using the TILLING approach. *PLoS One* 5:e15776. doi: 10.1371/journal.pone.0015776

Depristo, M. A., Banks, E., Poplin, R., Garimella, K. V., Maguire, J. R., Hartl, C., et al. (2011). A framework for variation discovery and genotyping using next-generation DNA sequencing data. *Nat. Genet.* 43, 491–501. doi: 10.1038/ng.806

Edgar, R. C. (2004). MUSCLE: multiple sequence alignment with high accuracy and high throughput. *Nucleic Acids Res.* 32, 1792–1797. doi: 10.1093/nar/gkh340

García, A., Aguado, E., Garrido, D., Martínez, C., and Jamilena, M. (2020a). Two androecious mutations reveal the crucial role of ethylene receptors in the initiation of female flower development in *Cucurbita pepo*. *Plant J.* 103, 1548–1560. doi: 10.1111/TPJ.14846

García, A., Aguado, E., Martínez, C., Loska, D., Beltrán, S., Valenzuela, J. L., et al. (2020b). The ethylene receptors CpETR1A and CpETR2B cooperate in the control of sex determination in *Cucurbita pepo*. *J. Exp. Bot.* 71, 154–167. doi: 10.1093/jxb/erz417

García, A., Aguado, E., Parra, G., Manzano, S., Martínez, C., Megías, Z., et al. (2018). Phenomic and genomic characterization of a mutant platform in *Cucurbita pepo*. *Front. Plant Sci.* 9:1049. doi: 10.3389/fpls.2018.01049

Harkey, A. F., Watkins, J. M., Olex, A. L., DiNapoli, K. T., Lewis, D. R., Fetrow, J. S., et al. (2018). Identification of transcriptional and receptor networks that control root responses to ethylene. *Plant Physiol.* 176, 2095–2118. doi: 10.1104/pp.17.00907

Houben, M., and Van de Poel, B. (2019). 1-aminocyclopropane-1-carboxylic acid oxidase (ACO): the enzyme that makes the plant hormone ethylene. *Front. Plant Sci.* 10:695. doi: 10.3389/fpls.2019.00695

Hu, B., Li, D., Liu, X., Qi, J., Gao, D., Zhao, S., et al. (2017). Engineering non-transgenic gynoecious cucumber using an improved transformation protocol and optimized CRISPR/Cas9 system. *Mol. Plant* 10, 1575–1578. doi: 10.1016/j.molp.2017.09.005

Inaba, A., Liu, X., Yokotani, N., Yamane, M., Lu, W. J., Nakano, R., et al. (2007). Differential feedback regulation of ethylene biosynthesis in pulp and peel tissues of banana fruit. *J. Exp. Bot.* 58, 1047–1057. doi: 10.1093/jxb/erl265

Ji, G., Zhang, J., Zhang, H., Sun, H., Gong, G., Shi, J., et al. (2016). Mutation in the gene encoding 1-aminocyclopropane-1-carboxylate synthase 4 (CitACS4) led to andromonoecy in watermelon. *J. Integr. Plant Biol.* 58, 762–765. doi: 10.1111/jipb.12466

Kim, I. S., Okubo, H., and Fujieda, K. (1992). Endogenous levels of IAA in relation to parthenocarpy in cucumber (*Cucumis sativus* L.). *Sci. Hortic.* 52, 1–8. doi: 10.1016/0304-4238(92)90002-T

Kumar, S., Stecher, G., Li, M., Knyaz, C., and Tamura, K. (2018). MEGA X: molecular evolutionary genetics analysis across computing platforms. *Mol. Biol. Evol.* 35, 1547–1549. doi: 10.1093/molbev/msy096

Li, H., and Durbin, R. (2009). Fast and accurate short read alignment with Burrows-Wheeler transform. *Bioinformatics* 25, 1754–1760. doi: 10.1093/bioinformatics/btp324

Li, S., Xu, H., Ju, Z., Cao, D., Zhu, H., Fu, D., et al. (2018). The RIN-MC fusion of MADs-box transcription factors has transcriptional activity and modulates expression of many ripening genes. *Plant Physiol.* 176, 891–909. doi: 10.1104/pp.17.01449

Li, S. B., Xie, Z. Z., Hu, C. G., and Zhang, J. Z. (2016). A review of auxin response factors (ARFs) in plants. *Front. Plant Sci.* 7:47. doi: 10.3389/fpls.2016.00047

Livak, K. J., and Schmittgen, T. D. (2001). Analysis of relative gene expression data using real-time quantitative PCR and the 2-ΔΔCT method. *Methods* 25, 402–408. doi: 10.1006/meth.2001.1262

Manzano, S., Aguado, E., Martínez, C., Megías, Z., García, A., and Jamilena, M. (2016). The ethylene biosynthesis gene CitACS4 regulates monoecy/andromonoecy in watermelon (*Citrullus lanatus*). *PLoS One* 11:e0154362. doi: 10.1371/journal.pone.0154362

Manzano, S., Martínez, C., García, J. M., Megías, Z., and Jamilena, M. (2014). Involvement of ethylene in sex expression and female flower development in watermelon (*Citrullus lanatus*). *Plant Physiol. Biochem.* 85, 96–104. doi: 10.1016/j.plaphy.2014.11.004

Manzano, S., Martínez, C., Megías, Z., Garrido, D., and Jamilena, M. (2013). Involvement of ethylene biosynthesis and signalling in the transition from male to female flowering in the monoecious *Cucurbita pepo*. *J. Plant Growth Regul.* 32, 789–798. doi: 10.1007/s00344-013-9344-6

Manzano, S., Martínez, C., Megías, Z., Gómez, P., Garrido, D., and Jamilena, M. (2011). The role of ethylene and brassinosteroids in the control of sex expression and flower development in *Cucurbita pepo*. *Plant Growth Regul.* 65, 213–221. doi: 10.1007/s10725-011-9589-7

Martin, A., Troadec, C., Boualem, A., Rajab, M., Fernandez, R., Morin, H., et al. (2009). A transposon-induced epigenetic change leads to sex determination in melon. *Nature* 461, 1135–1138. doi: 10.1038/nature08498

Martínez, C., and Jamilena, M. (2021). To be a male or a female flower, a question of ethylene in cucurbits. *Curr. Opin. Plant Biol.* 59:101981. doi: 10.1016/J.PBI.2020.101981

Martínez, C., Manzano, S., Megías, Z., Barrera, A., Boualem, A., Garrido, D., et al. (2014). Molecular and functional characterization of CpACS27A gene reveals its involvement in monoecy instability and other associated traits in squash (*Cucurbita pepo* L.). *Planta* 239, 1201–1215. doi: 10.1007/s00425-014-2043-0

Martínez, C., Manzano, S., Megías, Z., Garrido, D., Picó, B., and Jamilena, M. (2013). Involvement of ethylene biosynthesis and signalling in fruit set and early fruit development in zucchini squash (*Cucurbita pepo* L.). *BMC Plant Biol.* 13:139. doi: 10.1186/1471-2229-13-139

Montero-Pau, J., Blanca, J., Bombarely, A., Ziarsolo, P., Esteras, C., Martí-Gómez, C., et al. (2018). De novo assembly of the zucchini genome reveals a whole-genome duplication associated with the origin of the *Cucurbita* genus. *Plant Biotechnol. J.* 16, 1161–1171. doi: 10.1111/pbi.12860

Muday, G. K., Rahman, A., and Binder, B. M. (2012). Auxin and ethylene: collaborators or competitors? *Trends Plant Sci.* 17, 181–195. doi: 10.1016/j.tplants.2012.02.001

Müller, M., and Munné-Bosch, S. (2011). Rapid and sensitive hormonal profiling of complex plant samples by liquid chromatography coupled to electrospray ionization tandem mass spectrometry. *Plant Methods* 7:37. doi: 10.1186/1746-4811-7-37

Nakatsuka, A., Murachi, S., Okunishi, H., Shiomi, S., Nakano, R., Kubo, Y., et al. (1998). Differential expression and internal feedback regulation of 1-aminocyclopropane-1-carboxylate synthase, l-aminocyclopropane-1-carboxylate oxidase, and ethylene receptor genes in tomato fruit during development and ripening. *Plant Physiol.* 118, 1295–1305. doi: 10.1104/pp.118.4.1295

Niwa, T., Suzuki, T., Takebayashi, Y., Ishiguro, R., Higashiyama, T., Sakakibaraa, H., et al. (2018). Jasmonic acid facilitates flower opening and floral organ development through the upregulated expression of SlMYB21 transcription factor in tomato. *Biosci. Biotechnol. Biochem.* 82, 292–303. doi: 10.1080/09168451.2017.1422107

Oh, Y., Baldwin, I. T., and Galis, I. (2013). A jasmonate ZIM-domain protein NaJAZd regulates floral jasmonic acid levels and counteracts flower abscission in *Nicotiana attenuata* plants. *PLoS One* 8:e57868. doi: 10.1371/journal.pone.0057868

Papadopoulou, E., Little, H. A., Hammar, S. A., and Grumet, R. (2005). Effect of modified endogenous ethylene production on sex expression, bisexual flower development and fruit production in melon (*Cucumis melo* L.). *Sex. Plant Reprod.* 18, 131–142. doi: 10.1007/s00497-005-0006-0

Pattyn, J., Vaughan-Hirsch, J., and Van de Poel, B. (2020). The regulation of ethylene biosynthesis: a complex multilevel control circuitry. *New Phytol.* 229, 770–782. doi: 10.1111/nph.16873

Reeves, P. H., Ellis, C. M., Ploense, S. E., Wu, M. F., Yadav, V., Tholl, D., et al. (2012). A regulatory network for coordinated flower maturation. *PLoS Genet.* 8:e1002506. doi: 10.1371/journal.pgen.1002506

Rudich, J., Halevy, A. H., and Kedar, N. (1969). Increase in femaleness of three cucurbits by treatment with Ethrel, an ethylene releasing compound. *Planta* 86, 69–76. doi: 10.1007/BF00385305

Ruduś, I., Sasiak, M., and Kępczyński, J. (2013). Regulation of ethylene biosynthesis at the level of 1-aminocyclopropane-1-carboxylate oxidase (ACO) gene. *Acta Physiol. Plant.* 35, 295–307. doi: 10.1007/s11738-012-1096-6

Růžička, K., Ljung, K., Vanneste, S., Podhorská, R., Beeckman, T., Friml, J., et al. (2007). Ethylene regulates root growth through effects on auxin biosynthesis and transport-dependent auxin distribution. *Plant Cell* 19, 2197–2212. doi: 10.1105/tpc.107.052126

Schubert, R., Dobritzsch, S., Gruber, C., Hause, G., Athmer, B., Schreiber, T., et al. (2019). Tomato MYB21 acts in ovules to mediate jasmonate-regulated fertility. *Plant Cell* 31, 1043–1062. doi: 10.1105/tpc.18.00978

Shinozaki, Y., Hao, S., Kojima, M., Sakakibara, H., Ozeki-Iida, Y., Zheng, Y., et al. (2015). Ethylene suppresses tomato (*Solanum lycopersicum*) fruit set through modification of gibberellin metabolism. *Plant J.* 83, 237–251. doi: 10.1111/tpj.12882

Shinozaki, Y., Nicolas, P., Fernandez-Pozo, N., Ma, Q., Evanich, D. J., Shi, Y., et al. (2018). High-resolution spatiotemporal transcriptome mapping of tomato fruit development and ripening. *Nat. Commun.* 9:364. doi: 10.1038/s41467-017-02782-9

Stepanova, A. N., Yun, J., Likhacheva, A. V., and Alonso, J. M. (2007). Multilevel interactions between ethylene and auxin in *Arabidopsis* roots. *Plant Cell* 19, 2169–2185. doi: 10.1105/tpc.107.052068

Stintzi, A., and Browse, J. (2000). The *Arabidopsis* male-sterile mutant, opr3, lacks the 12-oxophytodienoic acid reductase required for jasmonate synthesis. *Proc. Natl. Acad. Sci. U.S.A.* 97, 10625–10630. doi: 10.1073/pnas.190264497

Sun, H., Wu, S., Zhang, G., Jiao, C., Guo, S., Ren, Y., et al. (2017). Karyotype stability and unbiased fractionation in the paleo-allotetraploid *Cucurbita* genomes. *Mol. Plant* 10, 1293–1306. doi: 10.1016/j.molp.2017.09.003

Swarup, R., Perry, P., Hagenbeek, D., Van Der Straeten, D., Beemster, G. T. S., Sandberg, G., et al. (2007). Ethylene upregulates auxin biosynthesis in *Arabidopsis* seedlings to enhance inhibition of root cell elongation. *Plant Cell* 19, 2186–2196. doi: 10.1105/tpc.107.052100

Till, B. J., Reynolds, S. H., Weil, C., Springer, N., Burtner, C., Young, K., et al. (2004). Discovery of induced point mutations in maize genes by TILLING. *BMC Plant Biol.* 4:12. doi: 10.1186/1471-2229-4-12

Trebitsh, T., Rudich, J., and Riov, J. (1987). Auxin, biosynthesis of ethylene and sex expression in cucumber (*Cucumis sativus*). *Plant Growth Regul.* 5, 105–113. doi: 10.1007/BF00024738

Trivellini, A., Ferrante, A., Vernieri, P., and Serra, G. (2011). Effects of abscisic acid on ethylene biosynthesis and perception in *Hibiscus rosa-sinensis* L. flower development. *J. Exp. Bot.* 62, 5437–5452. doi: 10.1093/jxb/err218

Vriezen, W. H., Feron, R., Maretto, F., Keijman, J., and Mariani, C. (2008). Changes in tomato ovary transcriptome demonstrate complex hormonal regulation of fruit set. *New Phytol.* 177, 60–76. doi: 10.1111/j.1469-8137.2007.02254.x

Wang, H., Schauer, N., Usadel, B., Frasse, P., Zouine, M., Hernould, M., et al. (2009). Regulatory features underlying pollination-dependent and-independent tomato fruit set revealed by transcript and primary metabolite profiling. *Plant Cell* 21, 1428–1452. doi: 10.1105/tpc.108.060830

Wang, K., Li, M., and Hakonarson, H. (2010). ANNOVAR: functional annotation of genetic variants from high-throughput sequencing data. *Nucleic Acids Res.* 38, e164. doi: 10.1093/nar/gkq603

Wang, Z., Dai, L., Jiang, Z., Peng, W., Zhang, L., Wang, G., et al. (2005). GmCOI1, a soybean F-box protein gene, shows ability to mediate jasmonate-regulated plant defense and fertility in *Arabidopsis*. *Mol. Plant Microbe Interact.* 18, 1285–1295. doi: 10.1094/MPMI-18-1285

Yue, P., Lu, Q., Liu, Z., Lv, T., Li, X., Bu, H., et al. (2020). Auxin-activated MdARF5 induces the expression of ethylene biosynthetic genes to initiate apple fruit ripening. *New Phytol.* 226, 1781–1795. doi: 10.1111/nph.16500

Zemlyanskaya, E. V., Omelyanchuk, N. A., Ubogoeva, E. V., and Mironova, V. V. (2018). Deciphering auxin-ethylene crosstalk at a systems level. *Int. J. Mol. Sci.* 19:4060. doi: 10.3390/ijms19124060

Zhang, J., Guo, S., Ji, G., Zhao, H., Sun, H., Ren, Y., et al. (2020). A unique chromosome translocation disrupting ClWIP1 leads to gynoecy in watermelon. *Plant J.* 101, 265–277. doi: 10.1111/tpj.14537

Zhang, J., Shi, J., Ji, G., Zhang, H., Gong, G., Guo, S., et al. (2017). Modulation of sex expression in four forms of watermelon by gibberellin, ethephone and silver nitrate. *Hortic. Plant J.* 3, 91–100. doi: 10.1016/j.hpj.2017.07.010

Zhang, Y., Zhang, X., Liu, B., Wang, W., Liu, X., Chen, C., et al. (2014). A GAMYB homologue CsGAMYB1 regulates sex expression of cucumber via an ethylene-independent pathway. *J. Exp. Bot.* 65, 3201–3213. doi: 10.1093/jxb/eru176

Zuckerkandl, E., and Pauling, L. (1965). Molecules as documents of evolutionary history. *J. Theor. Biol.* 8, 357–366. doi: 10.1016/0022-5193(65)90083-4

Conflict of Interest: The authors declare that the research was conducted in the absence of any commercial or financial relationships that could be construed as a potential conflict of interest.

Publisher's Note: All claims expressed in this article are solely those of the authors and do not necessarily represent those of their affiliated organizations, or those of the publisher, the editors and the reviewers. Any product that may be evaluated in this article, or claim that may be made by its manufacturer, is not guaranteed or endorsed by the publisher.

frontiers in Plant Science

ORIGINAL RESEARCH
published: 14 February 2022
doi: 10.3389/fpls.2022.828923

Transcriptomic Variations and Network Hubs Controlling Seed Size and Weight During Maize Seed Development

Yanzhao Wang[1†], Lihong Nie[2†], Juan Ma[1†], Bo Zhou[1], Xiaohua Han[1], Junling Cheng[1], Xiaomin Lu[1], Zaifeng Fan[3], Yuling Li[4] and Yanyong Cao[1]*

[1]Henan Provincial Key Laboratory of Maize Biology, Institute of Cereal Crops, Henan Academy of Agricultural Sciences, Zhengzhou, China, [2]Institute of Industrial Crops, Henan Academy of Agricultural Sciences, Zhengzhou, China, [3]State Kay Laboratory of Agro-biotechnology and Key Laboratory of Pest Monitoring and Green Management-MOA, China Agricultural University, Beijing, China, [4]Henan Maize Engineering Technology Joint Center, Henan Agricultural University, Zhengzhou, China

OPEN ACCESS

Edited by:
Soraya Mousavi,
Consiglio Nazionale delle Ricerche (CNR)—Institute of Biosciences and Bioresources, Italy

Reviewed by:
Yongzhen Wu,
Ludong University, China
Fa Cui,
Ludong University, China

***Correspondence:**
Yanyong Cao
yanyongcao@126.com

[†]These authors have contributed equally to this work

Specialty section:
This article was submitted to Plant Breeding, a section of the journal Frontiers in Plant Science

Received: 04 December 2021
Accepted: 20 January 2022
Published: 14 February 2022

Citation:
Wang Y, Nie L, Ma J, Zhou B, Han X, Cheng J, Lu X, Fan Z, Li Y and Cao Y (2022) Transcriptomic Variations and Network Hubs Controlling Seed Size and Weight During Maize Seed Development. Front. Plant Sci. 13:828923. doi: 10.3389/fpls.2022.828923

To elucidate the mechanisms underlying seed development in maize, comprehensive RNA-seq analyses were conducted on Zhengdan1002 (ZD1002), Zhengdan958 (ZD958), and their parental lines during seven seed developmental stages. We found that gene expression levels were largely nonadditive in hybrids and that cis-only or trans × cis pattern played a large role in hybrid gene regulation during seed developmental stage. Weighted gene co-expression network (WGCNA) analysis showed that 36 modules were highly correlated ($r = -0.90$–0.92, $p < 0.05$) with kernel weight, length, and width during seed development. Forty-five transcription factors and 38 ribosomal protein genes were identified as major hub genes determining seed size/weight. We also described a network hub, *Auxin Response Factor 12* of maize (*ZmARF12*), a member of a family of transcription factor that mediate gene expression in response to auxin, potentially links auxin signal pathways, cell division, and the size of the seeds. The *ZmARF12* mutant exhibited larger seed size and higher grain weight. *ZmARF12* transcription was negatively associated with cell division during seed development, which was confirmed by evaluating the yield of protoplasts that isolated from the kernels of the mutant and other inbred lines. Transient knock-down of *ZmARF12* in maize plants facilitated cell expansion and division, whereas transient silencing of its potential interactor *ZmIAA8* impaired cell division. *ZmIAA8* expression was repressed in the *ZmARF12* over-expressed protoplasts. The mutant phenotype and the genetics studies presented here illustrated evidence that *ZmARF12* is a cell division repressor, and potentially determines the final seed size.

Keywords: ***Zea mays*, allele-specific expression, hub gene, seed development, seed size, seed weight, *ZmARF12***

INTRODUCTION

While seeds are well established as a major food source for humans around the world, they are also important raw materials for industry. Seed development, including seed size and weight, is crucial to the life cycle of higher plants, and impacts seed yields. In maize (*Zea mays* L.), seed development contains several phases: early development consisting of double

fertilization and syncytium formation, followed by cell differentiation, periods of mitosis and endoreduplication, accumulation of storage compounds, maturation, and desiccation (Wang et al., 2012). It is important to understand the molecular mechanisms regulating the various aspects of seed development in maize, including their size and weight, to improve seed yields.

High-resolution transcriptome technology has been used to monitor variations in gene expression during seed development. Transcriptomes of F_1 hybrids and their parents allow the investigation of gene expression patterns and variation in regulation, which have been proposed to play a role in heterosis. Two general modes of gene expression in hybrids, i.e., additive and nonadditive, are used to describe gene expression levels in F_1 hybrids, with respect to the average expression value (mid-parent value) of two parents. Nonadditive patterns in hybrids deviate significantly from the mid-parent values, while additive expression patterns do not. The differences in genetic background, tissues, developmental stages, and methodologies result in nonadditive expression pattern being predominant in many hybrids (Hoecker et al., 2008; Jahnke et al., 2010; Zhao et al., 2019); whereas additive expression is the most common in other known cases (Stupar and Springer, 2006; Paschold et al., 2012; Hu et al., 2016; Zhou et al., 2019).

The relative contribution of cis- and trans-acting regulatory changes can be investigated using allele-specific expression analysis (relative to parental ratios) on F_1 plants (Zhou et al., 2019). Generally, the predominant roles of cis-effects have often been demonstrated between species, whereas trans-effects are known to play a larger role within species (Wittkopp et al., 2004, 2008; Shi et al., 2012; Wu et al., 2016; Haas et al., 2020; Mattioli et al., 2020). Cis- and trans-effects occur simultaneously, and their compensatory effects facilitate the stability of gene expression an evolutionary timescale (Mattioli et al., 2020). The cis- and trans-acting regulation determine the differences in gene expression. The prevalence of cis-regulatory variation, subject to additive expression, has been observed in multiple tissues in maize (Stupar and Springer, 2006; Hu et al., 2016; Zhou et al., 2019), and in other species (Hughes et al., 2008; McManus et al., 2010; Cubillos et al., 2014; Haas et al., 2020). Nonadditive gene expression occurs when a combination of different alleles contributes to trans-acting interactions in a hybrid. In maize, studies on these hybrids have largely focused on root, meristem, leaf, silk, tassel, and one or two stages of seed development, with respect to seed, embryo, and endosperm tissues. It has not yet been possible to monitor the dynamic changes of additive and nonadditive expression patterns and variations in regulatory throughout the entire seed developmental phase.

Analysis of transcriptome dynamics aids the identification of gene co-expression modules and genes that act as critical network hubs and interpret the biological processes and pathways associated with development. Systems biology approaches, such as co-expression networks have been used to elucidate the patterns of transcriptome organization (Lin et al., 2019; Zhou et al., 2019). Zhang et al. (2016) identified co-expression modules that were highly correlated with seed weight enrichment during ovule development and DNA methylation. Their methodology comprised weighted gene co-expression network analysis (WGCNA) of parental inbred and reciprocal F_1 hybrids at 14 days after pollination (DAP14) and DAP17. They found that ARF, bZIP, G2-like, MADS-box, and orphan genes were involved in seed size determination. Downs et al. (2013) constructed a developmental gene expression network from microarray transcriptome profiles of 50 maize tissues, including the embryo and endosperm, across different stages of development, and found 24 modules that were strongly associated with tissue types and related biological processes. Sekhon et al. (2014) identified 19 gene co-expression modules for the whole seed, embryo, and endosperm at various developmental stages, and found that one module was rich in zein genes, and that many other genes were significantly and closely related to cell cycle and division, and starch accumulation.

Zhengdan958 (ZD958) is cultivated from Zheng58 (Z58) and Chang7-2 (C72) and has been widely grown in China since the year 2000. Zhengdan1002 (ZD1002) is developed from Zheng588 (Z588) and ZhengH71 (ZH71) in 2015 and improved the yields by 4.4–6.7% over ZD958. Z58 and C72 are representative inbred lines coming from the Reid and SPT heterotic groups, respectively. Z588 and ZH71 are developed from Z58 and C72, respectively. RNA-seq was used to characterize two commercial Chinese varieties of ZD958 and ZD1002, their four parents, and two other F_1 hybrid lines, at seven seed developmental stages. We analyzed these data to reveal the transcriptome variations between the F_1 hybrid and parental lines and to identify gene expression patterns and regulatory variations in hybrids during different seed developmental stages. We identified significant co-expression modules, hub genes, and networks that determined maize seed size and weight. We characterized a hub gene, *Auxin Response Factor 12* of maize (*ZmARF12*), which regulates seed size and seed yield in maize. We found that the transcripts of *ZmARF12* were negatively associated with cell division during kernel development; by evaluating protoplasts yields isolated from the kernels of the mutants and the four inbred lines. Transient silencing of *ZmARF12* and its interactor, *ZmIAA8*, in maize plants through virus-induced gene silencing (VIGS) also confirmed their effects on cell division. One of the *ZmARF12* mutants exhibited characteristically larger seed size and higher grain weight. In addition, the transient over-expression of *ZmARF12* in maize protoplast isolated from kernels constrained the expression of *ZmIAA8*. The mutant phenotype and the genetics studies described here demonstrate that *ZmARF12* represses cell division, and potentially plays roles in determining final seed size and yield. This work provides important insights into the gene expression and regulation patterns of commercial hybrids and the molecular networks responsible for maize seed development.

MATERIALS AND METHODS

Plant Materials and Field Trials

The four inbred lines Z58, Z588, C72, and ZH71 and their four F_1 hybrid combinations ZD958, ZD1002, Z58/ZH71, and Z588/C72, were used in this study. The trials took place in 2017 growing season, on the experimental fields of the Henan Academy of Agricultural Sciences, China. The eight maize lines were arranged in 10-row plots with 15 plants per row, with

three replications. The sampling time points for maize seeds were DAP0, DAP8, DAP10, DAP12, DAP20, DAP30, and DAP40. The 100-fresh kernel weight (FKW), 100-dry kernel weight (DKW), ten-kernel length (TKL), and ten-kernel width (TKW) were measured between DAP8 and DAP40 at the aforementioned time points. DKW was determined after drying the samples at 65°C in an oven for 1 week.

Seeds were obtained, with our thanks, from the Maize Genetics Cooperation Stock Center (for *ZmARF12* mutants: UFMu-04333, UFMu-09264, UFMu-09010, UFMu-09505, and UFMu-11213), University of Nebraska, Lincoln [cv. Va35 that were used for Brome mosaic virus (BMV) inoculation].

RNA Sample Collection and Sequencing

After sampling, the tissues were quickly frozen in liquid nitrogen and stored at −80°C until RNA isolation. Total RNA from whole developing kernels from the four parental lines and four F_1 hybrids at DAP0, DAP8, DAP10, DAP12, DAP20, DAP30, and DAP40, was extracted using the TRIzol reagent (Invitrogen, Carlsbad, CA, United States) following the manufacturer's instructions. RNA-seq was constructed using Illumina HiSeqTM4000. After filtering, clean sequence reads were aligned to the B73 reference genome[1] using HISAT v2.2.1.[2] Fragments per kilobase of transcript per million mapped read (FPKM) values were estimated using Cufflinks v2.2.1.[3]

Pearson's correlation (three biological replicates for each genotype) was calculated using the cor.test function from stats in R 4.0.1.[4] The transformed and normalized gene expression values with $\log_2$ (FPKM + 1) were used for the principal component analysis (PCA). PCA was performed using the fast.prcomp function from gmodels in R 4.0.1.

DNA Sample Collection and Resequencing

In order to select high-confidence variants for allele-specific expression analysis using a genomic control, the whole-genome resequencing was applied for four parental lines. During 6–10 leaf stage, five leaves from five individuals of each inbred line were selected, and genomic DNA was extracted using a CTAB method. Whole-genome resequencing was performed on an Illumina Hiseq X10 platform, with a resequencing depth of 30 X. Filtered reads were aligned with the maize B73 reference genome using BWA v0.7.15. Variant calling was performed for multiple-samples using the Genome Analysis Toolkit (v4.0.1.2); those exhibiting segregation distortion or sequencing errors were discarded. The software tool, ANNOVAR (Wang et al., 2010), was used to align and annotate the single-nucleotide polymorphisms (SNPs).

Identification of Differentially Expressed Genes and Gene Functional Analyses

Differential expression analysis was conducted using the edgeR package (v3.12.1). In each pairwise comparison, the differentially expressed genes (DEGs) were filtered using the expression levels: FPKM > 1, FDR (the Benjamini and Hochberg false discovery rate) < 0.05, $|\log_2$ fold change$| > 1$. The DEGs were analyzed using Gene Ontology (GO) with hypergeometric distribution test. The category biological processes of GO terms were retrieved from http://geneontology.org/. Significant biological process terms were defined if the FDR threshold was <0.05.

Gene Expression Pattern Analysis

Two-tailed homoscedastic variance *t*-tests were used to test if the F_1 expression were significantly different from the mid-parent expressions. All DEGs with $p < 0.05$ were considered to have been nonadditively expressed; and considered as additive expressions otherwise. The nonadditive DEGs were further categorized into three distinct classes, based on their deviations from the mid-parent value: over-dominance (above the higher inbred parent level), dominance (in-between the inbred parent levels), and underdominance (below the lower inbred parent level).

Cis- and Trans-Regulatory Expression Assignment

Only SNPs identified by both transcriptome and whole-genome resequencing were used to infer gene regulation patterns. In addition, the genes used to infer the allele ratio of hybrid expression had to meet two criteria: (1) both parents in the three biological replicates had different allele types, and the alleles were heterozygous for each replicate in the hybrids; (2) every SNP was supported by no less than 20 reads in the hybrids and parents. When a gene showed multiple regulatory patterns, one pattern whose proportion was larger than or equal to 60% could be considered the pattern of the gene. The regulatory divergence patterns were assigned using the method described in McManus et al. (2010).

Briefly, the relative allelic expression of each gene was tested in F_1 hybrid (named H set) and parent (named P set) using chi-square test against the null hypothesis of 1:1 respectively, and compared between F_1 and parent (named T set) using two-tailed *t*-tests. The difference was defined as significant in any set with the value of $p < 0.05$. The regulatory divergences were further classified into seven patterns using the following criteria:

Cis-only: significant differential expression in P and H set but not in T set.

Trans-only: significant differential expression in P and T set but not in H set.

Cis + trans: significant differential expression in P, H, and T set. The $\log_2$-transformed allelic expression ratio has the same sign in H and P set.

Cis × trans: significant differential expression in P, H, and T set. The $\log_2$-transformed allelic expression ratio has the opposite sign in H and P set.

Compensatory: significant differential expression in H and T set but not in P set. The cis- and trans-regulatory divergences compensate each other.

[1]ftp://ftp.ensemblgenomes.org/pub/release-40/plants/fasta/zea_mays/dna/
[2]http://daehwankimlab.github.io/hisat2/
[3]http://cole-trapnell-lab.github.io/cufflinks/install/
[4]http://www.r-project.org/

Conserved: no significant differential expression in P, H, or T set.

Ambiguous: all other patterns.

Identification of Gene Co-expression Modules and Hub-Genes for Seed Size and Weight

Gene co-expression module assignments were determined based on the FPKM data, using the WGCNA protocol (Langfelder and Horvath, 2008). To identify seed size and weight associated modules, we correlated module eigengenes with FKW, DKW, TKL, and TKW from DAP8 to DAP40. For each of the time points, the genes with mean FPKM > 1 for the 24 samples were analyzed. The soft threshold power β was set to nine for all network constructions except for DAP8 ($\beta = 6$). The dynamic tree cut algorithm with a minimum module size of 50 genes was used to cut the hierarchal clustering. mergeCutHeight = 0.15 was used to merge similar modules. A significant module was defined if the *p*-value for module-trait associations was <0.05.

The intramodular connectivity of each gene was calculated using function softConnectivity function of the WGCNA package, in R 4.0.1; top 30 genes with high connectivity values (sum of the correlation coefficient of one gene with all other genes within one module) were considered to be hub genes in one module. The gene networks of the hub genes were visualized using Cytoscape v3.6.1.

Plant Cultivation and Auxin Treatment

Nicotina. benthamiana Domin. plants were grown in growth chambers at 24/22°C (day/night) with a 16 light, 8 h dark cycle as described previously (Chen et al., 2017).

Every sample of five maize (*Z. mays L.* inbred lines B73 or Va35) seeds was placed between two sheets of germination paper, as previously described in Ortiz-Ramírez et al. (2018). Each germination paper cylinder was then transferred into a glass tube (150 × 50 mm in diameter) filled with an 800 × dilution of Peters Pro 20–20–20 water-soluble fertilizer (ICL specialty fertilizers, Summerville, SC, United States) to reach 1/4 of the paper height, and incubated in a growth chamber at 27/24°C (day/night) with a 16/8 h light/dark cycle, and approximately 50% humidity.

The auxin treatment was conducted by transferring the roots of the plants into the Hoagland's solution containing 5 μM NAA (Sigma, Saint Louis MO, United States) solution. The primary roots of αNAA exposure and the control plants were harvested at 0, 1, 2, and 3 h post-treatment, respectively.

Real-Time RT-PCR

Total RNA was purified from different samples using TRIzol reagent (Invitrogen, Carlsbad CA, United States), and then treated with RNase-free DNase I (TaKaRa, Dalian, China). The first-strand cDNA was synthesized using 2.0 μg of total RNA per 20 μl reaction and an oligo (dT) primer. Ten-fold diluted cDNA, a set of gene-specific primers (**Supplementary Table 2**) and a FastSYBR mixture (CWBIO, Beijing, China) were mixed for qPCR to determine the accumulation levels of the maize genes on an ABI 7500 Real-Time PCR system (Applied Biosystems Inc., Foster City, CA, United States). The expression level of *ZmUbi* mRNA was determined and used as an internal control. The relative expression level of each gene was calculated using the $2^{-\Delta\Delta Ct}$ method (Livak and Schmittgen, 2001). Differences between the treatments were then analyzed using Student's *t*-tests. All experiments were carried out at least three times.

Transient Silencing of *ZmARF12* and *ZmIAA8* Through Virus-Induced Gene Silencing

The BMV-derived VIGS system was previously described (Cao et al., 2012; Zhu et al., 2014). DNA fragments of 222, and 186 bp, representing the *ZmARF12* and *ZmIAA8* genes, were amplified using specific primer pairs (**Supplementary Table 2**). The resulting constructs of BMV-*ZmARF12*, BMV-ZmIAA8, and the control BMV-GFP, were then transformed into the *Agrobacterium tumefaciens* strain C58C1. The *N. benthamiana* leaves were infiltrated with *A. tumefaciens* cultures and collected for BMV virion preparation, as described previously (Zhu et al., 2014).

The third leaves of the three-leaf-stage (2 weeks old) Va35 plants were rub-inoculated with approximately 20 μg of partially purified BMV virion. More than 20 seedlings were used for each treatment, and the inoculated plants were grown inside a growth chamber at 18/20°C (day/night) for 7–14 days before being challenged with auxin treatments, or harvested for protoplasts isolation (Zhu et al., 2014). Systemic infection leaves (or equivalent leaves from mock-inoculated plants) from BMV-*ZmARF12*, BMV-ZmIAA8, or BMV-GFP inoculated plants were harvested from individual plants at 7- and 14-d post-inoculation (dpi), and subjected to qRT-PCR to evaluate the efficiency of the gene silencing.

Quantification of Cell Area and Number of Cell Layers

The maize leaves or kernel pellicles were collected to quantify the cells per square and the number of cell layers, according to a previously described method (de Jong et al., 2015). Fresh leaf disks or pellicle tissues, which were 7–8 mm in diameter, were fixed in formalin-acetic acid-alcohol solution (5% formaldehyde solution, 5% acetic acid, and 45% anhydrous ethanol), and dehydrated with an ethanol series prior to being embedded in Technovit. Sections of 4 μm thick leaf disks or kernel pellicles were then stained with a toluidine blue solution, respectively. The sections were observed and scanned with 3D HISTECH Pannoramic MIDI II scanner (Budapest, Hungary), and micrographs were made with CaseViewer™ digital microscopy system (3D HISTECH). These micrographs were employed for further analysis with the CaseViewer 2.4 application.

For analysis of the Va35 leaf disk, randomly selected 20× micrographs were used to estimate the number of cell layers, by drawing two lines across the central vascular bundle (L1) and the common vascular system (L2), respectively. The number of cells along the two lines were scored. Whereas for the

analysis of the cell numbers and number of cell layers within the pellicle, two lines were drawn across the outermost layers of the epidermis and along the longitudinal direction of the pellicle, separately. The total numbers of cells along the lines were numbered.

Maize Protoplasts Isolation and Transfection

The maize kernels were aseptically dissected from greenhouse-grown ears harvested DAP10 and subjected to protoplasts isolation and transfection using the previously described protocols (Ortiz-Ramírez et al., 2018; Hu et al., 2020). The prepared protoplasts were transfected with pGFP-ARF12 plasmid and incubated at 25°C for 12 h, then the protoplasts were harvested by centrifuging at 500 × *g*, and used for real-time RT-PCR to evaluate the expression profiles of *ZmARF12* and its interactor *ZmIAA8* as previously described (Cao et al., 2012).

RESULTS

Morphological Dynamics at Different Seed Developmental Stages

Seed morphology showed that ZD1002 and its paternal parent ZH71 exhibited larger seed size and heavier weights than ZD958 and C72, respectively, during the seven seed developmental stages (**Figure 1A**). ANOVA and Duncan's multiple comparisons of FKW, DKW, TKL, and TKW for DAP8–40 stages further revealed the differences between the seed morphological characteristics of ZH71 and C72 were obvious during the investigation, whereas the differences between Z588 and Z58 were comparatively smaller (**Supplementary Figure 1**; **Supplementary Table 1**). ZD1002 and ZD958 showed consistently significant differences in terms of FKW and TKL during seed developmental stages. Four F_1 hybrids showed significantly increased seed size and weight compared with their respective inbred parents.

Overview of Transcriptome Analysis of Eight Genotypes

To understand dynamics of the gene expression during seed developmental stages, 168 RNA libraries from eight lines with three replicates at seven stages were constructed. A total of 27,377 maize gene models were expressed with FPKM value ≥ 1 in at least one sample. The number of expressed genes ranged from 18,442 to 21,276 for 168 samples. The correlation of three biological replicates were high for eight maize lines at each developmental stage (0.9575–0.9999; **Supplementary Figure 2**).

The PCA revealed that the 56 samples (eight genotypes at seven stages) were assigned to seven stages, and that DAP0 was clearly distinguished from other six stages (**Figure 1B**). DAP8 was also found to be distinguishable from the other six stages. Except for DAP0 and DAP8, the neighboring two DAP stages showed similarities. Moreover, two stages were often overlapping, such as DAP10 and DAP12, and DAP30 and DAP40 (**Figure 1B**). The pairwise comparisons of the two neighboring stages also identified major transcriptional differences between DAP0 and DAP8, and DAP8 and DAP10 for eight genotypes (**Supplementary Figure 3A**).

In line with phenotypic variations, the number of DEGs between Z588 and Z58 (72–199) was much lower than that between ZH71 and C72 (408–810) across all developmental stages (**Supplementary Figures 3B,C)**. DNA resequencing revealed that ~7% SNPs are different between Z588 and Z58, whereas the proportion of differences between ZH71 and C72 was ~14% (**Supplementary Figure 4**). Differential expression analyses showed that the transcriptome profiles of ZD1002 and ZD958 were similar to that of their maternal parents during their early developmental stages (DAP8–12) but closer to paternal parents at the later stages (DAP20–40; **Supplementary Figure 3D**). In general, the total number of DEGs (4700–5,379) between F_1 hybrids and paternal parents was slightly higher than that between F_1 hybrids and maternal parents (4677–5,026; **Supplementary Figure 3D**). These indicated that paternal parents might have a relative higher contribution to the differences between F_1 hybrids.

The number of DEGs between two commercial varieties ZD958 and ZD1002 varied from 162 to 1,050 during the seven stages (**Supplementary Figure 3E**). Compared with ZD958, more downregulated genes were observed in ZD1002 across all developmental stages (**Supplementary Figure 3E**). The two hybrids showed the largest differences at DAP0, followed by DAP12 and DAP40. The former DEGs were most significantly involved in four terms related to photosynthesis associated processes (**Supplementary Figure 5**). At DAP12 and DAP40, DEGs between ZD1002 and ZD958 were significantly involved response to heat and temperature stimuli (**Supplementary Figure 5**).

Gene Expression Levels Are Largely Nonadditive in Hybrids

The significantly increased differences with respect to seed size and weight in F_1 hybrids relative to parental lines showed seed heterosis. The differences between F_1 expression and mid-parent expression levels allow to the assessment of additive and nonadditive patterns. For ZD1002, a large proportion of DEGs (55.38–78.15%) exhibited nonadditive expression at all seven stages (**Supplementary Figure 6A**). For ZD958 and the two other hybrid crosses, most of DEGs (63.41–85.27%) displayed additive expression at DAP0, whereas differentially expressed profiles were more likely to exhibit nonadditive patterns (56.65–80.23%) for the remaining stages (**Supplementary Figures 6B–D**). Among nonadditive DEGs, a relative high portion of dominance mode were observed in most stages of the four F_1 hybrids. For ZD1002, 53.36% of DEGs exhibited over-dominance pattern at DAP12, which was much higher than that of dominance (4.60%) and under-dominance (7.11%). The joint expression patterns of over-dominance and dominance or under-dominance and dominance were also found in our investigation. These supported those multiple modes of gene action with heterosis during seed development. In addition,

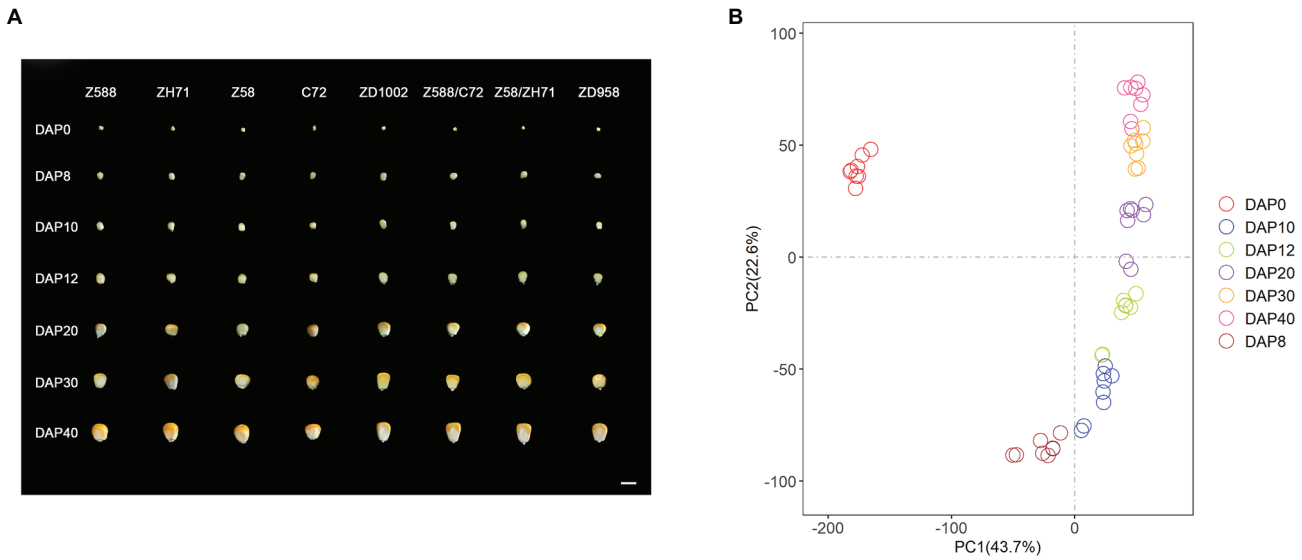

FIGURE 1 | (A) The geometry size, shape characteristics of the four inbred lines and the four hybrids were photographed at different days post pollination. Z588, Zheng588; ZH71, ZhengH71; Z58, Zheng58; C72, Chang7-2; ZD1002, Zhengdan1002; and ZD958, Zhengdan958. DAP0–DAP40 representing different days (0, 8, 10, 12, 20, 30, and 40 days) after pollination, respectively. Scale bar = 1 cm. **(B)** Principal component analysis (PCA) of the RNA-seq data at seven developmental stages. Mean fragments per kilobase of transcript per million mapped read (FPKM) values of three biological replicates are used for each genotype at each developmental stage. DAP represents days after pollination.

the transitional changes and proportions of gene expression patterns might result in the phenotypic differences between ZD958 and ZD1002 across seed development.

Regulatory Divergences During Seed Development

The sources of regulatory variation of genes can be inferred based on their allelic expression ratios in the F_1 hybrids and parents. In this context, DEGs between parents and hybrids whose SNPs were co-detected in genomic and transcriptomic levels were used to infer regulatory divergence assignment. Here, we showed the regulatory divergences between the two commercial varieties and further revealed their regulatory differences during seed development. For ZD1002, the cis-only regulatory difference was the main type at DAP0, DAP10, DAP12, and DAP20, accounting for 21.55–26.85% of DEGs (**Figures 2A,C–E**; **Supplementary Figure 7A**). For ZD958, the cis-only divergence type also accounted for the highest proportion (24.50–30.96%) of DEGs at DAP0 and DAP20 (**Figures 3A,E**; **Supplementary Figure 7B**). Three patterns including trans-only, trans + cis, and trans × cis contributed to the gene expression at DAP8 in ZD1002 (**Figure 2B**). Trans-only and compensatory were the main regulatory patterns at DAP8, DAP30, and DAP40 in ZD1002, respectively, whereas the proportion of trans × cis pattern was the highest at DAP12, DAP30, and DAP40 in ZD958 (**Figures 2, 3**; **Supplementary Figure 7**).

Co-expression Modules Highly Correlated With Seed Size and Weight

Seed size and weight are important traits of seed yield, and are direct reflections of seed development. To identify specific genes that are highly associated with seed size and weight, we constructed co-expression networks for each stage and correlated co-expression modules with seed size and weight related traits. At DAP8 and DAP10 stages, four modules were found to only be significantly correlated with TKW ($r = -0.49$–0.48, $p < 0.05$), and were considered a TKW-specific module (**Supplementary Figures 8A,B**). From the DAP12 to DAP40, 31 modules significantly correlated with seed size and weight were identified (**Supplementary Figures 8C–F**). The number of modules ranged from seven to nine for each stage. The correlation coefficient of these module-traits was high (−0.90 to 0.92). Ten of the 31 modules were significantly correlated with all four traits, with correlation coefficients between −0.88 and 0.92.

Hub Genes of Seed Size and Weight and Their Potential Networks

Hub genes are those that show the most connections in a network as indicated by their high correlation values, and they may play important roles in the determination of seed size and weight. Forty-five TF-encoding genes were identified as network hubs from DAP8 to DAP40 (**Figure 4A**). For example, there were five genes from ARF families (ARF3, ARF12, ARF14, ARF18, and ARF28), four MYBs (MYB44, MYB56, MYB73, and MYB79), three MYBRs (MYBR63, MYBR69, and MYBR70), and two bZIPs [abscisic acid-insensitive 5 (ABI5) and opaque2 heterodimerizing protein2 (OHP2); **Supplementary Figure 9**]. Twenty-five pairs of hub TFs showed potentially interactions with each other (the weight value of 0.11–0.29; **Supplementary Figure 9**).

Except for DAP10, 38 hub genes encoding ribosomal protein were found from DAP8 to DAP40 (**Figure 4A**;

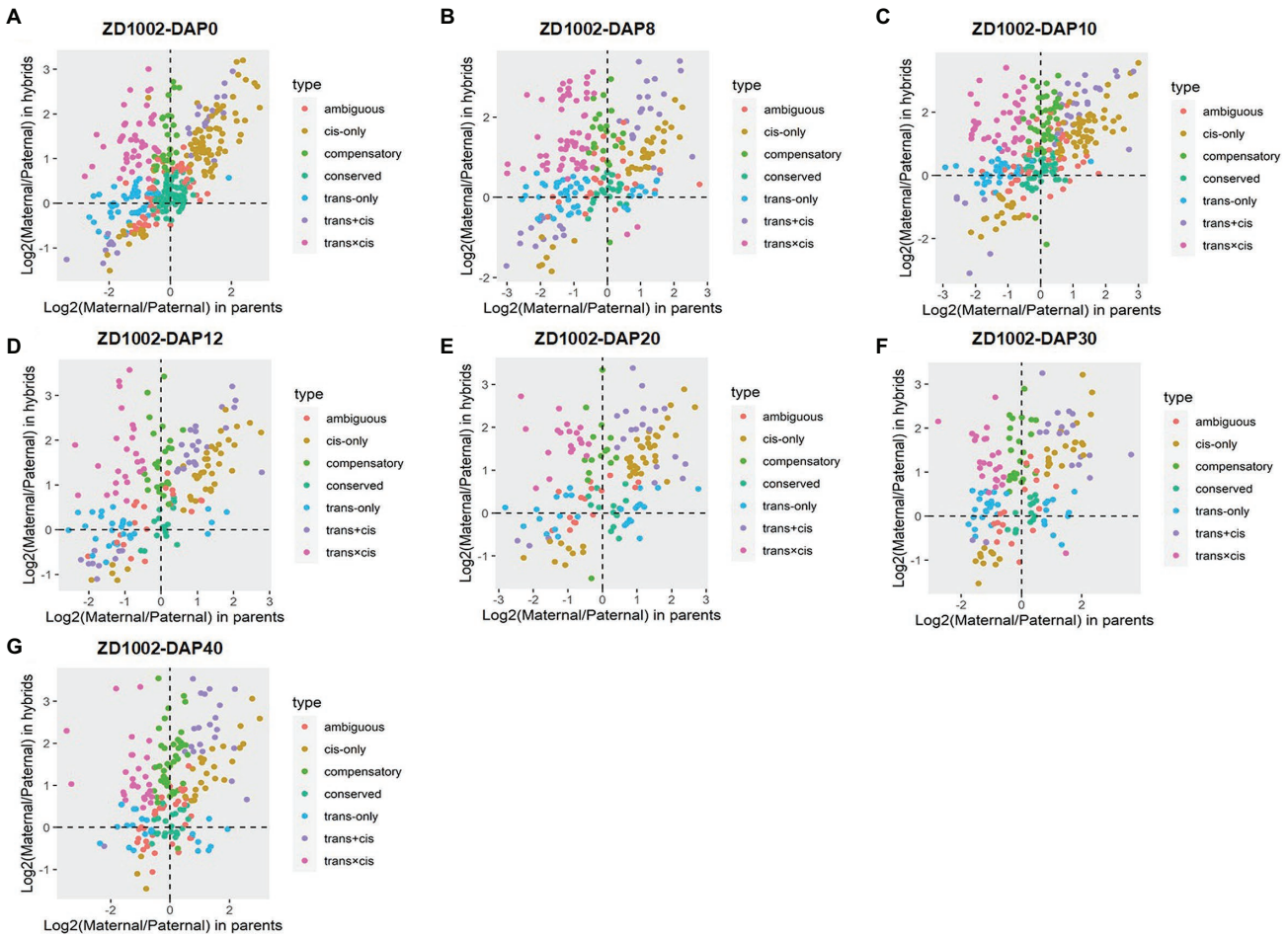

FIGURE 2 | Plots of allele-specific expression levels in Zhengdan1002 (ZD1002) and its parental data set at seven developmental stages. **(A–G)** represent 0 days after pollination (DAP0), DAP8, DAP10, DAP12, DAP20, DAP30, and DAP40, respectively. Each point represents a gene and is color-coded according to the types of regulatory divergence.

Supplementary Figure 10). There were 18 RP genes at DAP12, and among them 16 RP genes were found in the sienna3 module. Based on their gene networks, most of the hub RP genes were found to have high connections with each other, as 118 pairs of hub RP genes had high interactions, and their weight values ranged from 0.11 to 0.36 (**Supplementary Figure 10**). In the sienna3 module of DAP12, 103 pairs of hub genes encoding for RP were connected (0.11–0.20). Apart from inter-connections between hub RP genes, another 66 RP genes also showed interactions with these hub genes (**Supplementary Figure 10**). In addition, 49 TF genes including 11 hub TFs interacted with the 38 hub RP genes (**Supplementary Figure 10**).

Some zein genes, E3 ubiquitin-protein ligase, ubiquitin conjugating enzyme, chaperone proteins, and calcium-dependent protein kinases were also considered to be hub genes for seed size and weight (**Figure 4A**). Their inter-connections were also observed in our investigation (**Supplementary Figures 11–14**). The identification of hub genes and their networks could help to identify potential cross-talk in the regulation of maize seed development.

Transcription Profile of Hub Gene *ZmARF12* and Its Potential Interactor *ZmIAA8*

Auxin regulates cell division and is further involved in almost all the processes of plant growth and development, including seed size determination (Sun et al., 2017). The interactions between ARFs and IAAs is the key particular of auxin regulation (Korasick et al., 2014).

In *Arabidopsis*, ARF2 was thought to be negatively regulates auxin signal pathway and seed size through downregulation the cell division in the integument region of endosperm (Schruff et al., 2006). BIG GRAIN1, a positive regulator of auxin response in rice that involved in auxin transport, leads to significant increasement of seed size and plant biomass, seed weight, and finally the yield (Liu et al., 2015). However, the mechanisms underlying ARF and IAA control of seed development remains elusive.

Through WGCNA, we found that ARF12 was a network hub for seed size and weight (**Figure 4B**; **Supplementary Figure 9**); we have hence demonstrated the roles of ARF12 in determining maize seed size and weight. The mRNA

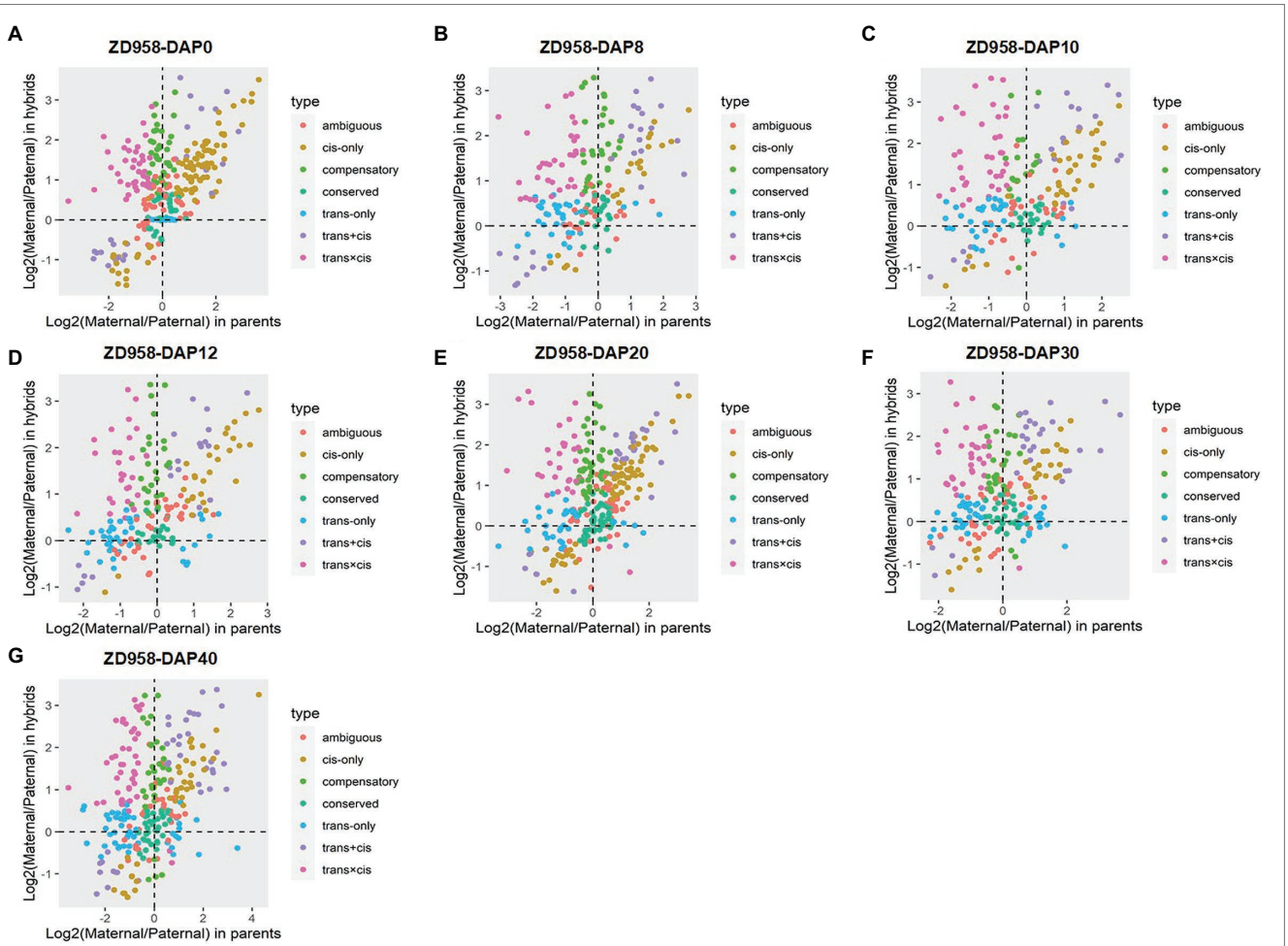

FIGURE 3 | Plots of allele-specific expression levels in Zhengdan958 (ZD958) and its parental data set at seven developmental stages. **(A–G)** represent DAP0, DAP8, DAP10, DAP12, DAP20, DAP30, and DAP40, respectively. Each point represents a gene and is color-coded according to the types of regulatory divergence.

accumulation of the *ZmARF12* in different tissues was observed, and real-time RT-PCR showed that it was relatively higher in the ear and tassel than in other tissues (**Supplementary Figure 15A**). To determine the response of *ZmARF12* to the exogenous auxin treatments, the expression levels in the seedling roots at different time points were evaluated after being subjected to 5 μM NAA solution using real-time RT-PCR. The results indicated that *ZmARF12* was upregulated in the first 2 h of treatments, but downregulated after 3 h of auxin treatment. Intriguingly, the mRNA abundance displayed a similar variation tendency in the mock treatment (**Supplementary Figure 15B**).

To explore the potential roles of *ZmARF12* in regulating the processes of grain production, we analyzed its expression levels at different seed developmental stages. The quantitative RT-PCR data showed that the transcriptional level of *ZmARF12* was rapidly reduced in the first 20 days, then reached a relatively stable level in the four hybrid lines and paternal lines C72 and ZH71. In contrast, the *ZmARF12* transcript level in the maternal lines Z58 and Z588 were consecutively upregulated with the embryo development, except for a slight decrease at DAP30 (**Supplementary Figure 15C**). The protein–protein interaction networks that possessed ARF12 had significant interactions with Aux/IAA-transcription factor 8 (IAA8), IAA26, and IAA28 (**Supplementary Figure 16**). IAA8 also showed connections with ARF12 in the WGCNA, with a weight value of 0.23 (**Figure 4B**). The expressions of *ZmIAA8*, in the four inbred lines and the four hybrids exhibited similar patterns, and were upregulated over the first 8 days, and then downregulated across the early stages (DAP8 to DAP30) of ear fertilization (**Supplementary Figure 15D**).

Transient Silencing of *ZmARF12* Facilitates Maize Cell Division Activity

To understand the potential roles of *ZmARF12* in regulating kernel development. The cell size was evaluated by examining the number of cells per surface unit and the number of cell layers in the leaves of *ZmARF12* in transient silenced plants. We used a BMV-based VIGS system to knock down *ZmARF12*

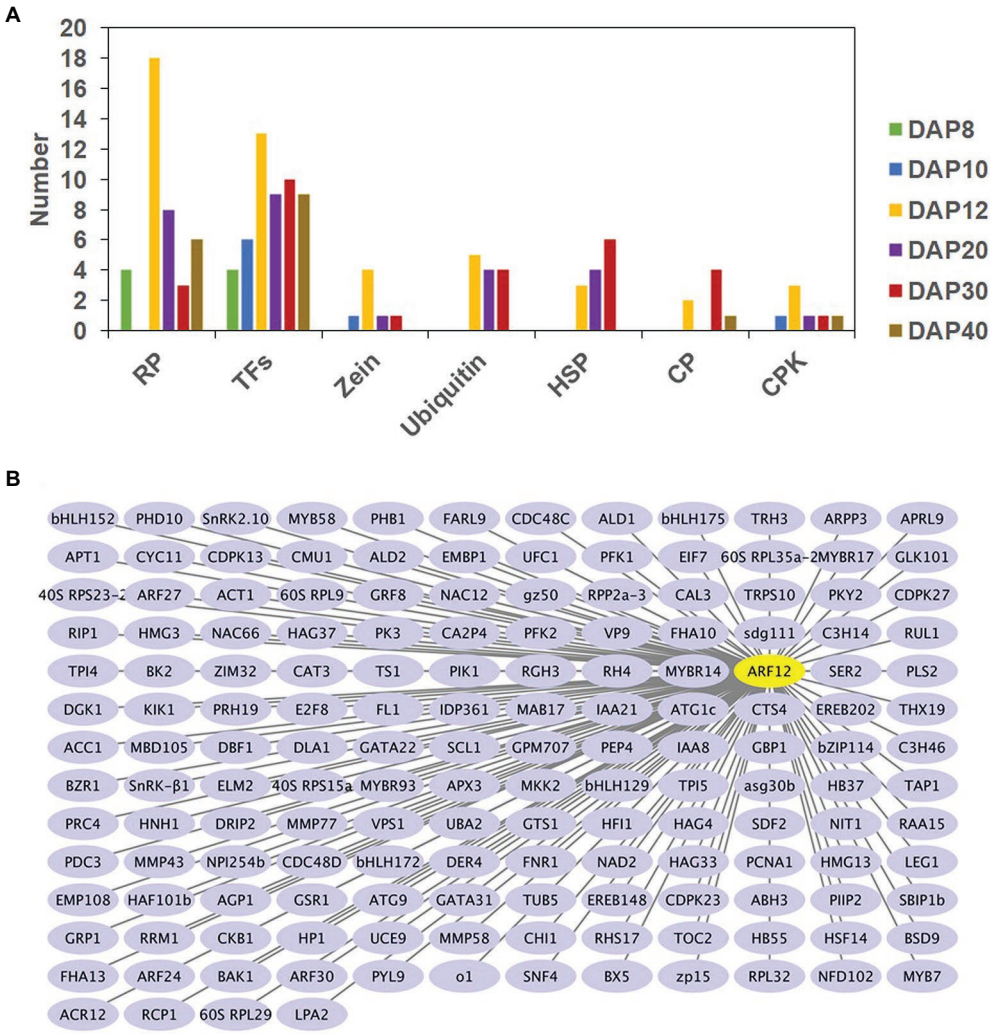

FIGURE 4 | Number of hub genes associated with seed size and weight at six developmental stages **(A)** and gene networks of ARF12 **(B)**. RP, TF, ubiquitin, HSP, CP, and CPK are abbreviations of ribosomal proteins, transcription factors, ubiquitin associated proteins, heat shock proteins, chaperone proteins, and calcium-dependent protein kinase, respectively. DAP8–40 represents 8–40 d after pollination, respectively. Cytoscape representation of co-expressed genes with edge weight ≥ 0.20 is shown. Only genes with annotations are displayed.

expression. The *ZmARF12* VIGS vector BMV-*ZmARF12* and control plasmid BMV-GFP were introduced into *N. benthamiana* to replicate the BMV virion. The Va35 plants were inoculated with the purified virus particles to transiently silence *ZmARF12* as previously reported (Cao et al., 2012; Zhu et al., 2014). The qRT-PCR results indicated that the expression of *ZmARF12* in the *BMV-ZmARF12* inoculated plants was about 30–35% that of the control plants (**Figure 5A**). In the transient silenced plants, the expression levels of *ZmARF11*, *ZmARF23*, and *ZmARF24*, which share 42.30, 49.96, and 61.17% homology with *ZmARF12* (Xing et al., 2011; **Supplementary Figure 17**), were not affected (**Supplementary Figure 18**). These results demonstrated that silencing had been successfully achieved. Additionally, the transient silencing of *ZmIAA8* facilitated the expression of its potential interacting gene, *ZmARF12* (**Figure 5A**; **Supplementary Figure 18**).

At 14 dpi, the second systemic leaves above the inoculated leaves were harvested for analysis of cell expansion and division. The *ZmARF12*-silenced plants had more cells, and more cell layers, compared to those in the control plants (**Figure 5C**; **Supplementary Figure 19**). In contrast, transient silencing of *ZmIAA8* impaired the cell division in the systemic leaves (**Supplementary Figure 19**). These findings suggested that *ZmARF12* might repress cell division during maize leaf growth.

ZmARF12 Might Be a Regulator of Cell Division During Seed Development

Between the two paternal inbred lines, ZH71 exhibited a larger seed size and heavier weight than C72 during the process of seed development (**Figure 1A**; **Supplementary Figure 1**). The expression of *ZmARF12* in both inbred lines decreased after

pollination; however, in compared with C72, ZH71 decreased more significantly at DAP10 stage (**Supplementary Figure 15C**). To further speculate whether the changes of seed weight and size were correlated with the expression level of *ZmARF12* in the different inbred lines, cell division was evaluated by examining the cell numbers per surface unit, and the number of cell layers in the grain pericarp at DAP10. The kernel pellicle of ZH71, which bore bigger kernels, had a smaller average cell size (larger cell size per unit), but more cell layers than those seen in C72, Z588, and Z58 (**Figure 6**).

The five *ZmARF12* mutants (UFMu-04333, UFMu-09264, UFMu-09010, UFMu-09505, and UFMu-11213) obtained from Maize Genetics COOP were employed to elucidate the potential role of *ZmARF12* in regulating the kernel development process. Among the five mutants, UFMu-09010 exhibited larger kernel sizes (**Figures 7A–C**), higher KWE (kernel weight per ear), and HKW (hundred kernel weight, HKW) than those of wild-type W22 (**Figure 7D**). The protoplasts were isolated from the maize kernels of different inbred lines at DAP10 to further demonstrate the function and regulation of *ZmARF12*. The kernel meristem protoplast yield (per mg of tissue) was measured; the data showed that the muARF12 and ZH71 kernels yielded more protoplasts per mg tissue than other lines (**Figure 7E**). To test the regulatory influence of *ZmARF12* on the expression of *ZmIAA8*, the protoplasts were transfected with transient expression vector that harboring *ZmARF12* gene. The real-time RT-PCR was performed on the total RNA that extracted from the transfected protoplasts and un-transfected protoplasts as the CK experiment. The data indicated that *ZmARF12* was successfully transiently over-expressed in the transfected protoplasts, and that the expression of *ZmIAA8* in the protoplast cells transformed with *ZmARF12* was significantly lower than that observed in the CK data (**Figure 7F**). These data indicated that *ZmARF12* might be a regulator of cell division during seed development.

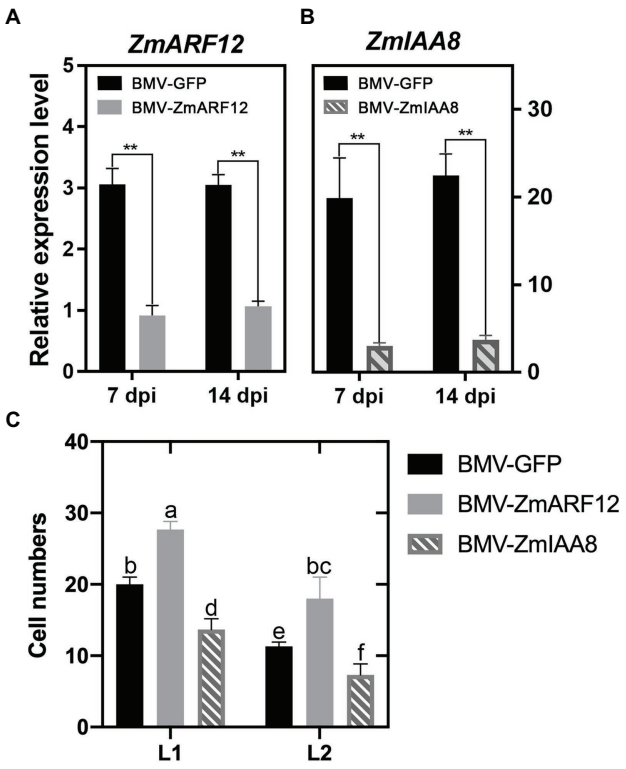

FIGURE 5 | Transient silencing of *Auxin Response Factor 12* of maize (*ZmARF12*) facilitates the cell division of maize leaves. The 7-day-old cv. Va35 maize plants were inoculated virions of either the chimeric brome mosaic virus (BMV-GFP) or BMV-GFP with a *ZmARF12* insert (BMV-ZmARF12) or a *ZmIAA8* insert (BMV-ZmIAA8) to knock-down *ZmARF12*, *ZmIAA8* using brome mosaic virus (BMV) induced gene silencing, respectively. **(A,B)** The first and second systemic leaves above the virus-inoculated leaves were harvested for analysis of the silencing efficiency of *ZmARF12*, *ZmIAA8* at 7 days post-inoculation (dpi) and 14 dpi, respectively. Each value is shown as the average of six independent experiments ± SD. $^{**}p < 0.01$ (according to a paired Student's *t*-test); ns, not significant. **(C)** Quantification of cell number per surface unit and number of cell layers of the second systemic leaves above inoculated leaves of *ZmARF12*-, *ZmIAA8*-silenced and control plants. Values are the means ± SD, different letters indicate significant difference ($p < 0.05$) as determined by Tukey–Kramer test.

DISCUSSION

Examining intra-specific transcriptomic variations can provide insights into phenotypic variation. With the aid of transcriptome technology, we investigated the differential expression dynamics between different genotypes, and monitored the gene expression and regulatory patterns in hybrids during seed development.

The genes that were differentially expressed between the hybrids and their parents exhibited both additive and nonadditive expression patterns; the proportions of which differed between the studied hybrids and seven developmental stages. Several studies have reported high proportions of additive expression patterns in F_1 hybrids (Jahnke et al., 2010; Hu et al., 2016). This was consistent with our observations that most of the DEGs (ZD958, Z58/ZH71, and Z588/C71) exhibited additive gene action at the start of pollination (DAP0). Nonadditive expression prevailed in the subsequent developmental stages of the three heterotic crosses, across the seven stages of ZD1002 seed development studied; in line with previous reports on maize seedlings, immature ears, primary roots, and embryos (Song and Messing 2003; Auger et al., 2005; Springer and Stupar, 2007; Hoecker et al., 2008). The shift from additive to nonadditive patterns between DAP0 and subsequent developmental stages was contrary to the results of many studies, as reviewed by Baranwal et al. (2012). In younger vegetative and reproductive stages, nonadditive expression accounted for major proportions of differential expression profiles (Baranwal et al., 2012). Differential expression activity has been reported to be significantly reduced, and additive expression as dominant, during the mature stages of vegetative development (Baranwal et al., 2012). Ko et al. (2016) found that temporal shifts in ZmCCA1-binding targets correlated with nonadditive and additive expressions during the early and late stages of seedling development. The shifts between additive and nonadditive expressions might be transitory, or a switch, to accelerate the rate of seed development in this work.

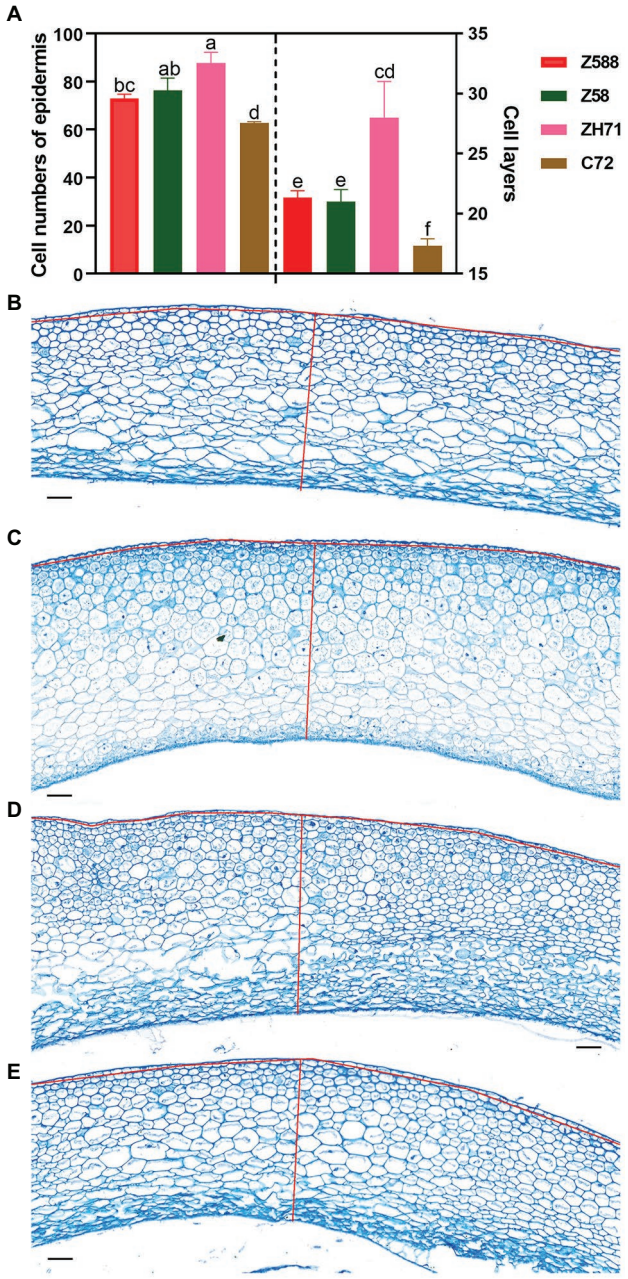

FIGURE 6 | Cell division of the kernel pellicle of the four inbred lines at early seed developmental stage. **(A)** To determine the cell number and number of cell layers in the kernel pellicle, kernels were collected from plants that grown in three different blocks with three replicates per genotype (Z588, Zheng588; ZH71, ZhengH71; Z58, Zheng58; and C72, Chang7-2) per block at 10 d after pollination. Each value is shown as the average of six independent experiments ± SD. Different letters indicate significant difference ($p < 0.05$) as determined by Tukey–Kramer test. Micrographs of the kernel pellicle from Z588 **(B)**, Z58 **(C)**, ZH71 **(D)**, and C72 **(E)**. For estimation of the numbers of cells and layers, the number of cells along the red line were scored. The scale bar represents 50 μm.

We noted additive and nonadditive DEGs were mainly affected by cis-only regulatory variation in more development stages for ZD1002 (**Supplementary Figure 20**). However, cis or cis coupled with trans × cis or other patterns mainly resulted in additive DEGs, whereas trans × cis largely affected nonadditive DEGs in ZD958 (**Supplementary Figure 20**). The results observed here were inconsistent with previous studies that trans-only regulatory variations were involved in nonadditive patterns, whereas cis-only patterns contributed to mid-parent expression (Zhou et al., 2019; Haas et al., 2020). Several investigations implicated that cis-regulatory variation in important roles for phenotypic evolution (Wittkopp and Kalay, 2012; Díaz-Valenzuela et al., 2020; Haas et al., 2020; Zhao et al., 2020). These changes of regulatory patterns were main drivers of the dynamic differences in seed size and weight between ZD1002 and ZD958.

Understanding the molecular mechanisms controlling seed development, seed size, and weight are important for improving maize seed yields. We constructed a set of co-expression modules with respect to the different developmental stages, and found 36 modules to be significantly and highly correlated modules with seed size and weight. Different modules recruited genes. Many genes were considered to be network hubs, with RP families and TFs comprising the two largest categories. RP-gene regulation of seed size has been reported in *Arabidopsis* and maize, identified through the analysis of mutants. Tian et al. (2017) reported that *NtRPL17* played an important role in establishing the size of embryos/seeds, by regulating cell cycle progression. In maize, emp5 mutants encode a PPR-DYW protein that is required for the editing of multiple transcripts in mitochondria, and the editing events, particularly the C-to-U editing at the rpl16-458 site, are critical to the mitochondrial functions and, hence, to seed development in maize (Liu et al., 2013). The *dek44* mutant produces small kernels with delayed development, and Dek44 encodes for the mitochondrial RPL9 (Qi et al., 2019).

Many of the TF families have been discovered to play roles in seed development (Bemer et al., 2010; Le et al., 2010; Agarwal et al., 2011). However, only a few TFs have been implicated in seed size and weight determination. Through WGCNA, Zhang et al. (2016) found that some ARF members were significantly correlated with seed weight, indicating their important roles in maize seed development. Congruently, several ARF genes were identified as being significant in our co-expression modules for seed size and weight. The seed size and grain weight of the *ZmARF12* mutant, UFMu-09010, were increased over those of the wild-type plants (**Figures 7A–D**). These observations were per mg tissue of the early stage fertilized seeds of the mutants, which yielded more protoplasts than other lines (**Figure 7E**). Overall, the expression of *ZmARF12* in the four inbred lines and their progenies exhibited a decreasing trend during the early stage of kernel fertilization (**Supplementary Figure 15**). The transcript levels of *ZmARF12* were negatively associated with cell division during kernel development (**Figure 6**). This was also confirmed by evaluating the yields of protoplasts that isolated from the kernels of other four inbred lines at DAP10 (**Figure 7E**). In addition, transient silencing of *ZmARF12* in maize Va35 plants facilitated cell expansion and division (**Figure 5**; **Supplementary Figure 19**), similar results were observed in the mutant UFMu-09010 (data not shown). The mutant phenotype

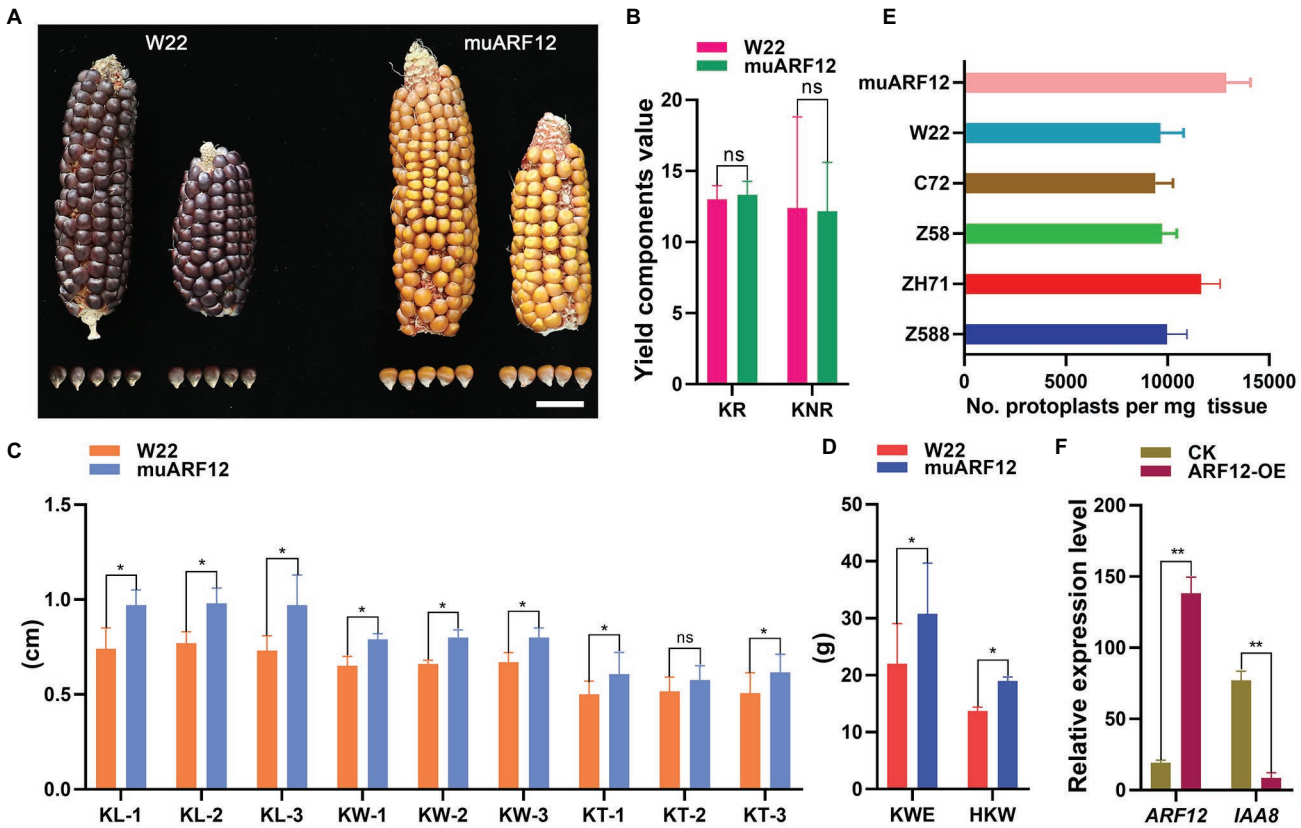

FIGURE 7 | *Auxin Response Factor 12* of maize regulating cell division during kernel development. Comparison of seeds generated by wild-type and ZmARF12 mutants by evaluating the differences of phenotypes of the kernels **(A)** and the yield related traits **(B–D)**. Scale bar = 2 cm; KR, kernel rows; KNR, kernel number per row; KL, kernel length; KW, kernel weight; KT, kernel thickness; EW, ear weight; and HKW, hundred kernel weight. **(E)** Protoplasts yield of per mg tissues that isolated from the kernels of *ZmARF12* mutant, W22 and other four inbred lines at 10 days after pollination (DAP10). **(F)** The effects of ZmARF12 on the expression of ZmIAA8 were evaluated by transient over-expressing ZmARF12 in the protoplasts that isolated from maize kernels at DAP10. Each value is shown as the average of six independent experiments ± SD. $^{*}p < 0.05$, $^{**}p < 0.01$ (paired Student's *t*-test); ns, not significant. Different letters on the columns show significant difference ($p < 0.05$) as determined by Tukey–Kramer test.

and VIGS studies described here provide evidence that *ZmARF12* might repress cell division during kernel fertilization process, and have potential roles in determining the final seed size.

Auxin is a central plant hormone that regulates many processes, including pattern formation, cell division, and cell expansion (Chapman and Estelle, 2009; Vanneste and Friml, 2009; Weijers and Wagner, 2016); in which signaling is mediated by ARFs and Aux/IAA repressors that regulate the expression of a multitude of auxin response genes (Berleth et al., 2004). The transcript levels of ZmIAA8 increased within the first DAP8 and then decreased again in the following days of kernel fertilization (**Supplementary Figure 15D**), this initial increase of *ZmARF12* expression levels was also observed in the two maternal inbred lines, Z588 and Z58 (**Supplementary Figure 15C**). Mounting evidence indicates that ARFs regulate gene expression in response to auxin stimuli, and that ZmIAA8 is transcriptional repressor for auxin response genes (Ma and Dooner, 2010). The overlap between the ZmIAA8 distribution and *ZmARF12* expression levels showed that the regulatory role of *ZmARF12* might also depend on the auxin trends during the kernel development. During the early stages of fertilization, maize kernel development mainly depends on cell division (Guo et al., 2010; Huang et al., 2019). The transient silencing of ZmIAA8 impairs cell division (**Figure 5**), suggesting that during the early stages of seed development, *ZmARF12* might be part of the auxin-dominated regulatory mechanism that associated with cell division.

As their predominant mechanisms, ARFs bind to auxin response elements (AuxREs) as promoters of auxin-regulated genes, and to mediate auxin signal pathways by activating or repressing gene transcription. It is thought that auxin regulates ARF function through its effects on gene expression and protein turnover of Aux/IAAs. Aux/IAAs can dimerize with ARFs, and repress the ability of ARFs to activate gene expression in protoplast transfection assays (Schruff et al., 2006). In this work, transient over-expression of the *ZmARF12* in the protoplasts was shown to impair the expression of ZmIAA8 (**Figure 7F**). The mechanism by which this occurs remains obscure. Thus, the identification of the direct interaction of *ZmARF12* with its dimerization partners will help elucidate the underlying mechanism of *ZmARF12* function.

CONCLUSION

To elucidate the underlying mechanism of maize seed development. Here, we report that transcriptional variations and network hub genes were involved in controlling seed size and weight through RNA-seq and weighted gene co-expression network analysis. The mutant phenotype and transient-silencing studies illustrated that *ZmARF12*, one of the network hubs, is a cell division repressor, and potentially determines the final seed size.

DATA AVAILABILITY STATEMENT

The original contributions presented in the study are publicly available. This data can be found here: National Center for Biotechnology Information (NCBI) BioProject database under accession numbers PRJNA728476 (DNA sequencing) and PRJNA649667 (transcriptome).

AUTHOR CONTRIBUTIONS

JM, ZF, YL, and YC designed the research, analyzed the data, and revised the final manuscript. YW and LN performed most experiments. BZ and XH helped with phenotype assessment. JC and XL helped with samples collection. JM and YC wrote the manuscript. All authors contributed to the article and approved the submitted version.

FUNDING

This work was supported by the National Key Research and Development Program of China (2016YFD0300309/03), the special fund for Henan Agriculture Research System (S2010-02-G01), Major scientific and technological project of Henan province (151100111100), Fund for Distinguished Young Scholars from Henan Academy of Agricultural Sciences (2020JQ01), and Science-Technology Foundation for Outstanding Young Scientists of Henan Academy of Agricultural Sciences (2020YQ04).

ACKNOWLEDGMENTS

The authors would like to thank the Maize Genetics Cooperation Stock Center for the seeds of *ZmARF12* mutants, Richard S. Nelson (Samuel Roberts Noble Foundation) for the BMV VIGS vector. We would like to thank Genedenovo Biotechnology Co., Ltd. (Guangzhou, China) for RNA-seq, DNA resequencing, and related data analyses.

SUPPLEMENTARY MATERIAL

The Supplementary Material for this article can be found online at: https://www.frontiersin.org/articles/10.3389/fpls.2022.828923/full#supplementary-material

REFERENCES

Agarwal, P., Kapoor, S., and Tyagi, A. K. (2011). Transcription factors regulating the progression of monocot and dicot seed development. *Bioessays* 33, 189–202. doi: 10.1002/bies.201000107

Auger, D. L., Gray, A. D., Ream, T. S., Kato, A., Coe, E. H., and Birchler, J. A. (2005). Nonadditive gene expression in diploid and triploid hybrids of maize. *Genetics* 169, 389–397. doi: 10.1534/genetics.104.032987

Baranwal, V. K., Mikkilineni, V., Zehr, U. B., Tyagi, A. K., and Kapoor, S. (2012). Heterosis: emerging ideas about hybrid vigour. *J. Exp. Bot.* 63, 6309–6314. doi: 10.1093/jxb/ers291

Bemer, M., Heijmans, K., Airoldi, C., Davies, B., and Angenent, G. C. (2010). An atlas of type I MADS box gene expression during female gametophyte and seed development in *Arabidopsis*. *Plant Physiol.* 154, 287–300. doi: 10.1104/pp.110.160770

Berleth, T., Krogan, N. T., and Scarpella, E. (2004). Auxin signals-turning genes on and turning cells around. *Curr. Opin. Plant Biol.* 7, 553–563. doi: 10.1016/j.pbi.2004.07.016

Cao, Y., Shi, Y., Li, Y., Cheng, Y., Zhou, T., and Fan, Z. (2012). Possible involvement of maize Rop1 in the defense responses of plants to viral infection. *Mol. Plant Pathol.* 13, 732–743. doi: 10.1111/j.1364-3703.2011.00782.x

Chapman, E. J., and Estelle, M. (2009). Mechanism of auxin-regulated gene expression in plants. *Annu. Rev. Genet.* 43, 265–285. doi: 10.1146/annurev-genet-102108-134148

Chen, H., Cao, Y., Li, Y., Xia, Z., Xie, J., Carr, J. P., et al. (2017). Identification of differentially regulated maize proteins conditioning sugarcane mosaic virus systemic infection. *New Phytol.* 215, 1156–1172. doi: 10.1111/nph.14645

Cubillos, F. A., Stegle, O., Grondin, C., Canut, M., Tisné, S., Gy, I., et al. (2014). Extensive cis-regulatory variation robust to environmental perturbation in *Arabidopsis*. *Plant Cell* 26, 4298–4310. doi: 10.1105/tpc.114.130310

de Jong, M., Wolters-Arts, M., Schimmel, B. C., Stultiens, C. L., de Groot, P. F., Powers, S. J., et al. (2015). *Solanum lycopersicum* AUXIN RESPONSE FACTOR 9 regulates cell division activity during early tomato fruit development. *J. Exp. Bot.* 66, 3405–3416. doi: 10.1093/jxb/erv152

Díaz-Valenzuela, E., Sawers, R. H., and Cibrián-Jaramillo, A. (2020). Cis- and trans-regulatory variations in the domestication of the chili pepper fruit. *Mol. Biol. Evol.* 37, 1593–1603. doi: 10.1093/molbev/msaa027

Downs, G. S., Bi, Y. M., Colasanti, J., Wu, W., Chen, X., Zhu, T., et al. (2013). A developmental transcriptional network for maize defines coexpression modules. *Plant Physiol.* 161, 1830–1843. doi: 10.1104/pp.112.213231

Guo, M., Rupe, M. A., Dieter, J. A., Zou, J. J., Spielbauer, D. S., Duncan, K. E., et al. (2010). Cell number regulator1 affects plant and organ size in maize: implications for crop yield enhancement and heterosis. *Plant Cell* 22, 1057–1073. doi: 10.1105/tpc.109.073676

Haas, M., Himmelbach, A., and Mascher, M. (2020). The contribution of cis- and trans-acting variants to gene regulation in wild and domesticated barley under cold stress and control conditions. *J. Exp. Bot.* 71, 2573–2584. doi: 10.1093/jxb/eraa036

Hoecker, N., Keller, B., Muthreich, N., Chollet, D., Descombes, P., Piepho, H.-P., et al. (2008). Comparison of maize (*Zea mays* L.) F_1-hybrid and parental inbred line primary root transcriptomes suggests organ-specific patterns of nonadditive gene expression and conserved expression trends. *Genetics* 179, 1275–1283. doi: 10.1534/genetics.108.088278

Hu, Y., Song, D., Gao, L., Ajayo, B. S., Wang, Y., Huang, H., et al. (2020). Optimization of isolation and transfection conditions of maize endosperm protoplasts. *Plant Methods* 16:96. doi: 10.1186/s13007-020-00636-y

Hu, X., Wang, H., Diao, X., Liu, Z., Li, K., Wu, Y., et al. (2016). Transcriptome profiling and comparison of maize ear heterosis during the spikelet and floret differentiation stages. *BMC Genomics* 17, 959–977. doi: 10.1186/s12864-016-3296-8

Huang, Y. C., Wang, H. H., Huang, X., Wang, Q., Wang, J. C., An, D., et al. (2019). Maize VKS1 regulates mitosis and cytokinesis during early endosperm development. *Plant Cell* 31, 1238–1256. doi: 10.1105/tpc.18.00966

Hughes, R., Spielman, M., Schruff, M. C., Larson, T. R., Graham, I. A., and Scott, R. J. (2008). Yield assessment of integument-led seed growth following targeted repair of auxin response factor 2. *Plant Biotechnol. J.* 6, 758–769. doi: 10.1111/j.1467-7652.2008.00359.x

Jahnke, S., Sarholz, B., Thiemann, A., Kühr, V., Gutiérrez-Marcos, J. F., Geiger, H. H., et al. (2010). Heterosis in early seed development: a comparative

study of F_1 embryo and endosperm tissues 6 days after fertilization. *Theor. Appl. Genet.* 120, 389–400. doi: 10.1007/s00122-009-1207-y

Ko, D. K., Rohozinski, D., Song, Q., Taylor, S. H., Juenger, T. E., Harmon, F. G., et al. (2016). Temporal shift of circadian-mediated gene expression and carbon fixation contributes to biomass heterosis in maize hybrids. *PLoS Genet.* 12:e1006197. doi: 10.1371/journal.pgen.1006197

Korasick, D. A., Westfall, C. S., Lee, S. G., Nanao, M. H., Dumas, R., Hagen, G., et al. (2014). Molecular basis for AUXIN RESPONSE FACTOR protein interaction and the control of auxin response repression. *Proc. Natl. Acad. Sci. U. S. A.* 111, 5427–5432. doi: 10.1073/pnas.1400074111

Langfelder, P., and Horvath, S. (2008). WGCNA: an R package for weighted correlation network analysis. *BMC Bioinformatics* 9:559. doi: 10.1186/1471-2105-9-559

Le, B. H., Cheng, C., Bui, A. Q., Wagmaister, J. A., Henry, K. F., Pelletier, J., et al. (2010). Global analysis of gene activity during *Arabidopsis* seed development and identification of seed-specific transcription factors. *Proc. Natl. Acad. Sci. U. S. A.* 107, 8063–8070. doi: 10.1073/pnas.1003530107

Lin, F., Zhou, L., He, B., Zhang, X., Dai, H., Qian, Y., et al. (2019). QTL mapping for maize starch content and candidate gene prediction combined with co-expression network analysis. *Theor. Appl. Genet.* 132, 1931–1941. doi: 10.1007/s00122-019-03326-z

Liu, L., Tong, H., Xiao, Y., Che, R., Xu, F., Hu, B., et al. (2015). Activation of big grain1 significantly improves grain size by regulating auxin transport in rice. *Proc. Natl. Acad. Sci. U. S. A.* 112, 11102–11107. doi: 10.1073/pnas.1512748112

Liu, Y. J., Xiu, Z. H., Meeley, R., and Tan, B. C. (2013). Empty pericarp5 encodes a pentatricopeptide repeat protein that is required for mitochondrial RNA editing and seed development in maize. *Plant Cell* 25, 868–883. doi: 10.1105/tpc.112.106781

Livak, K. J., and Schmittgen, T. D. (2001). Analysis of relative gene expression data using real-time quantitative PCR and the $2^{-\Delta\Delta CT}$ method. *Methods* 25, 402–408. doi: 10.1006/meth.2001.1262

Ma, Z., and Dooner, H. K. (2010). A mutation in the nuclear-encoded plastid ribosomal protein S9 leads to early embryo lethality in maize. *Plant J.* 37, 92–103. doi: 10.1046/j.1365-313x.2003.01942.x

Mattioli, K., Oliveros, W., Gerhardinger, C., Andergassen, D., Maass, P. G., Rinn, J. L., et al. (2020). Cis and trans effects differentially contribute to the evolution of promoters and enhancers. *Genome Biol.* 21, 210–232. doi: 10.1186/s13059-020-02110-3

McManus, C. J., Coolon, J. D., Duff, M. O., Eipper-Mains, J., Graveley, B. R., and Wittkopp, P. J. (2010). Regulatory divergence in *Drosophila* revealed by mRNA-seq. *Genome Res.* 20, 816–825. doi: 10.1101/gr.102491.109

Ortiz-Ramírez, C., Arevalo, E. D., Xu, X., Jackson, D. P., and Birnbaum, K. D. (2018). An efficient cell sorting protocol for maize protoplasts. *Curr. Protoc. Plant Biol.* 3:e20072. doi: 10.1002/cppb.20072

Paschold, A., Jia, Y., Marcon, C., Lund, S., Larson, N. B., Yeh, C. T., et al. (2012). Complementation contributes to transcriptome complexity in maize (*Zea mays* L.) hybrids relative to their inbred parents. *Genome Res.* 22, 2445–2454. doi: 10.1101/gr.138461.112

Qi, W., Lu, L., Huang, S., and Song, R. (2019). Maize Dek44 encodes mitochondrial ribosomal protein L9 and is required for seed development. *Plant Physiol.* 180, 2106–2119. doi: 10.1104/pp.19.00546

Schruff, M. C., Spielman, M., Tiwari, S., Adams, S., Fenby, N., and Scott, R. J. (2006). The AUXIN RESPONSE FACTOR 2 gene of *Arabidopsis* links auxin signaling, cell division, and the size of seeds and other organs. *Development* 133, 251–261. doi: 10.1242/dev.02194

Sekhon, R. S., Hirsch, C. N., Childs, K. L., Breitzman, M. W., Kell, P., Duvick, S., et al. (2014). Phenotypic and transcriptional analysis of divergently selected maize populations reveals the role of developmental timing in seed size determination. *Plant Physiol.* 165, 658–669. doi: 10.1104/pp.114.235424

Shi, X., Ng, D. W., Zhang, C., Comai, L., Ye, W., and Chen, Z. J. (2012). Cis- and trans-regulatory divergence between progenitor species determines gene-expression novelty in *Arabidopsis* allopolyploids. *Nat. Commun.* 3:950. doi: 10.1038/ncomms1954

Song, R., and Messing, J. (2003). Gene expression of a gene family in maize based on non-collinear haplotypes. *Proc. Natl. Acad. Sci. U. S. A.* 100, 9055–9060. doi: 10.1073/pnas.1032999100

Springer, N. M., and Stupar, R. M. (2007). Allele-specific expression patterns reveal biases and embryo-specific parent-of-origin effects in hybrid maize. *Plant Cell* 19, 2391–2402. doi: 10.1105/tpc.107.052258

Stupar, R. M., and Springer, N. M. (2006). Cis-transcriptional variation in maize inbred lines B73 and Mo17 leads to additive expression patterns in the F_1 hybrid. *Genetics* 173, 2199–2210. doi: 10.1534/genetics.106.060699

Sun, Y., Wang, C., Wang, N., Jiang, X., Mao, H., Zhu, C., et al. (2017). Manipulation of *Auxin response factor 19* affects seed size in the woody perennial *Jatropha curcas*. *Sci. Rep.* 7, 40844–40855. doi: 10.1038/srep40844

Tian, S., Wu, J., Liu, Y., Huang, X., Li, F., Wang, Z., et al. (2017). Ribosomal protein NtRPL17 interacts with kinesin-12 family protein NtKRP and functions in the regulation of embryo/seed size and radicle growth. *J. Exp. Bot.* 68, 5553–5564. doi: 10.1093/jxb/erx361

Vanneste, S., and Friml, J. (2009). Auxin: a trigger for change in plant development. *Cell* 136, 1005–1016. doi: 10.1016/j.cell.2009.03.001

Wang, K., Li, M., and Hakonarson, H. (2010). ANNOVAR: functional annotation of genetic variants from next-generation sequencing data. *Nucleic Acids Res.* 38:e164. doi: 10.1093/nar/gkq603

Wang, G., Wang, G., Wang, F., and Song, R. (2012). *A Transcriptional Roadmap for Seed Development in Maize. Seed Development: OMICS Technologies toward Improvement of Seed Quality and Crop Yield*. Netherlands: Springer.

Weijers, D., and Wagner, D. (2016). Transcriptional responses to the Auxin hormone. *Annu. Rev. Plant Biol.* 67, 539–574. doi: 10.1146/annurev-arplant-043015-112122

Wittkopp, P. J., Haerum, B. K., and Clark, A. G. (2004). Evolutionary changes in cis and trans gene regulation. *Nature* 430, 85–88. doi: 10.1038/nature02698

Wittkopp, P. J., Haerum, B. K., and Clark, A. G. (2008). Regulatory changes underlying expression differences within and between *Drosophila* species. *Nat. Genet.* 40, 346–350. doi: 10.1038/ng.77

Wittkopp, P. J., and Kalay, G. (2012). Cis-regulatory elements: molecular mechanisms and evolutionary processes underlying divergence. *Nat. Rev. Genet.* 13, 59–69. doi: 10.1038/nrg3095

Wu, Y., Sun, Y., Wang, X., Lin, X., Sun, S., Shen, K., et al. (2016). Transcriptome shock in an interspecific F_1 triploid hybrid of *Oryza* revealed by RNA sequencing. *J. Integr. Plant Biol.* 58, 150–164. doi: 10.1111/jipb.12357

Xing, H. Y., Pudake, R. N., Guo, G. G., Xing, G. F., Hu, Z. R., Zhang, Y. R., et al. (2011). Genome-wide identification and expression profiling of auxin response factor (ARF) gene family in maize. *BMC Genomics* 12, 178–190. doi: 10.1186/1471-2164-12-178

Zhang, X., Hirsch, C. N., Sekhon, R. S., de Leon, N., and Kaeppler, S. M. (2016). Evidence for maternal control of seed size in maize from phenotypic and transcriptional analysis. *J. Exp. Bot.* 67, 1907–1917. doi: 10.1093/jxb/erw006

Zhao, N., Ding, X., Lian, T., Wang, M., Tong, Y., Liang, D., et al. (2020). The effects of gene duplication modes on the evolution of regulatory divergence in wild and cultivated soybean. *Mol. Front. J.* 11:601003. doi: 10.3389/fgene.2020.601003

Zhao, Y., Hu, F., Zhang, X., Wei, Q., Dong, J., Bo, C., et al. (2019). Comparative transcriptome analysis reveals important roles of nonadditive genes in maize hybrid An'nong 591 under heat stress. *BMC Plant Biol.* 19, 273–289. doi: 10.1186/s12870-019-1878-8

Zhou, P., Hirsch, C. N., Briggs, S. P., and Springer, N. M. (2019). Dynamic patterns of gene expression additivity and regulatory variation throughout maize development. *Mol. Plant* 12, 410–425. doi: 10.1016/j.molp.2018.12.015

Zhu, M., Chen, Y., Ding, X. S., Webb, S. L., Zhou, T., Nelson, R. S., et al. (2014). Maize Elongin C interacts with the viral genome–linked protein, VPg, of sugarcane mosaic virus and facilitates virus infection. *New Phytol.* 203, 1291–1304. doi: 10.1111/nph.12890

Conflict of Interest: The authors declare that the research was conducted in the absence of any commercial or financial relationships that could be construed as a potential conflict of interest.

Publisher's Note: All claims expressed in this article are solely those of the authors and do not necessarily represent those of their affiliated organizations, or those of the publisher, the editors and the reviewers. Any product that may be evaluated in this article, or claim that may be made by its manufacturer, is not guaranteed or endorsed by the publisher.

frontiers | Frontiers in Plant Science

ORIGINAL RESEARCH
published: 14 April 2022
doi: 10.3389/fpls.2022.842336

Conjunctive Analyses of Bulk Segregant Analysis Sequencing and Bulk Segregant RNA Sequencing to Identify Candidate Genes Controlling Spikelet Sterility of Foxtail Millet

Yongbin Gao[1,2], Lihong Du[3], Qian Ma[1], Yuhao Yuan[1], Jinrong Liu[3], Hui Song[3] and Baili Feng[1]**

[1] State Key Laboratory of Crop Stress Biology for Arid Areas, College of Agronomy, Northwest A&F University, Xianyang, China, [2] Dexing Township Agro-Pastoral Comprehensive Service Center, Nyingchi, China, [3] Anyang Academy of Agricultural Sciences, Anyang, China

OPEN ACCESS

Edited by:
Gianni Barcaccia, University of Padua, Italy

Reviewed by:
Charles Y. Chen, Auburn University, United States
Shoupu He, National Key Laboratory of Cotton Biology, Institute of Cotton Research (CAAS), China

***Correspondence:**
Hui Song
837181622@qq.com
Baili Feng
fengbaili@nwsuaf.edu.cn

Specialty section:
This article was submitted to Plant Breeding, a section of the journal Frontiers in Plant Science

Received: *23 December 2021*
Accepted: *28 February 2022*
Published: *14 April 2022*

Citation:
Gao Y, Du L, Ma Q, Yuan Y, Liu J, Song H and Feng B (2022) Conjunctive Analyses of Bulk Segregant Analysis Sequencing and Bulk Segregant RNA Sequencing to Identify Candidate Genes Controlling Spikelet Sterility of Foxtail Millet. Front. Plant Sci. 13:842336. doi: 10.3389/fpls.2022.842336

Foxtail millet has gradually become a model gramineous C_4 crop owing to its short growth period and small genome. Research on the development of its spikelets is not only directly related to the yield and economic value of foxtail millet but also can provide a reference for studying the fertility of other C_4 crops. In this study, a hybrid population containing 200 offspring was constructed from the Xinong8852 and An15 parental lines, and two extreme trait populations were constructed from the F2 generation for analysis of the spikelet sterility. The F2 population conformed to a 3:1 Mendelian segregation ratio, and it was thus concluded that this trait is likely controlled by a single recessive gene. Bulk segregant analysis sequencing (BSA-Seq) was used to determine the candidate regions and candidate genes related to the development of foxtail millet spikelets. Additionally, the functional analysis of differentially expressed genes in populations with different traits was conducted by bulk segregant RNA sequencing (BSR-Seq). Finally, conjunctive analysis of BSA-Seq and BSR-Seq results, combined with biological information analysis, revealed six genes on chromosome VII that were ultimately identified as candidate genes controlling foxtail millet spikelet development. This study provides a new reference for research on foxtail millet sterility and lays a solid foundation for the examination of fertility in other gramineous crops.

Keywords: foxtail millet, spikelet, sterility, BSA-seq, BSR-seq

INTRODUCTION

Foxtail millet originated in China and has a cultivation history of more than 10,000 years. It has high nutritional value because of its dual uses as food and animal feed. At the same time, because of its short growth period, wide adaptability, drought tolerance, and tolerance of barren land, foxtail millet is widely cultivated in temperate and tropical arid and semiarid regions of Eurasia, where it plays a vital role in ensuring regional food security (Shan et al., 2014; Verma et al., 2015). With the completion of whole-genome sequencing of foxtail millet (Pandian and Ramesh, 2019), it has

gradually become a model gramineous C_4 crop, as well as a model for studying drought and stress tolerance, owing to its small diploid genome, self-pollination, high reproductive coefficient, small plant height, simple cultivation methods, short growth cycle, and easy, rapid propagation (Doust et al., 2009; Jia and Diao, 2017; Yang et al., 2020).

The development of the floral organs of crops is directly related to crop fertility, and it is also the basis for the yield formation and economic value of crops. Their morphogenesis and development are affected by the environment and involve complex genetic regulatory networks (Wu and Xu, 2009). Researchers have studied the growth and development of floral organs in rice (Jeon et al., 2000), maize (Yi et al., 2021), and wheat (Debernardi et al., 2020) previously, and also established the classical ABC, quartet, and floral organ characteristic gene activity models (Kaufmann et al., 2005; Soltis et al., 2007; Wu and Xu, 2009), which have further revealed the molecular mechanism of floral organ development in gramineous crops. In recent years, the key genes involved in top spike abortion (Li et al., 2015; Xue et al., 2018), anther color (Han et al., 2019), and male sterility (Yang, 2013) have also been reported successively. However, few studies have examined the genes related to the spikelet of foxtail millet. Further exploration of spikelet development in foxtail millet will further clarify the mechanisms of foxtail millet fertility and provide new opportunities for fertility research on other C_4 crops, as well as for the utilization of foxtail millet heterosis.

Bulked segregant analysis sequencing (BSA-Seq) can be used to detect the allele frequency (AF) of single-nucleotide polymorphisms (SNPs) by constructing the DNA pool of offspring with extreme traits and using molecular markers to perform co-segregation analysis between markers and traits in the two pools. Thus, BSA-Seq enables the rapid identification of genes associated with qualitative traits controlled by a single gene or major genes associated with quantitative traits. Bulked segregant RNA sequencing (BSR-Seq) is the combination of BSA-Seq and RNA-Seq, and it has been utilized in the localization of the maize yellowing mutation gene (Liu et al., 2012), the localization of the wheat powdery mildew resistance gene PmSESY, and the study of maize male sterility (Su et al., 2016). Similarly, de Lima Castro et al. (2017) localized a novel locus in Andean bean that is associated with anthracnose resistance by using BSA-Seq. Li et al. (2019) found the casein kinase gene BrCKL8, a key gene for forming Chinese cabbage leaf heads, by using BSA and RNA-Seq combined analysis, revealing the critical pathway of head formation in this crop.

In this study, we used the Xinong8852 and An15 parental lines of foxtail millet to construct a single F2 population that contained 200 individual plants. After field investigation, the traits related to the fertility of the F2 population conformed to a 3:1 Mendelian segregation ratio, and it was thus concluded that this trait is likely controlled by a single recessive gene. Then, BSA-Seq was used to sequence the two populations with extreme traits, which revealed the AF of SNPs from the two populations. This was followed by a correlation analysis based on the differentially expressed genes (DEGs) obtained by BSR-Seq analysis. Thus, this study aimed to localize infertility-related genes and loci and analyze the molecular mechanism of floral organ sterility in foxtail millet.

MATERIALS AND METHODS

Planting and Selection of Test Materials

In our study, Xinong8852 (XAP1) and An15 (AYP1), as well as the F2 population constructed by their cross, were used as experimental materials and planted in the Crop Teaching Sample Area of Northwest A&F University (Yangling, China). The parents and F2 progeny were planted separately by dibble seeding. At the flowering stage of foxtail millet, the traits were observed, and one parent plant was marked. In the F2 generation, 30 plants with normal spikelet development (KY) and 30 with abnormal spikelet development (BY) were marked. After labeling, fresh leaves were selected from the parents and the extreme population at the same time and stored at −80°C for subsequent DNA extraction for BSA-Seq. Before reaching full bloom, samples were taken from the spikes, respectively, and stored at −80°C for subsequent RNA extraction for BSR-Seq.

Bulked Segregant Analysis Sequencing

DNA Extraction, Library Construction, and Sequencing

The modified cetyltrimethyl ammonium bromide (CTAB) method (Doyle, 1990) was used to extract DNA from fresh leaves from parental materials (AYP1 and XAP1) and extreme individuals in the F2 population. Two parental bulk samples were constructed from the DNA of the parents, and the KY and BY bulk samples were constructed by mixing the DNA of the progeny of normal and abnormal plants in the F2 generation, respectively. The total amount of DNA was detected using a NanoDrop instrument (OD260/280; NanoDrop, Wilmington, DE, United States), and the integrity and concentration of DNA samples were identified using Qubit Fluorometer (Thermo Fisher Scientific, Waltham, MA, United States) and agarose gel electrophoresis. High-quality samples were thus identified and sequenced by Beijing Ovison Gene Technology Co. Ltd. (Beijing, China) using an Illumina high-throughput sequencing platform (NovaSeq 6000; Illumina, San Diego, CA, United States).

Detection and Annotation of Single-Nucleotide Polymorphisms

After filtering the raw reads obtained by sequencing to remove the adapter sequences, BWA software (Li, 2013) was used to compare the obtained clean reads with the reference genome, and SAMtools (Li et al., 2009) was used to compare the results to sort and remove duplicates. After SNP detection using the Unified Genotyper model in GATK3.7, variant filtration was used to filter out the sites with SNP index values less than 0.3 and SNP depth values less than 7 in the bulked samples from offspring with extreme phenotypes. ANNOVAR software was used to annotate the filtered SNP detection results, and finally, the high-quality SNPs site set was obtained.

Screening and Functional Analysis of Target Genes

Single-nucleotide polymorphism index values were used to represent the sequence difference between the offspring population and their parents, and the SNP index value of each variant locus after quality control in the KY and BY bulk samples

was calculated. The loci with SNP index values less than 0.3 and SNP depths less than 7 in the KY and BY bulk samples were filtered, and the homozygous and non-missing SNP loci were then retained. At the same time, the differences between the SNP index values of the two progeny pools were calculated to obtain the delta (SNP index) values. After 1,000 permutation tests, 95% CI were applied as the screening threshold to determine candidate sites. Additionally, functional annotation and analysis of genes corresponding to candidate sites were performed.

Bulked Segregant RNA Sequencing

RNA Extraction, Library Establishment, and Sequencing

The RNA of the two parents and two bulk samples of offspring with extreme phenotypes were extracted using the Trizol method. The concentration and purity of the extracted RNA were detected using the NanoDrop instrument (OD260/280, OD260/230), and the integrity of RNA fragments was detected using the Agilent 2100 platform (Agilent Technologies, Santa Clara, CA, United States). Thus, four bulk samples were obtained for BSA-Seq. Then, after quality control, Beijing Ovison Gene Technology Co. Ltd. completed the sample database construction and sequencing using an Illumina high-throughput sequencing platform (Hiseqtm2500/4000, Illumina). FastQC (version 0.11.9) was used to evaluate the quality of the sequence data. The original data was filtered using Fastp software (version 0.20.0) to remove adapters, uncalled bases, and low-quality sequences to obtain high-quality data (Chen et al., 2018).

Read Mapping and Differential Expression Analysis

The genome of the foxtail millet line Yugu1 was used as the reference genome, and the filtered sequencing data were compared using Star software (Dobin et al., 2012). The gene expression level was assessed based on fragments per kilobase of transcript per million fragments mapped (FPKM) values, and the gene expression levels of each sample were analyzed using HTSeq software (Simon et al., 2015). After obtaining the gene expression matrix, read counts were normalized, and the corresponding *p*-values were calculated based on the negative binomial (Pascal) distribution. Finally, multiple hypothesis testing correction (*via* the Benjamini–Hochberg procedure) was performed to control the false discovery rate. DESeq2 (Love et al., 2014) was used to identify DEGs between BY and KY samples, BY and AYP1 samples, and BY and XAP1 samples, respectively. Finally, the DEGs were further screened, and the genes with consistent trends and significant differences between BY and KY and their parents were identified for functional analysis.

Functional Analysis of Differentially Expressed Genes

Gene Ontology (GO[1]) is an internationally standardized gene function classification system that can be used to classify DEGs according to their molecular function, biological process, and cell composition (cellular component) ontologies, respectively. We used GOseq software (Young et al., 2010) to perform GO annotation and enrichment analysis of DEGs. The Kyoto Encyclopedia of Genes and Genomes (KEGG[2]) not only comprises all characterized metabolic pathways but also comprehensively annotates the enzymes that catalyze each step of such reactions, including amino acid sequences and PDB library links (Kanehisa et al., 2008), among other features. To further explore the biological pathways associated with DEGs, we first used KEGG automatic annotation server (KAAS) to complete the KEGG pathway annotation of DEGs and obtained the KEGG background file for each whole foxtail millet gene. Then, we used the KEGG Enrichment function in TBtools (Chen et al., 2018) for enrichment analysis.

Bulk Segregant Analysis Sequencing and Bulk Segregant RNA Sequencing Association Analysis

The candidate loci identified by BSA-Seq were jointly compared with DEGs obtained from the BSR-Seq screen to identify the genes located in variant candidate regions and differentially expressed. Using databases such as the National Center for Biotechnology Information, combined with GO and KEGG annotations, further analysis of the functions and pathways of the selected candidate genes were used to determine the main genes that cause infertility in foxtail millet spikelets and analyze the molecular mechanism of this phenotype.

Real-Time Quantitative PCR Validation

In order to further verify the accuracy of the above experimental results and the expression of candidate genes in foxtail millet corresponding with differences in fertility, quantitative reverse transcription PCR (RT-qPCR) experiments were conducted using RNA extracted from the panicles of millet in the two progeny pools before flowering. Each sample (100 mg, three biological replicates) was used for the extraction of total RNA. RNA samples were treated with DNase I (New England Biolabs, Ipswich, MA, United States) to remove genomic DNA contamination, followed by cleanup using the GeneJET RNA Cleanup and Concentration Micro Kit (Thermo Fisher, Waltham, MA, United States). A NanoDrop2000 spectrophotometer (Thermo Fisher) and 1% agarose gel electrophoresis were used to evaluate the total RNA concentration and quality of each sample. The validated RNA was uniformly mixed to form the BY sample (from the BY pool) and KY sample (from the KY pool). The cDNA was then prepared from 1 μg of total RNA using All-in-one First-Strand cDNA Synthesis SuperMix (Invitrogen, Beijing, China), following the manufacturer's instructions, for RT-qPCR analysis. Actin was used as an internal reference gene, and all primers were designed with Primer 5 (**Supplementary Table 1**). All RT-qPCR assays were performed using Top SYBR® Premix Ex Taq™ II (Tli RNaseH Plus) (Tli RNaseH Plus; Takara, Dalian, China) *via* the Applied Biosystems ABI 7500 Fast real-time PCR machine (Applied Biosystems, Foster City, CA, United States). The cycling conditions were 95°C for 1 min, 40 cycles at 95°C for 15 s, and 60°C for 15 s. Each target gene had three technical replicates, and the relative expression level of the target gene was calculated by the $2^{-\Delta\Delta Ct}$ method.

[1]http://www.geneontology.org/

[2]http://www.kegg.jp

RESULTS

Spikelet Sterility Field Measurements

The ear growth and development of parents and 200 F2 plants were observed and recorded after the jointing stage of foxtail millet. We found that the spikelets of the two parents could develop normally, with KY plants having no significant difference from their parents in the development of spikelets and panicles, but for BY plants, the glume remained closed and the spikelet could not normally open (**Figures 1A,B**). After maturity, we investigated the fertility and main agronomic traits of 200 F2 plants (**Supplementary Table 2**) and found 150 normal spikelets and 50 abnormal spikelets (**Figure 1C**). A χ^2 test of the F2 survey results confirmed that the fertility segregation rate of the F2 generation was consistent with a 3:1 ratio (fertile:sterile, $\chi^2 < \chi^2_{0.05} = 3.84$, $p < 0.05$, **Supplementary Table 3**), and thus complied with Mendel's law of segregation for a single recessive allele. Thus, we speculate that this phenomenon may be mainly controlled by a locus with a pair of recessive and dominant alleles (Guan et al., 2016; Han et al., 2019) and preliminarily define this phenotype as infertility of floral organs caused by abnormal spikelet development. To further reveal the mechanism of the phenotype and locate the key genes, we conducted further analysis at the molecular level through a combination of BSA-Seq and BSR-Seq.

Bulked Segregant Analysis Sequencing

Sequencing Quality Assessment and Mapping Analysis

To determine which genetic differences led to the occurrence of foxtail millet spikelet sterility, we used high-throughput sequencing technology to perform whole-genome resequencing of four samples from two parents and two progeny pools with extreme traits; thus, 41,422,537,500 bp of raw data were generated in total. After quality control, 41,214,112,800 bp high-quality clean reads were obtained. The guanine cytosine (GC) content of these reads was 46.31–46.94%, and the quality of the sequencing data was high (Q20 $\geq$ 97.82%, Q30 $\geq$ 93.95%) (**Supplementary Table 4**). Next, we mapped the clean reads obtained from the four samples after quality control based on the reference genome, obtaining a total of 271,043,339 reads. The mapping results showed that the sample comparison rate was between 97.91 and 99.07%, with an average sequencing depth of parents of 10×, and the offspring pools exhibited approximately 30× depth; the 1× and 4× coverage percentages were 95.49 and 90.82, respectively (**Table 1**). The mapping data shows that the reference genome was evenly and randomly covered, which was conducive to the filtering and screening of SNPs in the next step.

Detection and Annotation of Single-Nucleotide Polymorphisms

ANNOVAR is an efficient software tool that can use the latest information to perform functional annotations of genetic variants detected from multiple genomes. We used it to annotate the functions of detected SNP. By screening the SNPs detected by the unified genotype model of gatk3.7 software, 1,945,742 SNPs were obtained. By further annotating the SNPs with ANNOVAR, it was found that 73,739 SNPs were located in the exon region, including "stop gain" mutations, which cause a full coding sequence gene to contain a stop codon; "stop-loss" mutations, which cause a gene to lose its stop codon; "synonymous" mutations, which do not affect the amino acid sequence; and "non-synonymous" mutations, which alter the amino acid sequence.

Location of Candidate Regions and Screening of Genes

To determine the mutation sites that exist in the BY bulk sample of foxtail millet, the SNP index method was used to analyze the detected SNPs. First, after filtering out the heterozygous SNPs from the filial generation, the SNP index was less than 0.3, with a depth less than 7, and the sites in each F2 pool lacked SNPs; we identified 926,529 such SNPs from 1,945,742 SNPs. Then, we found a total of 9,055 mutation sites outside the CI by calculating the delta SNP index in the KY and BY bulk samples and screening with a 95% CI (**Figure 2**), and the annotation of these sites indicated that 523 were located in exons, including mutations that caused the gene to gain or lose its stop codon.

In considering the polymorphisms associated with the occurrence of sterility, we filtered out the sites with synonymous mutations in 523 loci and obtained 3 regions and 211 polymorphisms sites related to sterility from chromosomes III, VI, and VII. By associating the location information of these 211 polymorphic sites with genome annotation information, we identified 90 candidate genes, 70 of which were located between 20,557,247 bp and 31,479,141 bp on chromosome VII, 19 of which were located between 33,984,600 bp and 35,805,805 bp on chromosome VI, and a single candidate gene located between 4,908,634 and 4,912,328 on chromosome III. To further analyze the subcellular localization, molecular function, and biological processes associated with these candidate genes, we performed GO annotation and enrichment analysis for 90 candidate genes. All genes were annotated with 705 GO terms, of which 54 genes were significantly enriched within 23 functional groups, including 13 biological processes, 3 cellular components, and 7 molecular functions. Among the biological processes, these genes are mainly involved in the reproduction process, the development of seeds and fruits, the development of the reproductive system, and the reproductive structure. Among the cellular components, these genes are mainly enriched in the components of the cell membrane. Lastly, among molecular functions, these genes are mainly involved in functions such as binding and catalytic activity.

Bulked Segregant RNA-Seq Analysis

Sequencing Data Analysis of Four cDNA Bulk Samples

In order to further clarify the transcription process associated with organ sterility in foxtail millet, we used the two parents and two extreme trait groups to construct four pools. After establishing three replicates in each bulked pool, we performed RNA sequencing of 12 cDNA libraries on an Illumina (HiSeq^{TM}2500/4000) high-throughput sequencing platform. After reads with low quality and adapter sequences were removed, we obtained 187,104,828 clean reads from

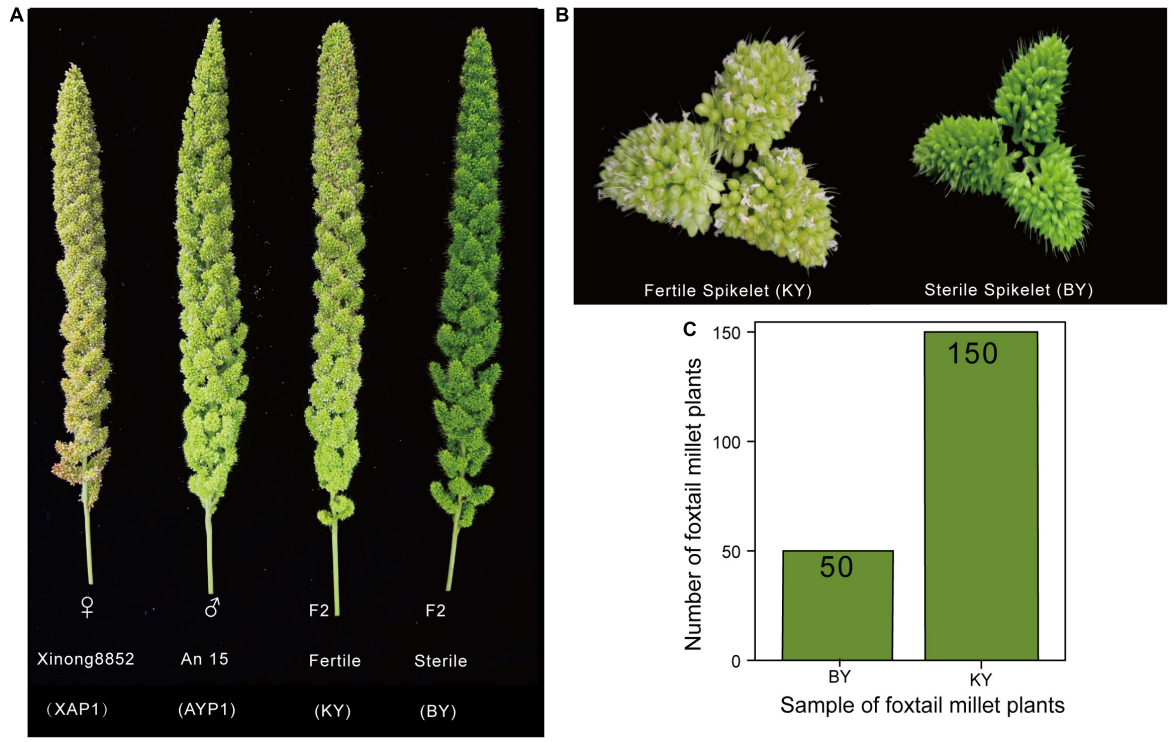

FIGURE 1 | The spike development of two parents and two F2 populations. **(A,B)** The spike and spikelet development of two parents and two F2 populations. **(C)** The number of plants with sterile spikelets and normal spikelets in the F2 population.

TABLE 1 | Quality statistics of mapping with the reference genome for BSA-Seq.

Sample	Mapped reads	Total reads	Mapping rate (%)	Average depth (×)	Coverage 1 × (%)	Coverage 4 × (%)
XAP1	36,115,655	36,886,738	97.91	10.57	95.49	90.82
AYP1	32,975,779	33,284,924	99.07	9.94	96.5	91.38
BY	109,123,265	110,367,772	98.87	29.19	98.42	97.76
KY	92,828,640	94,221,318	98.52	26.55	98.42	97.68

Mapped Reads: the total number of reads on the reference genome was compared.
Total reads: the total reads of valid sequencing data.
Mapping rate: the number of reads on the reference genome was compared by the number of reads in the valid sequencing data.
Average depth: the average sequencing depth, the total number of bases compared to the reference genome divided by genome size.
Coverage 1×: the proportion of bases whose coverage depth is not less than 1× in the whole genome.
Coverage 4×: the base coverage depth in the whole genome is no less than the base ratio of 4×.

193,102,338 raw reads from four samples (**Supplementary Table 5**). Then, the obtained clean reads were mapped to the reference genome of Yugu1 foxtail millet. The comparison revealed that the unique mapping degree reads rate was between 90.66 and 92.81% (**Table 2**).

Screening of Differentially Expressed Genes Between Different Bulk Samples

Through the principal component analysis of RNA-Seq data, we learned that all samples could be clustered by dimensionality reduction, which indicates that the repeatability between the groups of samples was good and that there was a big difference between the samples (**Figure 3A**). Based on this result, difference analysis was performed using the DESeq2 R package, and genes meeting thresholds of p-value > 0.05 and $|\log_2(\text{fold change})| > 1$ were selected as the DEGs. Spikelet sterility only appeared in the BY sample, but both parents and the KY sample showed normal spikelet phenotypes. We then compared the samples with abnormal floral organs with other samples with normal development to obtain genes related to floral organ sterility in foxtail millet. By comparing differential gene expression between BY with KY, BY with AYP1, and BY with XAP1, we obtained 1,814, 3,132, and 2,022 upregulated DEGs, and 4,537, 3,703 and 4,278 downregulated DEGs, respectively (**Figures 3B–D**).

Next, we looked for overlap among the three combinations and found their shared DEGs that were upregulated or downregulated for identification as candidate genes related to this study for further analysis. During this process, we obtained a total

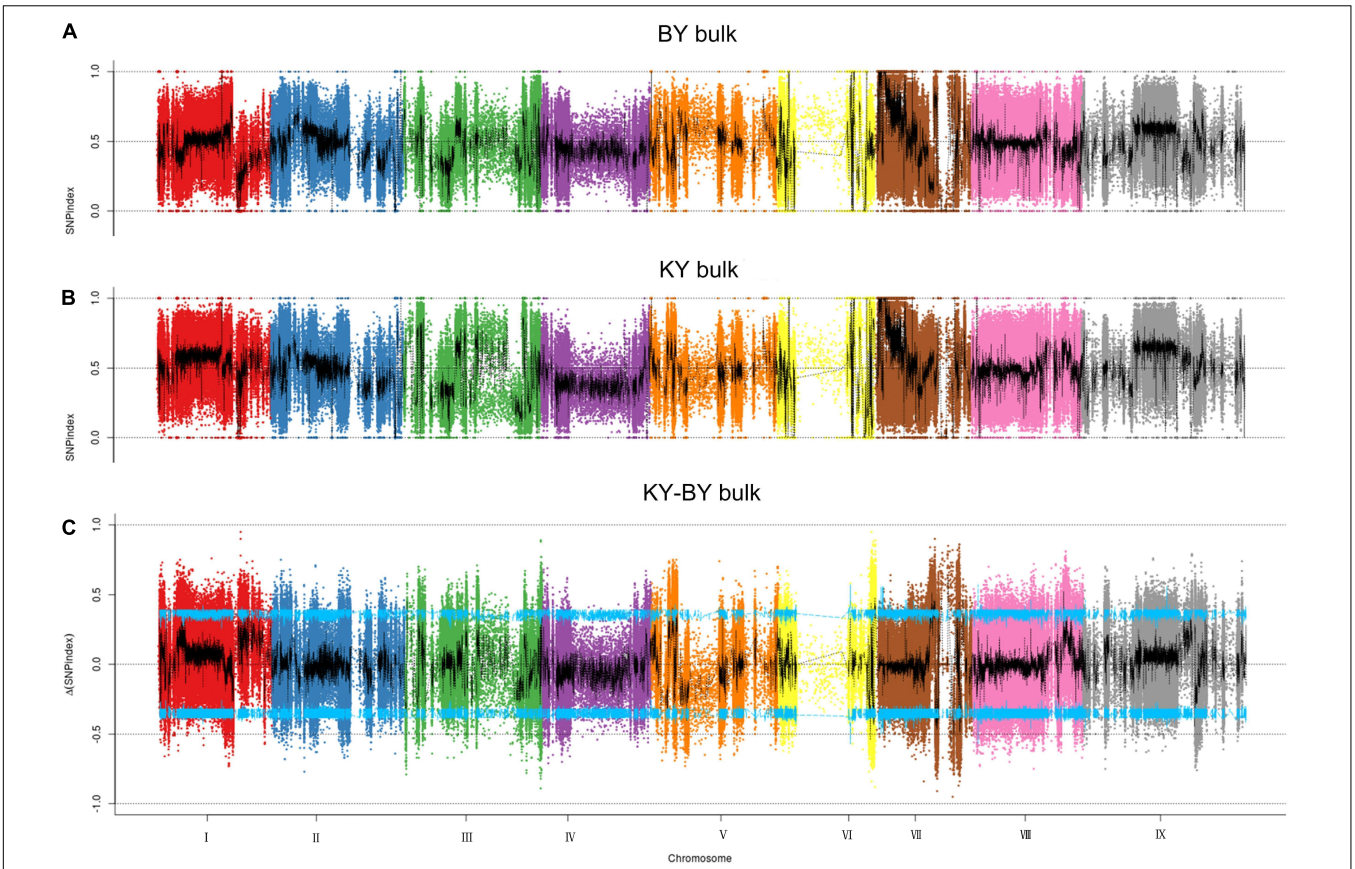

FIGURE 2 | Distribution of SNP index association values on chromosomes. **(A)** Distribution of single -nucleotide polymorphism (SNP) index values of BY bulk on chromosomes. **(B)** Distribution of SNP index values of KY bulk on chromosomes. **(C)** Distribution of Δ(SNP index) value on chromosomes, where the blue line represents the 95% CI.

TABLE 2 | Quality statistics of mapping with the reference genome for BSR-Seq.

Sample name	Total reads	Total mapping rate(%)	Multiple mapping (%)	Uniquely mapping (%)	Reads mapping to + (%)	Reads mapping to – (%)	Non-splice reads (%)	Splice reads (%)
XAP1	48,009,869	93.03	2.36	90.66	45.33	45.33	57.83	32.84
AYP1	47,835,947	94.76	1.96	92.81	46.41	46.41	61.74	31.06
KY	43,620,057	94.70	2.10	92.61	46.30	46.30	60.96	31.64
BY	47,638,955	93.79	3.23	90.57	45.28	45.28	57.76	32.81

Total reads: the total reads after quality control.
Total mapping rate: the rate of total reads that can be mapped to the reference sequence.
Multiple mapping: the reads that mapped to multiple positions in the reference sequence.Uniquely mapping: the reads that maps to a unique position in the reference sequence.
Reads mapping to +, reads mapping to –: the reads mapped to positive and negative chains, respectively.
Non-splice reads: the reads that mapped to only one exon.
Splice reads: the same reads section mapped to different exons.

of 294 shared upregulated DEGs (**Figure 3E**) and 1,779 shared downregulated DEGs (**Figure 3F**).

Gene Ontology and Kyoto Encyclopedia of Genes and Genomes Pathway Enrichment Analysis of Differentially Expressed Genes

To examine the molecular mechanism of foxtail millet spikelet development, we further analyzed 1,779 downregulated DEGs and 294 upregulated DEGs that were differentially expressed in BY samples compared with other samples.

The GO annotation was applied to the obtained DEGs, and the enrichment analysis was performed with a p-value < 0.05 threshold. The genes with relatively high expression in the BY sample were enriched for 25 GO terms, but those with relatively low expression were enriched for 112 GO terms. Among them, the relatively highly expressed genes in samples

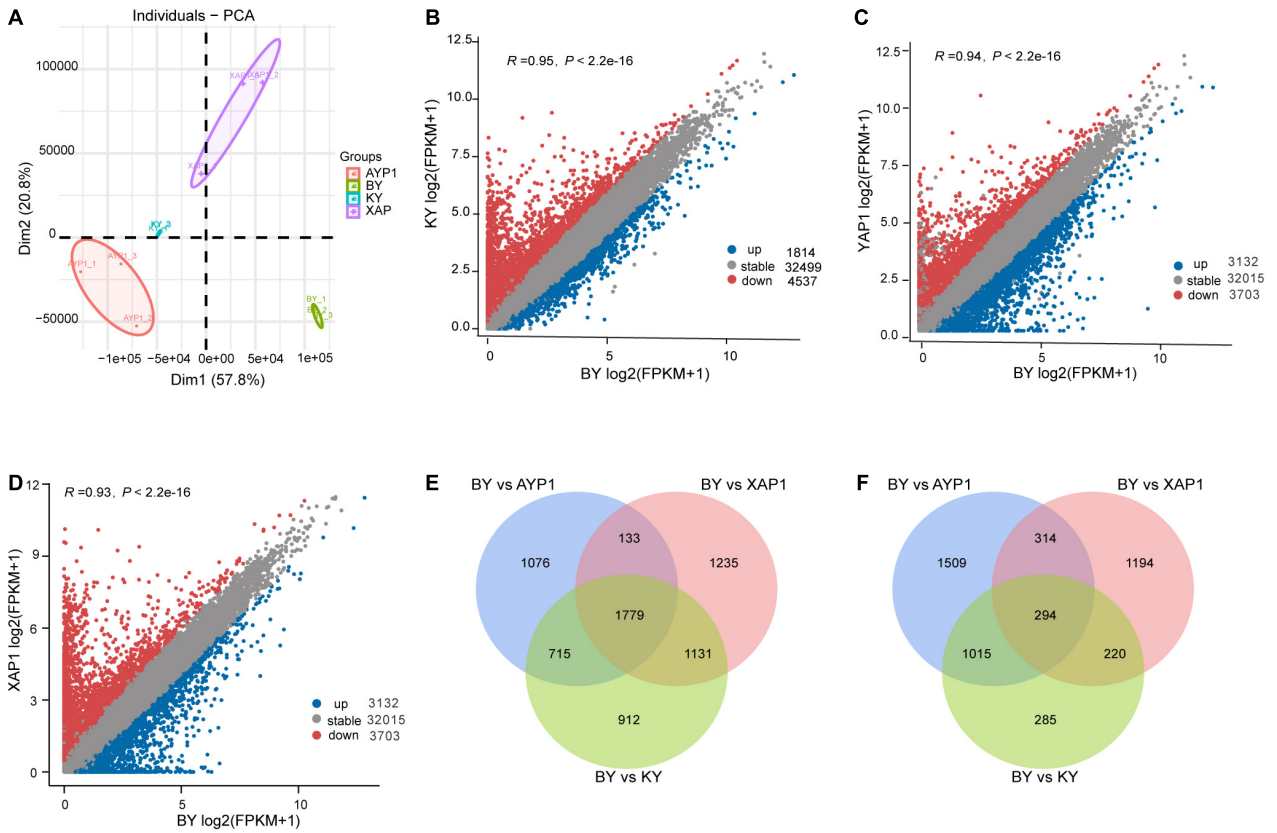

FIGURE 3 | Differences in gene expression among four different samples from two parents and two progeny pools. **(A)** Principal component analysis of four samples, and each sample contains three biological repeats. **(B–D)** The number of differential genes between different samples. Comparison of the expression of gene between BY with KY, BY with AYP1, BY with XAP1 samples. **(E)** The significantly downregulated genes in BY samples compared with other samples. **(F)** The significantly upregulated genes in BY samples compared with other samples.

with abnormal floret development were mainly enriched for the following terms: ion binding, oxidoreductase activity, heme binding, tetrapyrrole binding, nucleotide binding, nucleoside phosphate binding, and adenyl ribonucleotide binding, small molecule binding, anion binding, adenyl nucleotide binding, phosphatase activity, participation in defense response, obsolete oxidation-reduction process, and defense response to other organisms (**Figure 4A**). The relatively low-expression genes were mainly enriched for cell components, such as FANCM-MHF complex, with hydrolase, arylesterase, amine-lyase, strictosidine synthase, microtubule motor, acyl-[acyl-carrier-protein] desaturase, carbon-nitrogen lyase, and cytoskeletal motor, cation antiporter, and proton antiporter and other activities, and involved in biological processes, such as transmembrane transport and microtubule-based movement (**Figure 4B**).

Next, KEGG analysis was used for pathway enrichment analysis to analyze the metabolic pathways associated with these DEGs. The genes significantly upregulated in the BY samples were mainly enriched for the pathways of environmental adaptation, organismal systems, plant circadian rhythm, tyrosine metabolism, and plant-pathogen interaction (**Figure 4C**). The downregulated genes were associated with cyanoamino acid metabolism and isoquinoline alkaloids biosynthesis but were mainly enriched for the transcription factors, cytoskeleton proteins, fatty acid biosynthesis, biosynthesis of secondary metabolites, and homologous recombination pathways (**Figure 4D**).

The GO and KEGG enrichment analyses of the function and metabolic pathways of DEGs between samples with normal and abnormal spikelet development indicate that the development of foxtail millet spikelet is affected by multiple genes and multiple metabolic pathways.

Combined Analysis of Bulk Segregant Analysis Sequencing and Bulk Segregant RNA Sequencing

To further explore the main genes controlling spikelet abortion in foxtail millet and explore their function, the BSA-Seq and BSR-Seq results were analyzed jointly. Thus, we found that six candidate genes with mutations on chromosome VII were significantly differentially expressed between the samples with normal spikelet development and the samples with abnormal spikelet development, which included four downregulated genes and two upregulated genes (**Table 3**).

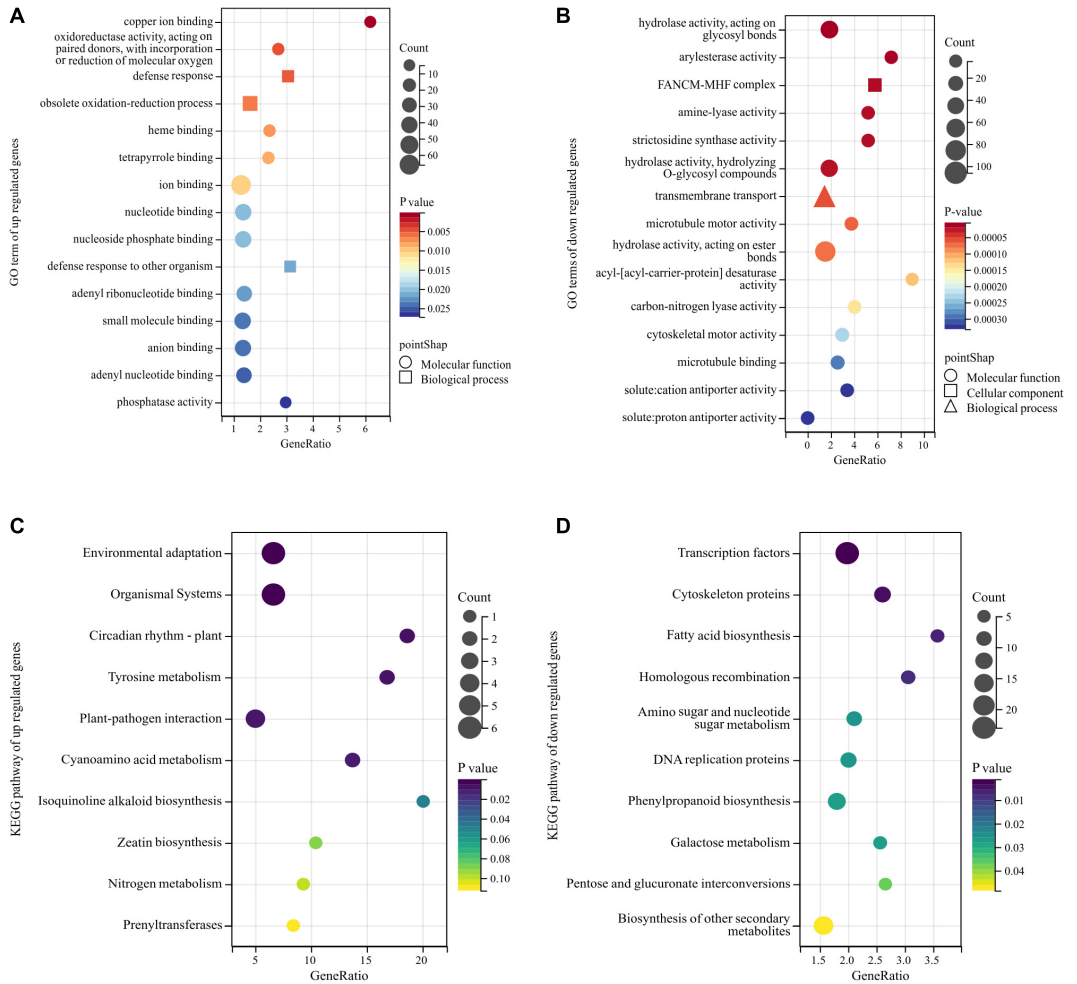

FIGURE 4 | Gene Ontology (GO) and Kyoto Encyclopedia of Genes and Genomes (KEGG) enrichment analyses of DEGs obtained by bulk segregant RNA sequencing (BSR-Seq). Among them, different colors represent the size of the *p*-value, the circular size represents the number of enriched genes, and different shapes represent different functional classifications. **(A,B)** The top 15 GO terms of upregulated and downregulated DEGs enrichment in GO enrichment analysis. **(C,D)** The top 10 pathways of upregulated and downregulated DEGs enrichment in KEGG enrichment analysis.

Then, we downloaded the gene sequence from NCBI and blasted it against the UniProt database to obtain the basic information on the six genes. Then, GO enrichment analysis was performed on the six obtained genes (**Figure 5**). Among them, the upregulated gene Setit009896mg was mainly related to hydrolase activity and participated in the metabolism of organic matter and carbohydrates. Additionally, among the significantly downregulated genes, Setit011801mg functions in actin-binding, cytoskeletal protein binding, and protein binding and participates in cellular component organization or biogenesis, cytoskeleton organization, and organelle organization. Setit009865mg is mainly related to transmembrane transport, and it is involved in transmembrane transport and the establishment of localization processes. Setit009909mg functions as a DNA-binding transcription factor and participates in the regulation of the transcription process.

In particular, the upregulated gene Setit009293mg was significantly enriched in biological processes and molecular functions and participates in pollination, pollen-pistil interaction, pollen recognition, pollen recognition, and protein serine/threonine kinase activity. In addition, the downregulated gene Setit011746mg was significantly enriched in biological processes and molecular functions, including rRNA methyltransferase activity, catalytic rRNA activity, RNA methyltransferase activity, and *S*-adenosylmethane-dependent methyltransferase activity, and participates in rRNA metabolic process, rRNA processing, and ribosome biogenesis.

Validation of Quantitative Reverse Transcription PCR of Candidate Genes Related to Millet Fertility

The expression patterns of the six candidate genes in foxtail millet with different fertility phenotypes were identified by RT-qPCR, which included a glucosidase activity gene (Setit009896mg), a protein phosphorylation gene (Setit009293mg), a gene related

TABLE 3 | Basic information of candidate genes.

Gene ID	Gene name	Chromosome position	Gene expression (up or down)
Setit009896mg	Beta-Glucosidase 12	ChrVII: 22,678,921–22,683,049	Up
Setit009293mg	Non-specific serine/threonine protein kinase	ChrVII: 30,845,482–30,849,804	Up
Setit009865mg	Sugar transport protein MST1	ChrVII: 21,688,075–21,691,295	Down
Setit011801mg	VQ motif-containing protein 11	ChrVII: 31,441,080–31,442,616	Down
Setit009909mg	ETHYLENE INSENSITIVE 3-like 5 protein	ChrVII: 21,771,669–21,773,573	Down
Setit011746mg	FBD domain-containing protein	ChrVII: 30,133,024–30,135,230	Down

to sugar transport (Setit009865mg), a serine/threonine-protein phosphatase PP2A-1 catalytic subunit gene (Setit011746mg), a gene related to DNA binding factor (Setit011801mg), and a gene related to ethylene (Setit009909mg).

Quantitative RT-PCR analysis showed that the expression of Setit009293mg (**Figure 6A**) and Setit009896mg (**Figure 6B**) in infertile samples was significantly higher than that in fertile samples ($p < 0.001$). However, the expression levels of Setit009865mg, Setit009909mg, and Setit011746mg were significantly lower than those of fertile samples ($p < 0.001$) (**Figures 6C,D,F**), and the expression of Setit011801mg was significantly lower than that of fertile samples ($p < 0.05$) (**Figure 6E**). Thus, the candidate genes' expression differences between samples were consistent with the BSR-Seq results, which supported our sequencing results.

DISCUSSION

In most crops, flower development directly affects its economic value. However, when crops are affected by the external environment or have various mutations, infertility is often a consequence. A thorough study of crop infertility and exploring its occurrence mechanism is not only important for improving crop yields and economic value but also for artificial interference breeding and the effective utilization of crop heterosis. Numerous studies have shown that the development of crop spikelets is a precise and complex regulated process, and any factor change in the process may lead to infertility (Litt and Kramer, 2010).

The development of spikelets in the panicle is one of the important characteristics of the development of foxtail millet from vegetative growth to reproductive growth, and it has a direct impact on the yield and quality of foxtail millet. Research on spikelet sterility in foxtail millet mainly focuses on male sterility. In 1967, the Yan male-sterile line was selected from a foxtail millet variety by the Yan'an Agricultural Science Institute (Li, 1997). In 1976, a dominant genic male-sterile line of foxtail millet was first discovered by the Chifeng Institute by Agricultural Sciences in Inner Mongolia from the F3 hybrid between Australian foxtail millet and Turpan foxtail millet. It was systematically determined that the genetic mechanism is the male-sterile gene Ms^{ch} in foxtail millet, and the existence of multiple alleles causing male sterility in foxtail millet was further confirmed at the level of cytogenetics (Hu et al., 1986; Ma et al., 1992). Li et al. (2010) tested and crossed 10 North China foxtail millet varieties with two high male-sterile lines (117A and Gao146A) and speculated that the sterility of these two sterile lines was controlled by one pair of major recessive genes and also affected by minor polygenes according to the fertility of F2 and BC1F1 segregation populations. Wang et al. (2007) conducted chromosome mapping of genes with 1066A sterile traits, which indicated that genes controlling this sterile trait are located on chromosome VI and recessive. With the continuous progress of research, more studies have shown that foxtail millet chromosome VI has genes related to fertility, especially male sterility (Hao et al., 2011; Jun et al., 2013; Jia et al., 2018). In recent years, the application of some new biotechnology in breeding has elucidated organ development of foxtail millet spikelets. Zhang et al. (2017) constructed an F2 mapping population by crossing narrow spikelet mutants with normal-type strains and using BSA-Seq position cloning technology and SSR molecular labeling. Thus, they localized the narrow spikelet mutant gene sins1 within the 7.709 Mb region between markers 3-2658 and CAAS3031. Xiang et al. (2017) examined foxtail millet loose-panicle mutants, showing that mutation of the Seita.5G387200 gene on chromosome II resulted in early termination of protein translation, leaving the siaux1 mutant with both lax primary branching pattern, low selfing, and floret fertility. Xue et al. (2018) identified two genes, Seita.1G106700 and Seita.1G107200, through phenotypic analysis and gene mapping of the spike tip abortion mutant sipaa1 associated with undeveloped or incomplete development of foxtail millet, demonstrating that spike tip abortion of foxtail millet may be caused by programmed cell death.

In our study, two populations with extreme traits associated with foxtail millet spikelet development were constructed by hybridization for BSA-Seq analysis. It was preliminarily determined that the three candidate regions on chromosomes III, VI, and VII and 90 genes with non-synonymous mutations in these three regions of the foxtail millet genome might be related to spikelet development. Nevertheless, no previous studies on the development of spikelet organs in these three candidate regions have been found (Wei et al., 2021). By analyzing the developmental transcription process of foxtail millet floral organs by BSR-Seq, more than 2,000 DEGs were identified between foxtail millet with spikelet sterility and normal-developing foxtail millet. This also showed that the infertility of foxtail millet spikelets may be caused by the mutual action of multiple genes. However, combined with segregation of the trait in the F2 population, it appears that the occurrence of this phenotype was probably affected by a

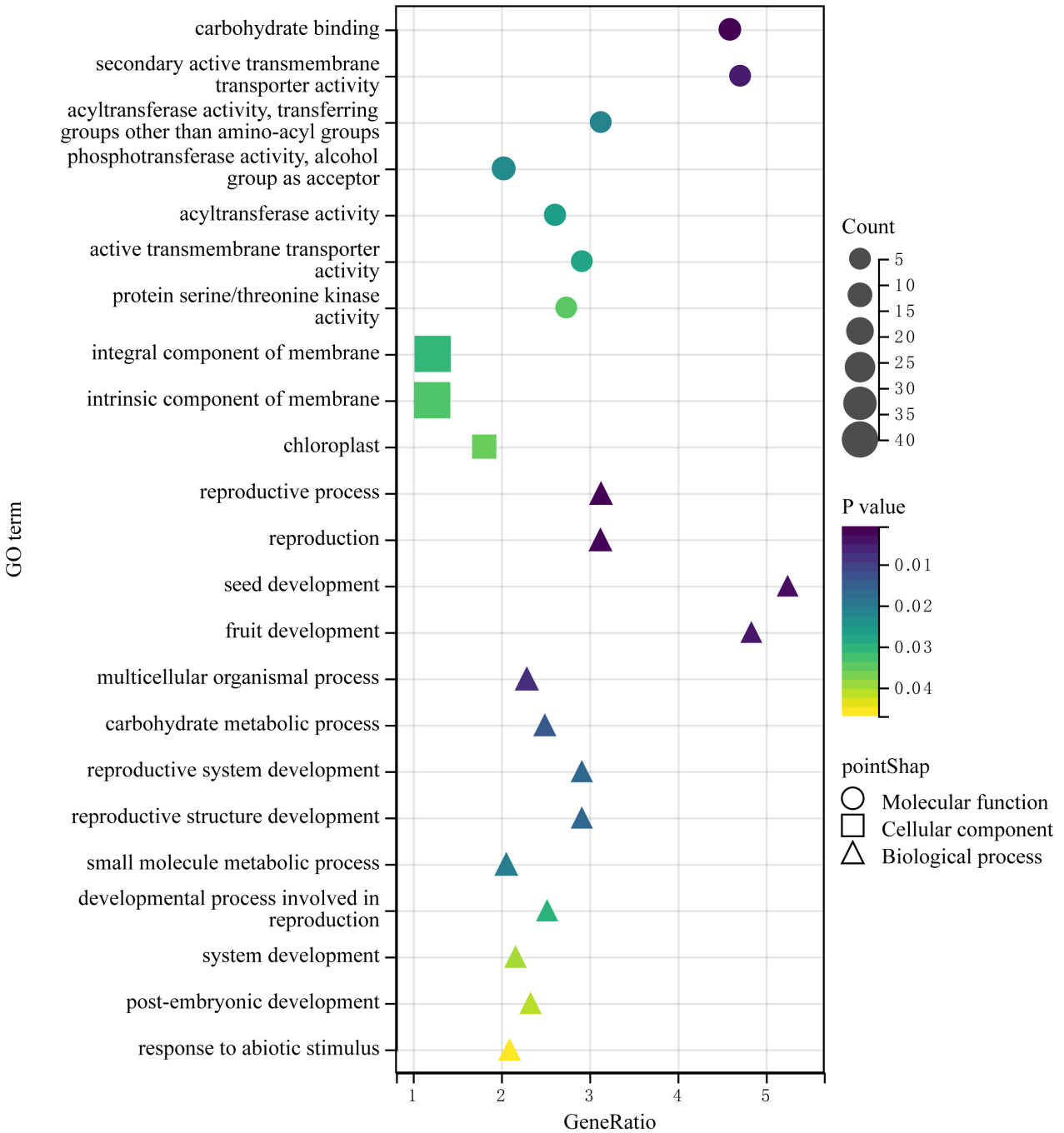

FIGURE 5 | The GO enrichment analysis of DEGs obtained by associating BSA-Seq and BSR-Seq. Among them, different colors represent the size of the *p*-value, the circular size represents the number of enriched genes, and different shapes represent different functional classifications.

pair of recessive main effect genes, and thus, changes in other genes may occur under the regulation of this locus. Through the combined analysis of the results of BSA-Seq and BSR-Seq, we obtained six candidate genes with different structures and functions. Among them were beta-glucosidase 12, non-specific serine/threonine protein kinase, FBD domain-containing protein, sugar transport protein MST1, VQ motif-containing protein 11, and ETHYLENE INSENSITIVE 3-like 5 protein, and proteins involved in carbohydrate metabolism, pollen recognition, WRKY transcription factor activity regulation, monosaccharide transmembrane transport, ethylene reaction pathway, floral meristem, and floral organ morphogenesis.

Among the candidate genes, monosaccharides and sucrose transporters play a pivotal role in saccharide transport from

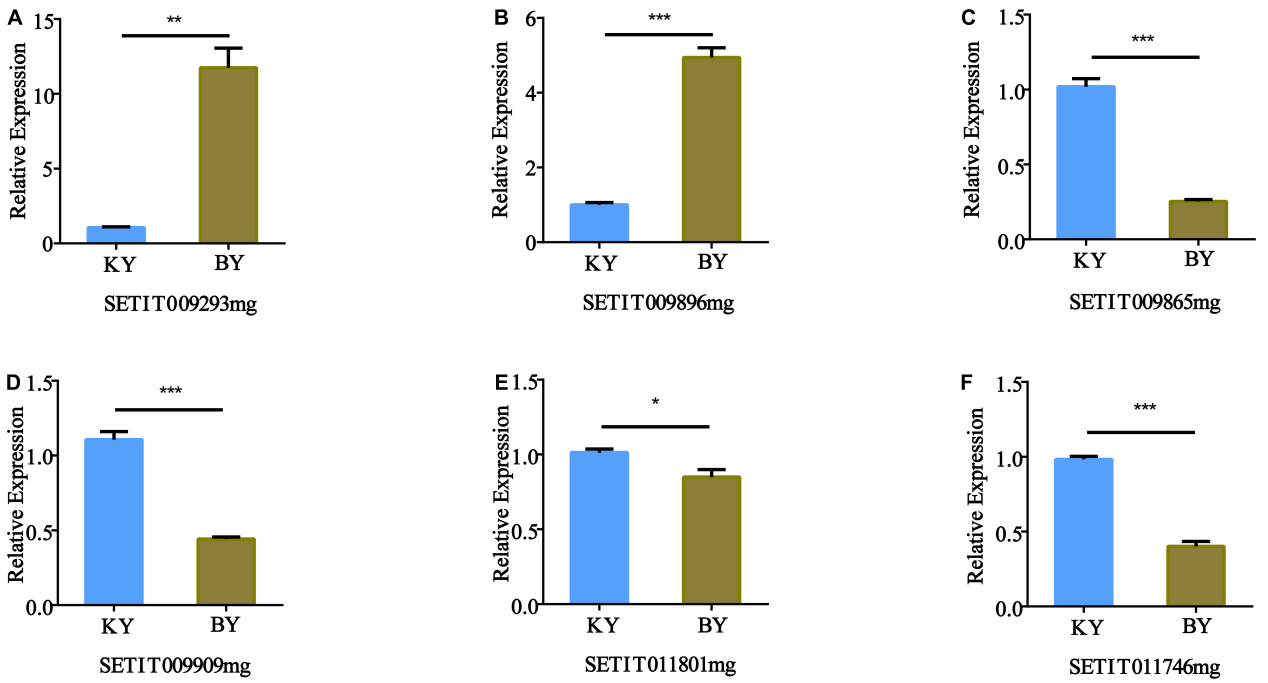

FIGURE 6 | Quantitative RT-PCR (RT-qPCR) validation of the expression of genes identified by BSA-Seq and BSR-Seq. The actin gene was used as an internal control. The transcription level of the spikes of the normal fertility sample (KY) was set at 1.0. Asterisks indicate significant differences at various thresholds (*$p < 0.05$, **$p < 0.01$, ***$p < 0.001$). Error bars represent the mean SE of three biological replicates. **(A–F)** Represent the relative expression of genes in different fertility samples.

source to sink (Smeekens, 2000). Studies on transgenic tobacco indicate that monosaccharide transporters may play an important role in photosynthate transport and morphogenesis (Leterrier et al., 2003). In rice, members of different monosaccharide transporter families often have different expression patterns.

TABLE 4 | The final candidate genes related to spikelet development.

Gene ID	Protein ID	FPKM		Description
		BY	KY	
Setit009896mg	K3Y6Q5	1.81	0.77	Glucosidase activity
Setit009293mg	K3Y505	1.38	0.24	Protein phosphorylation
Setit011746mg	K3YC02	0.29	0.62	Serine/threonine-protein phosphatase PP2A-1 catalytic subunit
Setit009865mg	K3Y6M4	2.21	6.54	Secondary carrier transporter
Setit011801mg	K3YC57	2.38	8.52	VQ motif-containing protein 11-like
Setit009909mg	K3Y6R8	1.15	9.71	DNA-binding transcription factor Activity transcription regulatory region sequence-specific DNA binding

FPKM: the number of genes expressed after FPKM standardization.

Expression of OsMST5 is only strongly detected in panicles before heading and has been suggested to be associated with pollen development (Ngampanya et al., 2003). Additionally, OsMST8 and OsMST4 are also actively involved in rice anther development (Wang et al., 2007). F-box motifs are widely present in protein interactions, and F-box proteins are involved in the regulation of various development processes such as plant photomorphogenesis, circadian clock regulation, self-incompatibility, floral meristem development, and floral organ identity determination (Hong et al., 2012). In *Arabidopsis*, the F-box protein COI1 recruits regulatory factors of defense response and pollen development through ubiquitination modification, while another F-box protein, UFO, regulates flower organ recognition by activating or maintaining the transcription of the class B organ recognition gene APETALA3 (Xie et al., 1998; Samach et al., 2010). The VQ motif-containing protein family is a plant-specific transcription regulation cofactor, which not only plays an important role in the regulation of plant growth, development, and responses to various external environmental stresses but also participates in regulating the growth and development of seed, hypocotyl, flower, and leaf tissues (Zhang and Wei, 2019). A study in *Arabidopsis* has shown that VQ proteins, as cofactors interacting with transcription factors (e.g., WRKY, MAPK), can usually interact with transcription factors or themselves to regulate various physiological and biochemical processes in plants (Cheng et al., 2012). Ethylene is a simple gas molecule with biological activity, which regulates the growth of plants and

many physiological processes, such as seed germination, root hair development, flowering, fruit ripening, organ senescence, and plant responses to biotic or abiotic stress (Bleecker and Kende, 2000). Ethylene-insensitive3 (EIN3) is a transcription factor, and its main target is ethylene response factor1 (ERF1), which is an early ethylene response gene encoding GCC-box-binding protein (Kosugi and Ohashi, 2000). Additionally, EIN3 protein acts upstream of ERF1 and specifically binds to a palindromic repeat in the ERF promoter to regulate a late ethylene response gene containing GCC-box in its promoter (Song et al., 2015).

As a reaction catalyzed by protein kinases, protein phosphorylation is one of the most important post-translational protein modifications, and it is related to the regulation of many biological activities and functions in cell signaling. When plants encounter stress, trauma, or stimulation by other cytokines and hormones, serine/threonine protein kinase is rapidly phosphorylated and activated at serine and threonine residues. It further activates downstream signal molecules through cascade phosphorylation, activates specific signal transduction pathways, and finally transmits external signals to the nucleus to activate or inhibit the expression of specific genes (Hasegawa et al., 2000; Afzal et al., 2008; Zipfel, 2008).

Based on the functional analysis of the above genes and the published literature, we speculated that the six candidate genes in **Table 4** are involved in the development of foxtail millet spikelet. Further analysis combined with RT-qPCR experimental results revealed that Setit009293mg exhibited the greatest change compared with other candidate genes between the different fertility samples, and GO enrichment analysis also showed Setit009293mg was mainly enriched in the processes of pollination and pollen-pistil interaction. Accordingly, we speculated that Setit009293mg was the most critical of the six candidate genes ultimately related to fertility. However, the development of millet spikelets is a complex process, which involves complex regulatory networks and multiple metabolic pathways (Wang et al., 2020; Shen et al., 2021). The occurrence of foxtail millet spikelet sterility might have been caused by non-synonymous mutations in the above gene located upstream, which led to the change of gene function, thus triggering a series of changes in downstream genes. The upregulation of Setit009293mg was associated with sterility, which affected the substrate of an rRNA methyltransferase activity-related gene (Setit011746mg), resulting in downregulation of its expression. However, owing to the occurrence of sterility in millet, the normal process from grain filling to maturity cannot be completed, resulting in a decrease in the expression of a gene regulating ethylene (Setit009909mg). At the same time, a gene related to the negative regulation of carbohydrate synthesis and thus related to the accumulation of organic matter in the growing process increased significantly (Setit009896mg), and a gene related to monosaccharide transport decreased significantly (Setit009865mg). The decrease of Setit011801mg expression in sterile samples may be a regulatory mechanism in the process of abiotic stress (Kim et al., 2013).

Through the combination of BSA-Seq and BSR-Seq, candidate genes related to millet spikelet development were preliminarily identified, and their functions and possible related pathways were preliminarily examined and confirmed by RT-qPCR. This study provides a reference for the improvement of millet yield and the study of yield-related traits in other gramineous crops. However, there are still some limitations in the functional verification and mechanism of action of genes in the experiment. In future research, we will continue to verify and explore the detailed mechanism of foxtail millet sterility based on the identified candidate genes.

CONCLUSION

Three regions associated with abnormal floret development were identified on chromosomes III, VI, and VII by BSA-Seq, and 90 candidate genes were identified. Combined with BSR-Seq results and biological analysis, six candidate genes related to foxtail millet sterility were finally determined, and Setit009293mg was considered to be the main gene controlling the sterility phenotype. This study lays a foundation for future breeding and map-based cloning of related genes in foxtail millet and other C_4 crops.

DATA AVAILABILITY STATEMENT

The original contributions presented in the study are publicly available. This data can be found here: PRJNA792301

AUTHOR CONTRIBUTIONS

YG: methodology, formal analysis, visualization, writing—review, and editing. LD: conceptualization and resources. QM: investigation and data curation. YY: validation, writing—review, and editing. JL: methodology and data curation. HS and BF: supervision and funding acquisition. All authors: contributed to the article and approved the submitted version.

FUNDING

This study was supported by the National Key Research and Development Program of China (Nos. 2020YFD1000800 and 2020YFD1000803), China Agriculture Research System (CARS-6-A26), and Research System of Minor Grain Crops in Shaanxi Province [NYKJ-2021-YL(XN)40].

SUPPLEMENTARY MATERIAL

The Supplementary Material for this article can be found online at: https://www.frontiersin.org/articles/10.3389/fpls.2022.842336/full#supplementary-material

REFERENCES

Afzal, A. J., Wood, A. J., and Lightfoot, D. A. (2008). Plant receptor-like serine threonine kinases: roles in signaling and plant defense. *Mol. Plant Microbe Interact.* 21, 507–517. doi: 10.1094/mpmi-21-5-0507

Bleecker, A. B., and Kende, H. (2000). Ethylene: a gaseous signal molecule in plants. *Annu. Rev. Cell Dev. Biol.* 16, 1–18. doi: 10.1146/annurev.cellbio.16.1.1

Chen, C., Chen, H., He, Y., and Xia, R. (2018). TBtools, a toolkit for biologists integrating various biological data handling tools with a user-friendly interface. *bioRxiv* [Preprint] 289660. doi: 10.1016/j.molp.2020.06.009

Cheng, Y., Zhou, Y., Yang, Y., Chi, Y. J., Zhou, J., Chen, J. Y., et al. (2012). Structural and functional analysis of VQ motif-containing proteins in *Arabidopsis* as interacting proteins of WRKY transcription factors. *Plant Physiol.* 159, 810–825. doi: 10.1104/pp.112.196816

de Lima Castro, S. A., Gonçalves-Vidigal, M. C., Gilio, T. A. S., Lacanallo, G. F., Valentini, G., da Silva Ramos Martins, V., et al. (2017). Genetics and mapping of a new anthracnose resistance locus in Andean common bean Paloma. *BMC Genomics* 18:306. doi: 10.1186/s12864-017-3685-7

Debernardi, J. M., Greenwood, J. R., Jean Finnegan, E., Jernstedt, J., and Dubcovsky, J. (2020). APETALA 2-like genes AP2L2 and Q specify lemma identity and axillary floral meristem development in wheat. *Plant J.* 101, 171–187. doi: 10.1111/tpj.14528

Dobin, A., Davis, C. A., Schlesinger, F., Drenkow, J., and Gingeras, T. R. (2012). Star: ultrafast universal RNA-seq aligner. *Bioinformatics* 29, 15–21. doi: 10.1093/bioinformatics/bts635

Doust, A. N., Kellogg, E. A., Devos, K. M., and Bennetzen, J. L. (2009). Foxtail millet: a sequence-driven grass model system. *Plant Physiol.* 149, 137–141. doi: 10.1104/pp.108.129627

Doyle, J. J. (1990). Isolation of plant DNA from fresh tissue. *Focus* 12, 13–15.

Guan, H., Xu, X., He, C., Liu, C., and Wang, L. (2016). Fine mapping and candidate gene analysis of the leaf-color gene ygl-1 in maize. *PLoS One* 11:e0153962. doi: 10.1371/journal.pone.0153962

Han, K., Du, X., Wang, Z., Lian, S., Wang, J., and Guo, E. (2019). Fine mapping of anther color gene Siac1 in foxtail millet. *Chin. Agric. Sci. Bull.* 35, 130–136. doi: 10.11924/j.issn.1000-6850.casb18110025

Hao, X., Wang, Z., Wang, G., Wang, G., Wang, X., Wang, L., et al. (2011). SSR marking of photosensitive male sterility genes in millet. *Acta Agric. Boreali Sin.* 26, 112–116.

Hasegawa, P. M., Bressan, R. A., Zhu, J. K., and Bohnert, H. J. (2000). Plant cellular and molecular responses to high salinity. *Annu. Rev. Plant Physiol. Plant Mol. Biol.* 51, 463–499. doi: 10.1146/annurev.arplant.51.1.463

Hong, M. J., Kim, D. Y., Kang, S. Y., Kim, D. S., Kim, J. B., and Seo, Y. W. (2012). Wheat F-box protein recruits proteins and regulates their abundance during wheat spike development. *Mol. Biol. Rep.* 39, 9681–9696. doi: 10.1007/s11033-012-1833-3

Hu, H., Ma, S., and Shi, Y. (1986). Discovery of dominant male sterility gene in millet (*Setaria italica*). *Acta Agron. Sin.* 2, 73–78+147. doi: 10.3321/j.issn:0496-3490.1986.02.001

Jeon, J. S., Jang, S., Lee, S., Nam, J., Kim, C., Lee, S. H., et al. (2000). *Leafy hull sterile1* is a homeotic mutation in a rice MADS box gene affecting rice flower development. *Plant Cell* 12, 871–884. doi: 10.1105/tpc.12.6.871

Jia, G., and Diao, X. (2017). Current status and perspectives of researches on foxtail millet (*Setaria italica* (L.)P. Beauv.): a potential model of plant functional genomics studies. *Chin. Bull. Life Sci.* 29, 292–301. doi: 10.13376/j.cbls/2017039

Jia, X., Yuan, X., Lu, P., Hou, D., and Dai, L. (2018). Cloning male sterility gene on chromosome 6 of foxtail millet. *Acta Agric. Boreali Sin.* 33, 65–70. doi: 10.7668/hbnxb.2018.01.011

Jun, W., Wang, Z.-L., Yang, H.-Q., Feng, Y., Guo, E.-H., Gang, T., et al. (2013). Genetic analysis and preliminary mapping of a highly male-sterile gene in foxtail millet (*Setaria italica* L. Beauv.) using SSR markers. *J. Integr. Agric.* 12, 2143–2148. doi: 10.1016/S2095-3119(13)60392-5

Kanehisa, M., Araki, M., Goto, S., Hattori, M., Hirakawa, M., Itoh, M., et al. (2008). KEGG for linking genomes to life and the environment. *Nucleic Acids Res.* 36, D480–D484. doi: 10.1093/nar/gkm882

Kaufmann, K., Melzer, R., and Theissen, G. (2005). MIKC-type MADS-domain proteins: structural modularity, protein interactions and network evolution in land plants. *Gene* 347, 183–198. doi: 10.1016/j.gene.2004.12.014

Kim, D. Y., Kwon, S. I., Choi, C., Lee, H., Ahn, I., Park, S. R., et al. (2013). Expression analysis of rice VQ genes in response to biotic and abiotic stresses. *Gene* 529, 208–214. doi: 10.1016/j.gene.2013.08.023

Kosugi, S., and Ohashi, Y. (2000). Cloning and DNA-binding properties of a tobacco Ethylene-Insensitive3 (EIN3) homolog. *Nucleic Acids Res.* 28, 960–967. doi: 10.1093/nar/28.4.960

Leterrier, M., Atanassova, R., Laquitaine, L., Gaillard, C., Coutos-Thévenot, P., and Delrot, S. (2003). Expression of a putative grapevine hexose transporter in tobacco alters morphogenesis and assimilate partitioning. *J. Exp. Bot.* 54, 1193–1204. doi: 10.1093/jxb/erg119

Li, H. (2013). Aligning sequence reads, clone sequences and assembly contigs with BWA-MEM. *arXiv* [Preprint]. arXiv:1303.3997

Li, H., Handsaker, B., Wysoker, A., Fennell, T., Ruan, J., Homer, N., et al. (2009). The sequence alignment/map format and SAMtools. *Bioinformatics* 25, 2078–2079. doi: 10.1093/bioinformatics/btp352

Li, H., Wang, Y., Tian, G., and Shi, Q. (2010). Genetic analysis on the sterile gene of highly m ale sterility line of Mille. *J. Hebei Agric. Sci.* 14, 96–99+104. doi: 10.16318/j.cnki.hbnykx.2010.11.032

Li, R., Hou, Z., Gao, L., Xiao, D., Hou, X., Zhang, C., et al. (2019). Conjunctive analyses of BSA-Seq and BSR-Seq to reveal the molecular pathway of leafy head formation in Chinese cabbage. *Plants* 8:603. doi: 10.3390/plants8120603

Li, W., Wisdom, Zhang, S., Fang, X., Wang, H., Jia, G., et al. (2015). Morphological effect and genomic mapping of Si-SP1 (small panicle 1) in foxtail millet. *J. Plant Genet. Resour.* 16, 581–587. doi: 10.13430/j.cnki.jpgr.2015.03.022

Li, Y. M. (1997). *Millet Breeding*. Beijing: China Agricultural Publishing House.

Litt, A., and Kramer, E. M. (2010). The ABC model and the diversification of floral organ identity. *Semin. Cell Dev. Biol.* 21, 129–137. doi: 10.1016/j.semcdb.2009.11.019

Liu, S., Yeh, C. T., Tang, H. M., Nettleton, D., and Schnable, P. S. (2012). Gene mapping *via* bulked segregant RNA-Seq (BSR-Seq). *PLoS One* 7:e36406. doi: 10.1371/journal.pone.0036406

Love, M. I., Huber, W., and Anders, S. (2014). Moderated estimation of fold change and dispersion for RNA-seq data with DESeq2. *Genome Biol.* 15:550. doi: 10.1186/s13059-014-0550-8

Ma, S., Cheng, H., and Hao, M. (1992). Genetic research on the male sterility gene M_s¯(ch) in millet. *Acta Agric. Boreali Sin.* 7, 9–14. doi: CNKI:SUN:HBNB.0.1992-03-001

Ngampanya, B., Sobolewska, A., Takeda, T., Toyofuku, K., Narangajavana, J., Ikeda, A., et al. (2003). Characterization of rice functional monosaccharide transporter, OsMST5. *Biosci. Biotechnol. Biochem.* 67, 556–562. doi: 10.1271/bbb.67.556

Pandian, S., and Ramesh, M. (2019). Decoding of finger millet genome: a milestone of millet genomics. *Signal Transduct. Insights* 8:1178643418820541. doi: 10.1177/1178643418820541

Samach, A., Klenz, J. E., Kohalmi, S. E., Risseeuw, E., and Crosby, W. L. (2010). The unusual floral organs gene of *Arabidopsis thaliana* is an f-box protein required for normal patterning and growth in the floral meristem. *Plant J.* 20, 433–445. doi: 10.1046/j.1365-313x.1999.00617.x

Shan, S., Li, Z., Newton, I. P., Zhao, C., Li, Z., and Guo, M. (2014). A novel protein extracted from foxtail millet bran displays anti-carcinogenic effects in human colon cancer cells. *Toxicol. Lett.* 227, 129–138. doi: 10.1016/j.toxlet.2014.03.008

Shen, H. M., Cheng, J. J., Wang, Y. M., Wu, N. L., Yang, Z. R., Zhao, X. W., et al. (2021). Dynamic gene expression analysis during panicle development in foxtail Millet. *Plant Physiol. J.* 57, 803–814. doi: 10.13592/j.cnki.ppj.2020.0590

Simon, A., Theodor, P. P., and Wolfgang, H. (2015). HTSeq—a Python framework to work with high-throughput sequencing data. *Bioinformatics* 2, 166–169. doi: 10.1093/bioinformatics/btu638

Smeekens, S. (2000). Sugar-induced signal transduction in plants. *Annu. Rev. Plant Physiol. Plant Mol. Biol.* 51, 49–81. doi: 10.1146/annurev.arplant.51.1.49

Soltis, D. E., Chanderbali, A. S., Kim, S., Buzgo, M., and Soltis, P. S. (2007). The ABC model and its applicability to basal angiosperms. *Ann. Bot.* 100, 155–163. doi: 10.1093/aob/mcm117

Song, J., Zhu, C., Zhang, X., Wen, X., Liu, L., Peng, J., et al. (2015). Biochemical and structural insights into the mechanism of DNA recognition by *Arabidopsis* ETHYLENE INSENSITIVE3. *PLoS One* 10:e0137439. doi: 10.1371/journal.pone.0137439

Su, A., Song, W., Xing, J., Zhao, Y., Zhang, R., Li, C., et al. (2016). Identification of genes potentially associated with the fertility instability of S-Type cytoplasmic

male sterility in maize *via* bulked segregant RNA-Seq. *PLoS One* 11:e0163489. doi: 10.1371/journal.pone.0163489

Verma, S., Srivastava, S., and Tiwari, N. (2015). Comparative study on nutritional and sensory quality of barnyard and foxtail millet food products with traditional rice products. *J. Food Sci. Technol.* 52, 5147–5155. doi: 10.1007/s13197-014-1617-y

Wang, T., Song, H., Li, P., Wei, Y., Hu, N., Chen, Z., et al. (2020). Transcriptome analysis provides insights into grain filling in foxtail millet (*Setaria italica* L.). *Int. J. Mol. Sci.* 21:5031. doi: 10.3390/ijms21145031

Wang, Y., Xu, H., Wei, X., Chai, C., Xiao, Y., Zhang, Y., et al. (2007). Molecular cloning and expression analysis of a monosaccharide transporter gene OsMST4 from rice (*Oryza sativa* L.). *Plant Mol. Biol.* 65, 439–451. doi: 10.1007/s11103-007-9228-x

Wei, W., Wang, P., Li, S., Fan, G., Zhao, F., Zhang, X., et al. (2021). Rapid identification of candidate genes controlling male-sterility in foxtail millet (*Setaria italica*). *Mol. Breed.* 41:73. doi: 10.1007/s11032-021-01269-2

Wu, X., and Xu, Q. (2009). Floral organ development and the function gene activity mode in angiosperms. *Plant Physiol. Newsl.* 45, 89–96.

Xiang, J., Tang, S., Zhi, H., Jia, G., Wang, H., and Diao, X. (2017). Loose panicle1 encoding a novel WRKY transcription factor, regulates panicle development, stem elongation, and seed size in foxtail millet [*Setaria italica* (L.) P. Beauv.]. *PLoS One* 12:e0178730. doi: 10.1371/journal.pone.0178730

Xie, D. X., Feys, B. F., James, S., Nieto-Rostro, M., and Turner, J. G. (1998). COI1: an *Arabidopsis* gene required for jasmonate-regulated defense and fertility. *Science* 280, 1091–1094. doi: 10.1126/science.280.5366.1091

Xue, H., Yang, J., Tang, S., Wisdom, Wang, R., Jia, G., et al. (2018). Morphological characterization and gene mapping of a panicle apical abortion mutant (sipaa1) in foxtail millet. *Sci. Agric. Sin.* 51, 1627–1640.

Yang, L. (2013). *Fine Mapping of the Male Sterility Gene SiMS1 in Millet*. Master's thesis. Beijing: Chinese Academy of Agricultural Sciences.

Yang, Z., Zhang, H., Li, X., Shen, H., Gao, J., Hou, S., et al. (2020). A mini foxtail millet with an *Arabidopsis*-like life cycle as a C_4 model system. *Nat. Plants* 6, 1167–1178. doi: 10.1038/s41477-020-0747-7

Yi, H., Zhang, C., Li, C., Wang, J., Yu, T., Liu, Y., et al. (2021). Identification and genetic analysis of two maize CMS-T mutants obtained from out-space-flighted seeds. *Genet. Resour. Crop Evol.* 68, 1937–1947. doi: 10.1007/s10722-021-01107-6

Young, M. D., Wakefield, M. J., Smyth, G. K., and Oshlack, A. (2010). Gene ontology analysis for RNA-seq: accounting for selection bias. *Genome Biol.* 11:R14. doi: 10.1186/gb-2010-11-2-r14

Zhang, G., and Wei, B. (2019). Characterization of VQ motif-containing protein family and their expression patterns under phytohormones and abiotic stresses in melon (*Cucumis melo* L.). *Plant Growth Regul.* 89, 273–285. doi: 10.1007/s10725-019-00534-x

Zhang, H., Tang, S., Ying-Tao, L. I., Zhi, H., Jia, G. Q., Zhang, W., et al. (2017). Morphological characterization and gene mapping of sins1(narrow spikelet 1) in foxtail millet. *J. Plant Genet. Resour.* 18, 538–545. doi: 10.13430/j.cnki.jpgr.2017.03.019

Zipfel, C. (2008). Pattern-recognition receptors in plant innate immunity. *Curr. Opin. Immunol.* 20, 10–16. doi: 10.1016/j.coi.2007.11.003

Conflict of Interest: The authors declare that the research was conducted in the absence of any commercial or financial relationships that could be construed as a potential conflict of interest.

Publisher's Note: All claims expressed in this article are solely those of the authors and do not necessarily represent those of their affiliated organizations, or those of the publisher, the editors and the reviewers. Any product that may be evaluated in this article, or claim that may be made by its manufacturer, is not guaranteed or endorsed by the publisher.

frontiers | Frontiers in Plant Science

MINI REVIEW
published: 03 May 2022
doi: 10.3389/fpls.2022.878074

Trends in Apomixis Research: The 10 Most Cited Research Articles Published in the Pregenomic and Genomic Eras

*Fabio Palumbo†, Samela Draga†, Alessandro Vannozzi, Margherita Lucchin and Gianni Barcaccia**

Laboratory of Plant Genetics and Breeding, Department of Agronomy, Food, Natural Resources, Animals and Environment (DAFNAE), University of Padua, Padua, Italy

OPEN ACCESS

Edited by:
Yong-Bi Fu, Agriculture and Agri-Food Canada, Canada

Reviewed by:
Tim Sharbel, University of Saskatchewan, Canada
Diego Hojsgaard, Leibniz Institute of Plant Genetics and Crop Plant Research (IPK), Germany

***Correspondence:**
Gianni Barcaccia
gianni.barcaccia@unipd.it

† These authors have contributed equally to this work

Specialty section:
This article was submitted to Plant Breeding, a section of the journal Frontiers in Plant Science

Received: *17 February 2022*
Accepted: *14 April 2022*
Published: *03 May 2022*

Citation:
Palumbo F, Draga S, Vannozzi A, Lucchin M and Barcaccia G (2022) Trends in Apomixis Research: The 10 Most Cited Research Articles Published in the Pregenomic and Genomic Eras. Front. Plant Sci. 13:878074. doi: 10.3389/fpls.2022.878074

Apomixis, or asexual reproduction by seed, represents an easy shortcut for life cycle renewal based on maternal embryo production without ploidy reduction (meiosis) and ploidy restitution (syngamy). Although the first studies officially published on this topic in scientific journals date back to the early 1930s, the identification and introduction of genes involved in asexual reproduction in species of agronomic interest still represent a major challenge. Through a bibliometric analysis of the research programs implemented in apomixis over the last 40 years, the present study was aimed to discuss not only the main findings achieved but also the investigational methods and model species used. We split the critical survey of the most cited original articles into pregenomic and genomic eras to identify potential trends and depict scenarios that have emerged in the scientific community working on apomixis, as well as to determine any correlation between the exponential increase in acquired basic knowledge and the development of advanced analytical technologies. This review found a substantial stagnation in the use of the same model species, with few exceptions, for at least 40 years. In contrast, the development of new molecular techniques, genomic platforms, and repositories has directly affected the approaches used in research, which has been directed toward an increasingly focused study of the genetic and epigenetic determinants of apomixis.

Keywords: asexual reproduction, MMC, meiosis, model species, bibliometric analysis

INTRODUCTION

Apomixis is highly desirable in agriculture as a reproductive strategy for cloning plants by seeds (Nogler, 1984). Because embryos derive from the parthenogenic development of apomeiotic egg cells, apomixis results in offspring that are exact genetic replicas of the parent. Introgression of apomixis from wild relatives to crop species and transformation of sexual genotypes into apomictically reproducing ones are long-held goals of plant breeding. It is generally accepted that the introduction of apomixis into agronomically important crops has revolutionary implications for agriculture. In recent years, many scientists have speculated on the isolation of genes controlling key steps of the apomictic pathway. Moreover, several papers have postulated the production of engineered plants exhibiting apomictic-like phenotypes. However, in model species only some

features of apomixis have been genetically engineered and none of the major crop plants has been edited or bred for apomixis (for review see Albertini et al. (2010), Pupilli and Barcaccia (2012), Vijverberg et al. (2019), Hojsgaard (2020), Ozias-Akins and Conner (2020), Scheben and Hojsgaard (2020), Schmidt (2020)). The only exception is represented by a very recent case concerning the transfer of the *PAR* allele from an apomictic dandelion to a sexual lettuce to induce egg cell division without fertilization (Underwood et al., 2022). Consequently, even in the modern era of functional genomics and systems biology, understanding the genetic control and molecular regulation of apomixis in plants appears much more complicated than expected.

This contribution addresses a critical review of the most cited articles published on apomixis in the pregenomic era (1980–2000) and genomic era (2001–2021). In genomics, the pregenomic and genomic eras refer to the time periods before and after the completion of the Human Genome Project. The working draft of the human genome was announced in 2000, and the papers describing it were published in February 2001 (Venter et al., 2001). Since then, the complete genomes of many reference organisms have been produced. These four decades are characterized by many scientific breakthroughs and methodological revolutions (e.g., availability of whole-genome and transcriptome assemblies, next-generation sequencing platforms, genome-editing tools and new breeding techniques). A massive set of cytological and ecological information, along with genetic and molecular data, has been collected mainly in model species (i.e., *Boechera holboellii*, *Hieracium* spp., *Hypericum perforatum*, *Paspalum* spp., *Ranunculus* spp., *Taraxacum officinale*), while Arabidopsis has often been used to elucidate the mechanisms of apomeiosis, parthenogenesis and apomixis. Several genes involved in the formation of unreduced embryo sacs and egg cells or responsible for the autonomous development of the embryo and endosperm have been cloned and characterized, but none of them were isolated in crop species (Pupilli and Barcaccia, 2012; Vijverberg et al., 2019; Hojsgaard, 2020; Ozias-Akins and Conner, 2020; Scheben and Hojsgaard, 2020; Schmidt, 2020). Hence, after four decades of substantial studies conducted in several laboratories with model plants, the asexual reproductive strategy called "gametophytic apomixis" still appears to be an unsolved puzzle. This situation has resulted in a loss of confidence by the major seed companies, making it difficult to acquire funds for conducting research on apomixis.

However, some novel views and original concepts are emerging. Noteworthy is the analogy between the Y-chromosome and apomixis-bearing chromosomes. Comparative genomic analyses have revealed common features such as the repression of recombination events, accumulation of transposable elements and degeneration of genes, from the most primitive to the most advanced evolutionary terms. Another emerging aspect is the link between apomixis and gene-specific silencing mechanisms, likely based on chromatin remodeling factors or transacting and heterochromatic interfering RNAs involved in both transcriptional and posttranscriptional gene regulation. More recently, merging lines of evidence regarding the role of auxin in cell fate specification of embryo sac and egg cell development have been reported in Arabidopsis, and some hypotheses have been postulated. From an evolutionary point of view, apomixis may now be regarded as a consequence of sexual failure rather than as a step toward clonal success (Albertini et al., 2019). Overall, these findings strengthen the hypothesis that apomixis as a whole may have evolved multiple times in angiosperm evolution following different developmental pathways deviating to different extents from sexuality (Barcaccia et al., 2020).

Here, the most cited publications on apomixis with the greatest potential impact on the scientific community working on this asexual mode of reproduction were analyzed. The goal was to make explicit their theoretical advances and/or practical applications and to depict the main trends in apomixis that have emerged from 20 years of studies in either the pregenomic or the genomic time period.

BIBLIOMETRIC ANALYSIS

A bibliometric analysis of the studies related to apomixis was conducted in December 2021 based on Scopus database, and the search was limited to articles [LIMIT-TO (DOCTYPE, "ar")] published between 1980 and 2021 in journals [LIMIT-TO (SRCTYPE, "j")] written in the English language [LIMIT-TO (LANGUAGE, "English")]. We first compared the results obtained by searching "apomixis" exclusively in the article title (TITLE) or considering the title, abstract, and keywords (TITLE-ABS-KEY). The former approach, more conservative, identified 280 articles (77 before 2000 and 203 after 2000). However, limiting the search for the term "apomixis" to the title alone led to the exclusion of several articles entirely related to asexual reproduction in plants. Conversely, extending the search of the term "apomixis" to the abstract and keywords increased the number of articles identified to 1,571, of which 377 were published before 2000 and 1,195 were published after 2000. However, some of these articles were not fully consistent with the topic. Considering that, from a practical point of view, it is challenging to manually double check the content of 1,571 articles, we analyzed the first 100 articles of each time frame (200 in total) to provide an estimated percentage of off-topic studies. A total of 12 and 11 articles from 1980–2000 and 2001–2021, respectively, were not related to apomixis in plants, as they mainly dealt with apomixis-like reproduction mechanisms in the animal kingdom. The geographical origin of these articles was random, and it is therefore quite unlikely that they could have an impact on the statistics presented in this study.

Based on these considerations, even if the second approach (i.e., searching "apomixis" within the title, abstract, or keywords) led to an overestimation of studies on apomixis, it was undoubtedly more comprehensive and was therefore employed for the selection of articles (**Supplementary Tables 1**, **2**). Heatmapper was then used to visualize the geographical distribution of the contributors (Babicki et al., 2016; **Figure 1A**).

Historically, the United States, Brazil and Germany represent the countries with the highest number of contributions in the

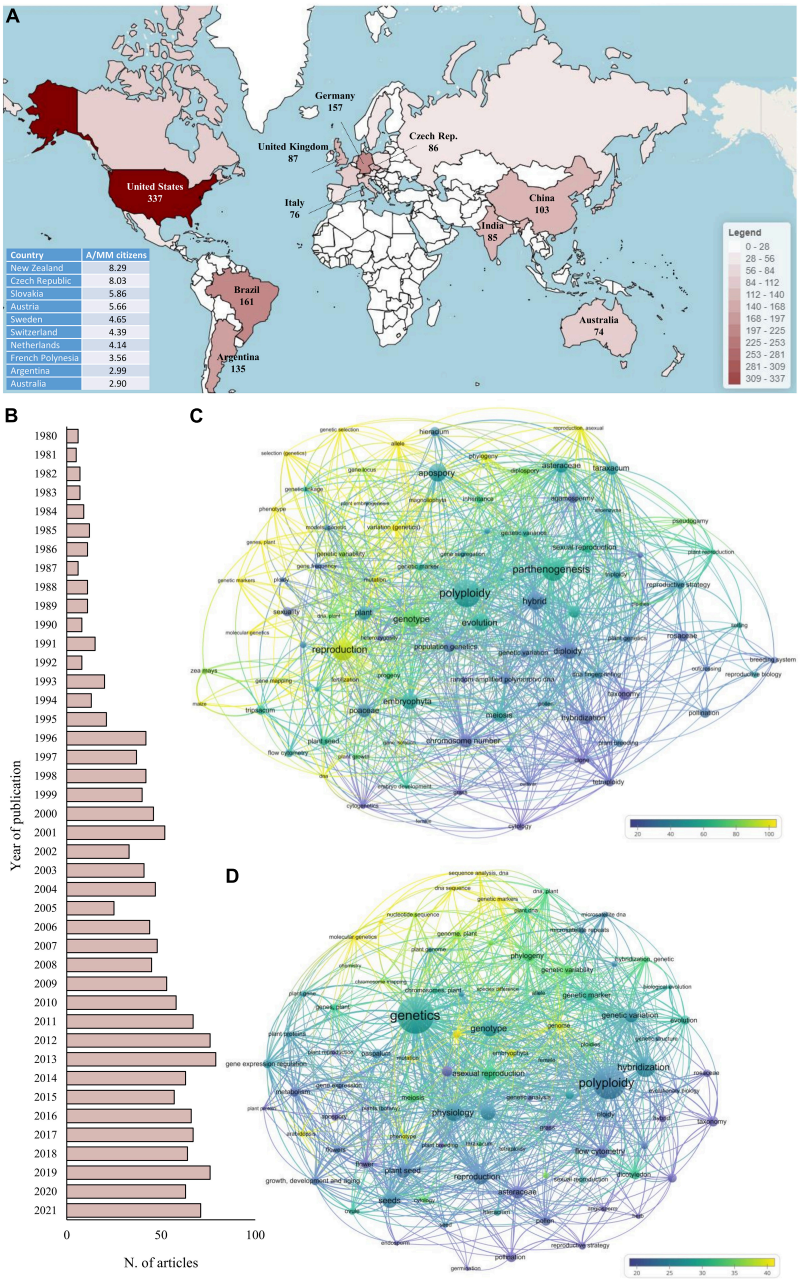

FIGURE 1 | Bibliometric analysis of the studies related to apomixis retrieved from the Scopus database, where the search was limited to articles published in English-based journals between 1980 and 2021. The search of the term "apomixis" was limited to the title, abstract and keywords. **(A)** The 10 countries with the highest number of contributions (in terms of published articles) to apomixis. The bottom left table indicates the top 10 countries with the highest number of articles per million citizens A/MM. **(B)** Contributions to apomixis by year. **(C,D)** Co-occurrence network analysis of the 100 most used keywords in apomixis-related articles published in 1980–2000 and 2001–2021, respectively. The font size of each keyword is proportional to the number of times the keyword has been used within the articles considered, while the color scale is based on the average number of citations received by the documents in which each specific keyword occurs.

field of apomixis. They alone contributed 41.6% of all articles published in the last 40 years on this topic, with 655 articles out of 1,571. Even restricting the analysis to the last 10 years (2012–2021), these first three positions remain unchanged, confirming, in absolute terms, the consolidated leadership of these countries in this research area. Clearly, normalizing these data according to the number of researchers working in the natural sciences fields would provide a more precise idea of the efforts made by each country in this specific topic. However, retrieving this type of data is quite challenging, if not impossible. Instead, an attempt to normalize the data was made by considering the population of each country. In this case, the pattern was completely reversed,

and countries such as New Zealand and the Czechia showed an article/citizen ratio four to ten times higher than that of the United States, Brazil and Germany.

In terms of time trends, the number of annual publications increased from 6 in 1980 to 75 in 2021, with a peak in 2013 (79), demonstrating a growing interest of researchers in this topic (**Figure 1B**). Notably, 22% (344) of all articles published in the last 40 years have been published in the last 5 years (2017–2021).

The keywords were also analyzed using a co-occurrence network analysis tool in VOSviewer software (van Eck and Waltman, 2010). To understand the dynamic change in their usage, the analysis was split into two sections considering the 100 most used keywords from 1980 to 2000 and from 2001 to 2021 (**Figures 1C,D**, respectively). The two keyword-based networks were organized considering both the use frequency of each keyword (as a function of the font size, namely, the larger the font size is, the greater the number of times the keyword has been used) and the average number of citations received by the documents in which each specific keyword occurred. Notably, excluding "apomixes," the most used keyword in the last two decades was "genetics." On the contrary, "genetics" never appeared in the ranking of the 100 most used keywords before 2000. However, in both periods, the articles containing keywords related to the field of genetics and molecular biology (e.g., "allele," "genome," "genetic markers," and "DNA sequence") were always the ones with the highest number of citations, highlighting the crucial role played by these two branches of biology in the study of apomixis. Apart from some laboratory analyses, i.e., cytometry, transversely used in the studies within the last 40 years, the use of keywords also reflected the evolution of the molecular methods used. From 1980 to 2000, the most popular keywords in the molecular genetics field were "allele," "mutation" and "gene mapping," while after 2000, studies were characterized by terms such as "genome," "gene expression" and "microsatellite DNA." The spread of capillary sequencers, NGS platforms and qPCR instruments at the turn of the century has shifted the focus of research toward more targeted and effective approaches to identifying the genetic determinants of apomixis.

Although not sufficiently exhaustive, the number of normalized citations per year (i.e., average number of citations/year) was used as an evaluation parameter in the choice and discussion of the most impactful articles on this topic. The absolute number of citations was not used, because it would have penalized the articles published in recent years. Finally, when choosing the most impactful articles (based on the average number of citations/year), we applied an additional filter based on consistency with the topic under consideration. As an example, the study by Silveira et al. (2009) is one of the articles with the highest average number of citations/year, but it does not provide information aimed at understanding apomictic mechanisms (i.e., it provides a list of reference genes to be used as control genes in qPCRs). For this reason, it was not included in the articles discussed in this review. Twenty articles were finally selected, 10 for each period.

PREGENOMIC ERA

Considering the 10 selected articles before 2000, we found that *Arabidopsis thaliana*, together with *Taraxacum*, represents the most studied plant species for scientific research on this topic. In the case of *Arabidopsis*, the scientific approaches used were commonly classical forward or reverse genetics with the analysis of mutants, gene mapping and functional characterization of candidate genes. Conversely, in *Taraxacum*, as in other species listed in the articles considered (i.e., *Erigeron annuus*, *Pennisetum squamulatum* or *Hieracium* spp.), more descriptive approaches were applied. In particular, microscopy, histology, flow cytometry, analysis of seed germination, plant genotyping by means of molecular markers (SSR, RAPD, AFLP or SCAR) have been frequently exploited. These tools were particularly useful to study the inheritance of apomixis, infer phylogenetic relationships between apomictic species or perform genetic mapping (**Table 1**).

Concerning basic research on the possible molecular mechanisms underlying apomixis, it is worth mentioning the efforts of Kiyosue et al. (1999). They isolated a mutation in *Arabidopsis*, *f644*, that allows for replication of the central cell and subsequent endosperm development without fertilization. By using a map-based strategy, the authors cloned and sequenced the *F644* gene and showed that it encodes a SET-domain polycomb protein. The latter, in turn, is the identical protein codified by *MEDEA* (*MEA*), a pivotal gene whose maternally derived allele is required for embryogenesis. These findings demonstrated the functions for plant polycomb proteins in the suppression of central cell proliferation and endosperm development. In another article, Chaudhury et al. (1997) analyzed other Arabidopsis mutants, *fis1*, *fis2* and *fis3*, in which certain processes of seed development were uncoupled from the double-fertilization event that occurs after pollination. The authors proposed a model in which the FIS1-FIS2-FIS3 interaction blocks endosperm development by acting in different stages of seed development. Their proposal assumed that this process in wild-type plants is initiated by a pollination-induced inactivation of the FIS1–FIS2–FIS3 complex (Chaudhury et al., 1997). The high number of citations per year reflects the importance of these two articles.

Another highly cited article, representing a milestone in apomixis research, is the contribution by Carman in 1997. He analyzed around 460 families of angiosperms and validated the hypothesis that the partial-to-complete replacement of meiosis by embryo sac formation in apomictic and polysporic species results from asynchronously expressed duplicated genes that control female development (Carman, 1997). Also, Carman further suggested that asexual reproduction in apomicts preserves primary genomes whilst sexual reproduction in polysporic and polyembryonic polyploids accelerates paleopolyploidization. Paleopolyploidization may sometimes eliminate the gene duplications required for apomixis while retaining those duplications required for polyspory or polyembryony.

Among the various scientific contributions listed in **Table 1** are the studies that have provided screening tools to determine the reproductive pathways in monocotyledons and dicotyledons.

TABLE 1 | List of the 10 most cited publications on apomixis between 1980 and 2000 and between 2001 and 2021.

Taxon	Method/s	Main results	References	C/Y[1]
Arabidopsis thaliana	Mutagenesis, cytological analyses (electron and optical microscopy), and ploidy analysis (fluorescence microscopy)	Developmental and genetic characterization of *fis1* (fertilization-independent seed), *fis2*, and *fis3* mutants indicates that these genes normally have a controlling role in seed development after pollination and double fertilization.	Chaudhury et al., 1997	29.3
Angiosperm families (460)	Phylogenetic associations among reproductive-anomalous species using statistical tests	Apomictic, polysporic and polyembryonic species are polyploid or paleopolyploid and probably possess duplicate genes for female development. The authors also indicate that such species are associated at the familial level and are evolutionarily linked.	Carman, 1997	26.9
Pennisetum squamulatum	Molecular markers (RAPD and SCAR)	Genetic mapping of 13 molecular markers in an interspecific hybrid population of 397 individuals segregating for apomixis and sexuality. Surprisingly, 12 of the 13 markers strictly cosegregated with aposporous embryo sac development, clearly defining a contiguous apospory-specific genomic region in which no genetic recombination was detected.	Ozias-Akins et al., 1998	12.7
Hieracium spp.	Histological and cytological analyses (scanning electron microscopy, confocal microscopy)	Apomixis was observed in two distinct and nearly obligate *Hieracium* species and compared with seed formation in a sexual species. Novel features previously unrecorded in apomictic members of the *Hieracum* genus were described. The outcomes of apomictic events were further analyzed with respect to the types of seedlings that germinate from apomictic seeds and from hybrid seeds derived from crosses between the sexual and apomictic plants.	Koltunow et al., 1998	8.0
Melastomataceae family (11 species)	Pollen analysis	Controlled pollinations and observations of pollen tube growth, pollen fertility and cytological data were studied in 11 species of Melastomataceae. The apomictic species had lower pollen fertility than the sexual species, showing that low pollen fertility may be a useful indicator of apomixis if analyzed using careful sampling supplemented by emasculation experiments. The apomictic species also showed meiotic irregularities, probably related to hybridization, polyploidy and low pollen fertility.	Goldenberg and Shepherd, 1998	7.4
Arabidopsis thaliana	Gene mapping, mutant complementation	Using a map-based strategy, the authors cloned and sequenced the *F644* gene, showing that it encodes a SET-domain polycomb protein identical to MEDEA (MEA), which is encoded by a gene whose maternal-derived allele is required for embryogenesis.	Kiyosue et al., 1999	21.9
Taraxacum spp.	Flow cytometry; alloenzymes	The inheritance of apomixis was studied in narrow crosses between diploid sexuals and triploid apomicts from the *Taraxacum* section *Ruderalia*, and the reproductive mode of the offspring was investigated. Of the 26 allozyme-confirmed F1 hybrids, diploids were significantly less frequent than triploids. Seed set was not observed in diploids but was observed in one-third of the triploid hybrids and all of the tetraploid hybrids. Partial apomixis was caused by semisterility and not by residual sexuality (facultative apomixis).	Tas and Van Dijk, 1999	7.7
Taraxacum spp.	Cytological analyses; flow cytometry, SSR	Four non-apomictic diploid and 10 non-apomictic triploid hybrids were pollinated with diploids, and the progenies were analyzed. Seed fertility was significantly reduced in two diploid hybrids. The authors identified different types of progenies, concluded that elements of apomixis, diplospory and parthenogenesis can be uncoupled and suggested that several loci are involved in the genetic control of apomixis in *Taraxacum*.	Van Dijk et al., 1999	8.2
Arabidopsis, Arabis, Hypericum and *Poa* spp.	Flow cytometry	Seed samples of 32 species (obligate and facultative sexuals and apomicts of monocots and dicots) were investigated by flow cytometry to reveal the pathway of reproduction. The screen is suited to selecting sporophytic or gametophytic mutants in sexual species, identifying pure sexual or obligate apomictic genotypes from facultative apomictic species, and analyzing the inheritance of individual reproductive processes.	Matzk et al., 2000	22.7
Erigeron annuus	AFLPs	Diplospory and parthenogenesis are unlinked and inherited independently; the absence of agamospermy in diploid F1s appears to be best explained by a combination of recessive-lethal gametophytic selection against the parthenogenetic locus and univalent inheritance of the region bearing diplospory.	Noyes and Rieseberg, 2000	9.6
Arabidopsis thaliana	SSR markers; genetic engineering	Mutation of the *Arabidopsis* gene *DYAD/SWITCH1* (*SWI1*), a regulator of meiotic chromosome organization, leads to apomeiosis. The alteration of a single gene in a sexual plant can result in functional apomeiosis, a major component of apomixis.	Ravi et al., 2008	10.4
Arabidopsis thaliana	Cytology and flow cytometry; genetic markers	The creation of the MiMe genotype and apomeiosis phenotype: MiMe plants undergo mitotic-like division instead of normal meiotic division, without affecting subsequent sexual processes.	D'Erfurth et al., 2009	16.4

(Continued)

TABLE 1 | (Continued)

Taxon	Method/s	Main results	References	C/Y[1]
Taraxacum officinale	Chemical analysis; AFLP and MS-AFLP analysis	Stress-induced methylation changes are common and are mostly heritable. Sequence-independent, autonomous methylation variation is readily generated. This highlights the potential of epigenetic inheritance to play an independent role in evolutionary processes, which is superimposed on the system of genetic inheritance.	Verhoeven et al., 2010	33.7
Arabidopsis thaliana	Histological analysis; immunoblotting and immunoprecipitation; cloning and genomic analysis of small RNAs	The *Arabidopsis* protein ARGONAUTE 9 (AGO9) controls female gamete formation by restricting the specification of gametophyte precursors in a dose-dependent, non-cell-autonomous manner. *AGO9*-dependent sRNA silencing is crucial to specifying cell fate in the *Arabidopsis* ovule, and epigenetic reprogramming in companion cells is necessary for sRNA–dependent silencing in plant gametes.	Olmedo-Monfil et al., 2010	30.7
Zea mays	Genotyping; *in situ* mRNA hybridizations	The DNA methylation pathway active during reproduction is essential for gametophyte development in maize and plays a critical role in the differentiation between apomictic and sexual reproduction. Downregulation of an ovule-specific chromatin-based silencing pathway in maize would result in apomixis. Apomeiosis and parthenogenesis in *Tripsacum* are genetically linked.	Garcia-Aguilar et al., 2010	10.6
Boechera spp.	Cytohistological analyses; SuperSAGE analysis	Apomixis-specific gene expression is characterized by a significant overrepresentation of transcription factor activity. The link between hybridization and asexuality provides a hypothesis for multiple evolutionary origins of apomixis in the genus *Boechera*.	Sharbel et al., 2010	9.7
Zea mays	Cytology and immunochemistry; digital gene expression tag profiling	Female germ cell development in maize is dependent upon conserved small RNA pathways acting non-cell-autonomously in the ovule. Interfering with this repression leads to apomixis-like phenotypes in maize. AGO104 influences the transcription of many targets in the ovaries, with a strong effect on centromeric repeats.	Singh et al., 2011	14.9
Pennisetum squamulatum	Flow cytometry; genetic engineering; histological analysis	The *PsASGR-BABY BOOM*-like (*PsASGR-BBML*) gene is expressed in egg cells before fertilization and can induce parthenogenesis and the production of haploid offspring in transgenic sexual pearl millet. A reduction in *PsASGR-BBML* expression in apomictic F1 transgenic plants results in fewer visible parthenogenetic embryos and a reduction in the embryo cell number compared with controls.	Conner et al., 2015	12.0
Taraxacum officinale	Flow cytometry; SSR, AFLP; demethylation experiment	Variations in DNA methylation contribute to heritable differences in flowering time within a single widespread apomictic clonal lineage of the common dandelion. Epigenetic mechanisms can facilitate adaptive divergence within genetically uniform asexual lineages.	Wilschut et al., 2016	8.5
Citrus spp.	DNA sequencing; bulk segregant analysis (BSA); local gene-based association analysis for the polyembryony locus; transcriptome sequencing	A comparative population analysis suggested that genomic regions harboring energy- and reproduction-associated genes are probably under selection in cultivated citrus. The genetic locus responsible for citrus polyembryony, a form of apomixis, is an 80-kb region containing 11 candidate genes; one of them, *CitRWP*, is expressed at higher levels in ovules of polyembryonic cultivars. A miniature inverted-repeat transposable element insertion in the promoter region of *CitRWP* cosegregated with polyembryony.	Wang et al., 2017	32.2

[1]*C/Y, citation/year.*

For each publication, the taxon used, the main methods involved, the main findings, the reference and the average number of citations per year are reported.

An emblematic example is the work of Matzk et al. The authors analyzed seed samples collected from 32 monocot and dicot species (apomicts along with obligate and facultative sexuals) *via* flow cytometry. Based on the cytometry estimates, they proposed a novel screen for the route of reproduction based on the ploidy levels of embryo and endosperm nuclei from mature seeds (Matzk et al., 2000).

The use of molecular markers for mapping gene loci involved in apomictic phenomena represents one of the most used approaches in the pregenomic era. For example, Ozias-Akins et al. by analyzing an interspecific hybrid population of 397 individuals that were segregated for apomixis and sexuality, identified 13 predictive markers (Ozias-Akins et al., 1998). Twelve of the 13 markers strictly cosegregated with aposporous embryo sac development, clearly defining a contiguous apospory-specific genomic region in which no genetic recombination was detected. Noyes and Rieseberg investigated the genetic basis of agamospermy in a segregating population of 130 F1 hybrids obtained from a cross between triploid agamospermous *Erigeron annuus* (2n = 27) and sexual diploid *E. strigosus* (2n = 18) (Noyes and Rieseberg, 2000). By means of linkage analyses performed on 387 segregating amplified fragment length polymorphisms (AFLPs), they found that four closely linked markers with polysomic inheritance were significantly associated with parthenogenesis. Moreover, they identified 11 co-segregating markers with univalent inheritance completely associated with diplospory.

Cytological analyses based on microscopy represent another essential tool in the study of apomixis. This is the case for the contribution by Koltunow in *Hieracium* and that of Goldenberg and Shepherd in the *Melastomataceae* family. In the first case, Koltunow et al. performed a detailed cytological study

of two distinct and nearly obligate species, *H. aurantiacum* and *H. piloselloides*. Also, they compared apomixis with seed formation in a sexual species to define the cellular basis for apomixis. In the light of this, they described novel features previously unrecorded in apomictic members of this genus and provided the basis for further molecular, cell biological and mechanistic studies investigating the control of apomixis (Koltunow et al., 1998). In the second study, controlled pollinations and observations of pollen tube growth, pollen fertility and cytological data were studied in 11 species of Melastomataceae (Goldenberg and Shepherd, 1998). The apomictic species had lower pollen fertility than the sexual ones, showing that low pollen fertility may be a useful indicator of apomixis if analyzed using careful sampling supplemented by emasculation experiments. The apomictic species also showed meiotic irregularities that were probably related to hybridization, polyploidy and low pollen fertility.

In *Taraxacum*, the inheritance of apomixis was studied in narrow crosses between diploid sexuals and triploid apomicts from the *Taraxacum* section *Ruderalia*, and the reproductive mode of the offspring was investigated. Of the 26 allozyme-confirmed F1 hybrids, diploids were significantly less frequent than triploids (Tas and Van Dijk, 1999). Seed set was not observed in any of the diploids, but it was observed in one-third of the triploid hybrids and in all the tetraploid hybrids. In a second article, the same authors crossed diploid sexual plants with four non-apomictic diploid and 10 non-apomictic triploid hybrids (obtained in a previous study) and analyzed the resulting progenies. The authors identified different types of progenies and concluded that elements of apomixis, diplospory and parthenogenesis can be uncoupled. This result is inconsistent with the single-locus model for apomixis in *Taraxacum* and suggests that several loci are involved in the genetic control of apomixis in *Taraxacum* (Van Dijk et al., 1999).

GENOMIC ERA

Pennisetum, *Taraxacum* and especially *Arabidopsis* continue to play a major role in post-2000 studies. In particular, *Arabidopsis* has been at the center of tremendous advances in our understanding of several fields, providing valuable information regarding the role of some candidate genes controlling apomixis. However, it should also be noted that crop species, such as corn and citrus, are starting to be studied. The identification of key genes involved in apomictic mechanisms in polyploids or interspecific hybrids has only been possible due to the introduction of genetic engineering techniques and sequencing platforms. Moreover, differently from the pregenomic era, the most cited articles in the post-2000 era almost exclusively addressed the functional characterization of genes and the *ad hoc* constitution of mutants. Finally, new hypotheses were proposed on the role of epigenetics, DNA methylation, miRNAs or siRNAs in reproductive mechanisms.

One of the milestones in the genetic study of apomixis is represented by the identification of the *DYAD/SWITCH1* (*SWI1*) locus, a regulator of meiotic chromosome organization, whose *dyad* allele leads to unreduced female gamete formation (apomeiosis). Most of the fertile diploid ovules were successfully fertilized by haploid pollen producing triploid seeds in dyad plants (Ravi et al., 2008). Another *Arabidopsis* mutant producing functional diploid gametes genetically identical to their mother was generated by combining three different mutations that worked to fully replace meiosis with a mitotic-like division. In particular, the mutated alleles characterizing the *MiMe* mutant (i.e., *MI*tosis instead of *ME*iosis) were *osd1*, *Atspo11-1* and *Atrec8*. The latter two led to a mitotic-like first meiotic division (by affecting the homologous recombination and the orientation of sister chromatids), while *osd1* prevented the second meiotic division. In contrast to the *dyad* mutation, both male and female gametes were unreduced such that selfed *MiMe* progeny were commonly tetraploid, while backcrossing diploid *MiMe* and wild-type plants produced triploid plants regardless of the use of male or female *MiMe* gametes (D'Erfurth et al., 2009). Further upstream, *AGO9*, a member of the ARGONAUTE family that is known to interact with miRNAs and siRNAs, was found to regulate early cell specification in the ovule. In particular, mutations in *AGO9* lead to the production of multiple abnormal somatic cells, some of which are able to initiate gametogenesis without undergoing meiosis (Olmedo-Monfil et al., 2010). When a single cell undergoes meiosis, it gives rise to a functional haploid megaspore. Also, identical results were obtained by mutating *SUPPRESSOR OF GENE SILENCING 3* (*SGS3*) and *RNA-DEPENDENT RNA POLYMERASE 6* (*RDR6*). The latter converts the ssRNA precursors of *trans*-acting siRNAs (ta-siRNAs) into dsRNA, while *SGS3* encodes an RNA-binding protein involved in the same pathway.

Strong homology of the components involved in silencing *via* DNA methylation was established between *Arabidopsis* and maize. Six loci that are specifically downregulated in ovules of apomictic plants were identified in maize-*Tripsacum* hybrids. Four of them encode chromatin-modifying enzymes (CMEs) that have been predicted (CHR106, DMT103, and DMT105) or shown (DMT102) to regulate DNA methylation. More precisely, CHR106 participates in the maintenance of methylation at both CG and non-CG sites, while the DNA methyltransferases DMT102, DMT105 and DMT103 act redundantly to maintain non-CG methylation. The set of deregulated genes also included *hdt104*, a member of the plant-specific histone deacetylase family, and *hon101*, a histone H1 linker protein gene. Specifically, loss-of-function alleles for *dmt102* and *dmt103*, homologous to the *Arabidopsis* CHROMOMETHYLASE and DOMAINS REARRANGED METHYLTRANSFERASE families, revealed apomictic phenotypes with unreduced gametes and the formation of multiple embryo sacs in the ovule (Garcia-Aguilar et al., 2010). Subsequent homology with *Arabidopsis* was identified as a dominant mutation resulting in the formation of functionally unreduced gametes in maize. *AGO104* is related to *Arabidopsis AGO9*; however, while *AGO9* acts to repress germ cell fate in somatic tissues, *AGO104* acts to repress somatic fate in germ cells. *AGO104* accumulates specifically in somatic cells surrounding the female meiocyte, suggesting a mobile signal rather than cell-autonomous control. Furthermore, *AGO104*

is necessary for non-CG methylation of centromeric and knob-repeat DNA and influences the transcription of many targets in the ovaries, with a strong effect on centromeric repeats (Singh et al., 2011). Another perspective affecting the onset of DNA methylation was reported for dandelions. Environmental stresses can trigger methylation changes, which may have evolutionary consequences, even in the absence of sequence variation. These changes are evidence that specific stresses can trigger specific methylation changes and that most of the induced changes are faithfully transmitted to offspring (Verhoeven et al., 2010). Further studies on dandelions substantiated the role of the methylation polymorphism during functional flowering time, confirming that epigenetic variation contributes to heritable phenotypic divergence in ecologically relevant traits in natural plant populations (Wilschut et al., 2016). Therefore, epigenetic variation plays a key role in the adaptive potential of populations to rapidly face changing environments or when genetic variation is limited. Additionally, a transcriptomic analysis supported the hypothesis of multiple evolutionary origins of apomixis and a possible link with hybridization was noted in an ancient hybrid of *Boechera* exhibiting a diplosporous type of *apomixis (Sharbel et al., 2010*). Apomixis-specific gene expression was characterized by a significant overrepresentation of transcription factor activity, showing that apomeiosis is associated with downregulation at the megaspore mother cell stage. On the other hand, apospory in *Pennisetum squamulatum,* a member of the Poaceae family, segregates *via* a single dominant locus transmitted by a large, hemizygous, non-recombining chromosomal region, the apospory-specific genomic region (*ASGR*). The ASGR contains multiple copies of the *PsASGR-BABY BOOM-like* (*PsASGR-BBML*) gene, a member of the BBM-like subgroup of the *APETALA 2/ETHYLENE RESPONSE FACTOR* (*AP2/ERF*) DNA-binding domain family. Additionally, the function of the *PsASGR-BBML* transgene was discovered: this gene is expressed in egg cells before fertilization and induces both parthenogenesis and the production of haploid offspring in sexual pearl millet (Conner et al., 2015). While the studies reported thus far have focused on gametophytic apomixis, asexual reproduction in the *Citrus* genus is largely based on sporophytic apomixis. Accessions of primitive, wild relative and cultivated *Citrus* species have been sequenced to shed light on the genetic locus responsible for polyembryony, resulting in 11 candidate genes. One of them, *CitRWP*, is expressed at higher levels in ovules of polyembryonic cultivars (Wang et al., 2017). *CitRWP*, also denoted *Cg4g018970*, encodes an RWP-RK domain similar to the *Arabidopsis* RKD family of proteins and acts as a regulator of egg cell-related genes. The extensive transcriptomic analysis by Wang et al. led to important insights suggesting that nucellar embryogenesis and sexual reproduction may employ similar genes or pathways.

CONCLUSION

Apomixis has aroused great scientific and intellectual curiosity, leading to an exponential increase in research studies. The prospect of introducing apomixis "as a whole" in crop species still remains the main goal, but the attempt to engineer species of agronomic interest has been unsuccessful. In terms of model species, the scenario has remained broadly unchanged since the 1980s: most studies are conducted on a few species, although in recent years, there have been some attempts to extend this research to agronomically important crops. In terms of methodologies, few clear differences were found between the pregenomic and genomic eras. The use of genetic engineering and sequencing platforms has begun to spread in the study of apomixis, but some methodologies, including flow cytometry and microscopy, still represent important research activities. Identification of the master regulatory switch triggering apomixis in sexual crops is a goal for plant breeders. The massive number of studies conducted in apomixis in the last 40 years requires a critical analysis aimed at integrating all the information produced. A new scenario is taking shape, and the exponential accumulation of knowledge related to apomictic mechanisms in model species is finally reaching application potential: genome editing. It is still too early to predict whether this new technology represents the beginning of a new era, but it would not be surprising to see that the 10 most cited articles in the next 20 years mainly concern the use of genomic editing approaches to transfer what has been learned thus far in model species into crops.

AUTHOR CONTRIBUTIONS

All authors listed have made a substantial, direct, and intellectual contribution to the work, and approved it for publication.

FUNDING

This study is part of the Mechanisms of Apomictic Development (MAD) project, under the Marie Sklodowska-Curie and Innovation Staff Exchange (Grant No. 872417) and funded by the EU H2020 Research and Innovation Program.

SUPPLEMENTARY MATERIAL

The Supplementary Material for this article can be found online at: https://www.frontiersin.org/articles/10.3389/fpls.2022.878074/full#supplementary-material

REFERENCES

Albertini, E., Barcaccia, G., Carman, J. G., and Pupilli, F. (2019). Did apomixis evolve from sex or was it the other way around? *J. Exp. Bot.* 70, 2951–2964. doi: 10.1093/jxb/erz109

Albertini, E., Barcaccia, G., Mazzucato, A., Sharbel, T. F., and Falcinelli, M. (2010). "Apomixis in the era of biotechnology," in *Plant Developmental Biology - Biotechnological Perspectives*, eds E. C. Pua and M. R. Davey (Berlin: Springer Berlin Heidelberg), 405–436. doi: 10.1007/978-3-642-02301-9_20

Babicki, S., Arndt, D., Marcu, A., Liang, Y., Grant, J. R., Maciejewski, A., et al. (2016). Heatmapper: web-enabled heat mapping for all. *Nucleic Acids Res.* 44, W147–W153. doi: 10.1093/nar/gkw419

Barcaccia, G., Palumbo, F., Sgorbati, S., Albertini, E., and Pupilli, F. (2020). A reappraisal of the evolutionary and developmental pathway of apomixis and its genetic control in angiosperms. *Genes* 11:859. doi: 10.3390/genes11080859

Carman, J. G. (1997). Asynchronous expression of duplicate genes in angiosperms may cause apomixis, bispory, tetraspory, and polyembryony. *Biol. J. Linn. Soc.* 61, 51–94. doi: 10.1006/bijl.1996.0118

Chaudhury, A. M., Ming, L., Miller, C., Craig, S., Dennis, E. S., and Peacock, W. J. (1997). Fertilization-independent seed development in *Arabidopsis thaliana*. *Proc. Natl. Acad. Sci. U S A.* 94, 4223–4228. doi: 10.1073/pnas.94.8.4223

Conner, J. A., Mookkan, M., Huo, H., Chae, K., and Ozias-Akins, P. (2015). A parthenogenesis gene of apomict origin elicits embryo formation from unfertilized eggs in a sexual plant. *Proc. Natl. Acad. Sci. U S A.* 112, 11205–11210. doi: 10.1073/pnas.1505856112

D'Erfurth, I., Jolivet, S., Froger, N., Catrice, O., Novatchkova, M., and Mercier, R. (2009). Turning meiosis into mitosis. *PLoS Biol.* 7:e1000124. doi: 10.1371/journal.pbio.1000124

Garcia-Aguilar, M., Michaud, C., Leblanc, O., and Grimanelli, D. (2010). Inactivation of a DNA methylation pathway in maize reproductive organs results in apomixis-like phenotypes. *Plant Cell* 22, 3249–3267. doi: 10.1105/tpc.109.072181

Goldenberg, R., and Shepherd, G. J. (1998). Studies on the reproductive biology of Melastomataceae in "cerrado" vegetation. *Plant Syst. Evol.* 211, 13–29. doi: 10.1007/BF00984909

Hojsgaard, D. (2020). Apomixis technology: separating the wheat from the chaff. *Genes* 11, 411. doi: 10.3390/genes11040411

Kiyosue, T., Ohad, N., Yadegari, R., Hannon, M., Dinneny, J., Wells, D., et al. (1999). Control of fertilization-independent endosperm development by the *MEDEA* polycomb gene in Arabidopsis. *Proc. Natl. Acad. Sci. U S A.* 96, 4186–4191. doi: 10.1073/pnas.96.7.4186

Koltunow, A. M., Johnson, S. D., and Bicknell, R. A. (1998). Sexual and apomictic development in *Hieracium*. *Sex. Plant Reprod.* 11, 213–230. doi: 10.1007/s004970050144

Matzk, F., Meister, A., and Schubert, I. (2000). An efficient screen for reproductive pathways using mature seeds of monocots and dicots. *Plant J.* 21, 97–108. doi: 10.1046/j.1365-313X.2000.00647.x

Nogler, G. A. (1984). "Gametophytic Apomixis," in *Embryology of Angiosperms*, ed. B. M. Johri (Berlin: Springer-Verlag), 475–518. doi: 10.1007/978-3-642-69302-1_10

Noyes, R. D., and Rieseberg, L. H. (2000). Two independent loci control agamospermy (apomixis) in the triploid flowering plant *Erigeron annuus*. *Genetics* 155, 379–390. doi: 10.1093/genetics/155.1.379

Olmedo-Monfil, V., Durán-Figueroa, N., Arteaga-Vázquez, M., Demesa-Arévalo, E., Autran, D., Grimanelli, D., et al. (2010). Control of female gamete formation by a small RNA pathway in Arabidopsis. *Nature* 464, 628–632. doi: 10.1038/nature08828

Ozias-Akins, P., and Conner, J. A. (2020). Clonal reproduction through seeds in sight for crops. *Trends Genet.* 36, 215–226. doi: 10.1016/j.tig.2019.12.006

Ozias-Akins, P., Roche, D., and Hanna, W. W. (1998). Tight clustering and hemizygosity of apomixis-linked molecular markers in *Pennisetum squamulatum* implies genetic control of apospory by a divergent locus that may have no allelic form in sexual genotypes. *Proc. Natl. Acad. Sci. U S A.* 95, 5127–5132. doi: 10.1073/pnas.95.9.5127

Pupilli, F., and Barcaccia, G. (2012). Cloning plants by seeds: inheritance models and candidate genes to increase fundamental knowledge for engineering apomixis in sexual crops. *J. Biotechnol.* 159, 291–311. doi: 10.1016/j.jbiotec.2011.08.028

Ravi, M., Marimuthu, M. P. A., and Siddiqi, I. (2008). Gamete formation without meiosis in Arabidopsis. *Nature* 451, 1121–1124. doi: 10.1038/nature06557

Scheben, A., and Hojsgaard, D. (2020). Can we use gene-editing to induce apomixis in sexual plants? *Genes* 11:781. doi: 10.3390/genes11070781

Schmidt, A. (2020). Controlling apomixis: shared features and distinct characteristics of gene regulation. *Genes* 11:329. doi: 10.3390/genes11030329

Sharbel, T. F., Voigt, M. L., Corral, J. M., Galla, G., Kumlehn, J., Klukas, C., et al. (2010). Apomictic and sexual ovules of *Boechera* display heterochronic global gene expression patterns. *Plant Cell* 22, 655–671. doi: 10.1105/tpc.109.072223

Silveira, R. D., Alves-Ferreira, M., Guimarães, L. A., Da Silva, F. R., and Carneiro, V. T. D. C. (2009). Selection of reference genes for quantitative real-time PCR expression studies in the apomictic and sexual grass *Brachiaria brizantha*. *BMC Plant Biol.* 9:84. doi: 10.1186/1471-2229-9-84

Singh, M., Goel, S., Meeley, R. B., Dantec, C., Parrinello, H., Michaud, C., et al. (2011). Production of viable gametes without meiosis in maize deficient for an ARGONAUTE protein. *Plant Cell* 23, 443–458. doi: 10.1105/tpc.110.079020

Tas, I. C. Q., and Van Dijk, P. J. (1999). Crosses between sexual and apomictic dandelions (*Taraxacum*). I. The inheritance of apomixis. *Heredity* 83, 707–714.

Underwood, C. J., Vijverberg, K., Rigola, D., Okamoto, S., Oplaat, C., Camp, R. H. M. O., et al. (2022). A *PARTHENOGENESIS* allele from apomictic dandelion can induce egg cell division without fertilization in lettuce. *Nat. Genet.* 54, 84–93. doi: 10.1038/s41588-021-00984-y

Van Dijk, P. J., Tas, I. C. Q., Falque, M., and Bakx-Schotman, T. (1999). Crosses between sexual and apomictic dandelions (*Taraxacum*). II. The breakdown of apomixis. *Heredity* 83, 715–721. doi: 10.1046/j.1365-2540.1999.00620.x

van Eck, N. J., and Waltman, L. (2010). Software survey: VOSviewer, a computer program for bibliometric mapping. *Scientometrics* 84, 523–538. doi: 10.1007/s11192-009-0146-3

Venter, C. J., Adams, M. D., Myers, E. W., Li, P. W., Mural, R. J., Sutton, G. G., et al. (2001). The sequence of the human genome. *Science* 291, 1304–1351. doi: 10.1126/science.1058040

Verhoeven, K. J. F., Jansen, J. J., van Dijk, P. J., and Biere, A. (2010). Stress-induced DNA methylation changes and their heritability in asexual dandelions. *New Phytol.* 185, 1108–1118. doi: 10.1111/j.1469-8137.2009.03121.x

Vijverberg, K., Ozias-Akins, P., and Schranz, M. E. (2019). Identifying and engineering genes for parthenogenesis in plants. *Front. Plant Sci.* 10:128. doi: 10.3389/fpls.2019.00128

Wang, X., Xu, Y., Zhang, S., Cao, L., Huang, Y., Cheng, J., et al. (2017). Genomic analyses of primitive, wild and cultivated citrus provide insights into asexual reproduction. *Nat. Genet.* 49, 765–772. doi: 10.1038/ng.3839

Wilschut, R. A., Oplaat, C., Snoek, L. B., Kirschner, J., and Verhoeven, K. J. F. (2016). Natural epigenetic variation contributes to heritable flowering divergence in a widespread asexual dandelion lineage. *Mol. Ecol.* 25, 1759–1768. doi: 10.1111/mec.13502

Conflict of Interest: The authors declare that the research was conducted in the absence of any commercial or financial relationships that could be construed as a potential conflict of interest.

Publisher's Note: All claims expressed in this article are solely those of the authors and do not necessarily represent those of their affiliated organizations, or those of the publisher, the editors and the reviewers. Any product that may be evaluated in this article, or claim that may be made by its manufacturer, is not guaranteed or endorsed by the publisher.

frontiers | Frontiers in Plant Science

ORIGINAL RESEARCH
published: 28 June 2022
doi: 10.3389/fpls.2022.904198

Integrate QTL Mapping and Transcription Profiles Reveal Candidate Genes Regulating Flowering Time in *Brassica napus*

Zigang Liu†, Xiaoyun Dong†, Guoqiang Zheng†, Chunmei Xu, Jiaping Wei, Junmei Cui, Xiaodong Cao, Hui Li, Xinlin Fang, Ying Wang and Haiyan Tian*

State Key Laboratory of Arid Land Crop Sciences, Gansu Agricultural University, Lanzhou, China

Flowering at the proper time is an important part of acclimation to the ambient environment and season and maximizes the plant yield. To reveal the genetic architecture and molecular regulation of flowering time in oilseed rape (*Brassica napus*), we performed an RNA-seq analysis of the two parents after vernalization at low temperature and combined this with quantitative trait loci (QTL) mapping in an F_2 population. A genetic linkage map that included 1,017 markers merged into 268 bins and covered 793.53 cM was constructed. Two QTLs associated with flowering time were detected in the F_2 population. qFTA06 was the major QTL in the 7.06 Mb interval on chromosome A06 and accounted for 19.3% of the phenotypic variation. qFTC08 was located on chromosome C06 and accounted for 8.6% of the phenotypic variation. RNA-seq analysis revealed 4,626 differentially expressed genes (DEGs) between two parents during vernalization. Integration between QTL mapping and RNA-seq analysis revealed six candidate genes involved in the regulation of flowering time through the circadian clock/photoperiod, auxin and ABA hormone signal, and cold signal transduction and vernalization pathways. These results provide insights into the molecular genetic architecture of flowering time in *B. napus*.

Keywords: flowering time, QTL mapping, RNA-seq, candidate genes, *Brassica napus*

OPEN ACCESS

Edited by:
Sara Zenoni,
University of Verona, Italy

Reviewed by:
Carlo Bergamini,
Council for Agricultural and Economics Research (CREA), Italy
Wangsheng Zhu,
China Agricultural University, China

***Correspondence:**
Zigang Liu
lzgworking@163.com

†These authors have contributed equally to this work

Specialty section:
This article was submitted to Plant Breeding, a section of the journal Frontiers in Plant Science

Received: *25 March 2022*
Accepted: *12 May 2022*
Published: *28 June 2022*

Citation:
Liu Z, Dong X, Zheng G, Xu C, Wei J, Cui J, Cao X, Li H, Fang X, Wang Y and Tian H (2022) Integrate QTL Mapping and Transcription Profiles Reveal Candidate Genes Regulating Flowering Time in Brassica napus. Front. Plant Sci. 13:904198. doi: 10.3389/fpls.2022.904198

HIGHLIGHTS

- Two QTLs associated with flowering time were identified in *Brassica napus*.
- The integration of QTL mapping and RNA-seq data allowed for the detection of six candidate genes that play important roles in the regulation of flowering.

INTRODUCTION

Brassica napus is a major oil crop and the largest source of high-quality vegetable oil worldwide. There are three types (spring, winter, and semi-winter), categorized by the amount of low-temperature exposure needed for the transition from vegetative growth to flowering. Semi-winter types require little exposure to the low temperatures and are planted primarily in the Yangtze River

basin of southern China. Spring rapeseed is planted in the high latitude region of China, and winter rapeseed is planted in the low latitude region. Winter rapeseed has many advantages over spring rapeseed, including grain yield, seed quality, resistance to adversity, etc., however, winter rapeseed cannot survive winter in northern China due to extreme low temperatures ($<-20°C$). Several varieties (e.g., NTS57, Ganyou 4, Ganyou 221) were bred *via* distant cross to introduce the cold-tolerance of winter turnip rape (*B. rapa*) to winter oilseed rape, enabling these varieties to overwinter in northern China, which is important to alleviate the shortage of vegetable oil and prevent sand from blowing from the fallow fields. These cold-tolerant varieties require prolonged exposure to low temperatures to initiate flowering. Vernalization is critical for flowering, and therefore also to grain yield, adaptation, and survival of winter crops.

Insufficient exposure to low temperatures resulting in inadequate vernalization delays the flowering of winter-type crops. It is possible to evaluate the degree of vernalization and obtain phenotypic data that can then be used to detect QTLs related to the vernalization of winter-type crops. A recombinant inbred line (RIL) wheat population was used to identify 15 QTLs linked to vernalization on nine chromosomes, and these QTLs accounted for 17 to 46% of phenotypic variation (Li et al., 2020). In total, five QTLs in four linkage groups accounted for 5.4 to 28.0% of the phenotypic variation in vernalization in an F_2 population derived from two varieties of perennial ryegrass (Jensen et al., 2005). In the rapeseed, flowering time was used to evaluate vernalization in 127 RIL population lines and identify QTLs linked to vernalization. In total, two QTLs (dtf7.1 and dtf1.1) in two linkage groups accounted for 53.1 and 8.3% of the phenotypic variation, respectively (Lee et al., 2021). One double haploid (DH) population was used to identify five consensus QTLs in the three environments, including two major QTLs located on chromosomes A03 and C08, respectively (Lee et al., 2021). Raman et al. (2012) used the flowering time to detect > 20 QTLs, including seven related to vernalization that accounted for 59.4% of the phenotypic variation. Four indexes of phenotype in the DH population in six environments were used to identify QTLs, and two vernalization QTLs in chromosomes A02 and A07 were identified (Shen et al., 2018). F_2 progeny and an $F_{2:3}$ population were used to identify 10 QTLs related to flowering time in four environments, one of which may be a novel QTL on chromosome A09 (Xu et al., 2020).

Several cold-tolerant *B. napus* varieties that can survive below $-25.6°C$ were bred in our laboratory. These strong winter types require more exposure to low temperatures for vernalization than do semi-winter and winter types, and this suggests that novel QTLs are responsible for regulating vernalization. In addition, if flowering time can be efficiently regulated using artificial measures, heterosis between two ecotypes (spring and strong winter types) can be exploited, and this is crucial for yield breeding of *B. napus*. Therefore, F_2 mapping of a spring-ecotype population derived from NTS57 and CY12 was used to detect QTLs related to the flowering time and vernalization for efficient breeding applications.

MATERIALS AND METHODS

An F_2 population was generated from a cross between two *B. napus* varieties, NTS57 (late-flowering, strong winter-type) and CY12 (early-flowering, spring-type), consisting of 174 individuals for QTL mapping. F_2 seeds were first sowed into plugs with 45 holes filled with nutrient soil in a greenhouse at the Gansu Agriculture University in Lanzhou of China. One seed per hole was sowed to foster seedlings, and 4 weeks after sowing them, they were transplanted into 25 cm diameter pots. The temperature in the phytotron was maintained in the range from 18 to 22°C. About 9 weeks after sowing, seedlings were transplanted into a phytotron with a constant temperature of 4°C and an 8-h light period and placed for 40 days in the phytotron. After vernalization accomplishment, seedlings were returned to the greenhouse, and the growth situation of seedlings was observed every day to accurately record the date of the first flowering. Leaf of 9 weeks' seedlings per F_2 individual was harvested. Per sample was quick-frozen in liquid nitrogen, and stored at −80°C to extract DNA for genotype detection and construction of a genetic map.

Seeds of two parents, i.e., 17NTS57 and CY12, were sown into pots in the greenhouse with temperature ranging from 18 to 22°C. The 9 weeks seedlings of the two parents were harvested (T0), and after harvesting, seedlings were placed into the phytotron with a temperature as low as 4°C for vernalization. Leaves of two parents were harvested on 20 days (T1) and 40 days (T2), respectively, after initiating vernalization. Leaves harvested were quick-frozen and stored at −80°C to extract RNA for transcriptome and qRT-PCR analysis.

Calculation of the Number of Days of First Flowering

Flowering time (FT), i.e., the number of days from sowing to the first flowering is a phenotypic date using QTL analysis, which was calculated using the following formula: FT = the date of first flowering from the date of sowing.

DNA Extraction and Targeted Sequencing

Following the protocols of Doyle and Doyle (1990), genomic DNA from the young expanded leaves was extracted from each F_2 plant. After quality assessment, each DNA sample was used to construct a library and perform targeted sequencing as described by GENOSEQ company (Wuhan, China). As sequence regions with known polymorphisms are attempted as targets for amplicon fragments, we utilized a total of 1,010 existing primer pairs from the previous SNP genotyping assays to target specific loci. These primers were mixed together in equal proportions. Mixed primers were diluted to ca. 54 nM aliquots and were used for multiplex PCR to amplify the intended target loci of each genome from F_2 progeny. Products in the amplified pools were modified by adding sequencing primer tags through secondary PCR. Modified pools were used to construct libraries for each individual. The effective concentration of libraries was determined by qRT-PCR. Libraries with more than 2 nM of the

effective concentration were selected for sequencing by Paired-end 150 bp Method in the Illumina HiSeq system. After filtering unclean reads from raw reads obtained by sequencing, clean reads were obtained, which were mapped to the reference genome (ZS11-v20200127) using the MEM algorithm in BWA software. The mapping rate, coverage scope, coverage depth, and coverage uniformity of the reference genome were assessed.

Linkage Map and QTL Analysis

Loci polymorphisms of the clean reads mapped to the reference were detected using GATK software (version 3.7), and single-nucleotide polymorphisms (SNPs) and insertions and deletions (InDels) were obtained to construct a linkage map of the F_2 population according to the methods of Xie et al. (2010). QTLs were detected by a composite interval mapping method using QTL Cartographer software (version 1.17j). The LOD thresholds of the QTLs were determined by a 1,000 permutation test at a 95% confidence level.

RNA-seq Analysis

RNA was extracted from the leaves of two parents (NTS57 and CY12) after treatment at low temperature for vernalization and used in the subsequent RNA-seq. Total RNA was extracted using TRIzol Reagent (Tiange Biotech, China) according to the manufacturer's instructions. The library construction and sequencing were performed by Gene Denovo Biotechnology Co. (Guangzhou, China) on an Illumina HiSeqTM2500 platform. The raw sequences generated from the Illumina sequencing were filtered to remove the adaptor sequences and low-quality sequence reads from the data sets. Clean reads were then mapped to the *B. napus* reference genome using TopHat2 (version 2.0.3.12) (Kim et al., 2013). The gene expression level was calculated by the reads per kb per million reads. Genes with a fold change ≥ 2 and a p-value < 0.01 were filtered as DEGs using the edgeR package[1]. Enrichment analysis of the DEGs was accomplished based on the gene ontology (GO) database and Kyoto Encyclopedia of Genes and Genomes (KEGGs) database. Both GO terms and KEGG pathways with a Q-value of ≤ 0.05 were significantly enriched by DEGs. The clustered profiles with a p-value of ≤ 0.05 were considered to be significant profiles. The RNA-seq raw data have been submitted to the SRA of NCBI with the accession number Sra552729.

Total RNA Extraction and Real-Time Quantitative PCR

Total RNA in leaves was extracted as per the manufacturer's instructions (TIANGEN Biotech (Beijing) Co., Ltd.), and RNA integrity was detected by the electrophoresis. The RNA was reverse-transcribed (PrimeScript™ RT Reagent Kit with gDNA Eraser, TaKaRa) to obtain single-stranded cDNA. In total, three replicates were performed for each sample. After measuring the concentration, the cDNA was stored at −20°C. The primers used for real-time quantitative PCR (qRT-PCR) were listed in **Supplementary Table 1**. qRT-PCR amplification reactions were performed using a LightCycler®96 RTPCR System (Roche, Basel, Switzerland) with SYBR qPCR Mix (Invitrogen, California, United States). *Actin-1* was used as an internal reference, and the relative expression of each gene was analyzed using the $2^{-\Delta\Delta Ct}$ method.

[1]http://www.r-project.org/

TABLE 1 | Statistical analysis of parents, F1, and F2 progeny for flowering time.

Parents Mean		F1	F2		
NTS57	CY12	Mean ± SD	Range	Mean ± SD	Heritability
121 ± 3.79	101 ± 2.52**	118 ± 4.44	93-123	109 ± 3.27	0.621

***Represents the extremely significant level between two parents.*

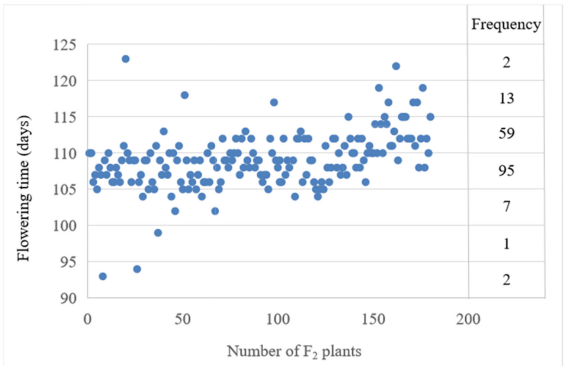

FIGURE 1 | Frequency and distribution of the phenotypic value of the flowering time and frequency in the interval spanning 10 days were labeled on the right.

RESULTS

Phenotypic Feature of Flowering Time

For the number of days from sowing to first flowering, i.e., flowering time, the phenotypic data showed significant differences between the two parents. The flowering time of the late-flowering parent NTS57 is 121 and 20 days later than the early-flowering parent CY12 (**Table 1**). The flowering time of F_2 individuals ranged from 93 to 123 days, with an interval of 30 days. The flowering time of F_2 plants exhibited normal distribution, showing features of quantitative hereditary traits. The broad sense heritability of FT trait among F_2 progeny is 0.621 (**Table 1**). The flowering time of three individuals in the F_2 population ranged from 2 to 8 days earlier than that of the early-flowering parent CY12, and that of two individuals was later than that of the late-flowering parent NTS57. These earlier- or later-flowering individuals are of higher value in the rapeseed breeding compared with the two parents (**Figure 1**).

A Targeted Sequence of F_2 Population and Variation Analysis

The mean coverage of the genome percentage and mean genome coverage depth of the parents and F_2 families were 0.08% and 108.29×, respectively. After filtrating, low-quality reads from raw reads obtained by the targeted sequencing of the two parents and 178 F_2 plants, there was an average of 308.56 thousand clean reads per plant, including 88.62 million bases. A total of 1,034 variants were obtained through comparison of the genotype of the two

parents, including 946 SNPs, 88 InDels, 563 transitions (i.e., 282 A/G and 281 C/T), and 378 transversions. Among InDels, one- and two-base deletions/insertions were the most common. These variants were distributed equally throughout the genome.

Construction of the Genetic Linkage Map

A total of 1,034 markers showing polymorphism between the two parents were used to construct a genetic linkage map, 1,017 of which were grouped into 19 linkage groups. The total length of the linkage map was 793.53 cM, and the average genetic distance between the two adjacent markers was 0.051 cM. Several markers lacking signs of recombination between adjacent markers were merged into one bin, and 268 bins were contained in this linkage map with an average genetic distance of 0.233 cM between the two adjacent bins. The linkage group with the longest genetic length was C06, which was also the linkage group with the largest number of bins (28). The linkage group with the lowest number of bins (2 bins containing 19 markers) was A10, and its genetic distance (6.43 cM) was the shortest (**Table 2**).

QTL Mapping of Flowering Time

A total of two QTLs (qFTA06 and qFTC08) associated with the flowering time were detected on two chromosomes (A06 and C08) in the F_2 population, with LOD values of 2.39 and 2.85, respectively. qFTA06 accounted for 19.3% of the phenotypic variation and was located on an 8.8 cM interval from 47.47 to 56.27 cM, mapping to the physical interval from 41.5 to 48.5 Mb on chromosome A06 of reference genome ZS11. qFTC08 accounted for 4.60% of the phenotypic variation and was located at the interval from 0.01 to 10.95 cM of the C08 linkage group (**Table 3** and **Figure 2**).

Illumina Sequencing and Mapped Clean Reads

To verify transcription-level changes, six cDNA libraries were constructed using total RNA extracted from the leaves of two winter rapeseed varieties, NTS57 and CY12, treated at low temperature for 20 (t1) and 40 (t2) days and continuous room temperature (t0). The *de novo* transcriptome assembly and annotation were implemented. A Phred quality score of > 30 (Q30) was > 92%, and the guanine-cytosine (GC) content was consistently 48% for the four samples, indicating that the sequencing results were satisfactory. Raw sequences from cDNA libraries were filtered to obtain high-quality clean reads. After trimming and removing low-quality reads and ribosomal RNAs, 845.5 million clean reads remained and were used for quantitative analysis of gene expression. These clean reads were mapped to the reference *B. napus* genome using Tophat 2 software (2.1.1 versions), and 77.96–81.35% of the clean reads were mapped successfully to the genome, including 65.61–68.24% of the unique mapped reads and 12.35–13.11% of the multiple mapped reads. The remaining 18.65–22.04% of the reads were unmapped to the genome (**Table 4**). A total of 78,197 genes were detected across all the samples of both varieties, including 6,387 new genes and 71,810 known genes.

Differences in Gene Expression Between Early- and Late-Flowering Varieties

To identify the important genes related to flowering time, the difference in gene expression between two varieties, early-flowering CY12 and late-flowering NTS57, was analyzed. NTS57 seedlings were maintained at low temperature for 20 days and contained 19,456 significant DEGs, including

TABLE 2 | Detailed information of the genetic map constructed in the F_2 population.

Chr	Length (cM)	No. markers	No. bins	Marker interval (cM)	Bin interval (cM)	Max interval (cM)
A01	35.072	87	18	0.408	2.063	5.735
A02	33.136	29	8	1.183	4.734	13.881
A03	57.528	27	5	2.213	14.382	37.445
A04	33.901	43	12	0.807	3.082	10.371
A05	16.362	48	8	0.348	2.337	5.335
A06	57.659	29	8	2.059	8.237	31.912
A07	36.537	36	6	1.044	7.307	14.325
A08	43.029	25	8	1.793	6.147	38.078
A09	42.131	49	11	0.878	4.213	7.265
A10	6.430	19	2	0.357	6.430	6.430
C01	42.278	81	19	0.528	2.349	11.356
C02	41.460	110	24	0.380	1.803	6.131
C03	58.663	52	12	1.150	5.333	15.542
C04	49.281	99	26	0.503	1.971	9.789
C05	24.294	43	13	0.578	2.025	7.159
C06	59.922	78	28	0.778	2.219	8.697
C07	59.180	31	13	1.973	4.932	28.748
C08	59.043	62	22	0.968	2.812	7.066
C09	37.622	69	25	0.553	1.568	11.062
Whole	793.528	1,017	268	0.974	4.418	14.544
Mean	41.765	53.526	14.105	0.051	0.233	0.765

TABLE 3 | Detailed information of QTL for flowering time.

QTL	Chr	Pos(cM)	LOD	R^2	Additive effect	Dominant effect	Confidence interval	Bin interval	Physical interval
qFTA06	A06	51.98	2.39	19.30%	8.22	1.42	47.47-56.27	c06b005-c06b008	41514735-48581582
qFTc08	C08	6.95	2.85	8.60%	–3.43	–0.48	0.01-10.95	C08b001-c08b006	859254-28988144

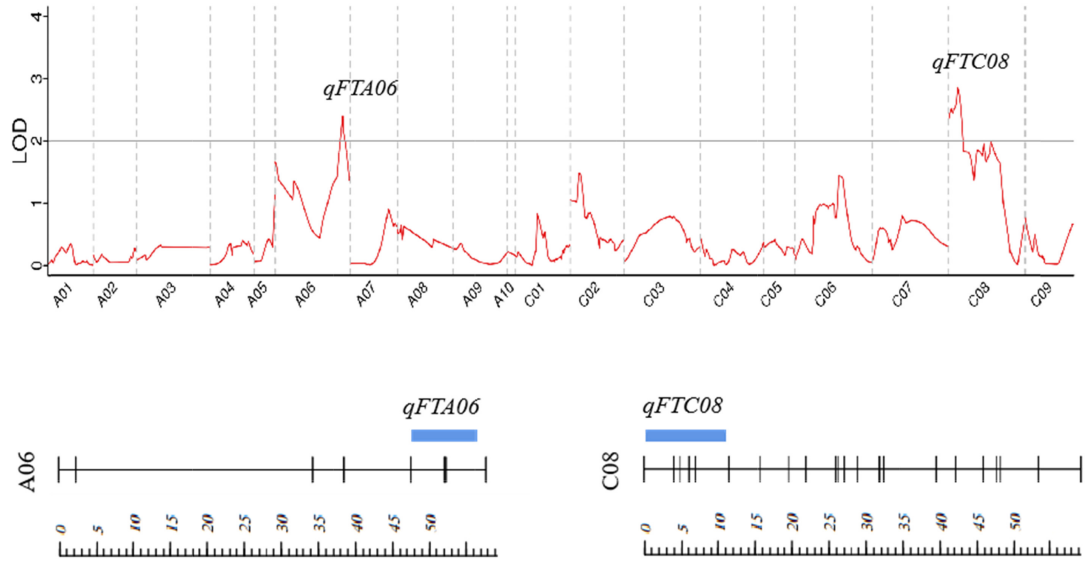

FIGURE 2 | Distribution of the putative QTLs for flowering time on the genetic map. Strips represent QTLs detected, and their location and length represent their location of QTL on the linkage map and interval span. The scale represents the genetic distance (cM).

TABLE 4 | Summary of the read numbers from the RNA-seq data for the four samples.

	Total reads	Unmapped reads		Unique mapped reads		Multiple mapped reads		Mapping ration
NTS57t0	144693890	29195649	20.18%	97189781	67.17%	18308460	12.65	79.82%
NTS57t1	155353088	30407162	19.57%	105202728	67.72%	19743198	12.71	80.43%
NTS57t2	128926068	26973068	20.92%	85748328	66.51%	16204672	12.57	79.08%
CY12t0	132109208	24637786	18.65%	90156636	68.24%	17314786	13.11	81.35%
CY12t1	128026106	28219780	22.04%	83998414	65.61%	15807912	12.35	77.96%
CY12t2	141845114	27246114	19.21	96320426	67.91%	18278574	12.89	80.79%

12,866 upregulated and 7,086 downregulated DEGs. NTS57 seedlings were maintained at low temperature for 40 days and contained 21,228 significant DEGs, including 11,103 upregulated and 10,125 downregulated DEGs (**Figure 3**). NTS57 seedlings were maintained at normal temperature and contained 10,820 DEGs, including 10,366 upregulated and 7,874 downregulated DEGs ($|\log2(TP/SP)| > 1$ and $P \leq 0.001$).

In total, 11,594 DEGs were common to both 20-day- and 40-day-exposed *B. napus*, including 6,654 upregulated and 4,940 downregulated DEGs. Of these, 4,626 DEGs (2,842 upregulated and 1,784 downregulated), were specific to low-temperature vernalization, and these were most likely the basis for variation in flowering time. Therefore, these 4,642 genes were used to further narrow the region containing QTLs related to the flowering time (**Figure 4**).

Analysis of the Crossover Between the Candidates Identified by QTL Mapping and RNA-seq Reduced the Number of Responsible Genes

RNA-seq analysis was used to narrow down the candidate genes identified *via* QTL mapping and identify specific DEGs associated with vernalization at low temperature in early- and late-flowering *B. napus* genotypes. A total of 4,642 specific genes were identified by RNA-seq., and we speculate that some important genes affecting variations in flowering time were included in these gene groups. Two QTLs related to the flowering time, qFTA06 and qFTC08, were found on the chromosomes A06 and C08, respectively. A total of 2,926 genes were distributed in two QTL regions, including 1,194 genes in the qFTA06 region and 1,732 genes in the qFTC08 region. Crossover analysis was used

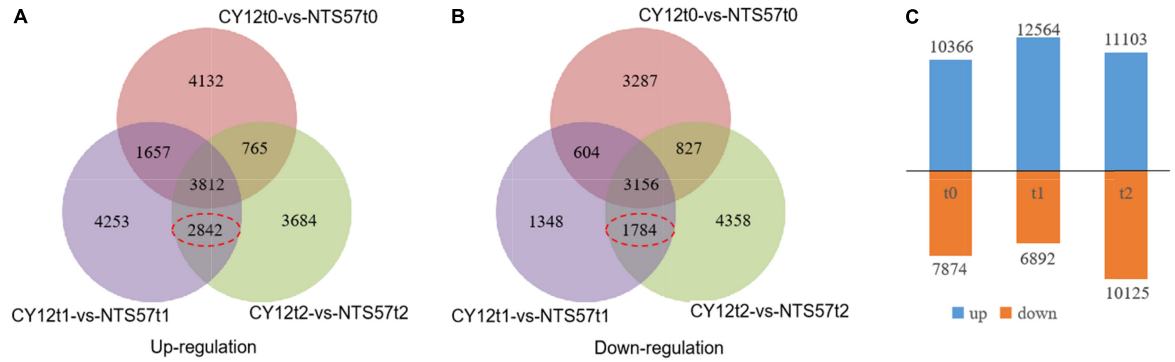

FIGURE 3 | Gene expression profiles and the differentially expressed genes (DEGs) identified between early- and late-flowering genotypes. The Venn diagram shows the numbers of upregulated **(A)** and downregulated **(B)** DEGs between two varieties with the different flowering times under three temperature treatments and the number of overlaps. The number of DEGs is shown in **(C)**.

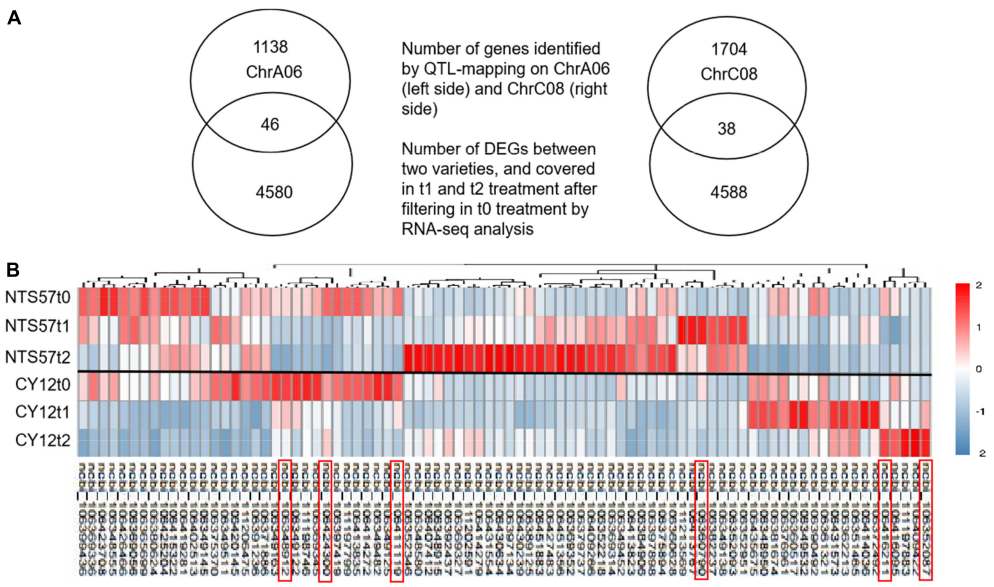

FIGURE 4 | Overlap in the DEGs identified using RNA-seq and located in QTLs. **(A)** The Venn diagram shows the number of genes located in QTLs related to the flowering time, the number of DEGs in the two varieties at low temperature, and the number of overlaps. **(B)** Heatmap showing clustered gene expression in early- and late-flowering genotypes. Different colors represent different expression levels in the late-flowering variety NTS57 and the early-flowering variety CY12 under three temperature treatments. The candidate genes selected that relate to flowering time are marked with a red rectangle.

to integrate QTL mapping and global transcriptomic data. In total, eighty-four DEGs in early- and late-flowering varieties at low temperature were found in two QTL regions related to the flowering time. Of these, 46 genes were located in the qFTA06 region, and 38 genes were located in the qFTC08 region. A total of fifty-six genes was upregulated and 28 genes were downregulated in the late-flowering genotype (**Figure 4**). In total, six genes were candidate genes affecting flowering and were involved in flower differentiation, flowering time, and floral organ formation. The IDs of the candidate genes and their annotations are listed in **Table 5**. *BnaC08G0115300ZS*, located in the qFTC08 region and encoding a rapid alkalinization factor (RALF32), belongs to a family of cysteine-rich plant peptide hormones that are involved in the multiple physiological and developmental processes such as growth and development of shoots, buds, anther, and pollen. RALF32 binds to CrRLK1L FERONIA (FER) to inhibit the development of the shoot apex (Abarca et al., 2021). *BnaC08G0356200ZS* encodes plant-specific Rop nucleotide exchange factor 6, which regulates many developmental processes such as the transition from vegetative growth to the reproduction of flowering plants through the auxin and ABA-signaling pathways (Zhang and McCormick, 2007; Kim et al., 2020). *BnaA06T0437200ZS* encodes a transcription activator GLK2-like (also called mitogen-activated protein kinase; MAPK) that belongs to the serine/threonine kinase family and is involved in the vernalization pathway in the cold signal perception and responsive networks (Gou et al., 2018; Xu and Chong, 2018; Chuang and Tan, 2019). *BnaC08G0010400ZS*

TABLE 5 | Candidate genes narrowed down by QTL-mapping and RNA-seq experiments and their annotations.

Candidate Gene	Regulation	Pfam_annnotation	Description
BnaA06G0363000ZS	Down	Protein of unknown function (DUF760)	UV-B-induced protein At3g17800, chloroplastic [Brassica rapa]
BnaA06G0437200ZS	Down	Myb-like DNA-binding domain	transcription activator GLK2-like [Brassica napus]
BnaA06G0332400ZS	Up	hypothetical protein	Flowering-promoting factor 1 OS = Sinapis alba GN = FPF1 PE = 2 SV = 1
BnaC08G0115300ZS	Down	Rapid ALkalinization Factor (RALF)	protein RALF-like 32 [Brassica oleracea var. oleracea] [Brassica oleracea]
BnaC08G0356200ZS	Up	PRONE (Plant-specific Rop nucleotide exchanger)	rop guanine nucleotide exchange factor 6 isoform X1 [Brassica napus]
BnaC08G0010400ZS	Down	DNA photolyase	cryptochrome-2 [Brassica napus];Cryptochrome-2 OS = Arabidopsis thaliana GN = CRY2 PE = 1 SV = 2

The 'down' or 'up' indicate the downregulation or upregulation of gene expression at the low temperature relative to that at the normal temperature.

encodes Cryptochrome 2 (CRY2), a conserved photoreceptor that accelerates flowering time by regulating the circadian clock (El-Din et al., 2003; Nefissi et al., 2011; Wu et al., 2021). *BnaA06T0363000ZS,* an ortholog of *At3G17800* that encodes a UV-B-induced protein with an unknown function, was significantly downregulated in two varieties of rapeseed during low-temperature vernalization. *BnaC08G0010400ZS* encodes a hypothetical protein that is a homolog of the flowering-promoting factor (FPF1) in *Arabidopsis*. FPF1 confers the promotion of flowering time by affecting auxin homeostasis.

Expression of Candidate Genes in the Early- and Late-Flowering Varieties

To investigate variation in candidate gene expression, total mRNAs were extracted from leaves of early- and late-flowering varieties treated at low temperature for 20 (t1) and 40 (t2) days for vernalization and from unvernalized samples as a control (t0). The mRNA levels of the candidate genes were detected using qRT-PCR. The expression of *BnaA06TG0363000ZS, BnaA06T0437200ZS*, and *BnaC08T0115300ZS* was significantly lower in the early-flowering variety than in the late-flowering variety. Conversely, the expression of *BnaA06G0332400ZS, BnaC08T0356200ZS*, and *BnaC08G0010400ZS* was significantly higher in the early-flowering variety than in the late-flowering variety (**Figure 5**). This pattern was consistent at both the RNA-seq and mRNA levels, indicating that the RNA-seq results were reliable in this study.

DISCUSSION

As a sessile organism, winter rapeseed is exposed to a wide range of ambient cues and must adjust its growth and development according to this environmental variation. For overwintering or biennial crops, flowering at the proper time and in season is vital to avoid ambient damage and improve crop yield (Xu and Chong, 2018). In the northern region of China, winter rapeseed is planted in early autumn and flowers the following spring. Winter is long and frosty; therefore, strong winter rapeseed genotypes are required to avoid premature flowering (Liu et al., 2021). Simultaneously, the winter low temperatures provide sufficient cold for vernalization to initiate floral transition the following spring. In China, winter rapeseed is primarily distributed in the Yangtze River valley. No existing winter variety can survive in this cold and arid region. Fortunately, several strong winter varieties were bred by our laboratory, and these varieties have been planted successfully in cold and arid regions. Flowering time is one of the most important adaptive traits in the winter rapeseed. In previous studies, populations developed by crossing early- and late-flowering *B. napus* genotypes (e.g., RILs, DH, F_2, $F_{2:3}$ posterities) were used in QTL analyses of the flowering time. Several QTLs associated with flowering time have been reported, and all but three of these (Chr. A01, A09, and C01) are distributed on 16 chromosomes (Fletcher et al., 2015; Jian et al., 2019; Scheben et al., 2020; Xu et al., 2020; Song et al., 2021 and **Supplementary Figure 1**). Both minor QTLs with small phenotypic contributions and major QTLs accounting for > 10% of the phenotypic variation have been reported. For example, Li et al. (2018) identified 100 QTLs associated with flowering time using a DH population containing 348 lines. These included 25 major QTLs located on chromosomes A06, A02, A03, and C06 that explained > 10% of the phenotypic variation. Two QTLs associated with flowering time were located on chromosomes A10 and C06 in an F_2 population (Li et al., 2018). In this study, two QTLs associated with flowering time were found in two regions on chromosomes A06 and C08 in F_2 progeny developed by hybridizing strong winter genotype (NTS57) and spring genotype (CY12), respectively. One of these, qFTC08, was found in the 28.1 Mb interval of chromosome C08 and accounted for 8.6% of the phenotypic variation. The other, qFTA06, is a major QTL found in the 7.06 Mb interval of chromosome A06 and accounts for 19.3% of the phenotypic variation. QTL analysis identified molecular markers correlating with flowering time and allowed for the selection of oilseed rape based on the molecular markers.

RNA-seq was used to detect DEGs in strong winter and spring types during vernalization. A total of 4,626 DEGs, including 2,842 upregulated and 1,784 downregulated DEGs, were identified, and their expression differed only at low temperatures during vernalization and not at normal temperatures. Several important genes for flowering time may be among these, and their differential expression may be the molecular basis of variation in flowering time between two varieties of oilseed rape. In QTL regions, qFTA06 and qFTC08, 1,138 and 1,704 genes were included, respectively. To narrow down genes that are important for flowering time, QTL mapping and RNA-seq results were integrated. In total, 2,842 genes were identified by QTL mapping

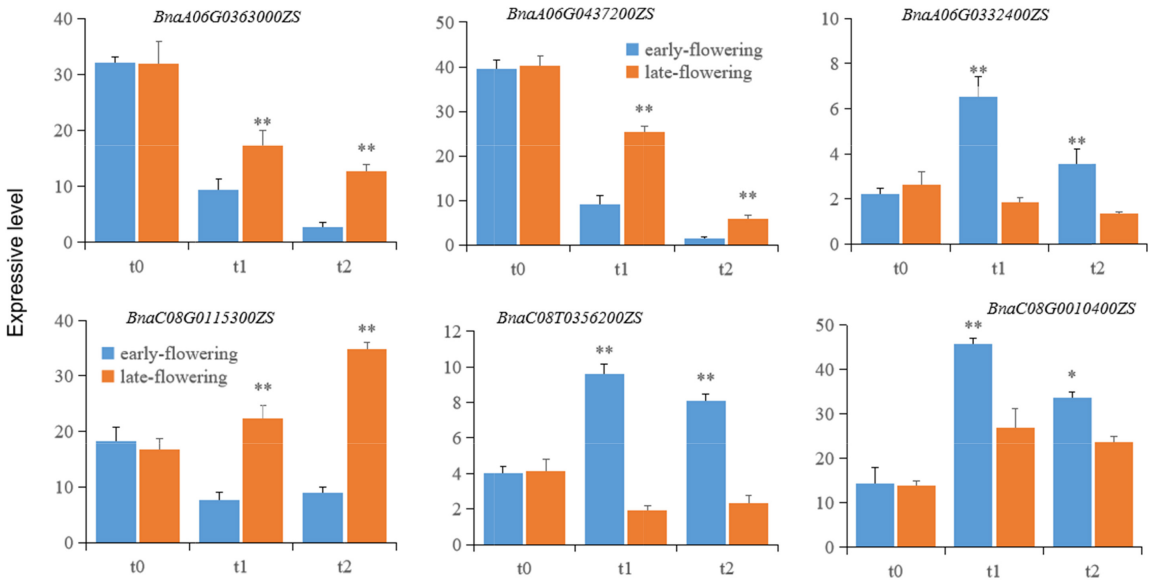

FIGURE 5 | The expression of putative genes related to flowering time in early- and late-flowering *B. napus* varieties during vernalization. Each candidate gene is labeled in the upper part of each panel. t0, t1, and t2 represent unvernalization and vernalization treatments for 20 and 40 days. Single and double asterisks (*,**) indicate statistical significance relative to the control at $p < 0.05$ and $p < 0.01$, respectively. The error bars represent the standard variations.

and 4,626 DEGs revealed by RNA-seq were crossed and 84 overlapping genes were identified. In a subsequent analysis of KO items and the KEGG pathway, six genes were identified as candidates involved in flowering.

The six genes included in the major flowering pathway regulate the circadian clock/photoperiod, vernalization, auxin and ABA signaling, and the MAPK cascade in the cold signal transduction pathway. *BnaC08G0115300ZS* encodes a plant peptide hormone involved in the differentiation of the shoot apex (Abarca et al., 2021). Shoot apices can differentiate into either flower buds and flowers or branch buds and branches. *BnaC08G0010400ZS* encodes a homolog of FPF1 that modulates flowering time (Wang et al., 2014), and overexpression of FPF1 causes early flowering (Ge et al., 2004). In rice, FPF1-like protein 4 (OsFPFL4) is a homolog of AtFPF1 that modulates auxin homeostasis to control flowering time (Guo et al., 2020). *BnaC08G0115300ZS* expression is higher in the late-flowering *B. napus* genotype than in the early-flowering genotype, suggesting that this gene suppresses flowering. *BnaC08G0356200ZS* encodes plant-specific Rop nucleotide exchange factor 6, which is involved in the regulation of the auxin and ABA-signaling pathway. The ABA-signaling pathway is involved in the regulation of photoperiod and circadian rhythms and promotes floral transition (de Montaigu et al., 2010). In our study, *BnaC08G0356200ZS* was upregulated and was higher in the early-flowering genotype, which implies that the upregulation of these two genes promotes oilseed rape flowering. *BnaA06G0437200ZS* encodes an ortholog of a transcription activator MAPK involved in the perception and transduction of the cold signal required for vernalization (Gou et al., 2018; Xu and Chong, 2018; Chuang and Tan, 2019). *BnaC08G0010400ZS* and *BnaA06T0363000ZS* regulate photoperiod and influence flowering (El-Din et al., 2003; Nefissi et al., 2011; Wu et al., 2021). In this study, these candidate genes were differentially expressed between early- and late-flowering genotypes during vernalization, which suggests that these candidate genes are important in regulating the floral translation of oilseed rape.

CONCLUSION

In this study, a genetic linkage map was constructed based on 1,017 markers that merged into 268 bins covering 793.53 cM. Two QTLs were detected that were distributed on the two chromosomes, including one major QTL on chromosome A06 that accounted for 19.3% of the phenotypic variation. RNA-seq analysis identified 4,626 DEGs between early- and late-flowering genotypes during vernalization. Integrated analysis using QTL mapping and RNA-seq identified 84 DEGs in the QTL regions. Of these, six candidate genes were involved in the regulation of flowering time and played an important role in the flowering-related pathways.

DATA AVAILABILITY STATEMENT

The original contributions presented in the study are included in the article/**Supplementary Material**, further inquiries can be directed to the corresponding author/s.

AUTHOR CONTRIBUTIONS

ZL, XD, GZ, HL, XF, YW, and HT conceived the study. GZ, CX, XC, and HL developed the experimental populations. JW and

JC completed the phenotyping, genotyping, and bioinformatic analyses. XD and GZ performed the linkage mapping. GZ completed the gene expression analyses. All authors contributed to the writing and/or editing of the manuscript and approved the final version of the manuscript.

FUNDING

This research was funded by the State Key Laboratory of Aridland Crop Science, Gansu Agricultural University (GSCS-2021-Z01), Industrial Support Plan Project of Gansu (2021CYZC-46), Young Doctoral Fund of Gansu (2021QB-035), Special funds from the central government to guide local scientific and technological development of China (ZCYD-2020-2-3), Ministry of Science and Technology of China (2018YFD0100500), and National Natural Science Foundation of China (31660404). The fund information (Ministry of Science and Technology of China) should been revised to (National Key Basic Research and Development Program of China).

SUPPLEMENTARY MATERIAL

The Supplementary Material for this article can be found online at: https://www.frontiersin.org/articles/10.3389/fpls.2022.904198/full#supplementary-material

REFERENCES

Abarca, A., Christina, M. F., and Zipfel, C. (2021). Family-wide evaluation of rapid alkalinization factor peptides. *Plant Physiol.* 187, 996–1010. doi: 10.1093/plphys/kiab308

Chuang, H., and Tan, H. (2019). MAP4K3/GLK in autoimmune disease, cancer and aging. *J. Biomed. Sci.* 26:82. doi: 10.1186/s12929-019-0570-5

de Montaigu, A., Toth, R., and Coupland, G. (2010). Plant development goes like clockwork. *Trends Genet.* 26, 296–306. doi: 10.1016/j.tig.2010.04.003

Doyle, J. J., and Doyle, J. L. (1990). *Isolation of Plant DNA from Fresh Tissue 12*. Madison, WI: Focus, 13–15.

El-Din, S., Alonso-Blanco, C., Peeters, A. J., Wagemaker, C., Weller, J. L., and Koornneef, M. (2003). The role of cryptochrome 2 in flowering in *Arabidopsis*. *Plant Physiol.* 133, 1504–1516. doi: 10.1104/pp.103.029819

Fletcher, R. S., Mullen, J. L., Heiliger, A., and McKay, J. K. (2015). QTL analysis of root morphology, flowering time, and yield reveals trade-offs in response to drought in *Brassica napus*. *J. Exp. Bot.* 66:25371500. doi: 10.1093/jxb/eru423

Ge, L., Chen, H., Jiang, J., Zhao, Y., Xu, M., Xu, Y., et al. (2004). Overexpression of OsRAA1 causes pleiotropic phenotypes in transgenic rice plants, including altered leaf, flower, and root development and root response to gravity. *Plant Physiol.* 135, 1502–1513. doi: 10.1104/pp.104.041996

Gou, X. Y., Liu, D. F., and Chong, K. (2018). Cold signaling in plants: insights into mechanisms and regulation. *J. Int. Plant Biol.* 60, 745–756. doi: 10.1111/jipb.12706

Guo, Y., Wu, Q., Xie, Z., Yu, B., Zeng, R., Min, Q., et al. (2020). OsFPFL4 is involved in the root and flower development by affecting auxin levels and ROS accumulation in rice (*Oryza sativa*). *Rice* 13:31912314. doi: 10.1186/s12284-019-0364-0

Jensen, L. B., Andersen, J. R., Frei, U., Xing, Y., Taylor, C., Holm, P. B., et al. (2005). QTL mapping of vernalization response in perennial ryegrass (*Lolium perenne* L.) reveals co-location with an orthologue of wheat VRN1. *Theor. Appl. Genet.* 110, 527–536. doi: 10.1007/s00122-004-1865-8

Jian, H., Zhang, A., Ma, J., Wang, T., Yang, B., Shuang, L. S., et al. (2019). Joint QTL mapping and transcriptome sequencing analysis reveal candidate flowering time genes in *Brassica napus* L. *BMC Genom.* 20:30626329.

Kim, D., Pertea, G., and Trapnell, C. (2013). TopHat2: accurate alignment of transcriptomes in the presence of insertions, deletions and gene fusions. *Geno. Biol.* 14:R36. doi: 10.1186/gb-2013-14-4-r36

Kim, E. J., Park, S. W., Hong, W. J., Silva, J., Liang, W., Zhang, D., et al. (2020). Genome-wide analysis of RopGEF gene family to identify genes contributing to pollen tube growth in rice (*Oryza sativa*). *BMC Plant Biol.* 20:95. doi: 10.1186/s12870-020-2298-5

Lee, N., Fukushima, K., Park, H. Y., and Kawabata, S. (2021). QTL analysis of stem elongation and flowering time in lettuce using genotyping-by-sequencing. *Genes* 12:947. doi: 10.3390/genes12060947

Li, R., Jeong, K., Davis, J. T., Kim, S., Lee, S., Michelmore, R. W., et al. (2018). Integrated QTL and eQTL mapping provides insights and candidate genes for fatty acid composition, flowering time, and growth traits in a F population of a novel synthetic allopolyploid. *Front. Plant Sci.* 9:30483289. doi: 10.3389/fpls.2018.01632

Li, Y., Xiong, H., Guo, H., Zhou, C., Xie, Y., Zhao, L., et al. (2020). Identification of the vernalization gene VRN-B1 responsible for heading date variation by QTL mapping using a RIL population in wheat. *BMC Plant Biol.* 20:331. doi: 10.1186/s12870-020-02539-5

Liu, Z. G., Zou, Y., Dong, X. Y., Wei, J. P., Xu, C. M., Mi, W. B., et al. (2021). Germinating seed can sense low temperature for the floral transition and vernalization of winter rapeseed (*Brassica rapa*). *Plant Sci.* 307:110900. doi: 10.1016/j.plantsci.2021.110900

Nefissi, R., Natsui, Y., Miyata, K., Oda, A., Hase, Y., Nakagawa, M., et al. (2011). Double loss-of-function mutation in EARLY FLOWERING 3 and CRYPTOCHROME 2 genes delays flowering under continuous light but accelerates it under long days and short days: an important role for *Arabidopsis* CRY2 to accelerate flowering time in continuous light. *J. Exp. Bot.* 62:21296763. doi: 10.1093/jxb/erq450

Raman, H., Raman, R., Eckermann, P., Coombes, N., Manoli, S., Zou, X., et al. (2012). Genetic and physical mapping of flowering time loci in canola (*Brassica napus* L.). *Theor. Appl. Genet.* 126, 119–132. doi: 10.1007/s00122-012-1966-8

Scheben, A., Severn-Ellis, A. A., Patel, D., Pradhan, A., Rae, S. J., Batley, J., et al. (2020). Linkage mapping and QTL analysis of flowering time using ddRAD sequencing with genotype error correction in *Brassica napus*. *BMC Plant Biol.* 20:546–558. doi: 10.1186/s12870-020-02756-y

Shen, Y., Xiang, Y., Xu, E., Ge, X., and Li, Z. (2018). Major co-localized QTL for plant height, branch initiation height, stem diameter, and flowering time in an alien introgression derived brassica napus DH population. *Front. Plant Sci.* 9:390. doi: 10.3389/fpls.2018.00390

Song, J., Li, B., Cui, Y., Zhuo, C., Gu, Y., Hu, K., et al. (2021). QTL mapping and diurnal transcriptome analysis identify candidate genes regulating flowering time. *Int. J. Mol. Sci.* 22:34299178. doi: 10.3390/ijms22147559

Wang, X., Fan, S., Song, M., Pang, C., Wei, H., Yu, J., et al. (2014). Upland cotton gene GhFPF1 confers promotion of flowering time and shade-avoidance responses in *Arabidopsis thaliana*. *PLoS One* 9:e91869. doi: 10.1371/journal.pone.0091869

Wu, X. M., Yang, Z. M., Yang, L. H., Chen, J. R., Chen, H. X., Zheng, S. X., et al. (2021). Lilium × formolongi cryptochrome 2 from regulates photoperiodic flowering in transgenic. *Int. J. Mol. Sci.* 29:34884732. doi: 10.3390/ijms222312929

Xie, W., Feng, Q., Yu, H., Huang, X., Zhao, Q., Xing, Y., et al. (2010). Parent-independent genotyping for constructing an ultrahigh-density linkage map based on population sequencing. *Proc. Natl. Acad. Sci. U.S.A.* 107, 10578–10583. doi: 10.1073/pnas.1005931107

Xu, S., and Chong, K. (2018). Remembering winter through vernalisation. *Nat. Plants* 4, 997–1009. doi: 10.1038/s41477-018-0301-z

Xu, Y., Zhang, B., Ma, N., Liu, X., Qin, M., Zhang, Y., et al. (2020). Quantitative trait locus mapping and identification of candidate genes controlling flowering time in *Brassica napus* L. *Front. Plant Sci.* 2020:33613591. doi: 10.3389/fpls.2020.626205

Zhang, Y., and McCormick, S. (2007). A distinct mechanism regulating a pollen-specific guanine nucleotide exchange factor for the small GTPase rop in *Arabidopsis thaliana*. *PNAS* 104, 18830–18835. doi: 10.1073/pnas.0705874104

Conflict of Interest: The authors declare that the research was conducted in the absence of any commercial or financial relationships that could be construed as a potential conflict of interest.

Publisher's Note: All claims expressed in this article are solely those of the authors and do not necessarily represent those of their affiliated organizations, or those of the publisher, the editors and the reviewers. Any product that may be evaluated in this article, or claim that may be made by its manufacturer, is not guaranteed or endorsed by the publisher.

frontiers | Frontiers in Plant Science

ORIGINAL RESEARCH
published: 08 July 2022
doi: 10.3389/fpls.2022.925467

Controlled Induction of Parthenogenesis in Transgenic Rice *via* Post-translational Activation of *PsASGR-BBML*

Gurjot Singh Sidhu[1†], *Joann A. Conner*[1,2*†] *and Peggy Ozias-Akins*[1,2]

[1] *Institute of Plant Breeding, Genetics, and Genomics, University of Georgia, Tifton, GA, United States,* [2] *Department of Horticulture, University of Georgia, Tifton, GA, United States*

Modern plant breeding programs rely heavily on the generation of homozygous lines, with the traditional process requiring the inbreeding of a heterozygous cross for five to six generations. Doubled haploid (DH) technology, a process of generating haploid plants from an initial heterozygote, followed by chromosome doubling, reduces the process to two generations. Currently established *in vitro* methods of haploid induction include androgenesis and gynogenesis, while *in vivo* methods are based on uni-parental genome elimination. Parthenogenesis, embryogenesis from unfertilized egg cells, presents another potential method of haploid induction. PsASGR-BABY BOOM-like, an AP2 transcription factor, induces parthenogenesis in a natural apomictic species, *Pennisetum squamulatum (Cenchrus squamulatus)* and *PsASGR-BBML* transgenes promote parthenogenesis in several crop plants, including rice, maize, and pearl millet. The dominant nature of *PsASGR-BBML* transgenes impedes their use in DH technology. Using a glucocorticoid-based post-translational regulation system and watering with a 100 μM DEX solution before anthesis, PsASGR-BBML can be regulated at the flowering stage to promote parthenogenesis. Conditional expression presents a novel opportunity to use parthenogenetic genes in DH production technology and to elucidate the molecular mechanism underlying parthenogenetic embryogenesis.

Keywords: *PsASGR-BBML*, parthenogenesis, haploid induction, glucocorticoid receptor, dexamethasone

OPEN ACCESS

Edited by:
Silvia Vieira Coimbra, University of Porto, Portugal

Reviewed by:
Pablo Bolaños-Villegas, University of Costa Rica, Costa Rica
Maria Pilar Valles, Aula Dei Experimental Station (CSIC), Spain

***Correspondence:**
Joann A. Conner
jconner@uga.edu

[†] These authors have contributed equally to this work and share first authorship

Specialty section:
This article was submitted to Plant Breeding, a section of the journal Frontiers in Plant Science

Received: *21 April 2022*
Accepted: *25 May 2022*
Published: *08 July 2022*

Citation:
Sidhu GS, Conner JA and Ozias-Akins P (2022) Controlled Induction of Parthenogenesis in Transgenic Rice via Post-translational Activation of PsASGR-BBML. Front. Plant Sci. 13:925467. doi: 10.3389/fpls.2022.925467

INTRODUCTION

Doubled-haploid (DH) technology is used extensively in some crop breeding programs to generate homozygous lines from a heterozygous cross in two generations as compared to five to six generations with traditional breeding (Dunwell, 2010). To obtain doubled-haploids, DH technology involves inducing plants from a haploid gametophyte, followed by chromosome doubling, typically using mitotic inhibitors such as colchicine. In cross-pollinated crops such as corn and *Brassica* spp., which show a high degree of heterosis, this technology is used to develop inbred lines which are then crossed to produce superior hybrids (Ferrie and Möllers, 2011; Chaikam et al., 2019). In self-pollinated crops, such as wheat and rice, DH technology can be used to produce homozygous pure-lines from heterozygous F_1 progeny (Weyen, 2008).

Methods to induce haploids are mainly divided into two categories—*in vitro* and *in vivo*. *In vitro* methods involve tissue-culture techniques to regenerate haploid cells from microspores or unfertilized egg cells, which are differentiated to produce embryos and ultimately haploid plants. Anther culture is a popular technique for haploid induction in crops such as rice (Mishra and Rao, 2016) but has several limitations, including genotype specificity within a species (Forster et al., 2007). Other agricultural species such as woody plants and leguminous crops are often recalcitrant to this technique (Murovec and Bohanec, 2012). The culturing of un-pollinated floral buds or isolated ovaries on tissue-culture media is a technique used for DH production in onion and sugar beet (Bohanec, 2009).

In vivo methods generate haploids through uni-parental genome elimination or by inducing parthenogenesis in unfertilized egg cells. In uni-parental genome elimination, the genome of one parent (inducer line) gets removed from the diploid zygote resulting from a cross between two parents. An inducer line, Stock-6, and its derivatives, have been widely used for haploid induction in maize since the advent of DH technology. Since first reported in 1959 (Coe, 1959), 60 years of intensive breeding have increased the haploid induction rate (HIR) of Stock-6 from 3% to about 15% (Uliana Trentin et al., 2020). Two major QTLs, *qhir1* and *qhir8,* respectively, explain 66 and 20% of the HIR genotypic variance (Prigge et al., 2012). *qhir1* carries a 4 bp insertion in the fourth exon of the *MATRILINEAL* (*MTL*)/*NOT LIKE DAD* (*NLD*)/*ZmPHOSPHOLIPASE A1* (*ZmPLA1*) gene, which encodes a patatin-like phospholipase expressed primarily in pollen (Gilles et al., 2017; Kelliher et al., 2017; Liu et al., 2017). The identification of *MTL*/*NLD*/*ZmPLA* provided an opportunity to engineer HI in other crops and potentially create new HI lines in maize. A *de novo MTL* mutation in a non-inducer maize line—*mtl*/*mtl* gave a maximum HIR of 12.5% and an average HIR of 6.7% (Kelliher et al., 2017). An engineered *mtl*/*mtl* rice mutant yielded an HIR of about 6% with a 20% seed-set (Yao et al., 2018), while Wang et al. (2019) observed an HIR of 3.63% with about 11.5% seed-set. Changes to wheat orthologous genes, *TaMTL-4A*, *TaMTL-4B*, and *TaMTL-4D,* and the *Setaria italica* ortholog *SiMTL*, result in HIR rates of 11.8–31.6 and 1.75–3.49%, respectively (Yao et al., 2018; Liu et al., 2019). *qhir8* was identified as a DUF679 membrane protein—ZmDMP (Zhong et al., 2019). Unlike *MTL/NLD/ZmPLA*, which is conserved across monocots, *DMP-like* genes exist both in monocots and eudicots. The identification of *ZmDMP* has allowed the engineering of HI within both monocots and dicots. Although a knock-out of wild-type *ZmDMP* resulted in a low HIR of about 0.15%, its combination with a *mtl*/*nld*/*zmpla1* mutation increased HIR by two to six-fold. This synergistic effect suggests that at least two distinct pathways play a role in Stock-6 based haploid induction (Jacquier et al., 2020). Arabidopsis mutants with loss-of-function of two *DMP-like* genes—*AtDMP8* and *AtDMP9*—have shown an average HIR of 1–3.2% (Zhong et al., 2020). Engineered *DMP* genes in *Medicago truncatula* and tomato have also been shown to produce HI (Wang et al., 2022; Zhong et al., 2022).

Uni-parental genome elimination in Arabidopsis was achieved by modifying the centromeric histone H3 (CENH3) protein, which epigenetically determines centromere location by creating chromatin onto which the kinetochore assembles (Ravi and Chan, 2010). Multiple variants of modified CENH3 have been identified that induce uni-parental genome elimination with varying efficiencies (Kuppu et al., 2020). In mature egg cells of Arabidopsis, variant CENH3 is recognized and selectively removed from centromeres creating a CENH3-depleted "weak" chromosome. During mitosis of hybrid zygotes, the CENH3-depleted centromeres do not compete as well for CENH3 and essential centromere proteins loading compared to normal centromeres leading to the missegregation/loss of weak centromeres and haploid induction (Marimuthu et al., 2021). In maize, complementing loss-of-function *cenh3*/*cenh3* mutants with a *tailswap-CENH3* resulted in an average HIR of 0.86% with a maximum HIR of 3.6% (Kelliher et al., 2016). Efforts to engineer CENH3-based haploid induction in bread wheat, an allohexaploid crop, were complicated by the presence of two *CENH3* genes (α and β). A paternal HIR rate of 7–8% was achieved by retaining six *CENH3*β alleles in wild-type state, a specific mutation in *CENH3*α*-A* (termed restored frameshift—*RFS*) coupled with knockout alleles for both *CENH3*α*-B* and *CENH3*α*-D* (Lv et al., 2020).

In parthenogenesis, the egg cell initiates embryogenesis without being fertilized by a sperm cell. Parthenogenesis in natural apomicts will retain the ploidy level of the maternal parent as the egg cells in the aposporous or diplosporous embryo sac are unrecombined and unreduced through the process of apomeiosis. Parthenogenesis in sexually reproducing diploid plants will produce meiotically recombined haploid progeny as embryogenesis will be initiated from meiotically reduced egg cells. *PsASGR-BBML*, the gene responsible for parthenogenesis in the natural apomict *P. squamulatum*, can induce parthenogenesis in sexual pearl-millet, rice, maize, and tobacco when expressed under the control of an egg cell-specific promoter (Conner et al., 2015, 2017; Zhang et al., 2020). The dominant phenotype of *PsASGR-BBML* transgenes limits its usefulness for DH technology. For the deployment of dominant parthenogenetic genes to commercial DH production pipelines, the function of PsASGR-BBML needs to be regulated such that parthenogenesis is turned on in parental lines from which haploids are desired but off in the resulting DH progeny.

The glucocorticoid receptor (GR) system has been used in plants for post-translational regulation (Yamaguchi et al., 2015). GR dependent post-translational activation systems have been successfully used to induce the downstream transcriptional responses of transcription factors such as BnBBM (Passarinho et al., 2008), LEAFY (William et al., 2004), and WUSCHEL (Leibfried et al., 2005) in Arabidopsis and OsMADS26 (Lee et al., 2008), WOX11 (Zhao et al., 2009) and WOX3 (Dai et al., 2007) in rice. A post-translational regulation system using the GR relies on a fusion construct where the gene of interest (GOI) is fused to the ligand-binding domain of rat GR. The GOI:GR fusion protein forms a cytoplasmic complex with heat shock protein 90 (HSP-90) and is retained in the cytoplasm until the application of dexamethasone (DEX), a synthetic steroid hormone. DEX binds to the GR domain and disrupts its interaction with HSP-90 which allows the GOI:GR fusion protein to relocate to the

nucleus, where the GOI induces the expression of its downstream targets. Successful regulation of parthenogenesis using a post-translational activation system requires DEX mediated activation of PsASGR-BBML:GR in the egg cell before fertilization.

Using a glucocorticoid-based post-translational regulation system, we demonstrate that *PsASGR-BBML:GR* driven by an Arabidopsis egg cell-specific promoter *AtDD45* (downregulated in *dif1*) can be regulated at the flowering stage to induce a high rate of parthenogenesis. This technique presents a new opportunity to use parthenogenetic genes in DH production technology and to potentially elucidate the molecular mechanism underlying parthenogenetic embryogenesis.

MATERIALS AND METHODS

Transformation Construct

The pCambia1300-*AtDD45::PsASGR-BBML:GR* transformation plasmid was based on the *DD45-gPsASGR-BBML* construct which was previously shown to induce parthenogenesis in rice (Conner et al., 2017). A GS-*PsASGR-BBML:GR* plasmid was produced containing a 1,089 bp synthetic DNA insert in pUC57 (GenScript USA Inc., Piscataway, NJ, United States). The GS-*PsASGR-BBML:GR* plasmid contained 125 bp of *PsASGR-BBML* exon 8 covering a unique *Bsu*36I restriction site in *DD45-gPsASGR-BBML*, a six nucleotide (two amino acid) buffer, an 852 bp GR domain sequence with one nucleotide change (T to A) to remove a *Bsu*36I restriction site from the GR domain without changing the amino acid, a TGA stop codon, and 99 bp of the *PsASGR-BBML* 3′ UTR covering a unique *Bgl*II site in *DD45-gPsASGR-BBML* (**Supplementary Figure 1**). The *DD45-gPsASGR-BBML* and GS-*PsASGR-BBML:GR* plasmids were digested with *Bsu*36I and *Bgl*II and the 244 bp *DD45-gPsASGR-BBML* fragment was replaced by the 1,084 bp GS-*PsASGR-BBML:GR* fragment through ligation, transformation, and verification to yield the *AtDD45::PsASGR-BBML:GR* cassette within pCambia1300 (**Figure 1**).

Plant Materials

In total 22 transgenic rice lines (*Oryza sativa Nipponbare*) were generated at the CALS Plant Transformation Facility, Cornell University, after transformation with *Agrobacterium tumefaciens* possessing the *AtDD45::PsASGR-BBML:GR* cassette cloned within the *pCambia1300* binary vector. Transgenic rice plantlets were moved to soil, hardened, and grown in the NESPAL greenhouse facility, Tifton, GA, maintained at 24–29°C (Conner et al., 2017). Plants were bottom-watered with low pH water (pH 5.2–5.8) and additionally fertilized with a 50 ml per pot solution of 3.96 g/L "Miracle-Gro® Water Soluble All Purpose Plant Food" and 7.8 ml/L "Ferti-Lome Chelated Liquid Iron and Other Micro Nutrients" as needed.

Seed Sterilization and Germination

Dehusked seeds were placed in a 15 ml Falcon tube and subjected to an 80% EtOH treatment for 1 min followed by a solution of 50% commercial bleach (5.25% hypochlorite) with 0.1% Tween-20 for 30 min with rotation. The seed was washed five times with sterile water and placed on 1 × MS (Murashige and Skoog) media with vitamins (PhytoTech Labs, Lenexa, KS, United States), 4 g/L Gelzan CM (Sigma–Aldrich, St. Louis, MO, United States), 2 ml/L PPM™ (Plant Cell Technology, Washington, DC, United States) and 2% sucrose. Seeds were germinated in a 27°C incubator with a 16 h-light–8 h-dark cycle.

DNA Extraction and Genotyping

CTAB-extracted DNA was isolated (Conner et al., 2013) and genotyped for *PsASGR-BBML:GR* using established primers 1792/1801 and PCR conditions (Conner et al., 2017).

Transgene Expression and Cloning

Total RNA was isolated from approximately 30 rice ovaries collected 1 day before anthesis using the RNeasy Plant Mini Kit (QIAGEN, Valencia, CA, United States). One microgram of total RNA was converted into cDNA using the SuperScript® III First-Strand Synthesis System kit (Invitrogen, Carlsbad, CA, United States). Expression analysis was performed using non-quantitative RT-PCR in a 25 μl PCR reaction consisting of 2 μl cDNA, 1X PrimeSTAR GXL Buffer, 200 μM dNTP, 0.2 μM p5022 (5′-AGCAAGAATAGGAAGTGTGGCA-3′)/p5023 (5′-TTGACGATGGCTTTTCCTAGCT-3′), and 0.625U PrimeSTAR GXL DNA Polymerase (Takara Bio Inc., CA, United States) for 35 cycles and an annealing temperature of 60°C. For *PsASGR-BBML:GR* transcript sequence verification, cDNA was amplified using primers 1792/1801, cloned into the Zero Blunt™ TOPO™ vector (Thermo Fisher Scientific, MA, United States), and sequenced by Psomagen, MD, United States.

Flow Cytometry

Bulk seed flow cytometry (BSFC) using five dissected embryos from mature seed for one sample, embryos from a single seed, and leaf flow cytometry were done according to Conner et al. (2017) with *Paspalum notatum* as the genome standard to determine ploidy level. Flow cytometry and ploidy level plots were generated using a BD Accuri C6 flow cytometer and software (BD Biosciences, San Jose, CA, United States). Background signal was removed through gating of signals that exhibited a strong correlation between FL2-A and FSC-A plotted on a logarithmic scale. Ploidy level plots are based on a linear Y-axis count number and a logarithmic X-axis FL2-A signal.

Seed Data

Three to four panicles collected from a study sample were randomly picked. The number of total mature seeds divided by the number of florets on the panicles multiplied by 100 gave seed set percentage data. The seed count was determined by the collection of all mature seeds from sample panicles. A fifty-seed weight was obtained for each plant sample. The weight of the total seed sample was measured and the seed count was calculated by [(total seed weight)/(50 seed weight)] × 50.

Whole Plant Dexamethasone Treatments

A 100 mM stock solution of dexamethasone (Sigma-Aldrich) was prepared in dimethyl sulfoxide (DMSO) (Sigma-Aldrich) and

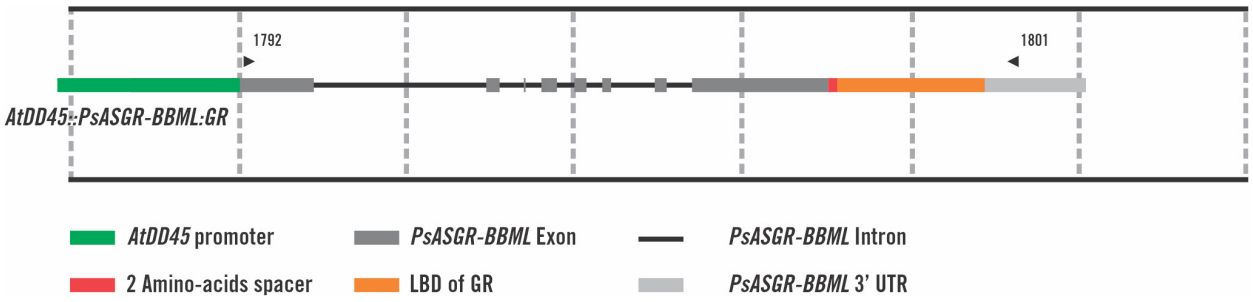

FIGURE 1 | Visual representation of the *AtDD45::PsASGR-BBML:GR* transgene cassette. The green rectangle denotes the *DD45* promoter from Arabidopsis. The gray rectangles denote the *PsASGR-BBML* exons, with black lines representing introns. The red rectangle denotes a two amino acid spacer between the last amino acid of *PsASGR-BBML* and the ligand-binding domain (LBD) of GR, which is represented by the orange rectangle. The light gray rectangle denotes the native *PsASGR-BBML* 3′ UTR. Positions of primers 1792 and 1801 are represented by small black triangles.

stored in aliquots at −20°C. For the initial DEX study, *PsASGR-BBML:GR* transgene positive plants were treated with 20, 50, or 100 μM DEX solution for 10–14 days, beginning at the boot stage for the first panicle of the plant sample and ending at the time when the first flush of flowering was complete. Flowering panicles were tagged. DEX working solutions were prepared by diluting the stock solution in low pH water (pH 5.2–5.8). The containers were watered with the minimum amount of DEX solution used daily by the rice plants, such that the containers were not dry but had a minimal amount of solution left. A fresh solution was added to the remaining solution daily. Transgene positive plants treated with 0.05 and 0.1% DMSO, and wild-type rice treated with all three concentrations of DEX and 0.05 and 0.1% DMSO were used as controls. For the second DEX study, plant treatment was started when the first plant in the treatment trial reached the boot stage and continued for 14 days. The treatments included 100 μM DEX, 0.1% DMSO, and only water.

In planta Floral Dexamethasone Treatment

Emasculated Florets

Florets from one panicle of a given T_1 plant were emasculated approximately 1 day before the first floral opening and ovaries were bathed with 5 μl of 100 μM DEX dispensed by pipette for three consecutive days. Florets from another panicle of the same plant were emasculated and treated with 0.1% DMSO. Ovaries were collected 5 days after emasculation and fixed overnight in FAA (47.5% ethanol, 3.7% formaldehyde, and 5% acetic acid). Fixed ovaries were dehydrated successively in 70, 85, and 100% ethanol for 2 h and transferred to 100% ethanol overnight. Dehydrated ovaries were cleared successively in 2:1 ethanol:methyl salicylate (MS), 1:2 ethanol:MS, and pure MS for 2 h for each treatment and then transferred to pure MS overnight. Cleared ovaries were observed under differential interference contrast (DIC) microscopy.

Un-Emasculated Florets

Floret tops from one panicle of a given T_1 plant were cut without disturbing the anthers and treated with 5 μl of 100 μM DEX for three consecutive days. Floret tops from another panicle from the same plant were cut in a similar way followed by 0.1% DMSO treatment. Upon maturity, seeds were collected and analyzed by BSFC.

RESULTS

In total, 22 independent *AtDD45::PsASGR-BBML:GR* lines, some with multiple plantlets, were generated and transferred to soil. Twenty-one lines had at least one *AtDD45::PsASGR-BBML:GR* transgene positive plant as determined by PCR with primers 1792/1801 (**Figure 1**). Expression of *PsASGR-BBML:GR* in rice ovaries 1 day before anthesis was confirmed by RT-PCR analysis from 10 independent lines. *PsASGR-BBML:GR* transcript sequence and splicing were verified from two lines. BSFC on 20 T_1 seed from DEX-untreated *PsASGR-BBML:GR* expressing T_0 lines did not show haploid embryo signal, verifying that in the absence of DEX, PsASGR-BBML:GR did not localize to the nucleus and parthenogenesis was not induced. Line 13B was not analyzed by BSFC due to a low seed set (**Table 1**).

Dexamethasone Treatment of T_1 Plants

Germination and transgene genotyping results are shown for T_1 seed from 10 T_0 lines (**Table 1**). A total of 66 out of 83 T_1 plants were genotyped as transgene positive, and all T_1 plants were confirmed to be diploid following flow cytometry on T_1 leaf tissue. Expression of *PsASGR-BBML:GR* in ovaries 1 day before anthesis was confirmed by RT-PCR for 13 T_1 plants from seven lines. One transgene positive T_1 plant from each T_0 line and two wild-type (WT) plants were treated with 100 μM, 50 μM, or 20 μM DEX through bottom watering (**Supplementary Figure 2**). Transgene positive plants treated with DMSO, WT plants treated with all three DEX concentrations, and untreated transgene positive plants were used as controls. Treatment began at the boot stage and continued for 10–14 days, encompassing the first flush of panicle flowering. Panicles from the treatment period were flagged and the seed was allowed to mature. Data for haploid embryo development was collected using BSFC on mature seed embryos and the percent seed set of flagged panicles is presented (**Table 2** and **Figure 2**).

TABLE 1 | Characterization of *AtDD45::PsASGR-BBML:GR* T_0 lines used in DEX induction studies.

Line	Transgene	Transcript expression *via* RT-PCR analysis	BSFC of T_1 seed	T_1 seeds germinated/ total sown	Transgene positive T_1/germinated
4C	+	Y	2n	12/15	7/12
6B	+	Y	2n	6/10	4/6
7B	+	Y	2n	7/10	5/7
8B	+	Y	2n	7/10	7/7
9B	+	Y	2n	8/10	7/8
10B	+	Y	2n	9/15	8/9
11B	+	Y	2n	10/10	7/10
13B	+	Y	Low seed	8/10	7/8
15B	+	Y	2n	8/15	7/8
22B	+	Y	2n	8/15	7/8

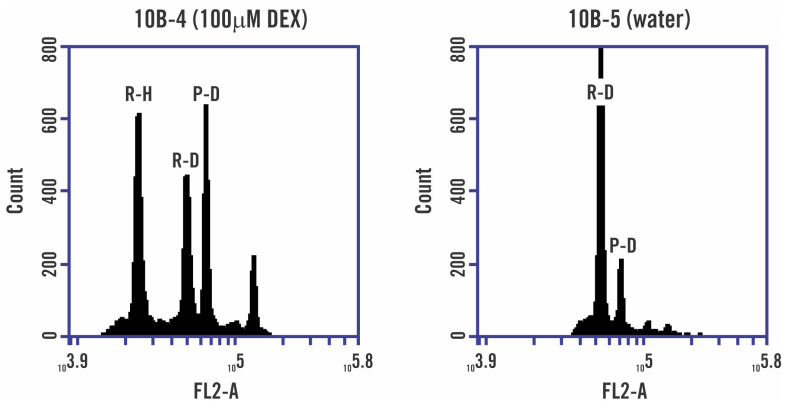

FIGURE 2 | Representative BSFC to identify parthenogenesis. Embryos from five seeds were bulked, processed, and analyzed with flow cytometry to determine if PsASGR-BBML:GR would induce haploid embryo development when induced with DEX. Line 10B-5, transgene positive, without DEX treatment did not display a haploid signal. 10B-4, transgene positive, with 100 μM DEX treatment displayed both haploid and diploid rice signals from bulked embryo tissue. R-H (rice haploid signal), R-D (rice diploid signal), and P-D (*Paspalum notatum* diploid signal). The plots shown are based on a linear Y-axis count number and a logarithmic X-axis FL2-A signal.

In total, seven of 10 transgenic lines exhibited T_2 seed showing haploid signal in BSFC when treated with the 100 μM DEX through bottom watering. Four lines showed haploid embryo formation at 50 μM DEX and two lines displayed haploid formation at 20 μM DEX treatment through bottom watering. Wild-type plants treated with DEX or DMSO, transgene positive plants treated only with DMSO or untreated WT and transgene positive plants did not display haploid signal in BSFC, indicating that both the *AtDD45::PsASGR-BBML:GR* transgene and inducer steroid DEX are required for successful induction of parthenogenesis. Wild-type plants treated with DMSO had an average and median seed-set of 95.6 and 95.9%, respectively, while DEX treated plants had an average and median seed-set of 84.3 and 90.1%, respectively. The overall seed set of transgene positive lines was reduced compared to WT plants and variable within T_1 plants within and between lines.

Identification of Transgene Homozygous Lines

From the initial 10 T_0 lines used for DEX treatment through bottom watering, lines 4C, 10B, 15B, and 22B were selected for further analysis as BSFC haploid signals in these lines were identified in T_2 seed when treated with 100 μM as well as 50 μM DEX through bottom watering. In total, thirty T_2 seeds were germinated and genotyped from four T_1 plants from each of the four lines. Six T_1 plants (4C-14, 10B-5, 10B-11, 10B-14, 15B-3, and 22B-13) generated only transgene positive T_2 plants and were considered homozygous for the transgene. A proportion of seedlings within 15B-3 and other 15B lines displayed an albino phenotype and were removed from further study. Of the transgene homozygous lines identified, T_1 line 10B-14 had been treated with 100 μM DEX through bottom watering, while T_1 line 10B-5 was an untreated bottom watering control. All 29 10B-5 offspring were diploid, while three 10B-14 seedlings were diploid and 20 seedlings were haploid.

New T_2 seedlings from homozygous lines 10B-11, 22B-13, and 4C-14, confirmed to be 100% transgene positive, were placed through another round of 100 μM DEX through bottom watering with untreated and DMSO controls. Seeds from the first 10 flowering panicles were collected and the seed number was calculated based on a 50 seed weight from each plant analyzed (**Supplementary Table 1**). T_2 lines from 10B-11 and 4C-14

TABLE 2 | BSFC results and seed set from DEX treatment through bottom watering of T_1 transgene positive plants.

100 μM DEX			50 μM DEX			20 μM DEX			DMSO			Untreated		
T_1 plant ID	BSFC[#]	Seed set	T_1 plant ID	BSFC[#]	Seed set	T_1 plant ID	BSFC[#]	Seed set	T_1 plant ID	BSFC[#]	Seed set	T_1 plant ID	BSFC[#]	Seed set
4C-1	3/4	32.7%	4C-5	4/4	34.9%	4C-7	0/5	51.9%						
6B-2	4/4	26.8%	6B-3	n/a	0.0%	6B-1	n/a	0.0%				6B-6	0/3	11.0%
7B-5	0/4	37.7%	7B-2	n/a	0.0%	7B-1	0/3	19.6%						
8B-3	0/4	23.6%	8B-2	0/4	18.8%	8B-1	0/5	51.1%	8B-4^	0/5	39.5%			
9B-3	4/4	45.0%	9B-2	0/3	13.9%	9B-1	1/5	53.5%	9B-4*	0/5	7.6%	9B-6	0/4	77.4%
10B-4	4/4	27.5%	10B-3	3/4	28.1%	10B-1	3/5	43.5%				10B-5	0/4	54.4%
11B-3	0/4	43.8%	11B-2	0/4	50.5%	11B-1	0/5	93.1%						
13B-3	3/4	45.5%	13B-2	n/a	0.0%	13B-1	n/a	0.0%	13B-5*	0/5	43.8%	13B-6	0/4	74.5%
15B-4	3/4	30.7%	15B-2	4/4	36.9%	15B-1	0/5	41.8%	15B-3^	0/4	45.9%			
22B-3	4/4	18.7%	22B-2	4/4	25.7%	22B-1	0/1	12.0%				22B-4	0/4	42.7%
WT-1	0/4	92.7%	WT-3	0/4	78.6%	WT-5	0/4	91.7%	WT-7*	0/4	96.8%			
WT-2	0/4	88.5%	WT-4	0/4	59.1%	WT-6	0/4	95.0%	WT-8*	0/4	95.0%			
									WT-9^	0/4	98.8%			
									WT-10^	0/4	91.8%			

[#]*Number of BSFC samples (5 embryos/sample) showing haploid signal/total number of samples.*

**Treatment with 0.05% DMSO/^treatment with 0.1% DMSO.*

showed more seed set from the three treatments than line 22B-13. As shown in **Figure 3**, all lines treated with 100 μM DEX showed significantly less seed set than plants within lines that were untreated or treated with DMSO only.

T_3 seeds were sterilized and germinated on MS media from three T_2 plants on three different days in DEX treatment before anthesis. The ploidy level of each germinated seedling was investigated by leaf flow cytometry. When an individual seed produced twin seedlings, each seedling was analyzed separately for ploidy level (**Table 3**). T_2 lines from 10B-11 showed the greatest average level of parthenogenesis (48%), followed by T_2 lines from 22B-13 (34%) and 4C-14 (22%). The rate of seed germination from heads decreased in all three lines the longer the plant was in DEX treatment before anthesis. While the rate of parthenogenesis and the number of twin haploid seedlings increased in lines from 10B-11 with the amount of time in DEX prior to anthesis, a similar trend was not identified in lines from 22B-13 or 4C-14.

Additional Technique to Induce Parthenogenesis

An *in planta* floral treatment was attempted on transgene positive T_1 plants 4C-11 and 4C-13, 10B-11 and 10B-13, and 22B-13. A total of 291 and 104 florets were treated with 100 μM DEX or 0.1% DMSO, respectively, and allowed to mature. Forty-five (13.4%) 100 μM DEX treated and 21 (20%) 0.1% DMSO treated florets produced seed, while an average of 81% seed set was observed on untreated florets. Seeds developed from 100 μM DEX treated florets of T_1 plants from the 10B line displayed haploid signal with BSFC while 0.1% DMSO and untreated seeds gave diploid signal only. In total, twenty-eight florets from the 10B-11 line were emasculated, treated with 100 μM DEX for 3 days, and fixed on the fifth day after emasculation. Seventeen ovaries showed clear parthenogenesis, i.e., the appearance of a parthenogenetic embryo along with the presence of intact polar nuclei (**Supplementary Figure 2**).

DISCUSSION

Doubled haploid technology has proven to be a valuable asset to modern hybrid breeding programs due to its ability to generate inbred lines in a considerably shorter period of time as compared to traditional breeding methods. Understanding the genetic principles of haploid induction, along with the ability to modify plants through transformation and CRISPR/Cas9 technology has allowed the genetic engineering of haploid induction in various crop plants. With the identification of parthenogenesis genes, a new haploid induction technology is possible that involves direct embryogenesis from unfertilized egg cells rather than uni-parental genome elimination after crossing. Parthenogenetic haploid induction in transgenic plants has been shown by using *PsASGR-BBML* transgenes, cloned from the apomixis locus of *P. squamulatum* (syn. *C. squamulatus*), in pearl millet, rice, maize, and tobacco (Conner et al., 2015, 2017; Zhang et al., 2020) and by egg-cell specific expression of the endogenous *OsBBM1* gene from rice (Khanday et al., 2019). A dicot apomixis

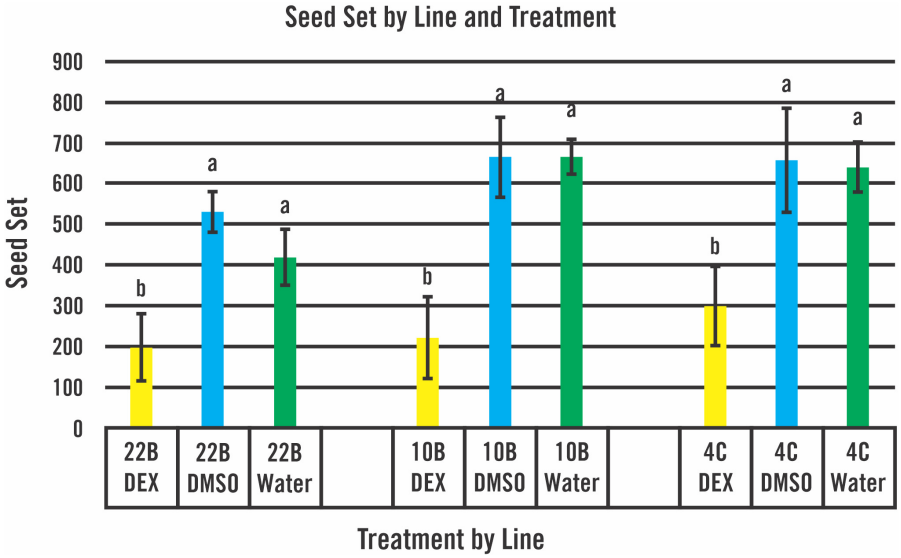

FIGURE 3 | Seed set of homozygous T_2 lines by treatment and line. A mature seed number was calculated for the first 10 flowering panicles. The number of plants treated for each line and treatment is found in **Supplementary Table 1**. Plants in all three lines treated with 100 μM DEX displayed significantly less mature seeds than plants treated with DMSO or no treatment controls. Error bars based on SD. Mean totals for seed set within a line not sharing a common letter were significantly different ($P < 0.01$) as determined by ANOVA using the Holm-Sidak comparison method.

locus parthenogenesis gene (*PARTHENOGENESIS [PAR]*) from *Taraxacum* has been identified but has yet to produce viable haploid seedlings in transgenic lettuce lines. Parthenogenesis has been confirmed through a haploid signal from developing seeds through flow cytometry and imaging of embryo-like structures in unpollinated ovaries (Underwood et al., 2022).

Regulating PsASGR-BBML function using a GR ligand-dependent post-translational regulation system, depends both on a functional PsASGR-BBML:GR fusion protein as well as the availability of the activating ligand occurring in the desired spatial and temporal frame. The PsASGR-BBML:GR fusion protein was expressed in rice egg cells using the Arabidopsis egg cell-specific promoter *AtDD45* (Steffen et al., 2007) which has been shown to be functional to produce haploid rice lines (Conner et al., 2017; Khanday et al., 2019). Lines displaying *PsASGR-BBML:GR* expression were identified through RT-PCR on RNA extracted from pre-anthesis rice ovaries. Studies of fusion proteins with GR ligand-dependent post-translational regulation within rice (Dai et al., 2007; Lee et al., 2008; Zhao et al., 2009) and GR dependent transcriptional activation in rice (Ouwerkerk et al., 2001) have been published. The rice studies used a range of DEX concentrations from 1 to 100 μM. This study shows that GR ligand-dependent post-translational regulation within gametophytic tissue can be accomplished in rice through bottom watering of plants with the chemical ligand solution. Various lines of *AtDD45::PsASGR-BBML:GR* watered with various DEX concentrations starting at the boot stage successfully induced parthenogenesis. The number of lines showing parthenogenesis was greatest at the 100 μM DEX treatment (70%) and decreased at the 50 μM (57%) and 20 μM (25%) DEX concentrations. DEX treatment through bottom watering is an easy method and its simplicity indicates that it could have a high potential for use in large-scale commercial DH development programs. Parthenogenesis could also be induced through an *in planta* floral treatment, which is a more direct placement of the DEX solution into the rice floret. This treatment consumes additional time and limits the seed set but greatly decreases the amount of DEX solution needed for the study.

The initial DEX through bottom watering treatment indicated that neither DEX nor DMSO treatment of wild-type plants greatly affected the seed set. However, *AtDD45::PsASGR-BBML:GR* lines treated with DEX tended to show less fecundity. This result is similar to decreased fecundity levels identified in rice and maize plants expressing *AtDD45-gPsASGR-BBML* or *gPsASGR-BBML* transgenes (Conner et al., 2017). Homozygous *AtDD45::PsASGR-BBML:GR* T_1 lines were identified and a second DEX through bottom watering study was initiated. As DEX concentration did not seem to affect WT plants, the 100 μM DEX concentration was chosen. Induction of parthenogenesis *via* DEX in homozygous T_2 lines shows a statistical decrease in seed set for the three transgenic lines when compared to DMSO treated or untreated plants in the line, which had similar amounts of seed set. While only based on a small study, the percent germination of seed in all 3 homozygous lines declined the longer the plant was treated with DEX before the first day of anthesis for that panicle. Similar to results from *AtDD45-gPsASGR-BBML* or *gPsASGR-BBML* transgenic lines in rice, the number of twin haploid seedlings found could be greater than the number of single haploid seedlings. It is yet to be determined if the *PsASGR-BBML* transgenes promote twinning of a developing zygote or if the leaky expression

TABLE 3 | Ploidy level of T_3 seedlings from homozygous T_2 lines treated with 100 μM DEX.

Plant	Days in DEX prior to anthesis	Seed number on MS plates	Percent germination	Parthenogenesis		Sexual reproduction		Percent parthenogenesis
				Number of seed producing one haploid seedling	Number seed producing twin haploid seedlings	Number of seed producing one diploid seedlings	Number of seed producing twin diploid and haploid seedlings	
10B-11-41	4	32	91	10	2	14	3	41
10B-11-31	6	32	75	9	0	12	2	39
10B-11-39	9	32	59	3	10	2	4	68
Total 10B-11				34		37		48
22B-13-33	6	36	78	1	17	5	5	21
22B-13-32	9	34	56	3	4	3	9	63
22B-13-31	11	36	58	3	11	5	2	24
Total 22B-13				23		45		34
4C-14-31	5	34	94	1	3	23	5	12.5
4C-14-33	7	33	76	3	5	15	2	32
4C-14-34	9	35	60	2	3	11	4	25
Total 4C-14				17		60		22

of the *PsASGR-BBML* transgenes converts synergid cells into egg/zygote cell fates. The identification of a seed containing both a diploid and a haploid seedling suggests the latter. The overall haploid induction rate for homozygous T_2 lines from 10B-11 was 48%, 34% for lines from 22B-13, and 22% for lines from 4C-14. The HI rate for these lines exceeds that of *mtl* engineered rice lines (4–6%) and is similar to or better than the dominant haploid induction rate of *PsASGR-BBML* or *OsBBM1* transgenes (Conner et al., 2017; Khanday et al., 2019). Additional studies can be undertaken to optimize the DEX treatment for concentration, timing, and testing of additional DEX-like steroids (Samalova et al., 2019).

Understanding the molecular pathways involved in PsASGR-BBML-induced parthenogenesis can also provide more options for improving the system's efficiency for both DH production and apomixis synthesis in crop plants. Although apomixis has been synthetically engineered in rice using different approaches, the understanding of the underlying molecular mechanisms is still limited (Khanday and Sundaresan, 2021). FIX (Fixation of hybrids) rice lines were engineered with CRISPR/Cas9 technology to create a quadruple gene mutation of *osd1/pair1/rec8/mtl* (Wang et al., 2019). The phenotype of *osd1/pair1/rec8* is designated *MiMe* (*Mitosis instead of Meiosis*) and creates both male and female clonal diploid gametes (d'Erfurth et al., 2009; Mieulet et al., 2016). The *mtl* phenotype creates embryo development of the diploid egg cell, leading to clonal seed. *S-Apo* (*Synthetic-Apomictic*) rice lines were engineered using CRISPR/Cas9 technology to create a *MiMe* phenotype along with an *OsBBM1* transgene promoting embryo development of the egg cell *via* parthenogenesis (Khanday et al., 2019). The frequency of apomictic/clonal seeds ranged from 0.2 to 0.4% in the FIX lines and 14–29% in the *S-Apo* lines.

The successful post-translational regulation of PsASGR-BBML reported in this study could be used for identifying downstream target genes by using differential expression analysis in DEX treated vs. untreated *AtDD45::PsASGR-BBML:GR* plants (Yamaguchi et al., 2015). Direct transcriptional targets of PsASGR-BBML can be identified by the simultaneous application of cycloheximide, an inhibitor of protein biosynthesis. This approach has been used to identify candidate genes activated by BBM:GR during somatic embryogenesis in Arabidopsis (Passarinho et al., 2008). Chromatin immunoprecipitation (ChIP) coupled with quantitative PCR or ChIP-seq could investigate the transcriptional targets of PsASGR-BBML, similar to a study of BBM in Arabidopsis using BBM: YFP/BBM-GFP instead of GR (Horstman et al., 2017). Protein pull-down using a GR-specific antibody could also determine if PsASGR-BBML is part of a larger protein complex. A recent study used a combination of glucocorticoid-based post-transcriptional regulation and ChIP-seq to determine that *OsBBM1* induces somatic embryogenesis by directly upregulating auxin-biosynthesis genes (Khanday et al., 2020).

The data presented shows that a glucocorticoid-based post-translational regulation system using a *PsASGR-BBML:GR* transgene can be activated at the flowering stage to promote a high rate of parthenogenesis and represents a novel opportunity to use parthenogenesis genes in DH production technology.

DATA AVAILABILITY STATEMENT

The original contributions presented in this study are included in the article/**Supplementary Material**, further inquiries can be directed to the corresponding author.

AUTHOR CONTRIBUTIONS

PO-A and JAC conceptualized the project. GS and JAC did the methodology, investigation, and analysis. JAC supervised the project. GS wrote the original draft. All authors revised and approved the manuscript.

FUNDING

This research was supported by the USDA-NIFA Award 2018-67013-27419 to JAC and PO-A.

ACKNOWLEDGMENTS

We thank Lovepreet Singh Chahal for support in the laboratory, Patrick Conner for statistical help, and Tracey Vellidis for figure creation.

SUPPLEMENTARY MATERIAL

The Supplementary Material for this article can be found online at: https://www.frontiersin.org/articles/10.3389/fpls.2022.925467/full#supplementary-material

Supplementary Figure 1 | Annotated GS-*PsASGR-BBML:GR* insert sequence.

Supplementary Figure 2 | DEX treatment and DIC screening for parthenogenesis.

Supplementary Table 1 | Individual plant data generated for second DEX study.

REFERENCES

Bohanec, B. (2009). "Doubled Haploids via Gynogenesis," in *Advances in Haploid Production in Higher Plants*, eds A. Touraev, B. P. Forster, and S. M. Jain (Dordrecht: Springer Netherlands), 35–46.

Chaikam, V., Molenaar, W., Melchinger, A. E., and Boddupalli, P. M. (2019). *Doubled haploid technology for line development in maize: technical advances and prospects*. New York, NY: Springer Verlag.

Coe, E. H. (1959). A Line of Maize with High Haploid Frequency. *Am. Natural.* 93, 381–382. doi: 10.1086/282098

Conner, J. A., Gunawan, G., and Ozias-Akins, P. (2013). Recombination within the apospory specific genomic region leads to the uncoupling of apomixis components in Cenchrus ciliaris. *Planta* 238, 51–63. doi: 10.1007/s00425-013-1873-5

Conner, J. A., Mookkan, M., Huo, H., Chae, K., and Ozias-Akins, P. (2015). A parthenogenesis gene of apomict origin elicits embryo formation from unfertilized eggs in a sexual plant. *Proc. Natl. Acad. Sci. U S A* 2015:1505856112. doi: 10.1073/pnas.1505856112

Conner, J. A., Podio, M., and Ozias-Akins, P. (2017). Haploid embryo production in rice and maize induced by PsASGR-BBML transgenes. *Plant Reprod.* 30, 41–52. doi: 10.1007/s00497-017-0298-x

Dai, M., Hu, Y., Zhao, Y., Liu, H., and Zhou, D.-X. (2007). A WUSCHEL-LIKE HOMEOBOX Gene Represses a YABBY Gene Expression Required for Rice Leaf Development. *Plant Physiol.* 144, 380–380. doi: 10.1104/pp.107.095737

d'Erfurth, I., Jolivet, S., Froger, N., Catrice, O., Novatchkova, M., and Mercier, R. (2009). Turning meiosis into mitosis. *PLoS Biol.* 7:e1000124. doi: 10.1371/journal.pbio.1000124

Dunwell, J. M. (2010). Haploids in flowering plants: origins and exploitation. *Plant Biotechnol. J.* 8, 377–424. doi: 10.1111/j.1467-7652.2009.00498.x

Ferrie, A. M. R., and Möllers, C. (2011). *Haploids and doubled haploids in Brassica spp. for genetic and genomic research*. New York, NY: Springer.

Forster, B. P., Heberle-Bors, E., Kasha, K. J., and Touraev, A. (2007). *The resurgence of haploids in higher plants*. Amsterdam: Elsevier Current Trends.

Gilles, L. M., Khaled, A., Laffaire, J. B., Chaignon, S., Gendrot, G., Laplaige, J., et al. (2017). Loss of pollen-specific phospholipase NOT LIKE DAD triggers gynogenesis in maize. *EMBO J.* 36, 707–717. doi: 10.15252/embj.201796603

Horstman, A., Li, M., Heidmann, I., Weemen, M., Chen, B., Muino, J. M., et al. (2017). The BABY BOOM transcription factor activates the LEC1-ABI3-FUS3-LEC2 network to induce somatic embryogenesis. *Plant Physiol.* 175, 848–857. doi: 10.1104/pp.17.00232

Jacquier, N. M. A., Gilles, L. M., Pyott, D. E., Martinant, J.-P., Rogowsky, P. M., and Widiez, T. (2020). Puzzling out plant reproduction by haploid induction for innovations in plant breeding. *Nat. Plants* 6, 610–619. doi: 10.1038/s41477-020-0664-9

Kelliher, T., Starr, D., Richbourg, L., Chintamanani, S., Delzer, B., Nuccio, M. L., et al. (2017). MATRILINEAL, a sperm-specific phospholipase, triggers maize haploid induction. *Nature* 542, 105–109. doi: 10.1038/nature20827

Kelliher, T., Starr, D., Wang, W., McCuiston, J., Zhong, H., Nuccio, M. L., et al. (2016). Maternal Haploids Are Preferentially Induced by CENH3-tailswap Transgenic Complementation in Maize. *Front. Plant Sci.* 7, 414–414. doi: 10.3389/fpls.2016.00414

Khanday, I., Santos-Medellín, C., and Sundaresan, V. (2020). Rice embryogenic trigger BABY BOOM1 promotes somatic embryogenesis by upregulation of auxin biosynthesis genes. *bioRxiv* 2020:265025. doi: 10.1101/2020.08.24.265025

Khanday, I., Skinner, D., Yang, B., Mercier, R., and Sundaresan, V. (2019). A male-expressed rice embryogenic trigger redirected for asexual propagation through seeds. *Nature* 565, 91–95. doi: 10.1038/s41586-018-0785-8

Khanday, I., and Sundaresan, V. (2021). Plant zygote development: recent insights and applications to clonal seeds. *Curr. Opin. Plant Biol.* 59:101993. doi: 10.1016/j.pbi.2020.101993

Kuppu, S., Ron, M., Marimuthu, M. P., Li, G., Huddleson, A., Siddeek, M. H., et al. (2020). A variety of changes, including CRISPR/Cas9-mediated deletions, in CENH3 lead to haploid induction on outcrossing. *Plant Biotechnol. J.* 18, 2068–2080. doi: 10.1111/pbi.13365

Lee, S., Woo, Y.-M., Ryu, S.-I., Shin, Y.-D., Kim, W. T., Park, K. Y., et al. (2008). Further characterization of a rice AGL12 group MADS-box gene, OsMADS26. *Plant Phys.* 147, 156–168. doi: 10.1104/pp.107.114256

Leibfried, A., To, J. P. C., Busch, W., Stehling, S., Kehle, A., Demar, M., et al. (2005). WUSCHEL controls meristem function by direct regulation of cytokinin-inducible response regulators. *Nature* 438, 1172–1172. doi: 10.1038/nature04270

Liu, C., Li, X., Meng, D., Zhong, Y., Chen, C., Dong, X., et al. (2017). A 4-bp Insertion at ZmPLA1 Encoding a Putative Phospholipase A Generates Haploid Induction in Maize. *Mol Plant* 10, 520-522. doi: 10.1016/j.molp.2017.01.011

Liu, H., Wang, K., Jia, Z., Gong, Q., Lin, Z., Du, L., et al. (2019). Efficient induction of haploid plants in wheat by editing of TaMTL using an optimized Agrobacterium-mediated CRISPR system. *J. Exp. Bot.* 71, 1337–1349. doi: 10.1093/jxb/erz529

Lv, J., Yu, K., Wei, J., Gui, H., Liu, C., Liang, D., et al. (2020). Generation of paternal haploids in wheat by genome editing of the centromeric histone CENH3. *Nat. Biotechnol.* 38, 1397–1401. doi: 10.1038/s41587-020-0728-4

Marimuthu, M. P., Maruthachalam, R., Bondada, R., Kuppu, S., Tan, E. H., Britt, A., et al. (2021). Epigenetically mismatched parental centromeres trigger genome elimination in hybrids. *Sci. Adv.* 7:eabk1151. doi: 10.1126/sciadv.abk1151

Mieulet, D., Jolivet, S., Rivard, M., Cromer, L., Vernet, A., Mayonove, P., et al. (2016). Turning rice meiosis into mitosis. *Cell Res.* 26, 1242–1254.

Mishra, R., and Rao, G. J. N. (2016). In-vitro Androgenesis in Rice: Advantages, Constraints and Future Prospects. *Rice Sci.* 23, 57–68. doi: 10.1016/j.rsci.2016.02.001

Murovec, J., and Bohanec, B. (2012). *Haploids and Doubled Haploids in Plant Breeding*. Houston, TX: InTech.

Ouwerkerk, P. B., de Kam, R. J., Hoge, H. J., and Meijer, A. H. (2001). Glucocorticoid-inducible gene expression in rice. *Planta* 213, 370–378. doi: 10.1007/s004250100583

Passarinho, P., Ketelaar, T., Xing, M., van Arkel, J., Maliepaard, C., Hendriks, M. W., et al. (2008). BABY BOOM target genes provide diverse entry points into cell proliferation and cell growth pathways. *Plant Mole. Biol.* 68, 225–237. doi: 10.1007/s11103-008-9364-y

Prigge, V., Xu, X., Li, L., Babu, R., Chen, S., Atlin, G. N., et al. (2012). New insights into the genetics of in vivo induction of maternal haploids, the backbone of doubled haploid technology in maize. *Genetics* 190, 781–793. doi: 10.1534/genetics.111.133066

Ravi, M., and Chan, S. W. L. (2010). Haploid plants produced by centromere-mediated genome elimination. *Nature* 464, 615–618. doi: 10.1038/nature08842

Samalova, M., Kirchhelle, C., and Moore, I. (2019). Universal Methods for Transgene Induction Using the Dexamethasone-Inducible Transcription Activation System pOp6/LhGR in Arabidopsis and Other Plant Species. *Curr. Prot. Plant Biol.* 4:e20089. doi: 10.1002/cppb.20089

Steffen, J. G., Kang, I.-H., Macfarlane, J., and Drews, G. N. (2007). Identification of genes expressed in the Arabidopsis female gametophyte. *Plant J.* 51, 281–292. doi: 10.1111/j.1365-313X.2007.03137.x

Uliana Trentin, H., Frei, U. K., and Lübberstedt, T. (2020). Breeding Maize Maternal Haploid Inducers. *Plants* 9:614.

Underwood, C. J., Vijverberg, K., Rigola, D., Okamoto, S., Oplaat, C., Camp, R. H., et al. (2022). A PARTHENOGENESIS allele from apomictic dandelion can induce egg cell division without fertilization in lettuce. *Nat. Genet.* 2022, 1–10. doi: 10.1038/s41588-021-00984-y

Wang, C., Liu, Q., Shen, Y., Hua, Y., Wang, J., Lin, J., et al. (2019). Clonal seeds from hybrid rice by simultaneous genome engineering of meiosis and fertilization genes. *Nat. Biotechnol.* 37, 283–286. doi: 10.1038/s41587-018-0003-0

Wang, N., Xia, X., Jiang, T., Li, L., Zhang, P., Niu, L., et al. (2022). In planta haploid induction by genome editing of DMP in the model legume Medicago truncatula. *Plant Biotechnol. J.* 20, 22–24. doi: 10.1111/pbi.13740

Weyen, J. (2008). *Barley and Wheat Doubled Haploids in Breeding*. New York, NY: Springer Netherlands, 179–187.

William, D. A., Su, Y., Smith, M. R., Lu, M., Baldwin, D. A., and Wagner, D. (2004). Genomic identification of direct target genes of LEAFY. *Proc. Natl. Acad. Sci. USA* 101, 1775–1780. doi: 10.1073/pnas.0307842100

Yamaguchi, N., Winter, C. M., Wellmer, F., and Wagner, D. (2015). Identification of direct targets of plant transcription factors using the GR fusion technique. *Methods Mole. Biol.* 1284, 123–138. doi: 10.1007/978-1-4939-2444-8_6

Yao, L., Zhang, Y., Liu, C., Liu, Y., Wang, Y., Liang, D., et al. (2018). OsMATL mutation induces haploid seed formation in indica rice. *Nat. Plants* 4, 530–533. doi: 10.1038/s41477-018-0193-y

Zhang, Z., Conner, J., Guo, Y., and Ozias-Akins, P. (2020). Haploidy in tobacco induced by PsASGR-BBML transgenes via parthenogenesis. *Genes* 11:1072. doi: 10.3390/genes11091072

Zhao, Y., Hu, Y., Dai, M., Huang, L., and Zhou, D.-X. (2009). The WUSCHEL-related homeobox gene WOX11 is required to activate shoot-borne crown root development in rice. *Plant Cell* 21, 736–748. doi: 10.1105/tpc.108.061655

Zhong, Y., Chen, B., Li, M., Wang, D., Jiao, Y., Qi, X., et al. (2020). A DMP-triggered in vivo maternal haploid induction system in the dicotyledonous Arabidopsis. *Nat. Plants* 6, 466–472. doi: 10.1038/s41477-020-0658-7

Zhong, Y., Chen, B., Wang, D., Zhu, X., Li, M., Zhang, J., et al. (2022). In vivo maternal haploid induction in tomato. *Plant Biotechnol.* J. 20, 250–252. doi: 10.1111/pbi.13755

Zhong, Y., Liu, C., Qi, X., Jiao, Y., Wang, D., Wang, Y., et al. (2019). Mutation of ZmDMP enhances haploid induction in maize. *Nat. Plants* 5, 575–580. doi: 10.1038/s41477-019-0443-7

Conflict of Interest: The authors declare that the research was conducted in the absence of any commercial or financial relationships that could be construed as a potential conflict of interest.

Publisher's Note: All claims expressed in this article are solely those of the authors and do not necessarily represent those of their affiliated organizations, or those of the publisher, the editors and the reviewers. Any product that may be evaluated in this article, or claim that may be made by its manufacturer, is not guaranteed or endorsed by the publisher.

frontiers | Frontiers in Plant Science

ORIGINAL RESEARCH
published: 18 July 2022
doi: 10.3389/fpls.2022.938339

Quantitative Trait Loci Mapping Analysis for Cold Tolerance Under Cold Stress and Brassinosteroid-Combined Cold Treatment at Germination and Bud Burst Stages in Rice

Zhifu Guo[1†], Haotian Wang[1†], Jialu Yao[1†], Yishan Cheng[1], Wenzhong Zhang[2], Zhengjin Xu[2], Maomao Li[3], Jing Huang[4] and Minghui Zhao[2]**

[1] Key Laboratory of Agricultural Biotechnology of Liaoning Province, College of Biosciences and Biotechnology, Shenyang Agricultural University, Shenyang, China, [2] Rice Research Institute, College of Agronomy, Shenyang Agricultural University, Shenyang, China, [3] Rice Research Institute, Jiangxi Academy of Agricultural Sciences, Nanchang, China, [4] Department of Agronomy, College of Agriculture, Purdue University, West Lafayette, IN, United States

OPEN ACCESS

Edited by:
Gianni Barcaccia,
University of Padua, Italy

Reviewed by:
Samar Gamal Thabet,
Fayoum University, Egypt
Hua Zhang,
Zhejiang Academy of Agricultural Sciences, China

***Correspondence:**
Maomao Li
lmm3056@163.com
Minghui Zhao
mhzhao@syau.edu.cn

[†] These authors have contributed equally to this work

Specialty section:
This article was submitted to Plant Breeding, a section of the journal Frontiers in Plant Science

Received: 07 May 2022
Accepted: 07 June 2022
Published: 18 July 2022

Citation:
Guo Z, Wang H, Yao J, Cheng Y, Zhang W, Xu Z, Li M, Huang J and Zhao M (2022) Quantitative Trait Loci Mapping Analysis for Cold Tolerance Under Cold Stress and Brassinosteroid-Combined Cold Treatment at Germination and Bud Burst Stages in Rice. Front. Plant Sci. 13:938339. doi: 10.3389/fpls.2022.938339

Low temperature is one of the major abiotic stresses limiting seed germination and early seedling growth in rice. Brassinosteroid (BR) application can improve cold tolerance in rice. However, the regulatory relationship between cold tolerance and BR in rice remains undefined. Here, we constructed a population of 140 backcross recombinant inbred lines (BRILs) derived from a cross between a wild rice (Dongxiang wild rice, DXWR) and a super rice (SN265). The low-temperature germination rate (LTG), survival rate (SR), plant height (PH), and first leaf length (FLL) were used as indices for assessing cold tolerance under cold stress and BR-combined cold treatment at seed germination and bud burst stages. A high-resolution SNP genetic map, covering 1,145 bin markers with a distance of 3188.33 cM onto 12 chromosomes, was constructed using the GBS technique. A total of 73 QTLs were detected, of which 49 QTLs were identified under cold stress and 24 QTLs under BR-combined cold treatment. Among these, intervals of 30 QTLs were pairwise coincident under cold stress and BR-combined cold treatment, as well as different traits including SR and FLL, and PH and FLL, respectively. A total of 14 candidate genes related to cold tolerance or the BR signaling pathway, such as CBF/DREB (LOC_Os08g43200), bHLH (LOC_Os07g08440 and LOC_Os07g08440), WRKY (LOC_Os06g30860), MYB (LOC_Os01g62410 and LOC_Os05g51160), and BRI1-associated receptor kinase 1 precursor (LOC_Os06g16300), were located. Among these, the transcript levels of 10 candidate genes were identified under cold stress and BR-combined cold treatment by qRT-PCR. These findings provided an important basis for further mining the genes related to cold tolerance or the BR signaling pathway and understanding the molecular mechanisms of cold tolerance in rice.

Keywords: wild rice, QTL mapping, cold tolerance, brassinosteroids, germination and bud burst stages

INTRODUCTION

Rice (*Oryza sativa* L.) is one of the most important crops for food production, which grows in tropical, subtropical, and temperate regions worldwide (Cheng et al., 2007). Cold stress is one of the most severe environmental factors limiting the growth, development, and yield formation of rice. It affects almost all growth stages of rice, including germination stage, bud burst stage, seedling stage, tillering stage, booting stage, flowering stage, and grain filling stage (Fujino et al., 2004; Xu et al., 2015). The germination rate and post-germination early seedling growth are two important traits that directly contribute to seedling vigor (Fujino et al., 2008). Cold stress at the germination and bud burst stages is the major limitation due to high sensitivity to cold at these stages, especially for the direct-seeded rice. It impairs the seed germination and early seedling growth of rice, which in turn leads to uneven stand establishment of seedling, delay of panicle development, spikelet sterility, and subsequent yield loss (Satoh et al., 2016; Najeeb et al., 2020). Therefore, improving the cold tolerance of germination and bud burst stages is an important objective in rice cultivation and breeding.

Brassinosteroids (BR) are essential plant steroid hormones that play important roles in growth, development, and tolerance to stresses in plants. Many studies have reported that exogenous BR application can obviously improve cold tolerance in plants (Chung et al., 2014; Sharma et al., 2017; Manghwar et al., 2022). In *Arabidopsis thaliana*, loss-of-function mutations of *brassinosteroid insensitive 1* (*BRI1*) and *brassinazole resistant 1* (*BZR1*) and overexpression of *brassinosteroid insensitive 2* (*BIN2*) result in decreased cold tolerance, whereas overexpression *of BRI1* and *BZR1* enhances cold tolerance (Li et al., 2017; Manghwar et al., 2022). In addition, BR biosynthetic genes *BR6ox2*, *DWF4*, and *CPD* are rapidly downregulated under cold stress (Chung et al., 2014; Eremina et al., 2016). In rice, soaking with BR can effectively alleviate the damage of rice seeds under cold stress, and spraying with BR can also improve cold tolerance of rice seedlings (Hwang and Back, 2019; Wu et al., 2020; Sadura and Janeczko, 2021). However, few genes related to both cold tolerance and BR in rice have been reported to date. The regulatory relationship between cold tolerance and BR in rice remains undefined.

Cold tolerance is a very complex quantitative trait associated with a massive number of biochemical and physiological processes and environment factors, which is genetically controlled by multiple quantitative trait loci (QTLs) or genes (Zhang et al., 2014). QTL mapping is one of the most common methods to identify the QTLs and genes related to cold tolerance in plants. Many genomic regions on all 12 rice chromosomes have been reported to contain some QTLs related to cold tolerance at different development stages (Miura et al., 2001; Fujino et al., 2004, 2008; Yang et al., 2021). For instance, *Ctb1* is the first cloned QTL for cold tolerance in rice. *Ctb1* encodes a F-box protein, which improves cold tolerance by associating with a subunit of the E3 ubiquitin ligase (Skp1) at the booting stage of rice (Saito et al., 2010). CTB4a, a leucine-rich repeat receptor-like kinase, increases ATP synthase activity and ATP content by interacting with the β-subunit of ATP synthase, which enhances seed setting and improves yield under low-temperature stress conditions (Zhang et al., 2017). In addition, COLD1 functions as a GTPase-accelerating factor and regulates G-protein signaling under cold stress in rice. COLD1 interacts with regulator of GTPase-activating protein 1 (RGA1), rapidly activates inward current and Ca^{2+} concentration, and ultimately enhances cold tolerance at the seedling stage in japonica rice (Ma et al., 2015). However, these are not sufficient to mine the useful genes and reveal the molecular mechanisms of cold tolerance in rice. With the rapid development of high-throughput sequencing technologies, faster and simpler ways to obtain single-nucleotide polymorphism (SNP) molecular markers based on sequencing technologies are increasingly used to perform QTL mapping, such as genotyping-by-sequencing (GBS), bulked segregant analysis (BSA), and bulked segregant RNA-seq (BSR). The introduction of these technologies has accelerated the identification of millions of SNPs across the whole genome (Jiang et al., 2016; Mielczarek and Szyda, 2016). In particular, GBS is becoming popular for QTL mapping, genetic diversity, and genomic selection, which has been successfully applied in QTL mapping for cold tolerance, salinity tolerance, aluminum tolerance, rice blast resistance, pericarp color, and some agronomic trait in rice (Spindel et al., 2013; Arbelaez et al., 2015; De Leon et al., 2016).

Wild rice (*Oryza rufipogon* Griff) is the relative ancestor of the cultivated rice, which can be used as a donor of novel and favorable alleles for rice breeding (Nakagahra et al., 1997; Atwell et al., 2014; Zhang et al., 2020). QTL mapping has been extensively used to identify the novel loci from wild rice, and these loci are expected to be used for improving the agronomic traits of rice (Koseki et al., 2010; Mao et al., 2015). Dongxiang wild rice (DXWR) possesses an extremely high innate tolerance to low-temperature stress at the seedling, booting, and flowering stages, and its underground stem can tolerate −12.8°C (Li et al., 2010; Zhang et al., 2014). Some genes or QTLs related to cold tolerance have been isolated and characterized in DXWR (Liu et al., 2003; Tian et al., 2006; Li et al., 2010; Xiao et al., 2015; Deng et al., 2018; Liang et al., 2018, 2019; Bai et al., 2021). Therefore, DXWR is an ideal germplasm for improving the cold tolerance of rice by hybridization, backcrossing, or genetic transformation.

In this study, we constructed a backcross recombinant inbred line (BRIL) population of 140 individuals derived from a cross between the DXWR and a super rice SN265 with excellent agronomic traits. On this basis, we used the GBS technique to construct a high-resolution genome-wide SNP genetic map for identification of cold-tolerant QTLs and candidate genes under cold stress and BR-combined cold treatment at the germination and bud burst stages. This study has important reference value for the discovery of cold tolerance genes and understanding of the regulation relationship between cold tolerance and BR in rice.

MATERIALS AND METHODS

Plant Materials

The recipient parent SN265, a super rice variety with excellent agronomic traits from north China, was crossed with the donor

parent DXWR, and the F_1 plants were backcrossed with SN265 four times to develop the BC_4F_1 generation. The resulting BC_4F_1 lines were selfed and advanced by using the single seed descent method to generate 140 BRIL individuals in the F_8 generation (BC_4F_8).

Phenotypic Characterization for Cold Tolerance

The evaluation of cold tolerance at germination and bud burst stages was conducted based on previous studies with minor changes (Kim et al., 1999; Qiao et al., 2004; Akhtamov et al., 2020; Najeeb et al., 2020; Pan et al., 2020). Seeds of each accession from the BRILs were placed in a drying oven at 50°C for 72 h to break dormancy, and surface-sterilized in 1% NaClO solution for 10 min, followed by washing three times in sterilized distilled water. Then, 50 seeds were soaked with sterilized distilled water (for cold treatment) and 0.1 μmol/L BR solution (for BR-combined cold treatment) in a petri dish (15 cm) at a constant temperature of 20°C for 24 h, respectively. The 50 pre-soaked seeds were stressed at 10°C for 10 days, and then moved to a greenhouse at 25°C for recovery. The germinated seeds of each accession were counted daily and defined as the low-temperature germination rate (LTG). The germination rate was calculated as follows: Germination rate (%) = (number of germinated seeds/total number of seeds) × 100%. Cold tolerance based on the LTG was graded on a scale of 1–9 as follows: 1, more than 90%; 3, 80–90%; 5, 50–79%; 7, 1–49%; and 9, 0%.

The survival rate (SR) is the percentage of rice seedlings survived from the germination stage to the early seedling stage under cold stress. The pre-soaked seeds were germinated in a growth chamber at a constant temperature of 30°C for 24 h. The germinated seeds with 5-mm coleoptiles were stressed at 10°C for 7 days and then moved to a greenhouse at 25°C for 10 days to allow early seedlings to resume normal growth. The SR was calculated as follows: Survival rate (%) = (number of survival seedlings/number of buds) × 100%. At least five pots of 30 plants were assessed for each line. Cold tolerance based on the SR was graded on a scale of 1–9 as follows: 1, more than 90%; 3, 70–90%; 5, 50–70%; 7, 10–49%; and 9, less than 10%.

Cold stress can directly influence the growth of coleoptile length, leaf length, and plant height at the bud burst stage. Therefore, phenotypic evaluation of cold tolerance at the bud burst stage is significant (Qiao et al., 2004; Najeeb et al., 2020; Pan et al., 2020). In the current study, cold tolerance was evaluated based on the phenotypic changes of plant height (PH) and first leaf length (FLL) at the bud burst stage. The PH and FLL of the early seedlings after recovering for 10 days were measured. The average of the three replicates of 10 seedlings for each treatment was analyzed. For cold treatment, the data obtained under normal temperature (25°C) were used as control. Cold tolerance scores based on the reduction rate of the PH and FLL were calculated as follows: reduction rate of PH and FLL = [(PH or FLL under normal temperature − PH or FLL under cold treatment)/PH or FLL under normal temperature] × 100%. For BR-combined cold treatment, both data obtained under normal temperature and cold treatment were used as controls, respectively. Cold tolerance scores depend on the reduction rate of PH and FLL = [(PH or FLL under normal temperature − PH or FLL under BR-combined cold treatment)/PH or FLL under normal temperature] × 100%, or [(PH or FLL under BR-combined cold treatment − PH or FLL under cold treatment)/PH or FLL under BR-combined cold treatment] × 100%, respectively.

All experiments for evaluating cold tolerance at the bud burst stage were repeated three times under the same conditions, and the average cold tolerance scores from the three replicates were used for QTL mapping analysis. R software 3.5.1 was used to analyze frequency distributions and correlations of four phenotypic traits under their respective two treatments.[1] The "cor" function was used to calculate Pearson's correlation coefficient between any two treatments. The "hist" function computes a histogram of the average phenotypic scores of each individual under each treatment. The significance between any pair of treatment was classified as 0, 0.001, 0.01, 0.05, 0.1, and 1, which were denoted as "**," "**," "*," "." and "".

Genotyping and Single-Nucleotide Polymorphism Identification

Fresh young leaves were collected from 14-day-old seedlings of 140 BRILs along with their parental lines and subjected to DNA extraction using a DNA extraction kit (Aidlab, China). GBS technology was used to construct DNA fragment libraries from each BRILs and their parental lines. *Pst*I and *Msp*I (NEB) were used for digestion and T4 ligase (NEB) for ligation. The libraries were enriched by PCR amplification and sequenced using an Illumina HiSeq 4000 instrument (Huada Gene Technology Co. Ltd., Shenzhen, China). The data were analyzed by Tassel software (Glaubitz et al., 2014). The raw reads were then filtered and sorted according to indices, and the high-quality SNPs between parents were termed by alignment with Nipponbare reference genome.

Linkage Map Construction and Quantitative Trait Loci Mapping

The genotypic data from each BRILs with filtered SNP markers were used to construct linkage map using QTL IciMapping sofware v4.163. Furthermore, QTLs were mapped using the inclusive composite interval mapping of additive (ICIM-ADD) method. QTLs were computed by using a permutation test involving 1,000 runs at a significance level of $p = 0.05$. After completion of the permutation test, a window size of 10 cM and a walk speed of 1 cM were set to start analysis of composite interval mapping. The threshold for the logarithm of odds (LOD) scores was set to 3.0. QTL nomenclature was followed by the method of McCouch (2008).

Annotation and Validation of Candidate Genes

The QTL intervals were determined by the physical position of the SNP markers, flanking the respective QTLs. All candidate genes were predicted in the located QTL ranges based on

[1] www.R-project.org

the Rice Genome Annotation Project website.[2] The 3-day-old early seedlings with seeds from SN 265, DXWR, and three excellent cold-tolerant BRILs, and three non-excellent cold-tolerant BRILs at normal temperature, 12-h under cold stress, and 12-h BR-combined cold treatment (mentioned before for SR) were subjected to total RNA extraction using an RNA extraction kit (Aidlab, China). Three biological replicates were collected, immediately frozen in liquid nitrogen, and then stored at −80°C until further analysis. The real-time PCR (qRT-PCR) was performed to identify the expression patterns of 10 candidate genes. The qRT-PCR was carried out using a q225 Real-Time PCR System (Monad, China) under the following conditions: 95°C for 5 min; 30 cycles of 95°C for 10 s, 60°C for 30 s, and 72°C for 2 min; and 1 cycle of 72°C for 10 min. Each sample was analyzed in three biological and three technical replicates. The relative expression levels were calculated using the ΔΔCt method (Livak and Schmittgen, 2002). The *actin* gene of rice (LOC_Os03g50885) was used as a reference gene. ΔCt was the difference between the Cts (threshold cycles) of the target gene and Cts of the reference gene. ΔΔCt was calculated by subtracting ΔCt of the treatment group from ΔCt of the normal group. Fold change was calculated using the following formula: Fold change = $2^{-\Delta\Delta Ct}$. All primer sequences are listed in **Supplementary Table 1**.

RESULTS

Phenotypic Characterization Under Cold Stress and Brassinosteroid-Combined Cold Treatment

The BRIL population was evaluated under cold stress and BR-combined cold treatment at the germination and bud burst stages. The BRILs showed varying levels of cold tolerance and significantly contrasting responses in LTG, SR, PH, and FLL (**Figures 1**, **2**). For LTG, grade 5 had the highest number of BRILs under cold stress, followed by grades 3, 7, and 1. Under BR-combined cold treatment, the number of BRILs in grades 3 and 5 increased, whereas the number of BRILs in grade 7 decreased (**Figure 1B**). For SR, grade 3 had the highest number of BRILs under cold stress, followed by grades 1, 5, and 7. After BR-combined cold treatment, the number of BRILs in grades 1 and 5 increased, whereas the number of BRILs in grade 7 decreased (**Figure 1C**). Furthermore, the phenotypic changes of PH and FLL were analyzed under cold stress and BR-combined cold treatment (**Figure 2**). Under normal temperature, the range of PH was 5−8 cm, and most of BRILs were distributed in the range of 7−8 cm, while the range of FLL was 2−4 cm, and most of BRILs were distributed in the range of 3−4 cm. After cold stress and BR-combined cold treatment, the PH and FLL were significantly reduced in most BRILs, with the range of 4−7 cm for PH and 2−4 cm for FLL, respectively. Compared to cold stress, the number of BRILs with PH of a 6-cm range and FLL of both 2-cm and 3-cm ranges increased under BR-combined cold treatment (**Figures 2B,C**). These results indicated that the continuous single-peak pattern distributions were observed for all four investigated traits, which are consistent with quantitative traits controlled by multiple genes. In addition, the treatment of BR could improve the ranges of LTG, SR, PH, and FLL in some BRILs according to the number of alterations of BRILs.

[2]http://rice.plantbiology.msu.edu

Correlation Analysis of Low-Temperature Germination Rate, Survival Rate, Plant Height, and First Leaf Length

Pearson's correlation analysis revealed that all four traits in the BRIL populations showed continuous and approximately normal distributions. Under cold stress, highly significant positive correlations were observed between LTG and SR (r = 0.37, $p \leq 0.01$), and between PH and FLL (r = 0.39, $p \leq 0.01$), respectively. By contrast, there was a significant negative correlation between SR and PH (r = −0.21, $p \leq 0.05$). Under BR-combined cold treatment, the positive correlations between LTG and SR (r = 0.37, $p \leq 0.01$), as well as between PH and FLL (r = 0.39, $p \leq 0.01$), and a negative correlation between LTG and SR (r = 0.37, $p \leq 0.01$) were shown similar to those under cold stress. Additionally, under both cold stress and BR-combined cold treatment, all of LTG, SR, PH, and FLL showed highly significant positive correlations with r = 0.73 ($p \leq 0.01$), r = 0.73 ($p \leq 0.01$), r = 0.79 ($p \leq 0.01$), and r = 0.73 ($p \leq 0.01$), respectively (**Figure 3**).

Genetic Linkage Map of the Recombination Bin Markers

In total, 64.48 Gb of high-quality sequence data were obtained from 42.8 M raw reads *via* the GBS approach, and 96.19% of those reads were mapped to the Nipponbare reference genome. The ratio of Q20 for BRILs was above 90%, and the guanine–cytosine (GC) content was 43.55%; thus, the quality of the data met requirements for further analysis. Finally, a total of 10,836 unfiltered SNPs were validated for the determination of recombinant events. After filtration followed by the ABH plugin, a total of 1,145 recombination bin markers were obtained to construct a recombination map for the BRIL population.

A genetic linkage map was developed by mapping the 1,145 bin marker to the 12 rice chromosomes. The 12 rice linkage groups varied in the number of markers and marker density. The total genetic distance of linkage map was 3188.33 cM, with the individual linkage groups ranging from 186.74 to 346.46 cM in length. The highest number of markers was 117 on chromosome 4, and the lowest number was 77 on chromosome 7. The averaged genetic distance between markers was 0.3 cM, and the interval of genetic distance among markers ranged from 1.9 to 146.3 cM (**Table 1**).

Comprehensive Quantitative Trait Loci Mapping for Cold Tolerance in Backcross Recombinant Inbred Line Population

The 1,145 SNP markers were used in QTL mapping of cold tolerance based on LTG, SR, PH, and FLL, respectively. An LOD threshold of 3.0 was used to identify QTLs for each trait using the CIM analysis. A total of 73 QTLs were detected, of which 49

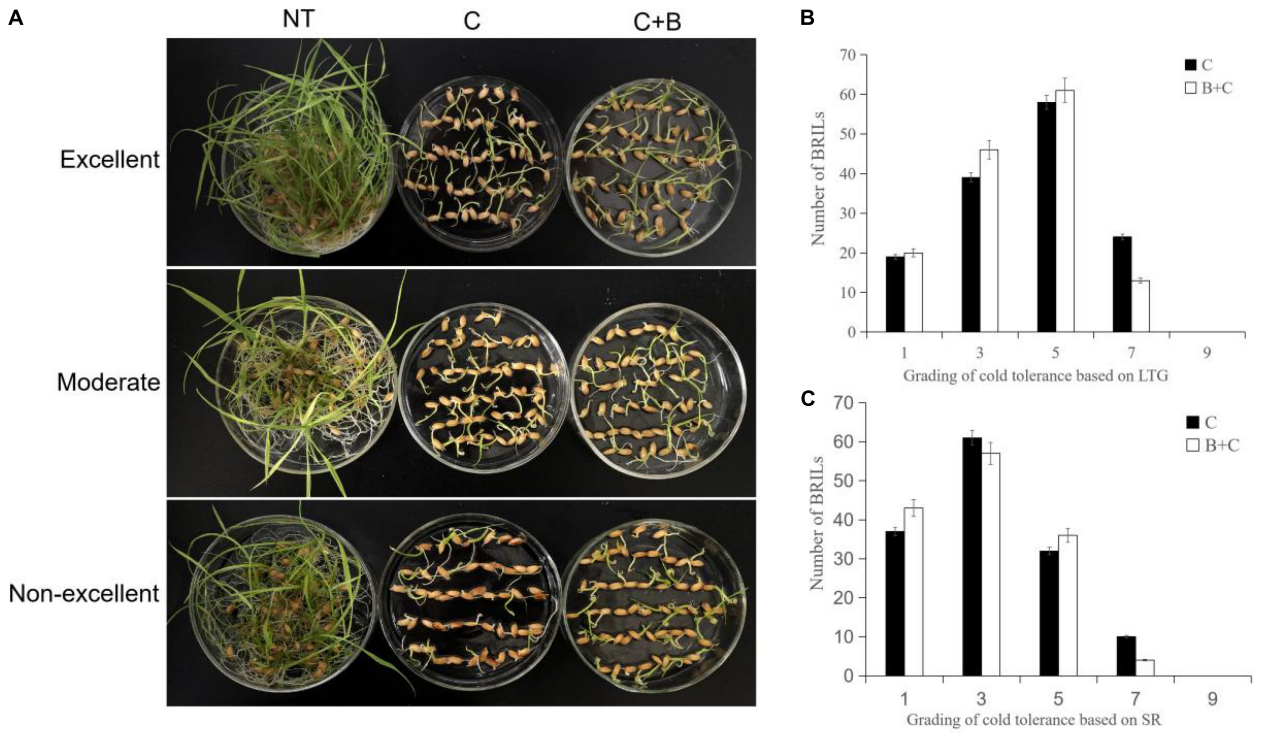

FIGURE 1 | Phenotypic characterization under cold stress and BR-combined cold treatment at the germination stage in BRILs. **(A)** Phenotypes of the representative BRILs with excellent, moderate, and non-excellent cold tolerance. **(B)** Grading of cold tolerance based on LTG. **(C)** Grading of cold tolerance based on SR. LTG, low-temperature germination rate; SR, survival rate; NT, normal temperature; C, cold stress; C + B, BR-combined cold treatment.

TABLE 1 | Summary of genetic linkage map characteristics in BRILs.

Chr	Number of bin markers	Genetic distance (cM)	Ave. genetic distance between markers (cM)	Ave. interval (cM)	Interval range (cM)
1	104	268.20	0.4	25.8	5.1–120.5
2	112	288.60	0.3	25.8	4.0–74.5
3	116	314.04	0.3	27.1	4.9–73.6
4	117	346.46	0.3	29.6	7.5–88.7
5	81	229.41	0.4	28.3	3.6–127.8
6	100	293.94	0.4	29.4	1.9–98.6
7	77	186.74	0.4	24.3	4.0–75.6
8	91	271.54	0.5	29.8	6.3–146.3
9	79	227.08	0.3	28.7	6.2–121.3
10	85	230.99	0.3	27.2	5.4–112.6
11	105	303.46	0.3	28.9	2.0–126.8
12	78	227.87	0.3	29.2	2.0–137.7
All	1,145	3188.33	0.3 (Ave.)	27.8 (Ave.)	1.9–146.3

Chr, chromosome number; Ave, average.

QTLs were identified under cold stress and 24 QTLs under BR-combined cold treatment. The phenotypic variation explained (PVE) by these QTLs ranged from 0.52 to 14.69%, while the range of LOD threshold was 3.02−9.38 (**Figure 4** and **Table 2**).

A total of four QTLs related to LTG were localized on chromosomes 7, 8, and 10, respectively. Among them, *qLTG7-1* with 3.93 LOD and 10.84% PVE was localized on chromosome 7 under cold stress, while *qLTG7-2*, *qLTG8-1*, and *qLTG10-1*, with the LOD ranging from 3.06 to 3.48 and PVE ranging from 4.74 to 12.41%, were localized on chromosomes 7, 8, and 10 under BR-combined cold treatment, respectively. The interval of *qLTG7-1* localized under cold stress coincided with the interval of *qLTG7-2* localized under BR-combined cold treatment (**Table 2**; **Supplementary Figure 1**).

For SR, a total of 43 QTLs were identified on all chromosomes, except chromosome 4, with LOD ranging from 3.05 to 9.38 and PVE ranging from 0.52 to 7.0%, 31 of which were localized

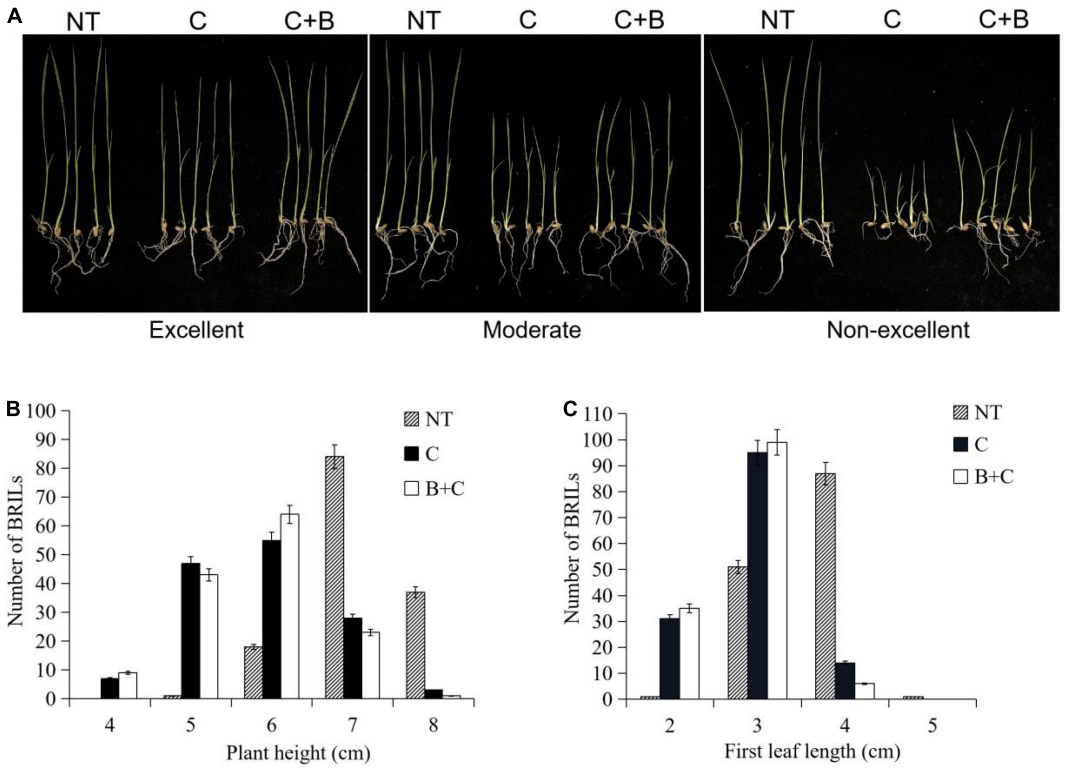

FIGURE 2 | Phenotypic characterization under cold stress and BR-combined cold treatment at the bud burst stage in BRILs. **(A)** Phenotypes of the representative BRILs with excellent, moderate, and non-excellent cold tolerance. **(B)** Ranges of the plant height in BRILs. **(C)** Ranges of the first leaf length in BRILs. NT, normal temperature; C, cold stress; C + B, BR-combined cold treatment.

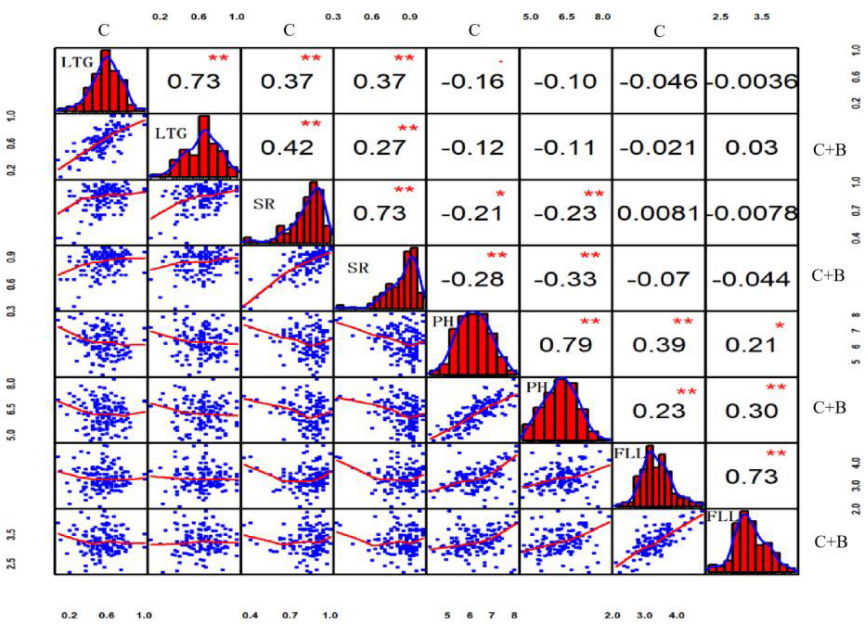

FIGURE 3 | Correlation analysis of LTG, SR, PH, and FLL under cold stress and BR-combined cold treatment. Plots on the diagonal line show phenotypic distribution of each trait as indicated; values above diagonal line are Pearson's correlation coefficients between traits; plots below diagonal line are scatter plots of compared traits. $^{**}P \leq 0.01$; $^{*}P \leq 0.05$. LTG, low-temperature germination rate; SR, survival rate; PH, plant height; FLL, first leaf length; C, cold stress; C + B, BR-combined cold treatment.

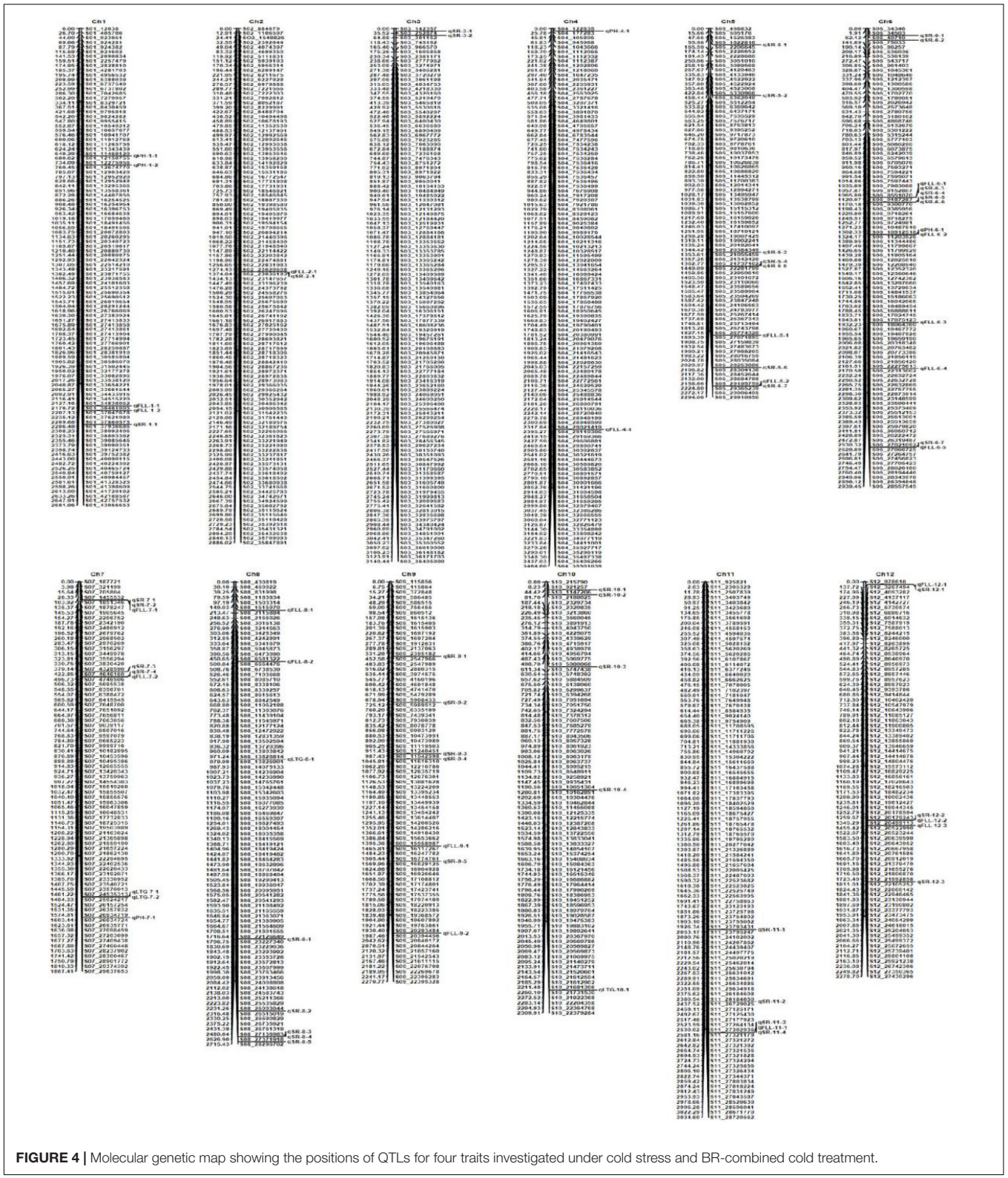

FIGURE 4 | Molecular genetic map showing the positions of QTLs for four traits investigated under cold stress and BR-combined cold treatment.

under cold stress and 12 were localized under BR-combined cold treatment, respectively. Intervals between some QTLs under both cold stress and BR-combined cold treatment were coincident, including *qSR5-4* and *qSR5-5*, *qSR6-4* and *qSR6-3*, *qSR6-6* and *qSR6-5*, *qSR7-1* and *qSR7-2*, *qSR8-4* and *qSR8-3*, and *qSR11-3* and *qSR11-4*, respectively (**Table 2**; **Supplementary Figure 2**).

TABLE 2 | QTL summary under different conditions for four traits.

Trait	Condition	QTL	Chr	Interval	LOD	PVE	Add
Germination rate	Cold	*qLTG7-1*	7	24535313–25924217	3.93	10.84	0.09
	Cold + BR	*qLTG7-2*	7	24535313–25924217	3.06	12.14	0.10
		qLTG8-1	8	13826814–13826901	3.24	6.40	–0.08
		qLTG10-1	10	21681306–21731530	3.48	4.74	–0.06
Seeding rate	Cold	*qSR1-1*	1	37869575–37936686	3.11	0.52	0.04
		qSR2-1	2	23029608–23036193	4.00	1.53	0.11
		qSR3-1	3	142357–252874	5.89	0.76	0.05
		qSR5-1	5	1622816–2206645	3.10	1.58	0.11
		qSR5-5	5	21737162–22281799	3.49	1.61	0.11
		qSR5-6	5	28253886–28304136	3.55	1.64	0.11
		qSR5-7	5	29195759–29365239	4.36	1.58	0.11
		qSR6-1	6	34503–49710	3.60	1.44	0.12
		qSR6-2	6	49710–75033	3.71	1.48	0.12
		qSR6-3	6	8551070–9187287	3.51	1.38	0.13
		qSR6-5	6	9187287–9300770	3.41	1.43	0.12
		qSR6-7	6	27021092–27066725	3.29	1.61	0.11
		qSR7-2	7	1455532–1851346	4.69	1.62	0.11
		qSR7-3	7	4328590–4646160	4.58	1.46	0.12
		qSR7-4	7	4646160–4746506	4.96	1.60	0.11
		qSR8-1	8	22126649–23227340	3.05	1.54	0.11
		qSR8-2	8	26093044–26515019	3.87	1.57	0.12
		qSR8-3	8	27136983–27371918	3.91	1.52	0.12
		qSR9-1	9	2395182–2547966	4.62	1.61	0.12
		qSR9-2	9	5908433–5989512	4.65	1.37	0.10
		qSR9-3	9	11240451–11542598	5.32	1.58	0.11
		qSR9-4	9	11542598–11616310	3.95	1.49	0.10
		qSR9-5	9	16774761–16829125	3.45	1.44	0.12
		qSR10-3	10	5080068–5747438	3.63	1.56	0.11
		qSR10-4	10	10051304–10162891	3.44	1.60	0.11
		qSR11-1	11	23793431–23795247	4.23	1.53	0.12
		qSR11-2	11	26184650–26729025	3.28	1.50	0.11
		qSR11-4	11	27302936–27321179	3.58	1.48	0.11
		qSR12-1	12	978610–3267494	4.14	1.55	0.12
		qSR12-2	12	20179243–20499113	3.99	1.56	0.12
		qSR12-3	12	21992858–22105252	3.60	1.55	0.11
	C + BR	*qSR3-2*	3	252874–381152	9.38	7.00	0.09
		qSR5-2	5	5330966–5362049	3.83	1.55	–0.04
		qSR5-3	5	20384349–21055459	3.33	2.76	–0.08
		qSR5-4	5	21737162–22281799	3.50	3.97	0.09
		qSR6-4	6	8551070–9187287	3.22	3.74	0.11
		qSR6-6	6	9187287–9300770	3.29	4.10	0.10
		qSR7-1	7	1455532–1851346	3.23	4.15	0.10
		qSR8-4	8	27136983–27371918	3.57	3.61	0.12
		qSR8-5	8	27371918–28296702	3.05	3.59	0.12
		qSR10-1	10	921257–1147206	4.85	4.20	0.09
		qSR10-2	10	1147206–2188025	3.31	3.91	0.09
		qSR11-3	11	27302936–27321179	3.59	4.11	0.10
Plant height	Cold	*qPH1-2*	1	12275956–12674770	3.89	11.71	0.05
	Cold + BR-N	*qPH1-1*	1	11469120–12150755	3.63	9.27	–0.05
		qPH4-1	4	122635–177283	4.73	8.94	–0.05
		qPH7-1	7	26934719–26934724	8.58	14.69	–0.07
	Cold + BR-C	*qPH6-1*	6	10912518–11203926	4.13	10.62	–0.05
First leaf length	Cold	*qFLL1-1*	1	34838052–36461005	3.34	1.37	–0.12
		qFLL2-1	2	23029608–23036193	3.35	1.39	–0.14

(Continued)

TABLE 2 | (Continued)

Trait	Condition	QTL	Chr	Interval	LOD	PVE	Add
		qFLL4-1	4	29021419–29110306	3.92	1.35	–0.13
		qFLL5-1	5	26774329–27071895	3.14	1.39	–0.14
		qFLL5-2	5	29195759–29365239	3.66	1.41	–0.14
		qFLL6-1	6	8551070–9187287	3.26	1.34	–0.14
		qFLL6-3	6	17075123–18064360	3.14	1.38	–0.14
		qFLL6-5	6	27021092–27066725	3.65	1.41	–0.13
		qFLL7-1	7	1455532–1851346	3.02	1.36	–0.14
		qFLL7-2	7	4646160–4746506	3.40	1.34	–0.14
		qFLL9-1	9	15958987–16117267	3.02	1.34	–0.12
		qFLL9-2	9	20293484–20394456	3.34	1.27	–0.13
		qFLL11-1	11	27302936–27321179	3.22	1.30	–0.14
		qFLL12-1	12	978610–3267494	3.77	1.37	–0.15
		qFLL12-2	12	20179243–20499113	3.82	1.42	–0.15
		qFLL12-3	12	20499113–20522990	4.11	1.44	–0.15
	Cold + BR-N	*qFLL1-2*	1	36461005–37047678	3.12	11.12	–0.07
		qFLL6-4	6	22275613–22313002	4.12	8.92	0.06
	Cold + BR-C	*qFLL6-2*	6	10912518–11203926	4.49	7.66	–0.07
		qFLL8-1	8	1515970–2115884	4.68	9.81	–0.09
		qFLL8-2	8	6581322–6664476	3.28	7.33	–0.07

Chr, chromosome number; LOD, logarithm of odds value; PVE, phenotypic variance explained; Add, additive effect; Cold, cold stress; Cold + BR, BR-combined cold treatment; Cold + BR-N, the data under normal temperature condition were used as the control; Cold + BR-C, the data under cold treatment condition were used as the control.

Unlike the LTG and SR, the data analysis of PH and FLL for QTL mapping needed to set different treatments as the controls (see Section "Materials and Methods" for details). For PH, only one QTL (*qPH1-2*) was localized on chromosome 1 under cold stress. Under BR-combined cold treatment, three QTLs (*qPH1-1*, *qPH4-1*, and *qPH7-1*) were identified on chromosomes 1, 4, and 7 with the control of PH under the normal-temperature condition, while one QTL (*qPH6-1*) was localized on chromosome 6 with the control of PH under cold stress. The LOD values of these QTLs ranged from 3.63 to 8.58, and their PVE values ranged from 8.94 to 14.69% (**Table 2**; **Supplementary Figure 3**).

For FLL, a total of 21 QTLs with LOD ranging from 3.02 to 4.68 and PVE ranging from 1.27 to 11.12% were identified on all chromosomes, except chromosomes 3 and 10. Among these 21 QTLs, 16 were localized in cold stress and five were localized in BR-combined cold treatment. Under BR-combined cold treatment, two QTLs (qFLL1-2 and *qFLL6-4*) were identified on chromosomes 1 and 6 using PH under normal-temperature conditions as control, while three QTLs (*qFLL6-2*, *qFLL8-1*, and *qFLL8-2*) were localized on chromosomes 6 and 8 with PH under cold stress as control (**Table 2**; **Supplementary Figure 4**).

Interestingly, intervals between some QTLs related to different traits were also coincident including *qSR2-1* and *qFLL2-1*, *qSR5-7* and *qFLL5-2*, *qSR6-4* and *qFLL6-1*, *qSR6-7* and *qFLL6-5*, *qSR7-2* and *qFLL7-1*, *qSR7-4* and *qFLL7-2*, *qSR11-3* and *qFLL11-1*, and *qFLL6-2* and *qPH6-1*, respectively.

Identification of Candidate Genes

According to the Rice Genome Annotation Project, the coincident QTL regions and QTLs with a higher LOD score (more than 5.0) were chosen to identify candidate genes using flanking markers. A total of 121 genes were located in the QTL regions mentioned previously, of which 60 were annotated with known functions, while the remaining 61 genes were identified as expressed proteins, hypothetical proteins, transposon, and retrotransposon proteins (**Supplementary Table 2**). Among these annotated candidate genes, 14 genes were possibly associated with cold tolerance or the BR signaling pathway based on the previously reported studies (**Table 3**). These genes included some transcription factors such as C-repeat-binding factor/DRE-binding factor (CBF/DREB, LOC_Os08g43200), basic helix–loop–helix (bHLH) transcription factor (LOC_Os07g08440 and LOC_Os05g50900), AP2 domain-containing proteins (LOC_Os06g44750 and LOC_Os06g09390), WRKY (LOC_Os06g30860), and MYB (LOC_Os01g62410 and LOC_Os05g51160), ethylene-responsive transcription factor (ERF, LOC_Os05g34730), and some other proteins including leucine-rich repeat (LRR) family protein (LOC_Os03g01410), heat shock factor-binding protein (LOC_Os06g16270), zinc finger-containing protein (LOC_Os06g09310), and extra-large G-protein-related (LOC_Os05g50910), and brassinosteroid insensitive 1 (BRI1)-associated receptor kinase 1 precursor (LOC_Os06g16300). Surprisingly, BRI1-associated receptor kinase 1 precursor, a protein associated with the BR signaling pathway, was just identified under BR-combined cold treatment. Furthermore, we validated the expression levels of 10 candidate genes under cold stress and BR-combined cold treatment using qRT-PCR. The results showed that the transcript levels of all genes, except LOC_Os05g50910 and LOC_Os05g34730, were significantly higher under both cold

TABLE 3 | Summary of the annotated candidate genes possibly associated with cold tolerance or the BR signaling pathway.

Condition	QTL	Chr	Locus name	Gene coordinates	Gene product
Cold/Cold + BR	qSR6-5/6	6	LOC_Os06g16300	9289219–9291362	BRASSINOSTEROID INSENSITIVE 1 Associated receptor kinase 1 precursor
Cold/Cold + BR	qSR8-3	8	LOC_Os08g43200	27321388–27320517	DREB dehydration-responsive element-binding protein
Cold	qFLL1-1	1	LOC_Os01g62410	36122778–36128487	MYB family transcription factor
Cold	qFLL5-2/qSR5-7	5	LOC_Os05g51160	29348631–29347196	MYB family transcription factor
Cold	qFLL6-3	6	LOC_Os06g30860	17917083–17915923	WRKY transcription factor 31
Cold + BR	qSR5-3	5	LOC_Os05g34730	20601854–20601261	Ethylene-responsive transcription factor ERF020
Cold	qSR7-3	7	LOC_Os07g08440	4338514–4342219	bHLH transcription factor
Cold	qFLL5-2/qSR5-7	5	LOC_Os05g50900	29211341–29208619	bHLH transcription factor
Cold/Cold + BR	qSR6-5/6	6	LOC_Os06g16270	9263601–9265449	Heat shock factor binding protein 2
Cold + BRs	qSR3-2	3	LOC_Os03g01410	294916–293668	Leucine rich repeat family protein
Cold	qFLL5-2/qSR5-7	5	LOC_Os05g50910	29213556–29219606	Extra-large G-protein-related
Cold	qFLL6-5/qSR6-7	6	LOC_Os06g44750	27025437–27029339	AP2 domain containing protein
Cold	qFLL7-2/qSR7-4	7	LOC_Os06g09390	4731330–4733911	AP2 domain containing protein
Cold	qFLL7-2/qSR7-4	7	LOC_Os06g09310	4678838–4680332	Zinc finger, C3HC4 type domain containing protein

Chr, chromosome number; Cold, cold treatment; Cold + BR, BR-combined cold treatment.

stress and BR-combined cold treatment than under normal temperature in all materials tested, while the transcript levels of LOC_Os06g16300, LOC_Os08g43200, and LOC_Os05g50900 under BR-combined cold treatment were slightly higher than those under cold stress. For two parents, LOC_Os05g50900, LOC_Os06g16300, and LOC_Os03g01410 showed higher expression levels in DXWR than in SN265 under cold stress and BR-combined cold treatment, whereas the opposite expression pattern was observed for LOC_Os06g30860 and LOC_Os06g09310. For the representative BRILs, LOC_Os05g50900, LOC_Os06g16300, LOC_Os08g43200, LOC_Os05g50900, and LOC_Os06g09390 showed higher transcript levels in three excellent BRILs than three non-excellent BRILs both under cold stress and BR-combined cold treatment (**Figure 5**; **Supplementary Figure 5**).

DISCUSSION

As a complex quantitative trait, cold tolerance in plants is controlled by various QTLs or genes. Thus, it is absolutely essential to mine more QTLs or genes to get a deeper understanding of molecular mechanisms for cold tolerance in plants (Zhang et al., 2014; Jha et al., 2017). Genetic diversity is the basis of the agronomic traits and stress resistance improvement in plants, and gene diversity is the most widely used index for measuring the level of genetic diversity. Wild species have high diversity of desirable genes for agronomic traits and resistance to stresses, and these allelic variations are important genetic resources for agronomic traits and stress resistance improvement (Koseki et al., 2010; Atwell et al., 2014). Common wild rice is the relative ancestor of the cultivated rice, which possesses abundant genetic diversity that can be used to improve agronomic traits and resistance to stress in cultivated rice. However, some gene resources might have been lost in cultivated rice after thousands of years of evolution and natural selection (Liu et al., 2003; Koseki et al., 2010; Liang et al., 2018, 2019; Zhang et al., 2020).

As previously mentioned, DXWR has a strong cold tolerance at the seedling, booting, and flowering stages, which is an ideal material for identifying and offering genes related to cold tolerance for rice improvement (Zhang et al., 2006). To date, many rice populations have been constructed using DXWR as the paternal parent, while many QTLs and candidate genes related to cold tolerance have been identified in these populations (Mao et al., 2015; Liang et al., 2018, 2019). In the current study, SN265, a super rice variety with excellent agronomic traits, was crossed with the donor parent DXWR to obtain F1 populations. To have a uniform background, the material was propagated by backcrossing the F1 populations with female parent SN265 for additional four times (BC_4F_1). Furthermore, the BC_4F_1 populations were selfed for multiple generations to generate an advanced BRIL population (BC_4F_8), and 140 BRIL individuals with abundant genetic diversity were chosen for cold tolerance evaluation and GBS sequencing. The backcrossing and selfing for multiple generations eliminated the background interference caused by different genetic bases, making the results of phenotypic evaluation and QTL mapping of cold tolerance more accurate and reliable.

Multiple studies have demonstrated that exogenous application of BR increased cold tolerance in plants. However, only several genes in BR biosynthesis and signaling pathways were reported to be involved in cold tolerance in Arabidopsis such as *BRI1*, *BZR1*, *BIN2*, *BR6ox2*, *DWF4*, and *CPD* (Chung et al., 2014; Eremina et al., 2016; Li et al., 2017; Sharma et al., 2017; Manghwar et al., 2022). In rice, few genes have been reported to be involved in both cold stress and BR biosynthesis or signaling pathways.

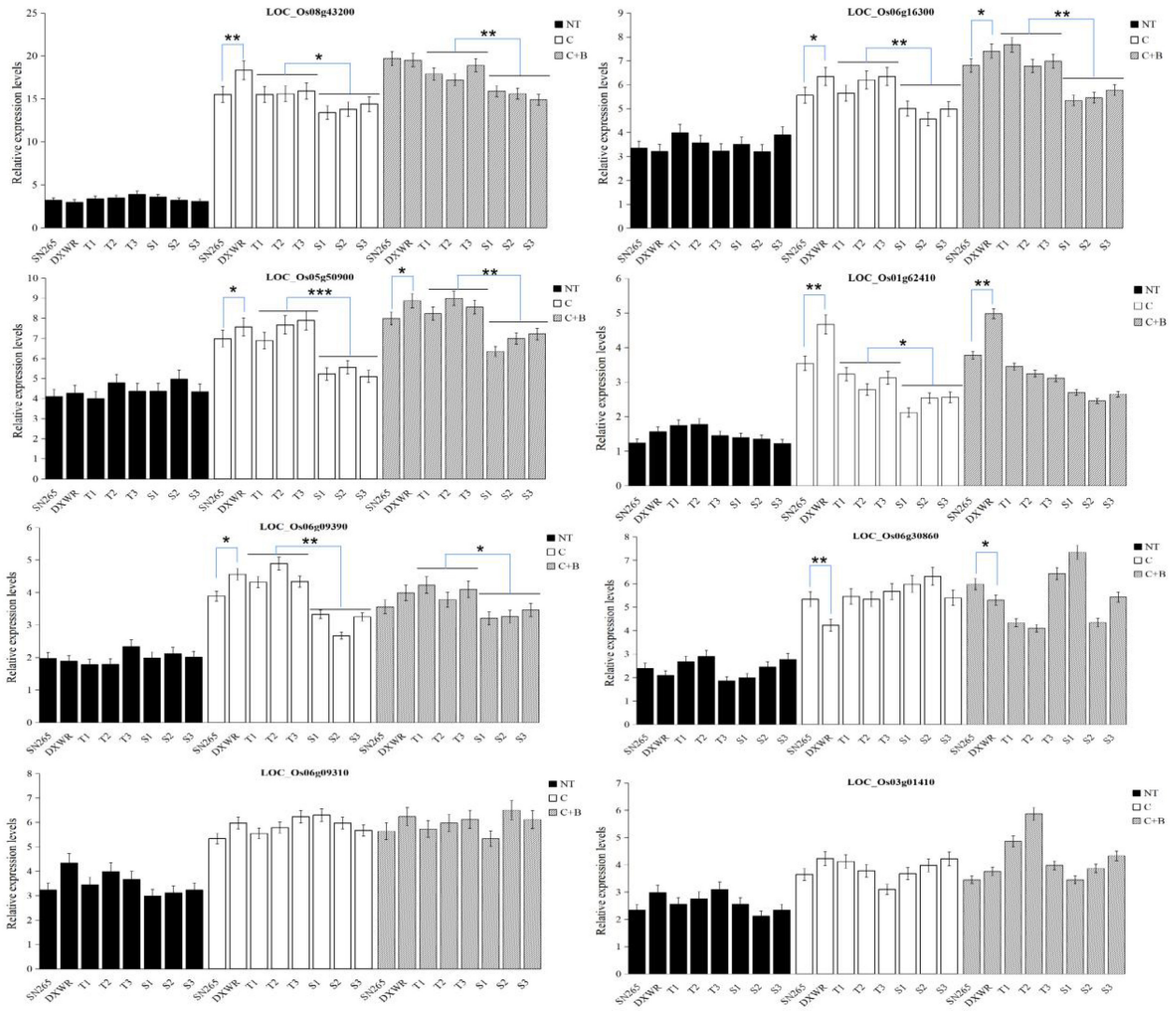

FIGURE 5 | Expression patterns of the candidate genes. Biological triplicates were averaged and statistically analyzed *via* Student's *t*-test (*$P < 0.05$; **$P < 0.01$; ***textitP < 0.001). NT, normal temperature; C, cold stress; C + B, BR-combined cold treatment.

In the current study, the exogenous application of BR improved the cold tolerance of some BRILs at germination and bud burst stages under cold stress, which provided a basis for identifying the QTLs related to cold stress and BR pathways.

The data of LTG and SR could be derived directly from the calculation of corresponding proportion under different treatments, and the analysis process does not need the controls (see Section "Materials and Methods" for details). Unlike LTG and SR, however, the measurements of PH and FLL for QTL mapping need to have a control so that the data could embody the changes under different treatment. Thus, the measurements of PH and FLL under cold stress set the data under normal-temperature condition as the control, whereas the measurements of PH and FLL under BR-combined cold treatment set the data under normal-temperature condition and cold stress as the controls, respectively. This was done to obtain more comprehensive QTLs (Kim et al., 1999; Qiao et al., 2004; Akhtamov et al., 2020; Najeeb et al., 2020; Pan et al., 2020).

In QTL mapping, intervals between some QTLs were coincident under different treatments (cold stress and BR-combined cold treatment), as well as different traits including SR and FLL, and PH and FLL, respectively. These coincident QTLs were probably more accurate. Furthermore, many candidate genes were identified by using the coincident QTL regions and those QTLs with higher LOD scores (more than 5.0). Among these genes, there were some transcription factors related to cold tolerance such as CBF/DREB (LOC_Os08g43200), bHLH (LOC_Os07g08440 and LOC_Os07g08440), WRKY (LOC_Os06g30860), MYB (LOC_Os01g62410 and LOC_Os05g51160), and ERF

(LOC_Os05g34730). In particular, DREB/CBF, bHLH, and WRKY transcription factors have been reported to be involved in BR signaling pathways. Under cold conditions, BR directs a bHLH transcription factor CESTA (CES) to contribute to the constitutive expression of the CBF regulators that control the expression of cold responsive genes in Arabidopsis (Eremina et al., 2016). BZR1, a key transcription factor in the BR signaling pathway, acts upstream of CBF1 and CBF2 to directly improve cold tolerance in Arabidopsis. Moreover, BZR1 also regulates WKRY6 to modulate plant response to cold stress (Li et al., 2017). In the current study, qRT-PCR was applied to preliminarily characterize the transcript levels of all transcription factor genes under cold stress and BR-combined cold treatment. The transcript levels of these genes, except LOC_Os05g34730, were upregulated both under cold stress and BR-combined cold treatment. For the representative BRILs, LOC_Os05g50900 (bHLH), LOC_Os08g43200 (DREB/CBF), and LOC_Os05g50900 (bHLH) showed higher transcript levels in the excellent BRILs than in the non-excellent BRILs under cold stress and BR-combined cold treatment. In addition to the transcription factors, some genes related to cold tolerance were also identified such as LRR protein, heat shock factor-binding protein, and zinc finger-containing protein. Interestingly, a BRI1-associated receptor kinase 1 precursor (LOC_Os06g16300) was also identified under BR-combined cold stress. BRI1 is a leucine-rich repeat receptor-like kinase that functions as the cell surface receptor for BR, and loss-of-function mutation of *BRI1* resulted in decreased cold tolerance in Arabidopsis (Eremina et al., 2016; Xu et al., 2022). Although the aforementioned candidate genes have been reported to be involved in cold tolerance or BR signaling pathways, few genes related to both cold stress and BR pathways have been studied in rice. In the current study, we initially demonstrated that the transcript levels of LOC_Os06g16300 (BRI1-associated receptor kinase 1), LOC_Os08g43200 (DREB/CBF), and LOC_Os05g50900 (bHLH) under BR-combined cold treatment were higher than those under cold stress. Further studies are needed to demonstrate whether these genes are involved in cold tolerance and BR pathways in rice. In conclusion, many QTLs and candidate genes were identified by GBS sequencing and mapping analysis, which provided an important basis for further mining the genes related to cold tolerance or BR pathways and studying the molecular mechanisms regulating cold tolerance in rice.

DATA AVAILABILITY STATEMENT

The original contributions presented in the study are publicly available. This data can be found here: NCBI, PRJNA836720.

AUTHOR CONTRIBUTIONS

ML and MZ designed and supervised the research work. ZG, MZ, and ML constructed the materials. ZG, HW, and JY determined phenotypic data, mapping analysis, and qRT-PCR experiments. YC and WZ performed the candidate gene association. JH and ZX contributed to revising the manuscript. All authors contributed to the article and approved the submitted version.

FUNDING

This work was supported by the Natural Science Foundation of Liaoning Province (2019JH3/10300327), the Liaoning Revitalization Talents Program (XLYC2008025), the Liaoning BaiQianWan Talents Program (2020921092), and the Basic Research Project of Education Department of Liaoning Province (LSNJC202022).

ACKNOWLEDGMENTS

We express our gratitude to the reviewers for helpful comments to improve the manuscript. We thank Ao Zhang from Shenyang Agricultural University for help with handling the data.

SUPPLEMENTARY MATERIAL

The Supplementary Material for this article can be found online at: https://www.frontiersin.org/articles/10.3389/fpls.2022.938339/full#supplementary-material

REFERENCES

Akhtamov, M., Adeva, C., Shim, K. C., Lee, H. S., Kim, S. H., Jeon, Y. A., et al. (2020). Characterization of quantitative trait loci for germination and coleoptile length under low-temperature condition using introgression lines derived from an interspecific cross in rice. *Genes* 11:1200. doi: 10.3390/genes11101200

Arbelaez, J. D., Moreno, L. T., Singh, N., Tung, C. W., Maron, L. G., Ospina, Y., et al. (2015). Development and GBS-genotyping of introgression lines (ILs) using two wild species of rice, *O. meridionalis* and *O. rufipogon,* in a common recurrent parent, *O. sativa* cv. Curinga. *Mol. Breed.* 35:81. doi: 10.1007/s11032-015-0276-7

Atwell, B. J., Wang, H., and Scafaro, A. P. (2014). Could abiotic stress tolerance in wild relatives of rice be used to improve *Oryza sativa*? *Plant Sci.* 215-216, 48–58. doi: 10.1016/j.plantsci.2013.10.007

Bai, L. W., Liu, J., Dai, L. F., Deng, Q. W., Chen, Y. L., Xie, J. K., et al. (2021). Identification and characterisation of cold stress-related proteins in *Oryza rufipogon* at the seedling stage using label-free quantitative proteomic analysis. *Funct. Plant Biol.* 48, 542–555. doi: 10.1071/FP20046

Cheng, S. H., Cao, L. Y., Zhuang, J. Y., Chen, S. G., Zhan, X. D., Fan, Y. Y., et al. (2007). Super hybrid rice breeding in China: achievements and prospects. *J. Integr. Plant Biol.* 49, 805–810. doi: 10.1111/j.1672-9072.2007.00514.x

Chung, Y., Kwon, S. I., and Choe, S. (2014). Antagonistic regulation of Arabidopsis growth by brassinosteroids and abiotic stresses. *Mol. Cells.* 37, 795–803. doi: 10.14348/molcells.2014.0127

De Leon, T. B., Linscombe, S., and Subudhi, P. K. (2016). Molecular dissection of seedling salinity tolerance in rice (*Oryza sativa* L.) using a high-density GBS-based SNP linkage map. *Rice* 9:52. doi: 10.1186/s12284-016-0125-2

Deng, Q. W., Luo, X. D., Chen, Y. L., Zhou, Y., Zhang, F. T., Hu, B. L., et al. (2018). Transcriptome analysis of phosphorus stress responsiveness in the seedlings

of Dongxiang wild rice (*Oryza rufipogon* Griff.). *Biol. Res*. 51:7. doi: 10.1186/s40659-018-0155-x

Eremina, M., Unterholzner, S. J., Rathnayake, A. I., Castellanos, M., Khan, M., Kugler, K. G., et al. (2016). Brassinosteroids participate in the control of basal and acquired freezing tolerance of plants. *Proc. Natl. Acad. Sci. U.S.A*. 113, E5982–E5991. doi: 10.1073/pnas.1611477113

Fujino, K., Sekiguchi, H., Matsuda, Y., Sugimoto, K., Ono, K., and Yano, M. (2008) Molecular identification of a major quantitative trait locus, qLTG3-1, controlling low-temperature germinability in rice. *Proc. Natl. Acad. Sci. USA*. 105, 12623–12628. doi: 10.1073/pnas.0805303105

Fujino, K., Sekiguchi, H., Sato, T., Kiuchi, H., Nonoue, Y., Takeuchi, Y., et al. (2004). Mapping of quantitative trait loci controlling low-temperature germinability in rice (*Oryza sativa* L.). *Theor. Appl. Genet*. 108, 794–799. doi: 10.1007/s00122-003-1509-4

Glaubitz, J. C., Casstevens, T. M., Lu, F., Harriman, J., Elshire, R. J., Sun, Q., et al. (2014). TASSEL-GBS: a high capacity genotyping by sequencing analysis pipeline. *PLoS One* 9:e90346. doi: 10.1371/journal.pone.0090346

Hwang, O. J., and Back, K. (2019). Melatonin deficiency confers tolerance to multiple abiotic stresses in rice via decreased brassinosteroid levels. *Int. J. Mol. Sci*. 20:5173. doi: 10.3390/ijms20205173

Jha, U. C., Bohra, A., and Jha, R. (2017). Breeding approaches and genomics technologies to increase crop yield under low-temperature stress. *Plant Cell Rep*. 36, 1–35. doi: 10.1007/s00299-016-2073-0

Jiang, Z., Wang, H., Michal, J. J., Zhou, X., Liu, B., Woods, L. C., et al. (2016). Genome wide sampling sequencing for SNP genotyping: methods, challenges and future development. *Int. J. Biol. Sci*. 12, 100–108. doi: 10.7150/ijbs.13498

Kim, K. M., Park, G. H., Kim, J. H., Kwon, Y. S., and Sohn, J. K. (1999). Selection of RAPD marker for growth of seedlings at low temperature in rice. *Mol. Cells* 9, 265–269.

Koseki, M., Kitazawa, N., Yonebayashi, S., Maehara, Y., Wang, Z. X., and Minobe, Y. (2010). Identification and fine mapping of a major quantitative trait locus originating from wild rice, controlling cold tolerance at the seedling stage. *Mol. Genet. Genomics* 284, 45–54. doi: 10.1007/s00438-010-0548-1

Li, F., Guo, S., Zhao, Y., Chen, D., Chong, K., and Xu, Y. (2010). Overexpression of a homopeptide repeat-containing bHLH protein gene (OrbHLH001) from Dongxiang Wild Rice confers freezing and salt tolerance in transgenic Arabidopsis. *Plant Cell Rep*. 29, 977–986. doi: 10.1007/s00299-010-0883-z

Li, H., Ye, K., Shi, Y., Cheng, J., Zhang, X., and Yang, S. (2017). BZR1 positively regulates freezing tolerance via CBF-dependent and CBF-independent pathways in arabidopsis. *Mol. Plant*. 10, 545–559. doi: 10.1016/j.molp.2017.01.004

Liang, Y., Yan, C., Zheng, J., Nan, W., Qin, X., and Zhang, H. (2019). Locating QTL associated with spike traits of dongxiang wild rice (*Oryza rufipogon* Griff.). *Euphytica* 215:26. doi: 10.1007/s10681-019-2349-x

Liang, Y., Zheng, J., Yan, C., Li, X., Liu, S., Zhou, J., et al. (2018). Locating QTLs controlling overwintering trait in Chinese perennial Dongxiang wild rice. *Mol. Genet. Genomics* 293, 81–93. doi: 10.1007/s00438-017-1366-5

Liu, F. X., Sun, C. Q., Tan, L. B., Fu, Y. C., Li, D. J., and Wang, X. K. (2003). Identifiification and mapping of quantitative trait loci controlling cold-tolerance of Chinese common wild rice (*O. rufifipogon* Griff.) at booting to flowering stages. *Chin. Sci. Bull*. 48, 2068–2071. doi: 10.1360/03wc0287

Livak, K. J., and Schmittgen, T. D. (2002). Analysis of relative gene expression data using real-time quantitative PCR. *Methods* 25, 402–408. doi: 10.1006/meth.2001.1262

Ma, Y., Dai, X., Xu, Y., Luo, W., Zheng, X., Zeng, D., et al. (2015). COLD1 confers chilling tolerance in rice. *Cell* 160, 1209–1221. doi: 10.1016/j.cell.2015.01.046

Manghwar, H., Hussain, A., Ali, Q., and Liu, F. (2022). Brassinosteroids (BRs) role in plant development and coping with different stresses. *Int. J. Mol. Sci*. 23:1012. doi: 10.3390/ijms23031012

Mao, D., Yu, L., Chen, D., Li, L., Zhu, Y., Xiao, Y., et al. (2015). Multiple cold resistance loci confer the high cold tolerance adaptation of Dongxiang wild rice (*Oryza rufipogon*) to its high-latitude habitat. *Theor. Appl. Genet*. 128, 1359–1371. doi: 10.1007/s00122-015-2511-3

McCouch, S. R. (2008). Gene nomenclature system for rice. *Rice* 1, 72–84. doi: 10.1007/s12284-008-9004-9

Mielczarek, M., and Szyda, J. (2016). Review of alignment and SNP calling algorithms for next-generation sequencing data. *J. Appl. Genet*. 57, 71–79. doi: 10.1007/s13353-015-0292-7

Miura, K., Lin, S. Y., Yano, M., and Nagamine, T. (2001). Mapping quantitative trait loci controlling low temperature germinability in rice (*Oryza sativa* L.). *Breed Sci*. 51, 293–299. doi: 10.1270/jsbbs.51.293

Najeeb, S., Ali, J., Mahender, A., Pang, Y. L., Zilhas, J., Murugaiyan, V., et al. (2020). Identification of main-effect quantitative trait loci (QTLs) for low-temperature stress tolerance germination- and early seedling vigor-related traits in rice (*Oryza sativa* L.). *Mol. Breed*. 40:10. doi: 10.1007/s11032-019-1090-4

Nakagahra, M., Okuno, K., and Vaughan, D. (1997). Rice genetic resources: history, conservation, investigative characterization and use in Japan. *Plant Mol. Biol*. 35, 69–77.

Pan, Y., Liang, H., Gao, L., Dai, G., Chen, W., Yang, X., et al. (2020). Transcriptomic profiling of germinating seeds under cold stress and characterization of the cold-tolerant gene LTG5 in rice. *BMC Plant Biol*. 20:371. doi: 10.1186/s12870-020-02569-z

Qiao, Y. L., Zhang, Y. Y., An, Y. P., Zhang, Y. R., Cao, G. L., and Han, L. Z. (2004). Screening method of cold tolerance at the budburst period in japonica rice. *J. Plant Genet. Res*. 5, 290–294. doi: 10.13430/j.cnki.jpgr.2004.03.017

Sadura, I., and Janeczko, A. (2021). Brassinosteroids and the Tolerance of Cereals to Low and High Temperature Stress: Photosynthesis and the Physicochemical Properties of Cell Membranes. *Int. J. Mol. Sci*. 23:342. doi: 10.3390/ijms23010342

Saito, K., Hayano-Saito, Y., Kuroki, M., and Sato, Y. (2010). Map-based cloning of the rice cold tolerance gene *Ctb1*. *Plant Sci*. 179, 97–102. doi: 10.1016/j.plantsci.2010.04.004

Satoh, T., Tezuka, K., Kawamoto, T., Matsumoto, S., Satoh-Nagasawa, N., Ueda, K., et al. (2016). Identifiification of QTLs controlling low-temperature germination of the East European rice (*Oryza sativa* L.) variety Maratteli. *Euphytica* 207, 245–254. doi: 10.1007/s10681-015-1531-z

Sharma, I., Kaur, N., and Pati, P. K. (2017). Brassinosteroids: a promising option in deciphering remedial strategies for abiotic stress tolerance in rice. *Front. Plant Sci*. 8:2151. doi: 10.3389/fpls.2017.02151

Spindel, J., Wright, M., Chen, C., Cobb, J., Gage, J., Harrington, S., et al. (2013). Bridging the genotyping gap: using genotyping by sequencing (GBS) to add high-density SNP markers and new value to traditional bi-parental mapping and breeding populations. *Theor. Appl. Genet*. 126, 2699–2716. doi: 10.1007/s00122-013-2166-x

Tian, F., Li, D. J., Fu, Q., Zhu, Z. F., Fu, Y. C., Wang, X. K., et al. (2006). Construction of introgression lines carrying wild rice (*Oryza rufifipogon* Griff.) segments in cultivated rice (*Oryza sativa* L.) background and characterization of introgressed segments associated with yield-related traits. *Theor. Appl. Genet*. 112, 570–580. 0165-2 doi: 10.1007/s00122-005-

Wu, W. P., Zhou, W. J., Tang, C. B., Liu, K., Zeng, H. L., and Wang, Y. (2020). Effects of Exogenous 2,4-Epibrassinolide on Germination and Physiological Characteristics of Rice Seeds under Chilling Stress. *Mol. Plant Breed*. 18, 4427–4434. doi: 10.13271/j.mpb.018.004427

Xiao, N., Huang, W. N., Li, A. H., Gao, Y., Li, Y. H., Pan, C. H., et al. (2015). Fine mapping of the *qLOP2* and *qPSR2-1* loci associated with chilling stress tolerance of wild rice seedlings. *Theor. Appl. Genet*. 128, 173–185. doi: 10.1007/s00122-014-2420-x

Xu, K., Jourquin, J., Njo, M. F., Nguyen, L., Beeckman, T., and Fernandez, A. I. (2022). The phloem intercalated with xylem-correlated 3 receptor-like kinase constitutively interacts with brassinosteroid insensitive 1-associated receptor kinase 1 and is involved in vascular development in *Arabidopsis*. *Front. Plant. Sci*. 12:706633. doi: 10.3389/fpls.2021.706633

Xu, M., Ye, X., Wang, W., Wei, C., Zhang, J., and Tu, J. (2015). Genetic analysis and molecular mapping of a high threshold and low temperature-sensitive mutant in rice (*Oryza sativa* L.) at the seedling stage. *Euphytica* 203, 71–82. doi: 10.1007/s10681-014-1260-8

Yang, L., Wang, J., Han, Z., Lei, L., Liu, H. L., Zheng, H., et al. (2021). Combining QTL-seq and linkage mapping to fine map a candidate gene in qCTS6 for cold tolerance at the seedling stage in rice. *BMC Plant Biol*. 21:278. doi: 10.1186/s12870-021-03076-5

Zhang, K., Su, J., Xu, M., Zhou, Z., Zhu, X., Ma, X., et al. (2020). A common wild rice-derived BOC1 allele reduces callus browning in indica rice transformation. *Nat. Commun*. 11:443. doi: 10.1038/s41467-019-14265-0

Zhang, Q., Chen, Q., Wang, S., Hong, Y., and Wang, Z. (2014). Rice and cold stress: methods for its evaluation and summary of cold tolerance-related quantitative trait loci. *Rice* 7:24. doi: 10.1186/s12284-014-0024-3

Zhang, X., Zhou, S. X., Fu, Y. C., Su, Z., Wang, X. K., and Sun, C. Q. (2006). Identifification of a drought tolerant introgression line derived from Dongxiang common wild rice (*O.rufifipogon* Griff.). *Plant Mol. Biol.* 62, 247–259. doi: 10.1007/s11103-006-9018-x

Zhang, Z., Li, J., Pan, Y., Li, J., Zhou, L., Shi, H., et al. (2017). Natural variation in CTB4a enhances rice adaptation to cold habitats. *Nat. Commun.* 8:14788.

Conflict of Interest: The authors declare that the research was conducted in the absence of any commercial or financial relationships that could be construed as a potential conflict of interest.

Publisher's Note: All claims expressed in this article are solely those of the authors and do not necessarily represent those of their affiliated organizations, or those of the publisher, the editors and the reviewers. Any product that may be evaluated in this article, or claim that may be made by its manufacturer, is not guaranteed or endorsed by the publisher.

frontiers | Frontiers in Plant Science

TYPE Original Research
PUBLISHED 21 September 2022
DOI 10.3389/fpls.2022.911993

OPEN ACCESS

EDITED BY
Gianni Barcaccia,
University of Padua, Italy

REVIEWED BY
Shuwei Liu,
Shandong University (Qingdao), China
Ajay Kumar Pandey,
National Agri-Food Biotechnology Institute, India

*CORRESPONDENCE
Jiewen Xing
jiewen.xing@cau.edu.cn
Yumei Zhang
zhangcui2003@163.com

†These authors have contributed equally to this work

SPECIALTY SECTION
This article was submitted to Plant Breeding, a section of the journal Frontiers in Plant Science

RECEIVED 03 April 2022
ACCEPTED 02 September 2022
PUBLISHED 21 September 2022

CITATION
Wang H, Han X, Fu X, Sun X, Chen H, Wei X, Cui S, Liu Y, Guo W, Li X, Xing J and Zhang Y (2022) Overexpression of *TaLBD16-4D* alters plant architecture and heading date in transgenic wheat. *Front. Plant Sci.* 13:911993. doi: 10.3389/fpls.2022.911993

Overexpression of *TaLBD16-4D* alters plant architecture and heading date in transgenic wheat

Huifang Wang[1†], Xiaofan Han[1†], Xiaofeng Fu[1], Xinling Sun[1], Hailong Chen[1], Xirui Wei[1], Shubin Cui[2], Yiguo Liu[1], Weiwei Guo[1], Ximei Li[1], Jiewen Xing[2*] and Yumei Zhang[1*]

[1]Shandong Provincial Key Laboratory of Dryland Farming Technology, Qingdao Agricultural University, Qingdao, China, [2]State Key Laboratory for Agrobiotechnology, Key Laboratory of Crop Heterosis Utilization (MOE), Beijing Key Laboratory of Crop Genetic Improvement, China Agricultural University, Beijing, China

Lateral organ boundaries domain (LBD) proteins, a class of plant-specific transcription factors with a special domain of lateral organ boundaries (LOB), play essential roles in plant growth and development. However, there is little known about the functions of these genes in wheat to date. Our previous study demonstrated that *TaLBD16-4D* is conducive to increasing lateral root number in wheat. In the present work, we further examined important agronomical traits of the aerial part of transgenic wheat overexpressing *TaLBD16-4D.* Interestingly, it was revealed that overexpressing *TaLBD16-4D* could lead to early heading and multiple alterations of plant architecture, including decreased plant height, increased flag leaf size and stem diameter, reduced spike length and tillering number, improved spike density and grain width, and decreased grain length. Moreover, auxin-responsive experiments demonstrated that the expression of *TaLBD16-4D* in wild-type (WT) wheat plants showed a significant upregulation through 2,4-D treatment. *TaLBD16-4D*-overexpression lines displayed a hyposensitivity to 2,4-D treatment and reduced shoot gravitropic response. The expressions of a set of auxin-responsive genes were markedly different between WT and transgenic plants. In addition, overexpressing *TaLBD16-4D* affected the transcript levels of flowering-related genes (*TaGI*, *TaCO1*, *TaHd1*, *TaVRN1*, *TaVRN2*, and *TaFT1*). Notably, the expression of *TaGI*, *TaCO1*, *TaHd1*, *TaVRN1*, and *TaFT1* displayed significant upregulation under IAA treatment. Collectively, our observations indicated that overexpressing *TaLBD16-4D* could affect aerial architecture and heading time possibly though participating in the auxin pathway.

KEYWORDS

***TaLBD16-4D*, plant architecture, heading time, auxin, wheat**

Introduction

Common wheat (*Triticum aestivum* L.) is one of the major globe cereal crops supplying approximately 20% of the daily calories and proteins for the world's population (Shiferaw et al., 2013; Tucker et al., 2017). Increasing grain yield of wheat is a major global challenge to provide sufficient food for the growing world population (Grassini et al., 2013; Jiang et al., 2017). To produce high yield of wheat, it needs not only the high yield potential determined by yield components (grain number per spike, number of fertile tillers per plant, and thousand grain weight) (Xue et al., 2008; Zhang et al., 2018) but also ideal plant architecture of morphological traits such as root system, plant height, branch or tiller number and angel, and flag leaf size and angle (Rogers and Benfey, 2015; Li et al., 2019). Of these, plant height is one of the most prominent architecture traits in crop plants, because of its role in planting density, harvest index, and lodging resistance that are closely associated with crop yield potential. Leaf size, especially flag leaf size, is a major contributor to grain yield in cereal crops, as it affects photosynthetic efficiency, carbohydrate synthesis, accumulation, and partitioning (Biswal and Kohli, 2013; Shahinnia et al., 2016). Also, plasticity of heading date (or flowering time) in wheat plays an important role in adaptation as it enables the regulation of plant development in different environments and guarantees the broad geographical range of wheat varieties. Selection for the optimum heading date to adapt their local growing conditions has also contributed to the increase of wheat yields globally (Kamran et al., 2014; Chen et al., 2020).

The molecular mechanisms regulating yield, plant architecture, and heading date have been extensively investigated and were demonstrated to be regulated by sophisticated phytohormone signaling pathways (Wang and Li, 2006; Ivanchenko et al., 2008; Hao et al., 2013; Renau-Morata et al., 2021). In particular, auxin plays critical roles in many, if not all, plant growth and developmental processes including apical dominance, phototropic and gravitropic responses, stem and leaf growth, flower development, and lateral and adventitious root formation (Okushima et al., 2005a; Vanneste and Friml, 2009; Kim et al., 2020). The auxin signaling pathway is tightly controlled at the cellular and tissue level mainly by transcription factors (Feng et al., 2012; Zhang et al., 2020). The LBD transcription factor is plant-specific and defined by the LOB domain, which has been designated to this functional group based on its nuclear localization and capacity to bind to DNA motifs (Husbands et al., 2007; Majer and Hochholdinger, 2011). The *LBD* family is composed of 42 members in *Arabidopsis*, 35 members in rice, 44 members in maize, and 24 members in barley while 94 members have been identified in wheat (Yang et al., 2006; Zhang et al., 2014; Guo et al., 2016; Xu et al., 2021). According to the structure of the LOB domain, the *LBD* family is classified into class I and class II subfamily. Class I protein members contain a zinc finger-like domain and a Leu-zipper-like coiled-coil motif, while class II members only have a conserved zinc finger-like domain (Landschulz et al., 1988; Shuai et al., 2002). The majority of *LBD* genes are expressed at the adaxial base of plant lateral organs and play an important role in the formation and development of plant lateral organs as well as metabolism in plants (Shuai et al., 2002; Chalfun-Junior et al., 2005).

Up to date, some members of the *LBD* family have been functionally identified in different species. Class I *LBD* genes included *AtLBD16*, *AtLBD18*, and *AtLBD29* that not only participate in auxin-dependent lateral and adventitious root formation downstream of *AtARF7* and *AtARF19* (Okushima et al., 2005b; Lee et al., 2009; De Smet et al., 2010) but also act as key regulators of callus formation in plant regeneration (Okushima et al., 2007; Fan et al., 2012). Transcript levels of *AtDDA1*/*AtLBD25* are reduced by exogenous indole-3-acetic acid (IAA or auxin) treatment, and the *dda1* mutant exhibits fewer lateral roots and aberrant hypocotyl elongation in the dark (Mangeon et al., 2011). *ASYMMETRIC LEAVES2* (*AS2*)/*LBD6* functions in the establishment of leaf polarity by repression of cell proliferation in the adaxial domain of *Arabidopsis* leaves (Semiarti et al., 2001; Iwakawa et al., 2007). *AtLBD30* is required for auxin-mediated development of embryogenesis and lateral organs (Rast and Simon, 2012). In maize, *Ramosa2* (*Ra2*, an ortholog of *AtLOB*) is involved in floral development (Bortiri et al., 2006). The *indeterminate gametophyte1* (*ig1*) gene of maize, encoding a LOB domain protein with high similarity to *ASYMMETRIC LEAVES2* of *Arabidopsis*, affects leaf development as well as embryo sac development (Evans, 2007). In rice, *OsCRL1* (an ortholog of *AtLBD29*) regulates crown and lateral root formation relying on the auxin signaling pathway (Inukai et al., 2005). *OsLBD3-7* acts as an upstream regulator of bulliform cell development to regulate leaf rolling (Li et al., 2016). *OsIG1* encodes a LOB domain protein and regulates floral organ and female gametophyte development (Zhang et al., 2015). Among class II *LBD* genes, *AtLBD37*, *AtLBD38*, and *AtLBD39* respond to exogenous nitrate and function in anthocyanin synthesis and nitrate metabolism (Rubin et al., 2009). *AtLBD41* participates in leaf dorsoventral determination (Chalfun-Junior et al., 2005). *OsLBD37* and *OsLBD38* delay the heading date by repressing the expression of the key regulator Ehd1 as well as the florigen genes *Hd3a* and *RFT1* and improve plant height and grain numbers and yield in overexpression plants (Li et al., 2017). Although extensive investigations of the *LBDs* in different species have provided better understanding of this gene family, the functional conservation and diversity of *LBD* genes in wheat remain largely unknown.

In our previous work, we found that *TaLBD16* (an ortholog of *AtLBD16*) contributes to the wide variation of lateral root number during wheat evolution, and overexpression of *TaLBD16-4D* can significantly increase lateral root number in wheat (Wang et al., 2018). As a continuation of this work, the

present study focused on the function and molecular mechanism of *TaLBD16-4D* in the aerial part of wheat. Our results demonstrated that constitutive overexpression of *TaLBD16-4D* led to pleiotropic effects on plant architecture, as well as early heading. Moreover, *TaLBD16-4D* overexpression plants displayed less sensitivity to 2,4-D treatment and decreased gravity response. Our findings showed that these changes could be ascribed to the attenuated auxin pathway in *TaLBD16-4D* overexpression plants. The identification of *TaLBD16-4D* can not only extend our understanding of the molecular and genetic regulation of wheat heading date and plant architecture but also serve as a new potential genetic regulator for breeding high yield wheat cultivars.

Materials and methods

Plant materials and growth conditions

Our previous research of *TaLBD16-4D* (Wang et al., 2018) provided *TaLBD16-4D*-overexpression transgenic wheat lines (OE1 and OE2) and wild-type (WT) Fielder for this study. For experiments in the greenhouse, the sterilized seeds of transgenic wheat plants and WT were incubated at 4°C for 3 days in the dark and then cultured at room temperature under dark conditions for 12 h. Uniformly germinated seeds were grown in a greenhouse with a 16-h/8-h light/dark photoperiod, a light intensity of 14,100 lx, a temperature regime of 24:18°C (light:dark), and 60% humidity. For field trials, transgenic wheat plants and WT used to evaluate yield-related traits were planted with three replicates under natural field conditions during long days in the region of Beijing (40.14°N, 116.19°E), and each replicate contained two rows that were 1.5 m long and 0.3 m apart with a sowing rate at 25 seeds per row. The irrigation and other management of field trials were in accordance with local standard practices.

Evaluation of agronomic characteristics and yield traits

The WT wheat plants and transgenic lines were planted in the experimental field with three replicates. For each replicate, the heading date (HD) of each genotype was calculated as days from the sowing date to the date when approximately 50% spikes were visible. Agronomic traits, including plant height, flag leaf length and width, spike length, and spikelet density, were examined before harvest. After maturity, grain number per spike (GNS) was given by 15 main spikes. Effective tillers of each plant were counted to determine the total number of wheat ears in each plant from 15 individual plants. Grain yield per plant was estimated by 10 plants. Thousand-grain weight (TGW), grain length (GL), and grain width (GW) were determined using a camera-assisted phenotyping system (Wanshen, Hangzhou).

Measurement of free IAA content

Uniformly germinated seeds from WT and transgenic wheat lines were grown in a greenhouse for 2 days. Next, the 2-day-old seedlings were transplanted to a culture box filled with 1/5th strength Hoagland solution. Solution was changed every 2 days. The endogenous content of IAA was quantified according to the method described by Yue et al. (2019). The roots and aerial part of WT and OE lines were collected respectively at 12 days after germination, frozen in liquid nitrogen, and stored at -80°C. For the extraction of free IAA, a 0.1-g sample was soaked with 4 ml extracting solution and shaken in the dark for 12 h at 4°C. Then, the sample was centrifuged at 10,000 rpm for 15 min at 4°C. The supernatant was removed to a new 10-mL tube with 3 mL extracting solution and stored at 4°C in darkness. The remaining sediment was reextracted twice for 30 min in the dark at 4°C. After reextraction every time, the sample was centrifuged again at 10,000 rpm for 15 min at 4°C. The three resulting supernatants were merged together (8 ml), placed on ice, and dried with nitrogen in the dark. Next, the dry sample was redissolved with 0.8 ml methanol. The powder of IAA (Sigma-Aldrich) was dissolved with different concentrations of methanol to construct the calibration curve. Finally, the above supernatants and standard solution were filtered with a 0.22-nm filter membrane. The determination of IAA was performed by Agilent Technologies 6400 high-performance liquid chromatography (HPLC). One milliliter of sample was used for detection. Each sample was analyzed with three biological replicates.

Auxin treatment at the seedling stage

The 2-day-old seedlings of WT and OE lines with the same vigor were transferred to a culture box filled with 1/5th strength Hoagland solution for 5 days in the greenhouse. The culture solution was changed every 2 days. Then, the 7-day-old uniform seedlings were treated with different concentrations of 2,4-D (0.001, 0.01, 0.1, 1, and 10 μM) and 1/5th strength Hoagland solution for another 5 days. Maximum root length was measured from the root tip to the root–shoot junction. Shoot length was measured from the tip of the longest leaf to the root–shoot junction. Shoot fresh mass was assessed using an automated electronic scale. The experiment was repeated three times, with at least eight plants per treatment group. For auxin-related gene expression analysis, leaves and root tissue were collected from the 5-day-old seedlings after 30 μM 2,4-D treatment for 0 or 12 h. For flower-related gene expression analysis, the 7-day-old uniform seedlings were cultured with 1/5th strength Hoagland solution, until the seedlings at the three-leaf stage were treated with 0.1 μM IAA for 0, 12, 16, or 24 h. The leaves at the three-leaf stage were used for gene expression analysis.

RNA extraction and reverse transcription qPCR analysis

Total RNA was extracted using the standard TRIzol RNA isolation protocol (Vazyme Biotech, Nanjing, China), according to the manufacturer's instructions. The RNA samples were digested with purified DNase I, and first-strand cDNA synthesis was performed using HiScript II One-Step RT-PCR Kit (Vazyme Biotech, Nanjing, China). Reverse transcription qPCR (RT-qPCR) was conducted using SYBR Color qPCR Master Mix (Vazyme Biotech, Nanjing, China) with the QuantStudio 3 Real-Time Fluorescence Quantitative PCR System (Thermo Fisher scientific, Waltham, USA). The RT-qPCR conditions and analytical methods were the same as those described by Wang et al. (2018). The specific gene primers for qPCR were designed according to the conserved region of three homeologs. The wheat *Actin* gene was used as an internal control (Shimada et al., 2009). The accession numbers of *TaActin* homoeologous genes were TraesCS1A02G274400, TraesCS1B02G283900, and TraesCS1D02G274400. Each sample was quantified in triplicate. A description of the genes and primer sequences is given in Supplementary Table 1.

Shoot gravitropic response analysis

Uniformly germinated seeds from WT and *TaLBD16-4D* OE lines were placed vertically on 0.6% agar medium for 2 days in the greenhouse. The 2-day-old seedlings were reoriented by 90° and grown for another 2 days. The shoot curvature was measured as the shoot gravitropic response. Each genotype was performed with three biological replicates, and the number of seedlings for each replicate was at least 10.

Statistical analysis

A one-way analysis of variance (ANOVA) with the least significant difference (LSD) test was conducted using IBM SPSS 19.0 for Windows (IBM, Armonk, NY, USA). Student's *t*-test was conducted using EXCEL 2019. All statistical tests were performed by two-sided significance tests with a 0.05, 0.01, or 0.001 significance level.

Results

Ectopic expression of *TaLBD16-4D* causes multiple phenotypic variations in wheat

Overexpression lines of *TaLBD16-4D* were previously generated with ORF driven by the maize *ubiquitin* (*Ubi*) promoter (Wang et al., 2018). In the present study, two homozygous overexpression (OE) lines (OE1 and OE2) in T_4 were used to elucidate the function of *TaLBD16* in the aerial part. At the seedling stage, various traits of OE1 and OE2 differed significantly from those of the wild type (WT) under greenhouse conditions, including shoot length, leaf width, leaf length, leaf area, total chlorophyll content (SPAD), shoot fresh weight, and growth rate. The shoot height and leaf length in lines OE1 and OE2 were both significantly lower than those in the wild type (Figure 1A; Supplementary Figures 1A-C), whereas the leaf width and total chlorophyll content (SPAD) in lines OE1 and OE2 were significantly higher (Supplementary Figures 1A, D, F). Furthermore, the leaf area and shoot fresh weight in OE lines were slightly lower than WT (Supplementary Figures 1A, E, G). In addition, overexpression of *TaLBD16-4D* accelerated the growth rate at the seedling stage, that is, OE1 and OE2 had entered the tillering stage when the wild type grew to the three-leaf stage (Figure 1A).

To further investigate the effects of *TaLBD16-4D* on yield and yield-related traits, we compared the traits between *TaLBD16-4D*-overexpression lines and WT under field conditions after the seedling stage. The most noticeable phenotype is the reduction of plant height, consistent with a decrease at the seedling stage. The plant heights of two OE lines were reduced by 31.38% and 31.02%, respectively (Figures 1B, G). Since wheat plant height is primarily determined by stem internode length, we measured the stems and internodes of transgenic lines. The results showed that the internode number in transgenic lines was one less than that in WT; at the same time, OE lines displayed significantly shortened internodes (Figure 1C; Supplementary Figure 2). These results revealed that overexpressing *TaLBD16-4D* led to decreased plant height of wheat by shortening the internode length together with the low node number. In addition, transgenic lines headed significantly early by 3.34 days, and showed reduced spike length by 20.45% and 15.83%, and increased spike density by 11.46% and 12.05%, respectively (Figures 1B, D, H, I; Table 1). Interestingly, the flag leaf width in OE lines was markedly higher, but flag leaf length in OE lines was much lower than WT, consistent with the phenotype of the first leaf at the seedling stage (Figure 1E; Table 1; Supplementary Figures 1C, D). Totally, the flag leaf area increased by 9.78% and 12.13% in the two OE lines, respectively (Figures 1E, J). Compared with the WT, the thousand-grain weights (TGW) of two OE lines were similar with those of WT, which might result from a trade-off between grain width increased by 3.7%~5.7% and grain length decreased both by 3.6%. Further examination showed that the grain yield per plant of both two overexpression lines were reduced by 23.11% and 33.56%, respectively, compared with the WT (Table 1), primarily because of lower grain number per spike and productive tillers per plant (Table 1).

10.3389/fpls.2022.911993

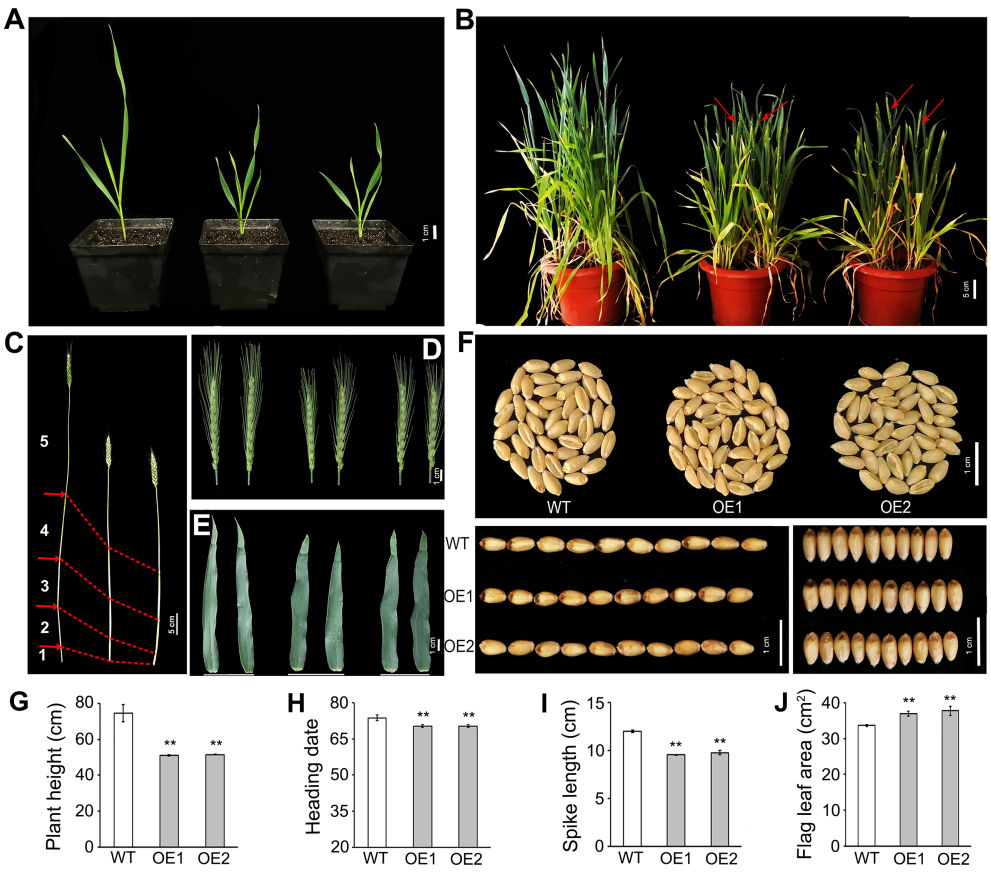

FIGURE 1
Pleiotropic effects of overexpressed *TaLBD16-4D* on wheat development. Comparisons of several important traits between the two *TaLBD16-4D*-overexpression transgenic plants (OE1 and OE2) and wild type (WT). **(A)** Photos of WT (left) and two OE lines (middle and right) taken when OE lines reached the tillering stage. **(B)** Phenotypic characteristic of WT (left) and two OE lines (middle and right) taken when OE lines reached the heading stage. Red arrow heads indicate spikes at the heading stage. **(C)** Main culms of WT (left) and two OE lines (middle and right). **(D)** Main spikes of WT (left) and two OE lines (middle and right). **(E)** Flag leaf of WT (left) and two OE lines (middle and right). **(F)** Morphology of grains in the WT and two OE lines. Comparison of plant height **(G)**, heading date **(H)**, spike length **(I)**, and flag leaf area **(J)** in WT and two OE lines, respectively. All values in G–J are the mean ± SD (n = 3). Statistical differences between WT and two OE lines are indicated by asterisks and were determined by Student's t-test and **P < 0.01.

TABLE 1 Measurements of yield and related-yield traits in the *TaLBD16-4D* transgenic and wild-type plants.

Traits	WT	OE1	OE2
Number of spikelets per spike	19.89 ± 0.29 (A)	17.60 ± 0.26 (B)	18.10 ± 0.44 (B)
Spike density	1.66 ± 0.04 (A)	1.85 ± 0.03 (B)	1.86 ± 0.08 (B)
Flag leaf width	1.84 ± 0.05 (B)	2.19 ± 0.03 (A)	2.26 ± 0.05 (A)
Flag leaf length	18.33 ± 0.55 (A)	16.83 ± 0.39 (B)	16.72 ± 0.53 (B)
Number of productive tillers per plant	14.03 ± 2.82 (A)	10.16 ± 0.24 (B)	9.63 ± 1.43 (B)
Grain number per spike on main stem	57.10 ± 1.27 (A)	45.77 ± 1.02 (B)	43.63 ± 1.86 (B)
Grain length	6.19 ± 0.12 (A)	5.97 ± 0.04 (B)	5.97 ± 0.02 (B)
Grain width	2.96 ± 0.01 (B)	3.07 ± 0.01 (A)	3.13 ± 0.01 (A)
Thousand grain weight	34.32 ± 0.12 (A)	33.51 ± 0.21 (A)	34.05 ± 0.45 (A)
Grain yield per plant	16.09 ± 1.40 (A)	12.37 ± 0.77 (B)	10.69 ± 2.58 (B)

A, B, ranked by LSD test at P ≤ 0.01.

TaLBD16-4D affects stem and leaf growth and development

TaLBD16-4D OE lines also exhibited multiple phenotypes related to stem and leaf. Compared with the WT, the two OE lines had fewer nodes and shortened internodes (Figure 1C; Supplementary Figure 2) but increased the thickness of the stem by 15.17% and 18.16%, respectively (Figures 2A, B). To investigate the effect of *TaLBD16-4D* at a cellular level, we performed paraffin sectioning of stem and leaves of these plants. Transverse histological sectioning analysis of the fourth stem internode showed significantly reduced cell numbers per unit area in OE1 (-41.47%) and OE2 (-28.41%) when compared with WT (Figures 2C, D), suggesting that cell sizes of the two OE lines were altered. Direct cell measurement exhibited that the cell perimeters were significantly increased in OE1 (+32.27%) and OE2 (+22.57%) (Figures 2C, E). In addition, leaf widths of both OE lines were significantly increased but leaf lengths were markedly reduced (Figure 1E; Supplementary Figure 1). Consistent with the transverse sectioning results of stems, transverse sectioning of the first leaf confirmed the significantly increased cell size (+10.22% in OE) and reduced cell numbers per unit area (-16.82% in OE) (Supplementary Figures 3A, C, D). Longitudinal sectioning of these leaves showed significantly reduced cell length in OE (-9.44%; Supplementary Figures 3B, E), which might cause decreased leaf length in transgenic lines. Notably, the OE plants had advanced vascular systems and parenchyma (Figure 2C; Supplementary Figure 3A), indicating an increased transport capacity and stores of photosynthate, which are crucial for grain weight. These results suggested that overexpression of *TaLBD16-4D* enhanced the size of stem diameter and leaf width probably by promoting cell enlargement. Indeed, although the OE plants were much shorter, the thousand grain weight of the two OE lines was almost identical to that of the WT.

TaLBD16-4D is involved in the auxin pathway and increased the IAA concentration

In *Arabidopsis thaliana*, *AtLBD16* is directly activated by auxin *via* AUXIN RESPONSE FACTOR 7 (ARF7) and ARF19 (ARF7/19) to induce the initiation of lateral root primordium (Okushima et al., 2007). Our previous study documented that the altered expression of *TaLBD16-4D* promotes the formation of lateral root (Wang et al., 2018). Synthetic auxins, such as 1-NAA, 2,4-D, and picloram, have been most commonly used for the identification of auxin receptors, auxin transport carriers,

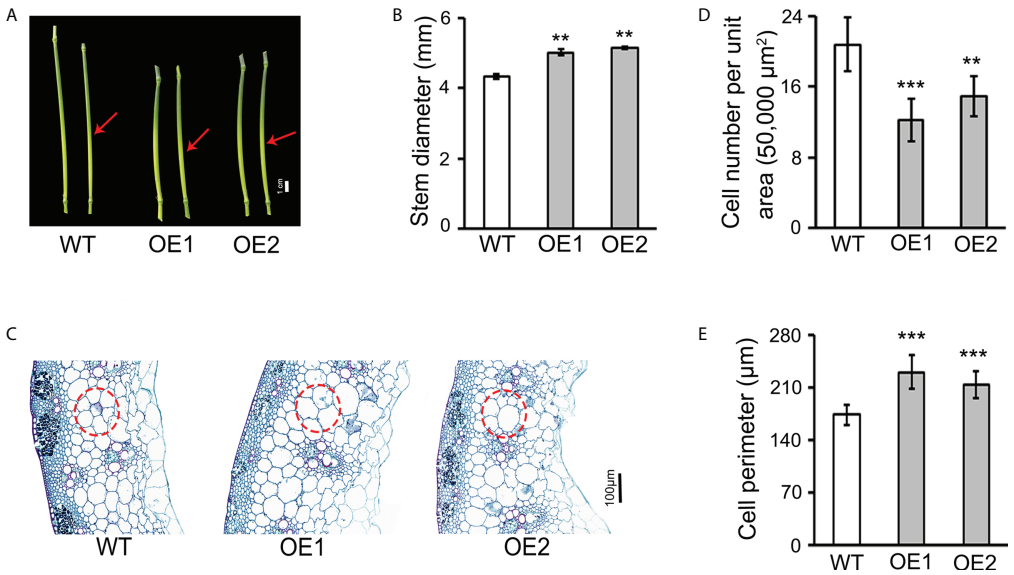

FIGURE 2
Overexpression of *TaLBD16-4D* altered wheat stem development. **(A)** Phenotypes of the fourth nodes and stems above the ground from the main culms for WT and *TaLBD16-4D*-overexpression plants grown in the field under natural long-day conditions. Arrowheads indicate the middle region of the fourth stem node used for observation. **(B)** Stem diameter of two OE lines and WT plants. **(C)** Transverse section analysis of the fourth stem node of *TaLBD16-4D*-overexpression and WT plants. Red circles indicate the major cell types selected for cell counting and measurement. **(D)** Cell number per unit area in c. **(E)** Cell size in c. For cell number (per unit area) counting, a total area of 50,000 μm^2 for each sample was investigated. For cell perimeter determination, representative cells within each of the red circle regions were selected for cell size measuring. Data reported are shown as mean ± SD (n = 7). Asterisks indicate statistically significant differences between WT and *TaLBD16-4D*-overexpression plants determined using Student's *t*-test. ** and *** indicate significant differences at the 0.01 and 0.001 levels, respectively.

transcription factor response to auxin, and cross talk among phytohormones, which are not subject to the many endogenous homeostatic and metabolic mechanisms that can affect IAA (Ljung et al., 2002). Synthetic auxins, including 2,4-D, can induce strong changes in expression of auxin-related genes that ultimately lead to auxin-insensitive response in the cereal seedling roots and/or shoots (Bian et al., 2012; Xu et al., 2017; Guo et al., 2021). Thus, it was speculated that the *TaLBD16-4D* gene might be involved in auxin-mediated growth events in wheat. To test this hypothesis, we analyzed the *TaLBD16-4D* gene expression patterns of WT after exogenous 2,4-D treatment *via* qRT-PCR. As shown in Figure 3A, the expression of the *TaLBD16* gene in root of the WT was significantly upregulated by 2,4-D treatment compared to that of the control.

To further elucidate the relationship between *TaLBD16-4D* gene and auxin, we treated two OE lines and WT with different concentrations of synthetic auxin (2,4-D). Seven-day-old seedlings were transferred to a nutrient solution containing various concentrations of 2,4-D for another 5 days. The maximum root lengths of the overexpression plants and WT were significantly inhibited by 0.001 and 10 μM of 2,4-D. However, no obvious changes in OE lines were displayed under 0.01 and 0.1 μM 2,4-D treatment, compared to untreated OE lines (Figure 3B). By contrast, the WT plants showed more sensitivity of accelerating effect to 2,4-D application than the OE lines, especially with a major change in maximum root length in response to 0.1 μM 2,4-D (Figure 3B). We also examined the shoot length and shoot fresh weight of WT and OE lines in response to 2,4-D. The shoot length of WT significantly decreased with increasing 2,4-D concentration compared to the untreated control (Figure 3C), while the two OE lines showed less sensitivity to 2,4-D application than that of WT, with only a minor change in root length in response to increasing 2,4-D concentrations from 0.01 to 1 μM (Figure 3C). Moreover, the shoot fresh mass of two OE lines also exhibited a minor change compared to that of WT which showed a drastic decrease trend under 0.001, 0.01, and 1 μM 2,4-D ($P < 0.01$; Figure 3D). These data indicated that *TaLBD16-4D*-overexpression plants were less sensitive to auxin than WT.

The auxin signaling pathway in *Arabidopsis* consists of ARFs and the AUXIN/INDOLE-3-ACETIC ACID (Aux/IAA)

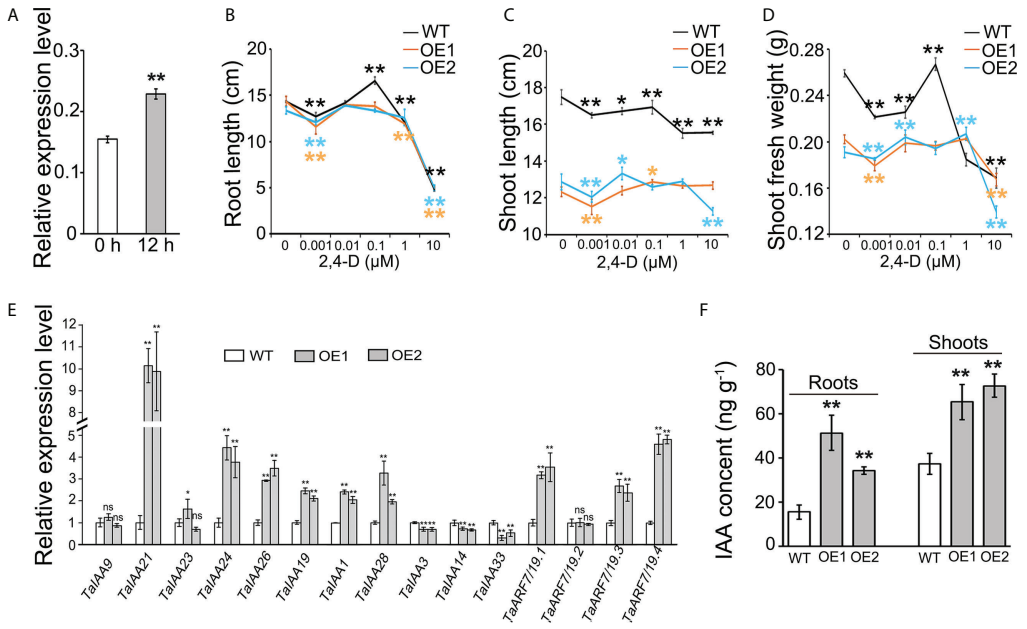

FIGURE 3
Effects of *TaLBD16-4D*-overexpressed wheat plants on the auxin pathway. **(A)** Expression patterns of the *TaLBD16-4D* gene in roots of WT under 2,4-D treatment. Five-day-old seedlings grown in a hydroponic culture were treated with 30 μM 2,4-D for 0 or 12 h. The expression of *TaActin* was used to normalize mRNA levels. The values are means ± SD of three biological replicates. Comparison of root length **(B)**, shoot length **(C)**, and shoot fresh mass **(D)** between *TaLBD16-4D* overexpression lines (OE1 and OE2) and WT with different concentrations of 2,4-D at the seedling stage. The 2,4-D concentrations were 0, 0.001, 0.01, 0.1, 1, and 10 μM, respectively. Three independent biological replicates were used (eight plants per biological replicate). Values are indicated as mean ± SD. **(E)** Expression analysis of 16 auxin signaling-related genes in the leaves of WT, OE1, and OE2, determined using qRT-PCR. The relative levels of each gene were normalized with the respective gene set as 1. *TaActin* was used as the internal standard. **(F)** Quantification of the IAA levels in the aerial part of WT and OE lines at the seedling stage. All values in d and e are indicated as mean ± SD (n = 3). Statistical differences between WT and two OE lines are indicated by asterisks and were determined using Student's *t*-test ns, not significant; $*P < 0.05$; $**P < 0.01$.

repressor family. At a low auxin level, ARF7/19 form a protein complex with AUXIN/INDOLE-3-ACETIC ACID (Aux/IAA) proteins, which represses the transcriptional activation activity of ARF7/19. In contrast, high accumulation of auxin induces the proteolysis of Aux/IAAs to activate ARF7/19-dependent transcription (Ito et al., 2016). To further identify the role of *TaLBD16-4D* in the auxin pathway in wheat, we investigated the expression patterns of auxin-responsive genes orthologous to *Arabidopsis* genes involved in the auxin signal transduction pathway, including 11 *TaAux/IAAs* (Qiao et al., 2017) and four *TaARF7/19s* (Wang et al., 2018). Of these genes, six *TaAux/IAAs* and three *TaARF7/19s* were significantly upregulated in the young leaves of *TaLBD16-4D* overexpression plants compared to WT (Figure 3E). Notably, the relative mRNA abundances of *TaIAA3*, *TaIAA14*, and *TaIAA33* in two OE lines were less than those in WT (Figure 3E). In addition, in comparison with WT, the IAA contents were significantly increased in both roots and aerial part of *TaLBD16-4D* overexpression plants (Figure 3F). Interestingly, the expression levels of genes involved in auxin biosynthesis (*TaTAR2.1*, *TaYUCCA1*, *TaYUCCA7*, *TaYUCCA8*, *TaSUR36*) and transport (*TaPIN*) were significantly upregulated in both leaves and roots of two OE lines (Supplementary Figure 4). Together, these data suggested that *TaLBD16-4D* might function as an important regulator impacting on auxin signaling, biosynthesis, and transport.

Previous studies revealed that the presence of auxin response elements (AuxREs) in the promoter region of *TaLBD16* orthologous genes in rice, *Arabidopsis*, and maize are crucial for their function in root development (Inukai et al., 2005; Okushima et al., 2007; Taramino et al., 2007). Thus, we decided to analyze the putative AuxREs in the promoter region of three *TaLBD16* homoeologous genes (*TaLBD16-4A*, *TaLBD16-4B*, and *TaLBD16-4D*). Based on the Chinese Spring reference genome, three identical AuxREs were detected among the promoters of these three homoeologous genes. In addition, one extra AuxRE was detected in the promoter of *TaLBD16-4B* (Supplementary Figure 5).

Overexpression of *TaLBD16-4D* impairs shoot gravitropism in wheat

Gravitropic response in shoot is also a typical auxin-related phenotype, which is associated with polar auxin transport leading to asymmetrical auxin distribution and differential growth between the upper and lower sides of responding organs (Li et al., 2007; Strohm et al., 2012; Song and Xu, 2013). To assess the gravity response of *TaLBD16-4D*-OE seedlings, the shoot angles of transgenic plants and WT were measured and compared. The seedlings grew vertically for 2 days after germination, and then the 2-day-old seedlings were placed horizontally for another 2 days. We analyzed the gravitropic curvature in these shoots on the first day and second day. The results demonstrated that *TaLBD16-4D* transgenic plants showed impaired gravitropic responses compared with WT (Figure 4A) and the gravitropic curvature of the two OE lines in each day was both significantly smaller than those of the wild-type seedlings (Figure 4B), indicating that overexpression of *TaLBD16-4D* impaired gravitropic responses of the seedling shoot.

Overexpressing *TaLBD16-4D* promotes wheat heading *via* influencing the expression of flowering-time genes

Changes in gene expression are often associated with phenotypic variation (Fay and Wittkopp, 2008). Given that *TaLBD16-4D* transgenic plants displayed early heading under long-day conditions (Figures 1B, H), we assumed that the expression of flowering-time genes might be influenced by *TaLBD16-4D*. In wheat, the heading is associated with the timing of floral transition, an important character in adapting to complicated environmental conditions (Cockram et al., 2007; Hu et al., 2020). The current consensus is that flowering promotion is subject to the vernalization and photoperiod pathways in wheat (Shim and Imaizumi, 2015). To investigate

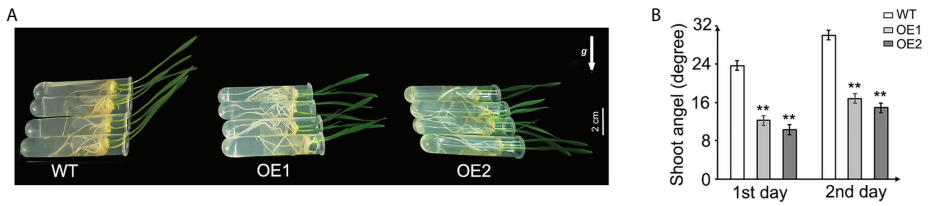

FIGURE 4
Gravitropism analysis of the *TaLBD16-4D*-overexpressing and WT plants. **(A)** Three-day-old seedlings of *TaLBD16-4D*-overexpressing (OE1 and OE2) and WT plants were grown vertically for 2 days and then horizontally grown for another 2 days. The arrow represents the direction of gravity. **(B)** The shoot angle of WT and *TaLBD16-4D*-overexpressed plants on the first day and second day. Three independent biological replicates were used (at least 10 plants per biological replicate). Values are mean ± SD (n = 3). Statistical differences between WT and two OE lines are indicated by asterisks and were determined using Student's *t*-test: **P < 0.01.

the roles of *TaLBD16-4D* in floral transition, we compared the expression patterns of six flowering-related genes (*TaGI*, *TaCO1*, *TaHd1*, *TaVRN1*, *TaVRN2*, and *TaFT1*) in leaves of the *TaLBD16-4D*-overexpression lines and WT at the three-leaf stage under long-day conditions. The analysis revealed that the two OE lines exhibited significantly upregulated expressions of *TaGI*, *TaCO1*, *TaHd1*, *TaVRN1*, and *TaFT1* and a downregulated expression of *TaVRN2* compared to WT (Figure 5). These results were consistent with the genetic network of wheat flowering-time genes in previous studies (Shimada et al., 2009; Hu et al., 2020) and also indicated that LBD16 might be important for floral transition acting upstream of the network.

To examine whether the expression profiles of flowering-related genes would be induced by auxin, qRT-PCR molecular assays were performed with the leaves of WT treated with IAA. We found that *TaGI*, *TaCO1*, *TaHd1*, *TaVRN1*, *TaVRN2*, and *TaFT1* exhibited significant dynamic expression changes in response to IAA treatment (Supplementary Figure 6). Meanwhile, the peak expression levels of these genes were different in response to IAA. Meanwhile, the peak expression levels of flowering-related genes were different in response to IAA. In brief, *TaGI* expression peaked at 16 h in response to IAA, while the transcripts of *TaCO1*, *TaHd1*, and *TaVRN2* peaked at 16 h. The expression of *TaVRN2* and *TaFT1* both peaked at 12 and 16 h in response to IAA (Supplementary Figure 6). These results suggested that flowering-related genes (*TaGI*, *TaCO1*, *TaHd1*, *TaVRN1*, *TaVRN2*, and *TaFT1*) in floral development processes might be regulated by auxin.

Discussion

Contribution of auxin to morphological changes by regulating the expression of the *TaLBD16-4D* gene in wheat

The phytohormone auxin is essential for plant growth and regulates a wide range of developmental processes. The underlying molecular mechanism of auxin signaling has been illuminated primarily in *Arabidopsis* (Song et al., 2009). A typical model for the auxin signal transduction pathway is that the Aux/IAA family interacts with auxin response factors (ARFs) at low auxin concentrations and inhibits the binding of ARF transcription factors to auxin-responsive elements (AuxREs) located in promoters of auxin-responsive genes, consequently repressing the expression of auxin-responsive genes (Ulmasov et al., 1997; Tian and Reed, 1999). At high auxin concentrations, auxin can promote the proteolytic degradation of the inhibitory Aux/IAA proteins by 26S proteasome (Tian et al., 2002; Kepinski and Leyser, 2004), and then ARFs are released from inhibition and regulate the transcription of auxin-responsive genes (Weijers and Jürgens, 2004). Previous studies have reported that several *LBD* genes, including *LBD16*, *LBD18*, *LBD29*, and

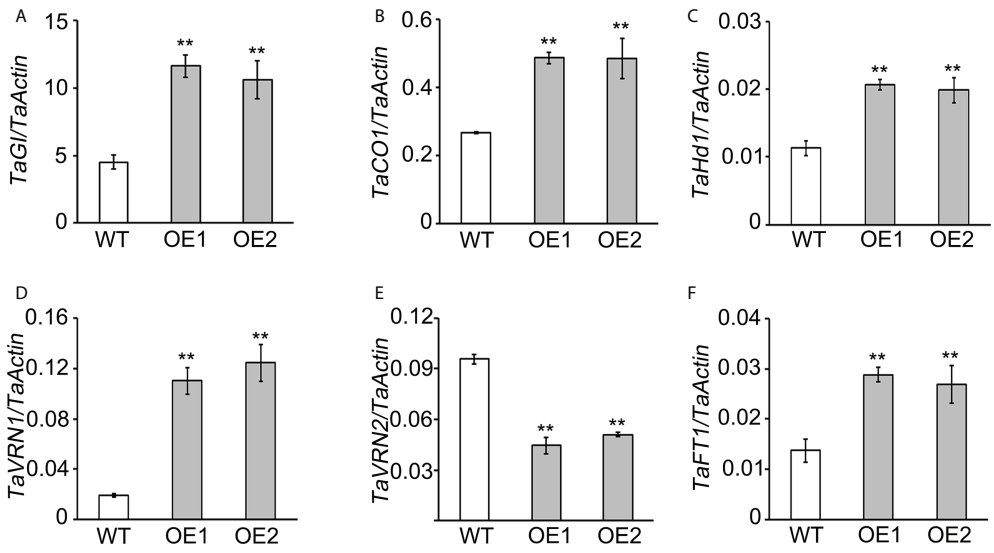

FIGURE 5
The expression analysis of flowering-related genes in WT plants and *TaLBD16-4D*-overexpressing transgenic lines. Expression levels of wheat flowering-related genes, including *TaGI* **(A)**, *TaCO1* **(B)**, *TaHd1* **(C)**, *TaVRN1* **(D)**, *TaVRN2* **(E)**, and *TaFT1* **(F)**, were determined by quantitative reverse transcription PCR (qRT-PCR). The third fully unfolded leaf at the three-leaf stage grown under long-day conditions. *TaActin* was used as an internal control for calculating the relative expression levels of the above genes. Values are shown as mean ± SD (n = 3). Statistical differences between WT and two OE lines are indicated by asterisks and were determined by Student's *t*-test **P < 0.01.

LBD33, play crucial roles in auxin-regulated lateral root development in *Arabidopsis*. For instance, under high auxin levels, auxin derepresses the activity of the transcriptional activators ARF7 and ARF19 through the degradation of Aux/IAAs such as IAA3, IAA14, IAA15, IAA19, and IAA28 and consequently directly activates the transcription of downstream genes including *LBD16* and *LBD29* to regulate lateral root development (Okushima et al., 2005b; Kim et al., 2020).

Up to date, the mechanism underlying the relationship between *LBD* genes and auxin to control plant growth and development of the aerial part is poorly understood. Our previous study has demonstrated that *TaLBD16* is specifically expressed in roots and contributes to increase the lateral root number. Moreover, the D genome plays a crucial role in the increased lateral root number of allohexaploid wheats compared to their allotetraploid progenitors (Wang et al., 2018). Interestingly, there were some variations of the amino acids among the three *TaLBD16* homoeologous genes and the expression of *TaLBD16-4D* was much higher than those of 4A and 4B genomes in the seedling roots of natural and synthetic allohexaploid wheats, which might be responsible for functional divergence of three *TaLBD16* homoeologous genes (Wang et al., 2018). In this study, one more AuxRE was detected on the *TaLBD16-4B* promoter (Supplementary Figure 5), which indicated a higher sensitivity to auxin. Despite of this, the higher expression of *TaLBD16-4D* revealed that more external or internal factors along with auxin finally determined the divergences in the expression of *TaLBD16* homologues. Since the LBD family is composed of 94 members in wheat (Xu et al., 2021) and *TaLBD16-4D* includes 14 homologous members sharing a high possibility of functional redundancy of this gene with structurally related transcription factors (Wang et al., 2018), we decided to study its function by obtaining the overexpressing transgenic lines instead of the *Talbd16* mutant. Furthermore, no sequence variation was found between the D genome of *Triticum aestivum* L. and its diploid ancestor (*Ae. tauschii*) (Wang et al., 2018). Although there might be unexpected effects due to its ectopic expression, we believe that the overexpression strategy can also largely demonstrate the direct or indirect function of *TaLBD16-D*. Here, the function of *TaLBD16-4D* in aerial architecture was analyzed by obtaining ectopic overexpressing transgenic wheat lines. It is well established that regulation of root growth is under the control of several hormones and the expression of various transcriptional regulators (Lavenus et al., 2016). Auxin is an important mediator of long-distance signaling for organ–organ communication, which can move over long distances from root to shoot that plays an essential role in most aspects of plant growth and development (Molnar et al., 2010; Li et al., 2021). Notably, it was found that *TaLBD16-4D* played an important role in auxin-mediated multiplate traits in wheat. First, the expression of *TaLBD16-4D* was increased by 2,4-D (Figure 3A) and the endogenous IAA content in both shoots and roots of transgenic seedling was significantly higher than that of WT (Figure 3F); Second, three putative AuxREs in the promoter region of *TaLBD16-4D* were identified from CS, which may help the upstream TaARFs regulate the expression of the *TaLBD16-4D* gene (Supplementary Figure 5). Third, *TaLBD16-4D*-overexpressing plants displayed auxin-related phenotypes, such as dwarfism, wider and shorter flag leaf, and abnormal panicle morphology, under normal conditions (Figure 1). Fourth, *TaLBD16-4D*-overexpression wheat showed less sensitivity in root growth, shoot length, and shoot fresh weight when treated with 2,4-D (Figures 3B–D) and impaired shoot gravitropic response (Figure 4). Fifth, expressions of genes regulating auxin biosynthesis, transport, and signaling were significantly changed between transgenic wheat plants and WT (Figure 3E; Supplementary Figure 4).

Influence of the *TaLBD16-4D* gene on heading time by the auxin-mediated photoperiodic pathway under long-day conditions

Wheat is a long-day plant grown widely across the world, and the differences in heading time among cultivars have led to a wide range of adaptability (Jackson, 2009; Shimada et al., 2009). Wheat cultivars that head early exhibit higher yield potential than cultivars that head later with the background of global warming, because the early-heading cultivars of wheat generally possess a longer post-heading and grain filling period and generate fewer total leaves per tiller but retain more green leaves and keep fewer leaves to senescence during anthesis (Tewolde et al., 2006). Heading time is tightly associated with the timing of floral transition. Numerous genetic studies in wheat have elucidated the regulatory network of heading-time (or flowering-time) genes involved in the vernalization and photoperiod pathway, which play important roles in floral induction (Worland, 2001; Kim et al., 2009; Song et al., 2015). *FLOWERING LOCUS T1*/*VERNALIZATION3* (*FT1*/*VRN3*) is an integrator of the vernalization and photoperiod pathways and functions as a flowering activator (Yan et al., 2006; Corbesier et al., 2007).

In the vernalization pathway, *VERNALIZATION1* (*VRN1*), *VERNALIZATION2* (*VRN2*), and *FT1*/*VRN3* are the key genes in wheat flowering regulation. *TaVRN2* is the flowering repressor to inhibit wheat flowering in winter by blocking the expression of *FT1* before vernalization (Yan et al., 2006; Li et al., 2011). The expression of *TaVRN1* is induced by vernalization, and it directly binds the promoters of *TaVRN2* and *TaFT1* to repress the expression level of *TaVRN2* and increase *TaFT1* expression to accelerate flowering (Yan et al., 2006; Deng et al., 2015). Although *TaVRN1*, *TaVRN2*, and *TaFT1* are naturally mutated in spring wheat varieties, there is a similar vernalization pathway of flowering regulation between spring wheat and

winter wheat, ultimately promoting flowering under long-day conditions with the absence of vernalization (Fu et al., 2005; Kippes et al., 2016; Finnegan et al., 2018). The role of GA in *Arabidopsis* flowering has been studied, and it has been shown to regulate flowering *via* the FT pathway (Hisamatsu and King, 2008; Wang et al., 2016). Recently, growth evidence has shown that auxin is also involved in floral stage transition and flowering opening. In *Arabidopsis*, increased distribution of auxin and upregulation of auxin transporter genes delayed flowering in the near-null magnetic field (Xu et al., 2018). Auxin is also involved in the flowering pathway in strawberry through its regulation of *auxin response factor4* (*ARF4*) expression, which can bind to the promoters of the floral meristem identity genes *APETALA1* (*AP1*) and *FRUITFULL* (*FUL*), inducing their expression (Dong et al., 2021). The involvement of *TaCYP78A5* in auxin synthesis pathway and auxin accumulation contributes to the delayed heading and flowering in wheat (Guo et al., 2022). However, it has not been reported whether there are correlations between the key flowering regulators and auxin in wheat.

Given that, the *LBD* gene family served as essential transcription factors to regulate multiple plant growth and development processes, including heading date (Wang et al., 2013; Xu et al., 2016). In previous research, *MdLBD11* in apple is classified into class I subclade, and overexpression of *MdLBD11* in *Arabidopsis* results in delayed flowering (Wang et al., 2013). OsLBD37 and OsLBD38 in rice act as class II type LBD proteins, and overexpression of either *OsLBD37* or *OsLBD38* results in delayed heading date and increased yield. In this work, we found that *TaLBD16-4D* might be involved in auxin pathway and overexpression of *TaLBD16-4D* in wheat also led to early heading. Notably, the transcript level of *TaLBD16-4D* was induced by 2,4-D, and the endogenous IAA content in both roots and shoots of *TaLBD16-4D* overexpression plants was significantly increased compared to those of WT (Figure 3A). Moreover, the expressions of *TaGI*, *TaCO1*, *TaHd1*, *TaVRN1*, *TaVRN2*, and *TaFT1* could be induced by IAA treatment, respectively (Supplementary Figure 6). For the critical regulators in the vernalization pathway, the expression level of activator *TaVRN1* was greatly upregulated in *TaLBD16-4D* OE lines, and the expression of the inhibitor *TaVRN2* was remarkably downregulated (Figure 5), which collaborated to promote the expression of *TaFT1* and led to early flowering. Meanwhile, the pivotal genes in the photoperiod pathway studied here included *TaGI*, *TaCO1*, *TaHd1*, and *TaFT1* (Shimada et al., 2009; Shaw et al., 2013; Hu et al., 2020). *TaLBD16-4D* might positively influence the expression of *TaGI*, *TaCO1*, and *TaHd1* under long-day conditions, which resulted in an upregulated expression of *TaFT1* to promote wheat flowering. Collectively, we deduced that *TaLBD16-4D* promotes wheat heading under long-day conditions probably through auxin-regulated flowering pathways. Therefore, it is necessary to further explore the molecular mechanism on how *TaLBD16-4D* participates in the auxin-mediated flowering pathway in wheat.

Data availability statement

The original contributions presented in the study are included in the article/Supplementary Material. Further inquiries can be directed to the corresponding authors.

Author contributions

YZ and JX designed the research. HW, XH, XS, XF, HC, SC, XW, YL, WG, and XL conducted the experiments. HW wrote the first draft. HW, XH, XF, and XS prepared the tables and figures. YZ and JX revised the manuscript. All authors read and approved the manuscript.

Funding

This work was supported by the Natural Science Foundation of China (31901546), the Key Research and Development Project of Shandong Province (2021LZGC025), the Agricultural Variety Improvement Project of Shandong Province (2019LZGC016), and the Foundation for High-level Talents of Qingdao Agriculture University (6631119057).

Conflict of interest

The authors declare that the research was conducted in the absence of any commercial or financial relationships that could be construed as a potential conflict of interest.

Publisher's note

Supplementary material

The Supplementary Material for this article can be found online at: https://www.frontiersin.org/articles/10.3389/fpls.2022.911993/full#supplementary-material

References

Bian, H., Xie, Y., Guo, F., Han, N., Ma, S., Zeng, Z., et al. (2012). Distinctive expression patterns and roles of the miRNA393/TIR1 homolog module in regulating flag leaf inclination and primary and crown root growth in rice (*Oryza sativa*). *N. Phytol.* 196 (1), 149–161. doi: 10.1111/j.1469-8137.2012.04248.x

Biswal, A. K., and Kohli, A. (2013). Cereal flag leaf adaptations for grain yield under drought: Knowledge status and gaps. *Mol. Breed.* 31 (4), 749–766. doi: 10.1007/s11032-013-9847-7

Bortiri, E., Chuck, G., Vollbrecht, E., Rocheford, T., Martienssen, R., and Hake, S. (2006). *ramosa2* encodes a LATERAL ORGAN BOUNDARY domain protein that determines the fate of stem cells in branch meristems of maize. *Plant Cell* 18 (3), 574–585. doi: 10.1105/tpc.105.039032

Chalfun-Junior, A., Franken, J., Mes, J. J., Marsch-Martinez, N., Pereira, A., and Angenent, G. C. (2005). *ASYMMETRIC LEAVES2-LIKE1* gene, a member of the AS2/LOB family, controls proximal–distal patterning in arabidopsis petals. *Plant Mol. Biol.* 57 (4), 559–575. doi: 10.1007/s11103-005-0698-4

Chen, Z., Cheng, X., Chai, L., Wang, Z., Du, D., Wang, Z., et al. (2020). Pleiotropic QTL influencing spikelet number and heading date in common wheat (*Triticum aestivum* l.). *Theor. Appl. Genet.* 133 (6), 1825–1838. doi: 10.1007/s00122-020-03556-6

Cockram, J., Jones, H., Leigh, F. J., O'Sullivan, D., Powell, W., Laurie, D. A., et al. (2007). Control of flowering time in temperate cereals: Genes, domestication, and sustainable productivity. *Exp. Bot.* 58 (6), 1231–1244. doi: 10.1093/jxb/erm042

Corbesier, L., Vincent, C., Jang, S., Fornara, F., Fan, Q., Searle, I., et al. (2007). FT protein movement contributes to long-distance signaling in floral induction of *Arabidopsis*. *Science* 316 (5827), 1030–1033. doi: 10.1126/science.1141752

Deng, W., Casao, M. C., Wang, P., Sato, K., Hayes, P. M., Finnegan, E. J., et al. (2015). Direct links between the vernalization response and other key traits of cereal crops. *Nat. Commun.* 6 (1), 1–8. doi: 10.1038/ncomms6882

De Smet, I., Lau, S., Voß, U., Vanneste, S., Benjamins, R., Rademacher, E. H., et al. (2010). Bimodular auxin response controls organogenesis in *Arabidopsis*. *Proc. Natl. Acad. Sci.* 107 (6), 2705–2710. doi: 10.1073/pnas.0915001107

Dong, X., Li, Y., Guan, Y., Wang, S., Luo, H., Li, X., et al. (2021). Auxin-induced *AUXIN RESPONSE FACTOR4* activates *APETALA1* and *FRUITFULL* to promote flowering in woodland strawberry. *Hortic. Res.* 8 (1), 115. doi: 10.1038/s41438-021-00550-x

Evans, M. M. (2007). The indeterminate gametophyte1 gene of maize encodes a LOB domain protein required for embryo sac and leaf development. *Plant Cell* 19 (1), 46–62. doi: 10.1105/tpc.106.047506

Fan, M., Xu, C., Xu, K., and Hu, Y. (2012). LATERAL ORGAN BOUNDARIES DOMAIN transcription factors direct callus formation in *Arabidopsis* regeneration. *Cell Res.* 22 (7), 1169–1180. doi: 10.1038/cr.2012.63

Fay, J., and Wittkopp, P. (2008). Evaluating the role of natural selection in the evolution of gene regulation. *Heredity* 100 (2), 191–199. doi: 10.1038/sj.hdy.6801000

Feng, Z., Zhu, J., Du, X., and Cui, X. (2012). Effects of three auxin-inducible LBD members on lateral root formation in arabidopsis thaliana. *Planta* 236 (4), 1227–1237. doi: 10.1007/s00425-012-1673-3

Finnegan, E. J., Ford, B., Wallace, X., Pettolino, F., Griffin, P. T., Schmitz, R. J., et al. (2018). Zebularine treatment is associated with deletion of *FT-B1* leading to an increase in spikelet number in bread wheat. *Plant Cell Environ.* 41 (6), 1346–1360. doi: 10.1111/pce.13164

Fu, D., Szűcs, P., Yan, L., Helguera, M., Skinner, J. S., Von Zitzewitz, J., et al. (2005). Large Deletions within the first intron in *VRN-1* are associated with spring growth habit in barley and wheat. *Mol. Genet. Genom.* 273 (1), 54–65. doi: 10.1007/s00438-004-1095-4

Grassini, P., Eskridge, K. M., and Cassman, K. G. (2013). Distinguishing between yield advances and yield plateaus in historical crop production trends. *Nat. Commun.* 4 (1), 1–11. doi: 10.1038/ncomms3918

Guo, F., Huang, Y., Qi, P., Lian, G., Hu, X., Han, N., et al. (2021). Functional analysis of auxin receptor *OsTIR1/OsAFB* family members in rice grain yield, tillering, plant height, root system, germination, and auxinic herbicide resistance. *N. Phytol.* 229 (5), 2676–2692. doi: 10.1111/nph.17061

Guo, L., Ma, M., Wu, L., Zhou, M., Li, M., Wu, B., et al. (2022). Modified expression of *TaCYP78A5* enhances grain weight with yield potential by accumulating auxin in wheat (*Triticum aestivum* l.). *Plant Biotechnol. J.* 20 (1), 168–182. doi: 10.1111/pbi.13704

Guo, B.-j., Wang, J., Lin, S., Tian, Z., Zhou, K., Luan, H.-y., et al. (2016). A genome-wide analysis of the *ASYMMETRIC LEAVES2/LATERAL ORGAN BOUNDARIES (AS2/LOB)* gene family in barley (*Hordeum vulgare* l.). *J. Zhejiang Univ-sc. B* 17 (10), 763–774. doi: 10.1631/jzus.B1500277

Hao, J., Yin, Y., and Fei, S.-z. (2013). Brassinosteroid signaling network: Implications on yield and stress tolerance. *Plant Cell Rep.* 32 (7), 1017–1030. doi: 10.1007/s00299-013-1438-x

Hisamatsu, T., and King, R. W. J. J. (2008). The nature of floral signals in Arabidopsis. II. Roles for *FLOWERING LOCUS T (FT)* and gibberellin. *J. Exp. Bot.* 59 (14), 3821–3829. doi: 10.1111/j.1439-037X.2006.00189.x

Husbands, A., Bell, E. M., Shuai, B., Smith, H. M., and Springer, P. S. (2007). LATERAL ORGAN BOUNDARIES defines a new family of DNA-binding transcription factors and can interact with specific bHLH proteins. *Acids Res.* 35 (19), 6663–6671. doi: 10.1093/nar/gkm775

Hu, R., Xiao, J., Zhang, Q., Gu, T., Chang, J., Yang, G., et al. (2020). A light-regulated gene, *TaLWD1L-a*, affects flowering time in transgenic wheat (*Triticum aestivum* l.). *Plant Sci.* 299, 110623. doi: 10.1016/j.plantsci.2020.110623

Inukai, Y., Sakamoto, T., Ueguchi-Tanaka, M., Shibata, Y., Gomi, K., Umemura, I., et al. (2005). Crown rootless1, which is essential for crown root formation in rice, is a target of an AUXIN RESPONSE FACTOR in auxin signaling. *Plant Cell* 17 (5), 1387–1396. doi: 10.1105/tpc.105.030981

Ito, J., Fukaki, H., Onoda, M., Li, L., Li, C., Tasaka, M., et al. (2016). Auxin-dependent compositional change in mediator in ARF7-and ARF19-mediated transcription. *Proc. Natl. Acad. Sci.* 113 (23), 6562–6567. doi: 10.1073/pnas.1600739113

Ivanchenko, M. G., Muday, G. K., and Dubrovsky, J. G. (2008). Ethylene–auxin interactions regulate lateral root initiation and emergence in arabidopsis thaliana. *Plant J.* 55 (2), 335–347. doi: 10.1111/j.1365-313X.2008.03528.x

Iwakawa, H., Iwasaki, M., Kojima, S., Ueno, Y., Soma, T., Tanaka, H., et al. (2007). Expression of the ASYMMETRIC LEAVES2 gene in the adaxial domain of arabidopsis leaves represses cell proliferation in this domain and is critical for the development of properly expanded leaves. *Plant J.* 51 (2), 173–184. doi: 10.1111/j.1365-313X.2007.03132.x

Jackson, S. D. (2009). Plant responses to photoperiod. *N. Phytol.* 181 (3), 517–531. doi: 10.1111/j.1469-8137.2008.02681.x

Jiang, Y., Schmidt, R. H., Zhao, Y., and Reif, J. C. (2017). A quantitative genetic framework highlights the role of epistatic effects for grain-yield heterosis in bread wheat. *Nat. Genet.* 49 (12), 1741–1746. doi: 10.1038/ng.3974

Kamran, A., Iqbal, M., and Spaner, D. (2014). Flowering time in wheat (*Triticum aestivum* l.): A key factor for global adaptability. *Euphytica* 197 (1), 1–26. doi: 10.1007/s10681-014-1075-7

Kepinski, S., and Leyser, O. (2004). Auxin-induced SCF^{TIR1}-Aux/IAA interaction involves stable modification of the SCF^{TIR1} complex. *Proc. Natl. Acad. Sci.* 101 (33), 12381–12386. doi: 10.1073/pnas.0402868101

Kim, S. H., Bahk, S., An, J., Hussain, S., Nguyen, N. T., Do, H. L., et al. (2020). A gain-of-function mutant of IAA15 inhibits lateral root development by transcriptional repression of *LBD* genes in arabidopsis. *Front. Plant Sci.* 11, 1239. doi: 10.3389/fpls.2020.01239

Kim, D.-H., Doyle, M. R., Sung, S., and Amasino, R. M. (2009). Vernalization: Winter and the timing of flowering in plants. *Annu. Rev. Cell. Dev. Biol.* 25, 277–299. doi: 10.1146/annurev.cellbio.042308.113411

Kippes, N., Chen, A., Zhang, X., Lukaszewski, A. J., and Dubcovsky, J. (2016). Development and characterization of a spring hexaploid wheat line with no functional *VRN2* genes. *Theor. Appl. Genet.* 129 (7), 1417–1428. doi: 10.1007/s00122-018-3141-3

Landschulz, W. H., Johnson, P. F., and McKnight, S. L. (1988). The leucine zipper: A hypothetical structure common to a new class of DNA binding proteins. *Science* 240 (4860), 1759–1764. doi: 10.1126/science.3289117

Lavenus, J., Guyomarc'h, S., and Laplaze, L. (2016). PIN transcriptional regulation shapes root system architecture. *Trends Plant Sci.* 21 (3), 175–177. doi: 10.1016/j.tplants.2016.01.011

Lee, H. W., Kim, N. Y., Lee, D. J., and Kim, J. (2009). LBD18/ASL20 regulates lateral root formation in combination with LBD16/ASL18 downstream of ARF7 and ARF19 in arabidopsis. *Plant Physiol.* 151 (3), 1377–1389. doi: 10.1104/pp.109.143685

Li, C., Distelfeld, A., Comis, A., and Dubcovsky, J. (2011). Wheat flowering repressor VRN2 and promoter CO2 compete for interactions with NUCLEAR FACTOR-y complexes. *Plant J.* 67 (5), 763–773. doi: 10.1111/j.1365-313X.2011.04630.x

Li, H., Li, J., Song, J., Zhao, B., Guo, C., Wang, B., et al. (2019). An auxin signaling gene *BnaA3. IAA 7* contributes to improved plant architecture and yield heterosis in rapeseed. *N. Phytol.* 222 (2), 837–851. doi: 10.1111/nph.15632

Li, G., Testerink, C., and Zhang, Y. (2021). How roots and shoots communicate through stressful times. *Trends Plant Sci.* 26 (9), 940–952. doi: 10.1016/j.tplants.2021.03.005

Li, P., Wang, Y., Qian, Q., Fu, Z., Wang, M., Zeng, D., et al. (2007). *LAZY1* controls rice shoot gravitropism through regulating polar auxin transport. *Cell Res.* 17 (5), 402–410. doi: 10.1038/cr.2007.38

Li, C., Zhu, S., Zhang, H., Chen, L., Cai, M., Wang, J., et al. (2017). OsLBD37 and OsLBD38, two class II type LBD proteins, are involved in the regulation of heading date by controlling the expression of *Ehd1* in rice. *Biophys. Res. Commun.* 486 (3), 720–725. doi: 10.1016/j.bbrc.2017.03.104

Li, C., Zou, X., Zhang, C., Shao, Q., Liu, J., Liu, B., et al. (2016). *OsLBD3-7* overexpression induced adaxially rolled leaves in rice. *PloS One* 11 (6), e0156413. doi: 10.1371/journal.pone.0156413

Ljung, K., Hull, A. K., Kowalczyk, M., Marchant, A., Celenza, J., Cohen, J. D., et al. (2002). Biosynthesis, conjugation, catabolism and homeostasis of indole-3-acetic acid in *Arabidopsis thaliana*. *Plant Mol. Biol.* 49 (3), 249–272. doi: 10.1023/A:1015298812300

Majer, C., and Hochholdinger, F. (2011). Defining the boundaries: structure and function of LOB domain proteins. *Trends Plant Sci.* 16 (1), 47–52. doi: 10.1016/j.tplants.2010.09.009

Mangeon, A., Bell, E. M., Lin, W.-c., Jablonska, B., and Springer, P. S. (2011). Misregulation of the LOB domain gene *DDA1* suggests possible functions in auxin signalling and photomorphogenesis. *J. Exp. Bot.* 62 (1), 221–233. doi: 10.1093/jxb/erq259

Molnar, A., Melnyk, C. W., Bassett, A., Hardcastle, T. J., Dunn, R., and Baulcombe, D. C. (2010). Small silencing RNAs in plants are mobile and direct epigenetic modification in recipient cells. *Science* 328 (5980), 872–875. doi: 10.1126/science.1187959

Okushima, Y., Fukaki, H., Onoda, M., Theologis, A., and Tasaka, M. (2007). ARF7 and ARF19 regulate lateral root formation *via* direct activation of *LBD/ASL* genes in arabidopsis. *Plant Cell* 19 (1), 118–130. doi: 10.1105/tpc.106.047761

Okushima, Y., Mitina, I., Quach, H. L., and Theologis, A. (2005a). AUXIN RESPONSE FACTOR 2 (ARF2): A pleiotropic developmental regulator. *Plant J.* 43 (1), 29–46. doi: 10.1111/j.1365-313x.2005.02426.x

Okushima, Y., Overvoorde, P. J., Arima, K., Alonso, J. M., Chan, A., Chang, C., et al. (2005b). Functional genomic analysis of the AUXIN RESPONSE FACTOR gene family members in *Arabidopsis thaliana*: Unique and overlapping functions of *ARF7* and *ARF19*. *Plant Cell* 17 (2), 444–463. doi: 10.1105/tpc.104.028316

Qiao, L., Zhang, L., Zhang, X., Zhang, L., Li, X., Chang, J., et al. (2017). Evolution of the aux/IAA gene family in hexaploid wheat. *J. Mol. Evol.* 85 (3), 107–119. doi: 10.1007/s00239-017-9810-z

Rast, M. I., and Simon, R. (2012). *Arabidopsis* JAGGED LATERAL ORGANS acts with ASYMMETRIC LEAVES2 to coordinate KNOX and PIN expression in shoot and root meristems. *Plant Cell* 24 (7), 2917–2933. doi: 10.1105/tpc.112.099978

Renau-Morata, B., Nebauer, S. G., García-Carpintero, V., Cañizares, J., Minguet, E. G., de los Mozos, M., et al. (2021). Flower induction and development in saffron: Timing and hormone signalling pathways. *Ind. Crops Prod.* 164, 113370. doi: 10.1016/j.indcrop.2021.113370

Rogers, E. D., and Benfey, P. N. (2015). Regulation of plant root system architecture: implications for crop advancement. *Curr. Opin. Biotechnol.* 32, 93–98. doi: 10.1016/j.copbio.2014.11.015

Rubin, G., Tohge, T., Matsuda, F., Saito, K., and Scheible, W.-R. (2009). Members of the LBD family of transcription factors repress anthocyanin synthesis and affect additional nitrogen responses in *Arabidopsis*. *Plant Cell* 21 (11), 3567–3584. doi: 10.1105/tpc.109.067041

Semiarti, E., Ueno, Y., Tsukaya, H., Iwakawa, H., Machida, C., and Machida, Y. (2001). The *ASYMMETRIC LEAVES2* gene of arabidopsis thaliana regulates formation of a symmetric lamina, establishment of venation and repression of meristem-related homeobox genes in leaves. *Development* 128 (10), 1771–1783. doi: 10.1242/dev.128.10.1771

Shahinnia, F., Le Roy, J., Laborde, B., Sznajder, B., Kalambettu, P., Mahjourimajd, S., et al. (2016). Genetic association of stomatal traits and yield in wheat grown in low rainfall environments. *BMC Plant Biol.* 16 (1), 1–14. doi: 10.1186/s12870-016-0838-9

Shaw, L. M., Turner, A. S., Herry, L., Griffiths, S., and Laurie, D. A. (2013). Mutant alleles of *Photoperiod-1* in wheat (*Triticum aestivum* l.) that confer a late flowering phenotype in long days. *PloS One* 8 (11), e79459. doi: 10.1371/journal.pone.0079459

Shiferaw, B., Smale, M., Braun, H.-J., Duveiller, E., Reynolds, M., and Muricho, G. (2013). Crops that feed the world 10. past successes and future challenges to the role played by wheat in global food security. *Food Secur.* 5 (3), 291–317. doi: 10.1007/s12571-013-0263-y

Shimada, S., Ogawa, T., Kitagawa, S., Suzuki, T., Ikari, C., Shitsukawa, N., et al. (2009). A genetic network of flowering-time genes in wheat leaves, in which an *APETALA1/FRUITFULL-like* gene, *VRN1*, is upstream of *FLOWERING LOCUS t*. *Plant J.* 58 (4), 668–681. doi: 10.1111/j.1365-313X.2009.03806.x

Shim, J. S., and Imaizumi, T. (2015). Circadian clock and photoperiodic response in *Arabidopsis*: From seasonal flowering to redox homeostasis. *Biochemistry* 54 (2), 157–170. doi: 10.1021/bi500922q

Shuai, B., Reynaga-Pena, C. G., and Springer, P. S. (2002). The *lateral organ boundaries* gene defines a novel, plant-specific gene family. *Plant Physiol.* 129 (2), 747–761. doi: 10.1104/pp.010926

Song, Y. H., Shim, J. S., Kinmonth-Schultz, H. A., and Imaizumi, T. (2015). Photoperiodic flowering: Time measurement mechanisms in leaves. *Annu. Rev. Plant Biol.* 66, 441–464. doi: 10.1146/annurev-arplant-043014-115555

Song, Y., and Xu, Z.-F. (2013). Ectopic overexpression of an auxin/indole-3-acetic acid (*Aux/IAA*) gene *OsIAA4* in rice induces morphological changes and reduces responsiveness to auxin. *Int. J. Mol. Sci.* 14 (7), 13645–13656. doi: 10.3390/ijms140713645

Song, Y., You, J., and Xiong, L. (2009). Characterization of *OsIAA1* gene, a member of rice Aux/IAA family involved in auxin and brassinosteroid hormone responses and plant morphogenesis. *Plant Mol. Biol.* 70 (3), 297–309. doi: 10.1007/s11103-009-9474-1

Strohm, A. K., Baldwin, K. L., and Masson, P. H. (2012). Multiple roles for membrane-associated protein trafficking and signaling in gravitropism. *Front. Plant Sci.* 3. doi: 10.3389/fpls.2012.00274

Taramino, G., Sauer, M., Stauffer, J. L.Jr., Multani, D., Niu, X., Sakai, H., et al. (2007). The maize (*Zea mays* l.) *RTCS* gene encodes a LOB domain protein that is a key regulator of embryonic seminal and post-embryonic shoot-borne root initiation. *Plant J.* 50 (4), 649–659. doi: 10.1111/j.1365-313X

Tewolde, H., Fernandez, C., Erickson, C. J. J. .A., and Science, C. (2006). Wheat cultivars adapted to post-heading high temperature stress. *J. Agron. Crop Sci.* 192 (2), 111–120. doi: 10.1093/jxb/ern232

Tian, Q., and Reed, J. W. (1999). Control of auxin-regulated root development by the arabidopsis thaliana SHY2/IAA3 gene. *Development* 126 (4), 711–721. doi: 10.1242/dev.126.4.711

Tian, Q., Uhlir, N. J., and Reed, J. W. (2002). Arabidopsis SHY2/IAA3 inhibits auxin-regulated gene expression. *Plant Cell* 14 (2), 301–319. doi: 10.1105/tpc.010283

Tucker, E. J., Baumann, U., Kouidri, A., Suchecki, R., Baes, M., Garcia, M., et al. (2017). Molecular identification of the wheat male fertility gene *Ms1* and its prospects for hybrid breeding. *Nat. Commun.* 8 (1), 1–10. doi: 10.1038/s41467-017-00945-2

Ulmasov, T., Murfett, J., Hagen, G., and Guilfoyle, T. J. (1997). Aux/IAA proteins repress expression of reporter genes containing natural and highly active synthetic auxin response elements. *Plant Cell* 9 (11), 1963–1971. doi: 10.1105/tpc.9.11.1963

Vanneste, S., and Friml, J. (2009). Auxin: A trigger for change in plant development. *Cell* 136 (6), 1005–1016. doi: 10.1016/j.cell

Wang, H., Pan, J., Li, Y., Lou, D., Hu, Y., and Yu, D. J. P. P. (2016). The DELLA-CONSTANS transcription factor cascade integrates gibberellic acid and photoperiod signaling to regulate flowering. *Plant Physiol.* 172 (1), 479–488. doi: 10.1104/pp.16.00891

Wang, H., Hu, Z., Huang, K., Han, Y., Zhao, A., Han, H., et al. (2018). Three genomes differentially contribute to the seedling lateral root number in allohexaploid wheat: Evidence from phenotype evolution and gene expression. *Plant J.* 95 (6), 976–987. doi: 10.1111/tpj.14005

Wang, Y., and Li, J. (2006). Genes controlling plant architecture. *Curr. Opin. Biotechnol.* 17 (2), 123–129. doi: 10.1016/j.copbio

Wang, X., Zhang, S., Su, L., Liu, X., and Hao, Y. (2013). A genome-wide analysis of the LBD (LATERAL ORGAN BOUNDARIES domain) gene family in malus domestica with a functional characterization of MdLBD11. *PloS One* 8 (2), e57044. doi: 10.1371/journal.pone.0057044

Weijers, D., and Jürgens, G. (2004). Funneling auxin action: Specificity in signal transduction. *Curr. Opin. Plant Biol.* 7 (6), 687–693. doi: 10.1016/j.pbi

Worland, T. (2001). *Genetic basis of worldwide wheat varietal improvement. the world wheat book: A history of wheat breeding* Vol. 1. Eds. A. P. Bonjean and W. J. Angus (Paris: Lavoisier publishing), 59–100.

Xue, W., Xing, Y., Weng, X., Zhao, Y., Tang, W., Wang, L., et al. (2008). Natural variation in *Ghd7* is an important regulator of heading date and yield potential in rice. *Nat. Genet.* 40 (6), 761–767. doi: 10.1038/ng.143

Xu, J., Hu, P., Tao, Y., Song, P., Gao, H., and Guan, Y. (2021). Genome-wide identification and characterization of the *Lateral organ boundaries domain* (*LBD*) gene family in polyploid wheat and related species. *PeerJ* 9, e11811. doi: 10.7717/peerj.11811

Xu, C., Luo, F., and Hochholdinger, F. (2016). LOB domain proteins: Beyond lateral organ boundaries. *Plant Mol. Biol.* 21 (2), 159–167. doi: 10.1016/j.tplants

Xu, Y.-X., Xiao, M.-Z., Liu, Y., Fu, J.-L., He, Y., and Jiang, D.-A. (2017). The small auxin-up RNA OsSAUR45 affects auxin synthesis and transport in rice. *Plant Mol. Biol.* 94 (1), 97–107. doi: 10.1007/s11103-017-0595-7

Xu, C., Zhang, Y., Yu, Y., Li, Y., and Wei, S. J. B. (2018). Suppression of arabidopsis flowering by near-null magnetic field is mediated by auxin. *Bioelectromagnetics* 39 (1), 15–24. doi: 10.1002/bem.22086

Yan, L., Fu, D., Li, C., Blechl, A., Tranquilli, G., Bonafede, M., et al. (2006). The wheat and barley vernalization gene *VRN3* is an orthologue of *FT*. *Proc. Natl. Acad. Sci.* 103 (51), 19581–19586. doi: 10.1073/pnas.0607142103

Yue, P., Wang, Y., Bu, H., Li, X., Yuan, H., Wang, A.J.P.B., et al. (2019). Ethylene promotes IAA reduction through PuERFs-activated PuGH3. 1 during fruit ripening in pear *(Pyrus ussuriensis)*. *Postharvest Biol. Tec.* 157, 110955–19586. doi: 10.1016/j.postharvbio.2019.110955

Yang, Y., Yu, X., and Wu, P. (2006). Comparison and evolution analysis of two rice subspecies *LATERAL ORGAN BOUNDARIES* domain gene family and their evolutionary characterization from arabidopsis. *Mol. Phylogenet. Evol.* 39 (1), 248–262. doi: 10.1016/j.ympev.2005.09.016

Zhang, J., Gizaw, S. A., Bossolini, E., Hegarty, J., Howell, T., Carter, A. H., et al. (2018). Identification and validation of QTL for grain yield and plant water status under contrasting water treatments in fall-sown spring wheats. *Theor. Appl. Genet.* 131 (8), 1741–1759. doi: 10.1007/s00122-018-3111-9

Zhang, J., Tang, W., Huang, Y., Niu, X., Zhao, Y., Han, Y., et al. (2015). Down-regulation of a *LBD*-like gene, *OsIG1*, leads to occurrence of unusual double ovules and developmental abnormalities of various floral organs and megagametophyte in rice. *J. Exp. Bot.* 66 (1), 99–112. doi: 10.1093/jxb/eru396

Zhang, F., Tao, W., Sun, R., Wang, J., Li, C., Kong, X., et al. (2020). PRH1 mediates ARF7-LBD dependent auxin signaling to regulate lateral root development in *Arabidopsis thaliana*. *PloS Genet.* 16 (2), e1008044. doi: 10.1371/journal.pgen.1008044

Zhang, Y.-M., Zhang, S.-Z., and Zheng, C.-C. (2014). Genomewide analysis of LATERAL ORGAN BOUNDARIES domain gene family in *Zea mays*. *J. Genet.* 93 (1), 79–91. doi: 10.1007/s12041-014-0342-7

frontiers | Frontiers in Plant Science

TYPE Mini Review
PUBLISHED 23 September 2022
DOI 10.3389/fpls.2022.976765

OPEN ACCESS

EDITED BY
Gianni Barcaccia,
University of Padua, Italy

REVIEWED BY
Ales Kovarik,
Academy of Sciences of the Czech Republic (ASCR), Czechia

*CORRESPONDENCE
Elvira Hörandl
elvira.hoerandl@biologie.uni-goettingen.de

SPECIALTY SECTION
This article was submitted to Plant Breeding, a section of the journal Frontiers in Plant Science

RECEIVED 23 June 2022
ACCEPTED 24 August 2022
PUBLISHED 23 September 2022

CITATION
He L and Hörandl E (2022) Does polyploidy inhibit sex chromosome evolution in angiosperms? *Front. Plant Sci.* 13:976765. doi: 10.3389/fpls.2022.976765

Does polyploidy inhibit sex chromosome evolution in angiosperms?

Li He[1] and Elvira Hörandl[2]*

[1]Eastern China Conservation Centre for Wild Endangered Plant Resources, Shanghai Chenshan Botanical Garden, Shanghai, China, [2]Department of Systematics, Biodiversity and Evolution of Plants, University of Göttingen, Göttingen, Germany

Dioecy is rare in flowering plants (5–6% of species), but is often controlled genetically by sex-linked regions (SLRs). It has so far been unclear whether, polyploidy affects sex chromosome evolution, as it does in animals, though polyploidy is quite common in angiosperms, including in dioecious species. Plants could be different, as, unlike many animal systems, degenerated sex chromosomes, are uncommon in plants. Here we consider sex determination in plants and plant-specific factors, and propose that constraints created at the origin of polyploids limit successful polyploidization of species with SLRs. We consider the most likely case of a polyploid of a dioecious diploid with an established SLR, and discuss the outcome in autopolyploids and allopolyploids. The most stable system possibly has an SLR on just one chromosome, with a strongly dominant genetic factor in the heterogametic sex (e.g., xxxY male in a tetraploid). If recombination occurs with its homolog, this will prevent Y chromosome degeneration. Polyploidy may also allow for reversibility of multiplied Z or X chromosomes into autosomes. Otherwise, low dosage of Y-linked SLRs compared to their multiple homologous x copies may cause loss of reliable sex-determination at higher ploidy levels. We discuss some questions that can be studied using genome sequencing, chromosome level-assemblies, gene expression studies and analysis of loci under selection.

KEYWORDS

angiosperms, dioecy, sex chromosomes, autopolyploidy, allopolyploidy

Introduction

Dioecy, the sexual system with separate female and male individuals, is phylogenetically widespread in angiosperms, but occurs only in 5–6% of species (Ming et al., 2011; Renner, 2014). Functional hermaphroditism with hermaphrodite flowers is the most common system, and the transition to dioecy can involve gynodioecy, monoecy, or other sexual systems (Darwin, 1877; Richards, 1997). Dioecy in many plants is under genetic control, with a sex-linked locus or region (SLR). We term

such chromosomes "SLR bearing," but here restrict the definition of sex chromosomes (following; Charlesworth, 2015) to mean chromosomes carrying completely sex-linked regions that include many genes and do not recombine. This distinction recognizes a key aspect of such "classical" sex chromosomes, their lack of recombination, which can arise in several different ways (Charlesworth, 2022), and which allows accumulation of deleterious mutations, resulting in degenerated sex chromosomes like those in mammals and *Drosophila* (Muller, 1918; Bachtrog, 2008). One hypothesis involves selection favoring the suppression of recombination between the sex-determining locus and linked sexually antagonistic polymorphic genes (Fisher, 1931; Rice, 1987). Suppression of recombination, however, might also result from neutral sequence divergence (Jeffries et al., 2021). Lenormand and Roze (2022) recently proposed a model for stepwise evolution of sex chromosomes via "lucky inversions" that prevent recombination. Genetic sex-determination has evolved independently multiple times in plants, but many have remained in the homomorphic state, suggesting that recombination has often not become suppressed, and that their SLRs carry just a sex-determining gene (or a few physically close and closely clinked sex-determining genes), explaining why degeneration have not occurred in these species. Eventually, ancestral sex chromosomes can be replaced by a new set of sex-determining chromosomes, and revert to autosomes (Vicoso, 2019; **Figure 1A**).

Many angiosperms are polyploid, having more than two chromosome sets (Van De Peer et al., 2017). Polyploidy is regarded an important evolutionary mechanism for angiosperms (e.g., Comai, 2005; Soltis and Soltis, 2009, 2016; Abbott et al., 2013; Hörandl, 2022). All angiosperms share an ancient genome duplication (Jiao et al., 2011), and 25–35% of species are more recently evolved polyploids of this already polyploid state (Landis et al., 2018). Unlike most animal polyploids, most polyploid plants are viable and can reproduce sexually (e.g., Levin, 2002; Comai, 2005). Asexual reproduction (apomixis) occurs in less than 1% of species and is not necessarily correlated to polyploidy (Mogie, 1992; Hojsgaard et al., 2014; Hojsgaard and Hörandl, 2019). In animals, the reason for the rarity of polyploidization is thought to be because it disturbs the "balance" system of sex determination by the X/autosome ratio (Muller, 1925). Such systems are found in species with extremely degenerated sex chromosomes in the heterogametic sex like the *Drosophila* Y (Orr, 1990). In this case, the heterogametic sex in a tetraploid (XXYY) will only produce heterozygous (XY) gametes if X-X and Y-Y pairs form preferentially at meiosis; since YY gametes are not viable, the heterogametic sex will be lost, resulting in rapid extinction (Orr, 1990; **Figure 1B**). Although sex chromosomes of angiosperms have been studied for a century (reviewed by Westergaard, 1958), less attention has been given to polyploidy in dioecious plants. A correlation analysis of polyploidy and sexual systems on c. 1000 angiosperm species found that polyploidy is associated with sexual dimorphism (gynodioecy, androdioecy, and dioecy), but not specifically with dioecy, and that patterns are highly clade-specific (Glick et al., 2016). For many dioecious tropical trees and shrubs, however, chromosome numbers and ploidy levels are unknown, and more work is needed.

Knowledge about sex chromosome evolution in polyploid plants is also scanty. Modern review articles about SLRs and genetic sex determination in plants focus on diploid systems (Feng et al., 2020; Charlesworth, 2021; Renner and Müller, 2021). The recently launched database,[1] included 166 angiosperm species with sex chromosomes or SLR-regions, of which 110 (66.3%) are classified as diploids, vs. only 20 (12%) as polyploids (Baránková et al., 2020), suggesting that polyploidy would not be highly correlated with sex chromosome evolution. However, the data are not yet clear enough, as 36 of the dioecious species (21.7%) have unknown ploidy levels (Baránková et al., 2020). Moreover, species-rich plant orders and families that experienced genome duplications before their diversification (Soltis et al., 2009), are hardly represented (only six cases in Brassicales, four in Poaceae, zero in Fabaceae, and Solanaceae), yet dioecy is present in all of them.

On the other hand, it is already known that several entirely dioecious lineages include polyploid series (Westergaard, 1958). Polyploidy may trigger shifts to dioecy (via different pathways reviewed by Ashman et al., 2013; Henry et al., 2018) speculated that whole-genome duplication could favor shifts to dioecy via evolution of sex-determining loci in duplicated genes. However, few such shifts are documented, except in *Fragaria* (Tennessen et al., 2016) where dioecy evolved in highly diploidized octoploids that arose from diploid, hermaphroditic progenitors (Tennessen et al., 2014). Most dioecious polyploids probably arose from diploid species with established SLR systems (e.g., *Salix polyclona*, He et al., 2022). Almost all angiosperms in which sex chromosome evolution is currently studied, including kiwi, papaya, persimmon, asparagus, strawberry, are cultivated plants (Henry et al., 2018), and little is known about sex chromosome evolution in natural polyploid systems. However, some examples (**Table 1**) include the tetraploids *Rumex acetosella* (Cunado et al., 2007) and hexaploid *Mercurialis annua* (Gerchen et al., 2022) all with male heterogamety. We briefly summarize sex chromosome evolution in diploids, and focus here on models of polyploidization from progenitors with established diploid non-degenerated systems (XY), and discuss how the presence of SLR-bearing chromosomes may affect new polyploids, and the cytological consequences, and whether polyploidy favors breakdown of dioecy, or causes reversals of X (or Z) chromosomes back to autosomes.

1 https://www.sexchrom.csic.es/

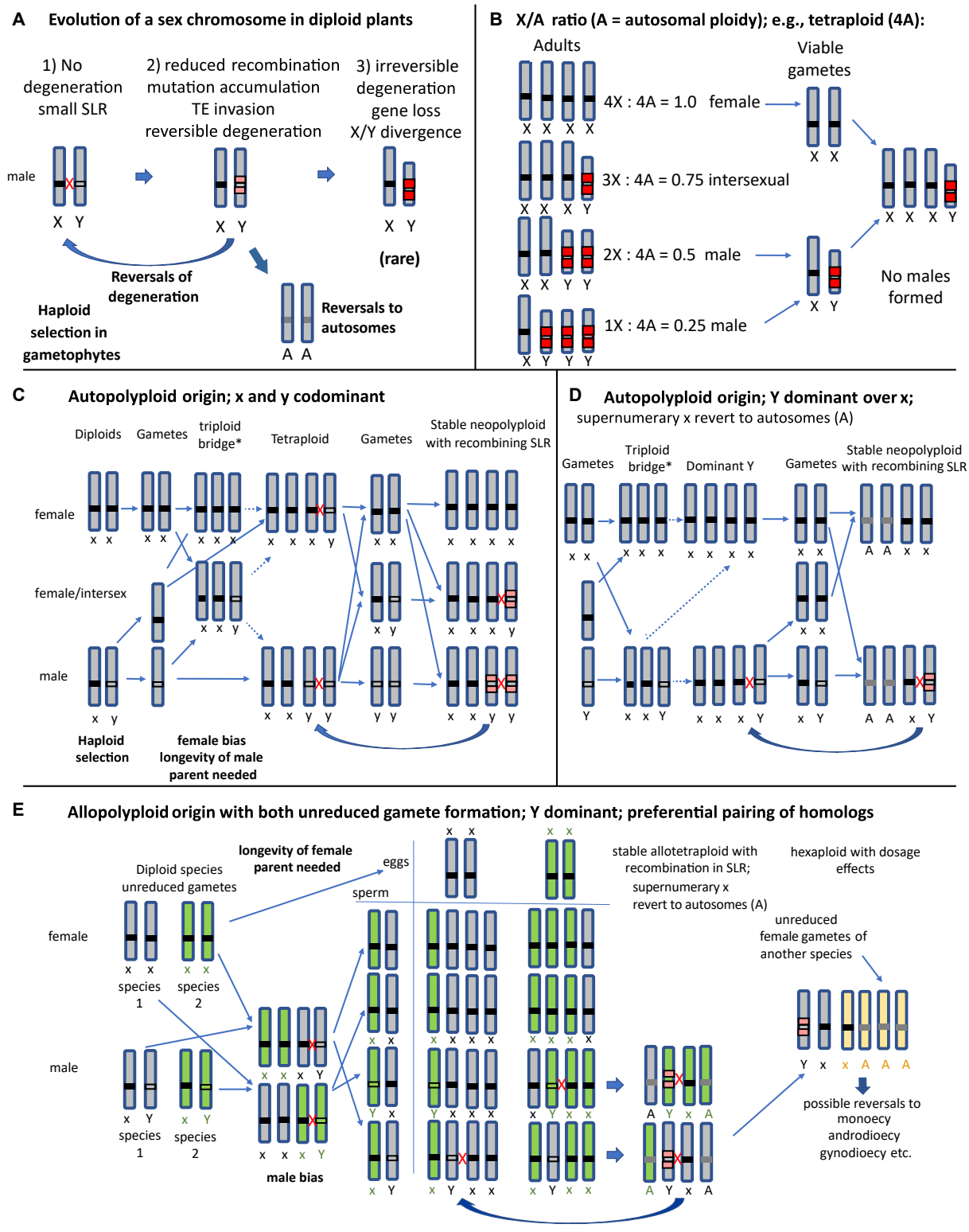

FIGURE 1
(Continued)

FIGURE 1
Evolutionary scenarios of SLR-bearing chromosomes and their homologs in different possible types of polyploid plants under male heterogamety, assuming different possible types of sex-determination; A, autosomes. The thick arrows indicate evolutionary changes, and the thin ones indicate crosses and gamete formation, and when the lines are dashed, this indicates that the cross has low fertility. Red crosses indicate recombination between chromosomes that pair at meiosis (for general meiosis behavior of polyploids see **Supplementary Figure 1**). **(A)** The three main phases of sex chromosome evolution in a diploid dioecious progenitor of a polyploid species; many plants appear to be in stages with no, or minor, degeneration. Reversals to autosomes can occur when the ancestral X-Y pair is replaces by a new set of sex-determining chromosomes. **(B)** Classical "balance" model by Muller (1925) for sex determination via the X/A ratio in species with degenerated sex chromosomes, as in many animals (including *Drosophila*, nematodes and, with female heterogamety, Lepidoptera) (Bachtrog et al., 2014), showing that polyploids can neither maintain stable X/Y ratios nor restore the heterogametic sex. This form of sex-determination appears to be rare in angiosperms. **(C)** An autopolyploid plant originated via unreduced female gametes (termed a "triploid bridge," because a triploid generation is initially formed by unreduced gametes of one parent, and can produce haploid, diploid, and triploid gametes; the * denotes low fertility of this generation). The diagram shows the expected progeny types assuming codominant expression of a Y-linked male-determining factor, and no preferential pairing of homologs (possible xyyy genotypes not shown). **(D)** Autopolyploid with a dominant Y-linked factor; xxxY genotypes represent fertile males. After some time two of the x may revert to autosomes A, whereas recombination between the xY pair prevents degeneration. **(E)** Allopolyploid origins via unreduced gametes of both parents (shown in green and gray), and with a dominant Y-linked maleness factor. Homologs of the same parent will preferentially pair at meiosis (see also **Supplementary Figure 1**). Initially only xxxY male allopolyploids can be formed and produce heterozygous male gametes (see text). Backcrossing with unreduced gametes of female parents can produce various tetraploid hybrid genotypes, including both xxxx females and xxxY males, resulting in stable populations. Here also two of the x may revert to autosomes **(A)**, and only one possible recombining xY pair (derived from the same progenitor) remains. Further hybridization with a third species can result in a hexaploid, which eventually results in reversal to a non-dioecious system.

TABLE 1 Examples of polyploid plants with known sex determination systems.

Taxa	Ploidy level	Male or female heterogamety	Sex determination system	References
Diospyros kaki	Hexaploid	Male	XXXXXX/XXXXXY or XXXXYY	Akagi et al., 2016
Fragaria chiloensis	Octoploid	Female	ZW/ZZ	Tennessen et al., 2016; Cauret et al., 2022
Melandrium album (Silene latifolia)	Tetraploid	Male	XXXX/XXXY	Warmke and Blakeslee, 1939
Mercurialis annua	Hexaploid	Male	XXXXXX/XXXXXY?	Gerchen et al., 2022
Rumex acetosella	Tetraploid	Male	XX/XY	Cunado et al., 2007
Salix polyclona	Tetraploid	Female	ZZZW/ZZZZ?	He et al., 2022

Sex chromosome evolution in diploid plants

In sessile organisms, separation of the sexes in different individuals reduces the chances of successful matings (Darwin, 1876; Hörandl and Hadacek, 2020). One factor favoring the evolution of dioecy in plants, and maintaining it over long evolutionary times, is prevention of self-fertilization and consequent inbreeding depression (Darwin, 1877; Renner, 2014). This is particularly important in wind-pollinated, long-lived plants, including tropical trees.

Dioecy and sex-linked regions evolved multiple times in angiosperms (Renner, 2014; Feng et al., 2020). Evolution from a functionally hermaphroditic ancestor requires two mutations, and both currently known plant sex-determining systems involve a gene whose action promotes one sex function and suppresses the other (review e.g., in Renner and Müller, 2021). Evolution via a turnover event in an ancestrally dioecious species will also usually involve an active maleness or femaleness factor, as the new factor must act in the presence of the ancestral one (Bull, 1983). *Rumex acetosa* and *R. thyrsiflorus* are exceptions, as sex in these species is determined by a balance system similar to that in *Drosophila* (Zuk, 1963). This balance system did not function in synthetic allopolyploid offspring (Zuk, 1963).

Charlesworth (2021) reviews three major phases of recombination and genetic degeneration (**Figure 1A**). Initially, SLRs are often small and do not show degeneration because there are too few sites in the completely non-recombining region, and purifying selection prevents mutation accumulation. A second phase may occur, in which recombination becomes suppressed in a larger region, allowing loss of gene functions, though the genes are still present; this weakens purifying selection on Y (or W) linked genes, allowing X-Y sequence divergence. If suppressed recombination persists for long enough in a large enough genome region, deletion of genes is expected to follow, producing highly degenerated sex chromosomes. The time needed for this stage of degeneration to be reached is unknown, and could differ between species, as it depends on mutation rates and population sizes (Bachtrog, 2008).

However, SLR regions of dioecious plants may be less subject to accumulation of deleterious mutations than in animals, because haploid gametophytes express up to 65% of genes (Joseph and Kirkpatrick, 2004; Gorelick, 2005; Cronk, 2022;

Mank, 2022). Hence, haploid selection is probably much stronger in plants than in animals (Otto et al., 2015), and could prevent sex chromosome degeneration. Indeed, YY (or WW) genotypes are viable in diploid dioecious plants at first phase (Ming et al., 2011), which is consistent with purifying selection eliminating deleterious mutations in haploid Y (or W) chromosomes in gametophytes (though other alternatives, including recent origins, or small sizes of sex-linked regions, are probably also important).

Degeneration will not happen if recombination occurs. Dioecy in plants restricts sexual selection mostly to post-pollination processes (Hörandl and Hadacek, 2020). Hence, selection might favor sexually antagonistic mutations in sex-linked genes less often than in animals. Therefore factors other than sexual antagonism may be required for dioecious plants to evolve extensive fully sex-linked regions and undergo degeneration (e.g., Lenormand and Roze, 2022).

Sex chromosomes in polyploid plants

Cytological mechanisms

Polyploids are divided into two major types, autopolyploids that originate within one species, and those originating after hybridization between species (allopolyploids). The chromosomes of new autopolyploids may form multivalents or rings, as they are not diverged and do not pair preferentially at meiosis (e.g., Stebbins, 1947; Comai, 2005). Allopolyploids have two diverged chromosome sets (homoeologs); chromosomes derived from the same parent species show preferential pairing, resulting in more or less regular bivalent formation, whereas homoeolog pairing is less frequent (Mason and Wendel, 2020; **Supplementary Figure 1**). Therefore, allopolyploids maintain fixed heterozygosity for the different alleles derived from the two parental species and carried by the homoeologous chromosomes (Comai, 2005; Glover et al., 2016). These mechanisms have consequences for SLR-bearing chromosomes.

Autopolyploids originate mainly via the "triploid bridge" process (**Figures 1C,D**; Ramsey and Schemske, 1998). The major constraint preventing establishment of such autopolyploids is male or female bias and reduced fertility in the triploid generation and possible general instability of meiosis, resulting in aneuploid progeny and low fertility (e.g., Comai, 2005). But its unreduced (triploid) gametes can fuse during fertilization with haploid gametes from a parent of the other sex, potentially establishing a cytologically stable autotetraploid. Various tetraploid sex chromosome configurations are possible, including xxyy (small captions mean codominant or recessive versus dominant Y) genotypes, which could produce xx, xy, and yy gametophytes and gametes (**Figure 1C**). If Y is dominant, xxxx females and xxxY males may emerge, constituting a stable population (**Figure 1D**), though sex-determination in autotetraploid dioecious plants with homomorphic sex chromosomes have been little studied (Spoelhof et al., 2017). In the heterogametic sex, the SLR-bearing chromosome can pair and (if the Y-linked region is not rearranged or otherwise prevented from recombining with the x) it may continue to recombine with any of the other three x chromosomes during meiosis, preventing degeneration (**Figures 1C,D**).

Allopolyploidization rarely involves a triploid bridge, but mostly arises after fertilization between unreduced gametes derived from two parental species or hybrids (Ramsey and Schemske, 1998). A first factor limiting production of such populations is that both parents must have the same XY or WZ system, which can differ within a genus (e.g., *Salix* and *Silene*) (Balounova et al., 2019; Martin et al., 2019; Gulyaev et al., 2022). Second, the newly formed polyploid will be in the minority and, as single individuals of dioecious plants cannot self-fertilize, they will backcross to the parents, which creates low fitness progeny (Levin, 1975; Ramsey and Schemske, 1998). Third, reproduction of the newly formed polyploid requires fertilization by a plant of the other sex (see **Figures 1C,E**); thus, they must live long enough to overlap with offspring generations. They will also have to form unreduced gametes, because only fusion of unreduced male and female gametes from the two dioecious parent species will produce tetraploids with the heterogametic sex (e.g., xx_1xY_2 male, $_1$ from species 1 and $_2$ from species 2). To produce males, the Y-linked male-determining gene must be dominant, because male xx_1yy_2 genotypes cannot be formed via unreduced gametes of allopolyploids because the female parent can only produce xx eggs and the male parent mostly xY pollen (**Figure 1E**). Somatic doubling is rare in nature (Ramsey and Schemske, 1998), and hence doubling of a x_1y_2 male diploid interspecific hybrid together with doubling a xx female is unlikely to happen frequently enough to establish populations. The xx_1xY_2 allotetraploid will produce male flowers and x_1Y_2 and x_1x_2 gametes. Its SLR-bearing chromosome Y will preferentially pair with the x from the same parent, resulting in four male heterozygous gamete classes. The formation of the next hybrid generation requires crossing with an unreduced female gamete derived from the other parent; only if this occurs, a stable cohort of allotetraploids with xxxY males and xxxx females can form. Most plants can produce fertile heterogametic males with only one copy of the Y chromosomes (XXXY) and females (XXXX) (e.g., *Melandrium album* = *Silene latifolia*) (Warmke and Blakeslee, 1939; Westergaard, 1958; Henry et al., 2018). This system can potentially be maintained for higher polyploids (Westergaard, 1958). Similar considerations apply to female heterogamety.

As in autopolyploids (**Figure 1E**), less differentiated Y chromosomes might recombine with the conspecific X and prevent further degeneration in polyploids (Charlesworth et al., 2021). On the other hand, the presence of duplicated sex chromosomes might increase recombination rates between the SLRs of autopolyploids (Pecinka et al., 2011; Glover et al., 2016). Furthermore, polyploidization can also increase the

recombination rate of X or Z chromosomes, maintaining their gene content (Wilson and Makova, 2009). However, natural selection likely reduces crossover rates of tetraploid homologs. Gates (1926) and Wright et al. (2015) suggested that the multiplied sex chromosomes (Z or X) in polyploids can gradually transform into autosomes, and this appears to have occurred in polyploid *Rumex acetosella*, which each retained have only one pair of sex chromosomes (XY for males) (Singh, 1968; Cunado et al., 2007). The dioecious octoploid *Fragaria* (e.g., *Fragaria chiloensis*) species that arose from hermaphroditic diploid progenitors also each have only one SLR on one of the homologues in each species studied (Tennessen et al., 2016; Cauret et al., 2022), while the others may have become autosomes. The "new" autosomes could still be just like the ancestral X or Z chromosome, or their genes might be lost due to diploidization.

Genetic degeneration

Tetraploid plants will regularly form diploid gametes, in which the effects of recessive deleterious mutations in one chromosome copy will be lessened by the function provided by the unmutated chromosome; this may mask mutations from selection (e.g., Otto and Gerstein, 2008), especially in high ploidy levels (e.g., hexaploid xxxxxY). Whether genes in a Y-linked region will degenerate more slowly in a polyploid than in a diploid plant, will probably depend on several factors, including the mutations' dominance coefficients, as well as any differences in recombination. Whether the masking effect could lead to an accumulation of deleterious recessive mutations in the pseudoautosomal region of sex chromosomein the heterozygous state needs to be investigated.

Consequences of polyploidy for the maintenance of dioecy

Polyploids have been observed to be associated with loss of dioecy of diploid progenitors, with changes occurring to monoecy, e.g., in hexaploid *Diospyros kaki* (Akagi et al., 2016), to hermaphroditism, e.g., in tetraploid *Empetrum* (Anderberg, 1994), or to monoecy and androdioecy in tetra- to dodecaploid *Mercurialis* (Pannell et al., 2004; Gerchen et al., 2022). In willows (*Salix*), shifts to diverse sexual systems occur in polyploids (Mirski, 2014; Mirski et al., 2017). These transitions to non-dioecious systems might be favored by selection for reproductive assurance by uniparental reproduction, especially in colonization scenarios (Ashman et al., 2013). However, also gene dosage effects and differential homeolog expression could cause lability if only one active Y interacts with multiple copies of x (unless all but one have turned into autosomes). Interestingly, introgression of a new Y chromosome from distantly related species happened at the origin of hexaploid, androdioecious *Mercurialis annua* (Gerchen et al., 2022). Such reversals to non-dioecious sexual systems may be indicators that polyploidization can prevent the maintenance of sex-determining systems for long evolutionary times, and this may be a further factor contributing to the rarity of degenerated sex chromosomes in plants. However, the shifts from dioecy to non-dioecious systems in several cultivated plants, including grape vines (Badouin et al., 2020) and papaya (Ming et al., 2007), do not involve ploidy changes, and could be due to human selection for major mutations (Henry et al., 2018). Loss of active sex-determiners, such as the maleness factors discussed above, could involve Y chromosome deletions, as observed in *Silene latifolia* (Kazama et al., 2016).

Discussion and outlook

Further work on polyploid dioecious plants with SLRs is clearly needed. Studies on neopolyploids (or synthetic polyploids) would help test whether dioecy in polyploids is rare because of constraints preventing their origination. Second, it should be tested whether auto- and allopolyploids differ in their heterogametic chromosome constitution, as predicted. Third, recombination between sex chromosome homologs, with non-recombining regions restricted in size, probably often prevents degeneration of plant sex chromosomes, alongside selection in the haploid pollen. The sizes of regions should be investigated for both XY and ZW systems, and the times when they evolved. Finally, the role of genetic or epigenetic effects in lability of sexual systems needs further study, specifically whether lability tends to be greater in higher polyploids with only one copy of the heterogametic chromosomes (XY or ZW).

Cytogenetic studies can identify heteromorphic sex chromosomes, and these will often be degenerated W or Y chromosomes, and also detectable from sex differences in genomic coverage, but in plants these appear to be the exception. Homomorphic sex chromosomes are more difficult to detect (Palmer et al., 2019; Baránková et al., 2020), sometimes not even with genome sequencing. Genome wide association studies (GWAS) can detect sex-linked regions, but will often find large partially sex-linked regions as well as completely sex-linked ones. Genetic differentiation between the sexes (F_{ST}) can provide a finer scale for use with less differentiated SLR-bearing chromosomes (Palmer et al., 2019; He et al., 2021) and even for polyploids (Kuhl et al., 2021). The highly accurate long HiFi (high-fidelity) reads produced by PacBio, combined with Hi-C, can generate haplotype-resolved genome assemblies of polyploids (Zhang et al., 2019; Cheng et al., 2021). Genome coverage, and of Ka/Ks ratios in divergence from related species to detect weakened efficacy of purifying selection, can detect and quantify degeneration of SLR protein-coding genes (as in examples outlined above). Analyses of gene expression via RNA seq, and epigenetic mechanisms controlling expression

(including cytosin-methylation and small RNAs activity) are important for understanding the expression of different sex phenotypes.

Author contributions

Both authors listed have made a substantial, direct, and intellectual contribution to the work, and approved it for publication.

Funding

This study was financially supported by the National Natural Science Foundation of China (grant no. 32171813). We acknowledge support by the Open Access Publication Funds of the Göttingen University.

Acknowledgments

We thank Susanne Renner for fruitful discussions, Deborah Charlesworth, and one referee for valuable comments and corrections on earlier versions of the manuscript.

Conflict of interest

The authors declare that the research was conducted in the absence of any commercial or financial relationships that could be construed as a potential conflict of interest.

Publisher's note

Supplementary material

The Supplementary Material for this article can be found online at: https://www.frontiersin.org/articles/10.3389/fpls.2022.976765/full#supplementary-material

References

Abbott, R., Albach, D., Ansell, S., Arntzen, J. W., Baird, S. J. E., Bierne, N., et al. (2013). Hybridization and speciation. *J. Evol. Biol.* 26, 229–246. doi: 10.1111/j.1420-9101.2012.02599.x

Akagi, T., Henry, I., Kawai, T., Comai, L., and Tao, R. (2016). Epigenetic regulation of the sex determination gene MeGI in polyploid persimmon. *Plant Cell* 28, 2905–2915. doi: 10.1105/tpc.16.00532

Anderberg, A. (1994). Phylogeny of the empetraceae, with special emphasis on character evolution in the genus empetrum. *Syst. Bot.* 19, 35–46. doi: 10.2307/2419710

Ashman, T. L., Kwok, A., and Husband, B. C. (2013). Revisiting the dioecy-polyploidy association: Alternate pathways and research opportunities. *Cytog. Gen. Res.* 140, 241–255. doi: 10.1159/000353306

Bachtrog, D. (2008). The temporal dynamics of processes underlying Y chromosome degeneration. *Genetics* 179, 1513–1525. doi: 10.1534/genetics.107.084012

Bachtrog, D., Mank, J. E., Peichel, C. L., Kirkpatrick, M., Otto, S. P., Ashman, T. L., et al. (2014). Sex determination: Why so many ways of doing it? *PLoS Biol.* 12:e1001899. doi: 10.1371/journal.pbio.1001899

Badouin, H., Velt, A., Gindraud, F., Flutre, T., Dumas, V., Vautrin, S., et al. (2020). The wild grape genome sequence provides insights into the transition from dioecy to hermaphroditism during grape domestication. *Gen. Biol.* 21:223. doi: 10.1186/s13059-020-02131-y

Balounova, V., Gogela, R., Cegan, R., Cangren, P., Zluvova, J., Safar, J., et al. (2019). Evolution of sex determination and heterogamety changes in section otites of the genus silene. *Sci. Rep.* 9:1045. doi: 10.1038/s41598-018-37412-x

Baránková, S., Pascual Díaz, J., Sultana, N., Alonso Lifante, M., Balant, M., Barros, K., et al. (2020). Sex-chrom, a database on plant sex chromosomes. *New Phytol.* 227, 1594–1604. doi: 10.1111/nph.16635

Bull, J. J. (1983). *Evolution of Sex Determining Mechanisms*. Menlo Park, CA: The Benjamin/Cummings Publishing Company, Inc.

Cauret, C. M. S., Mortimer, S. M. E., Roberti, M. C., Ashman, T.-L., and Liston, A. (2022). Chromosome-scale assembly with a phased sex-determining region resolves features of early Z and W chromosome differentiation in a wild octoploid strawberry. *G3 (Bethesda, Md)* 12:jkac139. doi: 10.1093/g3journal/jkac139

Charlesworth, D. (2015). Plant contributions to our understanding of sex chromosome evolution. *New Phytol.* 208, 52–65. doi: 10.1111/nph.13497

Charlesworth, D. (2021). When and how do sex-linked regions become sex chromosomes? *Evolution* 75, 569–581. doi: 10.1111/evo.14196

Charlesworth, D. (2022). Some thoughts about the words we use for thinking about sex chromosome evolution. *Philos. Trans. R. Soc. London Seri. B Biol. Sci.* 377:20210314. doi: 10.1098/rstb.2021.0314

Charlesworth, D., Bergero, R., Graham, C., Gardner, J., Keegan, K., and Dyer, K. A. (2021). How did the guppy Y chromosome evolve? *PLoS Genet.* 17:e1009704. doi: 10.1371/journal.pgen.1009704

Cheng, H., Concepcion, G., Feng, X., Zhang, H., and Li, H. (2021). Haplotype-resolved de novo assembly using phased assembly graphs with hifiasm. *Nat. Methods* 18, 170–175. doi: 10.1038/s41592-020-01056-5

Comai, L. (2005). The advantages and disadvantages of being polyploid. *Nat. Rev. Genet.* 6, 836–846. doi: 10.1038/nrg1711

Cronk, Q. (2022). Some sexual consequences of being a plant. *Philos. Trans. R. Soc. London Seri. B Biol. Sci.* 377, 20210213–20210213. doi: 10.1098/rstb.2021.0213

Cunado, N., Cuñado, N., Navajas Pérez, R., de la Herrán, R., Ruiz Rejón, C., Ruiz Rejón, M., et al. (2007). The evolution of sex chromosomes in the genus rumex (polygonaceae): Identification of a new species with heteromorphic sex chromosomes. *Chrom. Res.* 15, 825–833. doi: 10.1007/s10577-007-1166-6

Darwin, C. (1876). *Cross and Self-Fertilization of Plants*. London: John Murray.

Darwin, C. (1877). *The Different Forms of Flowers on Plants of the Same Species*. London: John Murray. doi: 10.5962/bhl.title.110054

Feng, G. Q., Sanderson, B. J., Keefover-Ring, K., Liu, J. Q., Ma, T., Yin, T. M., et al. (2020). Pathways to sex determination in plants: How many roads lead to rome? *Curr. Opin. Plant Biol.* 54, 61–68. doi: 10.1016/j.pbi.2020.01.004

Fisher, R. A. (1931). The evolution of dominance. *Biol. Rev.* 6, 345–368. doi: 10.1111/j.1469-185X.1931.tb01030.x

Gates, R. (1926). Polyploidy and sex chromosomes. *Nature* 117, 234. doi: 10.1038/117234a0

Gerchen, J. F., Veltsos, P., and Pannell, J. R. (2022). Recurrent allopolyploidization, Y-chromosome introgression and the evolution of sexual systems in the plant genus mercurialis. *Philos. Trans. Biol. Sci.* 377:20210224. doi: 10.1098/rstb.2021.0224

Glick, L., Sabath, N., Ashman, T. L., Goldberg, E., and Mayrose, I. (2016). Polyploidy and sexual system in angiosperms: Is there an association? *Am. J. Bot.* 103, 1223–1235. doi: 10.3732/ajb.1500424

Glover, N. M., Redestig, H., and Dessimoz, C. (2016). Homoeologs: What are they and how do we infer them? *Trends Plant Sci.* 21, 609–621. doi: 10.1016/j.tplants.2016.02.005

Gorelick, R. (2005). Theory for why dioecious plants have equal length sex chromosomes. *Am. J. Bot.* 92, 979–984. doi: 10.3732/ajb.92.6.979

Gulyaev, S., Cai, X.-J., Guo, F.-Y., Kikuchi, S., Applequist, W., Zhang, Z.-X., et al. (2022). The phylogeny of salix revealed by whole genome re-sequencing suggests different sex-determination systems in major groups of the genus. *Ann. Bot.* 129, 485–498. doi: 10.1093/aob/mcac012

He, L., Guo, F. Y., Cai, X. J., Chen, H. P., Lian, C. L., Wang, Y., et al. (2022). Evolutionary origin and establishment of the diploid-tetraploid complex in *Salix polyclona*. *Authorea*. doi: 10.22541/au.165769042.25880844/v1 [Epub ahead of print].

He, L., Jia, K.-H., Zhang, R.-G., Wang, Y., Shi, T.-L., Li, Z.-C., et al. (2021). Chromosome-scale assembly of the genome of salix dunnii reveals a male-heterogametic sex determination system on chromosome 7. *Mol. Ecol. Res.* 21, 1966–1982. doi: 10.1111/1755-0998.13362

Henry, I. M., Akagi, T., Tao, R., and Comai, L. (2018). One hundred ways to invent the sexes: Theoretical and observed paths to dioecy in plants. *Ann. Rev. Plant Biol.* 69, 553–575. doi: 10.1146/annurev-arplant-042817-040615

Hojsgaard, D., and Hörandl, E. (2019). The rise of apomixis in natural plant populations. *Front. Plant Sci.* 10:358. doi: 10.3389/fpls.2019.00358

Hojsgaard, D., Klatt, S., Baier, R., Carman, J. G., and Hörandl, E. (2014). Taxonomy and biogeography of apomixis in angiosperms and associated biodiversity characteristics. *Crit. Rev. Plant Sci.* 33, 414–427. doi: 10.1080/07352689.2014.898488

Hörandl, E. (2022). Novel approaches for species concepts and delimitation in polyploids and hybrids. *Plants* 11:204. doi: 10.3390/plants11020204

Hörandl, E., and Hadacek, F. (2020). Oxygen, life forms, and the evolution of sexes in multicellular eukaryotes. *Heredity* 125, 1–14. doi: 10.1038/s41437-020-0317-9

Jeffries, D., Gerchen, J., Scharmann, M., Pannell, J. R., and Pannell, J. (2021). A neutral model for the loss of recombination on sex chromosomes. *Philos. Trans. Biol. Sci.* 376:20200096. doi: 10.1098/rstb.2020.0096

Jiao, Y., Wickett, N. J., Ayyampalayam, S., Chanderbali, A. S., Landherr, L., Ralph, P. E., et al. (2011). Ancestral polyploidy in seed plants and angiosperms. *Nature* 473, 97–100. doi: 10.1038/nature09916

Joseph, S. B., and Kirkpatrick, M. (2004). Haploid selection in animals. *Trends Ecol. Evol.* 19, 592–597. doi: 10.1016/j.tree.2004.08.004

Kazama, Y., Ishii, K., Aonuma, W., Ikeda, T., Kawamoto, H., Koizumi, A., et al. (2016). A new physical mapping approach refines the sex-determining gene positions on the silene latifolia Y-chromosome. *Sci. Rep.* 6:18917. doi: 10.1038/srep18917

Kuhl, H., Guiguen, Y., Hoehne, C., Kreuz, E., Du, K., Klopp, C., et al. (2021). A 180 Myr-old female-specific genome region in sturgeon reveals the oldest known vertebrate sex determining system with undifferentiated sex chromosomes. *Philos. Trans. R. Soc. B Biol. Sci.* 376:20200089. doi: 10.1098/rstb.2020.0089

Landis, J. B., Soltis, D. E., Li, Z., Marx, H. E., Barker, M. S., Tank, D. C., et al. (2018). Impact of whole-genome duplication events on diversification rates in angiosperms. *Am. J. Bot.* 105, 348–363. doi: 10.1002/ajb2.1060

Lenormand, T., and Roze, D. (2022). Y recombination arrest and degeneration in the absence of sexual dimorphism. *Science (New York, NY)* 375, 663–666. doi: 10.1126/science.abj1813

Levin, D. A. (1975). Minority cytotype exclusion in local plant populations. *Taxon* 24, 35–43. doi: 10.2307/1218997

Levin, D. A. (2002). *The Role of Chromosomal Change in Plant Evolution*. Oxford: Oxford University Press.

Mank, J. E. (2022). Are plant and animal sex chromosomes really all that different? *Philos. Trans. R. Soc. London Seri. B Biol. Sci.* 377:20210218. doi: 10.1098/rstb.2021.0218

Martin, H., Carpentier, F., Gallina, S., Godé, C., Schmitt, E., Muyle, A., et al. (2019). Evolution of young sex chromosomes in two dioecious sister plant species with distinct sex determination systems. *Gen. Biol. Evol.* 11, 350–361. doi: 10.1093/gbe/evz001

Mason, A. S., and Wendel, J. F. (2020). Homoeologous exchanges, segmental allopolyploidy, and polyploid genome evolution. *Front. Genet.* 11:1014. doi: 10.3389/fgene.2020.01014

Ming, R., Bendahmane, A., and Renner, S. S. (2011). Sex chromosomes in land plants. *Ann. Rev. Plant Biol.* 62, 485–514. doi: 10.1146/annurev-arplant-042110-103914

Ming, R., Yu, Q., Moore, P. H., and Moore, P. (2007). Sex determination in papaya. *Semin Cell Dev. Biol.* 18, 401–408. doi: 10.1016/j.semcdb.2006.11.013

Mirski, P. (2014). Exceptions from dioecy and sex lability in genus salix. *Dendrobiology* 71, 167–171. doi: 10.12657/denbio.071.017

Mirski, P., Brzosko, E., Jedrzejczyk, I., Kotowicz, J., Ostrowiecka, B., and Wroblewska, A. (2017). Genetic structure of dioecious and trioecious salix myrsinifolia populations at the border of geographic range. *Tree Genet Genom.* 13:15. doi: 10.1007/s11295-016-1096-6

Mogie, M. (1992). *The Evolution of Asexual Reproduction in Plants*. London: Chapman and Hall.

Muller, H. J. (1918). Genetic variability, twin hybrids and constant hybrids, in a case of balanced lethal factors. *Genetics* 3, 422–499. doi: 10.1093/genetics/3.5.422

Muller, H. J. (1925). Why polyploidy is rarer in animals than in plants. *Am. Natur.* 59, 346–353. doi: 10.1086/280047

Orr, H. A. (1990). Why polyploidy is rarer in animals than in plants revisited. *Am. Natur.* 136, 759–770. doi: 10.1086/285130

Otto, S. P., and Gerstein, A. C. (2008). The evolution of haploidy and diploidy. *Curr. Biol.* 18, R1121–R1124. doi: 10.1016/j.cub.2008.09.039

Otto, S. P., Scott, M. F., and Immler, S. (2015). Evolution of haploid selection in predominantly diploid organisms. *Proc. Natl. Acad. Sci. U.S.A.* 112, 15952–15957. doi: 10.1073/pnas.1512004112

Palmer, D., Rogers, T., Dean, R., Wright, A. E., and Wright, A. (2019). How to identify sex chromosomes and their turnover. *Mol. Ecol.* 28, 4709–4724. doi: 10.1111/mec.15245

Pannell, J., Obbard, D., Buggs, R. J. A., and Buggs, R. J. A. (2004). Polyploidy and the sexual system: what can we learn from mercurialis annua? *Biol. J. Linn. Soc.* 82, 547–560. doi: 10.1111/j.1095-8312.2004.00340.x

Pecinka, A., Fang, W., Rehmsmeier, M., Levy, A. A., and Scheid, O. M. (2011). Polyploidization increases meiotic recombination frequency in *Arabidopsis*. *BMC Biol.* 9:24. doi: 10.1186/1741-7007-9-24

Ramsey, J., and Schemske, D. W. (1998). Pathways, mechanisms, and rates of polyploid formation in flowering plants. *Ann. Rev. Ecol. Syst.* 29, 467–501. doi: 10.1146/annurev.ecolsys.29.1.467

Renner, S., and Müller, N. A. (2021). Plant sex chromosomes defy evolutionary models of expanding recombination suppression and genetic degeneration. *Nat. Plants* 7, 392–402. doi: 10.1038/s41477-021-00884-3

Renner, S. S. (2014). The relative and absolute frequencies of angiosperm sexual systems: Dioecy, monoecy, gynodioecy, and an updated online database. *Am. J. Bot.* 101, 1588–1596. doi: 10.3732/ajb.1400196

Rice, W. R. (1987). The accumulation of sexually antagonistic genes as a selective agent promoting the evolution of reduced recombination between primitive sex chromosomes. *Evolution* 41, 911–914. doi: 10.1111/j.1558-5646.1987.tb05864.x

Richards, J. A. (1997). *Plant Breeding Systems*. London: Chapman and Hall. doi: 10.1007/978-1-4899-3043-9

Singh, R. B. (1968). A dioecious polyploid in rumex acetosella. *J. Heredity* 59, 168–170. doi: 10.1093/oxfordjournals.jhered.a107676

Soltis, D. E., Albert, V. A., Leebens-Mack, J., Bell, C. D., Paterson, A. H., Zheng, C. F., et al. (2009). Polyploidy and angiosperm diversification. *Am. J. Bot.* 96, 336–348. doi: 10.3732/ajb.0800079

Soltis, P. S., and Soltis, D. E. (2009). The role of hybridization in plant speciation. *Ann. Rev. Plant Biol.* 60, 561–588. doi: 10.1146/annurev.arplant.043008.092039

Soltis, P. S., and Soltis, D. E. (2016). Ancient WGD events as drivers of key innovations in angiosperms. *Curr. Opin. Plant Biol.* 30, 159–165. doi: 10.1016/j.pbi.2016.03.015

Spoelhof, J., Soltis, P., Soltis, D. E., and Soltis, D. (2017). Pure polyploidy: Closing the gaps in autopolyploid research. *J. Syst. Evol.* 55, 340–352. doi: 10.1111/jse.12253

Stebbins, G. L. (1947). Types of polyploids: their classification and significance. *Adv. Genet.* 1, 403–429. doi: 10.1016/S0065-2660(08)60490-3

Tennessen, J., Govindarajulu, R., Ashman, T.-L., and Liston, A. (2014). Evolutionary origins and dynamics of octoploid strawberry subgenomes revealed by dense targeted capture linkage maps. *Gen. Biol. Evol.* 6, 3295–3313. doi: 10.1093/gbe/evu261

Tennessen, J., Govindarajulu, R., Liston, A., and Ashman, T.-L. (2016). Homomorphic ZW chromosomes in a wild strawberry showdistinctive recombination heterogeneity but a small sex-determining region. *New Phytol.* 211, 1412–1423. doi: 10.1111/nph.13983

Van De Peer, Y., Mizrachi, E., and Marchal, K. (2017). The evolutionary significance of polyploidy. *Nat. Rev. Genet.* 18, 411–424. doi: 10.1038/nrg.2017.26

Vicoso, B. (2019). Molecular and evolutionary dynamics of animal sex-chromosome turnover. *Nat. Ecol. Evol.* 3, 1632–1641. doi: 10.1038/s41559-019-1050-8

Warmke, H. E., and Blakeslee, A. F. (1939). Sex mechanism in polyploids of melandrium. *Science* 89, 391–392. doi: 10.1126/science.89.2313.391

Westergaard, M. (1958). The mechanism of sex determination in dioecious flowering plants. *Adv. Genet.* 9, 217–281. doi: 10.1016/S0065-2660(08)60163-7

Wilson, M., and Makova, K. (2009). Genomic analyses of sex chromosome evolution. *Ann. Rev. Genom. Hum. Genet.* 10, 333–354. doi: 10.1146/annurev-genom-082908-150105

Wright, K. M., Arnold, B., Xue, K., Surinova, M., O'Connell, J., and Bomblies, K. (2015). Selection on meiosis genes in diploid and tetraploid *Arabidopsis arenosa*. *Mol. Biol. Evol.* 32, 944–955. doi: 10.1093/molbev/msu398

Zhang, X., Zhang, S., Zhao, Q., Ming, R., Tang, H., and Tang, H. (2019). Assembly of allele-aware, chromosomal-scale autopolyploid genomes based on Hi-C data. *Nat. Plants* 5, 833–845. doi: 10.1038/s41477-019-0487-8

Zuk, J. (1963). An investigation on polyploidy and sex determination within the genus rumex. *Acta Soc. Bot. Policy* 32, 5–67. doi: 10.5586/asbp.1963.001

frontiers | Frontiers in Plant Science

TYPE Original Research
PUBLISHED 30 September 2022
DOI 10.3389/fpls.2022.1012682

OPEN ACCESS

EDITED BY
Fulvio Pupilli,
National Research Council (CNR), Italy

REVIEWED BY
Kitty Vijverberg,
Naturalis Biodiversity Center, Netherlands
Ross Andrew Bicknell,
The New Zealand Institute for Plant and Food Research Ltd, New Zealand
Vladimir Brukhin,
Theodosius Dobzhansky Center for Genome Bioinformatics, Russia

*CORRESPONDENCE
Ingrid Garbus
igarbus@criba.edu.ar

†These authors have contributed equally to this work

SPECIALTY SECTION
This article was submitted to Plant Breeding, a section of the journal Frontiers in Plant Science

RECEIVED 05 August 2022
ACCEPTED 14 September 2022
PUBLISHED 30 September 2022

CITATION
Pasten MC, Carballo J, Gallardo J, Zappacosta D, Selva JP, Rodrigo JM, Echenique V and Garbus I (2022) A combined transcriptome - miRNAome approach revealed that a *kinesin* gene is differentially targeted by a novel miRNA in an apomictic genotype of *Eragrostis curvula*. *Front. Plant Sci.* 13:1012682. doi: 10.3389/fpls.2022.1012682

A combined transcriptome - miRNAome approach revealed that a *kinesin* gene is differentially targeted by a novel miRNA in an apomictic genotype of *Eragrostis curvula*

María Cielo Pasten[1†], José Carballo[1†], Jimena Gallardo[1,2], Diego Zappacosta[1,2], Juan Pablo Selva[1,3], Juan Manuel Rodrigo[1,2], Viviana Echenique[1,2] and Ingrid Garbus[1*]

[1]Centro de Recursos Naturales Renovables de la Zona Semiárida (CERZOS), Universidad Nacional del Sur-Consejo Nacional de Investigaciones Científicas y Técnicas (CONICET), Bahía Blanca, Argentina, [2]Departamento de Agronomía, Universidad Nacional del Sur (UNS), Bahía Blanca, Argentina, [3]Departamento de Biología, Bioquímica y Farmacia, Universidad Nacional del Sur (UNS), Bahía Blanca, Argentina

Weeping lovegrass (*Eragrostis curvula* [Shrad.] Nees) is a perennial grass typically established in semi-arid regions, with good adaptability to dry conditions and sandy soils. This polymorphic complex includes both sexual and apomictic cytotypes, with different ploidy levels (2x-8x). Diploids are known to be sexual, while most polyploids are facultative apomicts, and full apomicts have also been reported. Plant breeding studies throughout the years have focused on achieving the introgression of apomixis into species of agricultural relevance, but, given the complexity of the trait, a deeper understanding of the molecular basis of regulatory mechanisms of apomixis is still required. Apomixis is thought to be associated with silencing or disruption of the sexual pathway, and studies have shown it is influenced by epigenetic mechanisms. In a previous study, we explored the role of miRNA-mRNA interactions using two contrasting *E. curvula* phenotypes. Here, the sexual OTA-S, the facultative Don Walter and the obligate apomictic Tanganyika cDNA and sRNA libraries were inquired, searching for miRNA discovery and miRNA expression regulation of genes related to the reproductive mode. This allowed for the characterization of seven miRNAs and the validation of their miRNA-target interactions. Interestingly, a *kinesin* gene was found to be repressed in the apomictic cultivar Tanganyika, targeted by a novel miRNA that was found to be overexpressed in this genotype, suggestive of an involvement in the reproductive mode expression. Our work provided additional evidence of the contribution of the epigenetic regulation of the apomictic pathway.

KEYWORDS

***Eragrostis curvula*, apomixis, sRNA libraries, miRNA, miRNA-mRNA interaction**

Introduction

Apomixis can be described as asexual reproduction through seeds, and it comprises three central stages: apomeiosis (absence of meiosis), parthenogenesis (absence of fertilization) and autonomous endosperm development or pseudogamy (Nogler, 1984; Schmidt, 2020). It has been observed that apomixis is inherited as a dominant trait, and that the three developmental stages are controlled by independent loci in several species (Grossniklaus, 2001; Vijverberg and van Dijk, 2007).

There is a wide variety of apomictic mechanisms, which can be explained by the fact that apomixis emerged independently multiple times during evolution. It is theorized that apomixis arises from spatial and temporal changes in the expression of genes involved in sexual reproduction. The regulation guided by the availability of specific expression of the genes PAR1 and PsASGR-BabyBoom-Like has been observed for parthenogenesis in Pennisetum and Taraxacum (Underwood et al., 2022, Khanday et al., 2019). However, these genes *per se* are insufficient to transfer apomixis to economically important crops, since no genes linked to apomeiosis were found in apomictic species.

It has been found that the reproductive state can be influenced by environmental cues (Rodrigo et al., 2017; Gao, 2018; Schmidt, 2020). In numerous species, differences in photoperiod, salt stress and heat stress result in similar responses, adding to the now accepted notion that reproduction adjustments can take place, and that they appear to have a significant role in the adaptation of facultative apomicts (Gounaris et al., 1991; Hussey et al., 1991; Carman et al., 2015; Klatt et al., 2016).

There is evidence that shows that DNA methylation, chromatin modifications and noncoding RNAs have a central role in the regulation of gene expression at transcriptional and post-transcriptional levels (Pikaard and Scheid, 2014; Wei et al., 2017; Higo et al., 2020; Brukhin and Albertini, 2021; Carballo et al., 2021). The study of epigenetics in the last years has established that these mechanisms are key to the understanding of numerous processes in plants. Among the noncoding RNAs, the most abundant and important group are the small RNAs (sRNAs), that target coding or non-coding RNAs for silencing, *via* guided degradation or translational repression (Borges and Martienssen, 2015; Nejat and Mantri, 2018). MicroRNAs (miRNAs) are a large class of sRNAs derived from DICER-LIKE (DCL) processing of single-stranded precursors, known to participate mostly in post-transcriptional gene silencing (PTGS) (Borges and Martienssen, 2015). miRNAs regulate gene expression by specifically targeting messenger RNAs (mRNA) in association with the RNA-induced silencing complex (RISC), consisting mainly of ARGONAUTE (AGO) proteins, mainly AGO1, AGO4 and AGO10 (Neumeier and Meister, 2021) and acting either *via* direct degradation or *via* inhibition of translation, pairing with the 3' UTR region of the target (Melo and Melo, 2013).

miRNAs have central regulatory roles and affect processes such as reproduction, fertility, and leaf and flower morphogenesis, among others (Aukerman and Sakai, 2003; Palatnik et al., 2003; Schwab et al., 2005; Li et al., 2015; Ripoll et al., 2015). In *A. thaliana, Z. bungeanum* and some species of the genus Boechera, specific miRNAs have been identified (miR156/157, miR167 y miR172c) related to functions such as flower organogenesis, reproductive mode, and male and female fertility (Xing et al., 2013; Ru et al., 2006; Amiteye et al., 2011; Fei et al., 2021). Differential expression analyses of miRNAs in regards to ploidy and reproductive mode have also taken place (Amiteye et al., 2013; Ortiz et al., 2019).

Eragrostis curvula [Shrad.] Nees (weeping lovegrass), is a perennial grass belonging to the Poaceae family, native of Southern Africa, and it is commonly found in semi-arid regions around the world due to its ability to adapt to drought conditions and low fertility soils (Covas, 1991). This species constitutes a morphologically and evolutively diverse group, and it includes cytotypes with different ploidy levels (2x to 8x), which can reproduce sexually or by diplosporous apomixis (obligate or facultative) (Leigh, 1960; Voigt and Burson, 1983).

Due to its specific apomictic development, *E. curvula* has become one of several models for the study of apomictic mechanisms and was widely studied over the last years, obtaining information about its genome (Carballo et al., 2019), cytoembriology (Zappacosta et al., 2014), the position of the apomixis locus (Zappacosta et al., 2019), expression of candidate genes (Cervigni et al. 2008a, and Cervigni et al. 2008b; Garbus et al., 2017; Selva et al., 2017; Selva et al., 2020). More recently, the methylation status of facultative, fully sexual and fully apomictic genotypes was assessed, finding that facultative genotypes have a higher number of methylated positions (Carballo et al., 2021). Even when the methylation status could be interpreted as a consequence of the different reproduction systems rather than the cause (Mau et al., 2022), the tetraploid nature and the independent genetic origin of the three genotypes analyzed in the mentioned study is supporting the hypothesis that links the methylation status with the reproductive mode. This behavior shows the importance of epigenetic mechanisms in more dynamic reproductive conditions.

The scarce diploid plants of *E. curvula* (2n = 2x = 20) reproduce sexually, while polyploids mostly undergo facultative pseudogamous diplosporous apomixis (Leigh, 1960; Voigt and Burson, 1983). In this process, a megasporocyte avoids meiosis and experiences two rounds of mitotic division, generating four non-reduced nuclei at maturity: two synergid cells, an egg cell and one polar nucleus (Crane, 2001). The development of the non-reduced tetranucleate embryo sac is specific of this grass, that also undergoes parthenogenesis but requires fertilization of the polar nucleus for the development of the endosperm (Grimanelli et al., 2001; Crane, 2001).

In a previous study conducted using two contrasting *E. curvula* phenotypes, the sexual OTA-S and the apomictic Tanganyika, we investigated the role of miRNA-mRNA interactions in apomixis using a transcriptomic library and small RNA libraries (Garbus et al., 2019). Two genes were identified, a MADS-box transcription factor gene and a transposon, that were found to be repressed in the sexual genotype, most likely due to interactions with miRNAs, suggesting that a repressive effect on gene expression exerted by miRNAs might be involved in the expression of apomixis in *E. curvula* (Garbus et al., 2019).

In the current study we expanded the comprehension of the participation of miRNAs in the expression of apomixis in *E. curvula*, through its known function in mRNA degradation, by including the facultative apomictic material Don Walter. In this way, we analyzed the differential expression of miRNAs and their targets focusing on all the possible comparisons among the sexual cultivar OTA-S, the apomictic cultivar Tanganyika and the facultative Don Walter. There were described seven miRNAs, including their mature sequences, the pri-miRNA and pre-miRNA precursors, as well as their specific interaction with their target mRNAs. A specific regulation by genotype for the transcript for a *kinesin* gene that was found, being repressed in the apomictic cultivar Tanganyika, whereas the related miRNA expression was the opposite, i.e., overexpressed in the mentioned genotype. Our results support the previous evidence of the role of miRNAs in transcript regulation in apomixis.

Materials and methods

Plant materials

The experiments were carried out using three tetraploid (2n = 4x = 40) *E. curvula* cultivars: the sexual OTA-S (USDA: PI574506), the full apomictic Tanganyika (USDA: PI234217) and the facultative apomictic Don Walter. The plants were grown in the greenhouse in 10 L pots, under natural light conditions (38°43'0″S, 62°16'0″O), at 25°C +/- 4°C.

cDNA and sRNA libraries

To conduct the analyses reported in this work, we made use of the cDNA libraries previously constructed by our laboratory for genotypes OTA-S, Tanganyika and Don Walter (Garbus et al., 2017; Selva et al., 2020). OTA-S and Tanganyika cDNA libraries were constructed, sequenced and assembled as reported in Garbus et al. (2017). Briefly, libraries were obtained from spikelets with basal flowers at the beginning of anthesis, containing embryo sacs at all developmental stages, in biological duplicates for each genotype, naming O2P1 and O2P2 those derived from OTA-S, whereas the ones constructed from Tanganyika were called T3P1 and T3P2.

These libraries were deposited in the Sequence Reads Archive (SRA) database at NCBI as BioProject 358210 (Biosamples SAMN06167423 and SAMN06167424), whereas the Transcriptome Shotgun Assembly (TSA) project has been deposited at DDBJ/EMBL/GenBank under the accession GFVM00000000. cDNA libraries from the cultivar Don Walter were made in triplicates from spikelets with basal flowers at the beginning of anthesis, containing embryo sacs at all developmental stages, and were named DW1, DW2 and DW3. The procedures followed for library construction are described in Selva et al. (2020). The TSA Assembly project was deposited at DDBJ/EMBL/GenBank under the accession GIQX00000000.

Concerning small RNAs, libraries from OTA-S and Tanganyika were available (Garbus et al., 2019). They were constructed starting from the small RNA fraction obtained in the separation from the large RNA fraction used for the cDNA libraries (Garbus et al., 2017; Garbus et al., 2019), and thus biological replicates for each genotype lead to the sRNA libraries called O2P1, O2P2, T3P1 and T3P2. The procedure followed for library construction, sequencing and analysis is detailed in Garbus et al. (2019).

On the other hand, sRNA libraries from Don Walter were constructed aiming at this study, as detailed in the next section.

Small RNA libraries from Don Walter construction, sequencing and processing

Starting from 30 mg of fresh tissue from each sample, ground to a fine powder using liquid nitrogen, the total RNA was extracted as two fractions, small and large RNA, which include RNA sequences smaller and larger than 200 bp, respectively, using a commercial NucleoSpin® miRNA kit (Macherey-Nagel, Düren, Germany) according to the manufacturer's instructions (Selva et al., 2020). The small RNA fraction was sequenced in biological triplicates, DW1, DW2 and DW3, in 50 bp single end reads through Illumina MiSeq platform in the Polo d'Innovazione di Genomica, Genetica e Biologia (Polo GGB), in Siena, Italy.

After sequencing, the adapters of the raw reads were removed and trimmed using Cutadapt (Martin, 2011) with the following parameters: Phred quality score cutoff 30, minimum read length 18. The reads of the seven samples were collapsed to remove redundancy, using the script collapse_reads.pl. These libraries were deposited in the Sequence Reads Archive (SRA) database at NCBI as BioProject PRJNA855479 (Biosamples SAMN29493390, SAMN29493391 and SAMN29493392).

miRNA prediction and target identification

The software miRDP2 was used to predict miRNAs, using the Don Walter genome assembly to discover novel and known miRNAs. The first step in miRDP2 was to align reads against the Rfam database in order to identify and discard known rRNA, tRNA, scRNA, snRNA and snoRNAs. miRDP2 reports the mature, pri-miRNA and pre-miRNAs.

The plot of the hairpins was performed using the RNAplot script from ViennaRNA package 2.0 (Lorenz et al., 2011). The predicted mature miRNA file was indexed and each sample was mapped with the software Bowtie (Langmead, 2010) with 0 mismatches to quantify mature miRNAs. A matrix with the reads mapping on the predicted mature miRNA was constructed, and filtered when a mature miRNA was absent in at least 5 samples and the sum of all the mapping reads were less than 10. The R package DESeq2 (Love et al., 2014) was used to perform the normalization and the expression analysis. A principal component analysis was conducted to reduce complexity and compare all the samples. Comparisons were made between the full apomictic cultivar Tanganyika and the sexual cultivar OTA-S, and the facultative cultivar Don Walter, hereafter referred as APOvsSEX and APOvsFAC, respectively. The facultative cultivar Don Walter was further compared to the sexual OTA-S, hereafter referred as FACvsSEX. A mature miRNA was considered to be differentially expressed when the log2FoldChange was >1 and <1 for upregulated and downregulated mature miRNAs, respectively, and when padj<0.05.

Target identification was performed by the software psRNAtarget (Dai et al., 2018) using the genome annotation and the predicted mature miRNAs as input. Finally, in order to correlate the miRNA target with the transcript expression level, a differential expression analysis was conducted using previously sequenced transcriptomic reads from the three genotypes (Garbus et al., 2017; Selva et al., 2020). For these data sets, the software hisat2 (Kim et al., 2019) was used for mapping, and DESeq2 (Love et al., 2014) was used to perform the expression analysis.

DNA and RNA extraction

DNA and RNA were extracted from the cultivars OTA-S, Tanganyika and Don Walter aiming to validate the *in silico* observations. To carry out this purpose, three plants from each cultivar were grown reproducing the conditions applied for the construction of the libraries. The DNA was extracted from fresh leave tissue in biological triplicates for each cultivar, following a protocol based on cetyltrimethylammonium bromide (CTAB). Briefly, plant material was initially frozen and powdered in liquid nitrogen using a plastic pestle in a 1.5 ml Eppendorf tube. A total of ~50 mg of powdered tissue was incubated at 65°C in preheated CTAB extraction buffer containing 100 mM Tris HCl pH 8, 1.4 M NaCl, 20 mM EDTA pH 8, 2% CTAB (w/v) and 0.5% (v/v) β-mercaptoethanol. Then, chloroform was added to reach the proportion 2:1, collecting the supernatant obtained after a centrifugation step. Finally, DNA was precipitated with one volume of isopropanol, washed with 70% (v/v) ethanol and resuspended in ultrapure water.

RNA extraction was conducted in biological triplicates from spikelets from the three cultivars, collected following the same criteria used to obtain the samples for library construction. Briefly, spikelets with basal flowers at the beginning of anthesis were collected based on the reproductive calendar shown in Selva et al. (2017), where all developmental stages are represented, from early archespores to mature female gametophytes, evaluated through observations under a stereoscopic microscope (Leica S APO) of several collected spikelets. RNA isolation was performed using a TRIzol based protocol. Approximately 35 mg of tissue from biological triplicates per sample was frozen and homogenized in liquid nitrogen using a plastic pestle in a 1.5 ml Eppendorf tube. Then, they were mixed with TRIzol™ Reagent (Invitrogen). Following the addition of chloroform, RNA was precipitated from the upper layer with isopropanol and washed with ethanol. The samples were resuspended in 20–25 µl of DEPC water and stored at −80°C. RNA was quantified in a DeNovix DS-11 spectrophotometer (Denovix Inc., USA), whereas its integrity was checked by agarose gel electrophoresis.

cDNA and stem-loops based cDNA synthesis

RNA was used for the synthesis of cDNA, as well as stem-loop cDNA. The cDNA synthesis was performed aiming for the validation of transcripts' differential expression, using the ImProm II™ Reverse Transcription System (Promega) following the supplier's instructions.

Stem-loop synthesis was aimed at miRNA quantification (Chen et al., 2005), and was also conducted using the ImProm-II™ Reverse Transcription System, but in this case instead of using random primers, a specific stem loop of ≈50 bp was designed for each of the miRNAs intended to be validated and quantified. Stem-loop primers were designed manually, as described in Garbus et al. (2019) (Table 1).

Reactions were conducted from 20 ng of RNA, in biological triplicates for OTA-S, Tanganyika and Don Walter. Briefly, each 20 µl reaction was incubated in a BioRad Thermocycler for 5 min at 25°C followed by 60 min at 42°C and finally 15 min at 70°C to inactivate the reverse transcriptase, and cooled at 4°C.

TABLE 1 Primers designed for stem-loop miRNAs amplification.

Primer	Sequence	Size (bp)	tm (°C)
mat_810_DREB2	TGTGTTCTCAGGTCGCCCCCG	21	70.9
ST_mat_810_DREB2	GTCGTATCCAGTGCAGGGTCCGAGGTATTCGCACTGGATACGACcggggg	50	80.5
mat_42_KINESIN	GTGTTCTTTGCATCTTGGTCAAGC	24	60.7
ST_42_KINESIN	GTCGTATCCAGTGCAGGGTCCGAGGTATTCGCACTGGATACGACgcttga	50	76.7
mat_422_PATATIN	AGGTGATTTTTGGATTATGTTCAG	24	55.0
ST_mat_422_PATATIN	GTCGTATCCAGTGCAGGGTCCGAGGTATTCGCACTGGATACGACctgaac	50	76.5
mat_181_DdrPOL	GGAATGTTGTCTGGTTCAAGG	21	59.2
ST_mat_181_DdrPOL	GTCGTATCCAGTGCAGGGTCCGAGGTATTCGCACTGGATACGACccttga	50	77.4
mat_676_GAMYB	AGAGTTGGAGGAAAACAAACC	21	58.1
ST_mat_676_GAMYB	GTCGTATCCAGTGCAGGGTCCGAGGTATTCGCACTGGATACGACggtttg	50	76.5
mat_601_SQUA	TGACAGAAGAGAGTGAGCAC	20	58.7
ST_mat_601_SQUA	GTCGTATCCAGTGCAGGGTCCGAGGTATTCGCACTGGATACGACgtgctc	50	77.1
mat_750_GRF8	TCCACAGGCTTTCTTGAACTG	21	60.1
ST_mat_750_GRF8	GTCGTATCCAGTGCAGGGTCCGAGGTATTCGCACTGGATACGACcagttc	50	76.5
URP	CCAGTGCAGGGTCCGAGGT	19	69.3

PCR and RT-PCR

Primers based on the sequence of the transcripts differentially regulated among libraries (Table 2), were designed using the IDT Interphase (https://www.idtdna.com/PrimerQuest/Home/Index).

Amplification of the genomic sequence of the corresponding transcripts, as well as the miRNA precursors, was conducted using DNA. The reactions were run using a MyCycler Thermal Cycler (Bio-Rad, Hercules, CA, USA), and prepared with 0.3 µl of 40 mM dNTPs mix, 3 µl of 10× reaction buffer, 0.6 µl of each forward and reverse primer (10 pmol/µl), 0.2 µl of DNA polymerase, 1 µl of template genomic DNA (40 ng/µl), in a final reaction volume of 15 µl. The DNA polymerases used were either Taq Pegasus (PB-L) or GoTaq DNA Polymerase (Promega), both containing 5U enzyme/µl. The protocol followed for DNA amplification consisted of an initial DNA denaturation step at 95°C for 2-5 min, followed by 33 cycles at 95°C for 30 s, 30 s at the optimal annealing temperature for each primer pair, and 72°C for 30s. The final step consisted of a final extension of 3 min at 72°C. The primer annealing temperatures were optimized for each primer pair, starting from one degree below the lower melting temperature between both primers.

RT-PCR reactions were performed to verify and visualize the amplification among genotypes of the differentially regulated transcripts predicted *in silico*. Reactions were developed basically as described for the PCR ones, but starting from 2 µl of a 1/20 cDNA dilution.

PCR and RT-PCR amplification bands were separated by electrophoresis in a 1.5% (m/v) agarose gel and visualized using ethidium bromide in a VP High Performance UV Transilluminator.

Stem-loop miRNA amplification

The stem-loop miRNA amplification was performed from the cDNA amplified from the specific stem-loop sequences for each miRNA, using the miRNA sequences as the forward primers and an URP primer (Universal Reverse Primer), based on the stem-loop sequence, as the reverse primer (Table 1). The amplification reactions were conducted essentially as described for PCR, but starting from 2 µl of a 1/20 dilution of the retrotranscription reaction already described.

miRNAs precursor amplification

Specific primers for pri-miRNAs and pre-miRNAs were designed based on Don Walter genomic sequences, predicted by the mirDP2 software (Table 3). The amplification was carried out using a different forward primer for pri-miRNA and pre-miRNA, and the same reverse primers for both.

qPCR reactions

The experiments carried out to validate the differential regulation of transcripts and miRNAs described *in silico* for the three genotypes, were conducted through Quantitative Real-Time PCR (qPCR), using the thermocycler CFX Connect Real-Time PCR System (Bio-Rad). Reactions were performed in a final volume of 20 ul, and contained 50 pmol of forward and reverse primers, 3 µl of 200-fold diluted cDNA and 10 µl of Real Mix (Biodynamics, Argentina). The *E. curvula*

10.3389/fpls.2022.1012682

TABLE 2 Transcripts and/or gene based primers, designed for PCR and qPCR amplification.

Primer	Sequence	Size (bp)	Tm (°C)
GAMYB_F1	CCACTTCCGTCTCTGATCTTCT	22	61.4
GAMYB_R1	TCCGGGCGAAGGACTTG	17	64.4
GAMYB_F2	GGGCATGATGGCAGAGAG	18	61.4
GAMYB_R2	GCTCATAAATCAGTTCAGAGAATCATAG	28	56.4
GAMYB_RT_F3	CGCGGTGCAGAAGATGAG	18	61.0
GAMYB_RT_R3	CCTCGTGTTCCAGTAGTTCTTG	22	60.2
SQUA_F1	ATGGACCGCAAGGACAAGTC	20	62.8
SQUA_R1a	CGCCTCGCACACCTTGT	17	63.3
SQUA_R3	CTCCTCTTGATGTCGTCGAAC	21	60.4
SQUA_F4	GGAGTTCGACGACATCAAGAG	21	60.4
SQUA_R4	ATGTGTGAGAAACTTTACTACTTGC	25	55.9
SQUA_RT_Fe5	CCAAGCGCTACCACAAGA	18	59.6
SQUA_RT_R5	CTCCGACAGCTCATGGAAC	19	61.0
PAT_F1	CACTCAGATCAGAAGCACAAGA	22	58.7
PAT_R1	CGGTGCCAATGGAGATGAT	19	60.2
PAT_F2	GTAACCCGGATTTCAACCCT	20	60.6
PAT_R2	AGTGATCATCTTCCAACAACCT	22	58.2
GRF8_F1	AACTGTAATCCTGGACGTTTCA	22	58.2
GRF8_R1	AGGAGCATTCGCGACAAA	18	58.7
GRF8_F2	GCACCAGGCCCTGATCTA	18	62.7
GRF8_R2	GTGTGGCAGTGCGATGATAC	20	60.0
GRF8_RT_F4	TCAATCCGTGGAGTACCTTTG	21	59.7
GRF8_RT_R4	GTAGCGACCACGGTTTAAGT	20	58.8
DdRPolII_F3	CATACTGAAACCAAGGCCTATTTG	24	57.9
DdRPolII_R3	CATTGTCGAACTCACCCTTCT	21	59.7
DREB2_F2	GTGCTCTTCCCACGAATGA	19	60.1
DREB2_R2	ACCCTTCTTGGAACCCTTTG	20	61.4
DREB2_RT_F4	GGCCTCTAATCTGGGAAAGAAG	22	60.7
DREB2_RT_R4	CCTCACGCCACGGAATC	17	62.2
KIN_F1	GGAGGCCACCGACGACG	17	68.4
KIN_R1	GTGCCCAGCCTGAGTAGAGATA	22	62.9
KIN_F6	CGGTGGTGCAGAAACTGATA	20	59.4
KIN_R6	CGGACATCATGCCAGAAAGA	20	60.0

housekeeping gene UBICE (Ubiquitin conjugating enzyme transcript) was used to normalize the specific gene expression levels, as in Selva et al., 2020. The thermal cycling used for these amplifications consisted of 95°C for 2 min, 40 cycles at 94°C for 10 s, 15 s at the optimal annealing temperature for each primer pair and finally at 30s at 72°C. Reactions were conducted on technical triplicates of biological duplicates for the three assayed genotypes. Dissociation curve profiles were used to verify the specificity of each reaction. Normalization of transcript levels between cDNA samples was undertaken using the 2-ΔΔCt method (Livak and Schmittgen, 2001). The statistical analysis of the qPCR fold change in the expression of genes among different treatments was done through the Student's t-test, where a p-value of 0.05 was considered to be significant.

Results

Don Walter small RNA libraries characterization

Small RNAs libraries from inflorescences of the cultivar Don Walter were constructed for this work, whereas those from Tanganyika and OTA-S have been reported in Garbus et al., 2019. Thus, we started from a brief characterization of Don Walter sRNA libraries. There were obtained 2,541,355 raw reads for DW1, and 2,929,269 and 2,140,845 for DW2 and DW3 respectively. After trimming, a total of 2,114,363 (83.1%), 2,556,295 (87,2%) and 1,802,287 (84,1%) reads were retained for each library. As expected, reads with 21 and 24 bp were overrepresented in the three samples (Figure 1).

TABLE 3 Primers designed based on miRNA precursors identified in the Don Walter genome.

Primer	Sequence	Tm (°C)
pcs_pri_mat181F	GTGGAATGTTGTCTGGTTCAAG	58.9
pcs_pre_mat181	GGAATGTTGTCTGGTTCAAGG	59.2
pcs_rev_mat181	GAATGAAGCCTGGTCCGA	60.6
pcs_pri_mat42F	ACTTGCTAAGGAAGATCGTAGTG	57.7
pcs_pre_mat42F	GTGTTCTTTGCATCTTGGTCA	57.6
pcs_rev_mat42	TAGCATTCAAACACTTGAGCAC	56.6
pcs_pri_mat422F	AGATTGAACCTAAGCTTAGATA	51.0
pcs_pre_mat422F	GGTGATTTTTGGATTATGTTCAG	54.0
pcs_rev_mat422	AAGTTCTAGGCACATTGGC	56.6
pcs_pri_mat676F	ACTGTTATGACTAGGTTCTATC	51.9
pcs_pre_mat676	AGAGTTGGAGGAAAACAAACC	58.1
pcs_rev_mat676	TGAGATATTGGAGAAAAACAAG	52.1
pcs_pri_mat750F	ATGCTCTCCACAGGCTTTC	59.6
pcs_pre_mat750F	TCCACAGGCTTTCTTGAAC	57.7
pcs_rev_mat750	GGACTTTCTTGAACCATCAACAC	58.9
pcs_pri_mat810F	GGCGAGCTGCGAACACAT	62.4
pcs_pre_mat810F	GGGGCGAGCTGCGAACACATG	68.6
pcs_rev_mat810	CGGGGGCGACCTGAGAACACA	70.9
pcs_pri_mat601	CGGTGATTTCCATGGCTAACT	59.5
pcs_pre_mat601	TGACAGAAGAGAGTGAGCAC	58.7
pcs_rev_mat601	ACTGACAGAGAGAGAAGTGAGC	60.4

miRNA prediction and expression

To identify miRNA sequences and its precursors, the reads from the seven samples, i.e., three from the facultative Don Walter, two from the sexual OTA-S and two from the full apomictic Tanganyika cultivar, were merged in a single file. After trimming and filtering, a total of 171,339,858 reads passed the quality control. Since miRDP2 pipeline requires unique sequences, the input file was collapsed into 30,124,624 unique reads attaching their frequency to the header.

The miRDP2 software predicted 953 miRNAs that were used as reference to map each sample through the Bowtie software. A count matrix was constructed to quantify the expression of the mature miRNAs in the samples. After filtering, a PCA plot and a heatmap were constructed using the normalized matrix as input, showing the similarity within samples with the same reproductive behavior (Supplementary Figures 1, 2). Finally, the same matrix was used to show the expression of all the miRNAs in each sample (Figure 2). The differential expression analysis showed that 51, 108 and 51 mature miRNAs were up-regulated in APOvsSEX, APOvsFAC and FACvsSEX comparisons, respectively. On the other hand, the down-regulated miRNAs were 52, 57 and 99 for the APOvsSEX, APOvsFAC and FACvsSEX, respectively.

Target identification and transcript expression analysis

Target identification was performed through psRNATarget software (Dai et al., 2018) using the improved scoring schema V2 (2017). A total of 13,770 targets were found, which were putatively regulated by 682 unique mature miRNAs. In parallel, the expression of the transcripts was assessed. The reads were mapped against the transcripts using hisat2 (Kim et al., 2019) in order to quantify its expression. The differential expression analysis showed that 220, 2,162 and 542 transcripts were upregulated for the APOvsSEX, APOvsFAC and FACvsSEX, respectively; whereas the downregulated transcripts for the same comparisons were 195, 798 and 1,520, respectively.

Transcripts regulated by miRNAs

Based on the psRNAtarget results, we focused especially on those possible transcript-miRNA interactions in which the differential expression of transcripts and miRNAs among genotypes followed opposite direction, i.e., when transcripts showed to be up-regulated in a particular comparison, the miRNA resulted down-regulated and *vice versa*. Hence, 5, 14,

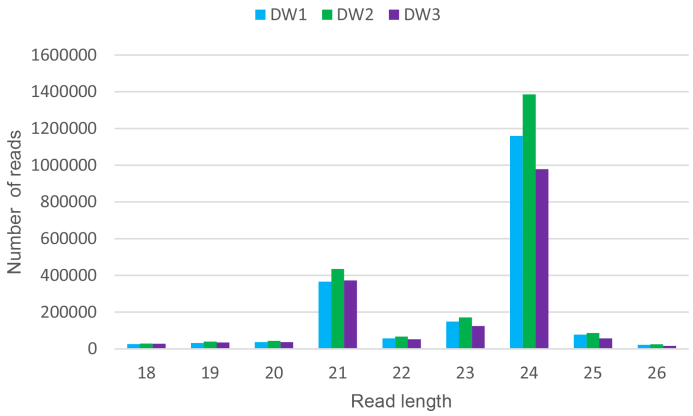

FIGURE 1
Read length distribution of the three Don Walter sRNA libraries. For each read length, the absolute read count per individual library is shown. The x-axis shows read lengths, and the y-axis shows the frequency of occurrence of reads of each length. The over-representation of 21 and 24 bp reads is evidenced.

and 16 target transcripts were found to be down-regulated while its mature miRNA was found to be up-regulated in the APOvsSEX, APOvsFAC and FACvsSEX comparisons, respectively. On the other hand, 14 and 6 targets were found up-regulated for the APOvsFAC and FACvsSEX comparison, while the mature miRNAs were found to be down-regulated. No miRNA-mRNA interactions were identified for the comparison APOvsSEX.

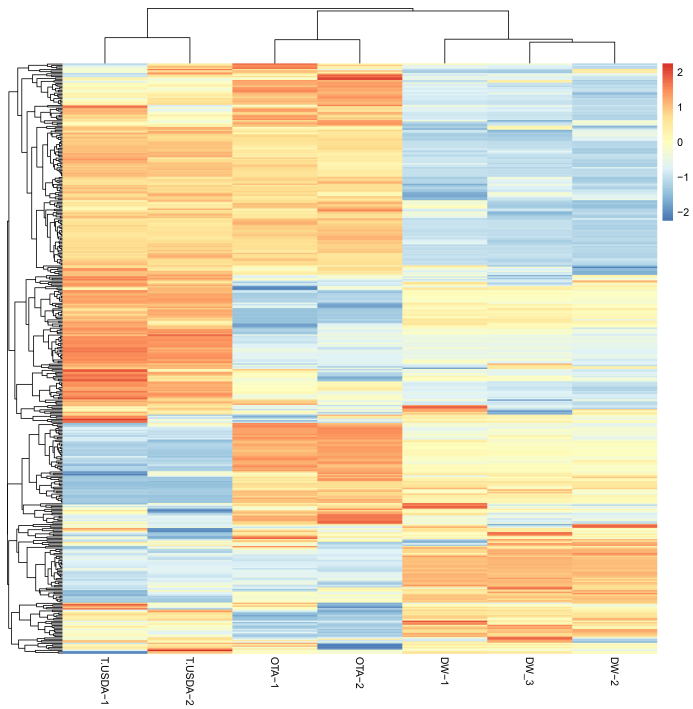

FIGURE 2
Heatmap showing the expression of the miRNAs in the seven samples analyzed. The count matrix was transformed in the log2 scale and normalized according to the library size. The considered samples are shown in the x-axis. In the color scale, orange and blue represent up-and down-expressed miRNAs respectively.

Genomic DNA and transcript expression analysis

The *in silico* analysis revealed the existence of ≈60 possible miRNA-target interactions that could be involved in the regulation of the reproductive mode in *E. curvula* (Supplementary Table 1). For validation purposes, after transcript annotation, seven miRNA-target interactions were selected mainly guided by their possible known function, discarding in this initial approach those transcripts without annotation and/or corresponding to hypothetical proteins (Table 4). Thus, for the comparison APOvsFAC with the target down-regulated and the miRNA up-regulated, the expression of the genes *Kinesin-like protein KIN-14D*, *Patatin-like protein 2* and *Dehydration-Responsive Element Binding Protein 2A* (DREB2A) (Supplementary Figure 3A–C) was explored, whereas for the target up-regulated and miRNA down-regulated combination, the expression of *Growth-regulating factor 8* (GRF8) and *Squamosa-promoter binding protein-like protein 13* genes was inquired (Supplementary Figure 3D, E). The expression of the genes for *DNA-Directed RNA polymerase II subunit RPB1* (DRdRNApolII) and *GAMYB transcription factor* were investigated because they were differential for the comparison FACvsSEX, with the target being down-regulated and miRNA up-regulated (Supplementary Figure 3F, G).

Initially, PCR reactions were conducted aiming to amplify the mentioned genes from genomic DNA for the three cultivars in biological triplicates, leading to the predicted amplification bands, using one or more specific primer combinations (Table 5, Figure 3). Interestingly, the kinesin transcript was differentially expressed among genotypes, being absent in the apomictic cultivar Tanganyika, in accordance with the prediction of being down-regulated in the APOvsSEX comparison (Figure 3A). However, the primer combination used for the other transcripts resulted in no amplification bands (Table 5, Figure 3B–G). In order to confirm the absence of expression, qPCR reactions were conducted. UBICE was amplified from all the cDNA samples with no significant difference in expression among them. However, the Cts obtained for the assayed cDNA samples were close to that of the negative controls, indicative of the absence of expression. Kinesin was not subjected to qPCR, since the observed amplification bands were conclusive.

Validation of novel and conserved miRNAs

The expression of the miRNA predicted to be interacting with the mentioned transcripts was analyzed through RT-PCR

TABLE 4 miRNA-mRNA interactions selected for the analysis.

	miRNA	Target	Transcript	Size (bp)	Protein	ID	Size (AA)	miRNA from the libraries	Transcript target site	Conserved miRNA	*E. curvula* miRNA
APOvsFAC	Up-regulated	Down-regulated	maker-Backbone_4151-snap-gene-0.33	4062	Kinesin-like protein KIN-14D	Q0E2L3.2	977	miRNA_42	371-394	-	Ecu-miRNA_novel_1
			maker-Backbone_1301-augustus-gene-1.1	1699	Patatin-like protein 2	A2YW91.1	405	miRNA_422	310-084	-	Ecu-miRNa_novel_2
			maker-Backbone_2520-snap-gene-0.20	1737	DREB2A	JAF93766	343	miRNA_810	532-552	Zma-miR398b	Ecu-miR398
	Down-regulated	Up-regulated	augustus_masked-Backbone_566-processed-gene-1.5	2073	Growth-regulating factor 8	Q6AWY1.1	409	miRNA_601	719-738	Zos-miR156e	Ecu-miR156c
			maker-Backbone_1343-snap-gene-1.63	1093	Squamosa-promoter binding protein-like protein 13	AQQ11858	195	miRNA_830	719-739	Tae-miR156a	Ecu-miR156d
FACvsSEX	Up-regulated	Down-regulated	maker-Backbone_4804-snap-gene-0.1	3972	DNA-directed RNA polymerase II subunit RPB1	P18616.3	1839	miRNA_181	3540-3560	Osa-miR166e	Ecu-miR166
			maker-Backbone_7431-snap-gene-0.35	2017	Transcription factor GAMYB	OEL28920	432	miRNA_676	2081-2101	Osa-miR2275b	Ecu-miR2275c

The transcripts identified in the Don Walter transcriptome that resulted up or down regulated from the comparisons APOvsSEX and FACvsSEx were annotated as well as the miRNAs that targeted them, when they were conserved. Protein name and ID were retrieved from the UNIport database.

TABLE 5 PCR amplicons expected and predicted sizes obtained from DNA and cDNA with several combinations of transcript-based primers.

	miRNAs	Target	Target gene	Forward primer	Reverse primer	Expected DNA amplicon size (bp)	Obtained DNA amplicon size (bp)	Expected cDNA amplicon size (bp)	Obtained cDNA amplicon size (bp)
APOvsFAC	Down-regulated	Up-regulated	Squamosa-promoter binding protein-like protein 13	SQUA_F1	SQUA_R1a	x	(-)	320	(-)
				SQUA_RT_F5	SQUA_R3	x	(-)	141	(-)
				SQUA_F4	SQUA_R4	572	~600	572	(-)
				SQUA_RT_F5	SQUA_RT_R5	x	(-)	121	(-)
			Growth-regulating factor 8	GRF8_F1	GRF8_R1	1028	~1000	580	(-)
				GRF8_F2	GRF8_R2	1028	~1000	350	(-)
				GRF8_RT_F4	GRF8_RT_R4	853	~850	175	(-)
	Up-regulated	Down-regulated	Patatin-like protein 2	PAT_F1	PAT_R1	1131	~1150	916	(-)
				PAT_F2	PAT_R2	931	~950	749	(-)
			Dehydration-Responsive Element Binding Protein 2A (DREB2A)	DREB2_F2	DREB2_R2	834	~850	229	(-)
				DREB2_RT_F4	DREB2_RT_R4	x	(-)	221	(-)
			Kinesin-like protein KIN-14D	KIN_F1	KIN_R1	1076	~1100	636	(-)
				KIN_F6	KIN_R6	1048	~1050	300	O, DW: 300; T: (-)
FACvsSEX	Up-regulated	Down-regulated	Transcription factor GAMYB	GAMYB_F1	GAMYB_R1	1165	~1150	1062	(-)
				GAMYB_F2	GAMYB_R2	1317	multiple bands	363	(-)
				GAMYB_RT_F3	GAMYB_RT_R3	322	~300	219	(-)
			DNA-directed RNA polymerase II subunit RPB1	DdRPolII_F3	DdRPolII_R3	1204	~1200	1009	(-)

A total of 7 miRNA–target combinations that arise from the APOvsFAC and FACvsSEX comparisons with opposite miRNA/target regulation have been tested.

and qPCR, revealing that all the miRNAs were expressed, whereas differential expression was only detected from the miRNA that targets the kinesin transcript (Figure 4).

miRNAs were further validated through the amplification from DNA of their pri-miRNA and pre-miRNA precursors, predicted from the Don Walter genome (Figure 3A–G), whereas their hairpin structures are shown in Figure 5. The sequences of the mature and star miRNAs as well as their precursor are reported in Supplementary Table 2.

The expression of all the tested miRNAs, as well as their precursors and the validation of their hairpin structures, together with the absence of amplification for most of the searched transcripts strongly suggests that a miRNA-target regulation exists for all the combinations tested.

Discussion

Eragrostis curvula (Schrad.) Nees, commonly known as weeping lovegrass, is a perennial grass from the Poaceae family, widely cultivated in the semiarid region of Argentina as a forage grass (Covas, 1991). *E. curvula* has a basic chromosome number of x=10, and it includes genotypes with different ploidy levels. While the diploid cytotypes are scarce and sexual in nature, tetraploid plants and plants with higher ploidy levels reproduce by pseudogamous diplosporous apomixis, defined as asexual reproduction through seeds (Leigh, 1960; Voigt and Burson, 1983; Noirot et al., 1997). Apomixis has been described in over 400 angiosperms, and it leads to the creation of clones of the mother plant (Nogler, 1984). However, this attribute is absent in most species of agricultural importance. The study of the genetic regulation of this mechanism would be important for the development of tools that could enable its transference to key species, such as wheat, rice or maize, in order to fixate important agronomic traits through generations (Hanna and Bashaw, 1987). The purpose of this work was focused on analyzing the epigenetic mechanisms that could be playing a role in diplosporous apomictic reproduction in this species.

Studies suggest that, instead of an independently originated trait, apomixis arises as the result of modifications in the temporal or spatial regulation of the sexual pathway in seed development, which produces variations or omissions in critical developmental stages (Koltunow and Grossniklaus, 2003; Schmidt, 2020). With this theory in mind, the expression of a gene or genes in specific cells from the nucellus could determine if sexual or apomictic processes, or both, will take place in that ovule, proposing that apomixis-related genes must be absent or

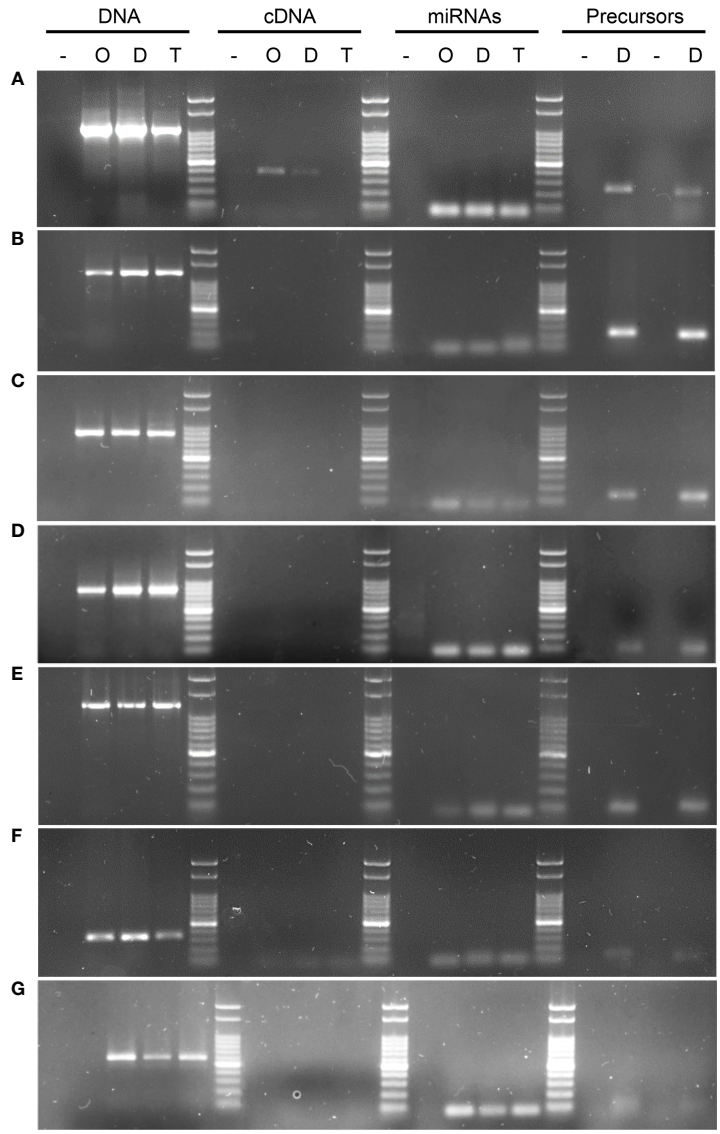

FIGURE 3
PCR and RT-PCR amplifications using gene, transcript, miRNA, pri-miRNA and pre-miRNA based primers. The image shows DNA from the target genes could be amplified in all of the tested samples, whereas when cDNA was the template, this led to amplification bands for 1 of the 7 transcripts tested using several primers combinations (Table 5). **(A)** KINESIN, which showed amplification in cDNA, and was absent only in Tanganyika, **(B)** PATATIN, **(C)** GRF8, **(D)** DREB2, **(E)** DdRNAPolII1B, **(F)** GAMYB, **(G)** SQUAMOSA. *UBICE* gene was used for normalization of cDNA expression. The amplification using miRNA, pri-miRNA and pre-miRNA based primers allowed the validation of the novel and reported miRNAs tested in this study.

unexpressed for the sexual processes to take place (Koltunow, 1993; Koltunow and Grossniklaus, 2003).

Genomic and transcriptomic studies were performed in the past to discover the molecular mechanisms involved in apomixis. Even though several advances were made in the last years, candidate genes related to meiosis could not be found through these approaches so far. Moreover, the involvement of epigenetic factors is being studied, as they can occur rapidly and are particularly frequent as a result of polyploidization and hybridization, and they could also help explain the parallel and independent occurrence of apomixis several times during evolution (Koltunow and Grossniklaus, 2003; Comai, 2005). In the year 2010, García-Aguilar et al., 2010 observed that a deregulation of DNA methylation produced apomeiotic-like phenotypes in reproductive cells of maize. Also, in apomictic genotypes of Boechera subjected to stress, Taraxacum-type diplospory arised in the female gametophyte. In studies with the same genotypes, the suppression of DNA methylation before

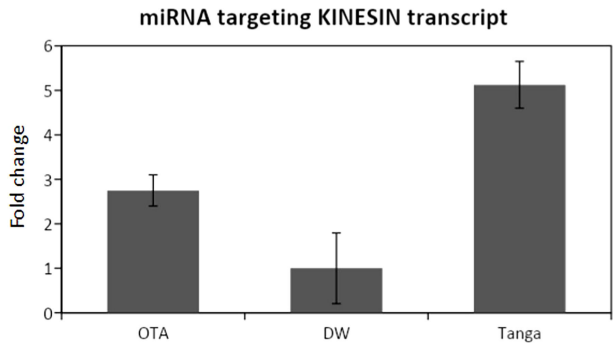

FIGURE 4
qPCR analysis for the miRNA that targets the Kinesin transcript. DW: Don Walter. Tanga: Tanganyika. The miRNA is overexpressed in the apomictic cultivar Tanganyika ($p<0.05$). Data was normalized with respect to the genotype that showed the lower expression.

the formation of the MMC triggered Antennaria-type mitotic diplospory (Gao, 2018). In *E. curvula*, it has been observed that environmental signals have an influence over the number of sexual embryo sacs (Rodrigo et al., 2017), and that polyploidization involves an increase in genome methylation, and it could lead to gene silencing, in order to preserve the functional characteristics of the diploid (Ochogavía et al., 2009; Zappacosta et al., 2014; Carballo et al., 2021).

As mentioned previously, miRNAs are known to play central regulatory roles during plant development, and they are part of diverse biological processes such as flower and leaf morphogenesis, response to stress, reproductive cell identity, fertility, etc. (Aukerman and Sakai, 2003; Palatnik et al., 2003; Sunkar and Zhu, 2004; Schwab et al., 2005; Ru et al., 2006; Olmedo-Monfil et al., 2010; Amiteye et al., 2011; Li et al., 2015; Ripoll et al., 2015; Fei et al., 2021).

Our work established that the gene *kinesin* is differentially expressed among genotypes, being absent in the apomictic genotype Tanganyika. A BLAST analysis of the transcript revealed that it is homolog of Kinesin14D. Moreover, the expression of the miRNA postulated to be regulating kinesin, was found to be upregulated in the genotype Tanganyika. This is a novel miRNA identified in this work, referred in the manuscript Ecu-miRNA_novel_1, and its existence was confirmed by the amplification of the precursors pri-miRNA and pre-miRNA and the predicted hairpin structure. Kinesins act as microtubule-based molecular motors involved in several biological processes such as cell division, intracellular transport, and cell shape determination (Zhu and Dixit, 2012; Ali and Yang, 2020). *Kinesin* genes are distributed in 14 families, with Kinesin7 and Kinesin14 being the most represented in land plants (Richardson et al., 2006). It is proposed that land plants may have evolved novel Kinesin14 motors to account for microtubule-based functions that are plant-specific or are typically performed by Dynein in other eukaryotes, as is spindle formation and the expansion of the phragmoplast (Zhu and Dixit, 2012; Gicking et al., 2018).

The Kinesin14 family includes many members that are up-regulated during mitosis and function during cell division and localization of plastids, thus influencing plant development (Gicking et al., 2018). ATK1 and ATK5 are two minus-end-directed Kinesin14 proteins that localize in the spindle apparatus. *A. thaliana atk1* mutants exhibit abnormalities in meiosis, such as extended spindle poles and reduced male fertility (Chen et al., 2002), as well as mild spindle bipolarity defects during mitosis (Marcus et al., 2003). The lack of spindle bipolarity in *atk1-1* leads to abnormal chromosome segregation during meiosis, whereas in mitosis this defect is corrected by anaphase, perhaps due to functional compensation by other minus-end-directed kinesins such as ATK5 (Nebenführ and Dixit, 2018). Mitotic spindles in the *atk5-1* mutant are abnormally broad (Ambrose et al., 2005). Furthermore, maize mutants in a Kinesin14 member, that is likely a functional homolog of ATK1, showed extended spindle poles and altered spindle length and width during meiosis (Higgins et al., 2016).

A study conducted in *Citrullus lanatus*, showed that 38 Kinesin genes were overexpressed in the reproductive organs, being 20 preferentially expressed in the female flower, and 9 specifically expressed in the male flowers, thus suggesting that they play critical roles in the growth and development of reproductive tissues (Tian et al., 2021). Interestingly ClKIN14D, homologous to Kinesin14D, was found to be overexpressed in male flowers and repressed in female flowers (Tian et al., 2021).

The analysis of protein motifs of the Kinesin translated from Don Walter transcriptome, revealed that it contains a calponin-homology domain (CH), thus classified as KCH, a

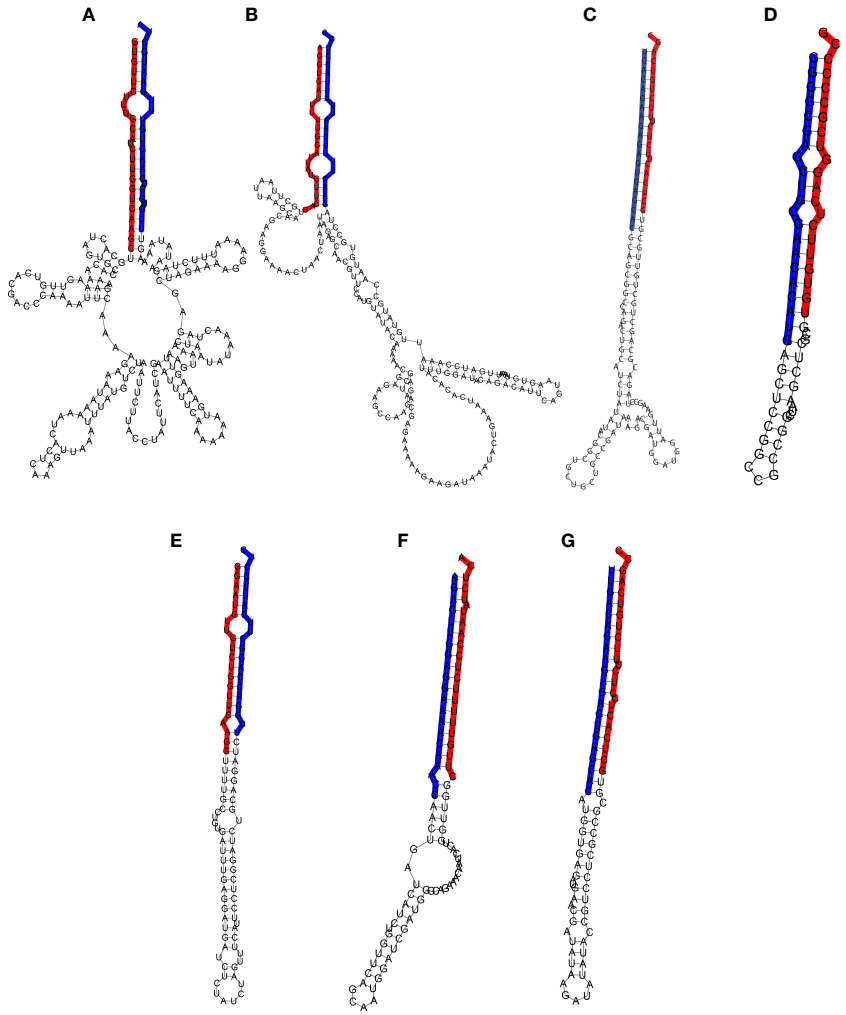

FIGURE 5
Hairpin structure of the miRNA precursors. The mature and star sequences are highlighted in blue and red, respectively. **(A)** Pre-Ecu-mir novel_1, **(B)** Pre-Ecu-mir novel_2, **(C)** Pre-Ecu-mir156c, **(D)** Pre-Ecu-mir398, **(E)** Pre-Ecu-mir166, **(F)** Pre-Ecu-mir 2275c, **(G)** Pre-Ecu-mir156d (Table 4).

unique subset of Kinesin14 that can bind to both microtubules and actin filaments in land plants (Umezu et al., 2011). KCHs are most abundant in developing tissues and are thought to participate in cell division and elongation (Frey et al., 2010). Identified KCHs showed to be mostly expressed in mature pollen, being proposed that they are the main actors for the movement of sperm cells in the pollen tube (Schattner et al., 2021). The expression of OsKCH1 was quantified in rice, revealing that the highest abundance of transcripts was found in primary leaf, primary root, and the developing flower (Frey et al., 2010).

In this bibliographic context it is clear that kinesins are involved in plant reproduction and, thus, is plausible that the miRNA-target interaction that impedes the translation of the kinesin transcript is contributing to a defective sexual expression and leading to an apomictic phenotype in Tanganyika. Moreover, Kinesins were reported to be targeted by miR1863 (Smita et al., 2021) in grapevine and by sly-miR171a in *Solanum lycopersicum* (López-Galiano et al., 2019). It is not unexpected that kinesins, with a main role in mitosis and meiosis, are determinant in plant growth and fertility.

The expression of the orthologous gene from Arabidopsis, At1g73860, was demonstrated to be tissue-specific for the microgametogenesis, specifically expressed in mature pollen (Honys and Twell, 2004; Klepikova et al., 2016), thus arguing in favor of a specific role in the reproductive pathway.

In addition, the rice orthologous Os02g0229600, was found highly expressed in mature pollen as well as in pre-flowering panicles (Sakai et al., 2011).

Whether the epigenetic mechanisms are the cause or the result of changes in the reproductive behavior is still under discussion (Hand and Koltunow, 2014; Mau et al., 2022), but under the light of our results, the fact that the kinesin gene is involved in apomixis in *E. curvula* cannot be denied. Thus, this gene is disclosed as a strong candidate for further studies allowing the design of strategies to inquire into apomixis mechanisms in this or other species.

Concerning the other analyzed genes, the absence of mRNA expression combined with the observed miRNA expression demonstrated miRNA-target interactions for all of them. Out of the analyzed transcripts, DNA-directed RNA polymerase II subunit RPB1 (DdRNAPolII1B), Squamosa-promoter binding protein-like 13 (SBP13), Growth-regulating factor 8 (GRF8) and Dehydration-Responsive Element Binding Protein 2A (DREB2A) are targeted by the conserved miRNAs with identity to Osa-miR166e, Tae-miR156a, Zma-miR396d and Zma-miR398b respectively, whereas the other transcripts are regulated by miRNAs firstly described in this work, and validated through the amplification of the pri-miRNAs and pre-miRNAs (Table 4).

Interestingly, several of our analyzed transcripts were previously demonstrated to be regulated by miRNAs. miR156 was reported to target SBP genes (Poethig, 2010; Wang, 2014; Garbus et al., 2019), and was shown to be highly conserved, playing an important role in plant development (Poethig, 2010). It is highly expressed during the juvenile phase and declines during vegetative phase change (Poethig, 2010), leading to an increased expression of SBPs genes that act by promoting the development of adult vegetative traits and floral induction (Wang, 2014). Overexpression of miRNA156 in *A. thaliana* produces nearly full sterility, and the rescue of SPL function brings back normal reproductive behavior (Zheng et al., 2019). It is also known that miRNA156's expression is fine-tuned since its temporal and spatial expression change during the reproductive development (Wu and Poethig, 2006; Zheng et al., 2019). We can hypothesize that the expression of miRNA156 could have different expression patterns related to the reproductive mode. Additional analyses testing its expression in different developmental stages of apomictic and sexual plants should be conducted to confirm this assumption.

The transcription factor GAMYB (Gibberellin-and-Abscisic acid-regulated MYB), involved in flowering time and flower organ development (Sunkar and Zhu, 2004), was also reported to be involved in another development *via* regulating the expression of phenylalanine ammonia lyase (PAL) (Woodger et al., 2003). It was proposed that miR319a-regulated GAMYB might also be involved in the browning inhibition of fresh-cut apples by H2S treatment (Chen et al., 2020). Other study states that, in *Oryza sativa*, miR1026 and miR159 target DdRNAPolII1B and GAMYB, respectively, being both up-regulated under stress conditions. The gene Patatin-like protein 2 (PLP2), related to lipid metabolism, was proposed to be targeted by miR6478 (Chen et al., 2020). DNA-directed RNA polymerase II has been reported to be targeted by miR172 in the genus Mimulus (Barozai et al., 2011).

This study provided small RNA libraries available for the scientific community for further analysis of miRNA regulation, at the time that it postulates and validates the presence in the genome of the facultative apomictic cultivar Don Walter of five conserved and two novel miRNAs, given by their evidenced pri-miRNA, pre-miRNA and hairpin structures, being functional as mRNA expression repressors. Moreover, a Kinesin gene expression could be related to miRNA differential regulation in the obligate apomictic genotype Tanganyika.

This work contributed new supporting evidence about the participation of miRNAs in the regulation of genes that are determinant for reproduction in *E. curvula*.

Data availability statement

The datasets presented in this study can be found in online repositories. The names of the repository/repositories and accession number(s) can be found in the article.

Author contributions

Conception: IG, VE. Experimental design: IG, JC. Materials: JS, JR, DZ, JC. Experimental procedures: MP, JG, JC. Bioinformatic data processing: JC, IG. Analysis and interpretation: IG, JC, MP. Writing: IG, JC, MP. Critical review: VE. All authors contributed to the article and approved the submitted version.

Funding

PIP 2021 – 2023 (Code: 11220200100306CO) Identificación de interacciones miRNA-mRNA basada en el análisis del degradoma orientada a la caracterización de su rol en la regulación epigenética de la apomixis diplospórica en pasto llorón (Eragrostis curvula) to IG: laboratory supplies financement. PICT Raíces 2017 - 0879. Genómica estructural para acceder a la región condicionante de la apomixis en Eragrostis curvula. to VE and Mario Cáccamo (NIAB, UK): laboratory supplies and sequencing services financement H2020-MSCA-RISE-2019, Mechanisms of Apomictic

Developments (MAD) to VE in Argentina: sequencing services and open access publication fees. PGI 24/A261 Estudio de las bases genéticas y epigenéticas asociadas a la apomixis en Eragrostis curvula (Shrad.) Nees to V.E: laboratory supplies.

Conflict of interest

The authors declare that the research was conducted in the absence of any commercial or financial relationships that could be construed as a potential conflict of interest.

Publisher's note

All claims expressed in this article are solely those of the authors and do not necessarily represent those of their affiliated organizations, or those of the publisher, the editors and the reviewers. Any product that may be evaluated in this article, or claim that may be made by its manufacturer, is not guaranteed or endorsed by the publisher.

Supplementary material

The Supplementary Material for this article can be found online at: https://www.frontiersin.org/articles/10.3389/fpls.2022.1012682/full#supplementary-material

SUPPLEMENTARY FIGURE 1
Heatmap of the clustering of samples based on distance matrix. Heatmap showing the distance matrix obtained on logarithm transformed counts, showing similarities and dissimilarities between the seven samples DW-1, DW-2, DW-3, T.USDA-1, T.USDA-2, OTA-1, OTA-2. In the color scale, red and blue represent more and less distance between samples, respectively.

SUPPLEMENTARY FIGURE 2
Principal component analysis plot. PCA plot showing the similarity within samples with the same reproductive behavior. The variance of principal components PC1 and PC2 are represented in the x and y axis, respectively.

SUPPLEMENTARY FIGURE 3
Alignment between miRNAs and their targeted transcripts. miRNA - target interaction between. **(A)** Ecu-miRNA_novel_1 and kinesin-like protein KIN-14D, **(B)** Ecu-miRNA_novel_2 and patatin-like protein 2, **(C)** Ecu-miR156c and Growth-regulating factor 8, **(D)** Ecu-miR398 and DREB2A, **(E)** Ecu-miR166 and DNA-directed RNA polymerase II subunit RPB1, **(F)** Ecu-miR2275c and Transcription factor GAMYB, and **(G)** Ecu-miR156d and Squamosa-promoter binding protein-like protein 13 (Table 4).

References

Ali, I., and Yang, W.-C. (2020). The functions of kinesin and kinesin-related proteins in eukaryotes. *Cell Adhesion Migration* 14 (1), 139–152. doi: 10.1080/19336918.2020.1810939

Ambrose, J. C., Li, W., Marcus, A., Ma, H., and Cyr, R. (2005). A Minus-End–directed kinesin with plus-end tracking protein activity is involved in spindle morphogenesis. *Mol. Biol. Cell* 16 (4), 1584–1592. doi: 10.1091/mbc.e04-10-0935

Amiteye, S., Corral, J. M., Vogel, H., Kuhlmann, M., Mette, M. F., and Sharbel, T. F. (2013). Novel MicroRNAs and microsatellite-like small RNAs in sexual and apomictic boechera species. *MicroRNA* 2 (1), 46–63. doi: 10.2174/2211536611302010006

Amiteye, S., Corral, J. M., Vogel, H., and Sharbel, T. F. (2011). Analysis of conserved microRNAs in floral tissues of sexual and apomictic boechera species. *BMC Genomics* 12 (1), 1–16. doi: 10.1186/1471-2164-12-500

Aukerman, M. J., and Sakai, H. (2003). Regulation of flowering time and floral organ identity by a MicroRNA and its APETALA2-like target genes. *Plant Cell* 15 (11), 2730–2741. doi: 10.1105/tpc.016238

Barozai, M. Y. K., Din, M., and Baloch, I. A. (2011). Identification of microRNAs in ecological model plant *Mimulus*. *J. Biophys. Chem.* 02 (03), 322–331. doi: 10.4236/jbpc.2011.23037

Borges, F., and Martienssen, R. A. (2015). The expanding world of small RNAs in plants. *Nat. Rev. Mol. Cell Biol.* 16 (12), 727–pp.741. doi: 10.1038/nrm4085

Brukhin, V., and Albertini, E. (2021). Epigenetic modifications in plant development and reproduction. *Epigenomes* 5 (4), 25. doi: 10.3390/epigenomes5040025

Carballo, J., Santos, B. A. C. M., Zappacosta, D., Garbus, I., Selva, J. P., Gallo, C. A., et al. (2019). A high-quality genome of eragrostis curvula grass provides insights into poaceae evolution and supports new strategies to enhance forage quality. *Sci. Rep.* 9 (1), 1–15. doi: 10.1038/s41598-019-46610-0

Carballo, J., Zappacosta, D., Marconi, G., Gallardo, J., Di Marsico, M., Gallo, C. A., et al. (2021). Differential methylation patterns in apomictic vs. sexual genotypes of the diplosporous grass eragrostis curvula. *Plants* 10 (5), 946. doi: 10.3390/plants10050946

Carman, J. G., de Arias, M. M., Nelson, S. M., Zhao, X., Gao, L., Srivastava, M., et al. (2015). "Hot on the trail of the sex-apomixis switch in boechera (Brassicaceae)," in *In Proceedings of the Plant and Animal Genome Conference* (San Diego, USA: PAG XXIV). Available at: https://pag.confex.com/pag/xxiii/webprogram/Paper14382.html

Cervigni, G. D. L., Paniego, N., Díaz, M., Selva, J. P., Zappacosta, D., Zanazzi, D., et al. (2008b). Expressed sequence tag analysis and development of gene associated markers in a near-isogenic plant system of eragrostis curvula. *Plant Mol. Biol.* 67 (1-2), 1–10. doi: 10.1007/s11103-007-9282-4

Cervigni, G. D. L., Paniego, N., Pessino, S., Selva, J. P., Díaz, M., Spangenberg, G., et al. (2008a). Gene expression in diplosporous and sexual eragrostis curvula genotypes with differing ploidy levels. *Plant Mol. Biol.* 67 (1-2), 11–23. doi: 10.1007/s11103-008-9305-9

Chen, C., Liu, C., Jiang, A., Zhao, Q., Zhang, Y., and Hu, W. (2020). miRNA and degradome sequencing identify miRNAs and their target genes involved in the browning inhibition of fresh-cut apples by hydrogen sulfide. *J. Agric. Food Chem.* 68 (31), 8462–8470.

Chen, C., Marcus, A., Li, W., Hu, Y., Calzada, J.-P. V., Grossniklaus, U., et al. (2002). The arabidopsis ATK1 gene is required for spindle morphogenesis in male meiosis. *Development* 129 (10), 2401–2409. doi: 10.1242/dev.129.10.2401

Chen, C., Ridzon, D. A., Broomer, A. J., Zhou, Z., Lee, D. H., Nguyen, J. T., et al. (2005). Real-time quantification of microRNAs by stem–loop RT–PCR. *Nucleic Acids Res.* 33 (20), e179–e179. doi: 10.1093/nar/gni178

Comai, L. (2005). The advantages and disadvantages of being polyploid. *Nat. Rev. Genet.* 6 (11), 836–846. doi: 10.1038/nrg1711

Covas, G. (1991). "Introducción del pasto llorón en la Argentina in El pasto llorón, su biología y manejo," in *Cerzos y dpto. de agronomía* (Bahía Blanca: Universidad Nacional del Sur), 1–6.

Crane, C. F. (2001). ""Classification of apomictic mechanisms"," in *The flowering of apomixis: from mechanisms to genetic engineering*, vol. 24 . Eds. Y. Savidan, J. G. Carman and T. Dresselhaus (Mexico: CIMMYT, IRD, EU DG VI (FAIR), 43.

Dai, X., Zhuang, Z., and Zhao, P. X. (2018). psRNATarget: a plant small RNA target analysis serve Release. *Nucleic Acids Res.* 46 (W1), 49–54. doi: 10.1093/nar/gky316

Fei, X., Lei, Y., Qi, Y., Wang, S., Hu, H., and Wei, A. (2021). Small RNA sequencing provides candidate miRNA-target pairs for revealing the mechanism of apomixis in zanthoxylum bungeanum. *BMC Plant Biol.* 21 (1), 1–13. doi: 10.1186/s12870-021-02935-5

Frey, N., Klotz, J., and Nick, P. (2010). A kinesin with calponin-homology domain is involved in premitotic nuclear migration. *J. Exp. Bot.* 61 (12), 3423–3437. doi: 10.1093/jxb/erq164

Gao, L. (2018). *Pharmacologically induced meiosis apomeiosis interconversions in boechera, arabidopsis and vigna* (Utah: Utah State University).

Garbus, I., Romero, J. R., Selva, J. P., Pasten, M. C., Chinestra, C., Carballo, J., et al. (2017). *De novo* transcriptome sequencing and assembly from apomictic and sexual eragrostis curvula genotypes. *PloS One* 12 (11), e0185595. doi: 10.1371/journal.pone.0185595

Garbus, I., Selva, J. P., Pasten, M. C., Bellido, A. M., Carballo, J., Albertini, E., et al. (2019). Characterization and discovery of miRNA and miRNA targets from apomictic and sexual genotypes of eragrostis curvula. *BMC Genomics* 20 (1), 1–13. doi: 10.1186/s12864-019-6169-0

García-Aguilar, M., Michaud, C., Leblanc, O., and Grimanelli, D. (2010). Inactivation of a DNA methylation pathway in maize reproductive organs results in apomixis-like phenotypes. *Plant Cell* 22 (10), 3249–3267. doi: 10.1105/tpc.109.072181

Gicking, A. M., Swentowsky, K. W., Dawe, R. K., and Qiu, W. (2018). Functional diversification of the kinesin-14 family in land plants. *FEBS Lett.* 592 (12), 1918–1928. doi: 10.1002/1873-3468.13094

Gounaris, E. K., Sherwood, R. T., Gounaris, I., Hamilton, R. H., and Gustine, D. L. (1991). Inorganic salts modify embryo sac development in sexual and aposporous cenchrus ciliaris. *Sexual Plant Reprod.* 4 (3), 188–192. doi: 10.1007/bf00190003

Grimanelli, D., Leblanc, O., Perotti, E., and Grossniklaus, U. (2001). Developmental genetics of gametophytic apomixis. *Trends Genet.* 17 (10), 597–604. doi: 10.1016/s0168-9525(01)02454-4

Grossniklaus, U. (2001). "From sexuality to apomixis: molecular and genetic approaches," in *The flowering of apomixis: From mechanisms to genetic engineering*, 168–211. Edited by Y. Savidan, J. G. Carman and T. Dresselhaus, Mexico D.F: CIMMYT, IRD, European Comission DG VI (FAIR).

Hand, M. L., and Koltunow, A. M. G. (2014). The genetic control of apomixis: Asexual seed formation. *Genetics* 197 (2), 441–450. doi: 10.1534/genetics.114.163105

Hanna, W. W., and Bashaw, E. C. (1987). Apomixis: Its identification and use in plant breeding 1. *Crop Sci.* 27 (6), 1136–1139. doi: 10.2135/cropsci1987.0011183x002700060010x

Higo, A., Saihara, N., Miura, F., Higashi, Y., Yamada, M., Tamaki, S., et al. (2020). DNA Methylation is reconfigured at the onset of reproduction in rice shoot apical meristem. *Nat. Commun.* 11 (1), 1–12. doi: 10.1038/s41467-020-17963-2

Higgins, D. M., Nannas, N. J., and Dawe, R. K. (2016). The maize divergent spindle-1 (dv1) gene encodes a kinesin-14A motor protein required for meiotic spindle pole organization. *Front. Plant Sci.* 7, 1277.

Honys, D., and Twell, D. (2004). Transcriptome analysis of haploid male gametophyte development in arabidopsis. *Genome Biol.* 5 (11), R85. doi: 10.1186/gb-2004-5-11-r85

Hussey, M. A., Bashaw, E. C., Hignight, K. W., and Dahmer, M. L. (1991). Influence of photoperiod on the frequency of sexual embryo saes in facultative apomictic buffelgrass. *Euphytica* 54 (2), 141–145. doi: 10.1007/bf00039600

Khanday, I., Skinner, D., Yang, B., Mercier, R., and Sundaresan, V. (2019). A male-expressed rice embryogenic trigger redirected for asexual propagation through seeds. *Nature* 565 (7737), 91–95. doi: 10.1038/s41586-018-0785-8

Kim, D., Paggi, J. M., Park, C., Bennett, C., and Salzberg, S. L. (2019). Graph-based genome alignment and genotyping with HISAT2 and HISAT-genotype. *Nat. Biotechnol.* 37 (8), 907–915. doi: 10.1038/s41587-019-0201-4

Klatt, S., Hadacek, F., Hodač, L., Brinkmann, G., Eilerts, M., Hojsgaard, D., et al. (2016). Photoperiod extension enhances sexual megaspore formation and triggers metabolic reprogramming in facultative apomictic ranunculus auricomus. *Front. Plant Sci.* 7. doi: 10.3389/fpls.2016.00278;

Klepikova, A. V., Kasianov, A. S., Gerasimov, E. S., Logacheva, M. D., and Penin, A. A. (2016). A high resolution map of the arabidopsis thaliana developmental transcriptome based on RNA-seq profiling. *Plant J.* 88 (6), 1058–1070. doi: 10.1111/tpj.13312

Koltunow, A. M., and Grossniklaus, U. (2003). Apomixis: A developmental perspective. *Annu. Rev. Plant Biol.* 54 (1), 547–574. doi: 10.1146/annurev.arplant.54.110901.160842

Koltunow, A. M. (1993). Apomixis: embryo sacs and embryos formed without meiosis or fertilization in ovules. *Plant Cell* 5 (10), 1425.

Langmead, B. (2010). Aligning short sequencing reads with bowtie. *Curr. Protoc. Bioinf.* 32, 11.7.1–11.7.14. doi: 10.1002/0471250953.bi1107s32

Leigh, J. H. (1960). Temperature, moisture and daylength effects in lovegrass (*Eragrostis curvula* (Schrad) nees). *S. Afr. J. Sci.* 56 (11), 268–269.

Livak, K. J., and Schmittgen, T. D. (2001). Analysis of relative gene expression data using real-time quantitative PCR and the 2–ΔΔCT method. *Methods* 25 (4), 402–408. doi: 10.1006/meth.2001.1262

Li, Z.-F., Zhang, Y.-C., and Chen, Y.-Q. (2015). miRNAs and lncRNAs in reproductive development. *Plant Sci.* 238, 46–52. doi: 10.1016/j.plantsci.2015.05.017

López-Galiano, M. J., Sentandreu, V., Martínez-Ramírez, A. C., Rausell, C., Real, M. D., Camañes, G., et al. (2019). Identification of stress associated microRNAs in *Solanum lycopersicum* by high-throughput sequencing. *Genes* 10 (6), 475. doi: 10.3390/genes10060475

Lorenz, R., Bernhart, S. H., Höner zu Siederdissen, C., Tafer, H., Flamm, C., Stadler, P. F., et al. (2011). ViennaRNA package 2.0. *Algorithms Mol. Biol.* 6 (1), 1–14. doi: 10.1186/1748-7188-6-26

Love, M. I., Huber, W., and Anders, S. (2014). Moderated estimation of fold change and dispersion for RNA-seq data with DESeq2. *Genome Biol.* 15 (12), 1–14. doi: 10.1186/s13059-014-0550-8

Marcus, A. I., Li, W., Ma, H., and Cyr, R. J. (2003). A kinesin mutant with an atypical bipolar spindle undergoes normal mitosis. *Mol. Biol. Cell* 14 (4), 1717–1726. doi: 10.1091/mbc.e02-09-0586

Martin, M. (2011). Cutadapt removes adapter sequences from high-throughput sequencing reads. *EMBnet.journal* 17 (1), p.10. doi: 10.14806/ej.17.1.200

Mau, M., Mandáková, T. M., Ma, X., Ebersbach, J., Zou, L., Lysak, M. A., et al. (2022). Evolution of an apomixis-specific allele class in supernumerary chromatin of apomictic boechera. *Front. Plant Sci.* 13. doi: 10.3389/fpls.2022.890038

Melo, C. A., and Melo, S. A. (2013). Biogenesis and physiology of MicroRNAs, Chapter 2, pp 5–24, in *Non-coding RNAs and Cancer*, Editor: M. Fabbri, Editorial: Springer, New York, NY doi: 10.1007/978-1-4614-8444-8_2

Nebenführ, A., and Dixit, R. (2018). Kinesins and myosins: Molecular motors that coordinate cellular functions in plants. *Annu. Rev. Plant Biol.* 69 (1), 329–361. doi: 10.1146/annurev-arplant-042817-040024

Nejat, N., and Mantri, N. (2018). Emerging roles of long non-coding RNAs in plant response to biotic and abiotic stresses. *Crit. Rev. Biotechnol.* 38 (1), 93–105. doi: 10.1080/07388551.2017.1312270

Neumeier, J., and Meister, G. (2021). siRNA specificity: RNAi mechanisms and strategies to reduce off-target effects. *Front. Plant Sci.* 11. doi: 10.3389/fpls.2020.526455

Nogler, G. A. (1984). Gametophytic apomixis. In: B.M. Johri (eds) *Embryology of Angiosperms*, (Berlin, Heidelberg: Springer). 475–518. doi: 10.1007/978-3-642-69302-1_10

Noirot, M., Couvet, D., and Hamon, S. (1997). Main role of self-pollination rate on reproductive allocations in pseudogamous apomicts. *Theor. Appl. Genet.* 95 (3), 479–483. doi: 10.1007/s001220050586

Ochogavía, A. C., Cervigni, G., Selva, J. P., Echenique, V. C., and Pessino, S. C. (2009). Variation in cytosine methylation patterns during ploidy level conversions in eragrostis curvula. *Plant Mol. Biol.* 70 (1-2), 17–29. doi: 10.1007/s11103-009-9454-5

Olmedo-Monfil, V., Durán-Figueroa, N., Arteaga-Vázquez, M., Demesa-Arévalo, E., Autran, D., Grimanelli, D., et al. (2010). Control of female gamete formation by a small RNA pathway in arabidopsis. *Nature* 464 (7288), 628–632. doi: 10.1038/nature08828

Ortiz, J. P. A., Leblanc, O., Rohr, C., Grisolia, M., Siena, L. A., Podio, M., et al. (2019). Small RNA-seq reveals novel regulatory components for apomixis in *Paspalum notatum*. *BMC Genomics* 20 (1), 1–17. doi: 10.1186/s12864-019-5881-0

Palatnik, J. F., Allen, E., Wu, X., Schommer, C., Schwab, R., Carrington, J. C., et al. (2003). Control of leaf morphogenesis by microRNAs. *Nature* 425 (6955), 257–263. doi: 10.1038/nature01958

Pikaard, C. S., and Scheid, M. O. (2014). Epigenetic regulation in plants. *Cold Spring Harbor Perspect. Biol.* 6 (12), a019315–a019315. doi: 10.1101/cshperspect.a019315

Poethig, R. S. (2010). The past, present, and future of vegetative phase change. *Plant Physiol.* 154 (2), 541–544. doi: 10.1104/pp.110.161620

Richardson, D. N., Simmons, M. P., and Reddy, A. S. (2006). Comprehensive comparative analysis of kinesins in photosynthetic eukaryotes. *BMC Genomics* 7 (1), 1–37. doi: 10.1186/1471-2164-7-18

Ripoll, J. J., Bailey, L. J., Mai, Q.-A., Wu, S. L., Hon, C. T., Chapman, E. J., et al. (2015). microRNA regulation of fruit growth. *Nat. Plants* 1 (4), 1–9. doi: 10.1038/nplants.2015.36

Rodrigo, J. M., Zappacosta, D. C., Selva, J. P., Garbus, I., Albertini, E., and Echenique, V. (2017). Apomixis frequency under stress conditions in weeping lovegrass (Eragrostis curvula). *PloS One* 12 (4), e0175852. doi: 10.1371/journal.pone.0175852

Ru, P., Xu, L., Ma, H., and Huang, H. (2006). Plant fertility defects induced by the enhanced expression of microRNA167. *Cell Res.* 16 (5), 457–465.

Sakai, H., Mizuno, H., Kawahara, Y., Wakimoto, H., Ikawa, H., Kawahigashi, H., et al. (2011). Retrogenes in rice (*Oryza sativa* l. ssp. japonica) exhibit correlated expression with their source genes. *Genome Biol. Evol.* 3, 1357–1368. doi: 10.1093/gbe/evr111

Schattner, S., Schattner, J., Munder, F., Höppe, E., and Walter, W. J. (2021). A tug-of-War model explains the saltatory sperm cell movement in *Arabidopsis*

thaliana pollen tubes by kinesins with calponin homology domain. *Front. Plant Sci.* 11. doi: 10.3389/fpls.2020.601282

Schmidt, A. (2020). Controlling apomixis: Shared features and distinct characteristics of gene regulation. *Genes* 11 (3), 329. doi: 10.3390/genes11030329

Schwab, R., Palatnik, J. F., Riester, M., Schommer, C., Schmid, M., and Weigel, D. (2005). Specific effects of MicroRNAs on the plant transcriptome. *Dev. Cell* 8 (4), 517–527. doi: 10.1016/j.devcel.2005.01.018

Selva, J. P., Siena, L., Rodrigo, J. M., Garbus, I., Zappacosta, D., Romero, J. R., et al. (2017). Temporal and spatial expression of genes involved in DNA methylation during reproductive development of sexual and apomictic. *Eragrostis curvula. Sci. Rep.* 7 (1), 1–11. doi: 10.1038/s41598-017-14898-5

Selva, J. P., Zappacosta, D., Carballo, J., Rodrigo, J. M., Bellido, A., Gallo, C. A., et al. (2020). Genes modulating the increase in sexuality in the facultative diplosporous grass *Eragrostis curvula* under water stress conditions. *Genes* 11 (9), 969. doi: 10.3390/genes11090969

Smita, S., Robben, M., Deuja, A., Accerbi, M., Green, P. J., Subramanian, S., et al. (2021). Integrative analysis of gene expression and miRNAs reveal biological pathways associated with bud paradormancy and endodormancy in grapevine. *Plants* 10 (4), p.669. doi: 10.3390/plants10040669

Sunkar, R., and Zhu, J.-K. (2004). Novel and stress-regulated MicroRNAs and other small RNAs from Arabidopsis[W]. *Plant Cell* 16 (8), 2001–2019. doi: 10.1105/tpc.104.022830

Tian, S., Jiang, J., Xu, G., Wang, T., Liu, Q., Chen, X., et al. (2021). Genome wide analysis of kinesin gene family in *Citrullus lanatus* reveals an essential role in early fruit development. *BMC Plant Biol.* 21 (1), 1–16. doi: 10.1186/s12870-021-02988-6

Umezu, N., Umeki, N., Mitsui, T., Kondo, K., and Maruta, S. (2011). Characterization of a novel rice kinesin O12 with a calponin homology domain. *J. Biochem.* 149 (1), 91–101. doi: 10.1093/jb/mvq122

Underwood, C. J., Vijverberg, K., Rigola, D., Okamoto, S., Oplaat, C., den Camp, R. H. M. O., et al. (2022). A PARTHENOGENESIS allele from apomictic dandelion can induce egg cell division without fertilization in lettuce. *Nat. Genet.* 54 (1), 84–93. doi: 10.1038/s41588-021-00984-y

Vijverberg, K., and van Dijk, P. J. (2007). Genetic linkage mapping of apomixis loci, In: E. Hörandl, U. Grossniklaus, P. J. van Dijk and T. F. Sharbel, eds. *Apomixis: evolution, mechanisms and perspectives*. Vienna, Austria: International Association for Plant Taxonomy, 137–158.

Voigt, P. W., and Burson, B. L. (1983). "Breeding of apomictic eragrostis curvula," in *Proceedings of the XIV international grassland congress* (CRC Press), 160–163.

Wang, J.-W. (2014). Regulation of flowering time by the miR156-mediated age pathway. *J. Exp. Bot.* 65 (17), 4723–4730. doi: 10.1093/jxb/eru246

Wei, J.-W., Huang, K., Yang, C., and Kang, C.-S. (2017). Non-coding RNAs as regulators in epigenetics (Review). *Oncol. Rep.* 37 (1), 3–9. doi: 10.3892/or.2016.5236

Woodger, F. J., Millar, A., Murray, F., Jacobsen, J. V., and Gubler, F. (2003). The role of GAMYB transcription factors in GA-regulated gene expression. *J. Plant Growth Regul.* 22 (2), 176–184. doi: 10.1007/s00344-003-0025-8

Wu, G., and Poethig, R. S. (2006). Temporal regulation of shoot development in *Arabidopsis thaliana* by miR156 and its target SPL3. *Development* 133 (18), 3539–3547. doi: 10.1242/dev.02521

Xing, S., Salinas, M., Garcia-Molina, A., Höhmann, S., Berndtgen, R., and Huijser, P. (2013). SPL 8 and mi R 156-targeted SPL genes redundantly regulate A rabidopsis gynoecium differential patterning. *Plant J.* 75 (4), 566–577.

Zappacosta, D., Gallardo, J., Carballo, J., Meier, M., Rodrigo, J. M., Gallo, C. A., et al. (2019). A high-density linkage map of the forage grass *Eragrostis curv*ula and localization of the diplospory locus. *Front. Plant Sci.* 10. doi: 10.3389/fpls.2019.00918

Zappacosta, D. C., Ochogavía, A. C., Rodrigo, J. M., Romero, J. R., Meier, M. S., Garbus, I., et al. (2014). Increased apomixis expression concurrent with genetic and epigenetic variation in a newly synthesized *Eragrostis curvula* polyploid. *Sci. Rep.* 4 (1), 1–7. doi: 10.1038/srep04423

Zheng, C., Ye, M., Sang, M., and Wu, R. (2019). A regulatory network for miR156-SPL module in *Arabidopsis thaliana*. *Int. J. Mol. Sci.* 20 (24), 6166. doi: 10.3390/ijms20246166

Zhu, C., and Dixit, R. (2012). Functions of the arabidopsis kinesin superfamily of microtubule-based motor proteins. *Protoplasma* 249 (4), 887–899. doi: 10.1007/s00709-011-0343-9

frontiers | Frontiers in Plant Science

TYPE Original Research
PUBLISHED 03 October 2022
DOI 10.3389/fpls.2022.999031

OPEN ACCESS

EDITED BY
Gianni Barcaccia,
University of Padua, Italy

REVIEWED BY
Handong Su,
Huazhong Agricultural University, China
Ravi Maruthachalam,
Indian Institute of Science Education and Research, Thiruvananthapuram, India

*CORRESPONDENCE
Mengliang Cao
mlcao@hhrrc.ac.cn

†These authors have contributed equally to this work and share first authorship

SPECIALTY SECTION
This article was submitted to Plant Breeding, a section of the journal Frontiers in Plant Science

RECEIVED 26 July 2022
ACCEPTED 16 September 2022
PUBLISHED 03 October 2022

CITATION
Xia Y, Wang Y, Hu Y, Zhan Y, Dan J, Tang N, Tian J and Cao M (2022) Double-seedlings and embryo-free seeds generated by genetic engineering.
Front. Plant Sci. 13:999031.
doi: 10.3389/fpls.2022.999031

Double-seedlings and embryo-free seeds generated by genetic engineering

Yumei Xia[1,2†], Yao Wang[3†], Yuanyi Hu[1,2†], Yijie Zhan[3], Junhao Dan[3], Ning Tang[1], Junyou Tian[3] and Mengliang Cao[1,2,3*]

[1]State Key Laboratory of Hybrid Rice, Hunan Hybrid Rice Research Center, Changsha, China, [2]National Center of Technology Innovation for Saline-Alkali Tolerant Rice in Sanya, Sanya, China, [3]Long Ping Branch, Graduate School of Hunan University, Changsha, China

Apomixis can fix the heterosis of Hybrid F_1, by maintaining its heterozygous genotype, and is an ideal way for the development of hybrid rice. In this paper, we designed an engineering strategy for realizing apomictic reproduction of hybrid rice in the way of induce adventitious embryos. An embryogenesis gene, *AtWUS*, controlled by the ovule-specific promoter, a ribonuclease gene *Barnase* driven by the egg cell-specific promoter *pDD45*, and an inactivation gene *ZmAA1* driven by the pollen-specific promoter *pG47* were simultaneously integrated into one T-DNA, and co-transformed with the second T-DNA carrying a *Barstar* gene. Double-seedlings were observed in transgenic line. Whole-genome sequencing and ploidy levels confirmed by flow cytometry showed that one of the double-seedlings was heterozygous diploid and the other seedling was homozygous haploid, which confirmed that embryogenesis in one of the double-seedlings arises from the zygote after fertilization and the other derived from an unfertilized gamete. Meanwhile we obtained embryo-free seeds at frequencies of 2.6% to 3.8% in T_1 generation, and 0.75% to 3% in T_2 generation. Though we did not obtained adventitious embryos in hybrid rice in this study, the phenomenon of double-seedlings and embryo-free seeds in transgenic line was informative and strongly suggested that endosperm development is an autonomously organized process in rice, independent of egg cell fertilization and embryo-endosperm communication. This provides novel insights into the induction of haploid embryos and lends theoretical support to successful clonal propagation using synthetic apomixis

KEYWORDS

apomixis, polyembryony, embryo-free seeds, haploid, endosperm development

Introduction

The wide commercial application of 'three-line' and 'two-line' hybrid rice has helped to guarantee the absolute grain security for 1.4 billion people in China (Ren et al., 2016; Mou, 2016). 'one-line' hybrid rice which could fix rice heterosis by means of apomictic reproduction and significantly reduce the cost of seed production, is the development direction of hybrid rice (Yuan, 2018).

Apomixis is an asexual propagation method through seeds in which the embryo is formed without the nuclear fusion of male and female gametes (Jia et al., 2015). In nature, apomixis and sexual reproduction could coexist in some apomictic species, such as *Hieracium*. when the sexual reproduction pathway fails, the expression of apomixis genes will be initiated, and the latter is an altered form of sexual reproduction (Catanach et al., 2006; Barcaccia and Albertini, 2013).

Apomictic pathway could be divided into either reduced gametophytic apomixis or diploid apomixis (Mu et al., 2001), the latter has been termed diplospory, apospory, and adventitious embryony (Koltunow, 1993; Mu et al., 2001; Conner et al., 2015). Somatic ovule cells that surround the embryo sac differentiate and have an embryogenic cell fate. With appropriate technical measures, somatic ovule cells of sexual plant might turn sexual reproduction into apomictic reproduction by aborting the egg cells and forming adventitious embryos.

Several genes, such as *BBM* (Boutilier et al., 2002; Anderson et al., 2017), *LEC* (Lotan et al., 1998; Kwong et al., 2003), and *WUS* (Mayer et al., 1998; Schoof et al., 2000) that could induce somatic embryogenesis in plants had been cloned in recent years. The *WUSCHEL* gene regulates the balance between stem cell proliferation and differentiation (Nardmann and Werr, 2006). Meanwhile, *WUS* is essential for regulating the growth of the stomium and septal cells during anther development, and for ovule development in *Arabidopsis* (Gros-Hardt et al., 2002; Deyhle et al., 2007). Upregulating *AtWUS* expression promotes somatic embryonic transition in Arabidopsis (Zuo et al., 2002), and improves regeneration of transgenic monocots (Gordon-Kamm et al., 2019), All these studies indicated that ectopically expressed *WUS* is able to transform tissues that are in a vegetative growth state into tissues with embryonic stem cell characteristics.

In this study, we first constructed one T-DNA containing three linked gene expression cassettes. The cassettes contained 1) the ribonuclease gene *Barnase* driven by the egg cell-specific promoter *AtDD45*, 2) the embryogenic gene *AtWUS* controlled by a somatic ovule cell-specific promoter, and 3) an inactivation gene *ZmAA1* driven by the pollen-specific promoter *pG47*. The second T-DNA carrying the *Barnase*-specific antagonist protein *Barstar* to inhibit the background expression of *Barnase* was constructed and then co-transformed with the first T-DNA into hybrid rice. We aimed to establish an engineering system by aborting the egg cells and forming adventitious embryos from somatic ovule cells such as the integument *via* expression of an embryogenic gene.

This study is a new exploration of a facultative apomictic reproductive system in hybrid rice. If this reproductive pathway transformation can occur in rice, it will provide a novel breakthrough for 'one-line' hybrid rice and will be valuable for fixing heterosis *via* synthetic apomixis in crops.

Results

Rationale of the experimental design

In order to induce somatic embryos and establish asexual reproduction, we constructed the p22W vector for *A. tumefaciens* with three expression cassettes in one T-DNA (Figure 1A): (1) the maize a-amylase gene *ZM-AA1* with the amyloplastic signal peptides under control of the pollen-specific *pG47* promoter to disrupt transgenic pollen production, which we have characterized previously (Xia et al., 2019); (2) the *Barnase* gene from *Bacillus amyloliquefaciens* that encodes a 12 kD small extracellular ribonuclease driven by the *Arabidopsis* egg cell-specific promoter *pDD45* to cause the death of egg cells (Steffen et al., 2007; Khanday et al., 2019); and (3) the *AtWUS* CDS under control of the rice ovule-specific promoter *Os02g51090* (Seagan and Lovett, 2014). We also introduced a *Barstar* expression cassette into the second T-DNA for transformation to inhibit the background expression of *Barnase* (Figures 1A, B). The *Barstar* gene encodes a *Barnase*-specific antagonist protein that is able to bind *Barnase*, rendering bacterially-expressed *Barnase* without enzymatic activity.

When the three cassettes are transformed into rice cells for designed genome engineering, the *ZM-AA1* cassette disrupts starch accumulation only in the transgenic pollen grains so that the transgenic pollen grains produced by the hemizygous transgenic plant are defective. In the absence of *Barstar*, the expression of *Barnase* usually causes host cell death, and ectopically expressed *AtWUS* will direct somatic cells into embryony, while the non-transgenic pollen grains are viable for pollination. The resulting transgenic plant produces male gametes (MG) of one genotype and female gametes (FG) of two genotypes. In the process of self-pollination, the nucellus cells form asexual embryos; egg cells, and sperm cells without the transgene form zygotic embryos, and the sperm cells without transgenes combine with the central cell to form endosperm, theoretically generating a 1:1 ratio of somatic embryos with transgenes and zygotic embryos without transgenes (Figure 1C).

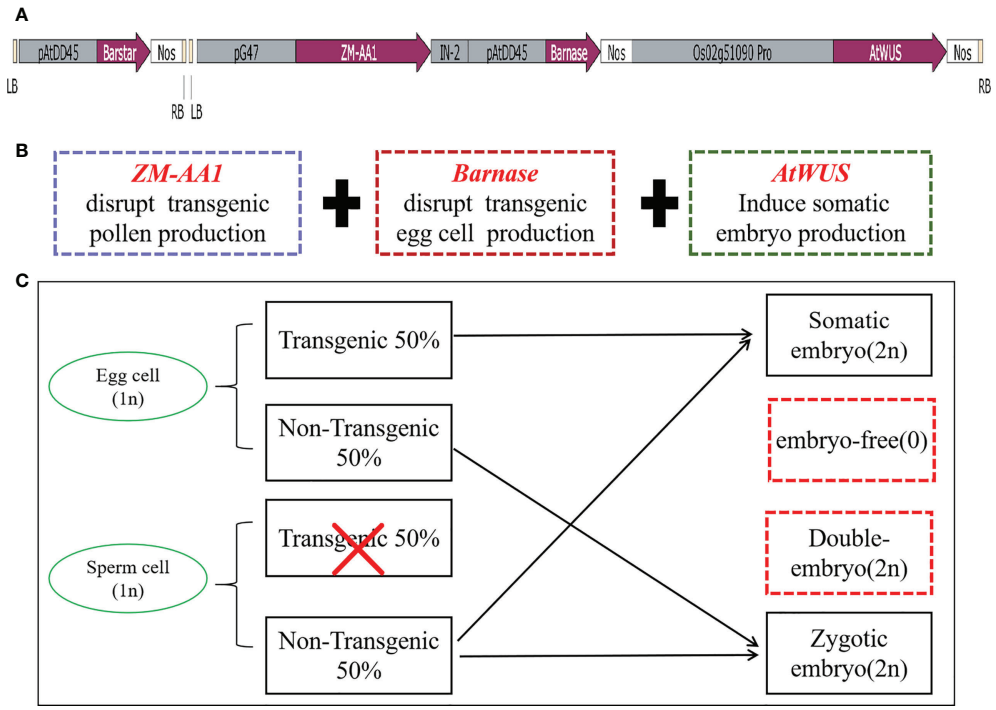

FIGURE 1
The transformation vector and model of the asexual seed propagation system. **(A)** Schematic diagram of the p22W vector construct containing two T-DNA regions. LB, left T-DNA border; pAtDD45, Arabidopsis DD45 promoter; Barstar, *Barstar* gene; NOS, nopaline synthase terminator; RB, right T-DNA border; pG47, pG47 promoter; ZM-AA1, *ZM-AA1* gene; IN-2, IN-2 terminator; Barnase, *Barnase* gene; Os02g51090pro, Os02g51090 promoter; AtWUS, Arabidopsis *WUS* gene. **(B)** The function of the three gene expression cassettes in the T-DNA. **(C)** Schematic model for generating asexual seed propagation in hybrid rice.

Ectopic expression of the *AtWUS* gene induced double-seedlings in transgenic hybrid rice

The vector p22W was transformed into the rice hybrid 9Y using an *Agrobacterium*-mediated method. Seeds from transgenic line which contained *AtWUS* gene (hereafter trans-line) were obtained for germination. Some seeds could grow two buds and roots independently in trans-line, and were called double-seedlings (Figure 2A). The induction frequency of double-seedling was 0.11% to 0.13% in T_1 generation and 0.21% to 0.45% in T_2 generation. While, no double-seedlings were observed in wild-type 9Y (Supplemental Table 1). The single-seedling isolated from the double-seedlings also generate double-seedlings in subsequent generations. This showed that single-seedlings and double-seedlings contain the same genetic factors to develop into double-seedlings. The embryogenic calli structures were found on the third leaf onwards of adult seedlings (Figure 2B), these findings are similar to ectopic expression of *BBM1* in rice (Khanday et al., 2019).

PCR amplification of the *AtWUS* and *Barstar* genes was then carried out in trans-line plants. Among the 85 analyzed T_1 progeny from trans-line, 28 of the seedlings were found to contain *AtWUS*, and *Barstar* gene. Among the 81 analyzed T_2 progeny from different family, 22 of the seedlings were found to contain both the *AtWUS* and *Barstar* genes (Supplemental Figure1A and Supplemental Table 1). Double-seedlings were *AtWUS* and *Barstar* gene transformation positive from trans-line.

To demonstrate the genetic origin of the double-seedlings, we performed whole-genome sequencing on a diploid F_1 wild-type 9Y plant, 22 T_1 progeny plants including two double-seedlings, 20 single-seedlings, and a control untransformed F_2 plant, 22 T_2-generation progeny plants including five double-seedlings, ten single-seedlings, and an untransformed F_3 control plant (Raw sequence data of these samples have been deposited in NCBI Short Read Archive with access number PRJNA870060). Analysis of sequence variants identified 1,302 SNPs in unique sequences distributed across the genome in the wild-type 9Y (Figure 2C). The 1,302 SNPs were determined to be

10.3389/fpls.2022.999031

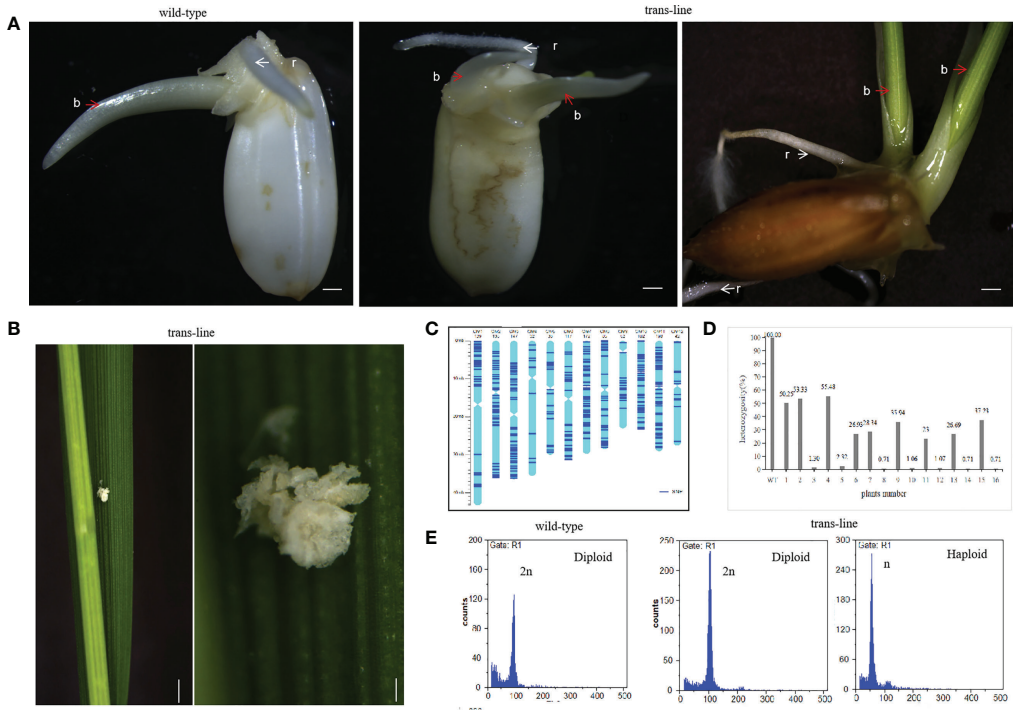

FIGURE 2
Recovery of double-seedlings in transgenic hybrid rice. **(A)** Seedlings in the wild-type (left; n=30) is normal with one bud (b; red arrow) and one root (r; white arrow). Double-seedlings in T_1-generation (n=2; middle) and T_2-generations (n=12; right) of could grown two buds(b; red arrow) and roots (r; white arrow) in trans-line. Scale bars, 1 mm. **(B)** Somatic embryo-like structures induced by *AtWUS* ectopic expression in trans-line leaves (n=20; left). Scale bars, 1 cm. The insets show magnified views of the somatic embryos (right). scale bars, 0.5 mm. **(C)** Determination of the genotype of wild-type 9Y using whole genome sequencing. The frame of each chromosome was constructed based on the *Oryza sativa* ssp. *japonica* genome version 6.0, with the scale on the left showing the length of the chromosome (Mb) and the names of the chromosomes shown across the top of the figure. The heterozygous SNP sites (AB) are marked in dark blue. **(D)** Genotyping analysis of trans-line. The plants are shown on the x-axis and the y-axis shows the heterozygosity. Wild-type 9Y (WT), F_1 generation (1) and F_2 generation progenies of 9Y (6) as control, double-seedlings from T_1-generation (n=2; 2-5) and T_2-generation (n=5; 7-16) were analysed. **(E)** Ploidy analysis of wild-type is diploid (n=3; left), one seedling of double-seedlings in trans-line is diploid (n=5; middle) and the other is haploid (n=5; right) by flow cytometry. The x-axis is the measure of relative fluorescence and the y-axis shows the number of nuclei.

heterozygous in control wild-type 9Y, and the heterozygosity of the wild-type was therefore set at 100%. The probability of F_2 progeny from 9Y plant retaining heterozygosity by random segregation for just one SNP is P=50%, the heterozygosity of any single F_3 progeny plant is P=25%. The maintenance of heterozygosity at all 1,302 SNPs on the different chromosomes by random segregation is $P=(0.5)^{1302} = 0$. All of the progeny were not contain the heterozygous genotype as wild-type 9Y, which means that no seeds with somatic embryo were obtained. The heterozygosity of double-seedlings were 53.33% to 55.48%, and another was 1.30% to 2.32% in T_1-generation. The heterozygosity of double-seedlings were from 23% to 37.23%, and another were 0.71 to 1.07% in T_2-generation (Figure 2D). These data suggest that one of double-seedlings is heterozygous arises from the zygote after fertilization, and that another is homozygous. The ploidy levels of the above double-seedlings were confirmed by flow cytometry; one shoot is diploid and the other shoot is haploid (Figure 2E), which confirms that embryogenesis in double-seedlings arises from the zygote after fertilization and the other shoot is derived from an unfertilized gamete.

Two plants from double-seedling were cultivated separately. Morphologies of the diploid and haploid were different at the heading stage and at maturity, haploids were more lower than diploid obviously (Figures 3A, B). We identified haploids by their small size compared with their diploid siblings as well as by their flowers. Due to defective meiosis, the haploids are sterile and the diploids were fertile with normal anther development (Figures 3C, D). Thus, ectopic expression of the *AtWUS* gene in the ovule is sufficient for the production of haploid plants. The diploids carry a non-identical set of alleles to the F_1 mother plant, confirming that one of the double-seedlings (diploid) is generated by sexual reproduction and the other (haploid) is generated by asexual reproduction.

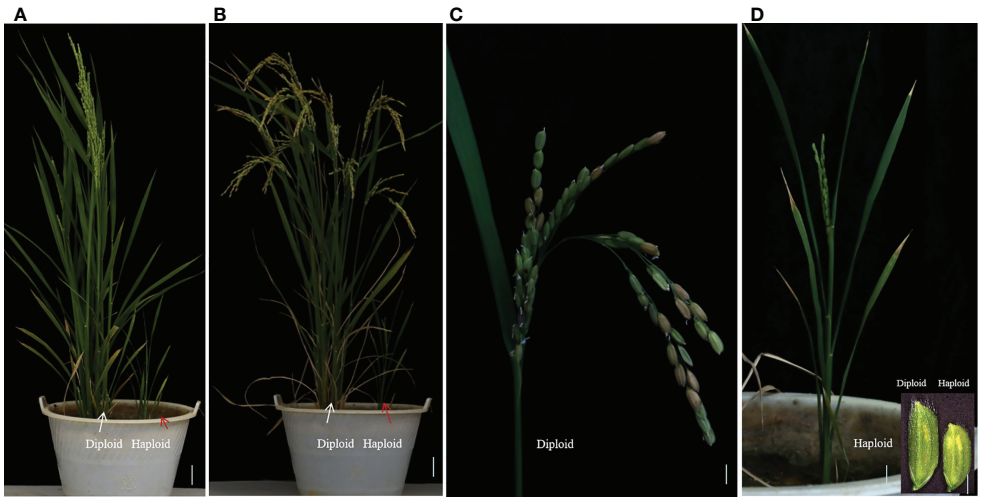

FIGURE 3
Characterization of double-seedlings in transgenic hybrid rice. **(A, B)** Two plants from double-seedlings are cultivated separately, Morphologies of the diploid (left; white arrow) and haploid (right; red arrow) is different at the heading stage **(A)** and at maturity. **(B)** Scale bars, 5 cm. **(C)** Panicle of the diploid in B is fertile. Scale bar, 2 cm. **(D)** panicle of haploid in B is sterile, and floret sizes of the diploid is larger than that of haploid plants. Scale bar, 2 cm. Inset scale bars, 2 mm.

Endosperm development is an autonomously programmed process in transgenic line

During plant sexual reproduction, a double fertilization event initiates embryo and endosperm formation. The embryos are readily observed in normal seeds (Figure 4A). After pre-germination treatment, the embryos start to germinate, but embryo-free seeds only contain endosperm and do not germinate after pre-germination (Figure 4B). *Barnase* gene expression cassette causes the death of the egg cell, and self-pollination of trans-line results in embryo-free seeds. We obtained embryo-free seeds at frequencies of 2.6% to 3.8% due to single fertilization in T_1 generation, and 0.75% to 3% in the T_2 generation, no embryo-free seeds were observed in wild-type 9Y (Supplemental Table 1). This showed that contain the same genetic factors to develop into embryo-free seeds.

Embryo and endosperm were observed in wild-type after a cross-section of the seeds, but just endosperm was observed with embryo-free seeds in trans-line (Figures 5A, B). Embryos showed normal development only in wild-type (Figure 5C). Endosperm turned into black when stained with I_2-KI in wild-type and trans-line (Figure 5D). Development of embryo was not observed in carpels of the plant in trans-line at 3 days after pollination (DAP), or show normal development. In control wild-type, the development of both embryo and endosperm in carpels (3DAPs) were observed (Figure 5E).

We identified embryo-free seeds by PCR amplification of the *AtWUS* gene, the transgene positive rate for detecting the *AtWUS* gene in embryo-free seeds was 91.3%. But the transgene-positive rate was 34.78% in T_1 progeny normal seeds from trans-line (Figures 4C, D). These results showed that embryo-free seeds were caused by transformation and carry the cassette: *Barnase* gene driven by the egg cell specific promoter *AtDD45*, which was lethal, so the egg cell was unable to form an embryo. However, the polar nuclei undergo fertilization to form normal endosperm in the embryo-free seeds. This showed that endosperm development is an autonomously programmed process that is independent of embryo formation.

Discussion

Apomixis not only accelerates breeding procedures and the fixation of heterosis but also enables farmers to reduce investment and receive more benefits. From the developmental perspective, most natural apomixis is classified as facultative, because it involves both sexual and asexual modes of reproduction for the advancement of generations; hence, apomixis is widely thought to be a controlled or deviant form of sexual reproduction (Hand and Koltunow, 2014; Susmita et al., 2021; (Van Dijk et al., 1999). This theory suggested that if the sexual pathway is not initiated in an ovule, the apomixis pathway remains functional to form embryos. Apomictic reproduction requires the formation of embryos containing somatic chromosomes without fertilization and the development of endosperm either with or without fertilization.

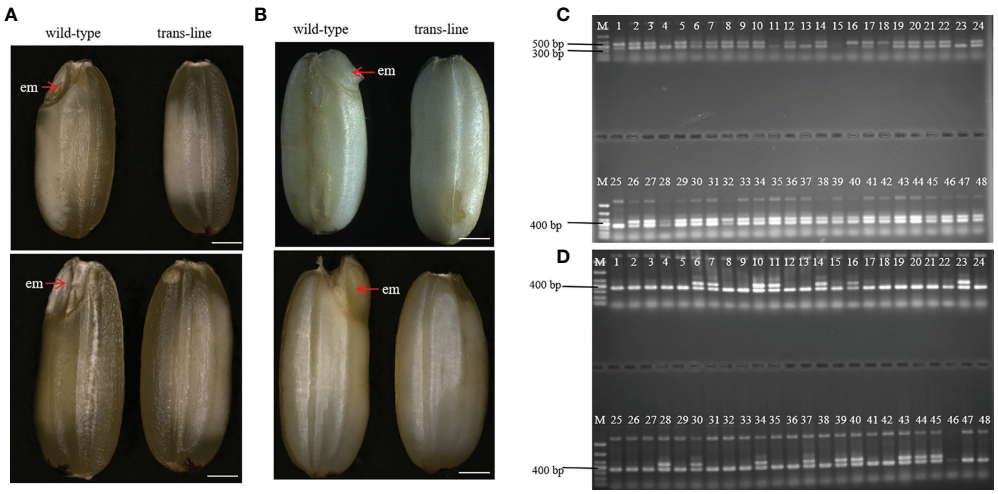

FIGURE 4
Identification and characterization of embryo-free seeds. **(A)** embryo-free seeds in trans-line and normal seeds in control wild-type are different in seed phenotype. Normal seeds with the embryo (em; red arrow) in control wild type (n=1000; left), but not in embryo-free seeds (n=59/1800; right). Scale bars, 1mm. **(B)** The embryo is germinated after the pre-germination treatment on normal seeds (left) and nothing changed in embryo-free seeds (right). Scale bars, 1 mm. **(C)** PCR detection of embryo-free seeds from trans-line, positive transgenic plantlets (lane 1) gave both a 456 bp fragment from *AtWUS* and a 364 bp fragment from the internal control *OSD1* gene. The 456 bp fragment from the *AtWUS* gene is not present in the control wild-type 9Y genome (lane 25), 91.3% percent of embryo-free seeds are transgene positive in trans-line (n=42/46; lanes 2-24, lanes 26-48). **(D)** Wild-type 9Y genome(lane 1, lane25) gave just a 364 bp fragment from the internal control *OSD1* gene. The 456 bp fragment from the *AtWUS* gene is amplified just at the percentage of 34.78% from normal seeds in trans-line (n=16/46; lanes 2-24, lanes 26-48).

In the case of adventitious embryony, non-zygotic embryos are formed outside the embryo sac and co-exist with sexual reproduction, because the sexual and asexual embryos share the nutritive endosperm produced from the sexual pathway for survival. Therefore, a seed containing multiple embryos is termed polyembryony (Hand and Koltunow, 2014).

In this study, double-seedlings were observed in transgenic line. one of double-seedlings was heterozygous diploid and the other seedling was homozygous haploid, which confirms that embryogenesis in double-seedlings arised from the zygote after fertilization and the other derived from an unfertilized gamete. *AtWUS* plays a key role in the occurrence of embryogenesis without fertilization. Thus, we guess other cells of the embryo sac such as synergids can develop into haploid embryo by expression of *AtWUS* gene driven by *Os02g51090* promoter, and it share the endosperm with the diploid embryo resulting from fertilization of egg cell and sperm cell. The plant of haploid is sterile and much smaller than that of diploid, when pre-germination in double-embryo seeds, haploid embryo can not compete with diploid embryo and death, this maybe why we observed double-seedlings at a low frequency.

In many other apomictic species, the development of functional endosperm takes place only when the pollen fertilizes the polar nuclei without egg cell fertilization (Bicknell and Koltunow, 2004). Rice is a sexually reproducing plant, and development of embryo-free seeds relies on the presence of haploid pollen that assures single fertilization and normal endosperm development. Embryo-free seeds obtained showed that in the absence of an embryo, endosperm can development normally as in the wild-type (Figure 5). These findings are similar to those previously reported in *Arabidopsis* (Xiong et al., 2021).

We suppose in this genetically regulated reproductive process, the egg cell develops into an embryo with fertilization and other cells of the embryo sac such as synergids develop into an embryo autonomously due to the ectopic expression of *AtWUS*, resulting in polyembryony. Because expression of *Barnase* in the egg cell causes a lethal egg cell and single fertilization occurs between the pollen and the polar nuclei without egg cell fertilization, resulting in embryo-free seeds (Figure 6).

The feasibility of fixing diploid clonal propagation of rice hybrids through seeds has been demonstrated by the MiMe strategy (Khanday et al., 2019; Wang et al., 2019). Hence, we are trying another engineering strategy for realizing apomictic reproduction of hybrid rice in the way of induce adventitious embryos. Though we did not obtained adventitious embryos in hybrid rice in this study, but the phenomenon of double-seedlings and embryo-free seeds in transgenic line were informative and strongly suggested that endosperm development is an autonomously organized process in rice. Nevertheless, the methods described here for asexual

10.3389/fpls.2022.999031

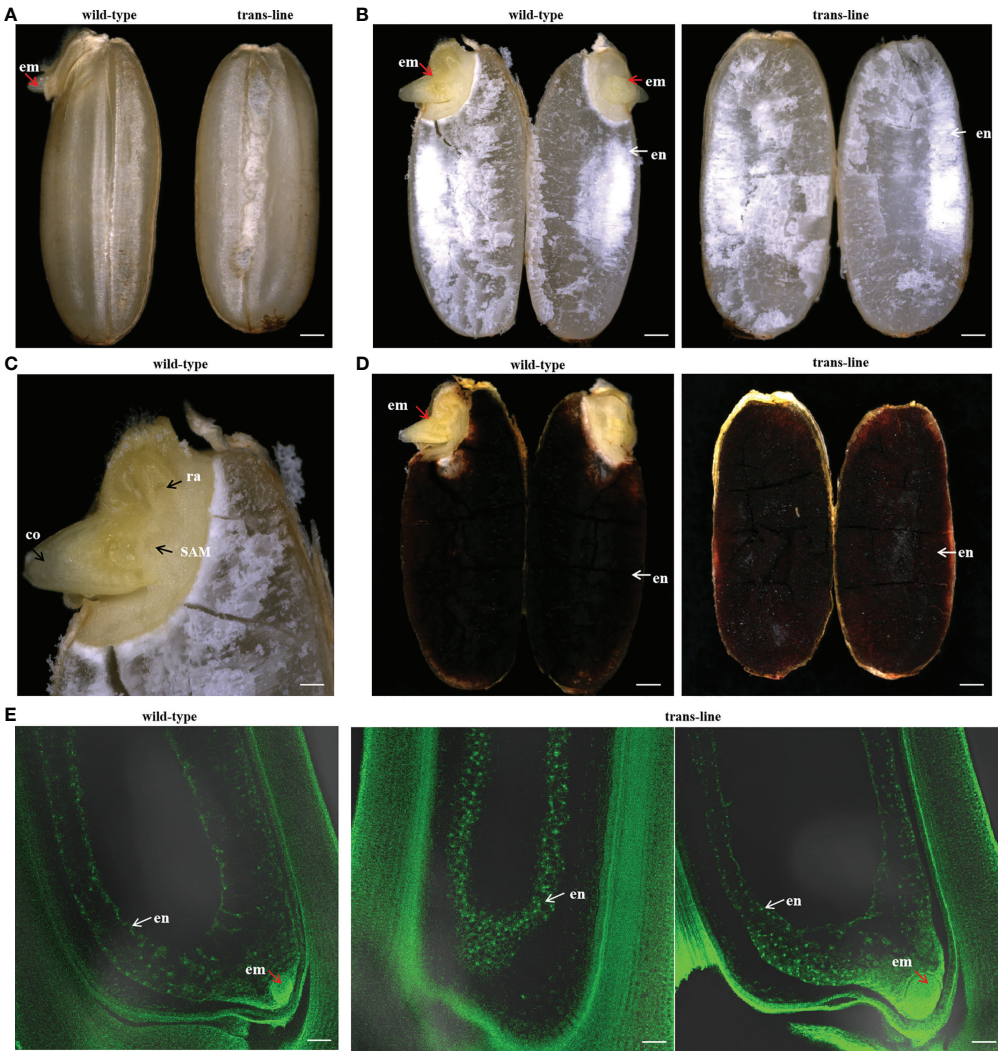

FIGURE 5
Development of embryo-free seeds in transgenic line. **(A)**Seeds were germinated normally with embryos (left; red arrow) one day after pre-germinated in wild-type 9Y (n=20), but embryo-free seeds without the germination of embryos formation (n=10/10; right) one day after pre-germinated in trans-line. Scale bars, 0.7 mm. **(B)** Embryo (left; em; red arrow) and endosperm (left; en; white arrow) are observed after a cross-section of seeds in wild-type (n=10; left), but just endosperm (right; white arrow) is observed with embryo-free seeds in trans-line (n=10; right). Scale bars, 0.7 mm. **(C)** Embryos show normal development in wild-type (n=10), co, coleoptile; ra, radicle; SAM, shoot apical meristerm. Scale bars, 0.25 mm. **(D)** Endosperm turned into black when is staining with I_2-KI in control wild-type (n=10; left) and trans-line(n=10; right). Scale bars, 0.7mm. **(E)** Development of embryo is not observed in carpels (n=1/20; middle) of the plant in trans-line at 3 days after pollination (DAP), or show normal development (n=19/20; right). In fertilized control wild-type carpels, the development of both embryo and endosperm in carpels (3DAPs) is observed (n=20; left). Scale bars, 35 μm.

propagation shed new light on the use of agro-biotechnology for crop improvement. Expressing of *AtWUS* gene will have further application for haploid induction to rapidly obtain homozygous lines for crop breeding such as maize and wheat.

To engineer a completely asexual system involving autonomous endosperm formation is essential in a sexually reproducing crop. Whereas embryo formation may or may not require fertilization. Our findings will also provide further support for successful clonal propagation in synthetic apomixis.

Materials and methods

Plant materials and growth conditions

The hybrid rice (*Oryza sativa*) variety 9You 418 (9Y) is widely grown and is relatively easy to transform for a hybrid, so it was used as the transgenic acceptor in this study and as a wild-type (WT) control. The WT control was grown in a paddy field in the city of Changsha during the natural rice-growing seasons

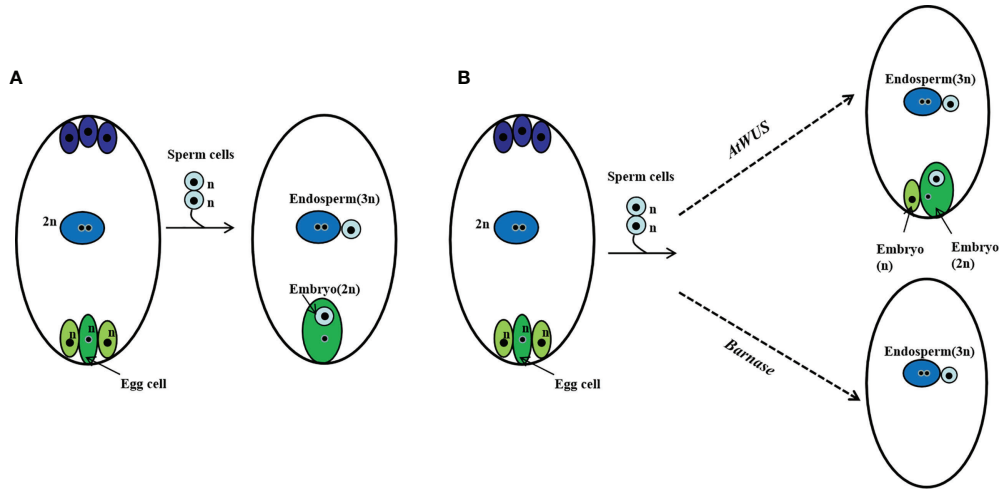

FIGURE 6
Schematic representation of polyembryony and embryo-free seed production. **(A)** Normal sexual reproduction and gamete fusion give rise to diploid progeny and triploid endosperm. **(B)** Ectopic expression of *AtWUS* induces other cells in the embryo sac to form embryos, the endosperm forms by fertilization of the central cell by a sperm cell. Asexual and sexual embryos share the endosperm formed during polyembryony. Ectopic expression of *Barnase* in the egg cell induces pollen single fertilization resulting in an embryo-free seed.

and maintained regularly. All lines created in this study were developed in the 9Y background. T_0-, T_1-, and T_2-generation lines were grown in pots in the greenhouse.

Plasmid construction and plant transformation

Left and right boundary sequences and multiple cloning sites were synthesized as oligonucleotides and ligated into pCAMBIA1300 (CAMBIA, Canberra, Australia) at the unique *Sac* II restriction enzyme site, generating the pC01 vector. The *Zm-AA1* expression cassette was excised as a single fragment by *Hind* III digestion from pFS4-11 (Xia et al., 2019), and was inserted into the pC01 vector that contained two T-DNA regions, generating pC02. The *Barstar* gene was inserted downstream of the *Arabidopsis DD45* promoter and upstream of the nopaline synthase terminator and cloned into the other T-DNA at the *Pac* I site, generating the vector pC03. The construct for egg-cell-specific expression of *Barnase* was made by cloning the *Barnase* gene between the *Arabidopsis DD45* promoter (Chen et al., 2012; Wu, 2012; Igawa et al., 2013) and the nopaline synthase terminator. The ovule-specific expression of *AtWUS* (AT2G17950) was engineered by cloning the full-length coding sequence (CDS) of *AtWUS* downstream of the rice ovule-specific *Os02g51090* promoter and upstream of the nopaline synthase terminator (Li et al., 2004; Seagan and Lovett, 2014). The two fragments were synthesized by GenScript and then cloned into pC03 downstream of *Zm-AA1* at the *Asc* I site to make p22W.

The p22W construct was introduced into *Agrobacterium tumefaciens* EHA105 and transformed into hybrid rice 9Y. Callus induction and plant regeneration were performed as previously described (Xia et al., 2019). Transgenic callus selected on medium containing the antibiotic hygromycin.

Pre-germination

T_1- and T_2-generation seeds were randomly sampled in a paper bag, and soaked in a covered container containing purified water at 37°C for 24 hours. The paper bag was removed, and the seeds were wreathed by a wet towel and allowed to sprout in the greenhouse at a temperature of 28°C for 24-48 hours. The seeds were then removed to a dish containing filter paper, and seed germination was observed for seven consecutive days.

Genomic DNA extraction and transgene determination

PCR amplification screens were used to confirm the presence of the *AtWUS* and *Barstar* genes in the transgenic plants. Total genomic DNA was extracted from leaf tissue of both transformed and untransformed plants using the CTAB pyrolysis method (Long et al., 2018). Total genomic DNA was extracted from seeds and endosperm tissue by the Inspection and Testing Center of the State Key Laboratory of Hybrid Rice in Changsha, Hunan Province, China. The PCR assays were performed using 2×Taq PCR Mix (Tiangen). The *AtWUS* CDS

sequence was amplified with the gene-specific primers *WUS*-F (5'-CTGAGACAGTTCGGAAAGATTGA-3') and *WUS*-R (5'-GAAGTTGTAAGGTGCAGATGAGTAA-3'). The rice *OSD1* gene (*Os02g37850*) was used as the internal control for normalization of gene expression. The *Barstar* gene sequence was amplified with the specific primers Bar-3F (5'-AATCCTTTCCCATTCCTCCCACT-3') and Bar-3R (5'-GCTTGCTTTGTTCAAACTGCCTC-3').

Imaging and microscopy

Plants and organs were photographed with a Cannon EOS5D MarkIII digital camera. Double-embryos, embryo-free seeds, and embryo-like structures were observed and imaged with a Leica MZ16FA microscope and a Zeiss SmartZoom5 microscope, respectively. Embryo-free seeds were analysised by I_2-KI staining after cross-section and imaged with a Zeiss SmartZoom5 microscope.

Cytological observation

For phenotypic analysis of embryo-free seeds, self-pollinated flowers from trans-line were collected at 3 DAP. carpels fixed in FAA solution for 24 h at room temperature and then stored in 70% ethanol. Prepare carpels using whole stain-clearing technique. The carpels were scanned with a confocal laser microscope (Zeiss LSM880).

Genotyping and statistical analysis

Genotyping by pinpoint sequencing of multiplex PCR products (Higentec, Changsha and GENOSEQ, Wuhan). We designed characteristic primers for the 1,048 target regions based on the rice genome sequence, and the specific primers were used to amplify 1,048 target regions at the same time by Multiplex-PCR (150-280 bp/per region). We then prepared libraries for next-generation sequencing of the PCR amplification products. Thus, we were able to obtain the genotypes for 5,400 SNP markers within the 1,048 target regions. Genotype calling was performed in the whole genome region using these SNPs which were heterozygous in the parent. The final list of 1,302 high-quality heterozygous SNPs were analyzed for segregation in the progeny plants and the recombination map was constructed for each chromosome (Higentec, Changsha).

Flow cytometry

Leaf cell ploidy was determined by estimating nuclear DNA content using flow cytometry (Ploidy Expert, Beijing). Nuclei for fluorescence-activated cell sorting analysis and DNA-content estimation were prepared using a method described previously (Wang et al., 2019).

Data availability statement

The original contributions presented in the study are publicly available. This data can be found here: NCBI, PRJNA870060.

Author contributions

MC and YX conceived and supervised the project. MC and YX designed the experiments. YX, YW, YH, YZ, JD, NT and JT performed the experiments. YX and YH wrote the manuscript with the help of MC. All authors read and approved the final manuscript.

Funding

This research was financially supported by the Natural Science Foundation of Hainan province (321MS108), the Natural Science Foundation of Changsha city(kq2202348), the Hainan Major Science and Technology Projects(ZDKJ202001) and the 2020 Research Program of Sanya Yazhou Bay Science and Technology City (202002006).

Conflict of interest

The authors declare that the research was conducted in the absence of any commercial or financial relationships that could be construed as a potential conflict of interest.

Publisher's note

Supplementary material

The Supplementary Material for this article can be found online at: https://www.frontiersin.org/articles/10.3389/fpls.2022.999031/full#supplementary-material

SUPPLEMENTARY FIGURE 1

PCR analysis of the transgene in particial progeny plants. **(A)** PCR analysis of the *AtWUS* gene in T_1-generation of trans-line. T_0 transgenic plantlets (lane 1), the wild type 9Y genome (lane 2), T_1 progeny plants(lanes 3-24), positive transgene gave both a 456 bp fragment from *AtWUS* and a 364 bp fragment from the internal control *OSD1* gene. The wild type 9Y genome just give a 364 bp fragment from the internal control *OSD1* gene. **(B)** PCR detection of the *Barstar* gene in T_1 plants of trans-line, T_0 transgenic plantlets (lane 1), The wild type 9Y genome (lane 2), T_1 progeny plants (lanes 3-24), positive transgene gave just a 345 bp fragment. **(C)** PCR analysis of the *AtWUS* gene in T_2-generation of trans-line. The wild type 9Y genome (lane 1), T_2 progeny plants (lanes 3-14). **(D)** PCR analysis of the *Barstar* gene in T_2-generation of trans-line. The wild type 9Y genome (lane 1), T_2 progeny plants(lanes 3-14).

SUPPLEMENTARY TABLE 1

Double-seedings and embryo-free seeds induction in transgenic rice.

SUPPLEMENTARY TABLE 2

Detecting the exogenous gene in transgenic rice.

References

Anderson, S. N., Johnson, C. S., Chesnut, J., Jones, D. S., Khanday, I., Woodhouse, M., et al. (2017). The zygotic transition is initiated in unicellular plant zygotes with asymmetric activation of parental genomes. *Dev. Cell.* 43, 349–358. doi: 10.1016/j.devcel.2017.10.005

Barcaccia, G., and Albertini, E. (2013). Apomixis in plant reproduction: A novel perspective on an old dilemma. *Plant Reprod.* 26, 159–179. doi: 10.1007/s00497-013-0222-y

Bicknell, R. A., and Koltunow, A. M. (2004). Understanding apomixis: recent advances and remaining conundrums. *Plant Cell.* 16, S228–S245. doi: 10.1105/tpc.017921

Boutilier, K., Offringa, R., Sharma, V. K., Kieft, H., Ouellet, T., Zhang, L., et al. (2002). Ectopic expression of BABY BOOM triggers a conversion from vegetative to embryonic growth. *Plant Cell.* 14, 1737–1749. doi: 10.1105/tpc.001941

Catanach, A. S., Erasmuson, S. K., Podivinsky, E., Jordan, B. R., and Bicknell, R. (2006). Deletion mapping of genetic regions associated with apomixis in hieracium. *Proc. Natl. Acad. Sci. U. S. A.* 103, 18650–18655. doi: 10.1073/pnas.0605588103

Chen, G. M., Wu, G., Wu, Y. H., and Lu, C. M. (2012). Developing transgenic plants with no seeds by transforming barnase gene. *J. Agric. Biotec.* 20, 113–120. doi: 10.3969/j.issn 1674-7968.2012.02.001

Conner, J. A., Mookkan, M., Huo, H., Chae, K., and Ozias-Akins, P. (2015). A parthenogenesis gene of apomict origin elicits embryo formation from unfertilized eggs in a sexual plant. *Proc. Natl. Acad. Sci. U. S. A.* 112, 11205–11210. doi: 10.1073/pnas.1505856112

Deyhle, F., Sarkar, A. K., Tucker, E. J., and Laux, T. (2007). WUSCHEL regulates cell differentiation during anther development. *Dev. Biol.* 302, 154–159. doi: 10.1016/j.ydbio.2006.09.013

Gordon-Kamm, B., Sardesai, N., Arling, M., Lowe, K., Hoerster, G., Betts, S., et al. (2019). Using morphogenic genes to improve recovery and regeneration of transgenic plants. *Plants (Basel)* 8, 38. doi: 10.3390/plants8020038

Gross-Hardt, R., Lenhard, M., and Laux, T. (2002). WUSCHEL signaling functions in interregional communication during arabidopsis ovule development. *Genes Dev.* 16, 1129–1138. doi: 10.1101/gad.225202

Hand, M. L., and Koltunow, A. M. (2014). The genetic control of apomixis: asexual seed formation. *Genetics* 197, 441–450. doi: 10.1534/genetics.114.163105

Igawa, T., Yanagawa, Y., Miyagishima, S. Y., and Mori, T. (2013). Analysis of gamete membrane dynamics during double fertilization of arabidopsis. *J. Plant Res.* 126, 387–394. doi: 10.1007/s10265-012-0528-0

Jia, N., Tang, Y. Y., Zeng, Y. R., Zhao, G. M., and Xu, Y. N. (2015). Research progress on apomixis in plants. *Biotec. Bull.* 31, 15–24. doi: 10.13560/j.cnki.biotech.bull.1985.2015.12.003

Khanday, I., Skinner, D., Yang, B., Mercier, R., and Sundaresan, V. (2019). A male-expressed rice embryogenic trigger redirected for asexual propagation through seeds. *Nature* 565, 91–95. doi: 10.1038/s41586-018-0785-8

Koltunow, A. M. (1993). Apomixis: Embryo sacs and embryos formed without meiosis or fertilization in ovules. *Plant Cell* 5, 1425–1437. doi: 10.1105/tpc.5.10.1425

Kwong, R. W., Bui, A. Q., Lee, H., Kwong, L. W., Fischer, R. L., Goldberg, R. B., et al. (2003). LEAFY COTYLEDON1-LIKE defines a class of regulators essential for embryo development. *Plant Cell* 15, 5–18. doi: 10.1105/tpc.006973

Li, J. H., Xu, Y. Y., Zhong, K., and Wang, H. (2004). Analysis of transgenic tobacco with overexpression of arabidopsis WUSCHEL gene. *J. Int. Plant Bio.* 46, 224–229. doi: 10.3321/j.issn:1672-9072.2004.02.015

Long, T., Yang, Y., Fu, D. B., and Wu, C. Y. (2018). A rapid method for isolation of high-quality total DNA using 2 ml centrifugal tube. *Bio* 101, e1010106. doi: 10.21769/BioProtoc1010106

Lotan, T., Ohto, M., Yee, K. M., West, M. A., Lo, R., Kwong, R. W., et al. (1998). Arabidopsis LEAFY COTYLEDON1 is sufficient to induce embryo development in vegetative cells. *Cell* 93, 1195–1205. doi: 10.1016/s0092-8674(00)81463-4

Mayer, K. F., Schoof, H., Haecker, A., Lenhard, M., Jürgens, G., and Laux, T. (1998). Role of WUSCHEL in regulating stem cell fate in the arabidopsis shoot meristem. *Cell* 95, 805–815. doi: 10.1016/s0092-8674(00)81703-1

Mou, T. M. (2016). The research progress and prospects of two-line hybrid rice in China (in Chinese). *Chin. Sci. Bull.* 61, 3761–3769. doi: 10.1360/N972016-01045

Mu, X. J., Cai, X., Sun, D. L., Shi, G. C., and Zhu, Z. Q. (2001). Apomixis and its application prospect. *Acta Agro. Sin.* 27, 590–599. doi: 10.3321/j.issn:0496-3490.2001.05.007

Nardmann, J., and Werr, W. (2006). The shoot stem cell niche in angiosperms: Expression patterns of WUS orthologues in rice and maize imply major modifications in the course of mono- and dicot evolution. *Mol. Biol. Evol.* 23, 2492–2504. doi: 10.1093/molbev/msl125

Ren, G. J., Yan, L. A., and Xie, H. A. (2016). Retrospective and perspective on indica three-line hybrid rice breeding research in China (in Chinese). *Chin. Sci. Bull.* 61, 3748–3760. doi: 10.1360/N972016-01109

Schoof, H., Lenhard, M., Haecker, A., Mayer, K. F., Jürgens, G., and Laux, T. (2000). The stem cell population of arabidopsis shoot meristems in maintained by a regulatory loop between the CLAVATA and WUSCHEL genes. *Cell* 100, 635–644. doi: 10.1016/s0092-8674(00)80700-x

Seagan, A. M., and Lovett, ,. S. J. (2014). A method of screening for genetic elements that induce parthenogenesis in plants. America: CN104039967A.

Steffen, J. G., Kang, I. H., Macfarlane, J., and Drews, G. N. (2007). Identification of genes expressed in the arabidopsis female gametophyte. *Plant J.* 51, 281–292. doi: 10.1111/j.1365-313X.2007.03137.x

Susmita, C., Kumar, S. P. J., Chintagunta, A. D., and Agarwal, D. K. (2021). Apomixis: A foresight from genetic mechanisms to molecular perspectives. *Botanical Rev* 88, 220–256. doi: 10.1007/s12229-021-09266-y

Van Dijk, P. J., Tas, I. C., Falque, M., and Bakx-Schotman, T. (1999). Crosses between sexual and apomictic dandelions (Taraxacum). II. the breakdown of apomixis. *Heredity (Edinb)* 83, 715–721. doi: 10.1046/j.1365-2540.1999.00620.x

Wang, C., Liu, Q., Shen, Y., Hua, Y., Wang, J., Lin, J., et al. (2019). Clonal seeds from hybrid rice by simultaneous genome engineering of meiosis and fertilization genes. *Nat. Biotechnol.* 37, 283–286. doi: 10.1038/s41587-018-0003-0

Wu, J. J. (2012). *Cell-to-cell communication involves in coordinated development of arabidopsis central cell and egg cell* (WuHan University).

Xia, Y. M., Tang, N., Hu, Y. Y., Li, D., Li, S. C., and Bu, X. L. (2019). A method for mechanized hybrid rice seed production using female sterile rice. *Rice* 12, 39. doi: 10.1186/s12284-019-0296-8

Xiong, H. X., Wang, W., and Sun, M. X. (2021). Endosperm development is an autonomously programmed process independent of embryogenesis. *Plant Cell* 33, 1151–1160. doi: 10.1093/plcell/koab007

Yuan, L. P. (2018). The strategy for hybrid rice development. *Hybrid Rice* 33, 1–2. doi: 10.16267/j.cnki.1005-3956.20180920.246

Zuo, J. R., Niu, Q. W., Frugis, G., and Chua, N. H. (2002). The WUSCHEL gene promotes vegetative-to-embryonic transition in arabidopsis. *Plant J.* 30, 349–359. doi: 10.1046/j.1365-313x.2002.01289.x

frontiers | Frontiers in Plant Science

TYPE Original Research
PUBLISHED 11 October 2022
DOI 10.3389/fpls.2022.994214

OPEN ACCESS

EDITED BY
Andrea Mazzucato,
University of Tuscia, Italy

REVIEWED BY
Paul M. Severns,
University of Georgia, United States
Messias Pereira,
State University of the North Fluminense Darcy Ribeiro, Brazil
Arthur Tugume,
Makerere University, Uganda

*CORRESPONDENCE
Songlin He
hsl213@163.com
Dezheng Kong
ylxyky@126.com

SPECIALTY SECTION
This article was submitted to Plant Breeding, a section of the journal Frontiers in Plant Science

RECEIVED 14 July 2022
ACCEPTED 20 September 2022
PUBLISHED 11 October 2022

CITATION
Jia W, Wang Y, Mi Z, Wang Z, He S and Kong D (2022) Optimization of culture medium for *in vitro* germination and storage conditions of *Exochorda racemosa* pollen. *Front. Plant Sci.* 13:994214. doi: 10.3389/fpls.2022.994214

Optimization of culture medium for *in vitro* germination and storage conditions of *Exochorda racemosa* pollen

Wenqing Jia[1,2], Yanli Wang[1,2], Zhaorong Mi[2], Zheng Wang[1], Songlin He[1,2]* and Dezheng Kong[1]*

[1]College of Forestry, Henan Agricultural University, Zhengzhou, China, [2]Postdoctoral Research Base, Henan Institute of Science and Technology, Xinxiang, China

Pollen morphology, pollen vigor, and long-term pollen storage are critical for plant cross-breeding and genetic improvement of *Exochorda racemosa*. We developed a protocol for viability determination and storage of *E. racemosa* pollen for breeding new varieties. The medium components for *E. racemosa* pollen germination was optimized by using an Orthogonal Assay Test Strategy (OATS). The germination rates of *E. racemosa* pollen were investigated after storing at different temperatures and different storage periods. The size of *E. racemosa* pollen was medium with three germination ditches, and the sculptural type of pollen was striate. Red ink and 2,3,5-triphenyl tetrazolium chloride (TTC) can effectively distinguish viable pollen from the unviable pollen of *E. racemosa*. The most suitable medium (CK2) for *E. racemosa* was composed of 150 g· L^{-1} sucrose, 100 mg·L^{-1} boric acid, 150 mg· L^{-1} $Ca(NO_3)_2$ and 50 mg· L^{-1} GA_3. Low-temperature stress produced the greater inhibition of pollen tube growth compared with high-temperature conditions. The CK2 medium at pH 6.5 resulted in the highest pollen germination rate and most extended pollen tube length. The optimal temperature for storage of dried pollen was −80°C ($P < 0.01$), and the germination rate was 53.60% after storage for 390 days. Thawing in a 35°C water bath produced the best viability of *E. racemosa* pollen after storage at −20°C and −80°C. The short-term storage of *E. racemosa* fresh pollen at 4°C was better than that at −20°C and −80°C ($P < 0.01$). It is possible to evaluate pollen quality and store pollen grains for *E. racemosa* by the parameters defined in this study.

KEYWORDS

***Exochorda racemosa*, ultra-morphology, pollen germination, storage, pH, temperature**

Introduction

Exochorda racemosa (Lindl.) Rehder (Rosaceae) is a 2 to 5 m tall tree species native to China. *E. racemosa, E. serratifolia* and *E. giraldii* are also named pearlbush because their inflorescence resembles a string of pearls (Schneider, 2012; Kim et al., 2014; Song et al., 2016; Zhang et al., 2018). *E. racemosa* has white blooms with fan-shaped petals in spring, and its fruits are golden yellow, five-sided capsules (Zhang et al., 2011; Palancean et al., 2015; Zhang et al., 2018). The flowers and tender leaves of *E. racemosa* are used as a high-quality food (Zhang et al., 2018). In addition to having high ornamental, food and medicinal value, *E. racemosa* is also resistant to heat, cold and drought.

Hybridization is an important means of plant speciation (Soltis and Soltis, 2009; Goulet et al., 2017), and it also contributes to increasing intraspecific genetic diversity and the transfer of genetic adaptations (Abdullah Yousuf Akhond et al., 2000; Soltis and Soltis, 2009). Each of the 6-20 key species in the genus *Rosa* contributes a specific trait to modern rose cultivars through hybridization. For example, *Rosa gallica* and other robust polyploid species lend the trait of cold hardiness, and *Rosa chinensis* brings recurrent blooming (Bendahmane et al., 2013). *E. racemosa* is a relatively common garden plant with high ornamental value, but is susceptible to powdery mildew (Zhang et al., 2018). Therefore, it is urgent to genetically improve the powdery mildew resistance of *E. racemosa* through hybridization. However, studies on pollen viability, fertilization ability and storage are very important for hybrid breeding programs, as pollen quality is a key factor in seed set (Wood, 2017; Kaur and Singhal, 2019). Pollen viability, especially the staining rate obtained by the pollen staining method, is not always correlated to the germination rate because pollen may retain metabolic capacity but lose germination ability (Wang et al., 2021). Therefore, the best method to evaluate pollen viability may be a combination of staining and germination test. A germination test is an effective and convenient method to study the applied aspects of pollen biology (Atlagić et al., 2012; Jia et al., 2015; Alexander, 2019). The pollen germination is highly sensitive to not only media components including calcium (Wood, 2017; Sorkheh et al., 2018), boron ions (Shekari et al., 2016; Gokbayrak and Engin, 2017) and sugar (Jia et al., 2020; Jia et al., 2021), but also environmental factors such as temperature (Memmott et al., 2007; Milatović et al., 2015; dos Santos Ferreira et al., 2021) and humidity (Iovane et al., 2021). The pH of the *in vitro* germination medium can also affect pollen germination and pollen tube growth in many plants (Therios et al., 1985; Burke et al., 2004; Mbogning et al., 2007).

Efficient pollen storage is important for artificial pollination, hybrid breeding and dealing with asynchronous flowering (Mesnoua et al., 2018a; Jia et al., 2021). The natural longevity of fresh pollen is typically only 5–15 days, which does not meet the needs of most hybridization procedures. Improving pollen storage methods can help prolong the lifespan of pollen and solve the problem of hybridizing plants with asynchronous flowering (Jia et al., 2020).

Previous research on *E. racemosa* has mainly focused on medicinal value, edible value and tissue culture (Yang and Kamp-Glass, 2000; Lee et al., 2006; Zhang et al., 2011; Zhang et al., 2018). Pollen quality is an important component of pollination biology and is significant in the selection of pollinating species and the identification of pollen pistils and fertilization (Liu et al., 2020). There is little information available on *E. racemosa* pollen quality and its determination. Although reference can be made to the pollen viability of other plant species, appropriate methods for measuring pollen viability for *E. racemosa* must be developed according to its specific pollen characteristics.

Protocols for determining *E. racemosa* pollen viability need to be optimized to perform controlled pollination and evaluate intra- and inter-cultivar incompatibility. Protocols are also needed to arrange the pollinating plants (varieties) for the main cultivars in orchards, as well as for clonal selection and genetic breeding trials. Our goal was to determine the optimal media for *E. racemosa* pollen germination and optimal conditions for pollen storage of *E. racemosa*. The objectives of this study were therefore to: (1) determine the optimal culture medium condition for *in vitro* pollen germination; (2) analyze the relationship between pollen viability estimates obtained through staining and estimates obtained from germination; and (3) determine the best *in vitro* conditions for pollen storage. The results of this study provide technical support for artificial pollination breeding and pollination tree configurations.

Materials and methods

Pollen collection

The flower buds of 8–10 years old *E. racemosa* at the pearl stage were collected from the Grand Canyon of Taihang Mountains in Northern China, and brought back to the laboratory. The anthers were isolated from the flower buds with tweezers and put in Petri dishes, which were later placed in a climatic chamber at 25°C to release pollen grains. After 36h, the fresh pollen grains released from anthers were filtered to eliminate waste using a metal mesh with 50 μm^2 openings. Subsequently, the fresh pollen grains were collected and divided into two parts: one part was used to determine the pollen germination rate, tube length and morphology, and another for preservation.

SEM observation on pollen morphology

The pollen grains were dehydrated in an air dry oven at 45°C for six hours, and then spread on the sample stage with black

double-sided cellophane tape and coated with gold by a sputter coater. The digital micrographs were taken by a SEM (FEI Quanta 200 scanning electron microscope) to analyze the shape and sculpture of pollen grains. The photos of pollen grains were taken at 500–3500 times magnification, and the polar and equatorial diameters of 30 randomly selected pollen grains were measured. The description of pollen morphology was mainly based on the glossaries described by Punt et al. (2007) and Halbritter et al. (2018).

Optimization of culture medium for *in vitro* pollen germination

An orthogonal experimental design ($L_9[3]^4$) was used to optimize the germination medium for *E. racemosa* pollen compared with a pure water culture medium (Table 1, CK1). The number '4' indicates four factors ([1] sucrose, [2] H_3BO_3, [3] GA_3 and [4] $Ca(NO_3)_2$), '3' means three levels ([1] sucrose (120, 150, and 180 g· L^{-1}), [2] H_3BO_3 (80, 100, and 120 mg· L^{-1}), [3] GA_3 (50, 75, and 100 mg· L^{-1}) and [4] $Ca(NO_3)_2$ (50, 100, and 150 mg· L^{-1})), and '9' means nine treatments (Table 1, M_1–M_9). All components of the medium for each treatment were dissolved in distilled water to prepare a liquid medium. Fresh pollen grains (150-200) were placed in a drop of liquid medium (50 μL) on a coverslip which was then inverted over the concave of a concave glass slide, and the slide was placed in Petri dishes covered with absorbent cotton soaked with water (hanging drop technique) (Addicott, 1943). The Petri dishes were incubated at 24°C in a humidity chamber under dark conditions. The germinated pollen grains were counted under a fluorescence microscope (BX53, Olympus, Japan) (10× magnification) after 5h of incubation. The pollen germination rate was determined by counting the number of germinating pollen grains of three slides (two concaves per slide). A pollen grain was considered germinated if the length of the pollen tube was longer than the diameter of the pollen grain (Jia et al., 2020). The pollen germination rate was calculated based on the formula: germination rate = (germinated pollen/total number of pollen grains) × 100.

Pollen staining

Pollen viability was determined by seven staining methods, including red ink (Brilliant crocein + Acid red 87) (Chen et al., 2010), carmine acetate (Mazzeo et al., 2014), TTC (2,3,5-triphenyl tetrazolium chloride) (Luo et al., 2020), MTT (2,5-diphenyl monotetrazolium bromide) (Rodriguez-Riano and Dafni, 2000), I_2-KI (iodine + potassium iodide) (Du et al., 2019), Alexander's stain (Alexander, 1969) and fluorescein diacetate (Dafni, 1992) (Table 2). Seven staining solutions were prepared according to Table 2. Two drops of staining solution were put on a glass slide and pollen samples were sprinkled on the drop with a slim brush. Then, the drop was carefully covered by a coverslip without trapping air after staining for 5–20 min (Table 2) under dark conditions. Viable pollen grains were counted under a fluorescence microscope (BX53, Olympus, Japan) (10× magnification). The deeply stained (Table 2) and normal pollen grains for each staining method were considered to be viable, whereas shriveled, lightly stained or colorless pollen grains were counted as non-viable. For each staining method, the pollen viability rate was determined using three glass slides (at least 200 grains per slide).

TABLE 1 Germination media of *E. racemosa* pollen grains in an orthogonal design assay.

Treatment	Sucrose (g·L^{-1})	Boric acid (mg·L^{-1})	$Ca(NO_3)_2$(mg·L^{-1})	GA_3(mg·L^{-1})	Germination rate (%)
M_1	120	80	50	50	61.54 ± 1.65 C
M_2	120	100	100	75	65.18 ± 1.05 B
M_3	120	120	150	100	54.05 ± 1.50 DE
M_4	150	80	100	100	67.05 ± 1.02 B
M_5	150	100	150	50	80.18 ± 2.52 A
M_6	150	120	50	75	65.20 ± 1.01 B
M_7	180	80	150	75	53.54 ± 1.10 E
M_8	180	100	50	100	56.66 ± 1.08 D
M_9	180	120	100	50	61.68 ± 2.14 C
CK1	0	0	0	0	15.68 ± 1.68 F
K1	60.50 B	60.71 B	61.13 B	67.15 A	
K2	70.81 A	67.58 A	64.88 A	61.55 B	
K3	57.29 C	60.31 B	62.59 B	59.25 B	
R	12.17	6.55	3.38	7.70	

Data shown are the mean ± SD. Different capital letters indicate significant differences at the 0.01 level. K1, K2, and K3 indicate the average pollen germination rate of E. racemosa at three levels of each factor; R represents the extreme difference at the level of the same factor.

TABLE 2 Method to assess pollen viability.

Staining method	Preparation of staining solution	Staining time (min)	Viable color or response
Red ink	1% red ink (Hero)	5	Red
Carmine acetate	1% carmine acetate: 1.0 g carmine acetate (Sigma) dissolved in 100 mL distilled water	5	Red
TTC	0.5% TTC: 0.5 g TTC (Sigma) dissolved in 100 mL 95% alcohol	20	Red
MTT	0.3% MTT: 0.3 g MTT (Sigma) dissolved in 100 mL PBS	20	Violet-purple
I_2-KI	0.5% I_2-KI (Macklin): 80 g potassium iodide KI and 10 g iodine I dissolved in 100 mL distilled water	20	Blue
Alexander's stain	10 mL 95% ethanol, 1 mL of 1% solution malachite green in 95% ethanol, 25 mL glycerol, 5 mL of 1% acid Fuchsin in water, 0.5 mL of 1% solution Orange G in water, 4 mL glacial acetic acid, and distilled water to a total of 100 mL (Macklin)	5	Dark purple
Fluorescein diacetate (FDA)	2 ml 20% saccharose in water with several drops of stock solution of FDA (2 mg FDA/1 ml acetone) (Macklin)	5	Green

Optimization of pH and temperature for *in vitro* pollen germination and pollen tube growth

The components of the control liquid medium (CK2) were 150 g· L^{-1} sucrose, 100 mg· L^{-1} boric acid, 150 mg· L^{-1} $Ca(NO_3)_2$ and 50 mg· L^{-1} GA_3. We adjusted only the pH of CK2 (4.5, 5.0, 5.5, 6.0, 6.5, 7.0, 7.5, and 8.0) to investigate the effect of pH on *in vitro* fresh pollen germination and pollen tube elongation. Temperature experiments were carried out in the same way with temperature gradients of 10°C, 20°C, 25°C, 30°C and 35°C. After 24 h of incubation under dark conditions, the pollen germination rate was calculated as stated before. The pollen tube length was measured using a fluorescence microscope (BX53, Olympus, Japan) with the help of Olympus cellSens standard software (Olympus, Japan). Each treatment for pH or temperature experiment contained three replicates. The germination rate and pollen tube length were based on at least 100 pollen grains per replicate.

Long-term pollen storage

The fresh pollen grains were dehydrated in a drying box at 30°C for 12 h. Pollen grains with an 8–9% water content were categorized as dried pollen. The dried pollen grains and fresh pollen grains (water content of 16–19%) were divided into four parts, and these were stored at 25°C (room temperature), 4°C, −20°C and −80°C. The water content of 0.2 g of pollen grains was determined at 105°C by drying to a constant weight, and the percentage water content of the pollen was calculated (Barnabas and Rajki, 1976). Pollen samples were immersed in liquid nitrogen before storage at −20°C and −80°C. Thirty centrifuge tubes with 0.2 g of pollen grains were placed at each temperature. One centrifuge tube was removed from each storage temperature for pollen germination assays after 5, 10, 30, 50, 70, 90, 120, 180, 270 and 390 days of storage. Stored pollen grains at −20 and −80°C were thawed in a 35°C water bath for 4 min.

All of the stored pollen grains were cultured in a liquid medium consisting of sucrose (150 g·L^{-1}), boric acid (100 mg·L^{-1}), $Ca(NO_3)_2$ (150 mg·L^{-1}) and GA_3 (50 mg·L^{-1}) by the hanging drop technique in an incubator. The conditions were 25 ± 1°C and 50% relative humidity (RH). After 5 h, the pollen germination rate was assessed using a fluorescence microscope (BX53, Olympus, Japan). The design of the germination experiment was completely randomized with three replications (three slides) per storage temperature for each storage time. The germination rates were measured by counting 200 pollen grains for each replication.

Thawing treatments

Dried pollen grains stored at −20°C and −80°C for 120 days were used as experimental materials to perform four thawing tests, which were 35°C water bath for rapid thawing (4 min), 4°C in a refrigerator for slow thawing (30 min), running tap water (18°C) (30 min), and 25°C for room temperature thawing (30 min), respectively. The pollen germination percentage and tube length were determined after thawing. For each thawing treatment, the experiment was repeated at least three times with three biological replications.

Statistical analysis

Data concerning pollen viability, germination and pollen tube length are average values of at least three replicates. All data were statistically analyzed by using SPSS 19.0. the data from experiments were expressed as mean values ± standard deviation. Orthogonal analysis of variance was carried out to determine the significance ($P < 0.01$) of the main effects (sucrose, H_3BO_3, GA_3 and $Ca(NO_3)_2$) on pollen germination, means grouping was with Duncan's test ($p < 0.01$). Data of different temperature, pH and storage time was subjected to one-way

analysis of variance (ANOVA). Differences between samples were determined by Fisher's least significant difference (LSD) test ($P < 0.01$). Moreover, the correlation between pollen viability by staining method and germination rates was statistically evaluated by Pearson's correlation coefficient (r) at a P values of 0.01. All of the figures were drawn using SigmaPlot 14.0 software.

Results

Pollen morphological characteristics

The shape and sculpture of pollen are useful characteristics for the identification of species and the determination of interspecific relationships in Exochorda spp. The average length of pollen grains of E. racemosa was 32.50 ± 3.67 µm, and the average width of the equatorial diameter was 15.60 ± 1.85 µm. The ratio of the length of the polar axis (P) to the equatorial diameter (E) in E. racemosa pollen was ≈2, so the shape of E. racemosa pollen was spheroidal, and the pollen size was medium. The pollen grains had three zonicolpate apertures, each with a width of approximately 3 µm from polar view, which dehisced from one pole to the other along the longitudinal axis (Figures 1A–C). The pollen had striate sculpturing (Figure 1D). Malformed and underdeveloped pollen accounted for 16.56% of the total pollen grains.

Optimization of pollen germination medium for *E. racemosa*

Sucrose concentration had a significant effect on pollen germination *in vitro* ($P < 0.01$), and there was an interaction between factors. Sucrose had the most significant effect (R = 12.17) on pollen germination, with an average range of 57.29–78.81%. The medium with 150 g· L^{-1}sucrose promoted higher germination compared to the medium containing 120 g·L^{-1} sucrose, 180 g·L^{-1}sucrose or no sucrose (Figures 2A–C). This indicated that sucrose was important in pollen germination. A germination rate of 80.18% occurred in M_5 medium, while in the pure water medium (CK1) (Table 1), the germination rate was only 15.68% (Figures 2A, B). Based on the ANOVA, sucrose was the most important factor affecting pollen germination, followed by GA_3, boric acid and Ca $(NO_3)_2$ (Tables 1, 3). The second level of sucrose, $Ca(NO_3)_2$ and boric acid had the highest average value of the three replications (xx = 70.81%, 67.58% and 64.88%, respectively) compared to their first and third levels (Table 1). GA_3 had the highest average value (xx = 67.15%) at the first level compared to the second and third levels (Table 1).

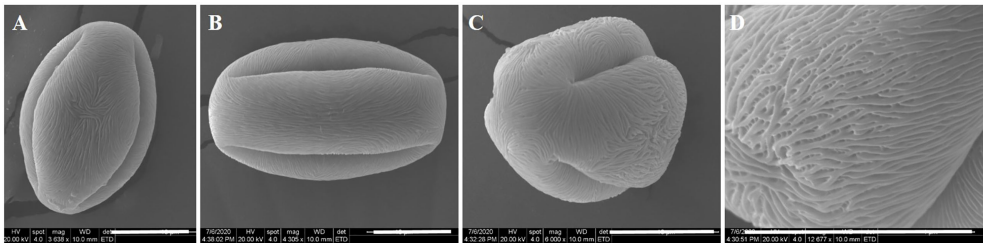

FIGURE 1
Ultra-morphology of pollen grains of *E. racemosa* under the SEM. **(A, B)** Equatorial view; **(C)** Polar view; **(D)** Exine sculptures. Bar = 10 µm.

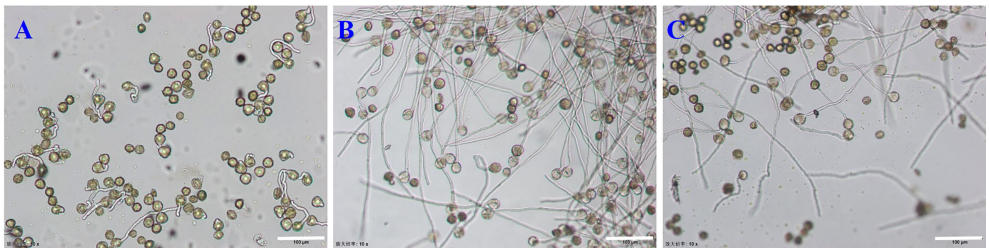

FIGURE 2
Germination rate of *E. racemosa* pollen in different culture media. **(A)** The CK1 medium; **(B)** The M_5 medium; **(C)** The M_7 medium. Bar = 150 µm.

TABLE 3 ANOVA results for the effects of different media on pollen germination of *E. racemosa*.

Source	Variance of square	df	Average of square	F value (*F*)	*P* value
Sucrose	545.29	2	272.64	74.49**	0.0001
Boric acid	284.43	2	142.21	38.86**	0.0001
$Ca(NO_3)_2$	32.13	2	16.06	4.39*	0.0467
GA_3	344.55	2	172.27	47.07**	0.0001
Standard error	32.94	9	3.66		
SUM	1206.38	8	150.80	41.20	0.0001

"*" indicates significant differences ($P < 0.05$). "**" indicates very significant differences ($P < 0.01$).

Optimization of pollen viability estimates for *E. racemosa*

Using existing staining methods, i.e., staining with magenta acetate, Alexander's stain, I_2-KI and MTT, did not distinguish between viable and non-viable pollen (Figures 3A–D). TTC, red ink and fluorescein diacetate can effectively distinguish viable pollen from the unviable pollen for E. racemosa (Figures 3E–H). For TTC staining, the viable pollen was dyed red (Figure 3E) with 79.6% pollen viability, which was similar to the pollen germination (80.18%). For the red ink stain method, red coloring was indicative of viable pollen grains with 82.30% pollen viability, which was similar to the pollen germination (80.18%), whereas the non-viable pollen grains were shriveled or lightly stained (Figure 3F). Fluorescein diacetate gave the highest pollen viability rates(86.25%) (Figures 3G, H), which was statistically different from actual pollen germination (80.18%). The correlations between pollen viability and *in vitro* germination tests were determined. A correlation matrix indicated that the germination rate of pollen grains was positively correlated with pollen viability by the TTC, red ink and fluorescein diacetate staining tests (Table 4). There were no significant differences ($P < 0.01$) in viability measured by TTC and red ink staining and *in vitro* germination test.

Effects of temperature and pH on pollen germination and pollen tube growth

The pollen germination rate and tube lengths were measured to determine the effects of low and high temperatures. Germination rates and tube length of E. racemosa pollen in hanging drop tests exhibited significant differences at different temperatures. The germination rate at 24 h was highest at 82.90% at 25°C, followed by 20°C, 30°C, 10°C and 35°C. Compared to incubation at 25°C, the pollen germination rate at 35°C decreased to 22.60%, while the pollen germination rate only decreased to 72.20% at 20°C. Pollen tube length after 24 h of incubation was highest at 3.2 mm at 25°C (Figures 4A, B). However, low-temperature stressed pollen grains exhibited degradation in tube growth. Under low-temperature stress, the tube length was reduced to 2.9 mm at 20°C and 0.8 mm at 10°C. Pollen tube length decreased to 2.6 mm at 30°C and 1.5 mm at 35°C under high-temperature stress. These results demonstrated that low-temperature stress significantly inhibited pollen tube growth compared to high-temperature conditions.

The pollen germination rate initially increased and then decreased as the pH level of the medium increased (Figure 4C). There were significant differences in pollen germination rates among the different pH levels. The pH 8.0 treatment produced

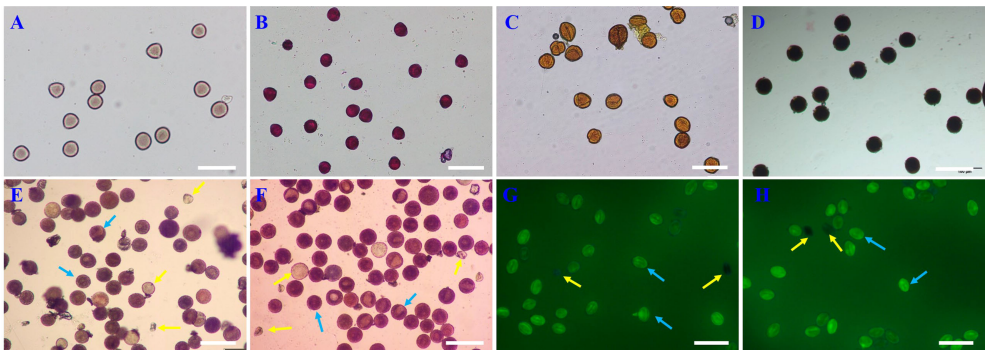

FIGURE 3
Comparison of the seven staining methods for *E racemosa* pollen. **(A)** Carmine acetate; **(B)** Alexander; **(C)** I-KI_2; **(D)** MTT; **(E)** TTC; **(F)** Red ink; **(G, H)** fluorescein diacetate. The yellow arrow indicates non-viable pollen; the blue arrow indicates viable pollen. Bar = 100 μm.

10.3389/fpls.2022.994214

TABLE 4 Correlation matrix between the *in vitro* pollen germination rate (%) and the pollen viability.

	Germination rate	TTC	Red ink	Fluorescein diacetate
Germination rate	1.000			
TTC	0.862**	1.000		
Red ink	0.538**	0.759**	1.000	
Fluorescein diacetate	0.623**	0.815**	0.884**	1.000

"**" indicates that the correlation appeared a very significant level.

the lowest (27.00%) pollen germination rate (Figure 4C). The pH 6.5 treatment had the highest (81.20%) pollen germination rate. This rate was not significantly different from the germination rate (78.90%) in the pH 6.0 treatment. The longest pollen tube length occurred at pH 6.5 and the shortest pollen tube length was recorded at pH 4.5 (Figure 4D).

Effects of storage temperatures and storage times on pollen germination

The effects of different storage temperatures and two different water contents on pollen germination are presented in Table 5. Pollen germination was significantly different following different storage temperatures. For dry pollen, the germination rate of pollen stored at 25°C decreased rapidly with increasing storage time, and pollen lost its viability after 180 days of storage. The pollen germination rate was reduced to 20.5% after storage at 4°C for 390 days. Under storage at −20°C and −80°C, the germination rate of pollen grains slowly decreased. After 390 days, pollen stored at −80°C maintained a germination rate of 53.6%, which was significantly higher than the rate of 40.3% when stored at −20°C. In this study, −80°C was the optimum temperature for storage of dried pollen. Our findings indicated that the longevity of dried pollen at −80°C was longer than 365 days. Similar to dried pollen, the germination rate for fresh pollens also decreased with increased storage time, but the germination rate decreased more rapidly at the four temperatures (Table 5). Fresh pollen

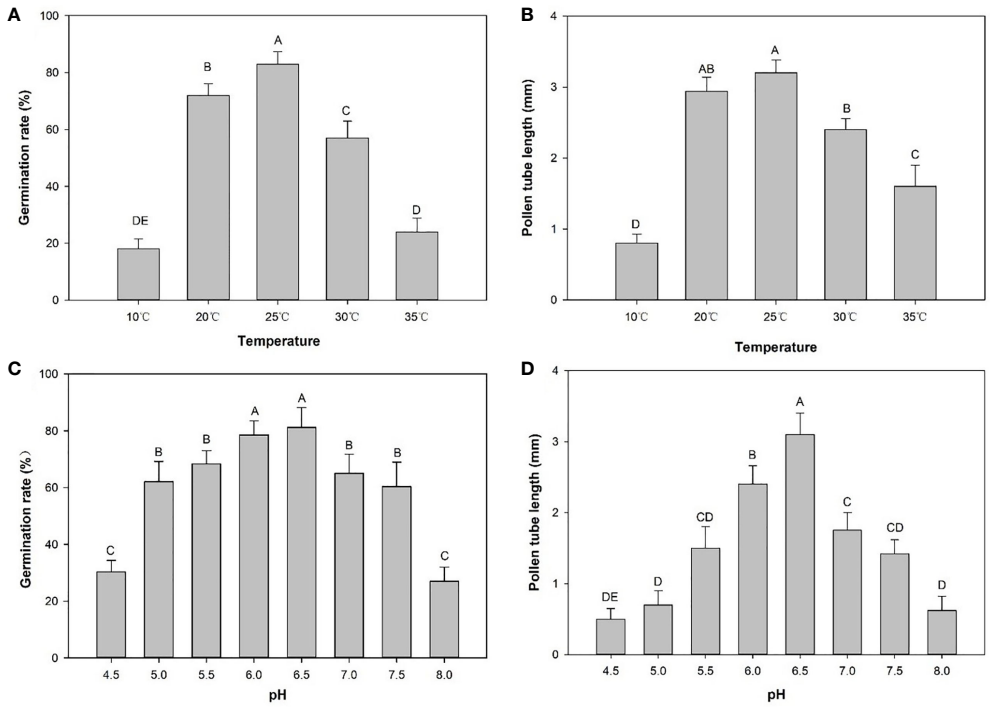

FIGURE 4
Germination rates (%) and pollen tube length (mm) in CK2 medium at different temperatures or pH values. **(A)** Germination rates at different temperatures. **(B)** Pollen tube lengths at different temperatures. **(C)** Germination rates at different pH values. **(D)** Pollen tube lengths at different temperatures. Distinct letters point out the statistically significant differences ($P < 0.01$) and error bars indicate the standard deviations.

10.3389/fpls.2022.994214

TABLE 5 Effects of storage temperature and storage times on *in vitro* pollen germination.

Storage temperature (°C)	Storage time (Days)									
	5	10	30	50	70	90	120	180	270	390
					Dried pollen					
25	61.0B	54.2D	37.2C	18.5D	10.2D	5.3D	2.6D	0.0D	0.0D	0.0D
4	79.2A	73.0C	68.0B	64.0C	60.0C	45.0C	40.0C	36.2C	27.5C	20.5C
−20	77.4A	77.1B	76.6A	72.5B	68.3B	65.6B	60.8B	53.6B	43.2B	40.3B
−80	78.5A	81.5A	78.0A	79.5A	78.0A	75.2A	74.7A	72.5A	60.5A	53.6A
					Fresh pollen					
25	36.0D	18.0D	0.0C	0.0C	0.0C	0.0C	0.0	0.0	0.0	0.0
4	66.0A	62.0A	50.0A	26.0B	12.0C	0.0C	0.0	0.0	0.0	0.0
−20	55.0C	46.1C	35.5B	20.8C	20.5B	10.0B	0.0	0.0	0.0	0.0
−80	59.2B	54.3B	47.6A	34.6A	27.8A	20.5A	8.9	0.0	0.0	0.0

Different capital letters indicate very significant difference ($P < 0.01$).

stored at 25°C lost its viability after 30 days of storage, while pollen grains almost lost most of their viability when stored at 4°C for 70 days (12.0%), at −20°C for 90 days (10.0%), and at −80°C for 120 days (8.9%). The germination rate of dried pollen was significantly higher than that of fresh pollen at different storage times at four storage temperatures. Therefore, it is necessary to reduce the water content of pollen before storage. Compared to 25°C, 4°C and −20°C, −80°C is the optimal storage temperature for dried pollen grains of E. racemosa.

Effects of thawing method on pollen germination

For the dried pollen grains at −80°C after 120 days of storage, the germination rate of pollen after thawing at 35°C was 75.5%. This was significantly higher than that after thawing at 25°C (Figure 5). There were no significant differences between the other thawing methods. For dried pollen grains at −20°C after 120 days of storage, the highest pollen germination rate (60.8%) was observed after thawing at 35°C, followed by thawing at 18°C (57.5%), 4°C (55.0%) and 25°C (52.0%) (Figure 5). After 120 days of storage at −80°C and −20°C, the pollen germination rate was the highest after thawing at 35°C, and the lowest after thawing at 25°C (Figure 5).

Discussion

Pollen morphology

The pollen morphological characteristics are typically stable, showing the common characteristics at the family, genera or specie level (Stafford and Knapp, 2006; Jia et al., 2015; Goncalves-Esteves et al., 2021). Walker (1974) reported that the sculptural types of primitive type pollen are simple, and the pollen sculptural types of advanced species are complex. Plant species with striate pollen are generally more advanced (Walker, 1974). Zhou et al. (1999) found that foveolate pollen is the most primitive, and species with striate pollen are more advanced among the nine species of *Spiraea*. We found that the pollen size of *E. racemosa* was medium and the pollen sculptural type of *E. racemosa* was striate which was similar to *Spiraea purpurea* (Lu et al., 2005). Therefore, we speculate that *E. racemosa* may be a more evolved species within the Spiraeoideae subfamily. However, the palynological data of the subfamily Spiraeoideae are poorly understood, and further research is required to clarify the taxonomic status and phylogenetical relationships of *E. racemosa*.

Pollen germination and pollen staining tests

It is significant to determine pollen germination requirements for cross-pollination (Kremer and Jemrić, 2006; Abdelgadir et al., 2012) because different plants have different requirements for pollen germination (Dane et al., 2004). Sucrose, H_3BO_3, Ca^{2+} and GA_3 are the most commonly used additions for *in vitro* pollen germination assays (Gokbayrak and Engin, 2017; Flores-Rentería et al., 2018). Among them, sucrose not only provides the necessary energy for pollen germination and pollen tube growth, but also maintains the osmotic pressure of the external environment and ensures pollen germination (Hirose et al., 2014). H_3BO_3 increases sugar uptake, translocation and metabolism by pollen cells, inducing Ca^{2+} entry from the outside environment and establishing the Ca^{2+} gradient required for the pollen tube tip growth gradient. Ca^{2+} helps regulate the polar growth and growth direction of pollen tubes (Ren et al., 2022). GA_3 functions in pollen germination and pollen tube growth. Low concentrations of GA_3 can significantly increase the pollen germination rate in apricot (Gokbayrak and Engin, 2017; Flores-Rentería et al., 2018).

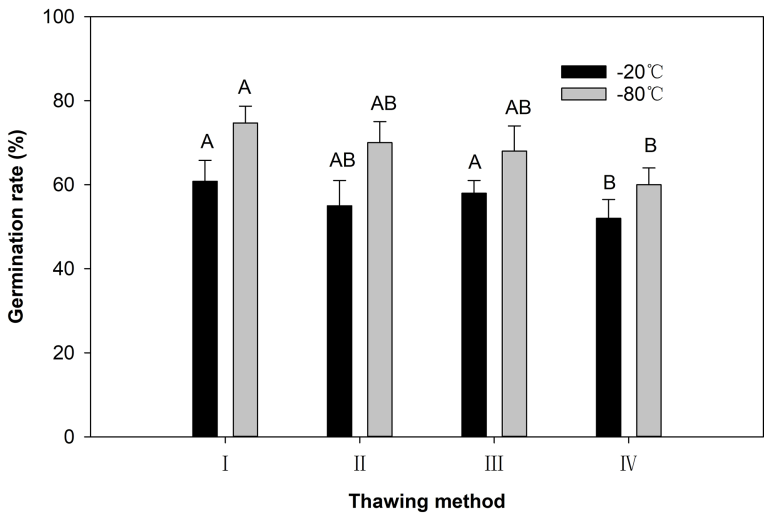

FIGURE 5
The pollen germination rate after different thawing ways. I: Thawing in a water bath at 35°C for 4 min; II: Thawing in a refrigerator at 4°C for 30 min; III: Thawing with running tap water at 18°C for 30 min; IV: Thawing at room temperature (25°C) for 30 min. Different capital letters indicate very significant difference ($P < 0.01$).

Our results showed that the pollen grains still germinated even in the presence of water only, but the germination rate was relatively low (15.68%). A possible explanation is that an ergastic substance stored in pollen provides nutrients for the pollen tube growth. By contrast, the germination rate of *E. racemosa* pollen increased significantly with the addition of sucrose, H_3BO_3, Ca^{2+} and GA_3. These data indicated that the nutrients stored in most *E. racemosa* pollen grains are insufficient to support pollen germination, and the germination of most pollen grains requires exogenous nutrients. The appropriate medium for pollen germination differs widely among plant species (Li et al., 2009; Yu et al., 2010; Luo et al., 2020; dos Santos Ferreira et al., 2021). The orthogonal experiments showed that sucrose and H_3BO_3 were the main factors affecting pollen germination, which was consistent with studies on pollen germination of *Paeonia ludlowii* (Jia et al., 2021), *Ketelee*ria *fortune* (Mesnoua et al., 2018a) and *Paeonia qiui* (Jia et al., 2020).

Staining is a common method used to estimate pollen viability due to its simplicity and speed. However, staining methods are not suitable for evaluating the pollen viability of all plant species (Impe et al., 2020; Luo et al., 2020). Of the seven staining methods tested in this study, only red ink, TTC and fluorescein diacetate could distinguish viable pollen from unviable pollen, and these showed a high correlation with the fresh pollen germination *in vitro*. The pollen viability indicated by red ink and fluorescein diacetate staining was somewhat higher than the actual pollen germination. These data were consistent with the results of Luo et al. (2020) in *Castanea mollissima* pollen grains and Pearson and Harney (1984) in *Rosa* pollen grains. There were no significant differences between the pollen viability estimated from the TTC test and the pollen germination. These results are consistent with those of Abdelgadir et al. (2012), who noted that TTC is an effective method for determining pollen viability in *Jatropha curcas*.

Plant reproductive development is susceptible to extreme temperatures (Mesnoua et al., 2018a; Sorkheh et al., 2018), and high or low temperatures during the reproductive period can lead to lower pollen germination. This can affect fruit and seed setting (Vasilakakis and Porlingis, 1985; Sukhvibul et al., 2000; Pirlak, 2002; Acar and Kakani, 2010). The optimal temperature for pollen germination of most plants ranges from 20°C to 28°C (Sorkheh et al., 2018; Beltrán et al., 2019; Iovane et al., 2021), and only a few species require higher (Mbogning et al., 2007; Cao et al., 2016; Fan et al., 2018) or lower (Li et al., 2005) temperatures. Excessively high or low incubation temperature can reduce pollen germination. Our study simulates the extreme temperature in spring in the Taihang Mountains, and the main purpose was to study the effect of high or low temperature on the pollen germination rate of *E. racemosa*. The results showed that the germination rate of pollen cultured at 10°C or 35°C was significantly lower than that of pollen cultured at 25°C, indicating that both low temperature and high temperature adversely affect pollen germination. Therefore, the effect of temperature on pollen germination should be considered during cross-pollination of *E. racemosa*.

The pH value of the germination medium is the main factor that affects pollen germination in many plants (Munzuroglu et al., 2003; Burke et al., 2004). Zaman (2009) and Fragallah et al. (2019) reported that pH levels affected pollen germination *in vitro*. Fragallah et al. (2019) reported that pollen growth was optimal

at pH 7.0 and worst at pH 5.3. A pH level of 8.5–9.0 was optimal for *in vitro* pollen germination in most cucurbit species (Zaman, 2009). In the present study, the pH value of the germination medium had a significant effect on the germination of *E. racemosa* pollen. This is the first report of the effects of different pH values on the germination of *E. racemosa*. The pollen germination rates increased and then decreased when the pH level increased from 4.5 to 8.0. The pollen germination rate was lowest when the pH of the medium was 4.5. The optimal pH value for pollen germination and pollen tube elongation was 6.5.

Pollen storage

Pollen preservation is important for producing new varieties through hybridization (Báez et al., 2002; Kadri et al., 2022). Pollen longevity can be extended when it has a low moisture content and when stored at low temperatures (Akond et al., 2012; Özcan, 2020). Our results showed that *E. racemosa* pollen stored at four temperatures had lost some germination capacity compared to the fresh pollen. These results are consistent with several other studies in which pollen stored at 25–30°C or 3–4°C in a refrigerator showed lower germination rate than fresh pollen from *Prunus persica* (Devi et al., 2018), *Carya illinoinensis* (Wang et al., 2021) and *Phoenix dactylifera* (Shaheen, 1986; Mortazavi et al., 2010; Maryam et al., 2015). Our results showed that dried pollen still germinates at 50% after 390 days of storage at −80°C, which is the optimal temperature for storage of *E. racemosa*. This suggests that the longevity of *E. racemosa* pollen may exceed 12 months at −80°C. Storing pollen at −20°C would also be a simple way to help maintain pollen potency. *In vitro* germination was significantly higher for pollen stored at −20°C for 390 days compared to 4°C storage, while pollen stored at 25°C for 180 days lost its ability to germinate. These observations were similar to pollen germination from six male varieties of *P. dactylifera*, with a significantly faster reduction in *in vitro* germination at 25°C compared to pollen stored at 4°C or −20°C (Mesnoua et al., 2018b). Jia et al. (2020) and Liu et al. (2020) also reported that pollen viability was significantly higher after −20°C storage than 4°C storage. Our results are also consistent with those of Liu et al. (2020) and Jia et al. (2020), where a higher pollen *in vitro* germination rate was obtained at −20°C, followed by lower germination rates following storage at 4°C and 25°C (Maryam et al., 2015; Jaskani and Naqvi, 2017).

The method used to thaw frozen pollen has an important influence on its germination rate and depends on the plant species and the water content of the pollen (Sun et al., 1998; Xu et al., 2000; Xue et al., 2000). The thawing method is as important as the storage temperature (Wen et al., 1999). Wen et al. (1999) studied the vitrified callus of *Freesia refracta* and concluded that thawing should be rapidly conducted at 40°C. Based on a review of research on the cryopreservation of plant material, Kulus and Zalewska (2014) concluded that slow thawing is usually less effective and more time-consuming than rapid warming. The results of four thawing tests on *E. racemosa* showed that the pollen germination rate and pollen tube length when pollen was thawed at 35°C were significantly better than pollen thawed at 25 °C. These results are not consistent with the results reported by Xu et al. (2000); Xue et al. (2000) and Wang et al. (2021), indicating pollen grains of different species may have different responses to thawing temperatures.

Conclusions

Red ink and TTC can effectively distinguish viable pollen from unviable pollen for *E. racemosa*. Sucrose in germination media can affect pollen germination. The best liquid medium for pollen germination was a medium containing 150 g· L^{-1} sucrose, 100 mg· L^{-1} boric acid, 150 mg· L^{-1} $Ca(NO_3)_2$ and 50 mg· L^{-1} GA_3. This medium resulted in a germination rate of 80.18%. A temperature of 25°C was optimal for pollen germination and pollen tube growth for *E. racemosa*. The length of pollen tubes was four times longer at 25°C compared to lengths at 10°C. The optimal pH for *in vitro* pollen germination was 6.5. The longevity of dried pollen was longer than that of fresh pollen. Storage of *E. racemosa* dried pollen at −80°C preserved pollen germination more effectively than storage at 25°C, 4°C and −20°C. Pollen longevity at −80°C exceeded 365 days. Thawing in a 35°C water bath for 4 min was the best thawing method for pollen stored at −20°C and −80°C.This paper systematically evaluates the influences of the parameters on pollen viability, pollen germination and pollen longevity, and provides theoretical direction for cross-breeding research in *E. racemosa*.

Data availability statement

The original contributions presented in the study are included in the article/supplementary material. Further inquiries can be directed to the corresponding authors.

Author contributions

We conceived and designed the experiments; WJ, YW and DK performed the experiments. YW, ZM, ZW and DK analyzed the data. WJ, ZW, ZM and SH wrote and revised the manuscript. All authors contributed to the article and approved the submitted version.

Funding

This work was supported by The National Key Research and Development Program of China (Grant no.

2018YFD1000401) and Henan Key Research and Development Plan (Grant no. 202102110082).

Conflict of interest

The authors declare that the research was conducted in the absence of any commercial or financial relationships that could be construed as a potential conflict of interest.

Publisher's note

All claims expressed in this article are solely those of the authors and do not necessarily represent those of their affiliated organizations, or those of the publisher, the editors and the reviewers. Any product that may be evaluated in this article, or claim that may be made by its manufacturer, is not guaranteed or endorsed by the publisher.

References

Abdelgadir, H., Johnson, S., and Van Staden, J. (2012). Pollen viability, pollen germination and pollen tube growth in the biofuel seed crop *Jatropha curcas* (Euphorbiaceae). *South Afr. J. Bot.* 79, 132–139. doi: 10.1016/j.sajb.2011.10.005

Abdullah Yousuf Akhond, M., Abul Hossain Molla, M., Obaidul Islam, M., and Ali, M. (2000). Cross compatibility between *Abelmoschus esculentus* and *A. moschatus*. *Euphytica* 114, 175–180. doi: 10.1023/A:1003985728630

Acar, I., and Kakani, V. G. (2010). The effects of temperature on *in vitro* pollen germination and pollen tube growth of pistacia spp. *Sci. Hortic.* 125, 569–572. doi: 10.1016/j.scienta.2010.04.040

Addicott, F. T. (1943). Pollen germination and pollen tube growth, as influenced by pure growth substances. *Plant Physiol.* 18, 270. doi: 10.1104/pp.18.2.270

Akond, A. M., Pounders, C. T., Blythe, E. K., and Wang, X. (2012). Longevity of crapemyrtle pollen stored at different temperatures. *Sci. Hortic.* 139, 53–57. doi: 10.1016/j.scienta.2012.02.021

Alexander, M. (1969). Differential staining of aborted and nonaborted pollen. *Stain Technol.* 44, 117–122. doi: 10.3109/10520296909063335

Alexander, L. (2019). Optimizing pollen germination and pollen viability estimates for *Hydrangea macrophylla*, dichroa febrifuga, and their hybrids. *Sci. Hortic.* 246, 244–250. doi: 10.1016/j.scienta.2018.11.008

Atlagić, J., Terzić, S., and Marjanović-Jeromela, A. (2012). Staining and fluorescent microscopy methods for pollen viability determination in sunflower and other plant species. *Ind. Crops prod.* 35, 88–91. doi: 10.1016/j.indcrop.2011.06.012

Báez, P., Riveros, M., and Lehnebach, C. (2002). Viability and longevity of pollen of nothofagus species in south Chile. *New Z. J. Bot.* 40, 671–678. doi: 10.1080/0028825X.2002.9512822

Barnabas, B., and Rajki, E. (1976). Storage of maize (Zea mays l.) pollen at -196 °C in liquid nitrogen. *Euphytica* 25, 747–752. doi: 10.1007/BF00041614

Beltrán, R., Valls, A., Cebrián, N., Zornoza, C., Breijo, F. G., Armiñana, J. R., et al. (2019). Effect of temperature on pollen germination for several rosaceae species: Influence of freezing conservation time on germination patterns. *PeerJ* 7, e8195. doi: 10.7717/peerj.8195

Bendahmane, M., Dubois, A., Raymond, O., and Bris, M. L. (2013). Genetics and genomics of flower initiation and development in roses. *J. Exp. Bot.* 64, 847–857. doi: 10.1093/jxb/ers387

Burke, J. J., Velten, J., and Oliver, M. J. (2004). *In vitro* analysis of cotton pollen germination. *Agron. J.* 96, 359–368. doi: 10.2134/agronj2004.3590

Cao, M. H., Yang, J. J., Su, J. Q., Lin, Z. J., and Lin, Y. H. (2016). Screening of rapid detection methods for pollen viability of wild canna tianbao. *Fujian Hot Crop Sci. Technol.* 43, 15–17. doi: CNKI:SUN:FJRK.0.2018-02-004

Chen, J., Zhang, Y. X., Tang, F. L., Liu, F. Q., Han, W. B., Liu, J. L., et al. (2010). Methodology study on measurement of alfalfa pollen vitality. *Acta Agrestia Sin.* 18, 297–301. doi: CNKI:SUN:CDXU.0.2010-02-031

Dafni, A. (1992). Pollination ecology: a practical approach. *Oxford Univ. Press* 3, 64–67. doi: 10.1046/j.1420-9101.1993.6050776.x

Dane, F., Olgun, G., and Dalgiç, Ö. (2004). *In vitro* pollen germination of some plant species in basic culture medium. *J. Cell Mol. Biol.* 3, 71–76.

Devi, I., Singh, H., Thakur, A., and Singh, J. (2018). Optimization of pollen storage conditions for low chill peach cultivars. *Indian J. Hortic.* 75, 560–566. doi: 10.5958/0974-0112.2018.00095.6

dos Santos Ferreira, M., Soares, T. L., Costa, E. M. R., da Silva, R. L., de Jesus, O. N., Junghans, T. G., et al. (2021). Optimization of culture medium for the *in vitro* germination and histochemical analysis of passiflora spp. pollen grains. *Sci. Hortic.* 288, 110298. doi: 10.1016/j.scienta.2021.110298

Du, G., Xu, J., Gao, C., Lu, J., Li, Q., Du, J., et al. (2019). Effect of low storage temperature on pollen viability of fifteen herbaceous peonies. *Biotechnol. Rep.* 21, e00309. doi: 10.1016/j.btre.2019.e00309

Fan, T. T., Guo, Z. H., Fu, H. J., Zhang, L., and Ding, Y. L. (2018). Germination and storage characteristics of *Pleioblastus pygmaeus* pollen. *For. Res.* 31 (3), 180–185. doi: 10.13275/j.cnki.lykxyj.2018.03.024

Flores-Rentería, L., Whipple, A. V., Benally, G. J., Patterson, A., Canyon, B., and Gehring, C. A. (2018). Higher temperature at lower elevation sites fails to promote acclimation or adaptation to heat stress during pollen germination. *Front. Plant Sci.* 9, 536. doi: 10.3389/fpls.2018.00536

Fragallah, S. A. D. A., Lin, S., Li, N., Ligate, E. J., and Chen, Y. (2019). Effects of sucrose, boric acid, pH, and incubation time on *in vitro* germination of pollen and tube growth of Chinese fir (*Cunnighamial lanceolata* l.). *Forests* 10, 102. doi: 10.3390/f10020102

Gokbayrak, Z., and Engin, H. (2017). Brassinosteroids and gibberellic acid: effects on *in vitro* pollen germination in grapevine. *OENO One* 51, 303–303. doi: 10.20870/oeno-one.2017.51.4.1862

Goncalves-Esteves, V., Cartaxo-Pinto, S., Marinho, E. B., Esteves, R. L., and Mendonca, C. B. F. (2021). Pollen morphology and evolutionary history of sapindales. *Braz. J. Bot.* 45, 341–66. doi: 10.1007/s40415-021-00719-7

Goulet, B. E., Roda, F., and Hopkins, R. (2017). Hybridization in plants: old ideas, new techniques. *Plant Physiol.* 173, 65–78. doi: 10.1104/pp.16.01340

Halbritter, H., Ulrich, S., Grímsson, F., Weber, M., Zetter, R., Hesse, M., et al. (2018). *Illustrated pollen terminology* (Berlin, Germany: Springer). doi: 10.1007/978-3-319-71365-6

Hirose, T., Hashida, Y., Aoki, N., Okamura, M., Yonekura, M., Ohto, C., et al. (2014). Analysis of gene-disruption mutants of a sucrose phosphate synthase gene in rice, OsSPS1, shows the importance of sucrose synthesis in pollen germination. *Plant Sci.* 225, 102–106. doi: 10.1016/j.plantsci.2014.05.018

Impe, D., Reitz, J., Köpnick, C., Rolletschek, H., Börner, A., Senula, A., et al. (2020). Assessment of pollen viability for wheat. *Front. Plant Sci.* 10, 1588. doi: 10.3389/fpls.2019.01588

Iovane, M., Cirillo, A., Izzo, L. G., Di Vaio, C., and Aronne, G. (2021). High temperature and humidity affect pollen viability and longevity in *Olea europaea* l. *Agronomy* 12, 1. doi: 10.3390/agronomy12010001

Jaskani, M. J., and Naqvi, S. A. (2017). "Storage and viability assessment of date palm pollen," in *Date palm biotechnology protocols volume II* (New York, NY: Springer), 3–13.

Jia, W., Guo, Y., Wang, Y., Zhu, X., Wang, Z., Liu, G., et al. (2020). Effects of storage conditions on pollen longevity of *Paeonia qiui*. *Trans. CSAE* 36, 307–315. doi: CNKI: SUN: NYGU.0.2020-14-038

Jia, W., Wang, Y., Guo, Y., Wang, Z., Qi, Q., Yan, S., et al. (2021). Characterization of pollen germination and storage of *Paeonia ludlowii*. *Sci. Silvae Sinicae* 57, 82–92. doi: 10.11707/j.1001-7488.20210209

Jia, W., Wang, S., and Li, L. (2015). Pollen morphology, storage condition and physiologically dynamic change during storage of *Camellia magniflora*. *Acta Bot. Boreal–Occident Sin.* 35, 754–760. doi: 10.7606/j.issn.1000-4025.2015.04.0754

Kadri, K., Elsafy, M., Makhlouf, S., and Awad, M. A. (2022). Effect of pollination time, the hour of daytime, pollen storage temperature and duration on pollen viability, germinability, and fruit set of date palm (*Phoenix dactylifera l.*) cv" deglet nour". *Saudi J. Biol. Sci.* 29, 1085–1091. doi: 10.1016/j.sjbs.2021.09.062

Kaur, D., and Singhal, V. (2019). Meiotic abnormalities affect genetic constitution and pollen viability in dicots from Indian cold deserts. *BMC Plant Biol.* 19, 1–11. doi: 10.1186/s12870-018-1596-7

Kim, K.-A., Cheon, K.-S., and Yoo, K.-O. (2014). Environmental characteristics of exochorda serratifolia s. Moore habitats. *Korean J. Plant Resour.* 27, 155–173. doi: 10.7732/kjpr.2014.27.2.155

Kremer, D., and Jemrić, T. (2006). Pollen germination and pollen tube growth in *Fraxinus pennsylvanica*. *Biologia* 61, 79–83. doi: 10.2478/s11756-006-0011-2

Kulus, D., and Zalewska, M. (2014). Cryopreservation as a tool used in long-term storage of ornamental species–a review. *Sci. Hortic.* 168, 88–107. doi: 10.1016/j.scienta.2014.01.014

Lee, H.-D., Lee, J.-W., Lee, C.-H., Kim, S.-D., Kim, H.-H., Kim, J.-H., et al. (2006). Effects of storage method, growth regulator, and inorganic salt on the seed germination of exochorda serratifolia s. Moore. *Hortic. Sci. Technol.* 24, 90–94.

Li, L., Liu, Y., and Liu, T. (2009). Study on the effects of the storage conditions on pollen viability of twelve kinds of spiraea. *Gansu Agric. Sci. Technol.* 8, 5–8. doi: 10.3969/j.issn.1001-1463.2009.08.002

Liu, X., Xiao, Y., Wang, Y., Chen, F., Huang, R., and Jiang, Y. (2020). The *in vitro* germination and storage characteristics of *Keteleeria fortunei* var. cyclolepis pollen provide a reference for cross breeding. *Protoplasma* 257, 1221–1230. doi: 10.1007/s00709-020-01509-w

Li, Y. Y., Xu, J., Shi, L., and Li, F. (2005). Examination of pollen germination and vitality of different cultivars of *Ziziphus mauritiana* in greenhouse. *J. Fruit Sci.* 6, 132–134. doi: 10.3969/j.issn.1009-9980.2005.06.031

Lu, L., Hong, W., and Zhongxin, W. (2005). Eight species of pollen morphology of clethraceae and violaceae, with reference to relationships among six families of dillenidae and staphyleaceae. *Acta Botanica Yunnanica* 27, 269–278. doi: 10.3969/j.issn.2095-0845.2005.03.005

Luo, S., Zhang, K., Zhong, W.-P., Chen, P., Fan, X.-M., and Yuan, D.-Y. (2020). Optimization of *in vitro* pollen germination and pollen viability tests for *Castanea mollissima* and *Castanea henryi*. *Sci. Hortic.* 271, 109481. doi: 10.1016/j.scienta.2020.109481

Maryam, M., Fatima, B., Haider, M. S., Abbas, S., Naqvi, M., Ahmad, R., et al. (2015). Evaluation of pollen viability in date palm cultivars under different storage temperatures. *Pak. J. Bot.* 47, 377–381.

Mazzeo, A., Palasciano, M., Gallotta, A., Camposeo, S., Pacifico, A., and Ferrara, G. (2014). Amount and quality of pollen grains in four olive (*Olea europaea* l.) cultivars as affected by 'on'and 'off'years. *Sci. Hortic.* 170, 89–93. doi: 10.1016/j.scienta.2014.02.030

Mbogning, J. B. D., Youmbi, E., and Nkongmeneck, B.-A. (2007). Morphological and *in vitro* germination studies of pollen grains in kola tree (Cola sp.). *Akdeniz Üniversitesi Ziraat Fakültesi Dergisi* 20, 311–318.

Memmott, J., Craze, P. G., Waser, N. M., and Price, M. V. (2007). Global warming and the disruption of plant–pollinator interactions. *Ecol. Lett.* 10, 710–717. doi: 10.1111/j.1461-0248.2007.01061.x

Mesnoua, M., Roumani, M., Bensalah, M., Salem, A., and Benaziza, A. (2018a). Optimization of conditions for *in vitro* pollen germination and pollen tube growth of date palm (*Phoenix dactylifera* l.). *J. Fundam. Appl. Sci.* 10, 158–167. doi: 10.4314/jfas.v10i1.11

Mesnoua, M., Roumani, M., and Salem, A. (2018b). The effect of pollen storage temperatures on pollen viability, fruit set and fruit quality of six date palm cultivars. *Sci. Hortic.* 236, 279–283. doi: 10.1016/j.scienta.2018.03.053

Milatović, D., Nikolić, D., and Radović, A. (2015). The effect of temperature on pollen germination and pollen tube growth of apricot cultivars. *III Balkan Symp. Fruit Growing* 1139, 359–362. doi: 10.17660/ActaHortic.2016.1139.62

Mortazavi, S., Arzani, K., and Moeini, A. (2010). Optimizing storage and *in vitro* germination of date palm (Phoenix dactylifera) pollen. *J. Agric. Sci. Technol. (JAST)* 12 (2), 181–189. doi: 10.1007/s10806-009-9189-y

Munzuroglu, O., Obek, E., and Geckil, H. (2003). Effects of simulated acid rain on the pollen germination and pollen tube growth of apple (*Malus sylvestris* miller cv. golden). *Acta Biolo. Hungarica* 54, 95–103. doi: 10.1556/ABiol.54.2003.1.10

Özcan, A. (2020). Effect of low-temperature storage on sweet cherry (*Prunus avium* l.) pollen quality. *HortScience* 55, 258–260. doi: 10.21273/HORTSCI14660-19

Palancean, A., Onika, E., and Rosca, I. (2015). Growth and development peculiarities of the species *Exochorda racemosa* in the republic of Moldova. *International Scientific Symposium Conservation of Plant Diversity*, ASM (Chisinau, Republic of Moldova: ArtPoligraf press), 88.

Pearson, H., and Harney, P. (1984). Pollen viability in Rosa. *HortScience* 19, 710–711.

Pirlak, L. (2002). The effects of temperature on pollen germination and pollen tube growth of apricot and sweet cherry. *Gartenbauwissenschaft* 67, 61–64.

Punt, W., Hoen, P., Blackmore, S., Nilsson, S., and Le Thomas, A. (2007). Glossary of pollen and spore terminology. *Rev. palaeobot. palynol.* 143, 1–81. doi: 10.1016/j.revpalbo.2006.06.008

Ren, R., Zhou, H., Zhang, L., Jiang, X., and Liu, Y. (2022). Ca^{2+} participates in programmed cell death by modulating ROS during pollen cryopreservation. *Plant Cell Rep.* 41, 1043–57. doi: 10.1007/s00299-022-02836-3

Rodriguez-Riano, T., and Dafni, A. (2000). A new procedure to asses pollen viability. *Sex. Plant Reprod.* 12, 241–244. doi: 10.1007/s004970050008

Schneider, S. (2012). Wilson's pearlbush (Exochorda giraldii var. wilsonii): A gem to the core. *Arnoldia* 69, 36–36. doi: 10.2307/42955532

Shaheen, M. (1986). Pistil receptivity in three cultivars of date palm (*Phoenix dactylifera* l.). *Proc. 1 Hot. Sci. Conf. st Tanta Univ. Egypt. Sept.* 11, 489–499.

Shekari, A., Nazeri, V., and Shokrpour, M. (2016). Pollen viability and storage life in *Leonurus cardiaca* l. *J. Appl. Res. Med. AROMA* 3, 101–104. doi: 10.1016/j.jarmap.2016.02.004

Soltis, P. S., and Soltis, D. E. (2009). The role of hybridization in plant speciation. *Annu. Rev. Plant Biol.* 60, 561–588. doi: 10.1146/annurev.arplant.043008.092039

Song, J.-H., Kong, M.-J., Oak, M.-K., and Hong, S.-P. (2016). A study on the distribution, external morphological characteristics and soil condition of *Exochorda serratifolia* s. Moore. *Korean J. Environ. Ecol.* 30, 929–938. doi: 10.13047/KJEE.2016.30.6.929

Sorkheh, K., Azimkhani, R., Mehri, N., Chaleshtori, M. H., Halász, J., Ercisli, S., et al. (2018). Interactive effects of temperature and genotype on almond (*Prunus dulcis* l.) pollen germination and tube length. *Sci. Hortic.* 227, 162–168. doi: 10.1016/j.scienta.2017.09.037

Stafford, P., and Knapp, S. (2006). Pollen morphology and systematics of the zygomorphic-flowered nightshades (Solanaceae; salpiglossideae sensu D'Arc and cestroideae sensu D'Arc Pro parte): A review. *Syst. Biodivers.* 4, 173–201. doi: 10.1017/S1477200005001787

Sukhvibul, N., Whiley, A. W., Vithanage, V., Smith, M. K., Doogan, V. J., and Hetherington, S. E. (2000). Effect of temperature on pollen germination and pollen tube growth of four cultivars of mango (Mangifera indica l.). *J. Hortic. Sci. Biotechnol.* 75 (2), 214–222. doi: 10.1080/14620316.2000.11511226

Sun, X., Xing, S., Lu, D., and Wang, J. (1998). Studies of the vitality of ginkgo pollen. *J. Fruit Sci.* 15 (1), 58–64.

Therios, I., Tsirakoglou, V., and Dimassi-Theriou, K. (1985). Physiological aspects of pistachio (*Pistacia vera* l.) pollen germination. *Rivista di ortoflorofrutticoltura italiana*, 161–70.

Vasilakakis, M., and Porlingis, I. (1985). Effect of temperature on pollen germination, pollen tube growth, effective pollination period, and fruit set of pear. *HortScience* 20, 733–735. doi: 10.21273/HORTSCI.20.4.733

Walker, J. W. (1974). Evolution of exine structure in the pollen of primitive angiosperms. *Am. J. Bot.* 61, 891–902. doi: 10.1002/j.1537-2197.1974.tb12315.x

Wang, X., Wu, Y., and Lombardini, L. (2021). *In vitro* viability and germination of *Carya illinoinensis* pollen under different storage conditions. *Sci. Hortic.* 275, 109662. doi: 10.1016/j.scienta.2020.109662

Wen, Y., Chunyan, L., Xiuling, B., Hengchun, L., and Li, W. (1999). Study on callus cryopreservation of freesia refracta klatt. *J. Northeast Nor. Univ.* 4, 70–72.

Wood, B. W. (2017). Flavonoids, alkali earth, and rare earth elements affect pecan pollen germination. *HortScience* 52, 85–88. doi: 10.21273/HORTSCI11426-16

Xue, M. N., Liu, H. Y., and Rao, G. R. (2000). Study on low temperature preservation of shatinyu's pollen. *Guihaia* 20, 367–370.

Xu, G. B., He, F., and Huang, X. G. (2000). Studied of *in vitro* culture and conservation of maidenhair tree (*Ginkgo bilobna* l.) germplasm. *J. Cent. South For Univ.* 20, 27–30. doi: 10.3969/j.issn.1673-923X.2000.01.005

Yang, G., and Kamp-Glass, M. (2000). *In vitro* culture initiation and proliferation of *Exochorda racemosa*. *HortScience* 35, 397. doi: 10.21273/HORTSCI.35.3.397C

Yu, Y., Zhang, H., Ma, L., and Tan, Z. (2010). Studies on the pollen vitality and storage capacity of *Physocarpus*. *Northern hortic.* 10, 71–72. doi: CNKI:SUN:BFYY.0.2010-10-027

Zaman, M. R. (2009). Effect of pH on *in vitro* pollen germination of fourteen cultivated and wild species of cucurbit. *J. Bio-Sci.* 17, 129–133. doi: 10.3329/jbs.v17i0.7120

Zhang, Y., Li, X., Dong, Z., Wang, M., Chen, G., Liu, X., et al. (2018). First report of powdery mildew caused by erysiphe alphitoides on *Exochorda racemosa* in China. *Plant Dis.* 102, 2037–2037. doi: 10.1094/PDIS-02-18-0227-PDN

Zhang, J., Li, X., Ren, L., Fang, C., and Wang, F. (2011). Chemical constituents from *Exochorda racemosa*. *China J. Chin. materia Med.* 36, 1198–1201. doi: 10.1007/s11606-010-1517-4

Zhou, L., Wei, Z., and Zheng, Y. (1999). Poll`en morphology of spiraeoideae in China (Rosaceae). *Acta Bota. Yunnanica* 21, 303–308. doi: 10.3969/j.issn.2095-0845.1999.03.004

Frontiers in
Plant Science

Cultivates the science of plant biology and its applications

The most cited plant science journal, which advances our understanding of plant biology for sustainable food security, functional ecosystems and human health.

Discover the latest Research Topics

See more →

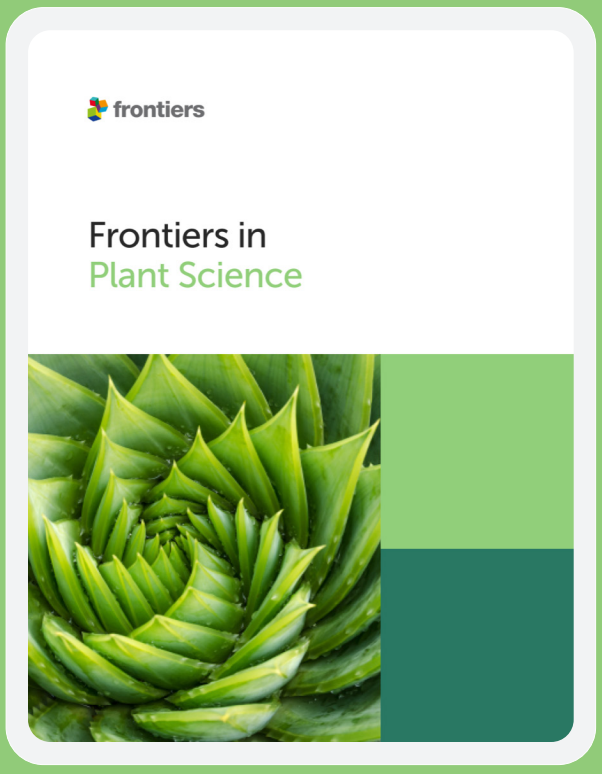

Frontiers

Avenue du Tribunal-Fédéral 34
1005 Lausanne, Switzerland
frontiersin.org

Contact us

+41 (0)21 510 17 00
frontiersin.org/about/contact